

Edinburgh Napier
UNIVERSITY



Assessing the toxicity of engineered
nanomaterials in the male reproductive
system: Developing an improved testing
strategy for hazard assessment

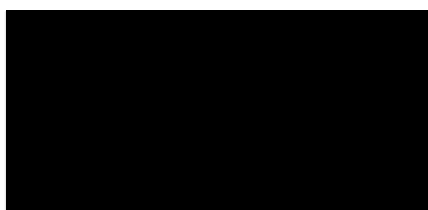
Bryony Louise Ross BSc, MSc, MRSB, ERT

January 2019

*A thesis submitted in partial fulfilment of the requirements of Edinburgh Napier
University, for the award of Doctor of Philosophy*

Declaration

I declare that the work in this thesis is the result of independent work, carried out by the author. Part of the research was conducted within work package 9 of the European Commission FP7 NMP project MARINA: Managing Risks of Nanoparticles (project number 263215) which ran from November 2011 – October 2015. The involvement of this project was limited to establishing cytotoxicity of a nanomaterial panel (within chapter 3) and all relevant work was entirely undertaken by the PhD applicant. Where people contributed, they are acknowledged in full. This thesis has not been submitted for any other degree or professional qualification.



Bryony L Ross, student no: [REDACTED]
January 21st, 2019

Abstract

Reproduction is the only certain constant within animals and maintaining the integrity of this process is key to ensuring survival of the species. However, male fertility rates in the Western world are in decline and the use of assisted reproductive techniques rising (Makarow and Hojgaard, 2010). With emerging technologies such as nanotechnologies presenting both enormous benefits alongside new risks, there is a clear need to understand and manage these potential novel threats to male reproductive health. However, the animal burden associated with such research is extreme, therefore consideration of how to reduce, refine or replace animal use in the associated developmental and reproductive toxicity (DART) testing is paramount.

This research aimed to assess the toxicity of engineered nanomaterials (ENM) in the male reproductive system and develop an improved testing strategy for hazard assessment of DART. Using a panel of highly representative ENM, assays to screen for toxicity in male testicular cell lines were established and optimised *in vitro*. Findings were then validated for reliability and reproducibility against those generated using similar test systems with cells from alternative organs of the body. Assessment of cell and endocrine function also provided a deeper understanding of cellular responses following acute sub-lethal ENM exposure.

Comparison of outcomes *in vitro* to *in vivo* was enabled by appraisal of tissues from animals exposed orally to the same ENM. Through this, a new method by which to stage tubules for histopathological analysis was developed, and for the first time a truly thorough morphological and stereological examination of tissues for markers of effect provided. Assimilation of key findings made it possible to conclude that silver ENM are reproductive toxicants and potential endocrine disruptors. The accumulated results were also used to guide development of a novel Integrated Approach to Testing and Assessment (IATA) for male reproductive toxicity from ENM.

Acknowledgements

Throughout the time I was researching and then writing this doctoral thesis, so many people in my life (friends, family and colleagues) have made the whole process possible and more importantly, an almost enjoyable 6 years! However, a number of these people need special recognition for their input and support.

First, thanks go to Prof. Lang Tran of IOM Edinburgh, for his encouragement to pursue completion of a PhD and facilitation of the MARINA project, within which part of this doctorate was completed. Lang always believed this was something I should complete and is due huge thanks for both helping make this happen, and for checking in so regularly on my progress. Thanks also goes to Prof. Rob Aitken, without whose influence I would never have found nanotechnology or toxicology as specialist subjects, and to Mrs Hilary Cowie, for her supportive attitude and management whilst my time was balanced between being a student and employed member of staff at IOM.

From Edinburgh Napier University, I would like to convey enormous thanks and gratitude to my supervisory team, Dr. Gary Hutchison, Dr. Eva Malone and Prof. Mick Rae for their guidance, wisdom, encouragement and patience with me through this process. Gary; having known you for a lot longer than the duration of this PhD there was never any doubt that you'd be the most supportive, kind, nurturing, wise and easy to get along with supervisor I could ask for. Thank you for giving me the chance to 'have a go' at this Doctorate malarkey, for your support through the tough parts, willingness to let me find my own path where needed, and for always making time to talk despite your increasingly manic schedule in recent years. Mick; thank you for your grounding influence, unwavering supply of sound advice, ability to remain stoic and offer endless reassurance that 'it's all dead easy really' even when I was throwing you the most asinine questions possible about PCR. For your cognisant questioning of my work as it emerged in thesis form, and latterly your much-needed pep talks, all of which were always sprinkled a plenty with humour and anecdotes. You've always made me think things might just turn out ok! Eva; thank you for being the voice of reason and reality in the group, for always helping to bring us back onto track in meetings and keeping the end

goal in sight, for keeping me hungry for the finish line by reminding me of what I was there to achieve when I felt lost, and for offering words of support and encouragement when I needed a boost. Your knowledge and input brought me so many different ways of thinking that I am hugely grateful for. You are all truly remarkable humans – I couldn't have asked for a better supervisory team.

In addition, massive thanks go to Dr. Lesley Young within the technical team at Edinburgh Napier university for her countless hours of help, sharing her knowledge and doing a huge amount to help keep the process of the PhD running, especially at times when I was running between study and full-time work. The lab work wouldn't have been possible to complete without your support, thank you. For their support on RT-PCR additional thanks go to Ms. Sadie Kemp and Dr. Katarzyna Siemienowicz for sharing their knowledge, reagents, and patience! For her expert advice and ideas on trouble-shooting for Western Blotting I would also like to thank Dr Jennifer Frazer. I would also like to thank two honours and masters students whom following my supportive role in their work in the histology lab were able to contribute to aspects of the studies within chapter 4; Erin Werner BSc honours student for her assistance with pilot RP-1 immunostaining, and Małgorzata Ślęzak for her contribution on toward expanding aspects of the histology-based work.

For their collaboration on the histology aspects of this doctorate, and training in animal-handling related to organ collection, I would like to extend thanks to Dr. Hans Bouwmeester and his colleagues at Wageningen University, and Prof. Flemming Cassee, Dr. Ilse Gosens and their colleagues at RIVM Netherlands. For sharing her wealth of knowledge around histological staining techniques, and assistance with scanning prepared slides I would like to thank Mrs Debbie Faichney at the University of Stirling. I would also like to thank Professor emeritus Randolph Richards for his expert advice and review on my histopathological analysis of tissues.

For their time helping me to understand semi-quantitative analysis of histological findings via the GRID analysis I would like to thank Prof. Richard Lea and Dr. Rebecca Sumner of the University of Nottingham.

I would like to thank from the bottom of my heart my parents, Prof. Lindsay Ross and Dr. Barbara Ross for their unwavering support – emotional, scientific, financial, editorial

and edible – through this process. I’m not sure they’ll ever know how grateful I am. Simply put, you’re the best humans I know, and I would have never completed without you both. For his willingness to take on a girl with ridiculously long working hours, high stress levels, ability to spend hours each day talking about testicles on a screen, often resulting in a ‘needy’ demeanour, thanks and love go to my fiancé Paul Burke – you’ve kept me laughing through this. I would also like to extend a huge thank you to my close friends Dr. Laura Gray and Dr. Karen Galea for their friendship, help, advice and company drowning ‘*a few*’ bottles of wine through this process. Laura thank you so much for the expert help on the statistics, and patience with my relentless questioning at all hours! Karen thank you for always checking in on my progress, and for your advice, support or simply offer of a much-needed open ear to chew over problems. I consider myself very lucky to have people like you both in my life.

For always being much needed calm in the storm, I must send love to my horses Blue & Gold; they are quite simply the best therapy. Lastly, for their voracious desire to walk on the keyboard, knock over coffee cups, and sit on the back of my study chair, I would like to thank my ‘co-authors’ Marshmallow and Bumblebee the cats. I like to tell myself they were trying to help...

Table of Contents

DECLARATION	I
ABSTRACT	II
ACKNOWLEDGEMENTS.....	I
TABLE OF CONTENTS	IV
LIST OF FIGURES	VIII
LIST OF TABLES	XVIII
ABBREVIATIONS	XXI
PRESENTATIONS AND PUBLICATIONS RELATING TO THIS THESIS	XXVIII
PAPERS AND BOOK CHAPTER CONTRIBUTIONS:	XXVIII
ORAL PRESENTATIONS:	XXVIII
POSTER PRESENTATIONS:	XXIX
CHAPTER 1: INTRODUCTION AND LITERATURE REVIEW	30
INTRODUCTION	30
MALE REPRODUCTIVE ANATOMY	30
MALE REPRODUCTIVE PHYSIOLOGY	34
NANOTECHNOLOGIES AND THE EMERGENCE OF NANOTOXICOLOGY.....	37
REPRODUCTIVE & DEVELOPMENTAL TOXICITY & DART TESTING.....	41
CURRENT UNDERSTANDING OF MALE REPRODUCTIVE NANOTOXICOLOGY	49
SUMMARY	71
OBJECTIVES OF THE RESEARCH PROGRAMME.....	73
CHAPTER 2: SELECTION, HANDLING AND PREPARATION OF THE ENGINEERED NANOMATERIAL PANEL.....	75
INTRODUCTION	75
SELECTION OF THE NANOMATERIAL PANEL.....	76
NANOMATERIAL WEIGHING AND HANDLING	77

PROTOCOL FOR WEIGHING NM-300 AG AND PREPARATION OF STOCK SOLUTION FOR DISPERSION	81
PROTOCOL FOR WEIGHING MATERIALS OTHER THAN NM-300 & PREPARATION OF STOCK SOLUTION FOR DISPERSION	81
DISPERSION PROTOCOLS FOR ENM	82
DISPERSION PROTOCOL (<i>IN VITRO</i>).....	82
DISPERSION PROTOCOL (<i>IN VIVO</i>)	83
OTHER PREPARATIONS OF ENM USED: ENM FEED MIXES (<i>IN VIVO</i>)	83
DISPOSAL OF ENM	84

CHAPTER 3: *IN VITRO* TOXICITY OF A PANEL OF ENM 85

INTRODUCTION	85
EXISTING KNOWLEDGE <i>IN VITRO</i>	85
EXISTING APPROACHES TO DART AND THE NEED FOR DEVELOPMENT OF <i>IN VITRO</i> APPROACHES	86
INITIAL STEPS TOWARD DEVELOPING <i>IN VITRO</i> METHODS TO APPRAISE REPRODUCTIVE TOXICITY OF ENM	88
OBJECTIVES	90
MATERIALS AND METHODS	91
THE NANOMATERIAL PANEL AND ITS PREPARATION.....	91
EXPRESSION OF DOSE FOR <i>IN VITRO</i> WORK.....	91
SELECTION AND ESTABLISHMENT OF OPTIMAL GROWTH CONDITIONS FOR THE TM3 LEYDIG CELL LINE...	92
CONTROL FOR HORMONE INTERFERENCE IN ASSAYS <i>IN VITRO</i>	93
CYTOTOXICITY ASSESSMENT	94
ALAMAR BLUE (AB) ASSAY.....	95
STATISTICAL ANALYSIS	97
RESULTS.....	98
COMPARISON OF CELL VIABILITY IN CHARCOAL-STRIPPED AND STANDARD FBS.....	98
TOXICOLOGICAL ASSESSMENT OF ENM PANEL: CELL PROLIFERATION ASSAYS.....	99
WST-1 ANALYSIS – PRISTINE COPPER OXIDE NANOTUBES (CUO).....	112
TIME COURSE APPRAISAL OF CYTOTOXICITY	113
DISCUSSION	123
OPTIMISATION OF PROTOCOLS: ASSAY INTERFERENCE AND FUTURE ENDOCRINE WORK.....	123
CYTOTOXICITY AND TIME- AND DOSE- DEPENDENT EFFECTS	124

CHAPTER 4: FUNCTIONAL CHANGES TO LEYDIG CELL BEHAVIOUR FOLLOWING ENM EXPOSURE 137

INTRODUCTION	137
OBJECTIVES	148
MATERIALS AND METHODS	149
RNA EXPRESSION VIA RP-QPCR	149
PROTEIN EXPRESSION VIA WESTERN BLOT	158

STATISTICAL ANALYSIS	165
RESULTS.....	167
RNA QUANTIFICATION AND INTEGRITY	167
GENORM 12 GENE PANEL ANALYSIS.....	168
PRIMER EFFICIENCY TESTING	170
PCR	172
WESTERN BLOTTING	176
DISCUSSION	181
PCR ANALYSIS FOR RNA EXPRESSION	182
WESTERN BLOT ANALYSIS	189
FINAL CONCLUSIONS AND NEXT STEPS	192

CHAPTER 5: HISTOLOGICAL ANALYSIS OF CHANGES TO RAT TESTIS FOLLOWING EXPOSURE TO ENM **194**

INTRODUCTION	194
TESTICULAR MORPHOLOGY IN DETAIL	195
SPERMATOGENESIS	200
THE SPERMATOGENIC CYCLE IN THE RAT	202
<i>EFFECTS OF ENM ON MALE REPRODUCTIVE HEALTH FOLLOWING ORAL EXPOSURE.....</i>	<i>203</i>
OBJECTIVES.....	210
MATERIALS AND METHODS	211
ANIMAL STUDY I: SILVER NANOPARTICLE TREATMENTS.....	211
ANIMAL STUDY II: SILICA NANOPARTICLE TREATMENTS.....	212
SELECTION OF TISSUE AND ITS PREPARATION	214
HAEMATOXYLIN AND EOSIN (H&E) STAINING.....	215
IMMUNOHISTOCHEMISTRY.....	216
IMAGE CAPTURE.....	220
MORPHOLOGICAL ANALYSIS OF TISSUES	221
IMMUNOHISTOCHEMICAL ANALYSIS:.....	221
STEREOLOGICAL ANALYSIS OF TUBULES I: BASIC MEASUREMENTS.....	222
STEREOLOGICAL ANALYSIS OF TUBULES II: STAGING AND RELATED MEASUREMENTS	222
STATISTICAL ANALYSIS	228
RESULTS.....	230
MORPHOLOGICAL ANALYSIS OF CONTROL TISSUES.....	230
MORPHOLOGICAL ANALYSIS OF TREATED TISSUES.....	232
IMMUNOHISTOCHEMICAL ANALYSIS OF TISSUES	242
STEREOLOGICAL ANALYSIS OF TUBULES I: SEMI-QUANTITATIVE ANALYSIS.....	252
COUNT DATA	252
COMPARISON OF CONTROL DATA.....	252
INITIAL MEASUREMENT RESULTS: TUBULE DIAMETER.....	253
INITIAL MEASUREMENT RESULTS: GERM CELL LAYER THICKNESS	255

STEREOLOGICAL ANALYSIS OF TUBULES II: STAGING AND RELATED MEASUREMENTS	257
NUMBER OF OBSERVATIONS.....	263
DAZL STAINING INTENSITY AND TUBULE STAGE	263
EVALUATION OF CONTROL DATA	265
CROSS-EVALUATION OF CONTROL DATA WITH PUBLISHED DATA TO DETERMINE RELIABILITY.....	266
TUBULE DIAMETER ANALYSIS	267
LUMEN VOLUME BY STAGE ANALYSIS:	270
THE EFFECT OF TUBULE SHAPE ON RECORDED VALUES	274
DISCUSSION.....	277
<u>CHAPTER 6: DISCUSSION.....</u>	298
ESTABLISHING SUITABLE ASSAYS FOR HIGH-THROUGHPUT SCREENING OF ENM CYTOTOXICITY	298
EVALUATION OF CELLULAR PARAMETERS RELATED TO FERTILITY AND ENDOCRINE FUNCTION	300
HISTOLOGICAL APPRAISAL OF RELEVANT FERTILITY & ENDOCRINE ENDPOINTS IN ANIMALS EXPOSED TO ENM <i>IN VIVO</i>.....	305
COMPARISON OF RESULTS <i>IN VITRO</i> TO <i>IN VIVO</i>	309
FORMATION OF AN INTEGRATED APPROACH TO TESTING AND ASSESSMENT (IATA) FOR MALE DART FOLLOWING EXPOSURE TO NANOMATERIALS.	315
CONCLUSIONS AND FUTURE WORK.....	318
<u>REFERENCE LIST</u>	320
<u>APPENDIX 1: PUBLISHED WORK FROM CHAPTER 3</u>	335
<u>APPENDIX 2: EXPERIMENTAL OUTLINE FOR WST-1 & ALAMAR BLUE ASSAYS.....</u>	336
<u>APPENDIX 3: PREPARATION OF RNA SAMPLES FOR PCR</u>	337
<u>APPENDIX 4: RNA SAMPLE QUANTIFICATION & INTEGRITY SCORING.....</u>	338

List of Figures

FIGURE 1: BASIC TESTICULAR ANATOMY, SHOWING THE MAJOR ARCHITECTURE OF THIS ASPECT OF THE MALE REPRODUCTIVE SYSTEM. FROM (BHIMJI AND LESLIE, 2018)	31
FIGURE 2: SCHEMATIC SHOWING STRUCTURE OF THE SEMINIFEROUS TUBULE. WITHIN TUBULES, SERTOLI CELLS (SC) SIT ON THE BASAL MEMBRANE, THEIR CYTOPLASM PROJECTING TOWARD THE CENTRAL LUMEN AT VARYING LENGTHS DEPENDING ON STAGE OF THE SPERMATOGENIC CYCLE, ‘NURSING’ DEVELOPING SPERMATOCYTES ALONG THEIR LENGTH. SC ARE CONNECTED VIA HIGHLY CONTROLLED CELLULAR JUNCTIONS TO FORM THE BLOOD TESTIS BARRIER. WITHIN THE INTERSTITIUM LIE BLOOD CAPILLARIES, LYMPHATIC VESSELS AND LEYDIG CELLS (LC), WHICH ARE RESPONSIBLE FOR GENERATION OF ANDROGENS TO SUPPORT SC IN MANAGING SPERMATOGENESIS, AMONGST OTHER ROLES IN MAINTENANCE OF THE MALE REPRODUCTIVE SYSTEM. FROM (BARRETT ET AL., 2019)	32
FIGURE 3: GONADAL HORMONE TARGETS, PATHWAYS, FEEDBACK LOOPS AND ROUTE OF METABOLISM AND EXCRETION IN MALES AND FEMALES. FROM: (NETTER, 1997).....	35
FIGURE 4: PHYSICO-CHEMICAL PROPERTIES OF NANOMATERIALS THAT SHOULD BE CONSIDERED WITH HIGH PRIORITY IN TOXICOLOGICAL ASSESSMENTS. FROM (JOHNSTON ET AL., 2010)	40
FIGURE 5: STAGES OF THE REPRODUCTIVE AND DEVELOPMENTAL CYCLE ACCORDING TO THE TWO MAJOR REGULATORY APPROACHES: US FOOD AND DRUG ADMINISTRATION (FDA) AND THE INTERNATIONAL CONFERENCE ON HARMONISATION (ICH). SEGMENTS I (FERTILITY), II (EMBRYOTOXICITY/TERATOGENICITY) AND III (PERI/POST-NATAL TOXICITY) REPRESENT THE FDA TESTING STRATEGY. STAGES A (PRE-MATING TO CONCEPTION), B (CONCEPTION TO IMPLANTATION), C (IMPLANTATION TO CLOSURE OF THE HARD PALATE), D (CLOSURE OF HARD PALATE TO END OF PREGNANCY), E (BIRTH TO WEANING) AND F (WEANING TO SEXUAL MATURITY) REPRESENT THE ICH APPROACH. NB. ICH STAGE C SPANS BOTH SEGMENT II AND III, AS INDICATED BY THE DOTTED WHITE LINE). ADAPTED FROM (SPIELMANN, 2009).	42
FIGURE 6: THE FOUR GENERATIONS OF NANOTECHNOLOGY. FROM (ROCCO, 2005)	75
FIGURE 7: DOUBLING TIME OF TM3 CELLS, SEEDING IN A T25 FLASK AT A DENSITY 1×10^6 CELLS IN 10ML MEDIA. N=1. VIABLE CELLS IDENTIFIED VIA TRYPAN BLUE EXCLUSION; COUNTS UNDERTAKEN WITH NEUBAUER COUNTING CHAMBER.	93
FIGURE 8: THE REDUCTION OF THE TETRAZOLIUM SALT WST-1 TO INSOLUBLE FORMAZAN IN METABOLICALLY ACTIVE CELLS. EC=ELECTRON COUPLING AGENT, RS=MITOCHONDRIAL SUCCINATE-TETRAZOLIUM-REDUCTASE SYSTEM. FROM (ROCHE, 2011).....	94
FIGURE 9: COMPARISON FOR SERUM TYPE – STANDARD FBS VS CHARCOAL STRIPPED FBS. VIABILITY OF CELLS FOLLOWING 24H EXPOSURE TO ZINC OXIDE (NM-110 & 111) USING THE WST-1 CYTOTOXICITY ASSAY. ALL VALUES CORRECTED FOR WST-1 INTERFERENCE WITH ASSAY. DOSES FROM $0.037-60.24 \mu\text{g}/\text{cm}^2$. N=3.	98
FIGURE 10: VIABILITY OF TM3 CELLS EXPOSED TO TITANIUM DIOXIDE ENM: NM-101, 103 & 104 FOR 24H ASSESSED USING THE WST-1 CYTOTOXICITY ASSAY (N=5). VIABILITY EXPRESSED AS % RELATIVE TO UNTREATED (ENDOGENOUS) CONTROL. DOSES $0.037-60.24 \mu\text{g}/\text{cm}^2$. ALL VALUES CORRECTED FOR WST-1 INTERFERENCE WITH ASSAY.	100
FIGURE 11: BOX AND WHISKERS REPRESENTATION OF VIABILITY OF TM3 CELLS CULTURED IN CHARCOAL STRIPPED SERUM, FOLLOWING 24H EXPOSURE TO TITANIUM DIOXIDE (NM-101, NM-103 AND NM-104) USING THE WST-1 CYTOTOXICITY ASSAY (N=6). DOSES $0.037-60.24 \mu\text{g}/\text{cm}^2$. ALL VALUES CORRECTED FOR WST-1 INTERFERENCE WITH ASSAY. DOSE 0 IS UNTREATED (NEGATIVE) CONTROL. WHERE A STATISTICALLY SIGNIFICANT LOSS IN VIABILITY OF CELLS WAS IDENTIFIED COMPARED TO CONTROL, ASTERISKS DEPICT LEVEL OF SIGNIFICANCE (* P=0.05, ** P=0.01, *** P=0.001 & **** P=0.0001).	100
FIGURE 12: VIABILITY OF CELLS CULTURED IN CHARCOAL STRIPPED SERUM, FOLLOWING 24H EXPOSURE TO ZINC OXIDE (NM-110 & 111) OR ZINC IONS (ZnSO_4), ASSESSED USING THE WST-1 CYTOTOXICITY ASSAY. VIABILITY EXPRESSED AS % RELATIVE TO UNTREATED (ENDOGENOUS) CONTROL. DOSES FROM $0.037-60.24 \mu\text{g}/\text{cm}^2$. N=5 FOR NM-110 & NM-111, N=3 FOR ZnSO_4 . ALL VALUES CORRECTED FOR WST-1 INTERFERENCE WITH ASSAY.	101
FIGURE 13: BOX AND WHISKERS REPRESENTATION OF VIABILITY OF TM3 CELLS CULTURED IN CHARCOAL STRIPPED SERUM, FOLLOWING 24H EXPOSURE TO ZINC ENM AND IONIC ZINC (NM-110, NM-111 AND ZnSO_4) USING THE WST-1	

CYTOTOXICITY ASSAY (N=6). DOSES 0.037-60.24 μ G/CM ² . ALL VALUES CORRECTED FOR WST-1 INTERFERENCE WITH ASSAY. DOSE 0 IS UNTREATED (NEGATIVE) CONTROL. ALL VALUES CORRECTED FOR WST-1 INTERFERENCE WITH ASSAY. N=5 FOR NM-110 & NM-111, N=3 FOR ZNSO ₄ . . WHERE A STATISTICALLY SIGNIFICANT LOSS IN VIABILITY OF CELLS WAS IDENTIFIED COMPARED TO CONTROL, ASTERISKS DEPICT LEVEL OF SIGNIFICANCE (* P=0.05, ** P=0.01, *** P=0.001 & **** P=0.0001).	102
FIGURE 14: NON-LINEAR CURVE SHOWING TOXICITY OF NM-110 TO TM3 CELLS. DOSES 0.037-60.24 μ G/CM ² . N=5. THE DATA OUTPUT WAS TESTED FOR NORMALITY USING BOTH THE D'AGOSTINO-PEARSON OMNIBUS NORMALITY TEST AND THE SHAPIRO-WILK NORMALITY TEST, RESIDUALS PLOTTED, AND OUTLIERS COUNTED USING THE ROUT COEFFICIENT. OUTLIERS IDENTIFIED ARE HIGHLIGHTED IN RED. THE LC ₅₀ VALUE WAS IDENTIFIED TO BE 3.813 μ G/CM ²	103
FIGURE 15: NON-LINEAR CURVE SHOWING TOXICITY OF NM-111 TO TM3 CELLS. DOSES 0.037-60.24 μ G/CM ² . N=5. THE DATA OUTPUT WAS TESTED FOR NORMALITY USING BOTH THE D'AGOSTINO-PEARSON OMNIBUS NORMALITY TEST AND THE SHAPIRO-WILK NORMALITY TEST, RESIDUALS WERE PLOTTED, AND OUTLIERS COUNTED USING THE ROUT COEFFICIENT. OUTLIERS ARE HIGHLIGHTED IN RED WHERE PRESENT. THE LC ₅₀ VALUE WAS IDENTIFIED TO BE 6.052 μ G/CM ²	104
FIGURE 16: VIABILITY OF CELLS CULTURED IN CHARCOAL STRIPPED SERUM, FOLLOWING 24H EXPOSURE TO SILICA DIOXIDE (NM-200 & 203), ASSESSED USING THE WST-1 CYTOTOXICITY ASSAY (N=6). VIABILITY EXPRESSED AS % RELATIVE TO UNTREATED (ENDOGENOUS) CONTROL. DOSES FROM 0.037-60.24 μ G/CM ² . ALL VALUES CORRECTED FOR WST-1 INTERFERENCE WITH ASSAY.	105
FIGURE 17: BOX AND WHISKERS REPRESENTATION OF VIABILITY OF TM3 CELLS CULTURED IN CHARCOAL STRIPPED SERUM, FOLLOWING 24H EXPOSURE TO SILICA DIOXIDE ENM (NM-200 & 203) USING THE WST-1 CYTOTOXICITY ASSAY (N=6). DOSES 0.037-60.24 μ G/CM ² . DOSE 0 IS UNTREATED (NEGATIVE) CONTROL. ALL VALUES CORRECTED FOR WST-1 INTERFERENCE WITH ASSAY. WHERE A STATISTICALLY SIGNIFICANT LOSS IN VIABILITY OF CELLS WAS IDENTIFIED COMPARED TO CONTROL, ASTERISKS DEPICT LEVEL OF SIGNIFICANCE (* P=0.05, ** P=0.01, *** P=0.001 & **** P=0.0001).	106
FIGURE 18: VIABILITY OF CELLS CULTURED IN CHARCOAL STRIPPED SERUM, FOLLOWING 24H EXPOSURE TO SILVER, SILVER DISPERSANT AND IONIC SILVER (NM-300, NM-300DIS AND AgNO ₃), ASSESSED USING THE WST-1 CYTOTOXICITY ASSAY (N=6). VIABILITY EXPRESSED AS % RELATIVE TO UNTREATED (ENDOGENOUS) CONTROL. DOSES FROM 0.037-60.24 μ G/CM ² . ALL VALUES CORRECTED FOR ENM AND WST-1 INTERFERENCE WITH ASSAY.	107
FIGURE 19: BOX AND WHISKERS REPRESENTATION OF VIABILITY OF TM3 CELLS CULTURED IN CHARCOAL STRIPPED SERUM, FOLLOWING 24H EXPOSURE TO SILVER (NM-300), SILVER DISPERSANT (NM-300DIS) AND IONIC SILVER (AgNO ₃) USING THE WST-1 CYTOTOXICITY ASSAY (N=6). DOSES 0.037-60.24 μ G/CM ² . ALL VALUES CORRECTED FOR ENM AND WST-1 INTERFERENCE WITH ASSAY. DOSE 0 IS UNTREATED (NEGATIVE) CONTROL. ALL VALUES CORRECTED FOR WST-1 INTERFERENCE WITH ASSAY. WHERE A STATISTICALLY SIGNIFICANT LOSS IN VIABILITY OF CELLS WAS IDENTIFIED COMPARED TO CONTROL, ASTERISKS DEPICT LEVEL OF SIGNIFICANCE (* P=0.05, ** P=0.01, *** P=0.001 & **** P=0.0001).	107
FIGURE 20: NON-LINEAR CURVE SHOWING TOXICITY OF NM-300 TO TM3 CELLS. DOSES 0.037-60.24 μ G/CM ² . N=6. THE DATA OUTPUT WAS TESTED FOR NORMALITY USING BOTH THE D'AGOSTINO-PEARSON OMNIBUS NORMALITY TEST AND THE SHAPIRO-WILK NORMALITY TEST, RESIDUALS WERE PLOTTED, AND OUTLIERS COUNTED USING THE ROUT COEFFICIENT. OUTLIERS ARE HIGHLIGHTED IN RED. THE LC ₅₀ VALUE WAS IDENTIFIED TO BE 7.885MG/CM ²	108
FIGURE 21: NON-LINEAR CURVE SHOWING TOXICITY OF AgNO ₃ TO TM3 CELLS. DOSES 0.037-60.24 μ G/CM ² . N=6. THE DATA OUTPUT WAS TESTED FOR NORMALITY USING BOTH THE D'AGOSTINO-PEARSON OMNIBUS NORMALITY TEST AND THE SHAPIRO-WILK NORMALITY TEST, RESIDUALS WERE PLOTTED, AND OUTLIERS COUNTED USING THE ROUT COEFFICIENT. OUTLIERS ARE HIGHLIGHTED IN RED. THE LC ₅₀ VALUE WAS IDENTIFIED TO BE 6.052 μ G/CM ²	109
FIGURE 22: VIABILITY OF CELLS CULTURED IN CHARCOAL STRIPPED SERUM, FOLLOWING 24H EXPOSURE TO CARBON NANOTUBES (NM-400, 401 & 403), ASSESSED USING THE WST-1 CYTOTOXICITY ASSAY (N=3). VIABILITY EXPRESSED AS % RELATIVE TO UNTREATED (ENDOGENOUS) CONTROL. DOSES FROM 0.037-60.24 μ G/CM ² . ALL VALUES CORRECTED FOR WST-1 INTERFERENCE WITH ASSAY.	110
FIGURE 23: BOX AND WHISKERS REPRESENTATION OF VIABILITY OF TM3 CELLS CULTURED IN CHARCOAL STRIPPED SERUM, FOLLOWING 24H EXPOSURE TO CARBON NANOTUBES (NM-400, NM-401 & NM-403) USING THE WST-1 CYTOTOXICITY ASSAY (N=3). DOSES 0.037-60.24 μ G/CM ² . ALL VALUES CORRECTED FOR WST-1 AND INTERFERENCE	

WITH ASSAY. DOSE 0 IS UNTREATED (NEGATIVE) CONTROL. WHERE A STATISTICALLY SIGNIFICANT LOSS IN VIABILITY OF CELLS WAS IDENTIFIED COMPARED TO CONTROL, ASTERISKS DEPICT LEVEL OF SIGNIFICANCE (* p=0.05, ** p=0.01, *** p=0.001 & **** p=0.0001). 111

FIGURE 24: BOX AND WHISKERS REPRESENTATION OF VIABILITY OF TM3 CELLS CULTURED IN CHARCOAL STRIPPED SERUM, FOLLOWING 24H EXPOSURE TO PRISTINE COPPER OXIDE USING THE WST-1 CYTOTOXICITY ASSAY (N=3). DOSES 0.037-60.24µg/cm². ALL VALUES CORRECTED FOR WST-1 INTERFERENCE WITH ASSAY. DOSE 0 IS UNTREATED (NEGATIVE) CONTROL. WHERE A STATISTICALLY SIGNIFICANT LOSS IN VIABILITY OF CELLS WAS IDENTIFIED COMPARED TO CONTROL, ASTERISKS DEPICT LEVEL OF SIGNIFICANCE (* p=0.05, ** p=0.01, *** p=0.001 & **** p=0.0001)..... 112

FIGURE 25: NON-LINEAR CURVE SHOWING TOXICITY OF PRISTINE CUO TO TM3 CELLS. DOSES 0.037-60.24µg/cm². N=3. THE DATA OUTPUT WAS TESTED FOR NORMALITY USING BOTH THE D'AGOSTINO-PEARSON OMNIBUS NORMALITY TEST AND THE SHAPIRO-WILK NORMALITY TEST, RESIDUALS WERE PLOTTED, AND OUTLIERS COUNTED USING THE ROUT COEFFICIENT. OUTLIERS ARE HIGHLIGHTED IN RED. THE LC₅₀ VALUE WAS IDENTIFIED TO BE 7.752MG/cm²..... 113

FIGURE 26: TIMECOURSE ASSAY FOLLOWING EXPOSURE TO TiO₂ (NM-101) AT THE HIGH DOSE RANGE 0.037MG/cm² TO 60.24MG/cm² IN THE PRESENCE OF ALAMAR BLUE (N=3). TIMEPOINTS REPRESENTED: A = T2H, B = T4H, C = T6H, D = T24H. WHERE A STATISTICALLY SIGNIFICANT LOSS IN VIABILITY OF CELLS WAS IDENTIFIED COMPARED TO CONTROL, ASTERISKS DEPICT LEVEL OF SIGNIFICANCE (* p=0.05, ** p=0.01, *** p=0.001 & **** p=0.0001)..... 114

FIGURE 27: TIMECOURSE ASSAY FOLLOWING EXPOSURE TO TiO₂ (NM-101) AT THE LOW DOSE RANGE 0.037MG/cm² TO 60.24MG/cm² IN THE PRESENCE OF ALAMAR BLUE (N=3). TIMEPOINTS REPRESENTED: A = T2H, B = T4H, C = T6H, D = T24H. WHERE A STATISTICALLY SIGNIFICANT LOSS IN VIABILITY OF CELLS WAS IDENTIFIED COMPARED TO CONTROL, ASTERISKS DEPICT LEVEL OF SIGNIFICANCE (* p=0.05, ** p=0.01, *** p=0.001 & **** p=0.0001)..... 115

FIGURE 28: TIMECOURSE ASSAY FOLLOWING EXPOSURE TO UNCOATED ZNO (NM-110) AT THE HIGH DOSE RANGE 0.037MG/cm² TO 60.24MG/cm² IN THE PRESENCE OF ALAMAR BLUE (N=3). TIMEPOINTS REPRESENTED: A = T2H, B = T4H, C = T6H, D = T24H. WHERE A STATISTICALLY SIGNIFICANT LOSS IN VIABILITY OF CELLS WAS IDENTIFIED COMPARED TO CONTROL, ASTERISKS DEPICT LEVEL OF SIGNIFICANCE (* p=0.05, ** p=0.01, *** p=0.001 & **** p=0.0001). 116

FIGURE 29: TIMECOURSE ASSAY FOLLOWING EXPOSURE TO UNCOATED ZNO (NM-110) AT THE LOW DOSE RANGE 0.037MG/cm² TO 60.24MG/cm² IN THE PRESENCE OF ALAMAR BLUE (N=3). TIMEPOINTS REPRESENTED: A = T2H, B = T4H, C = T6H, D = T24H. NOTE THE ADJUSTED Y AXIS ON (D) TO INCORPORATE INCREASED VARIABILITY IN READINGS. WHERE A STATISTICALLY SIGNIFICANT LOSS IN VIABILITY OF CELLS WAS IDENTIFIED COMPARED TO CONTROL, ASTERISKS DEPICT LEVEL OF SIGNIFICANCE (* p=0.05, ** p=0.01, *** p=0.001 & **** p=0.0001)..... 117

FIGURE 30: TIMECOURSE ASSAY FOLLOWING EXPOSURE TO COATED ZNO (NM-111) AT THE HIGH DOSE RANGE 0.037MG/cm² TO 60.24MG/cm² IN THE PRESENCE OF ALAMAR BLUE (N=3). TIMEPOINTS REPRESENTED: A = T2H, B = T4H, C = T6H, D = T24H. WHERE A STATISTICALLY SIGNIFICANT LOSS IN VIABILITY OF CELLS WAS IDENTIFIED COMPARED TO CONTROL, ASTERISKS DEPICT LEVEL OF SIGNIFICANCE (* p=0.05, ** p=0.01, *** p=0.001 & **** p=0.0001). 118

FIGURE 31: TIMECOURSE ASSAY FOLLOWING EXPOSURE TO COATED ZNO (NM-111) AT THE LOW DOSE RANGE 0.037MG/cm² TO 60.24MG/cm² IN THE PRESENCE OF ALAMAR BLUE (N=3). TIMEPOINTS REPRESENTED: A = T2H, B = T4H, C = T6H, D = T24H. NOTE THE Y AXIS SCALE ON (D) IS INCREASED TO INCORPORATE VARIANCE IN READINGS. WHERE A STATISTICALLY SIGNIFICANT LOSS IN VIABILITY OF CELLS WAS IDENTIFIED COMPARED TO CONTROL, ASTERISKS DEPICT LEVEL OF SIGNIFICANCE (* p=0.05, ** p=0.01, *** p=0.001 & **** p=0.0001)..... 119

FIGURE 32: TIMECOURSE ASSAY FOLLOWING EXPOSURE TO SILVER (NM-300) AT THE HIGH DOSE RANGE 0.037MG/cm² TO 60.24MG/cm² IN THE PRESENCE OF ALAMAR BLUE (N=3). TIMEPOINTS REPRESENTED: A = T2H, B = T4H, C = T6H, D = T24H. WHERE A STATISTICALLY SIGNIFICANT LOSS IN VIABILITY OF CELLS WAS IDENTIFIED COMPARED TO CONTROL, ASTERISKS DEPICT LEVEL OF SIGNIFICANCE (* p=0.05, ** p=0.01, *** p=0.001 & **** p=0.0001)..... 120

FIGURE 33: TIMECOURSE ASSAY FOLLOWING EXPOSURE TO SILVER (NM-300) AT THE LOW DOSE RANGE 0.037MG/cm² TO 60.24MG/cm² IN THE PRESENCE OF ALAMAR BLUE (N=3). TIMEPOINTS REPRESENTED: A = T2H, B = T4H, C = T6H, D = T24H. NOTE THE Y AXIS SCALE ON (C & D) IS INCREASED TO INCORPORATE VARIANCE IN READINGS. WHERE A STATISTICALLY SIGNIFICANT LOSS IN VIABILITY OF CELLS WAS IDENTIFIED COMPARED TO CONTROL, ASTERISKS DEPICT LEVEL OF SIGNIFICANCE (* p=0.05, ** p=0.01, *** p=0.001 & **** p=0.0001)..... 121

FIGURE 34: TIMECOURSE ASSAY FOLLOWING EXPOSURE TO SILVER DISPERSANT (NM-300DIS)) AT THE HIGH DOSE RANGE 0.037MG/cm² TO 60.24MG/cm² IN THE PRESENCE OF ALAMAR BLUE (N=1). TIMEPOINTS REPRESENTED: A = T2H, B

= T4H, C = T6H, D = T24H. WHERE A STATISTICALLY SIGNIFICANT LOSS IN VIABILITY OF CELLS WAS IDENTIFIED COMPARED TO CONTROL, ASTERISKS DEPICT LEVEL OF SIGNIFICANCE (* P=0.05, ** P=0.01, *** P=0.001 & **** P=0.0001).	122
FIGURE 35: LUTEINIZING HORMONE RECEPTOR AND ITS COMMON SECOND MESSENGER PATHWAYS. LH = LUTEINIZING HORMONE, G = G PROTEIN, AC = ADENYL CYCLASE, ATP = ADENOSINE TRIPHOSPHATE, CAMP = CYCLIC ADENOSINE MONOPHOSPHATE, PKA= PROTEIN KINASE A, PLC = PHOSPHOLIPID-SPECIFIC PHOSPHOLIPASE C, ERK 1/2= EXTRACELLULAR SIGNAL-REGULATED KINASE, PKC = PROTEIN KINASE C, AKT =PROTEIN KINASE B. FROM (CHOI AND SMITZ, 2014).	140
FIGURE 36: LOCATION AND ROLE OF SELECTED KEY PLAYERS IN STEROIDOGENESIS WITHIN THE LEYDIG CELL. REGULATORY AND STEROIDOGENIC PATHWAYS IN THE LEYDIG CELL. HIGHLIGHTED ARE RECEPTORS, ENZYMES AND MOLECULES OF INTEREST WHICH HAVE BEEN SELECTED FOR FURTHER ANALYSIS VIA FUNCTIONAL ASSAYS. LH-R: LH RECEPTOR, G: G PROTEIN, AC: ADENYL CYCLASE, PKA: PROTEIN KINASE A, STAR: STEROIDOGENIC ACUTE REGULATORY PROTEIN, PBR: PERIPHERAL BENZODIAZEPINE RECEPTOR, SR-BI: SCAVENGER RECEPTOR CLASS B TYPE 1, ES-10: CARBOXYESTERASE, HS-LIPASE: HORMONE SENSITIVE LIPASE, NCE: NEUTRAL CHOLESTEROL ESTERASE. IMAGE ADAPTED FROM (CHEN ET AL., 2007).	142
FIGURE 37: CONVERSION OF CHOLESTEROL TO PREGNENOLONE BY P450SCC.	144
FIGURE 38: KEY STEROID BIOSYNTHETIC PATHWAYS IN LEYDIG CELLS. ENZYMES EXAMINED USING PROTEIN AND RNA WORK ARE HIGHLIGHTED IN RED. P450SCC = SIDE CHAIN CLEAVAGE ENZYME; 3B-HSD = 3B-HYDROXYSTEROID. REPRODUCED FROM PAYNE (2007).	145
FIGURE 39: ANDROGEN RECEPTOR GENOMIC AND NON-GENOMIC MECHANISMS OF ACTION. FROM (SILVA ET AL., 2015)	147
FIGURE 40: AMPLIFICATION CONDITIONS FOR PCR	154
FIGURE 41: EXAMPLE ECL ACTIN STAIN (NM-110 & NM-111 N=1). 0,4 AND 8MG/μL REPRESENT DOSES OF 0, 1.26 AND 2.52μG/cm ²	162
FIGURE 42: GEL/MEMBRANE LAYOUT FOR STAINING AGAINST 4 ANTIBODIES AND ANALYSIS BY ECL. 0, 4 AND 8MG/μL REPRESENT DOSES OF 0, 1,26 AND 2.52μG/cm ²	162
FIGURE 43: WESTERN BLOT DETECTION METHODS. LHS IS ENHANCED CHEMILUMINESCENCE AS USED WITH THE GBOX SYSTEM, THE EQUATION REPRESENTING THE CHEMICAL CHANGE REQUIRED TO PRODUCE LIGHT. RHS IS FLUORESCENCE AS USED WITH THE LICOR SYSTEM, THE LOWER PORTION OF THE IMAGE REPRESENTING EXCITATION OF A FLUOROPHORE BOUND TO A SECONDARY ANTIBODY AND ITS SUBSEQUENT RELEASE OF LIGHT. IMAGE COMPILED FROM RESOURCES PROVIDED BY BIORAD AND GE LIFE SCIENCES.	163
FIGURE 44: DENSITOMETRY PLOT OF CHIP-BASED ELECTROPHORESIS FOR RNA SAMPLES FROM CELLS TREATED WITH NNM-110 AND NM-111 ZIN OXIDE NANOPARTICLES.....	167
FIGURE 45: GE NORM PAIRWISE VARIATION ACROSS 12 POTENTIAL REFERENCE GENES. OPTIMAL NUMBER OF TARGETS CONFIRMED TO BE 3, WITH V<0.15 FOR THIS NUMBER (SAMPLE N=18).	169
FIGURE 46: GE NORM M VALUES FOR 12 PANEL KIT. GAPDH, ACTB AND YWHAZ WERE CONFIRMED AS HAVING THE MOST STABLE EXPRESSION ACROSS ALL SAMPLES TESTED (SAMPLE N=18).....	169
FIGURE 47: MELT CURVES FOR GAPDH, YWHAZ AND ACTB (L TO R) AS SELECTED USING GE NORM ANALYSIS.	170
FIGURE 48: MELT CURVES GENERATED DURING PRIMER EFFICIENCY TESTING.	171
FIGURE 49: EXAMPLE MELT CURVE FOR PRIMERDESIGN CUSTOM PRIMER. CURVE SHOWN IS FOR STAR. BLUE REGION AT BASE IS NO TEMPLATE CONTROL DATA.....	172
FIGURE 50: MRNA EXPRESSION FROM TM3 CELLS EXPOSED TO NM-110 SHOWN AS LOG(2) RATIO FOLD DIFFERENCE COMPARED TO VEHICLE	173
FIGURE 51: MRNA EXPRESSION FROM TM3 CELLS EXPOSED TO NM-111 SHOWN AS LOG(2) RATIO FOLD DIFFERENCE COMPARED TO VEHICLE	174
FIGURE 52: MRNA EXPRESSION FROM TM3 CELLS EXPOSED TO NM-300 SHOWN AS LOG(2) RATIO FOLD DIFFERENCE COMPARED TO VEHICLE. GRAPHS SHOW ONLY LOWER DOSE (4μG/μL OR 1.26μG/cm ²) DATA BECAUSE CELLS TREATED WITH 8μG/μL (2.52μG/cm ²) DID NOT YIELD ANY RNA.....	175
FIGURE 53: STANDARDS FOR DERIVATION OF PROTEIN CONCENTRATION FROM PREPARED SAMPLES OBTAINED VIA BRADFORD ASSAY. LINEAR REGRESSION R ² FIT OF 0.9849.	177

FIGURE 54: WESTERN BLOT ANALYSIS FOR EXPRESSION OF ACTIN (LHS OF MEMBRANE) AND LH-R (RHS OF MEMBRANE) RECORDED ON LICOR USING FLUORESCENT SECONDARY ANTIBODIES. A) NM-110 N1 +T, B) NM-110 N2 +T, C) NM-110 N3 +T. 0,1,2,4,6 AND 8MG/ML REPRESENT 0, 0.32, 0.63, 1.26, 1.89 AND 2.52 MG/CM ² DOSES. ...	178
FIGURE 55: EXAMPLE OF WESTERN BLOT FOR NM-110 N3 +T, ORIGINALLY PROBED FOR LH-R AND ACTIN, WHICH WAS UNSUCCESSFULLY RE-PROBED FOR ANDROGEN RECEPTOR AND STAR. LOCATIONS WHERE THESE ANTIBODIES SHOULD HAVE BEEN ARE SHOWN ON THE IMAGE FOR ILLUSTRATION. 0,1,2,4,6 AND 8MG/ML REPRESENT 0, 0.32, 0.63, 1.26, 1.89 AND 2.52 MG/CM ² DOSES.	179
FIGURE 56: REPRESENTATIVE ECL CAPTURE OF ANTIBODY STAINS. L TO R: ACTIN, AR, LH-R & STAR. 0,4 AND 8MG/ML REPRESENT 0, 1.26 AND 2.52 MG/CM ² DOSES	180
FIGURE 57: MEAN EXPRESSION OF AR IN TM3 CELLS TREATED WITH NM-110, 111 AND 300 AS A % OF ACTIN EXPRESSION IN THE SAME SAMPLE. N=3.	180
FIGURE 58: ANDROGEN RECEPTOR EXPRESSION IN TM4 CELLS TREATED WITH NM-110 AND NM-111 (UNCOATED AND COATED) ZINC OXIDE AT DOSES OF 0, 1, 2, 4, 6 AND 8µG/ML, EQUIVALENT TO 0, 0.32, 0.63, 1.26, 1.89 AND 2.52µG/CM ² IN THE PRESENCE OF TESTOSTERONE STIMULATION. RECEPTOR EXPRESSION IS EXPRESSED AS A % OF β-ACTIN EXPRESSION IN CONTROL SAMPLE TO WHICH TESTOSTERONE STIMULUS HAS BEEN ADDED (CONTROL+T). AR EXPRESSION IS OVERLAID WITH CELL VIABILITY (% RELATIVE TO CONTROL) FOLLOWING 24 HOURS OF EXPOSURE TO ENM, RECORDED USING THE ALAMAR BLUE ASSAY. N=3. (YOUNG & FULTON, 2014).	191
FIGURE 59: ANDROGEN RECEPTOR EXPRESSION IN TM4 CELLS TREATED WITH SILVER ENM (NM-300) AT DOSES OF 0, 1, 2, 4, 6 AND 8µG/ML, EQUIVALENT TO 0, 0.32, 0.63, 1.26, 1.89 AND 2.52µG/CM ² IN THE PRESENCE OF TESTOSTERONE STIMULATION. RECEPTOR EXPRESSION IS EXPRESSED AS A % OF β-ACTIN EXPRESSION IN CONTROL SAMPLE TO WHICH TESTOSTERONE STIMULUS HAS BEEN ADDED (CONTROL+T). N=1. (YOUNG & FULTON, 2014).	192
FIGURE 60: GENERALISED MORPHOLOGY OF THE TESTES. THE INTERSTITIAL COMPARTMENT CONTAINS LEYDIG CELLS, BLOOD VESSELS AND CAPILLARIES, AS WELL AS LYMPHATIC VESSELS AND TESTICULAR MACROPHAGES (NOT VISIBLE). THE SEMINIFEROUS TUBULES, LINED BY PERITUBULAR MYOID CELLS, ARE COMPOSED OF TWO COMPARTMENTS – THE BASAL AND ADLUMINAL COMPARTMENTS. WITHIN THESE, GERM CELLS DEVELOP THROUGH SPERMATOGENESIS, A PROCESS WHICH IS MANAGED BY SERTOLI CELLS, BEFORE BEING SHED INTO THE CENTRAL LUMEN AT SPERMATION.....	195
FIGURE 61: ILLUSTRATION OF SERTOLI CELL MORPHOLOGY VIA IMMUNOFLUORESCENT MICROSCOPY (IF) (LEFT) AND SCHEMATIC REPRESENTATION OF ITS INTERACTION WITH GERM CELLS AT DIFFERENT STAGES DURING SPERMATOGENESIS TOGETHER WITH OTHER KEY FUNCTIONS (RIGHT). THE IF IMAGE SHOWS A SERTOLI CELL ISOLATED IN VITRO (WITH ATTACHED ELONGATING SPERMATIDS). CELL IS LABELLED FOR FILAMENTOUS ACTIN (RED) AND SOMATIC CELL-SPECIFIC TUBULIN (GREEN). THE CYTOPLASMIC ARMS WRAP GERM CELLS WITH THIN PROCESSES WHICH NURTURE CELLS THROUGH THEIR DIFFERENTIATION. THEY DO THIS VIA SPECIALISED CELL-CELL JUNCTIONS BETWEEN SERTOLI CELLS AND GERM CELLS (OR OTHER SERTOLI CELLS) CALLED ECTOPLASMIC SPECIALIZATIONS, LABELLED RED AROUND THE SPERMATID HEADS. BAR = 10µM. THE IMAGE SHOWING SERTOLI CELL INTERACTION AND FUNCTIONS DETAILS THE MANY FUNCTIONS IT SERVES: (1) TRANSPORT OF MICRONUTRIENTS ACROSS THE JUNCTIONAL COMPLEX; (2) MANAGEMENT OF WASTE AND RECYCLED LEFTOVER CYTOPLASM DURING GERM CELL DEVELOPMENT; (3) MAINTENANCE OF THE BLOOD–TESTIS BARRIER (BTB); (4) ESTABLISHMENT OF GERM CELL ADHESIONS AND COMMUNICATION; (5) INHIBITION OF IMMUNE REACTIONS AND MAINTENANCE OF IMMUNE PRIVILEGE; (6) INITIATION AND RESPONSE TO ENDOCRINE SIGNALLING PATHWAYS; (7) INITIATION AND REGULATION OF THE CYCLE OF THE SEMINIFEROUS EPITHELIUM; AND (8) MAINTENANCE OF STEM CELL HOMEOSTASIS. THE AUTOIMMUNOGENIC GERM CELLS REMAIN SEQUESTERED WITHIN THE ADLUMINAL COMPARTMENT BEHIND THE BTB, SURROUNDED BY SERTOLI CELLS WHICH SECRETE IMMUNOREGULATORY FACTORS (5) TO MODIFY ANY IMMUNE RESPONSE. TREG = T CELLS, M2 = MACROPHAGES. IMAGES REPRODUCED FROM FRANCA ET. AL. (2016).	198
FIGURE 62: ILLUSTRATION OF THE DIFFERENT KINDS OF CELLULAR JUNCTION IN THE EPITHELIUM OF RAT SEMINIFEROUS TUBULES.4 TYPES OF JUNCTION ARE REPRESENTED: TIGHT JUNCTIONS, ECTOPLASMIC SPECIALISATIONS, DESMOSOMES, AND GAP JUNCTIONS. EACH PLAYS A CRUCIAL BUT SLIGHTLY DIFFERENT ROLE IN MAINTENANCE OF THE BTB. IMAGE REPRODUCED FROM MRUK & CHENG (2015).	199
FIGURE 63: GERM CELL DEVELOPMENT THROUGH SPERMATOGENESIS IN THE RAT. THE PROLIFERATION PHASE INCLUDES 6 MITOTIC DIVISIONS FROM A1-A4 TYPE SPERMATOGONIA, INTERMEDIATE (I), B TYPE (B) AND FINALLY PRELEPOTENE SPERMATOCYTES (PL). MEIOSIS BEGINS WITH SMALL LEPTENE SPERMATOCYTES (L) ENTERING PROPHASE, CELL ENLARGING THROUGH ZYGOTENE (Z), EARLY- MID- AND LATE PACHYTENE (EP, MP, LP) SPERMATOCYTES. DIPLTENE	

SPERMATOCYTES (D) THEN UNDERGO THE FIRST MEIOTIC DIVISION (Me1) TO PRODUCE SECONDARY SPERMATOCYTES (SS). AFTER THE SECOND MEIOTIC DIVISION (Me2), HAPLOID CELLS BEGIN TO DIFFERENTIATE BY FORMING ROUND SPERMATIDS (RS) WHICH REPRESENT STEPS 1-7 OF SPERMATID DEVELOPMENT. RS BECOME ELONGATING SPERMATIDS FROM STEP 8 WHEN THE TAIL OF THE SPERMATID BEGINS TO FORM, CONTINUING TO DIFFERENTIATE UNTIL STEP 19 WHERE THEY ARE CONSIDERED TO BE MATURE SPERMATID AND READY FOR RELEASE. IMAGE ADAPTED FROM CREASY, 1997.	201
FIGURE 64: STAGES OF THE SPERMATOGENIC CYCLE WITHIN THE RAT. TO SHOW THE TRANSITIONAL CHARACTERISTICS, CELL NUCLEI ARE DEPICTED. STAGES ARE IDENTIFIABLE BY ROMAN NUMERALS. STEPS OF DEVELOPMENT FROM ROUND SPERMATIDS TO MATURE SPERMATID ARE LABELLED USING LETTERS AND NUMBERS. ROUND SPERMATIDS ARE SEEN WITHIN STEPS 1-8 OF SPERMATID DEVELOPMENT, AND ELONGATING SPERMATIDS FROM STEP 9-19. MITOSIS IS INDICATED BY 'M' AND MEIOSIS BY 'Me1' OR 'Me2'. SPERMATOGONIA ARE DEPICTED AS A, I OR B TYPE. SPERMATOCYTES ARE DEPICTED AS PRELEPTENE (PL), LEPTENE (L), ZYGOTENE (Z), PACHYTENE (P), DIPLTENE (Di) AND SECONDARY (SS). IMAGE REPRODUCED FROM HESS (1990).	203
FIGURE 65: BIOTIN LABELLED IMMUNOHISTOCHEMISTRY. SOURCE: VECTOR LABS (VECTORLABORATORIES, 2018).	217
FIGURE 66: SUBSET IMAGE PREPARATION FROM TISSUE SECTIONS WITHIN ZEN. A 50X MAGNIFICATION WAS APPLIED, THEN 5 SUBSET IMAGES WERE CAPTURED FROM THE 4 POLES OF THE SECTION PLUS THE MIDDLE.	220
FIGURE 67: EXAMPLE OF ANNOTATION AND MEASUREMENT PROCESS FOR STAGE, TUBULE DIAMETER AND LUMEN VOLUME APPLIED TO ALL SAMPLE IMAGES. TUBULES WERE STAGED AND MARKED SEQUENTIALLY WITH "NUMBER.STAGE" IN ZEN BLUE, BEFORE BEING EXPORTED TO IMAGEPRO PREMIER. TUBULE DIAMETER WAS THEN MEASURED ACROSS THE SHORTEST TRANSVERSE CROSS-SECTION OF TUBULE, AND LUMEN VOLUME CALCULATED BY DRAWING AN ROI AROUND THE EDGE OF THE LUMEN SPACE IN EACH TUBULE. REPRESENTATIVE IMAGE IS FROM ANIMAL I43 WITHIN THE NANO AMOR TREATMENT GROUP, TAKEN FROM THE WEST POLE OF THE SLIDE.	227
FIGURE 68: REPRESENTATIVE IMAGE OF TUBULE CONTAINING CELLS THAT HAVE SLOUGHED INTO THE CENTRE OF THE LUMEN. WHERE THIS WAS PRESENT, BOTH THE OVERALL LUMINAL VOLUME AND THE INNER LUMINAL VOLUME WERE CALCULATED WITHIN IMAGE PRO PREMIER, IN ORDER TO PROVIDE AID ANALYSIS OF WHETHER TAKING INTO ACCOUNT CELL SLOUGHING ALTERED ANY OUTCOMES OBSERVED RELATING TO TREATMENT.	227
FIGURE 69: REPRESENTATIVE IMAGE CAPTURED FROM A CONTROL ANIMAL TO ILLUSTRATE THE DIFFERENCES IN TUBULE SHAPE CAPTURED ON EACH SECTION OR VIRTUAL SLIDE. RED = ROUND TUBULE CUT EXACTLY PERPENDICULAR TO THE DIRECTION IT IS RUNNING IN, GREEN = ELLIPTICAL TUBULE, CUT AT AN OBLIQUE ANGLE TO THE DIRECTION OF THE TUBULE, BLUE = ELONGATED TUBE, CUT ON A SAGITTAL PLANE TO THE DIRECTION OF THE TUBE.....	228
FIGURE 70: REPRESENTATIVE MORPHOLOGY OF HEALTHY RAT TESTIS, TAKEN FROM CONTROL ANIMAL (H&E STAINED). A: GENERAL LAYOUT OF ROUND SEMINIFEROUS TUBULES, INTERSPERSED WITH POLYHEDRAL LEYDIG CELLS AND BLOOD VESSELS/CAPILLARIES. THE TUBULE IN THE CENTRE OF THE IMAGE IS AT STAGE VII. SCALE BAR REPRESENTS 50µm. B: HIGHER MAGNIFICATION REPRESENTATION OF THE SAME IMAGE. SCALE BAR REPRESENTS 20µm. C = CAPILLARY; LC = LEYDIG CELL; GC = GERM CELL LAYER; L = LUMEN; RB = RESIDUAL BODIES; S = SERTOLI CELL; M = PERITUBULAR MYOID CELL; P = PACHYTENE SPERMATOCYTE; PL = PRELEPTENE SPERMATOCYTE; RS = ROUND SPERMATID; ES = ELONGATING SPERMATID; SP = MATURE SPERMATID.	231
FIGURE 71: GENERALISED MORPHOLOGY OF HEALTHY RAT TESTIS WITH FOCUS ON INTERSTITIAL CELL POPULATIONS. A: ADULT LEYDIG CELL POPULATIONS SURROUNDING A CAPILLARY. B: ADULT LEYDIG CELLS LYING IN CLOSE ASSOCIATION TO A LARGER BLOOD VESSEL CONTAINING RED BLOOD CELLS. SCALE BAR REPRESENTS 20µm. C = CAPILLARY; BV = BLOOD VESSEL; LC = LEYDIG CELL; S = SERTOLI CELL; M = PERITUBULAR MYOID CELL; A= TYPE A SPERMATOGONIA; P = PACHYTENE SPERMATOCYTE; PL = PRELEPTENE SPERMATOCYTE; D = DIPLTENE SPERMATOCYTE; RS = ROUND SPERMATID; ES = ELONGATING SPERMATID; SP = MATURE SPERMATID.	232
FIGURE 72: GENERALISED MORPHOLOGY OF RAT TESTIS FROM ANIMALS TREATED WITH NM202 SILICA DIOXIDE. MORPHOLOGY APPEARS UNALTERED WHEN COMPARED TO CONTROL, INDICATING NO MAJOR STRUCTURAL DISTURBANCES TO THE TESTIS OF THESE ANIMAL FOLLOWING TREATMENT AT ANY DOSE LEVEL. A) NM202 LOW DOSE; B) NM202 MEDIUM DOSE; C) NM202 HIGH DOSE. SCALE BAR REPRESENTS 100µm.	233
FIGURE 73: IMAGE CAPTURED FROM AN ANIMAL TREATED WITH NM-300 SILVER NANOPARTICLES. A) GENERALISED LOSS OF TUBULAR ARCHITECTURE IN SOME TUBULES AND MAINTENANCE OF NORMAL ARCHITECTURE IN OTHERS (LEFT- AND RIGHT-HAND SIDE OF IMAGE). WITHIN THIS IMAGE, ROUND SPERMATIDS APPEAR TO BE DEGENERATING, AS ILLUSTRATED BY THEIR PATCHY APPEARANCE. B) PRESENCE OF PYKNOTIC NUCLEI (VERY DARK CELLS WHERE CHROMATIN	

IN THE NUCLEUS IS CONDENSED AND UNDERGOING APOPTOSIS). SCALE BAR REPRESENTS 50µM IN A, AND 20µM IN B.	235
FIGURE 74: IMAGE CAPTURED FROM AN ANIMAL TREATED WITH NM-300, ILLUSTRATING AREA OF FOCAL DYSMORPHISM IN TUBULES, ALONGSIDE TUBULES WHICH APPEAR TO BE HEALTHY AND SHOWING NORMAL GERM CELL POPULATIONS AND ARCHITECTURE (RED ASTERISKS). SCALE BAR REPRESENTS 100µM.	235
FIGURE 75: IMAGE CAPTURED FROM AN ANIMAL TREATED WITH NM-300 SILVER NANOPARTICLES, ILLUSTRATING GENERALISED LOSS OF TUBULAR ARCHITECTURE ACCOMPANIED BY INFLAMMATION WITHIN THE INTERSTITIUM. IMAGE B OFFERS A HIGHER MAGNIFICATION VIEW ON BOTH TUBULE AND INTERSTITIUM CONTENTS. SCALE BAR REPRESENTS 100µM IN A, AND 50µM IN B.	236
FIGURE 76: IMAGES CAPTURED FROM AN ANIMAL TREATED WITH NM-300 SILVER NANOPARTICLES, SHOWING RETENTION OF MATURE STEP 19 SPERMATIDS IN STAGE IX (A) AND X (B) TUBULES (RED ARROWS). RETENTION OF MATURE SPERMATIDS AFTER SPERMATION AT STAGE VIII IS A SENSITIVE INDICATOR OF TOXICITY. SCALE BAR REPRESENTS 20µM.	236
FIGURE 77: IMAGES FROM AN ANIMAL TREATED WITH NM-300 SILVER NANOPARTICLES, SHOWING WHAT COULD BE DEVELOPMENT OF MULTINUCLEATED GIANT CELLS WITHIN MORPHOLOGICALLY DEGENERATIVE TUBULES (RED CIRCLES). SCALE BAR REPRESENTS 50µM.	237
FIGURE 78: REPRESENTATIVE IMAGE OF FOCAL DYSMORPHISM WITHIN AgNO ₃ EXPOSED ANIMAL. GENERALISED LOSS OF CELLULAR ARCHITECTURE, AND PRESENCE OF PYKNOTIC NUCLEI (VERY DARK CELLS WHERE CHROMATIN IN THE NUCLEUS IS CONDENSED AND UNDERGOING APOPTOSIS) MAY BE SEEN THROUGHOUT THE TUBULE. SCALE BAR REPRESENTS 50µM.	238
FIGURE 79: REPRESENTATIVE IMAGE OF MORPHOLOGICALLY ABNORMAL TUBULES WITH LC HYPERPLASIA IN THE INTERSTITIUM WITHIN AgNO ₃ EXPOSED ANIMAL (HIGHLIGHTED WITH STAR). SCALE BAR REPRESENTS 100µM.	239
FIGURE 80: TUBULE OBSERVED WITHIN AgNO ₃ EXPOSED ANIMAL CONTAINING ALMOST NO GERM CELLS, THOSE CELLS LEFT LINING THE BASEMENT MEMBRANE ARE PRIMARILY SERTOLI CELLS. SCALE BAR REPRESENTS 50µM.	239
FIGURE 81: SLOUGHING OF TUBULAR CONTENTS INTO CENTRAL LUMEN, OBSERVED WITHIN AgNO ₃ EXPOSED ANIMALS. AS WITH OTHER SILVER TREATMENTS, MORPHOLOGICALLY DISTURBED TUBULES WERE OFTEN SEEN ALONGSIDE TUBULES WHICH WERE HEALTHY IN APPEARANCE (STAR). SCALE BAR REPRESENTS 50µM.	240
FIGURE 82: REPRESENTATIVE IMAGES OF FOCAL DYSMORPHISM WITHIN NANO AMOR EXPOSED ANIMAL. GENERALISED LOSS OF CELLULAR ARCHITECTURE IS OBSERVABLE WITHIN BOTH TUBULES, THESE AGAIN BEING SITUATED ADJACENT TO OTHER TUBULES WHICH APPEAR TO BE MORPHOLOGICALLY NORMAL. A NUMBER OF PYKNOTIC NUCLEI, IDENTIFIABLE AS VERY DARK CELLS WHERE CHROMATIN IN THE NUCLEUS IS CONDENSED AND UNDERGOING APOPTOSIS ARE ALSO VISIBLE ON IMAGE A. SCALE BAR REPRESENTS 50µM.	241
FIGURE 83: REPRESENTATIVE IMAGES OF NANO AMOR TREATED ANIMALS WHERE DILATED TUBULE LUMENS ARE PRESENT. A) TUBULES WITH DILATED LUMEN MAY BE SEEN ALONGSIDE OTHER TUBULES WITH SLOUGHING OF GERM CELL CONTENTS INTO THE CENTRAL LUMEN, OR COMPLETE OBLITERATION OF LUMEN AND TUBULAR ARCHITECTURE. B) HIGHER MAGNIFICATION VIEW OF TUBULES AT MULTIPLE STAGES WITH DILATED LUMENS, AND SOME MODERATE SLOUGHING OF GERM CELL CONTENTS. GERM CELL LAYER AROUND THE TUBULE EDGE APPEARS TO BE OTHERWISE NORMAL IN APPEARANCE. SCALE BAR REPRESENTS 200µM IN IMAGE A, AND 50µM IN IMAGE B.	241
FIGURE 84: TUBULE OBSERVED WITHIN ANIMAL EXPOSED TO NANO AMOR WHICH APPEARED TO HAVE RETENTION OF STEP 11 ELONGATING SPERMATIDS WITHIN THE LUMEN OF A STAGE XIV TUBULE. TUBULE STAGE IS IDENTIFIABLE BY PRESENCE OF MEIOTIC BODIES IN TOP PORTION. STEP 11 SPERMATIDS MAY BE SEEN IN THE VERY CENTRE OF THE CELLS SLOUGHED INTO THE LUMEN, IDENTIFIABLE AS BEING STEP 11 DUE TO THE PROTRUSION OF THE ACROSOME AND APEX AT A SHARP ANGLE FROM THE CAUDAL PORTION OF THE NUCLEUS. SPERMATIDS SEEN FROM STEP 13 TO 15 HAVE A MORE HOOKED APPEARANCE, WITH HIGHLY CONDENSED (APPEARING DARKER) AND POINTED NUCLEI.	242
FIGURE 85: REPRESENTATIVE IMAGES OF IMMUNOHISTOCHEMICAL STAINING FOR 3B-HSD WITHIN RAT TESTIS TISSUE FOLLOWING 3-4 MINUTES OF DAB EXPOSURE AND COLORIMETRIC REACTION DEVELOPMENT. SCALE BAR REPRESENTS 100µM. A) AgNO ₃ , B) NANO AMOR, C) NM-300 & D) CONTROL. RED ARROWS SHOW STAINING LOCALISED TO LEYDIG CELLS IN THE INTERSTITIUM. ASTERISKS AND RED CIRCLE DENOTE BACKGROUND STAINING WITHIN AgNO ₃ AND NANO AMOR TREATED ANIMALS THAT WAS VISIBLE THROUGHOUT MANY OF THE SECTIONS ANALYSED.	243

FIGURE 86: REPRESENTATIVE IMAGES OF IMMUNOHISTOCHEMICAL STAINING FOR LH-R WITHIN RAT TESTIS TISSUE FOLLOWING 3-4 MINUTES OF DAB EXPOSURE AND COLORIMETRIC REACTION DEVELOPMENT. SCALE BAR REPRESENTS 100µM. A) AGNO ₃ , B) NANO AMOR, C) NM-300 & D) CONTROL. RED ARROWS SHOW STAINING LOCALISED TO LEYDIG CELLS LOCATED WITHIN IN THE INTERSTITIUM BETWEEN SEMINIFEROUS TUBULES.....	244
FIGURE 87: REPRESENTATIVE IMAGES OF LH-R STAINED TISSUE CAPTURED FROM ANIMALS TREATED WITH NANOPARTICULATE SILVER. IMAGES A & B ARE BOTH CAPTURED FROM ONE ANIMAL (I44) TREATED WITH NANO AMOR; A SHOWS A HEALTHY AREA OF TESTICULAR TISSUE; IMAGE B SHOWS AN AREA OF FOCAL DYSMORPHISM WITHIN THE SAME SLIDE (RED ASTERISKS). IMAGE C SHOWS A STAGE XII SEMINIFEROUS TUBULE FROM AN NM-300 TREATED ANIMAL WHICH CLEARLY HAS DEGENERATING TISSUE SLOUGHING INTO THE LUMEN, WHILE IMAGE D SHOWS MEIOTIC DIVISIONS OF A STAGE XIV TUBULE AN ANIMAL TREATED WITH AgNO ₃ . IT IS NOTABLE THAT LH-R SPECIFIC STAINING IS COMPARABLE AND LOCALISED TO THE LEYDIG CELLS OF ALL IMAGES. SCALE BAR REPRESENTS 100µM IN A & B, AND 50µM IN C & D.	245
FIGURE 88: REPRESENTATIVE IMAGES OF IMMUNOHISTOCHEMICAL STAINING FOR AR WITHIN RAT TESTIS TISSUE FOLLOWING 9 MINUTES OF DAB EXPOSURE AND COLORIMETRIC REACTION DEVELOPMENT. AR POSITIVE SERTOLI CELL STAINING IS VISIBLE AS 'RINGS' OF DOTS AROUND THE OUTER EDGE OF THE SEMINIFEROUS EPITHELIUM IN TUBULES. SOME CLEAR BACKGROUND STAINING OF TISSUE IS VISIBLE WITHIN THE NM-300 TREATED IMAGE, THIS WAS PRESENT THROUGH MANY OF THE SLIDES. SCALE BAR REPRESENTS 100µM. A) AgNO ₃ , B) NANO AMOR, C) NM-300 & D) CONTROL.	246
FIGURE 89: A CLOSE MAGNIFICATION VIEW OF TISSUE FROM AN A) SILVER TREATED (NANO AMOR, I43) AND B) CONTROL (J20) ANIMAL FOLLOWING IHC STAINING FOR AR. BOTH SHOW CLEAR STAINING FOR AR ACROSS A NUMBER OF CELL TYPES. M = PERITUBULAR MYOID CELL (LONG AND THIN IN SHAPE), S = SERTOLI CELL (ROUND IN SHAPE), L = LEYDIG CELL, ASTERISK = CAPILLARY. SCALE BARS SHOW 20µM (LHS) AND 50µM (RHS) RESPECTIVELY.	247
FIGURE 90: TWO IMAGES CAPTURED FROM AN ANIMAL TREATED WITH NM-300, FOLLOWING IHC STAINING FOR AR. IMAGE A SHOWS A HEALTHY STAGE VIII TUBULE, WITH RED ASTERISKS INDICATING STAINING OF SERTOLI CELLS THAT HAVE MIGRATED TOWARD THE CENTRAL LUMEN TO ASSIST IN RELEASE OF MATURE SPERMATIDS AT SPERMATION. IMAGE B SHOWS AN UNHEALTHY STAGE VII TUBULE WITHIN A FOCAL AREA OF DYSMORPHISM FROM THE SAME SLIDE. DESPITE THE TUBULE APPEARING TO BE ABNORMAL, IT IS NOTABLE THAT POSITIVE AR STAINING IS STILL PRESENT AROUND THE BASEMENT MEMBRANE OF THE TUBULE (RED ASTERISKS).	247
FIGURE 91: REPRESENTATIVE IMAGES OF IMMUNOHISTOCHEMICAL STAINING FOR STAR WITHIN RAT TESTIS TISSUE FOLLOWING 3 MINUTES OF DAB EXPOSURE AND COLORIMETRIC REACTION DEVELOPMENT. SCALE BAR REPRESENTS 100µM. A) AGNO ₃ , B) NANO AMOR, C) NM-300 & D) CONTROL. AREAS OF GENERALISED OVER-STAINING ARE VISIBLE ON THE RIGHT-HAND SIDE OF IMAGE A AND THE BOTTOM RIGHT CORNER OF IMAGE C.	248
FIGURE 92: TWO IMAGES CAPTURED FROM ANIMALS TREATED WITH AgNO ₃ , AND FOLLOWING IHC STAINING FOR STAR. IMAGE A SHOWS A HEALTHY STAGE V-VI TUBULE, WITH RED DASHES OUTLINING THE AREA IN WHICH ROUND SPERMATID ACROSOMAL CAPS HAVE BEEN STAINED (ANIMAL K52). IMAGE B SHOWS A CLOSER VIEW OF THIS STAINING IN A DIFFERENT ANIMAL (K54). SCALE BAR REPRESENTS 50µM ON A AND 20µM ON B.	249
FIGURE 93: REPRESENTATIVE IMAGES OF IMMUNOHISTOCHEMICAL STAINING FOR DAZL WITHIN RAT TESTIS TISSUE FOLLOWING 3.5 MINUTES OF DAB EXPOSURE AND COLORIMETRIC REACTION DEVELOPMENT. SCALE BAR REPRESENTS 100µM. TUBULES ARE MARKED TO INDICATE i) HEAVILY STAINED TUBULES UNDERGOING SPERMATION AT STAGE VII (RED STARS), ii) MODERATELY STAINED TUBULES PRE- OR POST- SPERMATION AT STAGES VI-VII OR IX-XI (ORANGE PENTAGONS), OR iii) UNSTAINED TUBULES AT THE START (STAGE I-V) OR END (STAGE XII-XIV) OF THE CYCLE OF THE SEMINIFEROUS EPITHELIUM (BLUE TRIANGLES). A) AgNO ₃ , B) NANO AMOR, C) NM-300 & D) CONTROL.	250
FIGURE 94: TWO IMAGES CAPTURED FROM ANIMALS TREATED WITH NM-300 (LEFT) AgNO ₃ (RIGHT) FOLLOWING IHC STAINING FOR DAZL SCALE BAR REPRESENTS 100µM. BOTH IMAGES SHOW CLEAR FOCAL AREAS OF DYSMORPHISM WITHIN TESTICULAR SECTIONS. IT IS NOTABLE THAT DAZL STAINING WAS NOT AFFECTED BY MORPHOLOGICAL DISTURBANCE, UNLESS GERM CELLS WERE COMPLETELY ABSENT FROM TUBULES. THUS, IT WAS POSSIBLE TO USE DAZL STAINING TO ASSIST WITH STAGING OF DAMAGED TUBULES.....	250
FIGURE 95: REPRESENTATIVE IMAGES OF IMMUNOHISTOCHEMICAL STAINING FOR RP-1 WITHIN RAT TESTIS TISSUE FOLLOWING 3.5 MINUTES OF DAB EXPOSURE AND COLORIMETRIC REACTION DEVELOPMENT. SCALE BAR REPRESENTS 50µM. IMAGES WERE SELECTED AS THEY SHOW TUBULES WHICH INCLUDE CELLS EITHER SLOUGHED INTO THE CENTRAL LUMEN,	

OR CELLS WHICH HAVE INVADDED THAT TUBULAR LUMEN WHICH WOULD STAIN POSITIVELY FOR RP-1 SHOULD THEY BE NEUTROPHILS. A) AGNO ₃ , B) NANO AMOR, C) NM-300 & D) CONTROL.	251
FIGURE 96: SUMMARY OF CONTROL DATASETS FOR ANIMALS SACRIFICED AT DAY 29 AND DAY 85. LEFT: TUBULE DIAMETER. RIGHT: GERM CELL LAYER THICKNESS. A SIGNIFICANT DIFFERENCE WAS FOUND BETWEEN THE TWO GROUPS FOR TUBULE DIAMETER (P<0.0001) BUT NOT GERM CELL LAYER THICKNESS.	252
FIGURE 97: TUBULE DIAMETER MEASUREMENTS (+/- SEM) FROM ALL TREATMENTS EACH TREATMENT HAD 5 ANIMALS EXCEPT CONTROL FOR WHICH THERE WERE 8 ANIMALS. FROM TOP TO BOTTOM: A) AGNO ₃ (TUBULES MEASURED N=186), B) NM-300 (TUBULES MEASURED N=193), C) NANO AMOR (TUBULES MEASURED N=203), D) NM202 LOW DOSE (TUBULES MEASURED N=178), E) NM202 MEDIUM DOSE (TUBULES MEASURED N=199), F) NM202 HIGH DOSE (TUBULES MEASURED N=180), G) CONTROL (TUBULES MEASURED N=915), AND H) ALL TREATMENTS COMPARED TO CONTROL SHOWN AS A BOX AND WHISKERS PLOT ILLUSTRATING MINIMUM TO MAXIMUM VALUES AND MEDIAN FOR EACH GROUP.	254
FIGURE 98: GERM CELL LAYER THICKNESS MEASUREMENTS (+/- SEM) FROM ALL TREATMENTS EACH TREATMENT HAD 5 ANIMALS EXCEPT CONTROL FOR WHICH THERE WERE 8 ANIMALS. FROM TOP TO BOTTOM: A) AGNO ₃ (TUBULES MEASURED N=186), B) NM-300 (TUBULES MEASURED N=193), C) NANO AMOR (TUBULES MEASURED N=203), D) NM202 LOW DOSE (TUBULES MEASURED N=178), E) NM202 MEDIUM DOSE (TUBULES MEASURED N=199), F) NM202 HIGH DOSE (TUBULES MEASURED N=180), G) CONTROL (TUBULES MEASURED N=915), AND H) ALL TREATMENTS COMPARED TO CONTROL SHOWN AS A BOX AND WHISKERS PLOT ILLUSTRATING MINIMUM TO MAXIMUM VALUES AND MEDIAN FOR EACH GROUP.	256
FIGURE 99: ILLUSTRATIVE EXAMPLES OF TUBULE STAGING FROM I – XIV, ACCORDING TO DECISION KEY AND CRITERIA SPECIFIED WITHIN THE LITERATURE. SCALE BAR REPRESENTS 50µM ON LEFT-HAND SIDE IMAGES AND 10µM ON THE RIGHT-HAND SIDE. S (SERTOLI CELL NUCLEUS); A (TYPE-A SPERMATOGONIA); I (INTERMEDIATE SPERMATOGONIA); B (TYPE-B SPERMATOGONIA); PL (PRELEPTOTENE SPERMATOCYTE); P (PACHYTENE SPERMATOCYTE); L (LEPTOTENE SPERMATOCYTE); Z (ZYGOTENE SPERMATOCYTE); D (DIPLTENE SPERMATOCYTE); SS (SECONDARY SPERMATOCYTE); NU (NUCLEUS); ES (ELONGATING SPERMATID); RS (ROUND SPERMATID).	262
FIGURE 100: DEVELOPMENT OF DAZL STAINING ACCORDING TO TUBULE STAGE (SHOWN IN RED). INTENSITY OF DAZL STAIN INCREASES FROM STAGE V-VII, PEAKS AT STAGE VIII, THEN DECREASES FROM STAGE IX-XI, AND IS NOT PRESENT THROUGH STAGES XIII-IV OF THE NEXT CYCLE. IT IS A USEFUL STAIN TO AID ACCURACY OF STAGING TUBULES. SCALE BAR REPRESENTS 50µM.	264
FIGURE 101: DAB STAIN INTENSITY FOR DAZL ANTIBODY AS % OF TOTAL COUNTS ACCORDING TO STAGE OF TUBULE IN CONTROL ANIMALS (N=5).	265
FIGURE 102: DIAMETER OF THE SEMINIFEROUS TUBULE (SQUARES) AND VOLUME OF THE LUMEN (CIRCLES) AT VARIOUS STAGES OF THE SEMINIFEROUS EPITHELIUM CYCLE, SUPERIMPOSED ONTO THE DAZL IMMUNOSTAINING INTENSITY SCORES RECORDED. EACH VALUE REPRESENTS THE MEAN OF 5 ANIMALS (PLOTTED +/- SEM FOR COMPARISON TO FIGURE 40). NB. LUMEN VOLUME IS EXPRESSED DIRECTLY AS RECORDED (µM/CM ²), WITH THE INFLUENCE OF TUBULE SHAPE ON VOLUME OBSERVED CONSIDERED LATER WITHIN THIS ANALYSIS.	266
FIGURE 103: DIAMETER OF THE SEMINIFEROUS TUBULE AND VOLUME OF THE LUMEN PER UNIT LENGTH OF SEMINIFEROUS TUBULE AT VARIOUS STAGES OF THE CYCLE. EACH VALUE REPRESENTS THE MEAN OF FOUR ANIMALS (PLOTTED +/- SEM). WING & CHRISTENSEN, 1982. NB. LUMEN VOLUME IS EXPRESSED PER UNIT LENGTH OF THE SEMINIFEROUS TUBULE, PROBABLY IN ORDER TO TRY AND CORRECT FOR SHAPE DIFFERENCES BETWEEN TUBULE.	266
FIGURE 104: AVERAGE SEMINIFEROUS TUBULE DIAMETER (+/- SEM) OVERLAID ON DAZL STAINING INTENSITY SCORES, BOTH ACCORDING TO STAGE OF THE SEMINIFEROUS TUBULE CYCLE. DAZL STAINING INTENSITY SCORES FOLLOWED THE SAME PATTERN REGARDLESS OF WHETHER ANIMALS WERE EXPOSED TO ENGINEERED NANOMATERIALS OR NOT. TUBULE DIAMETERS RECORDED SHOWED SOME ALTERATION FROM THE PATTERN RECORDED IN CONTROL ANIMALS.	268
FIGURE 105: AVERAGE LUMEN VOLUME (+/- SEM) OVERLAID ON DAZL STAINING INTENSITY SCORES, BOTH ACCORDING TO STAGE OF THE SEMINIFEROUS TUBULE CYCLE. DAZL STAINING INTENSITY SCORES FOLLOWED THE SAME PATTERN REGARDLESS OF WHETHER ANIMALS WERE EXPOSED TO ENGINEERED NANOMATERIALS OR NOT. TUBULE DIAMETERS RECORDED SHOWED SOME ALTERATION FROM THE PATTERN RECORDED IN CONTROL ANIMALS.	271
FIGURE 106: KEY APOPTOTIC PATHWAYS WITHIN CELLS. ADAPTED FROM (IGNEY AND KRAMMER, 2002).	281
FIGURE 107: PROPOSED IATA FOR CONSIDERATION OF MALE DART FOLLOWING ENM EXPOSURE.	316
FIGURE 108: PROPOSED IATA, NOTE 1. DETAIL ON REQUIREMENTS FOR <i>IN VITRO</i> TOXICITY TESTING ENDPOINTS.	317

FIGURE 109: EXPERIMENTAL DESIGN FOR WST-1 ASSAY, BASED ON A 96 WELL PLATE. PLATE ROWS ARE ANNOTATED A-H, AND COLUMNS 1-12. PROTOCOL DENOTED BY GREY SHADING. IS NOTED IN SUPERScript AND OUTLINED IN FULL WITHIN THE BODY OF THE TEXT. 336

List of Tables

TABLE 1: SUMMARY OF GUIDELINES FOR DART TESTING. ADAPTED FROM BEEKHUIJZEN 2017 AND WITH REFERENCE TO ICH, EPA, REACH & THE EC PLANT BASED PRODUCT REGULATIONS (BEEKHUIJZEN, 2017, EPA, 2000, EPA, 2019, EMA, 2017, EC, 2006, EC, 2014).....	44
TABLE 2: <i>IN VIVO</i> AND <i>IN VITRO</i> REPRODUCTIVE AND DEVELOPMENTAL TOXICITY STUDIES OF SILVER (Ag) ENP, OUTLINING KEY PARAMETERS FROM EACH STUDY IDENTIFIED, INCLUDING STUDY TYPE, EXPOSURE TYPE AND METHOD, AND RELEVANT FINDINGS.....	53
TABLE 3: <i>IN VIVO</i> AND <i>IN VITRO</i> REPRODUCTIVE AND DEVELOPMENTAL TOXICITY STUDIES OF TITANIUM DIOXIDE (TiO ₂) ENP, OUTLINING KEY PARAMETERS FROM EACH STUDY IDENTIFIED, INCLUDING STUDY TYPE, EXPOSURE TYPE AND METHOD, AND RELEVANT FINDINGS	60
TABLE 4: <i>IN VIVO</i> AND <i>IN VITRO</i> REPRODUCTIVE AND DEVELOPMENTAL TOXICITY STUDIES OF SILICA ENP (Si), OUTLINING KEY PARAMETERS FROM EACH STUDY IDENTIFIED, INCLUDING STUDY TYPE, EXPOSURE TYPE AND METHOD AND RELEVANT FINDINGS DESCRIBED WITHIN THE PAPER.	64
TABLE 5: <i>IN VIVO</i> AND <i>IN VITRO</i> REPRODUCTIVE AND DEVELOPMENTAL TOXICITY STUDIES OF CARBON NANOTUBES (CNT), OUTLINING KEY PARAMETERS FROM EACH STUDY IDENTIFIED, INCLUDING STUDY TYPE, EXPOSURE TYPE AND METHOD AND RELEVANT FINDINGS DESCRIBED WITHIN THE PAPER.	67
TABLE 6: <i>IN VIVO</i> AND <i>IN VITRO</i> REPRODUCTIVE AND DEVELOPMENTAL TOXICITY STUDIES OF ZINC OXIDE ENM (ZnO), OUTLINING KEY PARAMETERS FROM EACH STUDY IDENTIFIED, INCLUDING STUDY TYPE, EXPOSURE TYPE AND METHOD AND RELEVANT FINDINGS DESCRIBED WITHIN THE PAPER.	69
TABLE 7: PANEL OF ENMS SELECTED FOR USE WITHIN THE MARINA PROJECT, AND THE PRESENT STUDY. TABLE INCLUDES ENM NAME AND JRC REFERENCE NUMBER, TOGETHER WITH FORM AND BASIC PHYSICO-CHEMICAL PARAMETERS PROVIDED BY THE MANUFACTURER AND FROM LITERATURE USING THE SAME ENM PANEL (JRC, 2011, KERMANZADEH ET AL., 2013, RIEGO SINTES, 2015, RASMUSSEN ET AL., 2013, RASMUSSEN ET AL., 2014, COMERO ET AL., 2011, VAN DER ZANDE ET AL., 2014A, CEFIC, 2012).....	79
TABLE 8: DOSE CONVERSIONS BETWEEN µG/ML AND µG/CM ² USED FOR CYTOTOXICITY STUDIES.....	92
TABLE 9: SUMMARY OF FINDINGS FROM WST-1 AND ALAMAR BLUE ON LEYDIG (TM3) AND SERTOLI (TM4) CELLS. RESULTS ARE REPORTED AS ‘-’ WHERE NO TOXICITY WAS IDENTIFIED, ‘(-)’ WHERE TOXICITY WAS IDENTIFIED ONLY AT THE HIGHEST POSSIBLE DOSE <i>IN VITRO</i> , AND ‘+’ WHERE CLEAR TOXICITY WAS SEEN. WHERE POSSIBLE, THE DOSE OVER WHICH A SIGNIFICANT DECREASE IN VIABILITY WAS SEEN IS REPORTED, AND FOR THOSE ENM ELICITING A CLEAR DOSE-RESPONSE TOXICITY TO TM3 CELLS, AND LC ₅₀ VALUE IS GIVEN.	135
TABLE 10: PCR REACTION MIX PREPARATION (PER WELL) AS PROVIDED BY PRIMERDESIGN. *WORKING CONCENTRATION OF PRIMERS = 300NM IN A 20µL REACTION.	153
TABLE 11: PRIMERS DESIGNED FOR PCR WORK.....	155
TABLE 12: USER-SUPPLIED PCR REACTION MIX PREPARATION/WELL	155
TABLE 13: SERIAL DILUTIONS OF UNTREATED CDNA TO GENERATE STANDARD CURVE FOR PRIMER EFFICIENCY DETERMINATION	156
TABLE 14: PRIMER DESIGN CUSTOM-DESIGNED PRIMERS.....	157
TABLE 15: PCR REACTION MIX, PREPARED ACCORDING.....	158
TABLE 16: ANTIBODY PREPARATION FOR WESTERN BLOTTING ANALYSIS. DETAILED IS PRIMARY ANTIBODY AND ITS PREPARATION FOR DETECTION IN EITHER FLUORESCENT (LICOR) OR ECL (GBOX) BASED SYSTEMS, ALONG WITH SECONDARY ANTIBODIES AND THEIR RESPECTIVE PREPARATION FOR EACH DETECTION METHOD.	164
TABLE 17: EFFICIENCY TESTING OF PRIMERS SOURCED FROM LITERATURE AND PRIMER-BLAST SEARCHING	172
TABLE 18: STATISTICAL ANALYSIS OF RT-qPCR FOR 4 GOI IN TM3 CELLS TREATED WITH NM-110, NM-111 AND NM-300. IT IS WORTH NOTING THAT AS LITTLE RNA WAS DETECTED IN SAMPLES TREATED WITH 8µG/µL NM-300, NO TUKEY’S MULTIPLE COMPARISONS TEST WAS COMPLETED.	176
TABLE 19: SUMMARY OF FINDINGS FROM PCR AND WESTERN ANALYSIS OF RNA AND PROTEIN EXPRESSION IN TM3 CELLS	181

TABLE 20: NANOMATERIALS USED IN ANIMAL TREATMENTS.....	212
TABLE 21: TISSUE SAMPLES SELECTED FOR ANALYSIS FROM THOSE PROVIDED BY RIKILT.....	214
TABLE 22: HAEMATOXYLIN AND EOSIN STAINING PROTOCOL.....	216
TABLE 23: PANEL OF ANTIBODIES SELECTED FOR EXAMINATION OF TISSUES COLLECTED BY IMMUNOHISTOCHEMISTRY.	218
TABLE 24: KEY CELL POPULATIONS, DISTINGUISHING FEATURES, MORPHOLOGICAL AND STEREOLOGICAL IDENTIFIERS PRESENT AT EACH STAGE OF THE SEMINIFEROUS TUBULE CYCLE USED IN STAGING TUBULES FOR MORPHOLOGICAL AND STEREOLOGICAL ANALYSIS.	224
TABLE 25: KEY CELL POPULATIONS PRESENT AT EACH STAGE THE SEMINIFEROUS CYCLE IN TUBULES TO SUPPORT DECISION KEY OUTLINED WITHIN TABLE 24 FOR STAGING OF TUBULES FOR MORPHOLOGICAL AND STEREOLOGICAL ANALYSIS. RELATIVE EXPECTED DAZL PROTEIN IMMUNOHISTOCHEMICAL STAIN IS ALSO NOTED AT THE BASE OF THE TABLE, BASED ON ROCCHIETTI-MARCH ET. AL. (2000). IMAGES REPRODUCED FROM HESS (HESS, 1990).....	226
TABLE 26: COUNT DATA FOR TUBULE OBSERVATIONS MADE PER STAGE OF SPERMATOGENESIS ASSIGNED ACROSS I) ALL DATA POOLED, AND II) EACH TREATMENT GROUP.....	263
TABLE 27: COMPARISON OF CONTROL DATA FROM ANIMALS HARVESTED AT DAY 29 COMPARED TO DAY 85 FOR TUBULE DIAMETER, GENERATED USING A MIXED-MODEL WHERE ANIMAL IS THE RANDOM EFFECT AND STAGE AND DAY ARE FIXED EFFECTS. ESTIMATES REPORTED BY THE MODEL FOR DAY29 AND 85 ARE SHOWN IN THE FIRST TWO ROWS OF THE TABLE, WITH THE DIFFERENCE BETWEEN THESE AND ASSOCIATED P-VALUE REPORTED IN THE BOTTOM ROW. N= 167.	265
TABLE 28: COMPARISON OF CONTROL DATA FROM ANIMALS HARVESTED AT DAY 29 COMPARED TO DAY 85 FOR LUMEN VOLUME, GENERATED USING A MIXED-MODEL WHERE ANIMAL IS THE RANDOM EFFECT AND STAGE AND DAY ARE FIXED EFFECTS. ESTIMATES REPORTED BY THE MODEL FOR DAY29 AND 85 ARE SHOWN IN THE FIRST TWO ROWS OF THE TABLE, WITH THE DIFFERENCE BETWEEN THESE AND ASSOCIATED P-VALUE REPORTED IN THE BOTTOM ROW. N=167.	265
TABLE 29: COMPARISON OF TUBULE DIAMETER IN TREATED ANIMALS TO CONTROLS GENERATED USING A MIXED-MODEL WHERE ANIMAL IS THE RANDOM EFFECT AND TUBULE STAGE AND TREATMENT ARE FIXED EFFECTS. ESTIMATES TOGETHER WITH THEIR STANDARD DEVIATION AND 90% CONFIDENCE INTERVAL ARE REPORTED BY THE MODEL FOR EACH TREATMENT ARE SHOWN IN THE FIRST 4 ROWS OF THE TABLE; THE DIFFERENCE BETWEEN EACH TREATMENT AND CONTROL AND ASSOCIATED P-VALUE ARE REPORTED IN THE BOTTOM 3 ROWS.....	268
TABLE 30: COMPARISON OF TUBULE DIAMETER IN TREATED ANIMALS TO CONTROLS FOR KEY STAGES OF THE SEMINIFEROUS EPITHELIUM CYCLE. RESULTS GENERATED USING A MIXED-MODEL WHERE ANIMAL IS THE RANDOM EFFECT AND TUBULE STAGE AND TREATMENT ARE FIXED EFFECTS. ESTIMATES TOGETHER WITH THEIR STANDARD DEVIATION AND 90% CONFIDENCE INTERVAL ARE REPORTED BY THE MODEL FOR EACH TREATMENT ARE SHOWN IN THE FIRST 4 ROWS OF THE TABLE; THE DIFFERENCE BETWEEN EACH TREATMENT AND CONTROL AND ASSOCIATED P-VALUE ARE REPORTED IN THE BOTTOM 3 ROWS.	269
TABLE 31: COMPARISON OF LUMEN VOLUME IN TREATED ANIMALS TO CONTROLS GENERATED USING A MIXED-MODEL WHERE ANIMAL IS THE RANDOM EFFECT AND TUBULE STAGE AND TREATMENT ARE FIXED EFFECTS. ESTIMATES TOGETHER WITH THEIR STANDARD DEVIATION AND 90% CONFIDENCE INTERVAL ARE REPORTED BY THE MODEL FOR EACH TREATMENT ARE SHOWN IN THE FIRST 4 ROWS OF THE TABLE; THE DIFFERENCE BETWEEN EACH TREATMENT AND CONTROL AND ASSOCIATED P-VALUE ARE REPORTED IN THE BOTTOM 3 ROWS.	271
TABLE 32: COMPARISON OF LUMEN VOLUME IN TREATED ANIMALS TO CONTROLS FOR KEY STAGES OF THE SEMINIFEROUS EPITHELIUM CYCLE. RESULTS GENERATED USING A MIXED-MODEL WHERE ANIMAL IS THE RANDOM EFFECT AND TUBULE STAGE AND TREATMENT ARE FIXED EFFECTS. ESTIMATES TOGETHER WITH THEIR STANDARD DEVIATION AND 90% CONFIDENCE INTERVAL ARE REPORTED BY THE MODEL FOR EACH TREATMENT ARE SHOWN IN THE FIRST 4 ROWS OF THE TABLE; THE DIFFERENCE BETWEEN EACH TREATMENT AND CONTROL AND ASSOCIATED P-VALUE ARE REPORTED IN THE BOTTOM 3 ROWS.	272
TABLE 33: COUNT DATA FOR TUBULES MEASURED WITH AND WITHOUT SLOUGHING OF CELLS INTO THE LUMINAL AREA. ...	273
TABLE 34: COUNT DATA FOR TUBULES MEASURED WITH AND WITHOUT SLOUGHING OF CELLS INTO THE LUMINAL AREA ACCORDING TO STAGE OF SPERMATOGENESIS. + = SLOUGHING PRESENT, - = NO SLOUGHING	273
TABLE 35: COMPARISON OF LUMEN VOLUME IN TREATED ANIMALS TO CONTROLS, WHERE LUMEN VOLUME WAS CORRECTED FOR CELLS SLOUGHED INTO THE CENTRAL LUMEN. GENERATED USING A MIXED-MODEL WHERE ANIMAL IS THE RANDOM EFFECT AND TUBULE STAGE AND TREATMENT ARE FIXED EFFECTS. ESTIMATES TOGETHER WITH THEIR STANDARD	

DEVIATION AND 90% CONFIDENCE INTERVAL ARE REPORTED BY THE MODEL FOR EACH TREATMENT ARE SHOWN IN THE FIRST 4 ROWS OF THE TABLE; THE DIFFERENCE BETWEEN EACH TREATMENT AND CONTROL AND ASSOCIATED P-VALUE ARE REPORTED IN THE BOTTOM 3 ROWS.	274
TABLE 36: COUNT DATA FOR SHAPE OF TUBULES MEASURED ACROSS ALL TREATMENTS. ROUND TUBULES WERE UNIFORM IN SHAPE AND DIAMETER, INTERMEDIATE TUBULES WERE MORE POLYHEDRAL THAN ROUND, WITH SOME ELONGATION AND DIFFERENCE IN DIAMETER DEPENDENT ON AXIS MEASURED, ELONGATED TUBULES WERE CLEARLY LONGER THAN WIDE WITH AN OVAL OR SAUSAGE SHAPED APPEARANCE. NUMBERS WITHIN BRACKETS REPRESENT % OF TREATMENT TOTAL (COLUMNS), WHILE NUMBERS OUT WITH BRACKETS REPRESENT % OF SHAPE TOTAL (ROWS).	275
TABLE 37: COMPARISON OF SHAPE EFFECTS ON TUBULE DIAMETER AND LUMINAL VOLUME. ANALYSIS CONDUCTED USING A MIXED MODEL, WHERE ANIMAL WAS THE RANDOM EFFECT AND SHAPE WAS THE FIXED EFFECT.....	275
TABLE 38: RE-TESTING TUBULE DIAMETER AND LUMEN VOLUME MEASUREMENTS IN TREATED ANIMALS TO CONTROLS FOR ROUND AND INTERMEDIATE SHAPED TUBULES. RESULTS GENERATED USING A MIXED-MODEL WHERE ANIMAL IS THE RANDOM EFFECT AND TUBULE STAGE AND TREATMENT ARE FIXED EFFECTS. ESTIMATES TOGETHER WITH THEIR STANDARD DEVIATION AND 90% CONFIDENCE INTERVAL ARE REPORTED BY THE MODEL FOR EACH TREATMENT ARE SHOWN IN THE FIRST 4 ROWS OF THE; THE DIFFERENCE BETWEEN EACH TREATMENT AND CONTROL AND ASSOCIATED P-VALUE ARE REPORTED IN THE NEXT 3 ROWS.	276
TABLE 39: SUMMARY OF MORPHOLOGICAL CHANGES OBSERVED WITHIN TISSUE SAMPLES FROM ANIMALS IN TWO STUDIES: I) ANIMALS TREATED WITH LOW, MEDIUM OR HIGH DOSE OF NM202 SILICA NANOPARTICLES; II) ANIMALS TREATED WITH ONE OF THREE DIFFERENT TYPES OF SILVER NANOPARTICLE (NM-300, NANO AMOR AND SILVER IONS AgNO ₃)	278
TABLE 40: JOHNSEN SCORE GRADING SYSTEM FOR TESTICULAR MORPHOLOGY	286
TABLE 41: RESULTS OF JOHNSEN SCORES ON SPERMATOGENESIS IN ANIMALS EXPOSED TO TWO TYPES OF SILVER ENM, SILVER IONS AND VEHICLE CONTROL. UNPUBLISHED DATA RECEIVED VIA PERSONAL COMMUNICATION (BOUWMEESTER AND VAN DER ZANDE, 2015).....	286
TABLE 42: COMPARATIVE SUMMARY OF FINDINGS FOR SILVER ENM. WHERE CELLS ARE BLANK, NO ASSAY WAS PERFORMED FOR THIS ENDPOINT. AR = ANDROGEN RECEPTOR, LHR = LUTEINISING HORMONE RECEPTOR, WB = WESTERN BLOT, IHC = IMMUNOHISTOCHEMISTRY, PCR = POLYMERASE CHAIN REACTION. *=ADDITIONAL RESULT FOR ANDROGEN RECEPTOR EXPRESSION, GENERATED FROM PILOT DATA USING TM4 CELLS.	310
TABLE 43: SAMPLE PREPARATION FOR PCR.....	337
TABLE 44: RNA SAMPLE QUANTIFICATION AND INTEGRITY SCORING USING SPECTROPHOTOMETRY AND CHIP-BASED GEL ELECTROPHORESIS.	338

Abbreviations

17β-HSD	<i>17β-hydroxysteroid dehydrogenase</i>
3-NT	<i>Neurotrophin 3</i>
3β-HSD	<i>3β-Hydroxysteroid dehydrogenase</i>
A549	<i>lung epithelial cell line</i>
AB	<i>Alamar Blue</i>
Ab	<i>Antibody</i>
ABC	<i>Avidin-biotinylated peroxidase enzyme complex</i>
AC	<i>adenyl/adenyl cyclase</i>
ACTB	<i>actin beta cytoplasmic</i>
ADME	<i>Absorption Distribution Metabolism and Excretion</i>
Ag	<i>silver</i>
Ag NP	<i>Silver ENM</i>
Ag⁺	<i>silver ions</i>
AgNO₃	<i>silver nitrate</i>
AKT	<i>protein kinase B</i>
Al	<i>aluminium</i>
AOPs	<i>Adverse Outcome Pathways</i>
A-R	<i>Androgen Receptor</i>
ATCC CRL-1714	<i>TM3 mouse Leydig cell line</i>
ATM/ATR	<i>ATM serine/threonine kinase</i>
ATP	<i>adenosine triphosphate</i>
ATP5B	<i>adenosine triphosphate synthase subunit</i>
Au NP	<i>gold nanoparticles</i>
B2M	<i>beta-2 microglobulin</i>
BALB/C	<i>albino laboratory-bred strain of house mouse</i>
Bax	<i>Apoptosis regulator</i>
BBB	<i>Blood Brain Barrier</i>
Bcl-xL	<i>B-cell lymphoma-extra large (transmembrane molecule in mitochondria)</i>
BFR	<i>brominated flame-retardants</i>
BSA	<i>Bovine Serum Albumin</i>
BTB	<i>Blood Testis Barrier</i>
C18-4	<i>mouse spermatogonial stem cell line</i>
C57 mice	<i>most widely used inbred strain of laboratory mouse</i>
C57BL6	<i>common inbred strain of laboratory mouse</i>
cAMP	<i>cyclic adenosine monophosphate</i>
CANX	<i>calnexin</i>
CASA	<i>Computer Assisted Sperm Analysis</i>
CB	<i>Carbon Black</i>
CD1	<i>outbred mice derived from a Swiss group of mice</i>
Cdc42	<i>gene that encodes Cell division control protein 42 homolog</i>
cDNA	<i>complementary deoxyribonucleic acid</i>
CeO₂	<i>cerium dioxide</i>

CLP	<i>Classification and Labelling of Packaging</i>
CNT	<i>Carbon Nanotubes</i>
CO₂	<i>carbon dioxide</i>
CuO	<i>copper oxide</i>
CYC1	<i>cytochrome c-1</i>
CYP11A1	<i>cholesterol side chain cleavage gene</i>
CYP17	<i>Cytochrome P450-C17 enzyme</i>
CYP17A1	<i>17α-hydroxylase/C₁₇₋₂₀ lyase gene</i>
CYP19A1	<i>gene that gives instructions for making aromatase</i>
DAB	<i>3,3'-diaminobenzidine</i>
DART	<i>Developmental And Reproductive Toxicity</i>
DAZ	<i>Deleted in AZoospermia</i>
DAZL/Dazl	<i>Deleted in AZoospermia-like</i>
DEP	<i>Diesel Exhaust Particles</i>
DHT	<i>di-hydrotestosterone</i>
DMEM	<i>Dulbecco's Modified Eagle's Medium/Nutrient Mixture</i>
DNA	<i>deoxyribonucleic acid</i>
DWCNT	<i>Double-Walled Carbon Nano Tubes</i>
EATS	<i>Endocrine Androgen Thyroid Steroidogenesis</i>
EC	<i>Electron Coupling</i>
EC	<i>Extracellular</i>
EC	<i>European Commission</i>
ECL	<i>androgen receptor</i>
ED	<i>Endocrine Disruptors</i>
EHS	<i>Environment Health and Safety</i>
EIF4A2	<i>eukaryotic translation initiation factor 4A2</i>
ELISA	<i>Enzyme-Linked Immunosorbent Assay</i>
EMA	<i>European Medicines Agency</i>
EMA ICH S5	<i>EMA ICH Reproductive Toxicology</i>
ENM	<i>Engineered Nano Materials</i>
ENP	<i>Engineered Nano Particle</i>
EOGRTS	<i>Extended One-Generation Reproductive Toxicity Study</i>
EPA	<i>Environmental Protection Agency</i>
ERK	<i>Extracellular signal-Regulated Kinase</i>
ES-10	<i>carboxylesterase</i>
EST	<i>Embryonic Stem cell Test</i>
EtOH	<i>ethanol</i>
EU	<i>European Union</i>
F344	<i>inbred strain of rats</i>
FAS	<i>death receptor</i>
FASL	<i>FAS ligand</i>
FBS	<i>Foetal Bovine Serum</i>
FCS	<i>Foetal Calf Serum</i>
FSH	<i>Follicle Stimulating Hormone</i>
GAPDH	<i>glyceraldehyde-3-phosphate dehydrogenase</i>
GC	<i>Germ cell</i>
GC-MS/MS	<i>Gas chromatography-mass spectroscopy</i>

GCPR	<i>G-coupled transmembrane receptor</i>
gDNA	<i>genomic deoxyribonucleic acid</i>
GHS	<i>Globally Harmonised System of Classification</i>
GI	<i>Gastro Intestinal</i>
GJ	<i>Gap Junction</i>
GLP	<i>Good Laboratory Practice</i>
GLP-1	<i>Glucagon-like peptide-1</i>
GLUTag	<i>intestinal L-cell line</i>
GDNF	<i>glial cell line-derived neurotrophic factor</i>
GnRH	<i>Gonadotrophin Releasing Hormone</i>
GOI	<i>Gene Of Interest</i>
GPx	<i>glutathione peroxidase</i>
GSH	<i>glutathione (reduced)</i>
GTPase	<i>Guanosine TriPhosphate-ase (family of hydrolase enzymes)</i>
H&E	<i>Haematoxylin and Eosin</i>
HARN	<i>High-Aspect Ratio Nanomaterials</i>
HeLa	<i>human cervical cancer cell line</i>
HEPA	<i>High Efficiency Particulate Air</i>
HEPES	<i>4-(2-hydroxyethyl)-1-piperazineethanesulfonic acid</i>
HepG2	<i>human liver cancer cell line</i>
HKG	<i>House Keeper Genes</i>
Hmcsr	<i>3-Hydroxy-3-Methylglutaryl Coenzyme A Reductase</i>
Hmcgs	<i>3-Hydroxy-3-Methylglutaryl-CoA Synthase 1</i>
HMG CoA	<i>3hydroxy-3-methylglutaryl-coenzyme</i>
HPA	<i>Hypothalamic Pituitary Adrenal</i>
HPG	<i>Hypothalamus Pituitary Gonad</i>
HRP	<i>Horseradish Peroxidase</i>
HSD17B3	<i>17b-hydroxysteroid dehydrogenase type 3</i>
Hsd3b1	<i>hydroxy-delta-5-steroid dehydrogenase, 3 beta- and steroid delta-isomerase 1</i>
HSDB3	<i>3b-hydroxysteroid dehydrogenase/D5-4 isomerase</i>
HSL / HS-Lipase	<i>Hormone Sensitive Lipase</i>
IATA	<i>Integrated Approaches to Testing and Assessment</i>
IC50	<i>Intermediate Concentration for a 50% reduction in viability</i>
ICH	<i>The International Council for Harmonisation of Technical Requirements for Pharmaceuticals for Human Use</i>
ICR	<i>Strain of albino mice originating in Switzerland</i>
IF	<i>Immunofluorescent microscopy</i>
IHC	<i>Immunohistochemistry</i>
INS-1	<i>pancreatic β-cell line</i>
INSL-3	<i>insulin-like peptide 3</i>
ITS	<i>Integrated Testing Strategy</i>
JRC	<i>Joint Research Council</i>
LC	<i>Leydig Cell</i>
LC/MS	<i>Liquid Chromatography–Mass Spectrometry</i>
LDH	<i>Lactate Dehydrogenase</i>
LDLR	<i>Low-Density Lipoprotein Receptor</i>

LH	<i>Luteinising Hormone</i>
LH-R	<i>Luteinising Hormone Receptor</i>
LHS	<i>Left Hand Side</i>
LIF	<i>Laser-Induced Fluorescence</i>
lipoid CAH	<i>lipoid adrenal hyperplasia</i>
LL-37	<i>human cathelicidin peptide</i>
LNCaP	<i>androgen sensitive human prostate adenocarcinoma cells</i>
LOAEL	<i>Lowest Observed Adverse Effect Level</i>
MA-10	<i>cell line derived from transplantable Leydig cell tumour</i>
MAP	<i>Mitogen-Activated Protein</i>
MAPK	<i>Mitogen-Activated Protein Kinase</i>
MARINA	<i>MANaging Risks of NANoparticles</i>
MDA	<i>Malondialdehyde</i>
Mdm2	<i>Mouse double minute 2</i>
mES	<i>mouse embryonic stem cells</i>
MHS	<i>mouse alveolar macrophage cell line</i>
MIQE	<i>Minimum Information for Publication of Quantitative Real-Time PCR Experiments</i>
Mltc-1	<i>Murine Leydig tumour cell line 1</i>
MoA	<i>Mechanism of Action</i>
MoO₃	<i>molybdenum trioxide</i>
mRNA	<i>messenger ribonucleic acid</i>
MSN	<i>Mesoporous Silica Nanoparticles</i>
mTOR	<i>mammalian target of rapamycin</i>
MTT	<i>tetrazolium dye (3-(4,5-dimethylthiazol-2-yl)-2,5-diphenyltetrazolium bromide)</i>
MWCNT	<i>Multi-Walled Carbon Nanotubes</i>
NADP	<i>Nicotinamide adenine dinucleotide phosphate</i>
NADPH	<i>nicotinamide adenine dinucleotide phosphate Hydrogen</i>
NaN₃	<i>sodium azide</i>
nano-Ag	<i>nano-silver</i>
NCBI-NIH Primer-BLAST	<i>National Center for Biotechnology Information National Institutes of Health Primer Basic Local Alignment Search Tool</i>
NCE	<i>Neutral Cholesterol Esterase</i>
NFκB	<i>nuclear factor kappa-light-chain-enhancer of activated B cells</i>
NIH/3T3	<i>mouse embryonic fibroblast cells</i>
NM	<i>Nanomaterial</i>
NM-100, 102	<i>nano silica dioxide</i>
NM-101	<i>nanomaterial form of titanium dioxide (anatase)</i>
NM-103	<i>nanomaterial form of titanium dioxide (hydrophilic)</i>
NM-104	<i>nanomaterial form of titanium dioxide (hydrophobic)</i>
NM-110, 111, 112	<i>nano zinc oxide</i>
NM-200, 203	<i>nano silica dioxide</i>
NM-211, 212	<i>nano cerium dioxide</i>
NM-300	<i>colloidal nanosilver</i>
NM-300dis	<i>nanosilver dispersant</i>
NM-400, 401, 402	<i>carbon nanotubes of varying length and diameter</i>
NM-600	<i>nano clay</i>

NMP	<i>Nanotechnologies, Materials and new Production Technologies</i>
NMRI mice	<i>Naval Medical Research Institute line of mice</i>
NOEL	<i>No Observed Effects Limit</i>
NP	<i>Nano Particles</i>
NR3C4	<i>Nuclear Receptor subfamily 3, group C, member 4</i>
NRT	<i>No Reverse Transcriptase</i>
nSi	<i>nano silica</i>
nSP70	<i>nano silica particles 70 nm (nSPxx for other sizes)</i>
NT2	<i>pluripotent testicular embryonic carcinoma cell line</i>
NTC	<i>No Template Controls</i>
O₂	<i>oxygen</i>
OECD	<i>Organisation for Economic Cooperation and Development</i>
OECD TG407	<i>OECD Repeated Dose 28-day Oral Toxicity Study in Rodents</i>
OECD TG408	<i>OECD Repeated Dose 90-Day Oral Toxicity Study in Rodents</i>
OECD TG416	<i>OECD Two Generation reproductive toxicity test</i>
OECD TG443	<i>OECD Extended one generation reproductive toxicity study</i>
OPPTS 870.3800	<i>Reproduction and Fertility effects test</i>
P450	<i>haem containing superfamily of enzymes</i>
P450arom	<i>Aromatase P450</i>
P450c17	<i>Cytochrome P450 17A1</i>
P450scc	<i>cholesterol side-chain cleavage enzyme</i>
PAP	<i>pen used for immunohistochemical and fluorescent staining</i>
PBPK	<i>Physiologically-based Pharmacokinetic</i>
PBR	<i>Peripheral Benzodiazepine Receptor</i>
PBS	<i>Phosphate Buffered Saline</i>
PBS-T	<i>Phosphate Buffered Saline -Tween</i>
PCR	<i>Polymerase Chain Reaction</i>
PEG	<i>Poly(L-lactide)-block-poly(ethylene glycol)methyl ether</i>
PKA	<i>Protein Kinase A</i>
PKC	<i>Protein Kinase C</i>
PLC	<i>phospholipid-specific phospholipase C</i>
PLLA	<i>Poly-L-Lactic Acid</i>
PND	<i>Post Natal Day</i>
PPP	<i>Plant Protection Products</i>
PTM	<i>Peritubular myoid cells</i>
PVDF	<i>nitrocellulose or polyvinylidene difluoride</i>
QSAR	<i>Quantitative Structure Activity Relationship</i>
Rac1	<i>gene that encodes a GTPase protein</i>
REACH	<i>Registration Evaluation Authorisation and Restriction of CHemicals</i>
RHS	<i>Right Hand Side</i>
RIKILT	<i>Rijkslandbouwschool (National Agricultural College), Wageningen</i>
RIA	<i>Radio Immuno Assay</i>
RIN	<i>Ribonucleic acid Integrity Number</i>
RNA	<i>ribonucleic acid</i>
ROI	<i>Region Of Interest</i>
ROS	<i>Reactive Oxygen Species</i>
RP-1	<i>mouse anti-rat granulocytes RP-1</i>

RPL13A	<i>Ribosomal Protein L13a</i>
rRNA	<i>ribosomal ribonucleic acid</i>
RS	<i>mitochondrial succinate-tetrazolium-reductase system</i>
RT	<i>Reverse Transcription</i>
RT-PCR	<i>Reverse Transcriptase Polymerase Chain Reaction</i>
RT-qPCR	<i>Reverse Transcriptase quantitative Polymerase Chain Reaction</i>
S5A	<i>5a-reductase</i>
SAS	<i>Synthetic Amorphous Silica</i>
SAS	<i>Statistical Analysis Software</i>
SC	<i>Sertoli Cell</i>
SCO	<i>Sertoli Cell Only</i>
SDHA	<i>Succinate Dehydrogenase complex subunit A</i>
SDS-PAGE	<i>Sodium Dodecyl Sulphate–Polyacrylamide Gel Electrophoresis</i>
SER	<i>Smooth Endoplasmic Reticulum</i>
Si	<i>silica</i>
Si NP	<i>Silica nanoparticles</i>
SiO₂	<i>silicon dioxide</i>
SOP	<i>Standard Operating Protocol</i>
SPF	<i>Specific Pathogen Free</i>
SR-B1	<i>Scavenger Receptor class B type 1</i>
SSA	<i>Specific Surface Area</i>
StaR	<i>Steroidogenic acute Regulatory protein</i>
SUN	<i>Sustainable Nanotechnologies</i>
SWCNT	<i>Single-Walled Carbon Nano Tubes</i>
T	<i>Testosterone</i>
TBECH	<i>1, 2-dibromo-4-(1, 2-dibromoethyl) cyclohexane</i>
TBS	<i>Tri-Buffered Saline</i>
TEER	<i>Transmembrane Electrical Resistance</i>
TEM	<i>Transmission Electron Microscopy</i>
TEX14	<i>testis-expressed gene 14</i>
TG	<i>Test Guidelines</i>
TGCC	<i>Testicular Germ-Cell Cancer</i>
TGF-β	<i>Transforming Growth Factor-β</i>
TGS	<i>Testicular Dysgenesis Syndrome</i>
TiO₂	<i>titanium dioxide</i>
TJ	<i>Tight Junction</i>
TM3	<i>mouse Leydig cell line</i>
TM4	<i>mouse Sertoli cell line</i>
TNF-α	<i>Tumour Necrosis Factor-α</i>
tpa	<i>tonnes per annum/year</i>
tRNA	<i>transfer ribonucleic acid</i>
TSPO	<i>translocator protein</i>
TUNEL	<i>terminal deoxynucleotidyl transferase dUTP nick end labelling</i>
Tween 20	<i>Polyoxyethylene Glycerol Trioleate and Polyoxyethylene (20) Sorbitan mono-Laurat</i>
UBC	<i>Ubiquitin C</i>
USDA	<i>United States Department of Agriculture</i>

V79	<i>Chinese hamster cell line</i>
WST-1	<i>Water Soluble Tetrazolium salt-1</i>
YWHAZ	<i>phospholipase A2</i>
Zn²⁺	<i>zinc ions</i>
ZnCl₂	<i>zinc chloride</i>
ZnO	<i>zinc oxide</i>
ZnSO₄	<i>zinc sulphate</i>
ZO-1	<i>Zonula Occludens-1 / Tight junction protein 1</i>
ΔΔCt	<i>delta delta Ct method</i>

Presentations and Publications

relating to this thesis

Papers and book chapter contributions:

Gary R Hutchison & **Bryony L Ross** (2014) 'Chapter 19: Current *in vitro* models for nanomaterial testing: The reproductive system' in Monteiro-Riviere & Tran, C.L. (eds) *Nanotoxicology: Progress toward nanomedicine*, 2nd edition, CRC Press

Karin S. Hougaard; Luisa Campagnolo; Pascale Chavatte-Palmer; Anne Tarrade; Delphine Rousseau-Raillard; Sarah Valentino; Margriet V Park; Wim H de Jong; Gerrit Wolterink; Aldert Piersma; **Bryony L Ross**; Gary Hutchinson; Jitka S Hansen; Ulla Vogel; Petra Jackson; Rémy Slama; Antonio Pietroiusti; Flemming Cassee (2015); A perspective on the developmental toxicity of inhaled nanoparticles; *Reproductive Toxicology* 56, pp118–140.

Lucian Farcas, Fernando Torres Andón, Luisana Di Cristo, Bianca Maria Rotoli, Ovidio Bussolati, Enrico Bergamaschi, Agnieszka Mech, Nanna Hartmann, Kirsten Rasmussen, Juan Riego Sintes, Jessica Ponti, Agnieszka Kinsner-Ovaskainen, François Rossi, Agnes Oomen, Peter Bos, Rui Chen, Ru Bai, Chunying Chen, Louise Rocks, Norma Fulton, **Bryony L Ross**, Gary Hutchison, Lang Tran, Sarah Mues, Rainer Ossig, Jürgen Schnekenburger, Luisa Campagnolo, Lucia Vecchione, Antonio Pietroiusti and Bengt Fadeel (2015), Comprehensive *in vitro* toxicity testing of a panel of representative oxide nanomaterials: first steps towards an intelligent testing strategy, *PLoS ONE* 10(5)

Oral Presentations:

ROSS, B.L. (2013) 'Toxicity of Engineered nanomaterials to the male reproductive system', Edinburgh Napier University Postgraduate Conference, Edinburgh

ROSS, B.L. (2015) 'Engineered nanomaterial toxicity to the male reproductive system', *NANOEH Conference*, South Africa

ROSS, B.L. (2015) 'Engineered nanomaterial toxicity to the male reproductive system', *Research in Progress seminar*, Edinburgh Napier University

ROSS, B.L. (2017) 'Can *in vitro* studies form an indicator for *in vivo* toxicity of engineered nanoparticles to the male reproductive system?', *Research seminar*, Edinburgh Napier University

Poster Presentations:

Bryony L Ross, Gary R Hutchison & Shirley Price (2013) "Tiered testing strategies for reproductive and developmental nanotoxicology: Development of a tool to guide experimental work", *British Toxicology Society Conference*, Solihull UK

Bryony L Ross, Eva M Malone, Hans Bouwmeester, Mieke van der Zande & Gary R Hutchison (2014) "Toxicity of Engineered nanomaterials to the male reproductive system", *Nanotox 2014 conference*, Antalya, Turkey

Bryony L Ross, Eva M Malone, Mick Rae, Hans Bouwmeester, Ilse Gosens, Flemming Cassee, Erin Werner, Malgorzata Ślęzak & Gary R Hutchison (2016) 'Development of *in vitro* strategies to predict *in vivo* toxicity of Engineered Nanoparticles to the Male Reproductive System', *IPTC 2016 Conference*, Singapore

Chapter 1: Introduction and Literature Review

Introduction

The reproductive system is complex in both males and females, and consequently reproductive toxicity can manifest as a diverse set of endpoints. As a result, it is necessary to understand normal reproductive anatomy and physiology to understand and investigate the potential toxicity of novel materials. Whilst the anatomy of the reproductive system has been relatively well studied, only recently has a more in-depth understanding begun to emerge on the complex cellular and hormonal processes underlying production of viable gametes (Gupta, 2011). Similarly, a fuller understanding of the integration of the reproductive system with, and dependency upon, multiple organs within the body is also relatively recent.

Male Reproductive Anatomy

Structures associated with male reproduction usually include paired testes, a duct system, accessory sex glands (seminal vesicles, prostate etc.), the scrotum (with thermoregulatory function) and a penis. The primary functions of the testis are spermatogenesis (production of male gametes), and steroidogenesis (production of steroid hormones, androgens). Unlike females, where the full complement of oogonia is present at birth, spermatogonia are proliferating continually and developing into spermatozoa for maximal sperm production (Evans and Ganjam, 2011).

The testis is divided into lobules of parenchyma which have avascular tubular and vascular interstitial compartments (Sharpe, 1983). Within the tubular compartment, the seminiferous tubules form highly convoluted loops beginning and ending with straight portions, forming the functional units of the compartment. The seminiferous tubules connect to the rete tubules, which in turn join efferent ductules which attach to the epididymis (Evans and Ganjam, 2011). The epididymis leads to the vas deferens (ductus deferens) and onto the ejaculatory duct (Fig. 1).

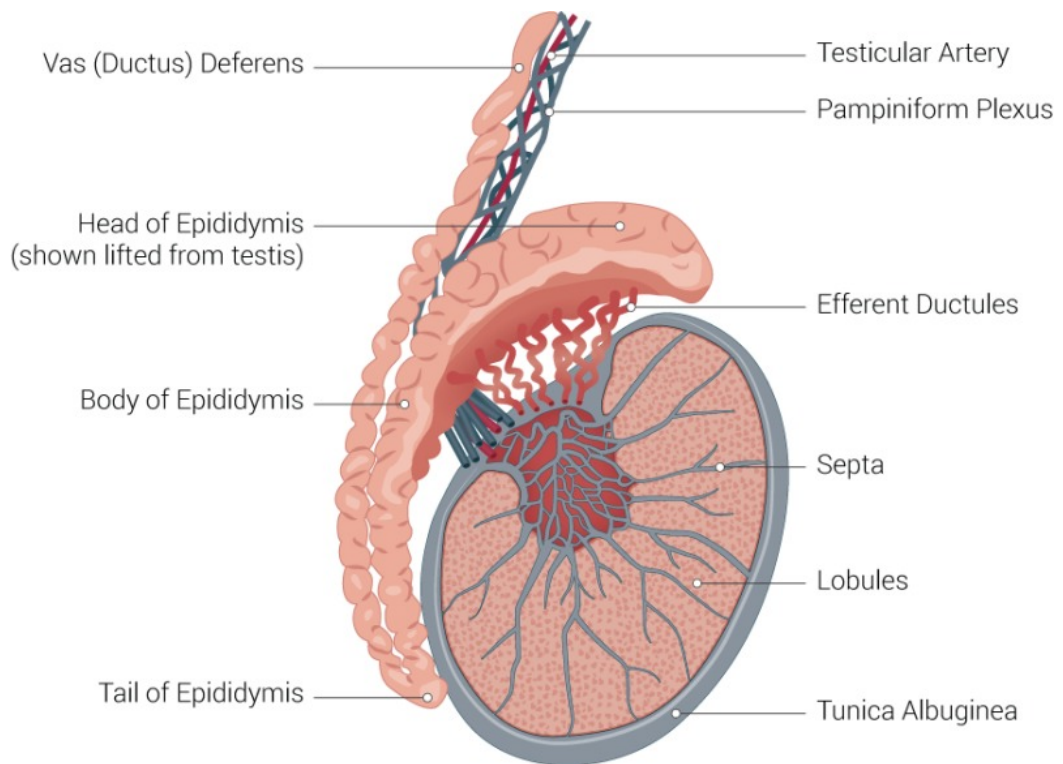


Figure 1: Basic testicular anatomy, showing the major architecture of this aspect of the male reproductive system. From (Bhimji and Leslie, 2018)

The vasculature of the testis begins with the internal spermatic artery, which originates from the abdominal aorta, running through the spermatic cord toward the testis. It gives off superior and inferior epididymal branches, supplying parts of the epididymis, before continuing as the testicular artery. On arrival at the testis, it moves in a line down the epididymal border, before forming a series of loops at the caudal pole leading to the rete testis, finally entering the testicular parenchyma. Here it divides into radiate arteries and then intertubular arterioles, which in turn supply intertubular and peritubular capillaries which run parallel to and circumferentially around the seminiferous tubules (Creasy and Chapin, 2013). The lymphatic system of the testis forms distinct vessels in the human, which enter the peritubular layer of the seminiferous tubules. Conversely, in the rat, they form channels between Leydig and peritubular cells of the seminiferous tubules but remain in the interstitial space (Creasy and Chapin, 2013). The veins leaving the testis form the pampiniform plexus as they enter the spermatic cord, which forms a heat exchange system, maintaining the testis at a few degrees below body temperature for optimal spermatogenesis (Fig. 1).

The seminiferous tubules contain germ cells at various stages of differentiation. They also contain Sertoli cells (SC), which provide structural support, nutrients and regulatory factors to the germ cells. SC divide the seminiferous epithelium into basal and luminal compartments - the basal compartment containing spermatogonia up to their pre-leptotene stage, and the ad-luminal compartment containing spermatocytes, spermatids and spermatozoa (Evans and Ganjam, 2011). Sperm are generated through a cycle that takes 6-9 weeks to complete in humans, during which a coordinated set of mitotic and meiotic divisions accompany elaborate cytodifferentiation and intercellular interactions (Schlatt and Ehmcke, 2014).

Junctions between SC create the blood-testes-barrier (BTB), forming an important immuno-privileged environment which prevents spermatozoa from entering the blood circulation or lymphatic systems. This prevents exposure of immunogenic sperm to the body's immune system, which can lead to autoimmune attack and disorders such as cryptic orchitis (Fig.2). Seminiferous tubules are surrounded by peritubular myoid cells which participate in important interactions with Sertoli cells (Evans and Ganjam, 2011).

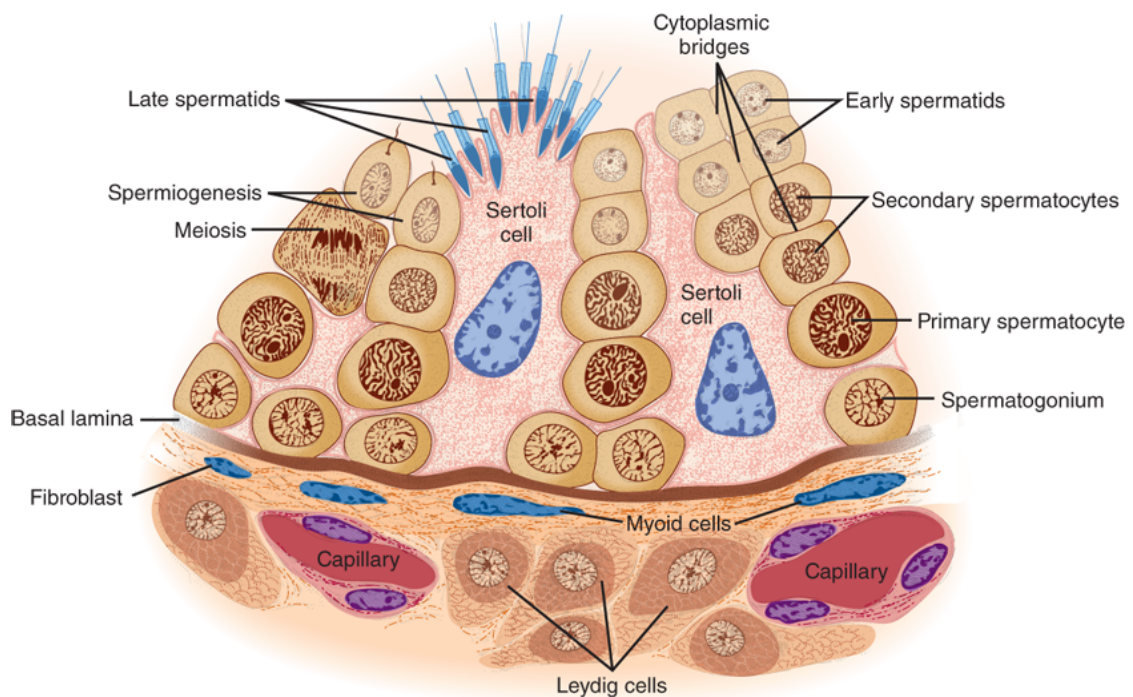


Figure 2: Schematic showing structure of the seminiferous tubule. Within tubules, Sertoli cells (SC) sit on the basal membrane, their cytoplasm projecting toward the central lumen at varying lengths depending on stage of the spermatogenic cycle, 'nursing' developing spermatozoa along their length. SC are connected via highly controlled cellular junctions to form the Blood Testis Barrier. Within the interstitium lie blood capillaries, lymphatic vessels and Leydig cells (LC), which are responsible for generation of androgens to support SC in managing spermatogenesis, amongst other roles in maintenance of the male reproductive system. From (Barrett et al., 2019)

The duct system of the testis, which conducts spermatozoa and associated secretory products away from the testis to the ejaculatory duct, consists of effluent ductules, the epididymal duct, and the vas deferens (Fig. 1). Upon maturation, spermatozoa are released from the cellular syncytium in which they are developed, and into the lumen of seminiferous tubules in a process called spermiation. From here, they enter the epididymis via efferent ductules, and during passage through the epididymis (a process which takes approximately 7 to 14 days) they acquire motility and undergo final maturation. At this stage, defective spermatozoa are also recognised and eliminated, before final secretory contributions are made to the seminal fluid prior to ejaculation (Evans and Ganjam, 2011).

The interstitial compartment of the testis contains venous and lymphatic systems, connective tissue, a few other key cell types (including specialised testicular macrophages) and Leydig cells (LC). Leydig cells are polyhedral cells, distributed within the interstitium, but often found loosely grouped around blood capillaries. Their primary role is the production of androgens, which not only play a key role in managing SC and in turn spermatogenesis, but also a number of important wider physiological roles. The capillaries around which LC tend to gather, and interstitial fluid from the lymphatic system are the primary mechanisms through which all hormones and nutrients are transported to and from the bloodstream to cells of the testis (Sharpe, 1983). There exist species differences in abundance of LC and it is important to take this into account when measuring response to toxicant exposure, if effects on number of LC are being used as an endpoint (Evans and Ganjam, 2011).

Management of male fertility is an exquisitely complex process, involving production of millions of spermatozoa daily, alongside associated sexual behaviour, and adjustments for external influences such as stress, nutrition or seasonality (Schlatt and Ehmcke, 2014). Much of this is heavily dependent on gonadotrophic hormones secreted by the adenohypophysis (anterior pituitary), which in turn are controlled by release of gonadotrophin releasing hormone (GnRH) from the hypothalamus. Because of the clear reliance of the major cells controlling function of the testis on external hormone influence, it is important to understand the basics of reproductive physiology, and in particular, the role of the Hypothalamus-Pituitary-Gonad axis in its control.

Male Reproductive Physiology

Control of reproduction is managed by the hypothalamus, pituitary and testes acting in concert, known as the Hypothalamus-Pituitary-Gonadal (HPG) axis.

In his 1955 monograph, Geoffrey Harris outlined his views and evidence for the neural mechanisms controlling the pituitary-gonadal axis (Harris, 1955). While the link between the pituitary and gonads was already well known at the time, relatively little was known about the neural influence on this from the hypothalamus. At the time, Harris outlined his fundamental hypothesis that “nerve fibres from the hypothalamus liberate some humoral substance(s) into the capillaries of the primary plexus in the median eminence and that this substance is carried by the portal vessels to excite or inhibit the cells of the pars distalis [adenohypophysis]” (Harris, 1955).

Since then, numerous refinements and additional complexities have been added to this model, leading to a much broader understanding of the neuroendocrine control of gonadal function (Plant, 2015). It is now well established that endocrine events regulating reproductive and sexual behaviours are distinct in males and females, as illustrated in Fig. 3. This occurs via a complex series of hormonal pathways, targets and feedback loops, enacting control both systemically and locally, via autocrine, paracrine and endocrine interactions.

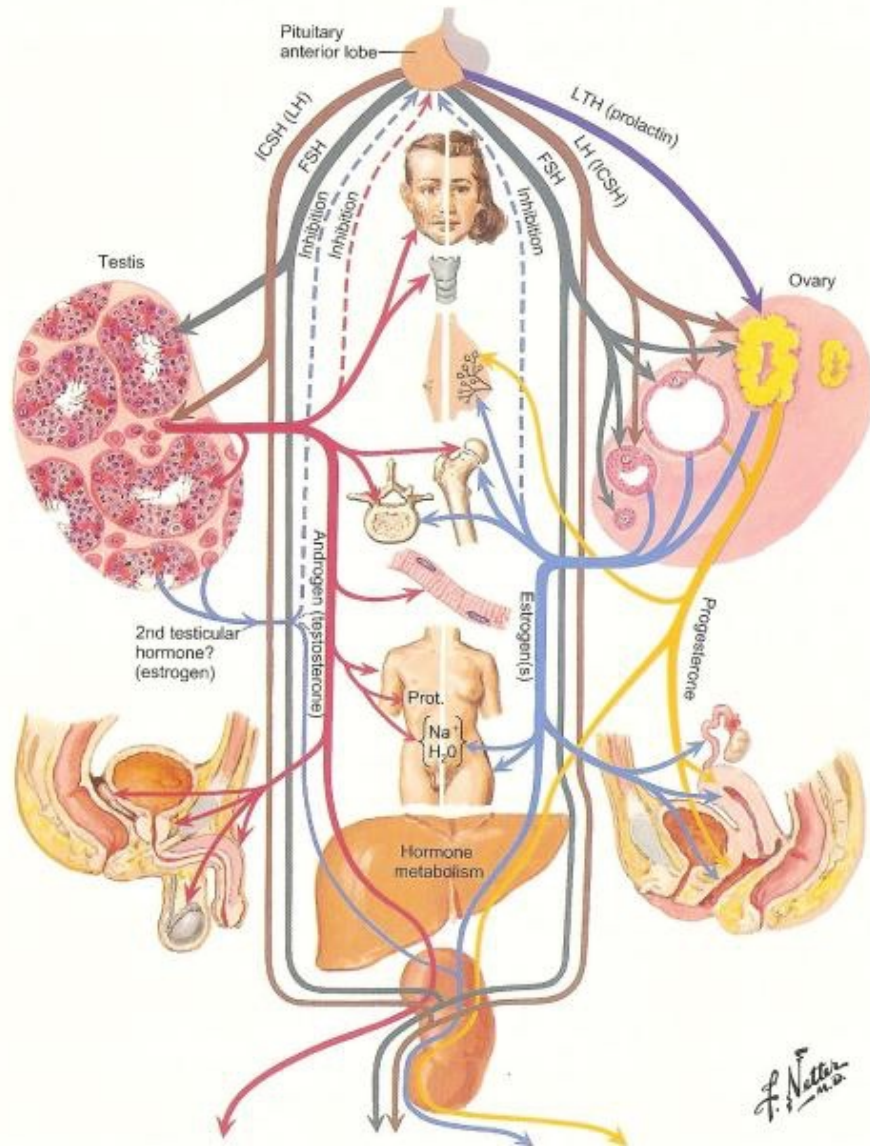


Figure 3: Gonadal hormone targets, pathways, feedback loops and route of metabolism and excretion in males and females. From: (Netter, 1997).

In males, pulsatile release of Gonadotrophin Releasing Hormone (GnRH) from the hypothalamus acts as a master on/off switch to the system by controlling release of luteinizing hormone (LH) and follicle stimulating hormone (FSH) from the adenohypophysis of the pituitary. This system is responsive to physiological and environmental changes that may require up- or down-regulation of the HPG axis and managing reproductive function accordingly. Recently it has emerged that timing of hypothalamic GnRH release is initiated in the KNDy neuronal network of the arcuate nucleus (representing a population of kisspeptin, neurokinin B & dynorphin neurones) by reciprocating interplay of stimulatory neurokinin B signals and inhibitory dynorphin inputs. This output is then thought to be relayed from the arcuate nucleus to the GnRH

neuronal network by release of kisspeptin from axonal terminals originating from KNDy neurons (Plant, 2015).

GnRH release leads to release of pulses of LH and FSH into the peripheral circulation throughout the day, facilitating LH-dependent testosterone production and FSH dependent Sertoli function (Gupta, 2011). FSH acts specifically on FSH receptors of SC within the seminiferous tubules of the testis, which in turn release a number of substances (e.g. androgen binding protein, glial cell line-derived neurotrophic factor (GDNF) and potentially oestradiol, amongst others) which regulate spermatogenesis by controlling expansion of germ cells (Carreau et al., 2006, Carreau et al., 2011).

LH acts on Leydig cells (LC) via the LH-receptor, in turn activate cAMP (cyclic adenosine monophosphate) and stimulate the production of androgens from cholesterol. Within the male, the primary gonadal androgens are testosterone (T) and di-hydrotestosterone (DHT). Locally, androgens prompt paracrine management of germ cell development by SC. This includes production of androgen binding protein by the SC which increases testosterone concentrations in the seminiferous tubules to lightly stimulate spermatogenesis. Systemically, the testis is responsible for 95% of testosterone circulating in post-pubertal males (Sherbet and Auchus, 2007). Upon diffusion into the circulation, testosterone equilibrates between protein bound (98%) and free fractions (2%), of which the free form is believed to be the active form (Sherbet and Auchus, 2007). Along with DHT, this circulating testosterone is responsible for maintenance of the male phenotype, management of androgen-controlled actions in the periphery, secondary sexual characteristics such as increased bone mass, muscle and body hair, as well as associated behaviours (Schlatt and Ehmcke, 2014).

The positive and negative feedback loops of the HPG axis shown in Fig. 3 maintain an environment conducive to normal reproductive function. At the most basic level, the feedback loops controlling LH and FSH production by feeding back at the hypothalamic level are inhibin and activin produced by SC, and testosterone produced by LC. Every site of production, pathway, target and feedback loop may be potentially disrupted by xenobiotics (Evans and Ganjam, 2011).

Interference of exogenous substances with the HPG axis has been shown to lead to sub-fertility or even infertility, depending on the severity of action and duration of exposure. Such substances are known as Endocrine Disruptors, and are defined “an exogenous chemical or mixture of chemicals that interferes with any aspect of hormone action” (Gore et al., 2014). For example, brominated flame-retardants (BFR) such as 1, 2-dibromo-4-(1, 2-dibromoethyl) cyclohexane (TBECH), are androgen receptor agonists, which interfere with androgen receptor signalling, leading to not only local effects in the testis but also systemic effects via the HPG axis (Kharlyngdoh et al., 2018). Another important family of compounds known for their endocrine disrupting action are phthalates. Excessive exposure to phthalates has been linked to both testicular dysgenesis syndrome (TGS) which manifests as effects on germ cell development, and to incidence of testicular germ-cell cancer (TGCC) (Jobling et al., 2011, Hutchison et al., 2008). Consideration of potential endocrine effects is therefore important when evaluating toxicity to any new substance.

Nanotechnologies and the emergence of nanotoxicology

Nanomaterials are “natural, incidental or manufactured materials containing particles, in an unbound state or as an aggregate or as an agglomerate and where, for 50 % or more of the particles in the number size distribution, one or more external dimensions is in the size range 1 nm - 100 nm” (EC, 2011). Humans have been exposed incidentally to naturally occurring NP such as those generated by volcanic activity for thousands of years. More recently, with the development of more advanced technologies, humans are now exposed to anthropogenic NP generated both unintentionally (e.g. diesel nanoparticles generated by automobile engines) and intentionally (engineered nanomaterials, ENM) (Oberdorster et al., 2005). Nanomaterials (NM) form a field of materials science, within which nanoparticles and nanostructures exist in a multitude of compositions, ranging from simple (e.g. pristine silver particles), to incredibly complex structures such as nano constructs used in medical technologies, modified by multiple surface ligands (Donaldson et al., 2004).

Harnessing the properties of NM can provide many benefits to society across a wide range of applications, from revolutionary medical solutions to advanced automotive parts, textiles and building materials (Aitken et al., 2011). Their small size means that their properties are often vastly different from their bulk counterparts (larger sized particles with the same chemical composition), typical examples including high tensile strength, low weight, high electrical and thermal conductivity, and unique electronic properties.

However, it is crucial to the responsible development of nanotechnologies to ascertain and understand any potential environment, health and safety (EHS) implications, and where necessary, implement strategies for their control. Because of the large gaps in our knowledge relating to potential risk, activity concerned with the EHS aspects of nanotechnologies has been growing for almost 2 decades. However, by comparison to many other modern environmental toxicants, research into the potential health and environmental impacts of nanotechnology remains in its infancy.

The advent of nanotoxicology

Investigation of EHS aspects of nanomaterials began using evidence gathered from many years of research within the mature field of particle toxicology. A seminal review which shaped much of the research following was that of the Royal Society and the Royal Academy of Engineering into the “opportunities and uncertainties” surrounding nanomaterials (RS-RAE, 2004). This highlighted potential risks to health and the environment arising from exposure, concluding that while for many nanotechnologies, there were no foreseeable risks to health or to the environment, for ‘nanoparticles and nanotubes’ there were potential risks which required further investigation and where appropriate, control. In the same year Donaldson and colleagues (Donaldson et al., 2004) proposed that there should exist a sub-category of toxicology specific to nanomaterials; nanotoxicology.

The nanotechnologies market is growing exponentially, and is expected to be worth \$125bn by 2025 (ResearchAndMarkets, 2018). In parallel with this growth, efforts have developed to understand and manage any associated risks. In 2009, one review identified over 600 research projects working in the area, a number of which will have

grown significantly since this time (Aitken R.J et al., 2009). However, it is only in recent years that data on nanotoxicology of the reproductive system began to emerge, making it a very new area for research.

Why are ENM different?

One key reason ENM are receiving much attention is their novel physico-chemical properties, which mean they pose novel challenges for researchers, risk assessors and regulators alike. Their key distinguishing property is that of size, or more accurately specific surface area (the total surface area per unit mass). This hugely increased surface reactivity has been linked to enhanced toxicity (RS-RAE, 2004, Oberdorster et al., 2005). In addition, their small size confers an increased potential to translocate resulting in an adsorption, distribution, metabolism and excretion (ADME) profile which may be vastly different to their bulk counterparts, and could allow them access across barriers in the body such as the blood-brain, placental barrier and BTB to access immunoprivileged sites and penetrate cells therein (Oberdorster et al., 2009, Takeda et al., 2009, Hankin et al., 2008). Furthermore, it is thought that those with a high aspect ratio (HARN) may conform to the fibre paradigm of toxicity (Tran CL 2008). Figure 4 summarises key properties of interest and their potential effects on ENM biointeractions.

Human exposure to ENM may be from a number of sources and via a number of routes, including inhalation, ingestion, trans-dermal permeation, or in some cases by injection (in the case of medicines). Following exposure, it is thought that ENM will interact with proteins at the site of entry termed the 'nano-bio interface', causing ENM to undergo continuous dynamic changes dependent on interactions (Savolainen et al., 2010, Colognato et al., 2012). The combination of this interface and the inherent properties of the ENM will determine its onward distribution. Potential adverse effects may therefore occur at the portal of entry, primary target organs (e.g. the lung or GI tract), and secondary target organs (e.g. the reproductive system or kidney).

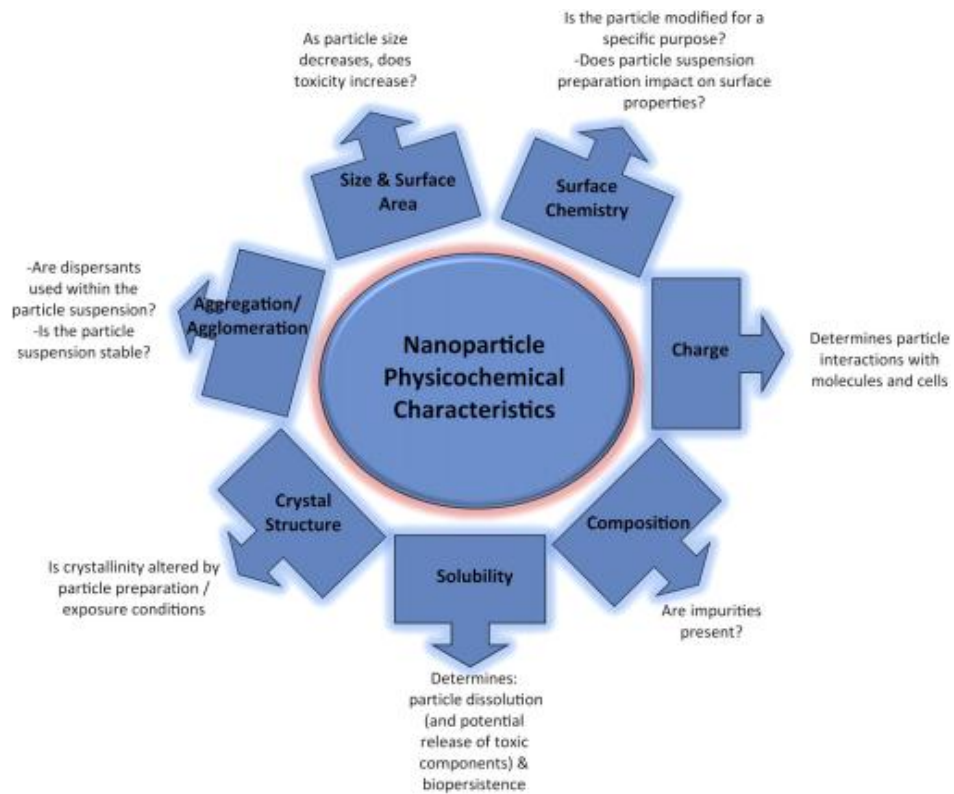


Figure 4: Physicochemical properties of nanomaterials that should be considered with high priority in toxicological assessments. From (Johnston et al., 2010)

The complex interaction of ENM with the physiological environment into which they are entered introduces a multitude of complexities which must be considered when appraising potential toxicity. For example, upon entry to the body ENM will be coated with a bio-corona (made up of a variety of biomolecules dependent on both the site of entry and characteristics of the ENM itself) which will evolve and change as the ENM passes through different compartments in the body (Pietrojusti et al., 2013). In addition, the novel physico-chemical characteristics and behaviour of ENM means they may interfere with toxicity testing, as has already been demonstrated for a number of key assays (Kroll et al., 2012).

With an obvious need for investigation of the interaction of ENM with biological systems, research using a multidisciplinary approach which combines chemistry, biology, physics, and engineering knowledge has begun in earnest. However, reproductive and developmental nanotoxicity is to date in its infancy, and although it is now gathering momentum, there remains relatively limited information on the interaction of ENM with this complex body system.

Reproductive & Developmental Toxicity & DART Testing

Reproductive toxicity is defined as an adverse effect induced by a substance on male or female reproductive ability or capacity, including developmental effects on the offspring and effects on or via lactation (UNECE, 2005). It is a younger field of science than many others; research into the reproductive and developmental effects of substances only began in earnest over the last 100 years. Disasters involving environmental and medical toxicants in the 1950s and 1960s contributed to the area of reproductive toxicity being more exhaustively scrutinised. The first of these was the thalidomide tragedy, where from 1957-1961 pregnant women were prescribed thalidomide to help with morning sickness in their first trimesters. Whilst the drug had minimal toxicity to the adult, it was highly embryotoxic, and over 10,000 babies were born with severe birth defects including phocomelia and amelia following exposure *in utero* (Gupta, 2011). This was shortly followed by the Minamata incident in Japan (1956), and ‘wonder wheat’ disaster in Iraq (1971) where around 3,000 and 100,000 people respectively who had eaten fish and wheat high in methylmercury saw severe neurological damage in their children (Gupta, 2011).

These, and other similar tragedies led to a growing interest in teratology, and increased efforts by both pharmaceutical and chemical regulators to ensure the safety of drugs and chemicals. As such, testing for developmental and reproductive toxicity (DART) is now a standard part of development and regulatory approval for any chemical, pharmaceutical or cosmetic product.

Categorisation of DART testing, and relevant regulatory frameworks for DART

DART testing covers two broad categories (developmental and reproductive) and three classes of toxicity (fertility, parturition and lactation). Depending on the study type, endpoints typically evaluated include reproductive function or capacity i.e. adverse effects on libido & sexual behaviour, the oestrus cycle or any aspect of spermatogenesis, hormonal activity or physiological response which would interfere with the capacity to fertilize, fertilization itself or development of the fertilized ovum up to and including implantation. Developmental endpoints include non-heritable effects on the offspring which interfere with normal development both peri- and post-natally; manifested, for

example, by altered body weight, developmental defects, and impaired mental or physical development up to and including puberty (ECHA, 2008) (Beekhuijzen, 2017).

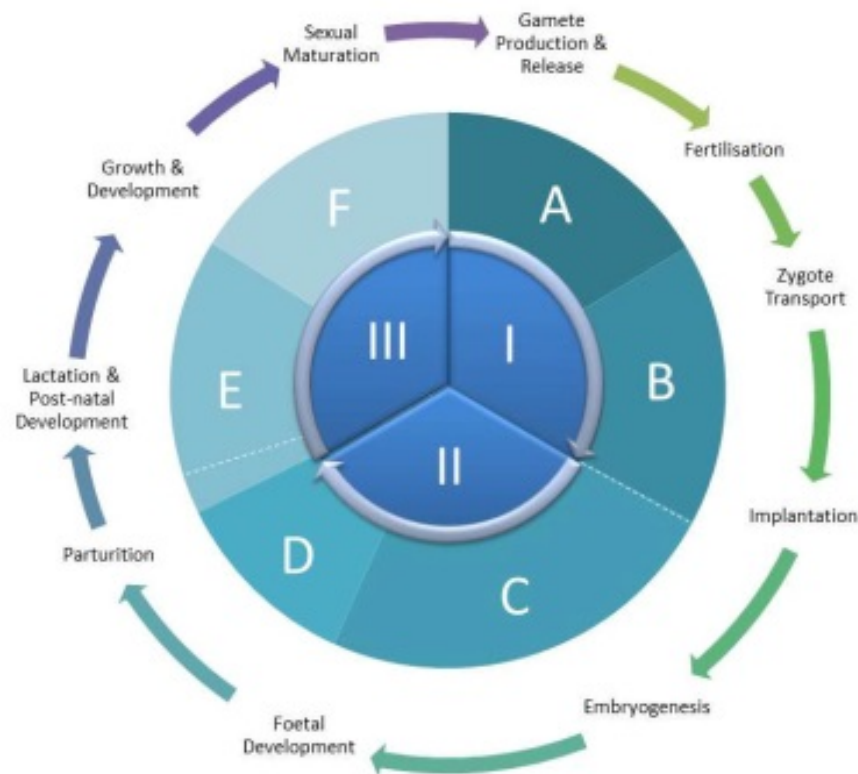


Figure 5: Stages of the reproductive and developmental cycle according to the two major regulatory approaches: US Food and Drug Administration (FDA) and the International Conference on Harmonisation (ICH). Segments I (fertility), II (embryotoxicity/teratogenicity) and III (peri/post-natal toxicity) represent the FDA testing strategy. Stages A (pre-mating to conception), B (conception to implantation), C (implantation to closure of the hard palate), D (closure of hard palate to end of pregnancy), E (birth to weaning) and F (weaning to sexual maturity) represent the ICH approach. NB. ICH stage C spans both segment II and III, as indicated by the dotted white line). Adapted from (Spielmann, 2009).

Despite the wide range of products to which DART testing may be applied (chemical, drugs, agrochemicals, industrial chemicals, food etc), the testing approach remains fairly similar in terms of endpoints evaluated. As an example, Fig. 5 provides an outline of the stages considered for DART testing, according to two both the European Medicines Agency and the US Food and Drug Administration (EMA, 2017, FDA, 1966). However, although endpoints are similar, approach may differ depending on industry, e.g. the chemical and agrochemical industries use similar methodologies as their exposures are more likely to be uncontrolled (for dose and duration) compared to the pharmaceutical industry, where control over exposure is key to a drug's efficacy and safety. Traditionally,

testing used within each segment or stage has been heavily dependent on *in vivo* methods. As such, the animal burden associated with conducting the suite of DART testing required for registration of a chemical, or approval of a drug is extremely large, several thousand animals being required to complete a full complement of DART testing for any given industry. Table 1 provides an outline of the major testing regimes for chemicals, pharmaceuticals and agrochemicals, along with an estimation of animal number required per test. For the agrochemical and pharmaceutical industries, testing requirements remain fairly static. Conversely, for industrial chemicals the EC regulation for the Registration, Evaluation Authorisation and restriction of Chemicals (REACH) implements an incremental approach to DART testing depending on tonnage production or import per year (as a proxy for likelihood of human exposure). Substances <1 tonne per year (tpa) do not require registration, and DART testing is scaled for those produced at >10tpa, >100tpa and >1000tpa (EC, 2006).

More recently, specific consideration has also been given to the potential for substances to interrupt the normal function of the endocrine system (endocrine disruptors, ED), which if affected can have direct influence on the reproductive system via the HPG axis. This has resulted in development of specific guidance for testing, at least for chemicals. One such piece of guidance is the OECD's 'Revised guidance document 150 on standardised test guidelines for evaluating chemicals for endocrine disruption' (OECD, 2018b). This contains a conceptual framework for testing and assessment of ED chemicals, alongside useful information on the applicability of existing Test Guidelines (TG) to identification of EDs via a weight of evidence approach.

Table 1: Summary of guidelines for DART testing. Adapted from Beekhuijzen 2017 and with reference to ICH, EPA, REACH & the EC Plant based Product regulations (Beekhuijzen, 2017, EPA, 2000, EPA, 2019, EMA, 2017, EC, 2006, EC, 2014)

INDUSTRY	TEST	When Required	Number of Animals ¹
Pharmaceutical	ICH S5 (R2) Section 4.1.1 Study of fertility and early embryonic development to implantation and Part II: Toxicity to Male Fertility	Completed before the initiation of large scale / long duration clinical trials (e.g. phase 3), as an evaluation of the reproductive organs is performed in earlier repeated-dose toxicity studies.	F0: 80 males and 80 females F1: Approx. 960 fetuses
	ICH S5 (R2) Section 4.1.3. Study for effects on embryo-foetal development in rats	EU & Japan: definitive developmental toxicity studies in 2 species are required for inclusion of women of childbearing potential (WOCBP) in any clinical study. However, there are defined situations where clinical trials with WOCBP may progress without these. US: assessments of embryo-foetal development may be deferred until before phase 3 clinical studies for WOCBP using precautions to prevent pregnancy.	F0: 88 females F1: Approx. 1,056 fetuses
	ICH S5 (R2) Section 4.1.3. Study for effects on embryo-foetal development in rabbits	See above	F0: 88 females F1: Approx. 792 fetuses
	ICH S5 (R2) Section 4.1.2. Study for effects on pre-and postnatal development, including maternal function	Should be submitted for marketing approval.	F0: 96 females F1: Approx. 1,152 pups
Chemical	OECD 421, Reproduction/Developmental Toxicity Screening Test (2016)	REACH Annex VIII (applicable for any registration of 10t or more / year)	F0: 48 females & 40 males F1: Approx. 480 pups
	OECD 422, Combined Repeated Dose Toxicity Study with the Reproduction/Developmental Toxicity Screening Test (2016)	REACH Annex VIII	F0: 48 females & 40 males F1: Approx. 480 pups
	OECD 414, Prenatal Developmental Toxicity Study in rats (2001)	REACH Annex IX (applicable for any registration of 100t or more / year)	F0: 88 females F1: Approx. 1,056 fetuses

		OECD 414, Prenatal Developmental Toxicity Study in rabbits (2001)	REACH Annex X (applicable for any registration of 1000t or more / year)	F0: 88 females F1: Approx. 792 fetuses
		OECD 443, Extended One-Generation Reproductive Toxicity Study (2012)	REACH Annex X	F0: 100 females & 100 males F1: Approx. 1,200 pups
Agrochemical	US	OPPTS 870.3700, Prenatal Developmental Toxicity Study in rats (1998)	Before registration	F0: 88 females F1: Approx. 1,056 fetuses
		OPPTS 870.3700, Prenatal Developmental Toxicity Study in rabbits (1998)	Before registration	F0: 88 females F1: Approx. 792 fetuses
		OPPTS 870.3800, Reproduction and Fertility Effects (1998)	Before registration	F0: 96 females & 96 males F1: Approx. 1,152 pups F2: approx. 1,152 pups
		OPPTS 870.3550 Reproduction/ Developmental Toxicity Screening Test (2000)	Must be reported	F0: min. 10 females & 10 males F1: min. 96 pups
	EU (Plant protection products, PPP)	EC 545/2011: Prenatal Developmental toxicity study (after OECD TG414)	Before registration	At least 20 females with implantation per group
		EC 545/2011: Multi-generation toxicity study (after OECD TG416, in rat and rabbit ²)	Before registration	F0: 96 females & 96 males F1: Approx. 1,152 pups F2: approx. 1,152 pups

¹ Number of animals estimated in part from Beekhuijzen (Beekhuijzen, 2018). Assumes a litter size of 12 rats/litter, and 9 rabbits. This excludes satellite animals for toxicokinetic studies.

² Animal number is only shown for rats against this row. It could be considered that the numbers for rabbit would reflect those reported in the OPPTS 870.3700

The applicability of DART frameworks to nanotechnologies

One important consideration faced by the nanotoxicology industry was whether existing DART frameworks take into account the novel properties and behaviour of ENM. This is especially relevant, because despite differences in the characteristics and often toxicity of materials on the nanoscale, many ENM share the same chemical identity as their bulk counterparts, making them no different on paper. Since then, the EC have confirmed that Regulation 1271/2008 in relation to the Classification and Labelling of Packaging (CLP) of substances and mixes applies to nanomaterials as substances in their own right, or special forms of the parent substance (EC, 2008). As such, it was not possible to wholly include 'nano' forms of a substance in their 'parent' substance's REACH registration dossier. In October 2018 the European Commission adopted regulation EU 2018/1881 which modified several REACH annexes (I, III, and VI-XII), including those relevant to DART, to assist with fulfilment of testing requirements when using ENM (EC, 2018). No mention of nanomaterials was identified in the agrochemical/Plant Protection Products (PPP) regulatory guidance. However, despite no specific mention, 5-fluorouracil-loaded PLLA-PEG/PEG nanoparticles are mentioned within the EMA's ICH S5 as an example of a compound which qualified for use of alternative assays.

DART and the 3Rs

Over recent years there has been increased demand for and effort put into developing non-animal methods to assess toxicity. This is in line with the principle of the 3Rs – Reduction, Refinement and Replacement of animals in scientific testing, first introduced by Russel & Burch (Russel and Burch, 1959). This initiative has been strongly supported in major regulatory frameworks such as the REACH regulations (Registration, Evaluation, Authorisation and Restriction of Chemicals) and the Globally Harmonised System of Classification Labelling and Packaging of Chemicals (GHS, CLP).

For DART testing, validation of alternative methods is problematic, as *in vitro* or *ex vivo* methods cannot for example address the contribution of the multitude of intra- and inter- cellular signalling pathways, auto- para- and endocrine effects of the hormonal HPG axis, influence of other hormonal systems such as the Hypothalamus-Pituitary-Adrenal (HPA) axis, or indeed the multiple other organs which influence reproduction *in*

vivo. Nor can it form a readily available replacement for mammalian models when considering whether maternal factors may be at play in toxicities. However, efforts to provide useful and relevant alternative testing strategies for ENM in reproductive toxicology are ongoing.

Part of the effort to reduce animal use comes in the form of Integrated Approaches to Testing and Assessment (IATA). IATAs are approaches based on multiple information sources that may be used for hazard identification and characterisation, one form of which is an Integrated Testing Strategy (ITS). Data included within an IATA may be from various sources, i.e. physicochemical properties, *in silico* models, grouping and read-across approaches, *in vitro* methods, *in vivo* tests and human data. Through this process, data generated from non-animal testing methods is expected to contribute to the reduction of animal testing (OECD, 2016). The latest amendments to REACH also make it clear the EC are open to use of non-validated non-animal testing methods, should they be “relevant and reproducible” (ECHA, 2017). The Chapter R7a (human health hazard identification) appendix for nanomaterials also mentions that Adverse Outcome Pathways (AOPs) specific to nanomaterials are under development at the OECD.

Whilst promising, there remain significant barriers in place to making better use of non-animal tests in establishing DART for ENM, including:

- i) Many *in vitro* test methods still require investigation for interference from ENM and associated optimisation,
- ii) The wide array of variations in nanomaterial, and previous lack of standardisation in gathering physico-chemical characterisation and basic toxicity analysis *in vitro* are rate limiters in driving power to Quantitative Structure Activity Relationship (QSAR) modelling *in silico*,
- iii) A lack of accurate and extensive toxicokinetic or Absorption, Distribution, Metabolism and Excretion (ADME) profiles for ENM makes it difficult to build Physiologically-based Pharmacokinetic (PBPK) models *in silico*, to help in predicting hazard for similar ENM.

Whilst the need for formation of integrated approaches to testing and assessment is undeniable, consideration of the barriers in place to achieving this and a work plan that contributes tangibly toward breaking these down must be prioritised in development of nanotoxicological research.

The ability of ENM to cross biological barriers

In order for ENM to have a direct effect on the production of spermatozoa, they must first reach, and second translocate the BTB. The BTB is formed by SC, which are linked by a variety of junction types (gap, tight, basal ectoplasmic specialisations etc), in order to provide a highly controlled environment the process of spermatogenesis within the adluminal compartment of seminiferous tubules of the testis. There is a myriad of considerations to take into account concerning distribution of ENM within the body, including the influence of its physico-chemical characteristics and dynamic biomolecule 'corona' (acquired on entry to the body) to its cross-barrier and cellular uptake, action and ultimately excretion (or accumulation) from any given organ. In relation to the ability of ENM to reach the testis and accumulate therein, evidence to date is mainly from radiolabelling of ENM, measurement of total elemental content in organs, or visualisation of ENM in organ tissues through electron microscopy.

Oberdorster *et al* followed the biodistribution of gold nanoparticles (Au NP) following intravenous injection to the tail vein in rats, observing that the smallest ENM tested (10nm Au) were able to translocate widely within the body including into the reproductive system (Oberdorster *et al.*, 2009). Transport to, and accumulation of ENM in the testis has been demonstrated both short- and long- term exposure to silver and silica ENM via oral and intravenous routes (van der Zande *et al.*, 2012, van der Zande *et al.*, 2014a, Buzulukov *et al.*, 2017, Garcia *et al.*, 2014). Interestingly, both van der Zande & Garcia found through elemental analysis that silver accumulated in the testis and was not excreted, even 4 months after treatment had ceased. This observation is not seen as frequently for ENM passing the blood-brain-barrier (BBB), suggesting that the BTB is less efficient following more prolonged challenge with ENM (Pietrojusti *et al.*, 2013). Evidence has also been presented for silica ENM accessing the testis following both oral and intravenous exposure routes (Morishita *et al.*, 2012, van der Zande *et al.*, 2014a). Morishita *et al* went on to characterise the intratesticular distribution of silica NPs using transmission electron microscopy (TEM) at 24 hours post exposure, identifying ENM within Sertoli cells and spermatocytes, including in the nuclei of spermatozoa (Morishita

et al., 2012). This adds weight to the argument that ENM can pass the BTB without producing noticeable testicular injury (at least in doing so).

How exactly ENM traverse the BTB is still not well understood. It is known that the BTB undergoes considerable restructuring during the process of germ cell translocation from basal to adluminal compartments to facilitate maturation, management of which is complex, involving an array of cellular signal transduction pathways (MAP kinase, TNF- α , TGF- β and others). The main mechanisms by which ENM may traverse the BTB are via passive transport, active transport or endocytosis, and it is thought that similar to the BBB, the BTB uses influx and efflux pumps to regulate the rate at which substances cross (Pietrojusti et al., 2013).

There is some thought that as cytokines produced in response to modulation by FSH and androgens help to modulate the BTB, disturbance of LC in which they are synthesised may be a contributing factor to passage of ENM into the adluminal compartment of seminiferous tubules (Lan and Yang, 2012, Pietrojusti et al., 2013). Recent research into the use of mesoporous silica nanoparticles as vehicles in which to transport and deliver male contraceptive drugs to the adluminal compartment of the testis has also highlighted endocytic vesicle-mediated pathways or GTPase (e.g. Rac1 or Cdc42)-mediated micropinocytosis as potential routes of entry (Chen et al., 2016). Although this area is still not well understood, it is clear that ENM are able to i) translocate to the testis via a variety of exposure routes and ii) cross the BTB, leading in some cases to accumulation.

Nanomaterial-specific evidence for DART

ENM are defined by differences in their physico-chemical characteristics and, and the form taken and their subsequent behaviour within biological systems can vary greatly. Metals and metal oxides are inorganic nanoparticles, examples of which include gold, silver, aluminium, titanium, molybdenum and silica. Recognising their particular importance either in terms of potential health effects, or as solutions to industry, this review focusses on studies relating to silver, titanium, zinc, silica and CNTs which are synthesised using a variety of both 'top down' and 'bottom up' methodologies and are utilised for a myriad of applications.

Silver ENM

Silver ENM (Ag NP) have applications in optics, electronics, textile engineering, water treatment and cosmetic products. In particular its antimicrobial properties have been harnessed for use in wound dressings, antimicrobial coatings on surgical masks and prostheses. A review of the literature returned by far the most literature for any material included, with a total of 27 relevant studies identified. Of these, 7 were conducted *in vitro* using cell lines, 6 *ex vivo* on murine and zebrafish embryos, and 14 *in vivo* on rodents (Table 2). Importantly, all studies reported adverse findings regardless of dose, exposure route, or exposure length.

In vivo, toxicity to the male reproductive organs is consistently reported. Eight studies expose both mice, rats and rabbits to Ag ENM via injection (intravenous, intraperitoneal and intramuscular), and another 6 expose rodents orally, either via food or gavage. The dosing regimens applied varied greatly, from sub-acute low-dose (1mg/kg) applications over 12 days (Garcia et al., 2014), through more standardised 28-day protocols with a range of doses from low to extremely high (1000mg/kg) (Kim et al., 2008) to low dose chronic approaches lasting over 120 days (Castellini et al., 2014). Although effects observed varied in line with the exposure route, characteristics of silver ENM chosen, dose regime and animal used, all studies reported adverse effects following exposure.

One relevant theme that appeared was that of ion dissolution from ENMs and the effects this may have on reported toxicity. Bar-Ilan *et al.* (2009) exposed zebrafish embryos to size-matched silver and gold nanoparticles, finding that Ag produced almost 100% mortality compared to a 3% mortality rate at the same time point post-exposure & highlighting the importance of nanoparticle chemistry in their toxicity (Bar-Ilan et al., 2009). As Au and Ag were both shown to be taken up by the embryos, the authors suggested that Ag toxicity is caused by the physico-chemical attributes of the ENM themselves, or that Ag⁺ ions formed during *in vivo* nanoparticle destabilisation. This hypothesis is corroborated by the findings of Powers *et al.* (2010), who undertook a comparison of the effects of Ag particles and ions on zebrafish embryos, finding that particles were less potent than ions (Powers et al., 2010). Li *et al.* (2010) conducted a similar study in mouse embryos at the blastocyst stage, and found that, as in the

zebrafish studies, embryonic toxicity from Ag particles was lower than from Ag ions (Li et al., 2010).

Research into the effect functionalization of Ag NPs may have on toxicity has also begun. It has been demonstrated that functionalising Ag NPs alters the activity and light responses of zebrafish embryos (Powers et al., 2011). This effect was further highlighted by Lee *et al* (2010), who applied Ag ENM with varied functional characteristics to zebrafish embryos, and reported that both type and dose of Ag ENM altered the type of abnormalities observed in embryos (Lee et al., 2007).

Studies *in vitro* report toxicity to male germ cells and defects in sperm function. Bradyich-Stolle *et al.* (2005) examined the suitability of a mouse spermatogonial stem cell line (C18-4) as a model to assess cytotoxicity, via the LDH and MTT assay using silver, molybdenum trioxide (MoO₃), and aluminium (Al) nanoparticles (Braydich-Stolle et al., 2005). They identified a concentration-dependent toxicity for all types of particles tested, with a toxicity ranking of Ag > Al > MoO₃. Similarly, Asare *et al* (2012) investigated toxicity of 20nm and 200nm Ag ENM to the human NT2 pluripotent testicular embryonic carcinoma cell line, identifying loss of cellular viability via the MTT assay, and DNA damage (assessed via Comet assay) (Asare et al., 2012). Although the outcomes of these studies suggest that these cell lines may be valuable models by which to assess the cytotoxicity of nanoparticles in the germ line *in vitro*, it must be noted that evidence that ENM interfere with the MTT has now emerged (Kroll et al., 2012). Consideration of ENM interference with toxicity assays is therefore important and will be considered in later chapters.

Other cell lines investigated include murine embryonic stem cells and fibroblasts, for which differential toxicity depending on whether Ag ENM were coated or not was reported (similarly to the findings of Braydich-Stolle et al, above) (Ahamed et al., 2008). Zhang et al (2015) also reported use of the complementary murine cell lines TM3 (Leydig) and TM4 (Sertoli), reporting that exposure of TM3 & TM4 cells to Ag ENM resulted in interference with cellular signalling pathways, as well as those related to and tight junction formation in the BTB (TM4), and testosterone synthesis (TM3), highlighting the potential for endocrine-disruption as a mechanism of action (Zhang et al., 2015a).

Table 2: *In vivo* and *in vitro* reproductive and developmental toxicity studies of Silver (Ag) ENP, outlining key parameters from each study identified, including study type, exposure type and method, and relevant findings

Study	ENM	Animal/Cell/(n)	Study Type	<i>in vivo</i> / <i>in vitro</i> ?		Exposure	Method	Outcomes
(Braydich-Stolle et al., 2005)	Ag NP 15nm, MoO ₃ NP 30nm, Al NP 30nm	Male mouse C18-4 cell line (established from type A spermatogonia isolated from 6-day old mouse testes)	Target organ toxicity		<i>in vitro</i>	Incubation	Cells exposed at 5,10,25,50,100mg/ml	Concentration. dependent toxicity for all types of NP tested, whereas comparative salts had no significant effect (CdCl ₂ , AlCl ₃ etc). Ag most toxic, MoO ₃ least toxic. Cell line a valid model for cytotoxicity of NP in germline cells <i>in vivo</i> .
(Asare et al., 2012)	Ag NP 20nm & 200nm	Male 8-oxoguanine DNA glycolyase knockout mice (Ogg1-/- KO), and Human NT2 pluripotent testicular embryonic carcinoma cell line (which mimics the repair status of human testicular cells vs oxidative damage and authors claim is thus a suitable model for human male reproductive toxicity studies)	Target organ toxicity		<i>in vitro</i>	Incubation	Cells exposed to NPs @ 10/50/100ug/ml for 24/48/72h	Ag NP and UF more cytotoxic and cytostatic than TiO ₂ , causing apoptosis, necrosis and decreased proliferation in concentration and time dependent manner. 200nm Ag NPs cause concentration-dep increase in DNA strand breaks in NT2 cells. ROS formation leading to oxidative purine DNA base damage (comet) not found to be a significant MoA
(Ahamed et al., 2008)	Ag NPs (size not stated)	murine mammalian cells, embryonic stem cells and embryonic fibroblasts	Target organ toxicity		<i>in vitro</i>	Incubation	Ag NPs added to culture media containing cells and incubated. Cells were harvested at 4, 24, 48, and 72 h after Ag NP treatment	Uncoated Ag NPs agglomerate and may be excluded from some organelles such as the nucleus and mitochondria while the coated Ag NPs do not agglomerate and are distributed throughout the cell. Both types of Ag NP stimulated apoptosis via up-regulation of cell cycle checkpoint protein p53, DNA damage repair proteins Rad51 and phosphorylated-H2AX expression. Surface chemistry of Ag NP induce different DNA damage responses, i.e., coated Ag NP induced more severe damage versus uncoated Ag NP.
(Yoisingnern et al., 2015)	Ag NPs av. diameter 40nm	BDF1 mice (8-12 weeks) / sperm	Target organ toxicity		<i>in vitro</i>	Incubation	dose of 0, 0.1, 1, 10, and 50µg/mL for 3h.	Found internalisation of Ag NPs in spermatozoa, with even distribution inc. within mitochondrial area, in a dose dependent fashion. Flow cytometry showed negative effect on sperm viability although authors could not deduce whether this was a particle or ion effect. Morphological analysis of spermatozoa showed Ag NPs significantly increased sperm abnormalities, including coiled tails, roll tail, and bent tails, in a dose-dependent manner. Acrosome reaction was also decreased significantly in Ag NP exposed sperm, something which is required for sperm capacitation pre-fertilization of oocyte. Authors also looked at IVF and ICSI and found negative effects associated with Ag NP exposure.

(Zhang et al., 2015a)	Ag NPs 10/20nm	Balb/c mice, 21 day old / TM3 TM4 and Spermatogonial Stem Cells (SSC)	Target organ toxicity	<i>in vitro</i>	Incubation		Time/dose dep effect of TM3/4 proliferation, membrane damage and ROS generation. 10nm worse than 20. Via PCR/WB saw in TM3 and TM4 cells Ag NPs activated the p53, p38, and pErk1/2 signalling pathways and significantly downregulated the expression of genes related to testosterone synthesis (TM3) and tight junctions (TM4). Furthermore, the exposure of TM3 and TM4 cells to Ag NPs inhibited proliferation and self-renewal of SSCs.
(Moretti et al., 2013)	Au and Ag NPs	human sperm	Target organ toxicity	<i>in vitro</i>	Incubation	Semen samples from 10 donors exposed to 30/60/122/250 and 500uM of Au and Ag NPs for 60 and 120 mins.	Examination for motility and viability showed dose dependent effect, with sig at 125+uM. Ag NPs seemed to be more potent tox than Au. Au NPs were localised within sperm, although Ag not detectable (maybe because they'd become ions?). However, toxicity not seen until higher levels of exposure (250-500uM) which are not usually easy to achieve <i>in vivo</i> .
(Lee et al., 2007)	Ag NP 5–46 nm	Zebrafish Embryos	Developmental	<i>ex vivo</i>	Incubation	Ag nanoparticle solutions (ranging from 0.04, to 0.71 nM) incubated chronically with cleavage-stage (8-cell) embryos in egg water for 120 hpf.	single Ag nanoparticles were transported into and out of embryos through chorion pore canals (CPCs). NPs trapped inside CPCs and the inner mass of the embryos, showing restricted diffusion. Toxicity and biocompatibility of Ag NPs and the types of abnormalities observed in zebrafish are highly dependent on the dose of Ag nanoparticles, with a critical concentration of 0.19 nM.
(Li et al., 2010)	Ag NPs 5-25nm & Ag+ ions	Mouse embryos @ blastocyst stage	Developmental	<i>ex vivo</i>	Incubation	Blastocysts treated with 50 microM Ag NP or Ag ions	<i>In vitro</i> exposure induces apoptosis and retards early post-implantation development after transfer to host mice. However, Ag NP embryonic cytotoxicity appeared lower than that induced by the Ag+ ion. The results collectively show that Ag NP has the potential to induce embryo cytotoxicity.
(Powers et al., 2011)	Ag NPs, Ag+ ions, 10nm citrate-coated Ag NP (Ag NP-C), and 10 or 50nm polyvinylpyrrolidone-coated Ag NPs (Ag NP-PVP).	Zebrafish Embryos	Developmental	<i>ex vivo</i>	Incubation	exposed developing zebrafish to Ag(+) or Ag NPs on days 0-5 post-fertilization, Ag NPs of different sizes and coatings: 10nm citrate-coated Ag NP (Ag NP-C), and 10 or 50nm polyvinylpyrrolidone-coated Ag NPs (Ag NP-PVP).	Ag NPs are less potent than Ag(+) with respect to dysmorphology and loss of viability, but nevertheless produce neurobehavioral effects that highly depend on particle coating and size, rather than just reflecting the release of Ag(+). Different Ag NP formulations are likely to produce distinct patterns of developmental neurotoxicity.
(Powers et al., 2010)	Ag(+) ranging from 10nM to 100microM	Zebrafish Embryos	Developmental	<i>ex vivo</i>	Incubation	Zebrafish from 0 to 5days post-fertilization to concentrations of Ag(+) ranging from 10nM to 100microM	Ag+ found to be a developmental toxicant. At low concentrations, Ag(+) acts as a neurobehavioral toxicant even in the absence of dysmorphology. Early behavioural impairment observed is predictive of subsequent decreases in survival.

(Bar-Ilan et al., 2009)	Ag / Au NPs (3, 10, 50, and 100 nm)	Zebrafish Embryos	Developmental	<i>ex vivo</i>	Incubation	Exposure to various sizes at a concentration of 100 or 250 µM, from 4 to 120 hours post fertilisation (hpf)	Ag NP produced almost 100% mortality at 120 hpf, while Au nanoparticles produced less than 3% mortality at the same time point. Au NP induced minimal sub-lethal toxic effects, but Ag NPs generate a variety of embryonic morphological malformations. Both Ag and Au were shown to be taken up by the embryos, suggesting that Ag toxicity is caused by the nanoparticles themselves or Ag ions that are formed.
(Taylor et al., 2014)	ligand-free Au and Ag NPs	Murine Blastomeres/Embryos	Developmental	<i>ex vivo</i>	injection	Embryo culture to the blastocyst stage was assessed.	Rate of development did not differ, and PCR for BAX, BCL2L2, TP53, OCT4, NANOG, DNMT3A showed comparable expression. Exposure of blastomeres to Ag+ ions in place of NPs caused immediate development arrest.
(Thakur et al., 2014)	Ag NPs	10-12-week-old Wistar rats (16)		<i>in vivo</i>	oral gavage		Found disorganisation of STs, germinal epithelium, loss spermatogenic cells (esp. spermatocytes and spermatids) and exfoliation of FCs to lumen. Atrophy of tubular lumen, with loss of epithelium and SCO were present. V few mature sperm seen. TEM showed damage to tubular basement membrane, and apoptotic GCs, with separation from basal laminae. TEM for sertoli cells showed dissociation of nuclei from basal portion, vacuoles in cytoplasm. NPs containing lysosomal bodies were seen in SC cytoplasm. Spermatogonia, round spermatids and elongating plus mature spermatids were all affected.
(Zhang et al., 2015b)	Ag NPs	Inst of Cancer Res neonatal mice 8 days old (PND8)	Target organ toxicity	<i>in vivo</i>	Abdominal sub-cut injection	injection of 5 doses over 13 days (PND 8 to 21).	Analysis showed Ag NPs were 10-40nm in size. LDH assay showed proportional association between dose and cell death in TM3/4 cells. Increased rate of abnormal sperm recorded, alongside sig reduction in testis weight per body weight and diameter of convoluted tubules at PND 28 and 42. PCR results showed drop in Cpy19a1 expression at PND 28/42 which recovered by PND 60. Cyp11a1 was upregulated in Ag NP treated. AMH was sig reduced in PND28 but recovered by PND42/60, indicating possible implications for development
(Sleiman et al., 2013)	Ag NP 60nm diameter	male Wistar rats (30)	Target organ toxicity	<i>in vivo</i>	gavage	Rats exposed at PND23-53 50 to 15ug/kg bw. by oral gavage and sacrificed at PND53 or 90	Ag NP exposure delayed puberty onset in both treated groups compared to control. High dose treatment produced reduction in total and daily sperm production at PND53, seen in both groups at PND90. Morphometric analysis showed disorganisation of seminiferous epithelium, sloughing of GCs and debris in lumen. No sig difference in epithelial height or lumen/tubule diameters recorded. No change in serum testosterone or oestradiol concentrations from control at PND53 or 90.
(Castellini et al., 2014)	Ag NPs (45 nm)	Rabbits	Target organ toxicity	<i>in vivo</i>	IV injection	Injection of 0.6 mg/kg bw. Looked at sperm quality of rabbits throughout a 126-day study	Reported sperm cells with a lower percent of motility, vigour and oxygen consumption and acrosome and mitochondrial damage. Ag NPs identified in spermatids and ejaculated sperm; however, no morphological effect seen nor was libido, serum testosterone, sperm concentration or semen volume altered

(Gromadzka-Ostrowska et al., 2012)	Ag NP (20 nm);	rats	Target organ toxicity	<i>in vivo</i>	IV injection	exposure to 5 mg/kg bw/day Ag NP (20 nm);	reported decreased sperm and germ count and DNA damage in germ cells
(Rezazadeh-Reyhani et al., 2015)	Ag NPs (50-60nm).	albino mice 10-12 weeks (24)	Target organ toxicity	<i>in vivo</i>	IP injection	exposed intraperitoneally to 0.5, 1 and 5mg/kg daily for 25 days	Histology showed alterations in tubular diameter and spermiogenesis index between control and treated. Ag NPs resulted in reduction of LCs in interstitium, and increased number of hypertrophied LCs. Testosterone LH and FSH assay showed dose dependent decrease in all three hormones. IHC for Hsp70-2 undertaken, as well as PCR. IHC showed increase in Hsp-70 expression at low dose, then dig decrease in med/high dose, which was confirmed by PCR. Sperm count, motility, chromatin condensation and DNA damage were assessed – decreases in count, motility, chromatin and loss in DNA integrity seen.
(Ahmed et al., 2017)	Ag NPs	adult albino rats (60)	Target organ toxicity	<i>in vivo</i>	IP injection	Effect after 7 or 28 days at L or H doses (100/1000mg/kg/day).	7day low group testes showed congested blood vessels covering tunica albuginea. Some tubules with disorganized separated germinal epithelium from their basement membranes. 28day low group had thickened connective tissue, capsule studded with Ag NPs & congested sub-capsular blood vessels. Decrease in the thickness of germinal epithelium lining some tubules, others with exfoliated germ cells & vacuolated cytoplasm. Sig decrease in Testosterone seen within Ag NP treated groups. There was downregulation of Dazl, Tnp2 and GDNF in Ag NPs received rats of groups II and III. Decrease in Ki-67 IHC as marker of cell proliferation. Increase in CD68 by IHC as compensatory mechanism by release of testicular macrophages. TEM showed vacuolisation of SC and LC.
(Garcia et al., 2014)	Ag NPs 10nm	CD1 mice	Target organ toxicity	<i>in vivo</i>	iv injection	injected 1mg/kg 10nm Ag NPs into CD1 mice for 12 days, and sacrificed at 15/60/120 days post exposure	Ag still detectable in testis at 120d post exposure. Treatment resulted in no changes in body and testis weights, sperm concentration and motility, fertility indices, or follicle-stimulating hormone and luteinizing hormone serum concentrations; however, serum and intratesticular testosterone concentrations were significantly increased 15 days after initial treatment. Histologic evaluation revealed significant changes in epithelium morphology, germ cell apoptosis, and Leydig cell size. Additionally, gene expression analysis revealed Cyp11a1 and Hsd3b1 mRNA significantly upregulated in treated animals.
(Fathi et al., 2018)	Ag NPs	200-250g adult Wistar rats (28)	Target organ toxicity	<i>in vivo</i>	IP injection	Single injection of 30/125/300mg/kg. 28 days after injection, 25 tubules from each animal were examined for histological changes.	Histomorphometry showed significant reduction in number of spermatogonia, sertoli and Leydig cells in M/H dose groups. No comment on morphology.

(Park et al., 2010)	Ag NPs. small (22/42/71) and large (323nm)	Mice	Target organ toxicity	<i>in vivo</i>	oral	Dosed at 1mg/kg of small (22/42/71) and large (323nm)	Saw testicular (and other multiple organ) presence of small but not large NPs. TGF- β (cytokine) and B cell (lymphocyte) distribution were increased in small exposed but not large exposed animals. Also looked at 28day rep dose of 42nm Ag NPs at 0.25/0.5/1mg/kg. Cytokine assay showed increases in IL-1/6/4/10/12 and TGF-B in a dose dep manner. B cell distribution and lymphocyte IgE production also increased.
(Miresmaeili et al., 2013)	Ag NPs	Wistar rats (32)	Target organ toxicity	<i>in vivo</i>	oral	dosing was 25/50/100/200mg/kg. every 12 hours over one cycle of spermatogenesis (48days)	Acrosome reaction evaluated by triple stain showed significant difference between control and exp group. Reduction in spermatogonia cells in highest dose group. 50-200 groups all showed significant reduction in number of primary spermatocytes and spermatids and spermatozoa. No significant effect on SC number.
(Layali et al., 2016)	Ag NPs	male Syrian rats (24)	Target organ toxicity	<i>in vivo</i>	oral	orally administered Ag NPs at concentrations of 0.07/0.14 and 0.28ug daily for 5 weeks.	Sperm count and motility significantly declined, especially in M/H dose groups. Malondialdehyde concentration in the seminal fluid of rats was significantly raised in M/ which they report indicates increased lipid peroxidation.
(Kim et al., 2008)	Ag NPs	Sprague Dawley Rats	Biodistribution	<i>in vivo</i>	oral	Twenty-eight-day oral toxicity, genotoxicity, and gender- related tissue distribution of silver nanoparticles	reported high distribution of Ag NPs to the testis
(Mathias et al., 2015)	Ag NPs	Wistar rats (30)	Target organ toxicity	<i>in vivo</i>	oral	Oral exposure with 15/30ug/kg/day 60nm Ag NPs from PND 12 to PND58, with sacrifice at PND102.	Onset of puberty was delayed in Ag NP treated animals. Interestingly, partner preference was altered in 15ug dosed animals – swing toward male partner seen in sexual partner preference testing. Acrosomal integrity (sperm function) decreased in a dose dependent manner. Sperm Plasma membrane integrity measured by eosin-y and nigrosin stain also showed decrease with increasing dose. Number of sperm abnormalities increased with Ag NP exposure. No change on serum hormone levels (testosterone, LH, FSH and oestradiol).

Titanium Dioxide ENM

Titanium dioxide (TiO₂) NPs are amongst the most commonly used metal oxide NPs. They tend to be available in either crystalline rutile or pure crystalline form, or as mixtures of crystalline anatase and rutile forms. They are best known as a component in sunscreens, pigments and paints. However, TiO₂ NP also have applications as drug delivery vehicles, photocatalysts, and in electronic data storage. Eighteen studies examining DART of TiO₂ NP were identified and are outlined within Table 3. Of these, 3 examine *in vitro* techniques involving cell lines (mouse TM3 Leydig cells, and human NT2 testicular embryonic carcinoma cells) or direct application to sperm, and five examine *in vivo* toxicity studies following exposure via inhalation (3), oral (8) or injection (4).

Both the *in vitro* and *in vivo* studies report varied outcomes following TiO₂ NP exposure, with some finding dose dependent toxicity and others reporting transient or no effects (Smith et al., 2015). *In vivo*, a number of findings were reported, including detection of reactive oxygen species (ROS) and oxidative stress (imbalance between oxidants and antioxidants in favour of oxidant presence), morphological markers of altered spermatogenesis within the testis, and changes to circulating hormone levels, implicating both potential for either direct damage to the organ by TiO₂ NP, or indirect effects via endocrine disruption. *In vitro*, It is interesting to note that the comparative study to examine the potential for TiO₂ NP, diesel exhaust particles and ultrafine carbon black to impair the male mouse reproductive system undertaken by Komatsu *et al.* (2008) identified TiO₂ as being more cytotoxic to TM3 Leydig cells than the other carbon based particles examined (Komatsu et al., 2008). Conversely, the comparative study undertaken by Asare *et al* (2012), found TiO₂ NP to be less toxic than Ag NPs or TiO₂ in its ultrafine form to male human NT2 testicular embryonic carcinoma cells (Asare et al., 2012).

This variation in outcome did not appear to be linked to exposure route, dose regimen, ENM size (where identifiable) or animal type as all reported a range of outcomes. Based on this it is possible that the variation in results could very well be linked to physical form, especially in the case of TiO₂ NP for which differences in toxicity dependent on crystalline form and pH of the exposure environment have been previously demonstrated (De Matteis et al., 2016). This highlights further the importance of

understanding ENM characteristics well in establishing their toxicity, and the need for standardised reference materials in toxicity testing.

Table 3: *In vivo* and *in vitro* reproductive and developmental toxicity studies of titanium dioxide (TiO₂) ENP, outlining key parameters from each study identified, including study type, exposure type and method, and relevant findings

Paper	ENM	Animal/Cell	Study Type	<i>In vitro</i> / <i>In vivo</i>	Exposure	Method	Outcomes
(Komatsu et al., 2008)	25–70 nm TiO ₂	Mouse Leydig TM3 Cells	Fertility (mech)	<i>in vitro</i>	Incubation	Cells exposed to different concentrations of the NP for 48h.	TiO ₂ taken up into cells. Dose dependent decrease in cell viability. TiO ₂ more toxic than the other NPs tested. TM3 cell proliferation suppressed by TiO ₂ .
(Asare et al., 2012)	21nm TiO ₂	Male 8-oxoguanine DNA glycosylase knockout mice (<i>Ogg1</i> ^{-/-} KO), and Human NT2 pluripotent testicular embryonic carcinoma cell line	Fertility (mech)	<i>in vitro</i>	Incubation	Cells exposed @ 10/50/100ug/ml for 24/48/72h	Ag NP and UF more cytotoxic and cytostatic than TiO ₂ , causing apoptosis, necrosis and decreased proliferation in concentration and time dependent manner. 200nm AgNPs cause concn. dependent increase in DNA strand breaks in NT2 cells. ROS formation leading to oxidative purine DNA base damage (comet) not found to be a significant MoA
(Pawar and Kaul, 2012)	TiO ₂ NP	buffalo sperm	Target organ toxicity	<i>in vitro</i>	incubation	1/10/100ug/ml concentrations (<100nm).	Significant decrease in cell viability and membrane after 6h incubation with NPs. Significant increase in sperm capacitation observed for TiO ₂ NP albeit at lower concentrations. In DNA fragmentation assay, dose-dependent increase in DNA fragmentation observed. Ultrathin cross-sections revealed TiO ₂ NPs inside head and plasma membrane of the buffalo spermatozoa as assessed by TEM.
(Jackson et al., 2011)	17nm TiO ₂	Mouse C57/6BomTac	Developmental	<i>in vivo</i>	Pulmonary	Pulmonary exposure during gestation days 8-18. Measurements taken 5 and 26d post exposure (maternal), and PND 2 and 22 (offspring)	No DNA strand breaks in mated mice or offspring. Changes in gene expression relating to retinoic acid in F offspring, but no effect on M offspring. Changes may be secondary response to maternal inflammation, but this is only a hypothesis.
(Boisen et al., 2012)	~100nm TiO ₂	Pregnant C57BL/6 mice	Fertility - F1	<i>in vivo</i>	inhalation	Pregnant C57BL/6 mice were exposed by whole-body inhalation to the nanoTiO ₂ UV-Titan L181 (~42.4 mg UV-Titan/m ³) or filtered clean air on gestation days (GD) 8-18. Female C57BL/6 F1 offspring raised to maturity and mated with unexposed CBA males. F2 descendants were collected and ESTR germline mutation rates estimated from full pedigrees (mother, father, offspring) of F1 female mice (192 UV-Titan-exposed F2 offspring and 164 F2 controls).	No evidence for increased ESTR mutation rates in F1 females exposed in utero to UV-Titan nanoparticles from GD8-18 relative to control females

(Yamashita et al., 2011)	Si NP 70 nm (nSP70), 300 nm (nSP300) and 1,000 nm (mSP1000), TiO ₂ & fullerene NP 65, 322, 1,140, 217 and 143 nm	Pregnant mice	Fertility	<i>in vivo</i>	Injection	To determine distribution, injection at GD16 and fluorescent examination 24h afterwards. To determine fetotoxicity, injection (100 µl, 0.8 mg per mouse) into pregnant mice at GD16 and GD17	SiNPs with <100 nm and nano-TiO ₂ 35 nm induce resorption of embryos and foetal growth restriction. Maternal body weight ↓ SP70 & TiO ₂ , but SP300, SP1000 and fullerenes did not show any changes. Modifying the surface of nSPs from –OH to –COOH or –NH ₂ functional groups can prevent these complications.
(Hougaard et al., 2010)	~21nm TiO ₂	Mouse C57/6BomTac	Developmental	<i>in vivo</i>	Pulmonary	Pulmonary exposure during gestation days 8-18	Long term lung inflammation seen in adult female mice. Negligible Ti in milk. Gestationally exposed offspring had moderate neurobehavioural alterations
(Tassinari et al., 2013)	TiO ₂ NPs	Sprague-Dawley rats (42)	Target organ toxicity	<i>in vivo</i>	oral	0,1,2 mg/kg dose. Measured tubular diameter and relative area of seminiferous tubules. Also looked at sex steroid and thyroid hormone serum levels., as well as tissue distribution.	Saw significant increase in testosterone levels at highest dose, but no histomorphological effect on testis.
(Orazizadeh et al., 2014)	TiO ₂ NP	NMRI mice (32)	Target organ toxicity	<i>in vivo</i>	oral	300mg/kg Ti TiO ₂ O2 for 35 days, and beta carotene (BC) treatment for 10 days before addition of TiO ₂ . 300mg/kg in 30g mouse = 0.1mg per mouse, equivalent to 19.5g in 65kg human.	Saw significantly lowered T levels in TiO ₂ treated, which seemed to be reversed somewhat in the BC group. Sperm number, motility and normality reduced in TiO ₂ only, but sig increased by comparison to this in BC+T. Histology showed sloughing, detachment of basement membrane and vacuoles in T group, T+B group had vacuoles and sloughing but much less. Johnsen's score for spermatogenesis gave much reduced score in T and T+B but not as much. Suggested beneficial effects on sertoli cell function due to loss of sloughing of GCs and vacuoles...also poss. due to restoration of Testosterone production...or antioxidative effect.
(Meena et al., 2015)	21nm TiO ₂	8wk old Wistar rats	Target organ toxicity	<i>in vivo</i>	IV injection	5/25/50 mg/kg weekly for 30 days	Oxidative stress markers SOD (reduced), Catalase (increased), GPx (decreased), lipid peroxidase (increased) following exposure, all dose dependently. Creatine kinase levels as markers of sperm maturity, dose dep elevated level seen with TiO ₂ is associated with an increased rate of functional abnormalities and increased cytoplasmic retention. Caspase-3 as marker of apoptosis – increased with dose, alongside decrease in total sperm count. Testosterone levels by ELISA were decreased with TiO ₂ – sig at M/H doses, DNA damage by comet and DNA fragmentation assay showed fragmentation at M/H doses. Only changes histology seen at highest dose – cellular inflammation. TiO ₂ NPs were seen in testis although description is not clear.

(Khorsandi et al., 2017)	TiO ₂	NMRI mice (32)	Target organ toxicity	<i>in vivo</i>	oral	75mg/kg Q or 300mg/kg TiO ₂ for 42 days, or 75mg/kg Quercetin for 7 days then add 300TiO ₂ for 35 days. Looked at potential benefits of quercetin (flavonoid polyphenol found in red onions and many other fruit/veg)	Claimed that TiO ₂ showed decreased T and sperm quality, along with vacuolisation, sloughing and detachment from B membrane. Lipid Peroxidase levels increased, and SOD/CAT levels decreased indicating oxidative stress. Authors claim Quercetin supplementation improved all of these parameters.
(Takeda et al., 2009)	TiO ₂ NP 25-70nm	pregnant ICR mouse dams	Target organ toxicity	<i>in vivo</i>	oral	Dams dosed with 100ul 1mg/ml TiO ₂ NP 25-70nm at 3,7,10 and 14 days post coitum	Aggregates of TiO ₂ NPs found in both LCs, SCs and spermatids at 4 days and 6 weeks of age. Morphology in TiO ₂ exposed mice showed focal disruption, with disorganised tubules, less mature sperm in lumens at spermiation. Also, SC count showed reduced numbers in treated. This effect was dose dependent.
(Smith et al., 2015)	TiO ₂ NP (anatase)	adult male mice	Target organ toxicity	<i>in vivo</i>	IP injection	2.5 or 5 mg/kg IP injection to adult male for 3 days followed by sacrifice 1/2/3/5 weeks or 24/48/230h later.	NPs found in scrotal adipose tissue 120h post injection. At 120 h and up to 3 weeks post injection, testicular histology revealed enlarged interstitial spaces. Numbers of apoptotic cells increased sig in all treated animals. Short term epididymal sperm abnormalities increased (not long term). Suggests transient effect – 4-8 days post injection effects were seen, 10 days -5 weeks post injection no effects detectable.
(Jia et al., 2014)	TiO ₂ NPs 25nm	60 Kunming mice (3weeks old).	Target organ toxicity	<i>in vivo</i>	oral	10/50/250mg/kg for 42 days from PND28-70	Abnormalities in epididymis sperm was much higher in exposed animals, loss of GC layer (high dose) and vacuoles (all dose) in seminiferous tubules seen, and significant decrease =in serum T levels. Also saw decrease in expression of 17b-HSD and P450 17a-HSD, with increase of CytP450-19 (key for translation of T to Oestradiol) was increased. Nano-TiO ₂ exposure does not alter the mRNA levels of P450scc, 3β-HSD and AR
Hong et al (2015) (Hong et al., 2015)	TiO ₂ NP	ICR mice (40) 5 weeks old	Target organ toxicity	<i>in vivo</i>	oral	2.5/5/10mg/kg bw	Exposure resulted in lesions of testis and epididymis, deductions in sperm concentration and sperm motility, and an increase of the number of abnormal sperm in mice. Lowered seminiferous tubule epithelium layer and degeneration, reductions of Leydig cells and mature sperm within the lumen, immature sperm, sperm breakages, acrosome fusion and/or pyknosis, and spermatolysis, cell pyknosis, necrosis and abscission, severe disorganization of tissue, and spano-sperm within the lumen. Caused major enzyme changes, and Ox stress marker changes. O ₂ •-, H ₂ O ₂ , MDA, and PC levels were significantly elevated with increasing TiO ₂ dose. Marked increase in testicular 8-OHdG level was observed, indicating that excessive ROS production led to DNA damage in the testis due to TiO ₂ NP-induced toxicity.

Silica ENM

Silica, the common name for materials composed of silicon dioxide (SiO_2), occurs in both crystalline and amorphous forms. Silica nanoparticles (Si NP) are currently being produced on an industrial scale as additives to cosmetics, drugs, printer toners, varnishes, and food (Napierska et al., 2010). Of the literature examined, eleven studies on Si NP were identified, of which 9 were *in vivo* and 2 *in vitro* (Table 4). Of the studies *in vitro*, one was via direct application of Si ENM to boar sperm which showed no direct effect of Si ENM on sperm function (Barkalina et al., 2014), and the other a murine embryonic stem cell test which reported concentration dependent inhibition of stem cell differentiation, but only following exposure to the smallest of 4 particle sizes tested (Park et al., 2009). Interestingly, no studies on male germ cell lines were identified.

The *in vivo* work of Yamashita *et al* (2011), who undertook a comparative study of adverse outcomes arising from prenatal exposure to Si, TiO_2 and fullerene NPs via acute intravenous injection is noteworthy (Yamashita et al., 2011). They showed that Si NPs <100nm and TiO_2 NPs <35nm induced resorption of embryos and foetal growth inhibition, but larger versions of the NPs and fullerenes did not induce any changes. In addition, they note the importance of functionalization of ENM to their toxicity, showing that surface modification with carboxyl groups could prevent the adverse outcomes described. In addition, Bara *et al* (2018) reported comparatively lower toxicity of mesoporous silica nanoparticles (MSN) to zinc oxide ENM to Swiss albino mice dams and pups following oral exposure during gestation (2 doses over gestational days 15-19). Interestingly, the group identified a decrease of testosterone levels in male pups compared to control at high but not low doses of MSN. They also examined steroidogenesis in pups post-puberty, and found changes in expression of key proteins, enzymes and receptors involved compared to control (Bara et al., 2018).

Table 4: *In vivo* and *in vitro* reproductive and developmental toxicity studies of Silica ENP (Si), outlining key parameters from each study identified, including study type, exposure type and method and relevant findings described within the paper.

Paper	ENM	Animal/Cell	Study Type	<i>In vitro</i> / <i>In vivo</i>	Exposure	Method	Outcomes
(Park et al., 2009)	Si NP 10,30,80 & 400nm	Embryonic stem cell test	Developmental	<i>in vitro</i>	Incubation	Mouse embryonic stem cells were exposed to silica nanoparticles at concentrations ranging from 1 to 100 microg/ml.	Concentration dependent inhibition of differentiation of stem cells into contracting cardiomyocytes by two Si NP of the two smaller primary sizes, while the two larger sizes had no effect up to the highest concentration tested.
(Barkalina et al., 2014)	mesoporous silica NPs:138, 270 & 280nm in size	boar sperm	Target organ toxicity	<i>in vitro</i>			Found no negative effect from MSNPs with hexagonal pore symmetry, functionalised with polyethyleneimine and amino- propyltriethoxysilane, on sperm function including motility, viability, acrosomal status and DNA fragmentation index.
(Kim et al., 2006)	magnetic SiO ₂ NPs 50nm thickness	mice	Target organ toxicity	<i>in vivo</i>	IP injection	Medical focus. IP admin to mice, for 4 weeks, 25,100,200mg/kg.	MNPs were found in testis (and brain through BBB). However, no histopathological findings were made.
(Chen et al., 2003)	NaCl modified Si NPs	Male Kunming white mice	Fertility	<i>in vivo</i>	Injection	injection to abdominal cavity or tail vein, concentrations 0-225mg/kg/bw. Sacrifice +96h	Si NP deposition identified in testes, glands and interstitial cells
(Kim et al., 2006)	Si NP 50nm	Male IRC Mice	Fertility	<i>in vivo</i>	Injection	intraperitoneal injection, 10,25,50,100mg/kg, 4 wks, sacrifice @ designated times	Small amount of Si NP found in testicle, gland and interstitial cells, no pathological changes in testes. No acute tox or mortality @ high concentrations. No apparent abnormalities in subsequent generations
(Yamashita et al., 2011)	Si NP 70 nm (nSP70), 300 nm (nSP300) and 1,000 nm (mSP1000), TiO ₂ & fullerene NP 65, 322, 1,140, 217 and 143 nm	Pregnant mice	Fertility - F1	<i>in vivo</i>	Injection	To determine distribution, injection at GD16 and fluorescent examination 24h afterwards. To determine fetotoxicity, injection (100 µl, 0.8 mg per mouse) into pregnant mice at GD16 and GD17	Si NPs with <100 nm and nano-TiO ₂ 35 nm induce resorption of embryos and foetal growth restriction. Maternal body weight ↓ SP70 & TiO ₂ , but SP300, SP1000 and fullerenes did not show any changes. Modifying the surface of Si NPs from -OH to -COOH or -NH ₂ functional groups can prevent these complications.
(Durnev et al., 2010)	Si NP 2-5nm	male F1(CBAx57Bl/6) mice or to outbred albino rats	Fertility (mech)	<i>in vivo</i>	Injection	1-5-µ granules in water suspension injected on days 1, 7, and 14 of gestation	A 24-h exposure in a dose of 5 mg/kg increased DNA damage in bone marrow cells. Si NPs ↓body weight gain in pregnant rats and new-born rats at different stages of the experiment but had no effect on other parameters of physical development of rat progeny and caused no teratogenic effects.

(Morishita et al., 2012)	Amorphous silica particles (nSP70, 70-nm diameter; nSP300, 300-nm diameter).	Balb/c mice testis	Target organ toxicity	<i>in vivo</i>	iv injection tail	injected intravenously through the tail vein with 100 IL (0.8 mg) of nSP70 or nSP300 on two consecutive days then TEM used to examine distribution qualitatively.	70nm but not 300nm Si were able to enter nuclei of spermatocytes (through BTB). This matched previous findings that 70nm Si can pass through blood-placenta barrier. For histology Mice were given 4 doses of 100 IL (0.4 or 0.8 mg) nSP70 or saline (control), IV through the tail vein every other day. Testes were collected 48 h or 1 week after the last administration. Found no histological changes. Did not examine hormone levels.
(Ren et al., 2016)	Si NPs diameter 57.66nm	C57 male mice	Target organ toxicity	<i>in vivo</i>	tracheal perfusion	2mg/kg every 3 days for 45 days (so 15x). Some sacrifice at 45days others at 75 days post first dose.	At d45, GC layer was thin, with vacuolisation and exfoliated cells in focal points. Claim Si NPs were visible in spermatogenic cells (I can't see from their images). Sperm motility and normality in the epididymis was decreased in Si NP treated comp to control at d45. These effects appeared to be reversible, with d75 testes and epididymis having normal morphology and sperm content. As with the histological findings, TUNEL apoptosis assay showed more apoptotic spermatocytes and spermatoblasts at d45 treated, but no change from normal at d75. Ox stress testing at d45 showed decreased SOD, but increased MDA and 3-NT. Day 75 SOD and 3-NT were no different to control but MDA was higher. Authors suggest possible mechanism for Si-NP induced apoptosis.
(Bara et al., 2018)	mesoporous silica NPs (no size given)	Swiss albino mice. 28F and 10M	Target organ toxicity	<i>in vivo</i>	oral	Exposed to ZnO NP 50/100mg/kg or bulk ZnO 100mg/kg, or MSN 50/250mg/kg. Oral gavage on 2 alternate days GD 15-19.	No histological changes in placenta seen in all treatments. Testes exposed to ZnO or high dose MSN prenatally showed changes including prominent epithelial vacuolization, decrease in seminiferous tubule diameter, low cellular adhesion of epithelia and alterations to spermatogenesis. Low dose MSN and bulk Zn groups had no changes. Testosterone increased in high bulk ZnO, lowered in high MSN, no changes in ZnO NP or low MSN. In female corpus luteum, StaR was decreased in high ZnO and MSN, P450 and LHR higher in MSN, No change in ZnO NP group for P450 or LHR. In offspring (post pubertal, gestational exposure) – ZnO NP and bulk Star higher, P450scc significantly higher in 200mg bulk ZnO, and non-significantly higher in ZnO NP. P450c17, 17B-HSD and LHR no change following ZnO NP. MSN exposure resulted in increased StaR, decreased P450scc, LHR, 17b-HSD and P450c17.
(Xu et al., 2014)	Si NPs	male ICR mice (8wks).	Target organ toxicity	<i>in vivo</i>	IV injection tail	Mice given Si NPs 20mg/kg every 3 days, 5x over 13-day period. Sacrificed at 15/35/60 days after 1 st dose.	Saw reversible changes to oxidative stress and quality/quantity of epididymal sperm (observed at 15/35d but not 60d). No changes to acrosome integrity, sperm numbers, spermatogonia numbers or levels of Testosterone, LH or FSH. Suggests damage is reversible.

Carbon Nanotubes

Carbon-based ENM have in a wide variety of forms, encompassing carbon allotropes such as fullerenes, and cylindrical carbon nanotubes (CNT). CNT are hollow tubes of carbon, with a unique molecular structure which affords them extraordinary properties, including high tensile strength, high electrical conductivity, high ductility, high heat conductivity, and relative chemical inactivity. They hold great promise for applications such as targeted drug delivery. However, CNT are a classical example of HARN, bearing structural similarities to other fibrous materials such as asbestos. Consequently, there is much interest in their potential toxicity to humans and animals, particularly via inhalation (Tran *et al*, 2008; Poland *et al*, 2008). Five studies were identified reporting reproductive and developmental endpoints, of which 1 was *in vitro*, 1 *ex vivo* and 3 *in vivo* (Table 5).

All studies appeared to agree that CNT are toxic to the male reproductive organs, however the extent reported once again varies with approach, CNT type and dose regimen. The study *in vitro* used Syrian hamster embryo cells, alongside V79 hamster lung cells to compare cytotoxicity and genotoxicity of single- double- and multi-walled CNTs (SWCNT, DWCNT, MWCNT). The authors reported that MWCNT were more cytotoxic and genotoxic than SWCNT or DWCNT (Darne *et al.*, 2014). However, it is notable that the authors used the micronucleus test as part of their assessment, to which interference from ENM has previously been highlighted (Kroll *et al.*, 2012). The *ex vivo* study examined developmental endpoints for acute and long-term exposure of zebrafish embryos to CNT, highlighted in Table 5 (Cheng *et al.*, 2009). They showed an immune response was generated following CNT exposure. While embryos were able to produce primordial germ cells and a second generation, the larvae of this generation had a lower survival rate than control thus implying a negative effect on reproductive potential.

Table 5: *In vivo* and *in vitro* reproductive and developmental toxicity studies of carbon nanotubes (CNT), outlining key parameters from each study identified, including study type, exposure type and method and relevant findings described within the paper.

Paper	ENM	Animal/Cell	Study Type	<i>in vivo</i> / <i>in vitro</i>	Exposure	Method	Outcomes
(Darne et al., 2014)	single and MW CNTs (nanocyl)	Syrian hamster embryo and immortalised V79 hamster lung cells	Target organ toxicity	<i>in vitro</i>	Incubation	examined cytotoxicity and genotoxicity endpoints.	Found MWCNTs more cytotoxic and genotoxic than SWCNT or DWCNTs. Notable that this group used the micronucleus test which has reported interference for ENM. Used the comet and DCF-DA test for free radical generation.
(Cheng et al., 2009)	CNT	Zebrafish Embryos	Developmental	<i>ex vivo</i>	Incubation	Zebra fish embryos exposed to 2 ng of fluorescein isothiocyanate (FITC) labelled, bovine serum albumin (BSA) coated MWCNT at the 1 cell stage. Examinations conducted at 30 minutes, 24, 48 and 96 hours post microinjection.	At early stages, the embryos generated an immune response by accumulating circulating white blood cells at the trunk region. The embryos were able to produce normal primordial germ cells and were able to produce a second generation. The larvae of the second generation however, had lower survival rates compared to the untreated groups, suggesting a negative effect on the reproduction potential.
(Nirmal et al., 2017)	hydroxyl-functionalised MWCNT	Wistar rat sperm	Target organ toxicity	<i>in vivo</i>	incubation	6 animals per group, 0.4mg/kg, 2mg/kg and 10mg/kg, 15 doses over 30 days.	Sperm count, motility and normality showed dose-dep decrease. Viability unchanged, acrosome unaffected and DNA quality same. Sperm abnormalities inc. curved tails and deformed heads. Histology showed dose dependent changes. Vacuolisation, reduced GC layer and oedema interstitially with dilated blood vessels. Test levels decreased in 2/10 treatment groups comp to control. Ox stress markers – SOD and GPx dose dep increase, GST and MDA sig increase treated 2/10.
(Bai et al., 2010)	COOH-MWCNTs and NH2-MWCNTs	mice	Target organ toxicity	<i>in vivo</i>	injection	five repeated intravenous injections of COOH-MWCNTs and NH2-MWCNTs in mice for 13 days	Exposure did not elicit any change in sperm counts, sperm motility and sperm morphology. Histological changes seen at d15 following dosing (vacuolisation, reduced GC layer etc) recovered after d60/90 washout period.
(Farombi et al., 2016)	f-MWCNTs	Wistar rats 50 pubertal (8-week-old)	Target organ toxicity	<i>in vivo</i>	injection	0.25/0.5/0.75 and 1mg/kg f-MWCNTs via IP injection for 5 days.	Markers of Ox stress increased significantly dose dependent manner in testes and sperm (SOD, CAT, GPx up but GST and GSH down). Plasma Test. Level significantly decreased with treatment. Histopathology showed increasing effects with dose – decreased GC layer, interstitial congestion, oedema, tubular degeneration. Similar effect seen in epididymis – hyperplasia and loss of sperm in lumen

Zinc Oxide

Zinc oxide (ZnO) ENM are frequently available as powders or dispersions. They exhibit antibacterial, anti-corrosive, antifungal and UV filtering properties, and are commonly used in the manufacture of rubber, concrete, food products, sunscreens and as coating agents by the paint industry. Of the 7 studies identified, 1 was *in vitro*, 1 *ex vivo* and 5 were *in vivo* (Table 6).

In vitro, Barkhordari *et al* (2013) found dose-dependent toxicity of ZnO ENM to human sperm samples following incubation for 180minutes (Barkhordari *et al.*, 2013). *Ex vivo*, a study exposing zebrafish embryos to micron-sized ZnO to of zebrafish embryos again highlighted the importance of dissolution of ions in toxicity, but interestingly, this time the authors reported that a solution of Zn²⁺ ions was less toxic than ZnO particles, suggesting that ROS generated by the ZnO led to its more potent toxicity (Zhu *et al.*, 2009).

Of the literature examined *in vivo*, two studies administered pregnant rats to ZnO ENM via differing exposure routes. Zhang *et al* and Jo *et al* both examined maternal and F1 effects of ZnO exposure (Zhang *et al.*, 2008, Jo *et al.*, 2013). Zhang *et al* (2008) used intratracheal instillation, and found lower pregnancy rates in exposed dams, but no significant neurological impairment of those pups born. Jo *et al* (2013) exposed dams by oral gavage, observing a reduced number of born/live pups, together with decreased birth weight and increased foetal resorption. They also undertook an investigation into biodistribution of ZnO ENM following exposure, finding ENM within the mammary tissue of dams, and within the liver and kidney of pups (but did not mention the testes).

In relation to target organ specific effects, two studies exploring oral exposure to ZnO ENM reported adverse morphology in the testis post-exposure, with evidence of damage to LC and developing spermatozoa (Moridian *et al.*, 2015, Talebi *et al.*, 2013). The combined observations of lowered circulating testosterone, and lowered numbers of LC also emphasises the potential for endocrine disturbance following ZnO ENM exposure.

Table 6: *In vivo* and *in vitro* reproductive and developmental toxicity studies of zinc oxide ENM (ZnO), outlining key parameters from each study identified, including study type, exposure type and method and relevant findings described within the paper.

Paper	ENM	Animal/Cell	Study Type	<i>in vivo</i> / <i>in vitro</i> ?	Exposure	Method	Outcomes
(Barkhordari et al., 2013)	ZnO NPs (no size given)	human sperm	Target organ toxicity	<i>in vitro</i>	incubation	15 sperm samples exposed to 10/1000/500 or 1000ug/ml for 45/90/180 minutes.	Cell death 20.8,21.2 and 33.2% after 45/90/180mins. Highest concentration gave highest tox. 180mins exposure sig worse than all other exposure times
(Zhu et al., 2009)	ZnO NPs	Zebrafish Embryos	Developmental	<i>ex vivo</i>	Incubation	Zebra fish embryos exposed to ZnO. Examined sedimentation of nanoscale ZnO in zebrafish culture medium and assessed the toxicity of settled ZnO NP aggregates on developing zebrafish embryos and larvae.	Within 48h micron-sized ZnO NP aggregates formed and settled out of the culture medium. These aggregates exerted dose-dependent toxicity to zebrafish embryos and larvae, reducing hatching rate and causing pericardial oedema. The observed toxicity of the ZnO NP aggregates was not likely a result solely of particle dissolution, as soluble Zn ²⁺ alone caused much less toxicity to zebrafish embryos than ZnO NP. The combination of both ZnO NP and Zn ²⁺ is likely to lead to the embryonic toxicity, possibly by increasing reactive oxidative species (ROS) and/or compromising the cellular oxidative stress response.
(Zhang et al., 2008)	ZnO NPs	Rats	Maternal/ F1	<i>in vivo</i>	Intratracheal Instillation	Pregnant rats exposed via intratracheal instillation at the dose of 7.5 mg/kg bw once a day for 5 days.	Pregnancy rates in Nano-ZnO group were lower than those of Control. Difference of birth numbers between groups was not significant. Body weights of young rats in Nano-ZnO group at the day of 4, 7 and 21 were higher than those of other groups. Results of water maze experiment showed that the Nano-ZnO group did not behave in a significantly altered manner to control. There was no statically significant difference between particle groups and Control group in experiments of plane righting reflex and air righting reflex.
(Moridian et al., 2015)	ZnO NPs (no size given)	32 NMRI mice	Target organ toxicity	<i>in vivo</i>	oral	5/50/300mg/kg ZnO NPs daily for 35 consecutive days (sperm cycle in mouse).	Found sig decrease in serum T levels in M/H dose groups, and slight decrease in L group. Same finding for diameter of Sem Tubule in L then M/H group. Took into account shrinkage of seminiferous tubules in paraffin embedded tissue (21%) – good practise. In M/JH groups total vol of seminiferous tubules, interstitial tissue and LC number were sig lower than control. Suggested loss of LCs may lead to loss Testosterone.

(Talebi et al., 2013)	ZnO NPs (no size given)	32 adult male NMRO mice	Target organ toxicity	<i>in vivo</i>	Oral	5, 50 or 300mg/kg dose	Sperm count and motility decreased sig compared to control, and abnormal sperm numbers increased sig in higher dose groups. Histomorphology analysis showed various findings: low dose had vacuolisation, med dose had GC degeneration, loss elongating spermatids, disorganisation of GC and sloughing, high dose had all of the above with atrophy and multinucleated giant cells present. Johnsen's score showed sig decrease in med and high dose groups. Morphometrics showed ST diameter and seminiferous epithelial height dig decreased in med and high doses (but no mention of staging here so is this really relevant?). Leydig cell numbers were also significantly reduced in low and med dose. No staging of tubules undertaken with this paper, nor characterisation of ZnO offered.
(Jo et al., 2013)	ZnO NPs <100nm	Rats	Maternal / F1	<i>in vivo</i>	Oral Gavage	Rats were exposed to 500 mg/kg bw of ZnO nanoparticles, beginning 2 weeks before mating and continuing until postnatal day 4.	Rats treated with nano-zinc oxide showed reduced number of born/live pups, decreased body weights of pups and increased foetal resorption. Zinc oxide nanomaterials were distributed to organs such as mammary tissue of dams and liver and kidney of pups.
(Mohamed and Abdelrahman, 2018)	ZnO NPs<100nm and <40nm	40 rats	Target organ toxicity	<i>in vivo</i>	Oral	Investigated the possible protective role of ZnO NPs on testicular and epididymal structure and sperm parameters in nicotine-treated rats. 40 rats, some had nicotine 1mg/kg and others nicotine+ZnO 40nm for a period of 30 days	Histology showed ZnO supplementation appeared to help prevent nicotine related damage (which showed as separation of seminiferous epithelium, congested blood vessels and possible pyknotic nuclei etc in ST). Epididymal samples showed mucosa around epididymis and congested blood vessels with mononuclear infiltration, some of which was reversed with ZnO. Ox stress measured via CAT, SOD, GSH and GPx were reduced in NP supplemented compared to nicotine alone, MDA levels were also lower in this group. Sperm morphology and count same result. StaR and P450scc expression significantly decreased in nicotine group, whereas ZnO NP supplemented group caused increase in both past control.

Summary

The foregoing review demonstrates that ENM of various types are able to access immunoprivileged areas relating to the reproductive system and influence reproduction and development in a number of ways. ENM can cross barriers such as the placenta and BTB, having been observed in both male and female reproductive organs. Exposure to ENM results in interference with aspects of fertility, including spermatogenesis and endocrine function. In addition, a number of ENM have been shown to impair embryonic development and to have adverse effects on the morphology and later reproductive function of offspring to maternally exposed animals.

Mechanistically, toxicity from exposure to ENM appears to potentially affect reproduction via a number of modes of action. Physico-chemical characteristics of ENM are clearly important, and functionalisation of ENM can often alter the toxicity and Mechanism of Action (MoA) observed. In addition, secondary release of ions via nanoparticle destabilisation appears to be an important consideration, as exemplified by some of the studies discussed. Likewise, it is sensible to expect that this will be the case for the BTB also, although no published literature is yet available.

Many ENM have been shown to elicit direct cytotoxicity to cells of the reproductive system and developing embryos. One MoA which has received much attention is that of oxidative stress, which can threaten germ cell, foetal and placental cells. ENM have also been demonstrated to elicit DNA damage via a number of mechanisms, direct and indirect. In addition, a role for inflammation in induction of reproductive and developmental toxicity has been suggested, and evidence to support this is emerging.

The literature published to date shows a great diversity in study design, with only one study from that reviewed using a test known to be validated (the developmental embryonic stem cell test, EST). Reporting varies hugely from study to study, as does choice of ENM in terms of its size, surface morphology & functionalization, controls used, dose regimens applied, exposure routes selected, and indeed whether such important aspects of each study are reported in full by their authors. Furthermore, components of studies also differ greatly in terms of model system, species of choice,

assays (and whether interference from ENM has been considered in their choice), biomarkers considered and end points under investigation. This makes comparison of studies difficult, as well as deduction of general rules for testing. To avoid further problems with comparison of studies, ideally all future research would include the following: i) Clear physico-chemical characterisation for all ENM reported on, ii) The use of well-characterised reference materials alongside test materials from which to make a comparison, iii) Inclusion of ionic controls for metallic ENM to elaborate further on whether any effect seen is ionic or particulate, iv) Consideration of potential for assay interference from ENM at every stage (*in vitro*), and v) where possible, consideration of ENM as endocrine disruptors, alongside investigation of their role in eliciting direct toxicity to the testis.

Overall, it is clear that ENM are able to interfere with male and female fertility, development and later reproductive success of offspring. However, the sheer complexity of the reproductive system, gaps in data and diversity in studies makes it hard to draw any solid conclusions or rules from the evidence on mechanisms or expected outcomes at the current time. There is therefore a clear need for structured testing of ENM developed for industrial or medical purposes to elucidate potential adverse effects to reproduction and development.

Objectives of the research programme

Based on the clear requirement for development of knowledge on male reproductive nanotoxicology, and the concurrent need to reduce, refine or replace the use of animal testing in research, the aim of this research is to investigate toxicity of ENM to the male reproductive system with a focus on development of non-animal testing approaches in line with the 3Rs principle.

The research will use a panel of commonly used reference engineered nanomaterials, alongside some highly relevant commercially available materials, selected as representative of the field. These have been well characterised, enabling generation of data which is directly comparable to that of other researchers using the same materials. During the research, the potential for interference of ENM with the assays will also be considered at each stage, as will the involvement in ionic dissolution from particles in their toxicity.

The work programme has four main sections:

1. Making use of established male gonadal cell lines, establishing suitable assays to screen ENM for cytotoxicity and the effects of time- and dose- on effect;
2. Using a sub-panel of ENM, investigation of functional cellular parameters relevant to both fertility and endocrine health will be undertaken on the same cell lines;
3. In parallel with 1 & 2, testicular tissues collected from animals exposed *in vivo* through a 28-day sub-chronic oral dosing regimen to two types of silver, three types of silica and a silver ionic control will be examined in detail for morphological and functional markers of effect;
4. The results *in vitro* will then be compared to those generated *in vivo*. Determination of comparability will guide a decision on ability of the *in vitro* tests to predict outcomes *in vivo*, and form one of the first steps in formation of an integrated approach to testing and assessment (IATA) for male DART following exposure to nanomaterials.

The output of this research will contribute to both building the knowledge base relating to male reproductive toxicity from ENM *in vitro*, and toward forming useful alternative models for predicting toxicity from engineered nanomaterials. Thus, the ultimate aim is to develop robust, reliable and repeatable *in vitro* test methods for the prediction of engineered nanomaterial (ENM) toxicity *in vivo*.

Chapter 2: Selection, handling and preparation of the Engineered Nanomaterial Panel

Introduction

To ensure comparability between tests, the same engineered nanomaterials have been used in all experiments in the present study. The ENMs selected were from two European Commission Framework 7 projects: MARINA (MANaging Risks of NANoparticles, FP7-NMP 263215), and SUN (Sustainable Nanotechnologies, FP7-NMP 604305). Any additional ENMs used were in support of the materials used within these projects. This short chapter outlines the materials used and rationale for their choice, together with providing materials and methods on their handling, dispersion and preparation for work both *in vitro* and *in vivo*.

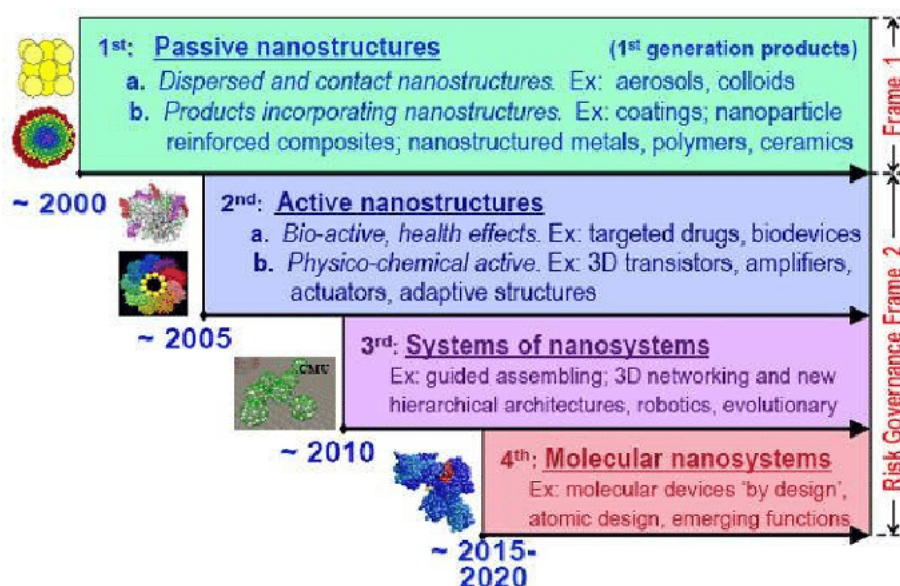


Figure 6: The four generations of nanotechnology. From (Rocco, 2005)

In the mid-2000s, Mike Rocco of the U.S. National Nanotechnology Initiative described 4 generations of nanotechnology development as part of a road mapping exercise for the future of the field (Fig. 6). These ranged from passive nanostructured materials (1st generation products) that may be added to existing products or materials to benefit their function e.g. as paint or fuel additives, or for incorporation to polymers and metals

to improve their performance, through active nanostructures with targeted health or structural effects, nanosystems capable of guided assembly and basic robotics, to 4th generation molecular systems controlled from the molecular level up, with much more complex functions. In order to orientate the work reported within this thesis, it is important to recognise that all ENM used are classified as first-generation ‘pristine’ nanomaterials; passive nanostructures that have been created and are in their pure, or unformulated, state.

Selection of the Nanomaterial Panel

Within the MARINA project, ENMs were selected based on scientific, regulatory and industrial relevance. These materials selected were available from the Nanomaterials Repository at the Joint Research Council (JRC). The JRC’s repository was founded to provide an independent source of control and reference ENMs in response to a previous lack of reference and control samples, which over time had led to a lack of harmonisation of procedures used to generate data for risk assessment of ENMs (Cotogno et al., 2016). As such, the materials provided were controlled to be from the same manufacturer, source and batch, as the degree to which ENMs with the same chemical identity but differing sources may be considered to be the “same” material has been debated (Motzkus et al., 2014). The materials selected for use have also been utilised in occupational health and safety testing within a number of other projects worldwide to help establish potential risk from first generation ENM.

Within the repository, various forms of materials with differing nanofoms but the same chemical identity have been made available, to assist with grouping and read-across. Within MARINA, 14 principal ENMs were selected for investigation: Titanium Dioxide (TiO₂ **NM-101, 103, 104, 105**); Silica Dioxide (SiO₂ **NM-200, 203**); Zinc Oxide (ZnO **NM-110, 111, 112**); Multi-walled Carbon Nanotubes (MWCNT **NM-400, 401, 403**); nano-Silver (nano-Ag **NM-300K**). In addition, 5 secondary materials were selected: other SiO₂ (NM-100, 102); cerium dioxide (CeO₂ **NM-211, 212**); and nanoclay (NM-600). Of these materials, those in **bold** were selected for use within the MARINA hazard theme testing and are used in the work described in this thesis. Many of these materials overlap with materials selected by the OECD Working Party on Manufactured Nanomaterials project

on the safety testing of a representative set of manufactured nanomaterials, providing additional relevance for their selection and use (OECD, 2010).

Materials were extensively characterised, both by the JRC and partners within the MARINA project (Riego Sintes, 2015, Rasmussen et al., 2013, Rasmussen et al., 2014, Comero et al., 2011). Characterisation includes (but is not limited to): Agglomeration/Aggregation; Water Solubility/ Dispersibility; Crystalline phase; Crystallite size; Representative Electron Microscopy; Particle size distribution; Specific surface area; Zeta potential; Surface chemistry; Photocatalytic activity; Redox potential; Radical formation potential; Elemental analysis and Storage stability over time and at different temperatures. Consequently, no further characterisation work was undertaken during the present study.

To complement those used in MARINA, some additional ENMs were used in specific sections of this doctoral work. These were: pristine Copper Oxide (CuO) ENM from the SUN project, selected because of its use in antimicrobial wood coatings (SPA, 2014), and synthetic amorphous silica (SAS), selected because of its industrial relevance and used *in vivo* as a comparative material to the reference ENM NM202 (van der Zande et al., 2014a).

Physico-chemical information on all ENMs used within the project is provided in Table 7. All ENMs with the prefix NM were sourced from the Joint Research Council's reference nanomaterial repository, prepared under Good Laboratory Practise (GLP) (Cotogno et al., 2016).

Nanomaterial Weighing and Handling

ENM from the JRC were distributed in vials under argon, all other materials were distributed in vials. ENMs were prepared slightly differently depending on whether they were provided as powder or dispersion (for example, NM-300). All vials were stored at room temperature in the dark. It was advised that materials should be used for a maximum of one week once open, however, this was not always practically possible due to the time span of the laboratory work and limited quantities of ENM available. It

should be noted that ENM used within the low dose Alamar Blue experiments and PCR work were all used out with the 1 week recommended timeframe as a result. All ENMs were weighed for preparation into dispersion using a 6-place micro balance with laminar flow HEPA filter system, situated within a fume hood equipped with air control system that was set up specifically for safe handling of ENM, and housed in a specially designated ENM weighing and handling room within Edinburgh Napier University.

Table 7: Panel of ENMs selected for use within the MARINA project, and the present study. Table includes ENM name and JRC reference number, together with form and basic physico-chemical parameters provided by the manufacturer and from literature using the same ENM panel (JRC, 2011, Kermanizadeh et al., 2013, Riego Sintes, 2015, Rasmussen et al., 2013, Rasmussen et al., 2014, Comero et al., 2011, van der Zande et al., 2014a, Cefic, 2012).

ENM	JRC ID and source (where available)	Chemical Number (where available)	Type of Material	FORM	Mean Primary Particle Size (nm)	Length and Diameter (nm)	Particle size distribution [nm]	Specific Surface Area [m ² /g]
NM-101 TiO ₂	JRCNM01001a	-	Titanium Dioxide	Anatase, thermal uncoated	5-6	N/A	<100 = 95%; <50 = 77%; <10 = 11%	320
NM-103 TiO ₂	-	-	Titanium Dioxide	Thermal hydrophobic	186	N/A	N/A	60
NM-104 TiO ₂	-	-	Titanium Dioxide	hydrophilic	67	N/A	N/A	60
NM 200 SiO ₂	JRCNM02000a	-	Silicon Dioxide, coated	Precipitated PR-A-02	47	N/A	N/A	189
NM-202 SiO ₂	-	-	Silicon Dioxide, uncoated	Thermal PY-B-01	10-25	N/A	N/A	204
NM-110 ZnO	BASF Z-Cote	1314-13-2, EINECS 215-222-5	Zinc Oxide, uncoated	uncoated	100	N/A	N/A	13
NM-111 ZnO	JRCNM01101a BASF Z-Cote HP1	1314-13-2, 2943-75-1 EINECS 215-222-5, 220-941-2	Zinc Oxide, coated	Coated with Triethoxycaprylsilane 130	140	N/A	N/A	15
NM-300	RAS GmbH	7440-22-4	Silver	Colloidal suspension, Polyoxylaurat Tween-20 capped (stabilising agent)	Ag <20 nm (15 nm mean). Nominal silver content 10w/w%	N/A	N/A	N/A
NM-300 DIS	RAS GmbH	-	Silver Dispersant	N/A	-	N/A	N/A	N/A

ENM	JRC ID and source (where available)	Chemical Number (where available)	Type of Material	FORM	Mean Primary Particle Size (nm)	Length and Diameter (nm)	Particle size distribution [nm]	Specific Surface Area [m ² /g]
NM-212 CeO ₂		-	Cerium Dioxide, uncoated	precipitated	>10 to 20	N/A	N/A	65
NM-400 CNT	JRCNM04000a Nanocyl	7782-42-5, EINECS 231-955-3	MWCNT, Short entangled	Multi-walled Carbon Nanotubes	N/A	L846nm D11nm	N/A	11
NM-401 CNT	JRCNM04001a	7782-42-5, EINECS 231-955-3	MWCNT, long entangled	Multi-walled Carbon Nanotubes	N/A	L4048nm, D67nm	N/A	11
NM-403 CNT	JRCNM04003a	-	MWCNT	Multi-walled Carbon Nanotubes	N/A	L443nm, D12nm	N/A	12
Pristine CuO	-	-	Copper Oxide	Pristine	3-35 (av. 12)	N/A	N/A	
Nano Amor	Industrial silver		Silver	PVP coated	<15nm	N/A	<15 = 75% 15-62 = 25%	
AgNO ₃	-	-	Silver nitrate, ionic	Ionic silver	N/A	N/A	N/A	N/A
ZnSO ₄	-	-	Zinc oxide, ionic	Ionic Zinc	N/A	N/A	N/A	N/A

Once the vial of any ENM had been opened, work to dispense the required weight to a separate vial from which to prepare dilutions was carried out quickly, ensuring that the stock solution vial was not open for any longer than absolutely necessary. During this time, the vial was kept upright to minimize the escape of argon. Clean glassware and spatulas were used for each handling of ENM.

Protocol for weighing NM-300 Ag and preparation of stock solution for dispersion

Vials of NM-300 contained 0.5 g silver in a dispersant composed of 5 ml de-ionised water (75%) with ammonium nitrate stabilizing agent (7%) and emulsifiers (8%), comprised of 4% Polyoxyethylene Glycerol Trioleate and 4% Polyoxyethylene(20) Sorbitan mono-Laurat (Tween 20). The silver concentration was roughly 10% w/w (100mg/ml), meaning that each vial contained 500 mg of silver. As the material was very viscous, weighing was recommended for dilution. For example, this meant that if 60mg of NM-300 was weighed (representing 6mg NM-300 at 10% w/v), 5.6ml of deionized and autoclaved water containing 2% FBS would be added to form the stock dispersion under clean conditions in a fume hood within the cell culture lab to produce a 2mg/ml stock solution.

Protocol for weighing materials other than NM-300 & preparation of stock solution for dispersion

For each ENM approximately 5-10mg of particles were weighed, to which 4-6 ml dispersion media were added under clean laboratory conditions (in a fume hood within the cell culture lab). For NM-110 and 111 (ZnO), an additional pre-wetting step with 0.5 vol.% ethanol (EtOH) was included, as this was essential to achieve a good suspension in the dispersion media. Practically, this meant that for 6mg of ZnO, 30 μ l of 0.5% ethanol would be added drop by drop and the powder mixed by rotating the tube in the hand for 30secs-1min. 5.97ml of deionized and autoclaved water containing 2% FBS was then added to form a 2mg/ml stock solution.

Dispersion Protocols for ENM

ENM toxicity testing often requires preparation of particle dispersion in liquid. For many ENMs, forming a stable dispersion in aqueous media is difficult due to their tendency to form agglomerates. Dispersibility may be improved using a number of approaches, from adjusting pH or ionic strength of the dispersant, to addition of solvents, or inclusion of de-agglomeration steps via mechanical stirring, shaking or ultrasonication (Hartmann et al., 2015).

Selection and application of a suitable protocol for ENM dispersion is important in order to provide better control over delivered dose, avoid generation of false positive results (via secondary toxicity from dispersants or chemicals added to aid dispersion), and avoid undesirable modifications of ENM caused by the dispersion process. In addition, from a regulatory point of view, harmonisation and standardisation of protocols and methods applied is vital to provide data which is comparable and reproducible (Hartmann et al., 2015).

Within this work, and in line with the agreed approach used by MARINA project partners, a dispersion protocol used in the NANOGENOTOX project was adopted (Joint Action co-funded by the Executive Agency for Health and Consumers - Grant Agreement n°2009 21 01 under the European Union 2nd Health Programme). This was selected as a good basis for a harmonized generic protocol for the dispersion of nanomaterials in aqueous media for the purposes of mammalian toxicological testing.

Dispersion protocol (*in vitro*)

ENM stock solutions were prepared to a concentration of 2 mg/ml in deionized and autoclaved water containing 2% FBS, and then sonicated (400W) for 16 minutes in a water bath at room temperature to assist dispersion. Water bath sonication was selected as it was considered to pose less risk of introducing contaminants or disrupting the structure of ENM than other available methods such as probe sonication (Hartmann et al., 2015). Working solutions were diluted to 200µg/ml, and from these, serial dilutions were prepared as outlined within Chapters 3 and 4. The described protocol ensured stable dispersion for up to 1 hour before considering re-dispersion due to

potential onset of agglomeration and/or sedimentation. However, any sedimented particles were easily re-dispersed by vortexing the dispersion for 10 seconds. ENM dispersions were prepared fresh for each particle treatment undertaken. Following the preparation of stock solutions, working concentrations were prepared in complete culture media (without FBS).

Dispersion protocol (*in vivo*)

Preparation of ENM dispersions and their use within *in vivo* experiments was undertaken at the laboratories of Wageningen University, Netherlands (as part of a larger *in vivo* study within the MARINA project), the testicular tissue from which was provided to Edinburgh Napier University for analysis. The team conducting the *in vivo* treatments followed the same dispersion protocol as stated above for NM-300, with some small differences. Van der Zande *et al* reported that “NM-300 particles were suspended in LC/MS grade water to a total silver concentration of 27 mg/mL, AgNO₃ was dissolved in LC/MS grade water to a final silver concentration of 2.7 mg/mL and matrix controls were equally diluted”. Pure liquid chromatography/mass spectrometry (LC/MS) grade water (Biosolve, Valkenswaard, The Netherlands) served as a matrix control for both NM-300 and AgNO₃. ENM suspensions/solutions were prepared freshly three times a week. As per the protocol used *in vitro*, suspensions were also sonicated after preparation for 20 min at 20°C at 100% output (4W specific ultrasound energy (240 J/m³) to minimise agglomeration, using a Branson 5510 water bath sonicator (Emerson, USA) (van der Zande et al., 2012).

Other preparations of ENM used: ENM feed mixes (*in vivo*)

The *in vivo* animal treatments were undertaken by either oral gavage, or via feed. For those which were undertaken by feed (NM202), this was achieved by mixing NM202 with feed, preparation of which was undertaken at the laboratories of Wageningen University, Netherlands. For this, Van der Zande *et al* summarised that “NM202 was mixed with standard feed and chocolate milk was added to increase palatability, which was assessed in a pilot experiment. SAS or NM-202 was mixed by hand-stirring to a thick

paste with chocolate milk (Chocomel, Nutricia, The Netherlands) and ground standard diet pellets (RMH-B, ABDiets, The Netherlands) in a ratio of 1:8:1 respectively, by weight. Total intended silica content was 99 mg/g and was fed in different amounts to rats to achieve the desired daily dosage” (van der Zande et al., 2014a, van der Zande et al., 2014b)

Disposal of ENM

Following use, all unused solutions containing ENM were disposed of in a way which avoided their release into the ecosystem (e.g. by being entered into the general drainage system) in line with the most recent guidance on the safe handling of nanomaterials. In this case, ENM containing solutions were decanted into sealed waste containers and stored in the dark at room temperature before specialist waste disposal via a third-party company.

Chapter 3: *In vitro* toxicity of a panel of ENM

Introduction

While the toxicity of various ENM has been demonstrated in numerous publications over the last 15 years, as outlined within Chapter 1, there remains a relative scarcity in available information and understanding of the effects ENM may have on the male reproductive system. From the available literature, several interesting *in vitro* focussed studies help in both highlighting the need to build knowledge in the area, and provision of further justification of the ENM panel selected, described in full within Chapter 2.

Existing knowledge *in vitro*

In two separate studies, Braydich-Stolle *et al.* showed that the mouse spermatogonial stem cell line C18-4 was adversely affected by metal nanoparticle exposure (Braydich-Stolle *et al.*, 2005, Braydich-Stolle *et al.*, 2010). Of the metal NP tested, smaller NPs had a greater effect and silver elicited the highest toxicity, with evidence of interference with cellular kinase interaction and cellular division following exposure. Furthermore, Asare *et al.* investigated cytotoxic and genotoxic effects of silver (Ag) and titanium dioxide (TiO₂) NPs to primary testicular cells from C57BL6 mice. They observed that Ag NPs were cytotoxic but minimally genotoxic, and that TiO₂ NPs did not affect cell number, proliferation nor elicit any significant genotoxicity (Asare *et al.*, 2012). Wiwanitkit *et al.* demonstrated that gold NPs were able to penetrate sperm heads and tails of a human sperm cell sample, causing an increase in immotile cells compared to control (Wiwanitkit *et al.*, 2009). Conversely, Makhluף *et al.* showed that bovine sperm cells incubated with a colloid solution of iron oxide NPs showed no adverse effects to motility or their ability to undergo the acrosome reaction, showing that the observed responses to ENM exposure are not necessarily uniform (Ben-David Makhluף *et al.*, 2006). Such variation in outcomes reported following metal nanoparticle exposure highlights the need for further investigation, with some concomitant consideration of the role physico-chemical characteristics have in determining hazard and thus any associated risk.

Komatsu *et al.* were one of the first groups to set the scene for further investigation of toxicity within the Leydig cell line, by examining uptake and toxicity of diesel exhaust

particles (DEP), TiO₂ and Carbon Black (CB) on the TM3 Leydig cell line. They showed that the particles were internalised by the cells, and that following this a number of effects were seen, from impairment of cell proliferation and viability, to alterations in testosterone production via interference with the steroidogenic acute regulatory (StAR) gene (Komatsu et al., 2008). Han *et al* recently reported that exposure of Leydig and Sertoli cell lines (details of exact cell lines used not published) to zinc oxide (ZnO) nanoparticles *in vitro* resulted in internalisation, time- and dose- dependent cytotoxicity through induction of apoptosis (Han et al., 2016). Finally, Zhang *et al* reported that silver nanoparticles inhibited viability and proliferation of TM3 Leydig and TM4 Sertoli cell lines in a dose- and time- dependent manner, by damaging cell membranes and inducing generation of reactive oxygen species (ROS) (Zhang et al., 2015a). They showed that toxicity increased with decreasing size of silver particle, and through PCR demonstrated that pathways related to apoptotic cell death (p53, pErk1/2) were upregulated and genes encoding receptors and enzymes involved in control of testosterone synthesis and action were downregulated (*AR, LH-R, CPY11A1, 3βHSD, CYP1Aa1, StaR*, amongst others).

This brief section not only outlines findings to date in relation to research carried out *in vitro* on male somatic cell lines into the hazard of ENM, but also highlights the relative scarcity of such information. As such, it serves to emphasise the need to broaden the knowledge base in the area by developing methodology and undertaking further research *in vitro*.

Existing approaches to DART and the need for development of *in vitro* approaches

The studies presented so far highlight not only evidence for direct reproductive toxicity, but also a potential endocrine disrupting role for ENMs, as it is clear that they may interfere with enzymes, proteins and receptors involved in endocrine regulation of steroidogenesis and thus function of the Hypothalamus-Pituitary-Gonadal axis. Consequently, testing for reproductive and endocrine endpoints is likely to be required to build a full hazard profile for ENMs.

As summarised in Chapter 1, current approaches to establishing the Developmental And Reproductive Toxicity (DART) of chemicals, agrochemicals and pharmaceuticals are very much reliant on *in vivo* methods. The animal burden associated with reproductive endpoints remains high both in the risk assessment of chemicals and development of medicines and medical devices, with the average number of animals required to fulfil a single DART test undertaken being between 560 and 2,450 (Beekhuijzen, 2017). Some attempts have been made to refine testing approaches to reduce the number of animals required; for example, by the replacement of OECD TG416 'Two generation reproductive toxicity test' with OECD TG443 'Extended one-generation reproductive toxicity study (EOGRTS)' where possible within the REACH Chemical Regulations (Beekhuijzen, 2017). However, to date there have been no stand-alone *in vitro* system or model developed in place of traditional reproductive toxicity, and currently there remain very few, if any, validated *in vitro* tests which may be used to contribute to building a hazard profile for a given chemical/pharmaceutical.

The challenge of building validated *in vitro* tests for reproductive endpoints is further complicated by complexity of the reproductive system and its reliance on and interaction with the rest of the body (via endocrine, neurological and immunological systems, amongst others), which made it incredibly difficult to develop validated *in vitro* tests that are representative of what may be achieved *in vivo*.

Currently, OECD TG443 'Extended one generation reproductive toxicity study' for chemicals, and the OPPTS 870.3800 'Reproduction and Fertility effects' test for agrochemicals are perhaps the most equipped of the standard *in vivo* reproductive toxicity tests to examine potential reproductive toxicity and endocrine disruption endpoints. Despite this, and the fact that on average they use over 1,000 animals each, the OECD recognise that information on mechanism of action for endocrine disruption probably still "needs to be obtained from *in vitro* EATS assays (Endocrine, Androgen, Thyroid, Steroidogenesis) or [other] *in vivo* lower tier tests" (OECD, 2018b). This highlights that while *in vivo* testing is still considered the gold standard in ensuring reproductive safety, the importance of *in vitro* testing in understanding *in vivo* outcomes

cannot be denied. It is further corroborated by the latest guidance on hazard testing of nanomaterials under REACH, which states that prior consideration of all available non-animal information should be made before any *in vivo* test is conducted, and that “relevant and reproducible *in vitro* test systems may be used” to contribute to hazard assessment (ECHA, 2017).

Finally, the rapid ongoing evolution of nanotechnologies means that the number of nanomaterials under development is growing exponentially. While many of these may share the same chemical identity, their varied physico-chemical modifications and functionalisation mean that it is not possible to simply assume hazard profile based on testing undertaken on pristine nanomaterials, yet the use of grouping and read-across in hazard testing is not without limits. This further highlights the need for robust, high-throughput *in vitro* assays that allow for a rapid screening of the vast number of existing and newly developed nanomaterial variants. Such *in vitro* testing systems could be used as an early warning system to better reduce the number of *in vivo* studies required, in line with the 3Rs principle of reduction, refinement and replacement of animal testing (Russel and Burch, 1959).

Initial steps toward developing *in vitro* methods to appraise reproductive toxicity of ENM

In order to minimise the animal burden of reproductive toxicity testing, it is important to develop reliable, reproducible *in vitro* methods and models by which to gain insight. As nanotoxicology is a relatively young field of research, development of such tests remains very much within its infancy. The initial step in establishing the usefulness of *in vitro* testing in predicting the potential for ENM to cause harm to the male reproductive system *in vivo* is to investigate cytotoxicity within a pre-defined testicular cell line.

Leydig cells are polyhedral cells present within the testicular interstitium. They hold key developmental, reproductive and immune system roles, and are responsible for production of androgens which act on both local and systemic targets. Locally, androgens produced by Leydig cells stimulate Sertoli cells, the ‘nurse’ cells which control the blood-testis-barrier (BTB) and manage the process of spermatogenesis inside

seminiferous tubules of the testis. For *in vitro* testing, the mouse Leydig cell line TM3 which was originally isolated from the BALB/C mouse was selected for use (Mather, 1980, Mather et al., 1982). The successful use of TM3 cells has been previously reported both in more general reproductive toxicity studies (Engeli et al., 2018, Yin et al., 2017), and in those using ENM (Komatsu et al., 2008, Talebi et al., 2013). TM3 cells are also complementary to the TM4 Sertoli cell line, having been isolated at same age and using the same methodology, thus presenting potential for investigation of more complex *in vitro* models through co-culture work. TM3 was therefore considered a good choice as an initial cell line representative of the Leydig cell.

Objectives

The objective of this chapter was to identify whether a key cell found within the testes, the Leydig cell, would be adversely affected following ENM exposure, with the aim of developing a reliable *in vitro* initial hazard screen test. The toxicity tests will determine an LC₅₀ (intermediate concentration for a 50% reduction in viability) in a Leydig cell line (TM3) following exposure to a range of ENM doses and exposure times, in order to guide development of further research to determine whether ENM alter normal cell function when at sub-lethal doses. To ascertain the impact of ENM physico-chemical properties the cells were exposed to a panel of ENM, with varying properties, to help identify potential commonality or differences in cell response.

The research questions to be addressed were therefore:

- 1) Using a basic assay for cytotoxicity, which ENM from a pre-established panel (if any) have adverse effects on TM3 cell viability?
- 2) For those ENM found to affect viability, can a timecourse assay using Alamar Blue help to establish the effect of time- and dose- on toxicity?
- 3) Through analysis of the results, is it possible to identify a sub-lethal concentration range and recommended exposure time for future investigation into the functional effects of ENM on TM3 cells?
- 4) Taking into account prior reports of ENM interference with assays *in vitro*, are the WST-1 and Alamar Blue assays suitable to assess cytotoxicity to TM3 Leydig cells from ENM?

Materials and Methods

The Nanomaterial Panel and its preparation

The panel of ENMs selected for analysis, methods for their handling, dispersion and preparation of serial dilutions are described in Chapter 2.

Expression of dose for *in vitro* work

Expression of dose in nanotoxicology presents a complex problem. Basic pharmacological principles dictate that response is proportional to the concentration of the affecter at its site of action. Historically, dose was therefore expressed in terms of mass per volume of diluent prepared (e.g. $\mu\text{g}/\mu\text{l}$). However, this makes the assumption that any material prepared for testing in suspension has clearly defined physico-chemical properties that remain unchanged during the dosing process. In reality however, it has been shown that the moment ENM make contact with any biological media, they become altered, for example via agglomeration, aggregation or the formation of protein coronae (Lundqvist et al., 2008, Lynch and Dawson, 2008, Bouwmeester et al., 2011). It also fails to take into account the difference between dose administered, and the dose which reaches the site of action (in this case cell monolayer surface). Dosimetry for nanoparticles can be affected by numerous factors, including shape, size, density, agglomeration, surface charge (zeta potential), as well as media properties such as density and viscosity, and other factors including gravitational settling from suspension or surface area of the test environment (Teeguarden et al., 2007).

In order to allow for the fact that *in vitro* testing was undertaken on a cellular monolayer within a fixed area, it is important as a bare minimum to take into account surface area. Therefore, although dose preparations were calculated in $\mu\text{g}/\text{ml}$, the final results are represented as $\mu\text{g}/\text{cm}^2$, as this provides a more realistic representation of the dose of ENM which is in contact with the surface area of the cells within a 2-D model. Table 8 outlines the conversion between the two dose modalities for the range of doses applied to cells.

Table 8: Dose conversions between $\mu\text{g/ml}$ and $\mu\text{g/cm}^2$ used for cytotoxicity studies

Initial Dose range, 96 well plate:							
$\mu\text{g/ml}$	0.125	1.25	12.5	25	50	100	200
$\mu\text{g/cm}^2$	0.037	0.37	3.76	7.53	15.06	30.12	60.24
Low Dose Range, 96 well plate:							
$\mu\text{g/ml}$	0.075	0.75	1.5	3	6	12	
$\mu\text{g/cm}^2$	0.023	0.23	0.47	0.94	1.875	3.75	

Selection and establishment of optimal growth conditions for the TM3 Leydig cell line

The TM3 mouse Leydig cell line (ATCC CRL-1714TM) was successfully cultured within a sterile environment using Dulbecco's Modified Eagle's Medium/Nutrient Mixture F-12 Ham 500ml with L-glutamine, 15mM HEPES, and sodium bicarbonate (DMEM), together with 10% foetal bovine serum (Gibco® FBS) and penicillin/streptomycin. Quality assurance work was undertaken to ensure a good working knowledge of both TM3 and TM4 cell lines.

As these cells are semi-immortalised, they do not behave exactly as a fully immortalised cell line and have required some additional time within the project to determine and implement optimum growth parameters (Fulton and Hutchison, 2012). Because of this, all work undertaken within this research was controlled for passage number (passage 3-9) and replicated at least 5 times to ensure statistical power in calculating results.

Normal behaviour in culture and doubling time, together with determination of optimum seeding density within assay plates was investigated. Cells were seeded into T25 culture flask (with a 25cm² growth area) at a density of 1x10⁶ cells/10mls media, and counts taken daily over 4 days in order to calculate their doubling time (Fig. 7). Viable cells were identified via Trypan Blue or Nigrosin exclusion, and cell counts undertaken using a Haemocytometer (Neubauer counting chamber). Throughout each count, % viability remained high (>96%), and by day 4, 7.52x10⁶ cells were counted. Doubling time was calculated using the following equation:

$$\text{Doubling Time} = \frac{\text{Duration} \times \log(2)}{\log(\text{final concentration}) - \log(\text{initial concentration})}$$

Doubling time for TM3 cells between passage 3 and 9 was calculated to be 32.96 hours.

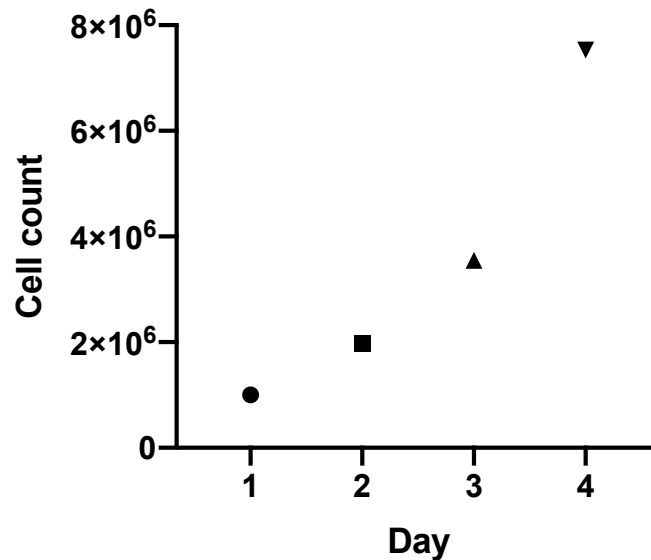


Figure 7: Doubling time of TM3 cells, seeded in a T25 flask at a density 1x10⁶ cells in 10mls media. n=1. Viable cells identified via Trypan Blue exclusion; counts undertaken with Neubauer counting chamber.

Control for hormone interference in assays *in vitro*

Charcoal stripping of FBS is used routinely for cell culture in endocrine studies, and involves its absorption with activated carbon, with the aim of minimising non-polar material such as lipophilic (lipid-related) materials (virus, certain growth factors, hormones and cytokines) regardless of molecular weight but has little effect on salts, glucose, amino acids, etc. without nonspecific loss of other serum components (ThermoFisher-Scientific, 2019a).

To ensure that cell growth and viability were not affected by use of charcoal stripped serum, a comparison of growth and assay performance of TM3 cells using both standard FBS and charcoal stripped FBS (c/s FBS) at two concentrations within medium (5% and 10%) was undertaken. Addition of 10% c/s FBS led to slower doubling times in TM3 cells, but addition of 5% c/s FBS resulted in no change in cell growth or behaviour (data not shown). Addition of Charcoal stripped FBS at 5% (Gibco® One Shot™ charcoal stripped Foetal Bovine Serum, USDA Approved) was therefore selected for use with the TM3 cell line in all investigations.

WST-1 assay

The WST-1 assay is a colourimetric assay, used to measure the activity of cellular enzymes in reducing the soluble tetrazolium dye WST-1 (4-[3-(4-Iodophenyl)-2-(4-nitrophenyl)-2H-5-tetrazolio]-1,3-benzene disulphonate) to insoluble formazan (Fig. 8). This bioreduction is undertaken by oxidoreductase enzymes in the cytosol of cells, dependent on glycolytic NADPH production by mitochondria. Reduction of WST-1 therefore increases with cellular metabolic activity, due the elevation of NADPH, thus, formazan production directly correlates to the number of metabolically active cells in the culture, measured by a scanning multiwell spectrophotometer (ELISA reader).

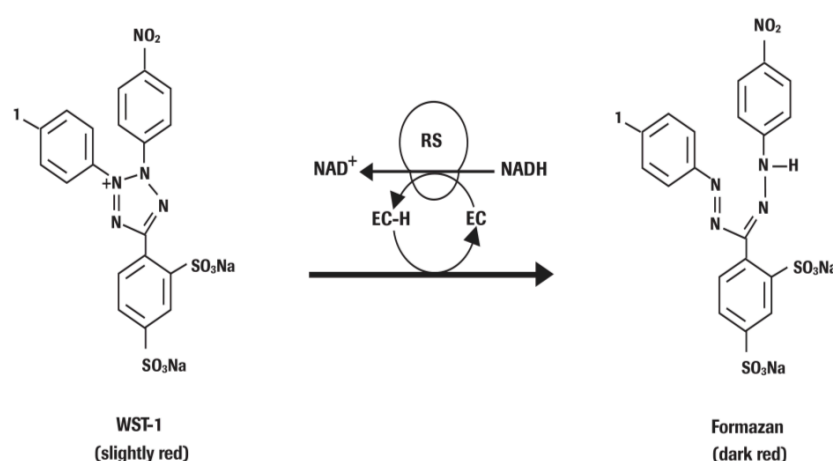


Figure 8: The reduction of the tetrazolium salt WST-1 to insoluble Formazan in metabolically active cells. EC=electron coupling agent, RS=mitochondrial succinate-tetrazolium-reductase system. From (Roche, 2011).

Initially, experiments to identify the optimal seeding density for TM3 cells to give the 2 days of growth in wells required to undertake the assay, without cells becoming over-confluent were undertaken. This was important for TM3 cells, as over confluence leads to cell growth up around the edges of the plate, creating an almost 'pancake-like' folding of the cell monolayer which would interfere with absorbance readings. TM3 Leydig cells were seeded in a 96 well plate at a density of 5×10^4 cells/well and allowed to incubate for 24h, until a confluent cellular monolayer had formed. ENM stock solutions were prepared to a stock concentration of 2mg/ml and sonicated to assist dispersion, described in detail within Chapter 2. Working solutions were diluted to an equivalent on-plate dose of $60.2 \mu\text{g}/\text{cm}^2$ from which serial dilutions were prepared down to $0.037 \mu\text{g}/\text{cm}^2$. Cells were exposed to ENM for a period of 24hrs according to the plate

plan in Appendix. 2. This allowed for every cell treatment to be made in triplicate, except the 'no cells' controls which were in duplicate.

After the incubation period, the old medium was discarded from the wells which were then rinsed with fresh medium before adding further media to a final volume of 100µl per well. 10µl of WST-1, cell proliferation reagent, was then added to each well and the 96 well plate incubated again for 2 hours at 37°C in a 5% CO₂ atmosphere. Following incubation, cell viability was estimated by measuring absorbance on a plate reader at 450nm. In total, a minimum of 5 replicates of the assay were carried out for each ENM.

The experimental design built in a number of controls, which are outlined below and noted on relevant wells of Appendix 2 in superscript:

1. Cells in medium without ENM + WST-1: negative control to show endogenous levels of WST-1 reduction from cells.
2. Cells + Triton X-100 + WST-1: positive control for loss of viability with no ENM Exposure.
3. Medium without cells + WST-1: negative control to ensure media does not interfere in the assay.
4. Nanoparticles in medium without cells + WST1: control to identify any interference with/inhibition of the assay from ENM.
5. Cells + Triton X-100 + ENM + WST-1: positive control for loss of viability following ENM Exposure.
6. Cells + nanoparticles +NO WST-1: negative control to show that ENM do not interfere in the assay.

Alamar Blue (AB) Assay

In addition to assessing cell viability using the WST-1 assay, the Alamar Blue assay was also used during exposure over a 24-hour timecourse. This used the same experimental and control setup as outlined for WST-1 to ensure that the source of any assay interference was identifiable. In this assay, viable cells reduce the non-fluorescent, membrane permeable blue compound Alamar Blue (resazurin) into a fluorescent pink

dye (resorufin), which is extruded into the medium. Alamar Blue (AB) is stable and water soluble so can be used for timecourse assays such as this. Successful reduction takes place only in metabolically active cells; thus fluorescence provides an indication of cell metabolic viability.

There is an overlap between the absorbance spectra of resazurin and resorufin. If test wells are fully reacted and there is no oxidised substrate present, then determination of the amount of reduced AB is $\text{Absorbance}_{570\text{nm}} - \text{Absorbance}_{600\text{nm}}$. However, during a time course assay this is not often the case, especially at earlier time points, and so using this calculation alone leads to generation of negative absorbance readings. Thus, to correct for the contribution of oxidised substrate, the following procedure was used to derive the amount of reduced AB at the prescribed reading filter (570nm):

1. Subtract absorbance of media only from AB in media to give Absorbance at the lower wavelength of 570nm (A_{LW}) and the higher wavelength of 600nm (A_{HW})
2. Use these values to calculate a correction factor (R_0):

$$R_0 = A_{\text{LW}} / A_{\text{HW}}$$

3. The % reduced AB is then given by:

$$AR_{\text{LW}} = A_{\text{LW}} - (A_{\text{HW}} \times R_0) \times 100$$

Thus, the following equation provides a corrected value for % difference in reduction:

$$\text{Percent difference in reduction} = \frac{A_{\text{LW}} - (A_{\text{HW}} \times R_0) \text{ for test well}}{A_{\text{LW}} - (A_{\text{HW}} \times R_0) \text{ positive growth control}} \times 100$$

The Alamar Blue assay was carried out in triplicate for ENMs identified as being of interest – i.e. those with positive results for cytotoxicity – NM-110 and 111 (ZnO), NM-300 (Ag), and NM-101 (TiO₂) as a reference material. Silver dispersant (NM-300DIS) was also examined in a single experiment as a cross check for interference or reactivity of the dispersant with AB.

Preparation of cells and dispersion of ENMs followed the same initial protocol as for cells exposed to ENM and then assessed using WST-1. At the time of exposure to ENMs,

Alamar blue was added to each well and fluorescence was then measured at 570nm using a plate reader at 2, 4, 6 and 24 hours in order to track changes in viability (reference absorbance 600nm). Plates were maintained in an incubator between readings. The values of viability were corrected using the equation above, as well as against endogenous (blank) expression.

In order to provide a direct comparison to results from the WST-1 assay, a full dose response was conducted using the original dose range (0.037-60.24 $\mu\text{g}/\text{cm}^2$). A second lower dose range of 0.023-3.75 $\mu\text{g}/\text{cm}^2$ was then investigated to identify sub-lethal concentrations that could be used for further assessment of cell impacts at non-lethal doses.

Statistical Analysis

Absorbance readings for both tests were initially processed using Microsoft Excel. As pilot data confirmed that some of the ENM interfered with absorbance in the assay, following input of raw data, all readings were corrected by subtracting absorbance of the ENM control wells (containing nanoparticles + WST-1) from the test wells (containing nanoparticles + cells + WST-1). Mean absorbance and standard deviation were calculated, and results were expressed as a % viability relative to untreated (endogenous) control cells.

Results were then imported to Graphpad Prism v7.0, and the data analysed using descriptive statistics, together with a Shapiro-Wilk test for normality (selected due to the lower experimental replicate number). To deduce whether treatment led to significant changes in cellular viability relative to untreated control, a one-way analysis of variance (ANOVA) was conducted, with a post-hoc Tukey or Dunnett's multiple comparison test to provide comparison between individual doses of ENM, and ENM doses and control; $P < 0.05$ *, $P < 0.01$ ** $P < 0.001$ ***. For comparisons with more than one contributing factor (e.g. charcoal stripped medium vs standard FBS, and nano-silver vs ionic silver) a 2-way ANOVA was used, with a post-hoc Dunnett's test for multiple comparisons between treatments and control.

Data was plotted as box and whiskers and scatter plots, to show the range in readings and identify where there was high variation. Where a potential dose-response relationship was identified, further analysis was undertaken using non-linear log(inhibitor) vs. response (three parameter) curve. The data output was tested for normality using both the D'Agostino-Pearson omnibus normality test and the Shapiro-Wilk normality test, residuals were plotted, and outliers counted using the ROUT coefficient.

Results

Comparison of cell viability in Charcoal-stripped and Standard FBS

Before carrying out cytotoxicity testing for all ENM, a comparison of viability between cells cultured in normal FBS and those cultured in charcoal stripped FBS was undertaken, by exposing cells to uncoated and coated ZnO (M110 and 111) at doses from 0.037-60.24 $\mu\text{g}/\text{cm}^2$ (n=3). Exposure to both ENM resulted in a clear dose-dependent toxicity, with no apparent difference in result between the two serum types, despite some variability around the point at which cells appeared to be losing viability (Fig. 9).

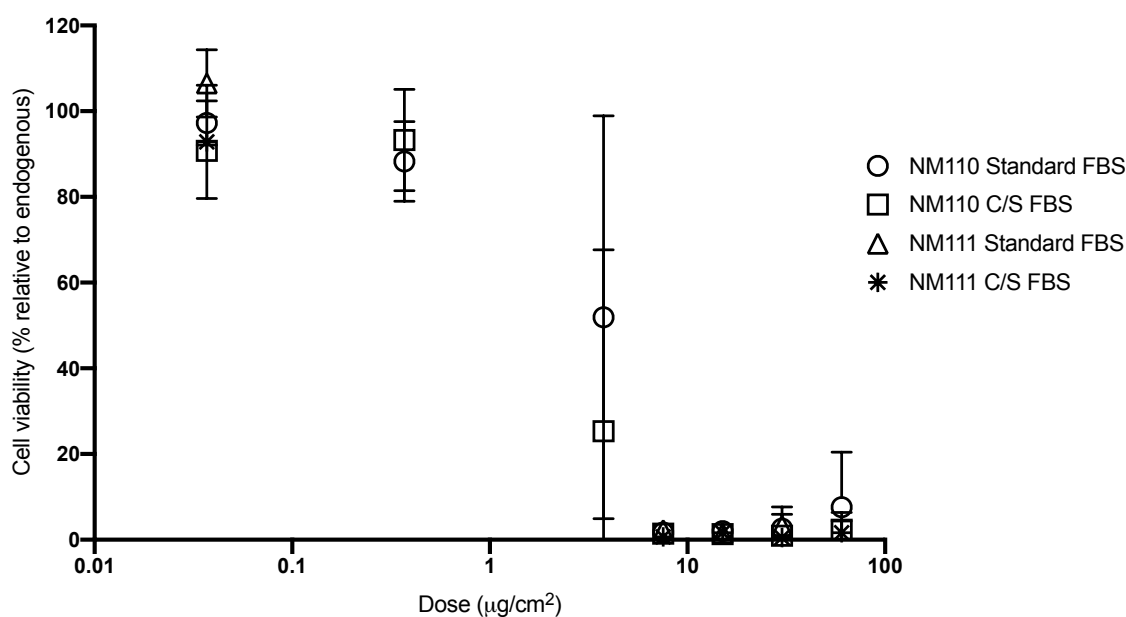


Figure 9: Comparison for serum type – standard FBS vs Charcoal Stripped FBS. Viability of cells following 24h exposure to Zinc Oxide (NM-110 & 111) using the WST-1 cytotoxicity assay. All values corrected for WST-1 interference with assay. Doses from 0.037-60.24 $\mu\text{g}/\text{cm}^2$. N=3.

To confirm that serum type did not influence cellular response to a toxic challenge, a 2-way ANOVA was undertaken. The results of this confirmed that serum type had no effect on result (n/s) whereas dose effect was significant (**** $p < 0.0001$) for NM-110. Cells exposed to NM-111 also showed a significant reduction in viability compared to dose (**** $p < 0.0001$). In this case, ANOVA also suggested influence of media on viability ($P = 0.0015^{**}$). However, this was due to wide variation around the onset of cellular toxicity (0.37 and $3.76 \mu\text{g}/\text{cm}^2$), which skewed the data and led to significance in the findings. In support of this, when a 2-way ANOVA was repeated excluding these doses, any significance associated with serum type was nullified, while dose effect remained significant ($p < 0.0001^{****}$). As a result, all future cell culture work was undertaken using 5% c/s FBS, selected as being optimal for cell culture.

Toxicological assessment of ENM Panel: cell proliferation assays

Assay Interference Testing

Examination of the controls outlined within the materials & methods section revealed the control wells (WST-1 & media) showed a marginal interference in absorbance reading caused by the dye; all results were therefore corrected for WST-1. For silver (NM-300, NM-300dis and AgNO_3), marginal interference from the ENM was also identified. To ensure this did not skew the results, an additional correction for silver particles was made for these materials.

Titanium Dioxide (NM-101, 103 & 104)

Fig. 10 shows the cytotoxicity assessment of TM3 cells exposed to three forms of titanium dioxide, NM-101 (anatase), NM-103 (hydrophilic) and NM-104 (hydrophobic) ($n = 6$) across a range of doses from $0.037 \mu\text{g}/\text{cm}^2$ to $60.24 \mu\text{g}/\text{cm}^2$. These are expressed as % cell viability relative to that in a healthy endogenous control (also reported as box and whiskers plots in Fig. 11).

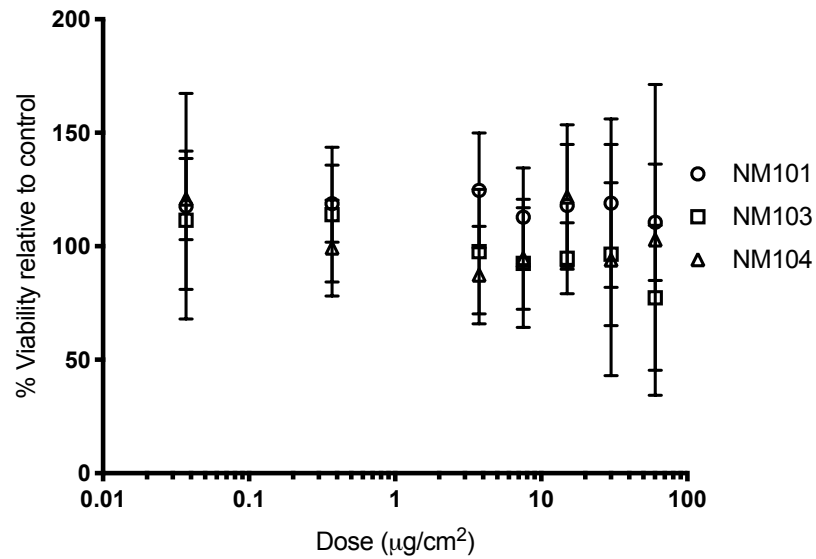


Figure 10: Viability of TM3 cells exposed to Titanium dioxide ENM: NM-101, 103 & 104 for 24h assessed using the WST-1 cytotoxicity assay (n=5). Viability expressed as % relative to untreated (endogenous) control. Doses 0.037-60.24µg/cm². All values corrected for WST-1 interference with assay.

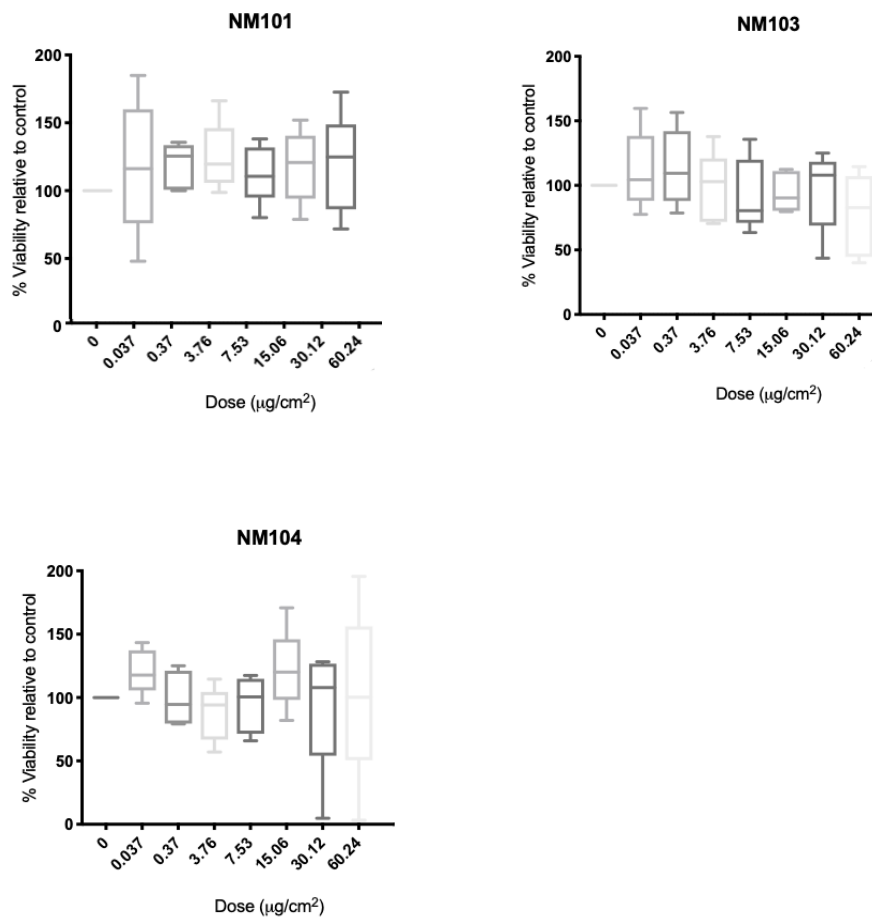


Figure 11: Box and Whiskers representation of viability of TM3 cells cultured in charcoal stripped serum, following 24h exposure to Titanium Dioxide (NM-101, NM-103 and NM-104) using the WST-1 cytotoxicity assay (n=6). Doses 0.037-60.24µg/cm². All values corrected for WST-1 interference with assay. Dose 0 is untreated (negative) control. Where a statistically significant loss in viability of cells was identified compared to control, asterisks depict level of significance (* p=0.05, ** p=0.01, *** p=0.001 & **** p=0.0001).

For NM-101, very little change in viability of cells was observed across the dose range, although the standard deviation on some doses was high. Statistical analysis of the results by ANOVA showed there was no significant difference between the readings ($P>0.05$).

For NM-103, little change in viability of cells was observed from 0.037-60.24 $\mu\text{g}/\text{cm}^2$, however at 60.24 $\mu\text{g}/\text{cm}^2$ mean viability decreased to 73%. Statistical analysis of the results showed that this decrease in viability was not statistically significant ($P >0.05$). Cells exposed to NM-104, showed little notable alteration in viability across the range of doses tested, albeit there was some variance in the results at higher doses reported. ANOVA confirmed no significant effect on viability with nanomaterial dose ($P>0.05$).

Zinc Oxide (NM-110, 111 & ionic control)

The cytotoxicity assessment conducted in parallel for the uncoated (NM-110) and coated (NM-111) forms of ZnO, together with ionic ZnSO₄ as a control material is summarised in Figures 12 & 13.

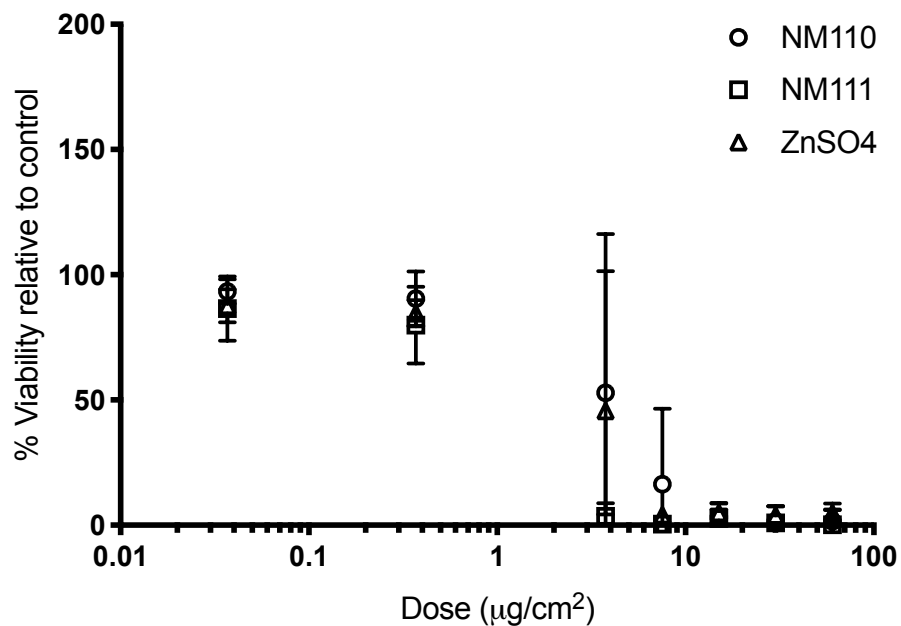


Figure 12: Viability of cells cultured in charcoal stripped serum, following 24h exposure to Zinc Oxide (NM-110 & 111) or zinc ions (ZnSO₄), assessed using the WST-1 cytotoxicity assay. Viability expressed as % relative to untreated (endogenous) control. Doses from 0.037-60.24 $\mu\text{g}/\text{cm}^2$. N=5 for NM-110 & NM-111, N=3 for ZnSO₄. All values corrected for WST-1 interference with assay.

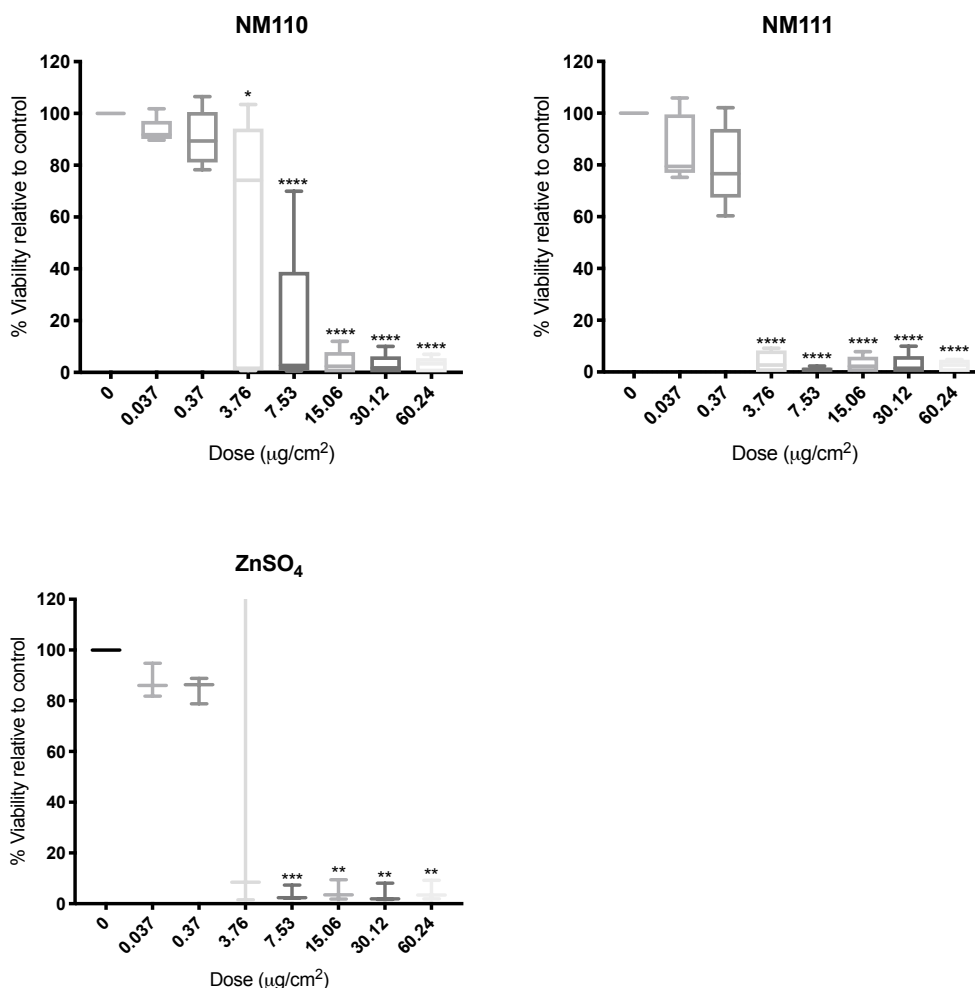


Figure 13: Box and Whiskers representation of viability of TM3 cells cultured in charcoal stripped serum, following 24h exposure to Zinc ENM and ionic Zinc (NM-110, NM-111 and ZnSO₄) using the WST-1 cytotoxicity assay (n=6). Doses 0.037-60.24µg/cm². All values corrected for WST-1 interference with assay. Dose 0 is untreated (negative) control. All values corrected for WST-1 interference with assay. N=5 for NM-110 & NM-111, N=3 for ZnSO₄. Where a statistically significant loss in viability of cells was identified compared to control, asterisks depict level of significance (* p=0.05, ** p=0.01, *** p=0.001 & **** p=0.0001).

The results show a clear dose-response toxicity, cell viability decreasing with increasing dose for both ENMs and ZnSO₄ ions. To further understand the nature of the dose-response observed, a non-linear curve was fitted to the results of NM-110 and NM-111 cell exposures in order to identify the nature of the relationship and understand the influence of potential outliers in the data. Figure 14 shows the raw data fitted to a log(inhibitor) vs. response (three parameter) curve.

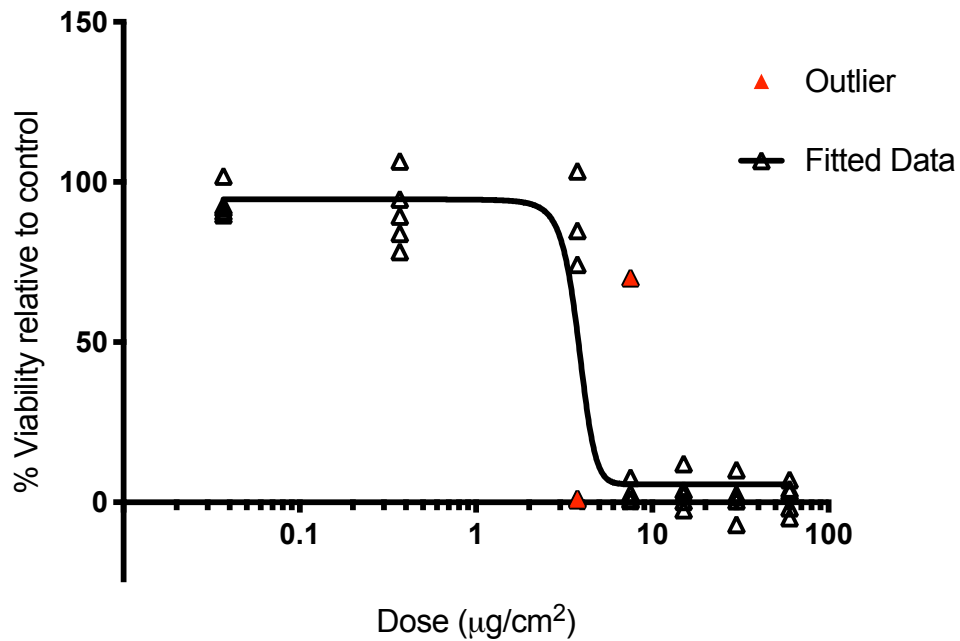


Figure 14: Non-linear curve showing toxicity of NM-110 to TM3 cells. Doses 0.037-60.24µg/cm². N=5. The data output was tested for normality using both the D'Agostino-Pearson omnibus normality test and the Shapiro-Wilk normality test, residuals plotted, and outliers counted using the ROUT coefficient. Outliers identified are highlighted in red. The LC₅₀ value was identified to be 3.813µg/cm².

Results of the curve fit for NM-110 gave an R² value of 0.8197 and revealed that the data did not appear to be normally distributed (p=0.0020** D'agostino-Pearson, p<0.0001**** Shapiro-Wilk). ROUT analysis identified key outliers within the 3.76 and 7.53µg/cm² doses, where the greatest variation was reported for this ENM (shown in red within Fig. 14). To further characterise the dose-response curve, the doses with high variation were removed and the data re-plotted to test whether the outliers were responsible for the lack of normality in distribution found via the D'Agostino-Pearson test. Results of this curve fit showed a much-improved fit (R²= 0.9843), found that the data was normally distributed without inclusion of outliers, and that there were no further outliers in the data. From this regression, it was possible to calculate an LC₅₀ value (concentration at which 50% of viability is lost) of 3.813µg/cm².

Results of the curve fit for NM-111 showed an R² value of 0.9662, that the data was normally distributed (n/s D'agostino-Pearson and Shapiro-Wilk), and ROUT analysis did not identify any outliers. The LC₅₀ value reported was 6.052µg/cm² (Fig. 15).

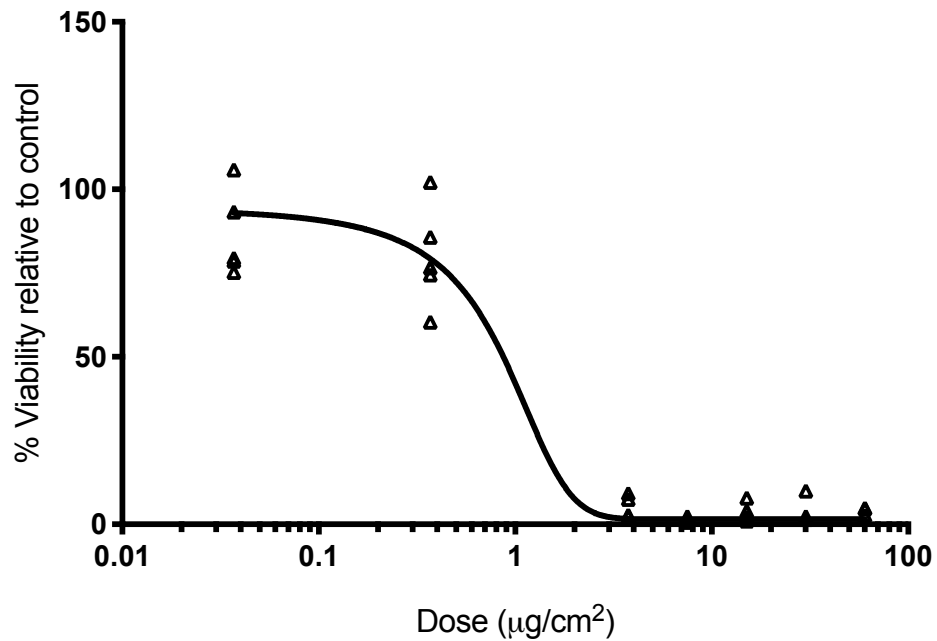


Figure 15: Non-linear curve showing toxicity of NM-111 to TM3 cells. Doses 0.037-60.24µg/cm². N=5. The data output was tested for normality using both the D'Agostino-Pearson omnibus normality test and the Shapiro-Wilk normality test, residuals were plotted, and outliers counted using the ROUT coefficient. Outliers are highlighted in red where present. The LC₅₀ value was identified to be 6.052µg/cm².

Significance of the dose-response toxicity was confirmed by one-way ANOVA, which showed a significant effect for NM-110 ($p < 0.001^{***}$), NM-111 ($P < 0.0001^{****}$) and ZnSO₄ ($P = 0.003^{***}$). Dunnett's multiple comparisons showed that this effect was significant from 3.76µg/cm² for both NM-110 ($p < 0.001^{***}$), 7.53µg/cm² for NM-111 ($p < 0.0001^{****}$) and ZnSO₄ ($p < 0.005^{**}$ increasing to $p < 0.0001^{****}$ from 7.53µg/cm²).

Cells exposed to NM-110 showed a high degree of variance in % viability between assay replicates at 3.76µg/cm² (Fig 13), the dose level at which a significant onset of toxicity was observed. In this case, the variation in response was so great that the effect of ENM exposure on viability was not statistically significant at any dose under 7.53µg/cm² ($P < 0.01^{**}$). Cells exposed to NM-111 also recorded wide variation in % viability between replicates at 0.37µg/cm². ANOVA confirmed a significant reduction in viability compared to control from 3.76µg/cm² ($P < 0.0001^{****}$). Data collected from ionic zinc (ZnSO₄) exposures revealed a similar dose response correlation with decreased cell viability with cells exposed NM-110 and 111, with a clear dose-dependent decrease in cell viability from 3.76µg/cm² upwards. A two-way ANOVA comparing NM-110 NM-111 and ZnSO₄ was undertaken to confirm results; this found no significant interaction between

treatments, but that viability was altered significantly with increasing dose ($p < 0.0001$ ****).

Silica Dioxide (NM 200 & 203)

Cytotoxicity assessments for two forms of silica dioxide (NM-200 and NM-203) are shown in Figures 16 and 17.

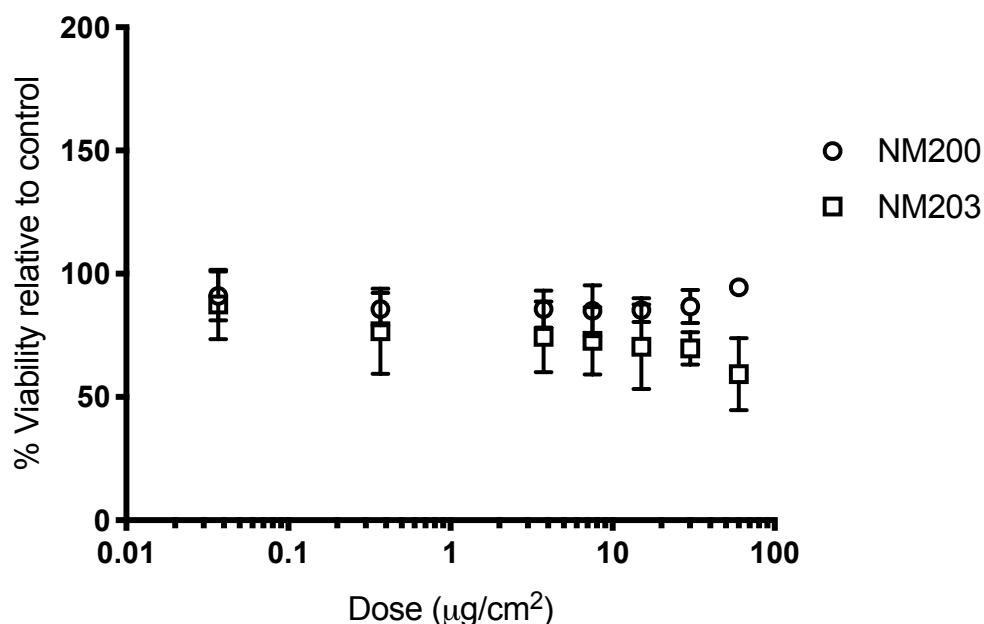


Figure 16: Viability of cells cultured in charcoal stripped serum, following 24h exposure to silica dioxide (NM-200 & 203), assessed using the WST-1 cytotoxicity assay ($n=6$). Viability expressed as % relative to untreated (endogenous) control. Doses from 0.037-60.24 $\mu\text{g}/\text{cm}^2$. All values corrected for WST-1 interference with assay.

The results indicate that there appears to be little effect on cell viability from NM-200, but NM-203 shows a decrease in cell viability at highest doses (Fig. 16). Little variation between replicates was observed, especially in comparison to other ENM tested. Statistical analysis confirmed that for NM-200 there was a small but statistically significant change in viability with increasing dose ($p=0.0223$ *), which Dunnett's multiple comparisons confirmed was significant from 0.37 $\mu\text{g}/\text{cm}^2$ ($p < 0.05$ *). This was likely due to the fact that there was very little variation across replicates, as shown in Fig. 17.

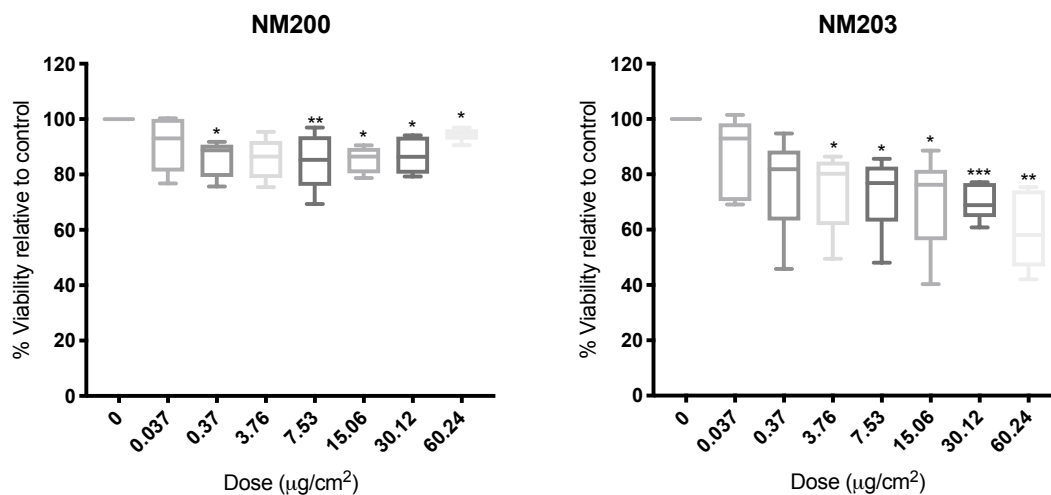


Figure 17: Box and Whiskers representation of viability of TM3 cells cultured in charcoal stripped serum, following 24h exposure to silica dioxide ENM (NM-200 & 203) using the WST-1 cytotoxicity assay (n=6). Doses 0.037-60.24µg/cm². Dose 0 is untreated (negative) control. All values corrected for WST-1 interference with assay. Where a statistically significant loss in viability of cells was identified compared to control, asterisks depict level of significance (* p=0.05, ** p=0.01, *** p=0.001 & **** p=0.0001).

The observed decrease in viability at the higher doses in cells exposed to NM-203 was found to be significant (P<0.001***), and multiple comparison analysis revealed that this effect became significant at a dose of 3.76µg/cm² (p<0.05*).

Silver, Silver Dispersant and Silver ions (NM-300, 300Dis and AgNO₃)

Cytotoxicity assessment was next undertaken for colloidal silver nanoparticles (NM-300) and a silver ionic control (AgNO₃). As silver was the only ENM provided in suspension as a colloid, its dispersant (NM-300dis) was also provided for testing to ensure that any effect observed following NM-300 exposure was independent of its dispersant. As previously outlined, all results displayed were corrected for WST-1 interference. In this case, results were also corrected for ENM, as the ENM control wells (ENM + WST-1) showed a marginal interference in absorbance reading. The results are summarised in Figs. 18 and 19.

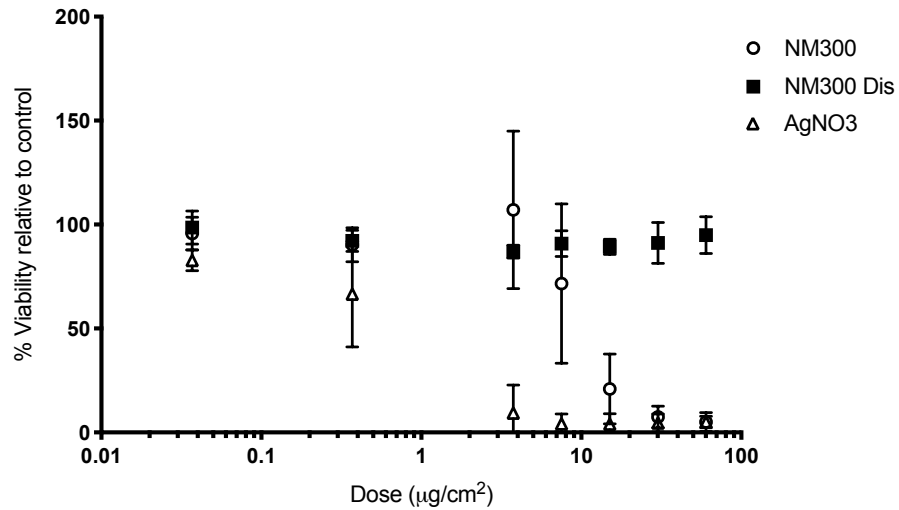


Figure 18: Viability of cells cultured in charcoal stripped serum, following 24h exposure to Silver, Silver Dispersant and ionic Silver (NM-300, NM-300DIS and AgNO₃), assessed using the WST-1 cytotoxicity assay (n=6). Viability expressed as % relative to untreated (endogenous) control. Doses from 0.037-60.24µg/cm². All values corrected for ENM and WST-1 interference with assay.

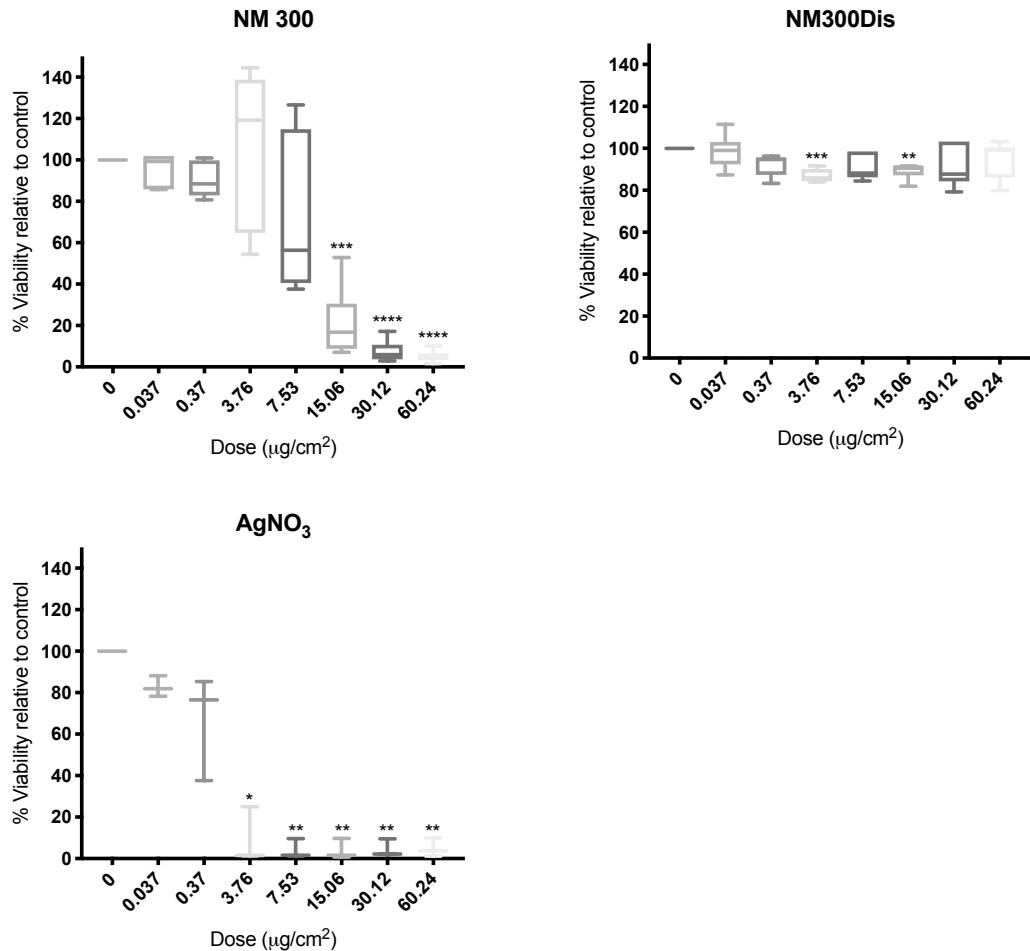


Figure 19: Box and Whiskers representation of viability of TM3 cells cultured in charcoal stripped serum, following 24h exposure to Silver (NM-300), Silver dispersant (NM-300Dis) and ionic Silver (AgNO₃) using the WST-1 cytotoxicity assay (n=6). Doses 0.037-60.24µg/cm². All values corrected for ENM and WST-1interference with assay. Dose 0 is untreated (negative) control. All values corrected for WST-1 interference with assay. Where a statistically significant loss in viability of cells was identified compared to control, asterisks depict level of significance (* p=0.05, ** p=0.01, *** p=0.001 & **** p=0.0001).

There was clear dose-response effect of silver ENM and ion exposure on TM3 cell viability, but no effect on viability from silver dispersant. To further understand the nature of the dose-response observed and the influence of potential outliers on the data, a non-linear (log(inhibitor) vs. response (three parameter)) curve was fitted to the results of NM-300 (Fig. 20).

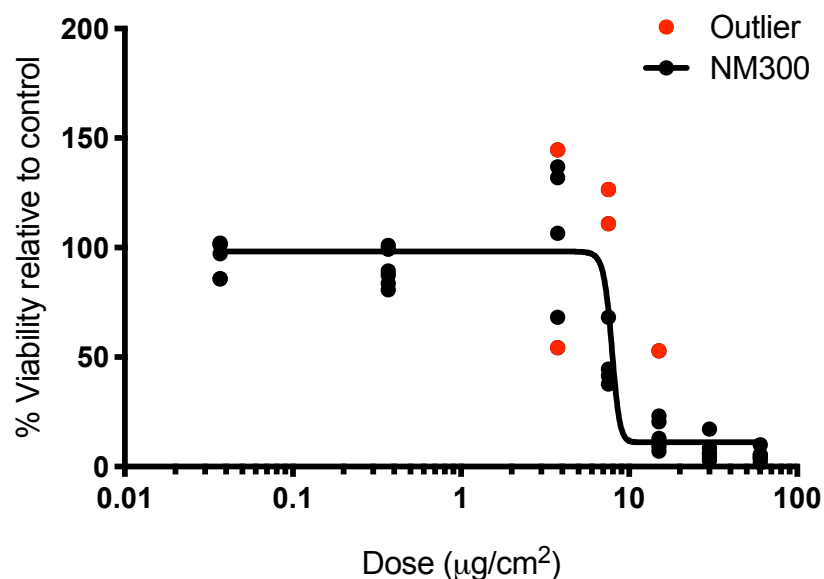


Figure 20: Non-linear curve showing toxicity of NM-300 to TM3 cells. Doses 0.037-60.24µg/cm². N=6. The data output was tested for normality using both the D'Agostino-Pearson omnibus normality test and the Shapiro-Wilk normality test, residuals were plotted, and outliers counted using the ROUT coefficient. Outliers are highlighted in red. The LC₅₀ value was identified to be 7.885µg/cm².

The curve fit for NM-300 gave an R² value of 0.7826 and reported that the data did not appear to be normally distributed (n/s D'agostino-Pearson, p=0021** Shapiro-Wilk). ROUT analysis identified key outliers within the 3.76 and 7.53µg/cm² doses, where the greatest variation was reported for this NM (shown in red within Fig. 20). To further characterise the dose-response curve, the 2 doses with high variation were removed and the data re-plotted. Results of this curve fit showed a much-improved curve fit (R² = 0.9802), normal distribution of the data and identified no further outliers. The regression gave an LC₅₀ value of 7.885µg/cm² for NM-300.

Results of the curve fit for AgNO₃ showed an R² value of 0.9398, and that the data was not normally distributed (n/s D'agostino-Pearson, p=0.0433* Shapiro-Wilk). ROUT analysis identified one outlier value at the 0.370µg/cm² dose (Fig. 21). To further characterise the dose-response curve, the doses with high variation were removed and the data re-plotted. Results of this curve fit revealed an improved R² value of 0.9802, and that there were no further outliers in the data. Regression analysis produced an LC₅₀ value of 0.282µg/cm² for AgNO₃.

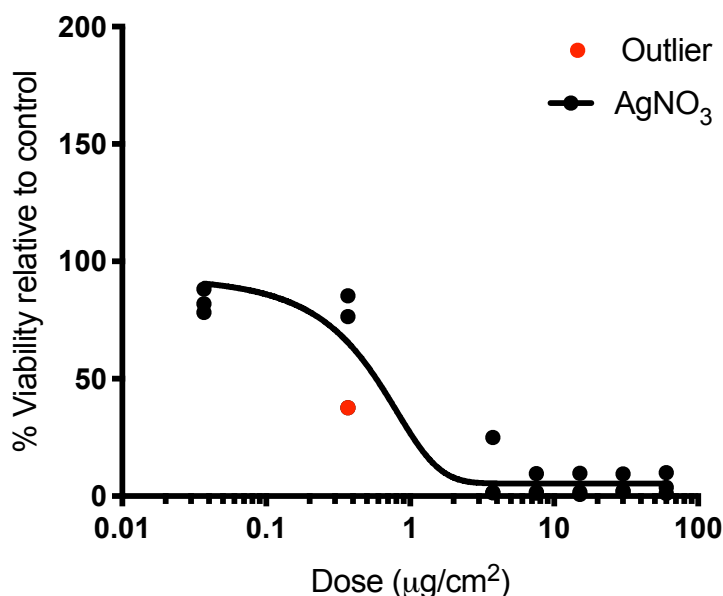


Figure 21: Non-linear curve showing toxicity of AgNO₃ to TM3 cells. Doses 0.037-60.24µg/cm². N=6. The data output was tested for normality using both the D'Agostino-Pearson omnibus normality test and the Shapiro-Wilk normality test, residuals were plotted, and outliers counted using the ROUT coefficient. Outliers are highlighted in red. The LC₅₀ value was identified to be 6.052µg/cm².

Toxicity of NM-300 and AgNO₃ was confirmed by one-way ANOVA, which showed a significant effect for NM-300 (p<0.001***) and AgNO₃ (p=0.0055**). For NM-300, results show a high degree of variance between replicates of the assay at 3.76µg/cm² and 7.53µg/cm², the dose around which a significant drop in viability was observed (Fig. 19). As such, toxicity was not statistically significant until 15.06µg/cm² (P<0.001***). The linear regression confirmed an LC₅₀ value of 7.85µg/cm².

ANOVA of NM-300Dis also showed significance in viability changes across the dose range (p=0.027*). A Dunnett's multiple comparison test suggested that there was significant change in viability following exposure for doses in the middle of the range of exposures (3.76 and 15.06µg/cm², P<0.05*).

For ionic silver (AgNO_3), significance in dose-response toxicity established by one-way ANOVA ($p=0.055^{**}$). Multiple comparisons confirmed that this change was significant from $3.76\mu\text{g}/\text{cm}^2$.

WST-1 Analysis – Carbon Nanotubes (NM-400, 401 and 403)

Cytotoxicity appraisal for three CNT of varying length and diameter (NM-400, 401 and 403) is summarised in Fig. 22 and 23.

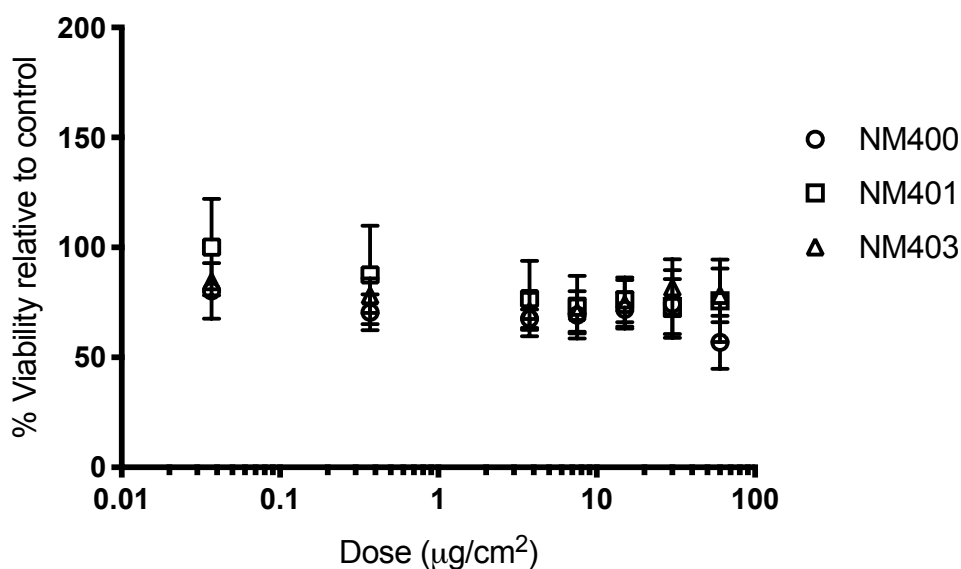


Figure 22: Viability of cells cultured in charcoal stripped serum, following 24h exposure to carbon nanotubes (NM-400, 401 & 403), assessed using the WST-1 cytotoxicity assay ($n=3$). Viability expressed as % relative to untreated (endogenous) control. Doses from 0.037 - $60.24\mu\text{g}/\text{cm}^2$. All values corrected for WST-1 interference with assay.

Initial appraisal of the graphed results shows limited change in TM3 cell viability following exposure to CNTs, except perhaps at the higher doses applied. One-way ANOVA indicated no significant change in viability for NM 400 and NM-401. However, a significant effect on viability was identified following exposure to NM-403 ($p=0.0443^*$). Further investigation confirmed there was no paired change in NM-400 or NM-401 and showed that significant differences were observed between untreated and $0.037\mu\text{g}/\text{cm}^2$ in NM-403 ($P=0.0093^{**}$).

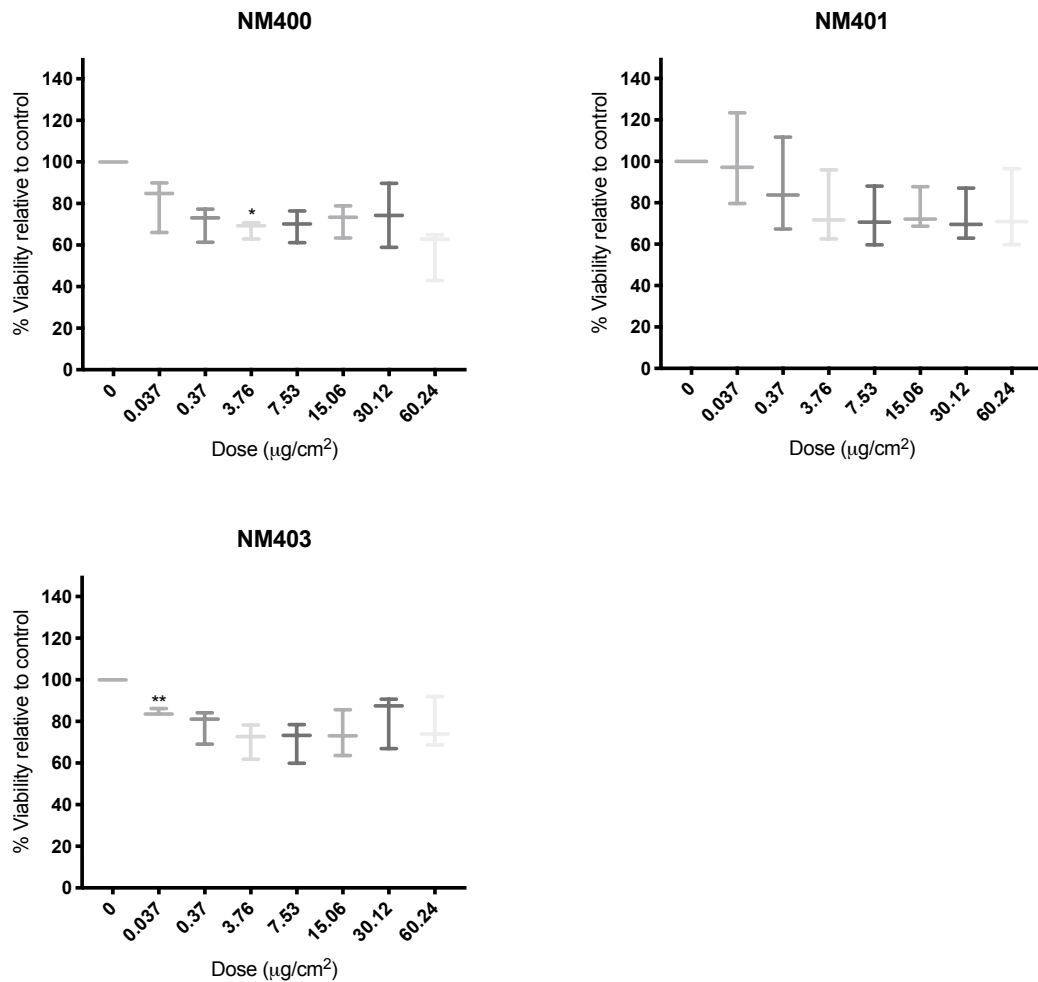


Figure 23: Box and Whiskers representation of viability of TM3 cells cultured in charcoal stripped serum, following 24h exposure to Carbon Nanotubes (NM-400, NM-401 & NM-403) using the WST-1 cytotoxicity assay (n=3). Doses 0.037-60.24μg/cm². All values corrected for WST-1 and interference with assay. Dose 0 is untreated (negative) control. Where a statistically significant loss in viability of cells was identified compared to control, asterisks depict level of significance (* p=0.05, ** p=0.01, *** p=0.001 & **** p=0.0001).

WST-1 Analysis – Pristine Copper Oxide Nanotubes (CuO)

Cytotoxicity assessment following exposure of TM3 cells to pristine copper oxide ENM is shown in Fig. 24.

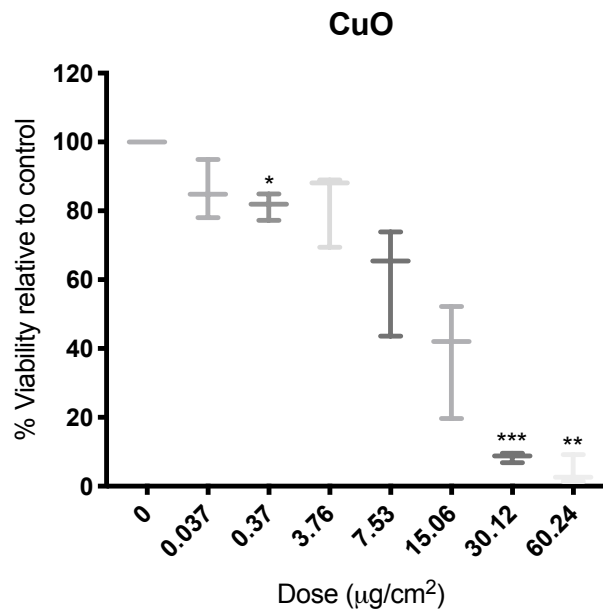


Figure 24: Box and Whiskers representation of viability of TM3 cells cultured in charcoal stripped serum, following 24h exposure to pristine copper oxide using the WST-1 cytotoxicity assay (n=3). Doses 0.037-60.24µg/cm². All values corrected for WST-1 interference with assay. Dose 0 is untreated (negative) control. Where a statistically significant loss in viability of cells was identified compared to control, asterisks depict level of significance (* p=0.05, ** p=0.01, *** p=0.001 & **** p=0.0001).

Exposure to CuO resulted in dose-response toxicity, with viability decreasing as dose increased. One-way ANOVA confirmed significance of this change (p=0.0150*), and Dunnett's multiple comparison confirmed showed that significant differences between untreated and 0.037, 30.12 and 60.24µg/cm² in NM-400. To further investigate the nature of this dose-response relationship, a non-linear curve was fitted to the results. Figure 25 shows the raw data fitted to a log(inhibitor) vs. response (three parameter) curve. The R² value of the line was 0.8591, with data reporting as normal in both tests undertaken, and no outliers identified. This allowed identification of an LC₅₀ value of 7.752µg/cm² for pristine CuO.

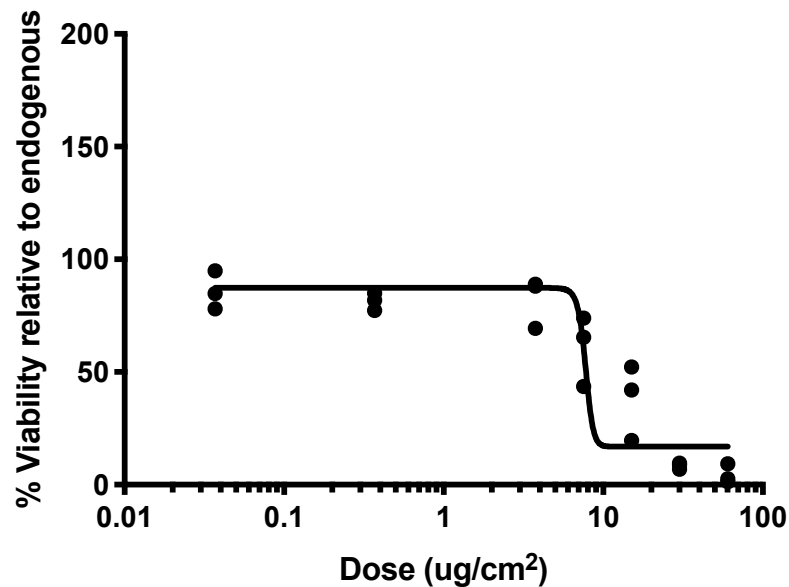


Figure 25: Non-linear curve showing toxicity of pristine CuO to TM3 cells. Doses 0.037-60.24 $\mu\text{g}/\text{cm}^2$. N=3. The data output was tested for normality using both the D'Agostino-Pearson omnibus normality test and the Shapiro-Wilk normality test, residuals were plotted, and outliers counted using the ROUT coefficient. Outliers are highlighted in red. The LC₅₀ value was identified to be 7.752 $\mu\text{g}/\text{cm}^2$.

Time Course Appraisal of Cytotoxicity

Following identification of nanomaterials that had a negative impact on cell viability and associated LC₅₀ values, it was appropriate to identify the impact of time on this response. Timecourse studies were undertaken for ENM of interest, namely titanium dioxide NM-101 (used as a control as WST-1 revealed no toxicity following exposure), both uncoated (NM-110) and coated (NM-111) zinc oxide, and silver (NM-300).

The study was conducted using the standard dose range (0.037 $\mu\text{g}/\text{cm}^2$ to 60.24 $\mu\text{g}/\text{cm}^2$) and a lower dose range (0.023 – 3.75 $\mu\text{g}/\text{cm}^2$) informed by the results of cytotoxicity evaluation using the WST-1 assay, with the aim of identifying sub-lethal doses which could be used to guide analysis of functional changes within the cells following ENM exposure.

All results underwent a correction for interference from ENM, as it was noted from 'no ENM' controls in initial assays that ENM appeared to interfere marginally in readings. It was also noted that for all ENM tested, there were seemingly erroneous readings and huge variance in results at t=24h, leading to questions around suitability of this timepoint for measurement of viability using the Alamar Blue assay.

TM3 Timecourse study - Titanium Dioxide (NM-101): High dose range

Following NM-101 treatment, analysis shows a dose- and time- response dependent effect on viability (Fig. 26). At 24h the variation in results is large and shows a decrease in toxicity at higher doses compared to earlier timepoints. As the results at the 24hour timepoint were such a departure from the pattern observable through the other times, the ANOVA was repeated without the 24hr time data. This showed time ($p=0.0065^{**}$) and dose ($p<0.0001^{****}$) were still significant.

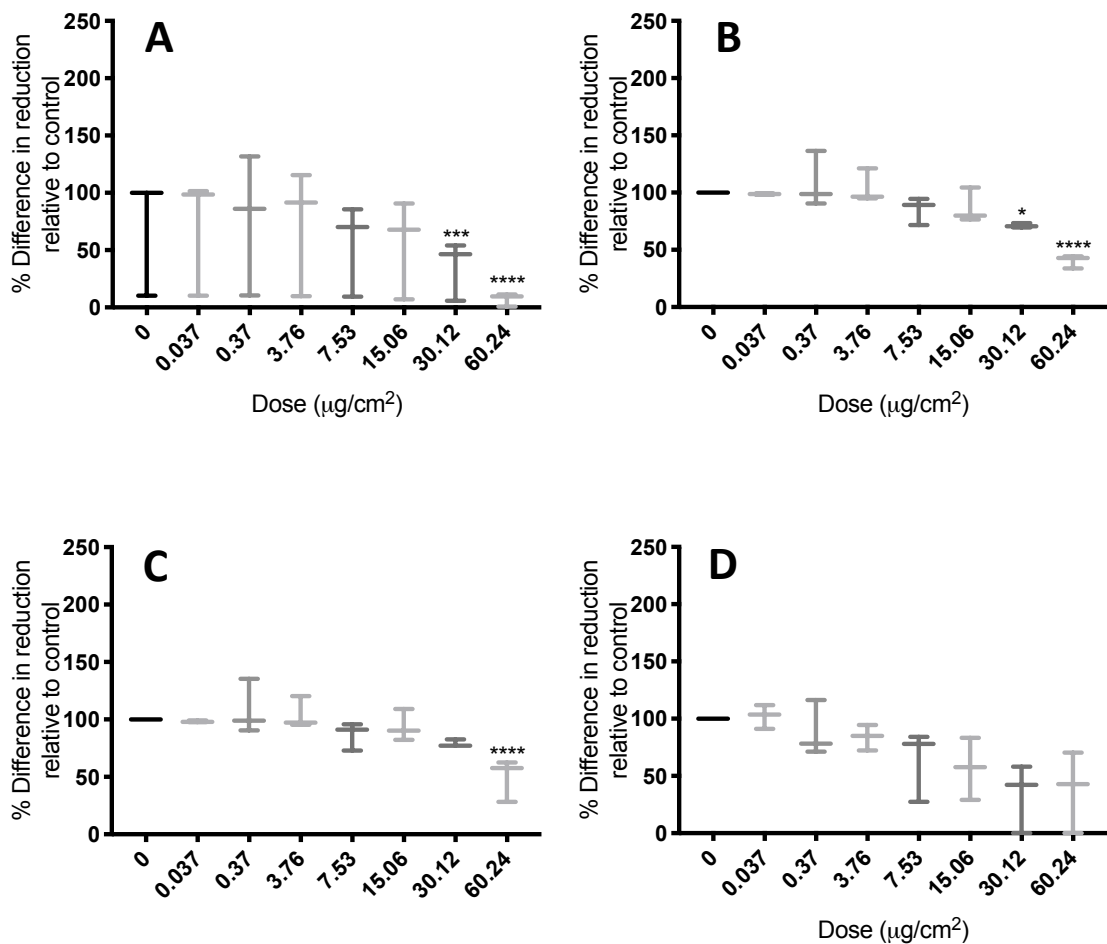


Figure 26: Timecourse assay following exposure to TiO₂ (NM-101) at the high dose range 0.037μg/cm² to 60.24μg/cm² in the presence of Alamar Blue (n=3). Timepoints represented: A = t2h, B = t4h, C = t6h, D = t24h. Where a statistically significant loss in viability of cells was identified compared to control, asterisks depict level of significance (* $p=0.05$, ** $p=0.01$, *** $p=0.001$ & **** $p=0.0001$).

TM3 Timecourse study - Titanium Dioxide (NM-101): Low dose range

At the low dose range of 0.023 – 3.75 $\mu\text{g}/\text{cm}^2$, NM-101 had little effect on the viability of cells except at the highest doses (Fig 27). Statistical analysis indicates that while there was no change in response with time, there was a significant effect from dose ($p=0.014^{**}$) on cells' ability to reduce Alamar blue. However, a Dunnett's test did not show any significant departure from control in any of the treatments at any timepoint, therefore it is likely that the findings of the ANOVA are influenced by the huge variance in readings at higher doses, which could quite easily skew results given ANOVA is based on the assumption of equal variance within all samples. Interestingly at the 24-hour measurement, higher doses of NM-101 seem to increase cell ability to reduce Alamar blue, before dropping off sharply at the highest dose.

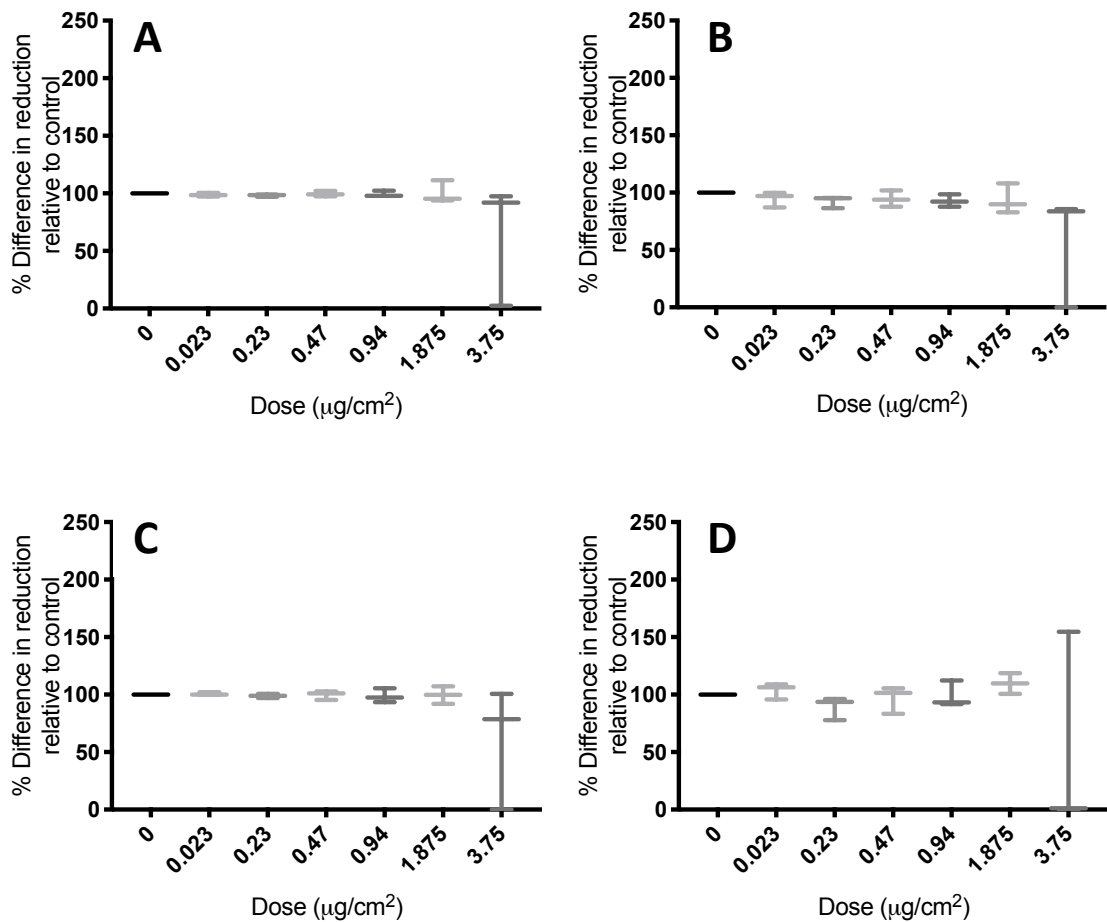


Figure 27: Timecourse assay following exposure to TiO_2 (NM-101) at the low dose range 0.037 $\mu\text{g}/\text{cm}^2$ to 60.24 $\mu\text{g}/\text{cm}^2$ in the presence of Alamar Blue ($n=3$). Timepoints represented: A = 2h, B = 4h, C = 6h, D = 24h. Where a statistically significant loss in viability of cells was identified compared to control, asterisks depict level of significance (* $p=0.05$, ** $p=0.01$, *** $p=0.001$ & **** $p=0.0001$).

TM3 Timecourse study – Zinc Oxide (NM-110): High dose range

For NM-110, a decrease in viability with increasing dose was present, which appeared to increase with time (Fig. 28). A clear reduction in viability of cells appears at a low dose (3.76µg/cm²) for 2h, 4h and 6h timepoints. Again, at 24h the variation in results is such that it is difficult to identify a clear pattern at first examination. 2-way ANOVA of the results revealed no interaction between time and dose, but was significant for time and dose effects individually (p<0.0001****). As previously, removal of the 24h timepoint from the analysis altered the outcome considerably, this time showing no significant effect of time on the result, but a significant decrease in cells' ability to reduce AB with increasing dose (P<0.0001****). Multiple comparisons showed no significant difference between data compared to control for the 2h timepoint, however at 4h and 6h the highest dose was found to be significantly different to control (p<0.001*** and p<0.01** respectively).

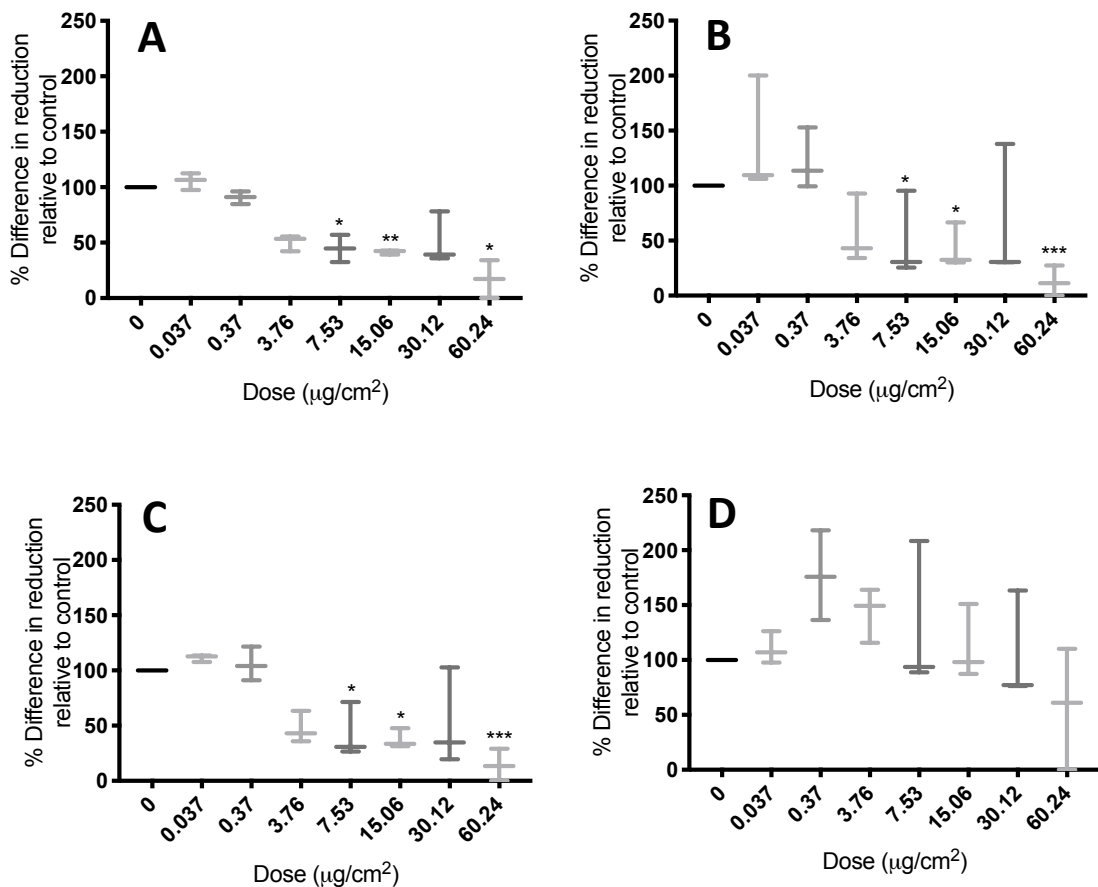


Figure 28: Timecourse assay following exposure to uncoated ZnO (NM-110) at the high dose range 0.037µg/cm² to 60.24µg/cm² in the presence of Alamar Blue (n=3). Timepoints represented: A = t2h, B = t4h, C = t6h, D = t24h. Where a statistically significant loss in viability of cells was identified compared to control, asterisks depict level of significance (* p=0.05, ** p=0.01, *** p=0.001 & **** p=0.0001).

TM3 Timecourse study - Zinc Oxide (NM-110): Low dose range

At the lower dose range, NM-110 treated cells appeared to show a clear decrease in viability in cells exposed to doses of 1.875 $\mu\text{g}/\text{cm}^2$ and above at 2h, 4h and 6h timepoints, becoming more pronounced as time progressed (Fig. 29). As with previous tests, the results at 24hours show an apparent increase in cellular activity, followed by sharp decrease at the highest dose, but with such heavy variation it was not immediately clear if this was a meaningful response. 2-way ANOVA using all datasets gives a significant outcome for both dose ($p=0.001^{**}$) and time ($p=0.0002^{***}$). However, it was clear that the 24hour timepoint results were skewing the statistical analysis. This was confirmed by ANOVA, which reported a significant effect of dose on reduction of Alamar blue ($p<0.0001^{****}$) but no effect of time on the outcome after removal of the 24h readings.

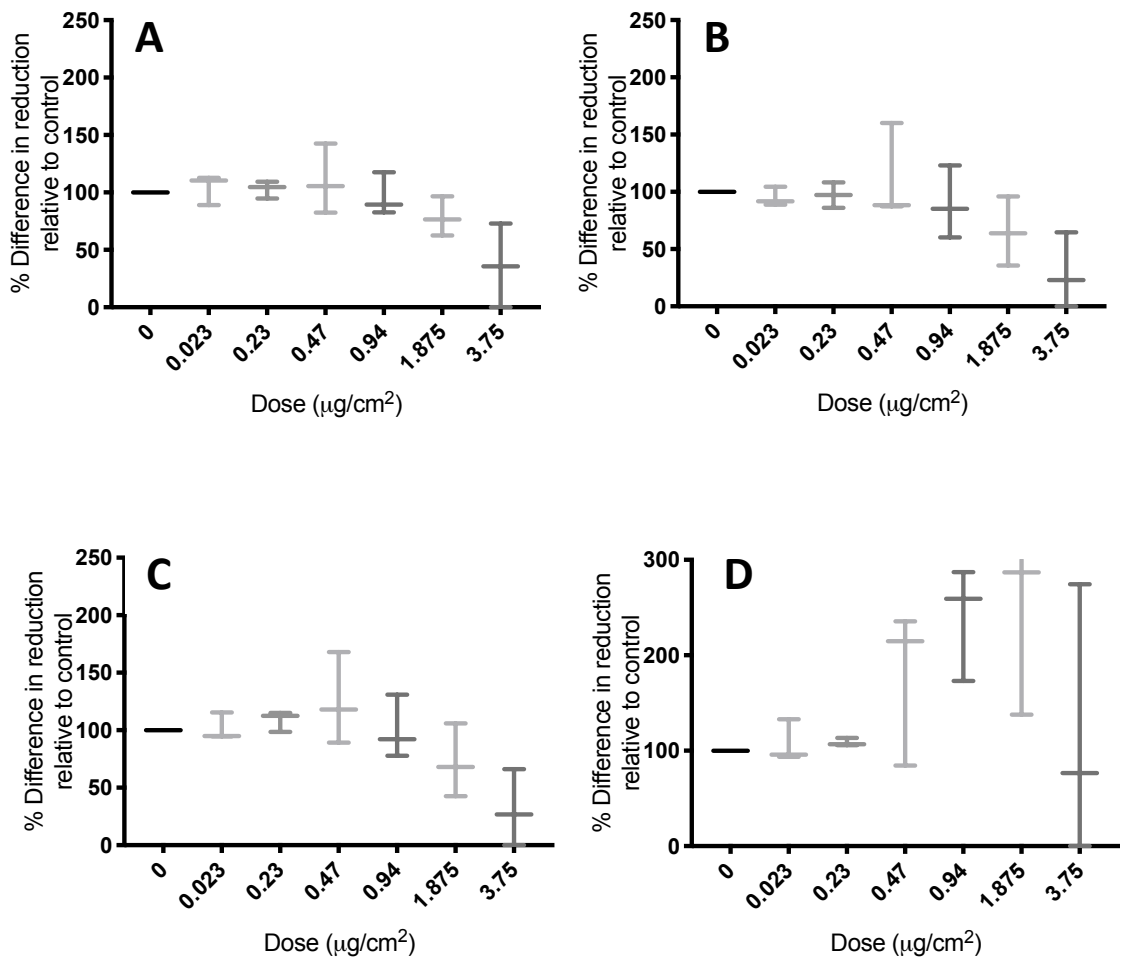


Figure 29: Timecourse assay following exposure to uncoated ZnO (NM-110) at the low dose range 0.037 $\mu\text{g}/\text{cm}^2$ to 60.24 $\mu\text{g}/\text{cm}^2$ in the presence of Alamar Blue (n=3). Timepoints represented: A = t2h, B = t4h, C = t6h, D = t24h. Note the adjusted Y axis on (D) to incorporate increased variability in readings. Where a statistically significant loss in viability of cells was identified compared to control, asterisks depict level of significance (* $p=0.05$, ** $p=0.01$, *** $p=0.001$ & **** $p=0.0001$).

TM3 Timecourse study - Zinc Oxide (NM-111): High dose range

NM-111 showed a dose-response toxicity over the high dose range, with loss of cell viability $>3.76\mu\text{g}/\text{cm}^2$ at t2h, t4h and t6h timepoints (Fig. 30). Again, at t24h the variation in results makes it difficult to interpret the outcome. 2-way ANOVA showed no interaction between time and dose on the result, but gave a significant outcome for effect of time and dose separately on the result ($\leq p < 0.0001$ ****). The 24hour timepoint appeared to be skewing the statistical analysis, and its removal revealed significance of time on ability of cells to reduce Alamar Blue ($p = 0.0218^*$) whilst maintaining significance in relation to dose effect ($p < 0.0001$ ****). For all timepoints, multiple comparisons showed a significant change in cells' ability to reduce AB at doses of $3.76\mu\text{g}/\text{cm}^2$ and above, with assigned significance of $p < 0.001$ *** at 2hours, and $p < 0.0001$ **** at 4 and 6 hours.

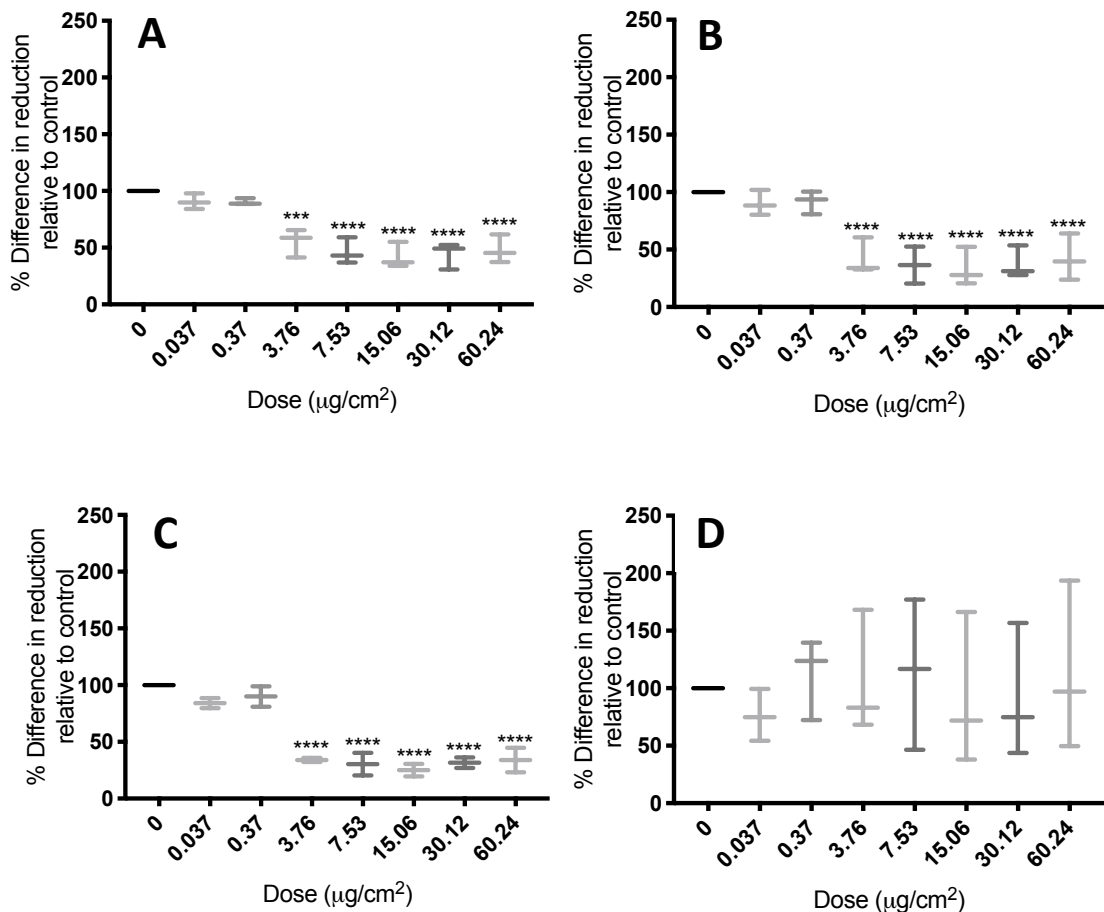


Figure 30: Timecourse assay following exposure to coated ZnO (NM-111) at the high dose range $0.037\mu\text{g}/\text{cm}^2$ to $60.24\mu\text{g}/\text{cm}^2$ in the presence of Alamar Blue ($n=3$). Timepoints represented: A = t2h, B = t4h, C = t6h, D = t24h. Where a statistically significant loss in viability of cells was identified compared to control, asterisks depict level of significance (* $p=0.05$, ** $p=0.01$, *** $p=0.001$ & **** $p=0.0001$).

TM3 Timecourse study - Zinc Oxide (NM-111): Low dose range

At a low dose range, NM-111 treated cells showed a decrease in viability at doses of $0.94\mu\text{g}/\text{cm}^2$ and above at 2, 4 & 6h readings, which seemed to become more marked as time progressed (Fig. 31). 2-way ANOVA of the full dataset reported a significant effect of time on results ($p=0.0001^{***}$) but no significant effect of dose on the outcome. As with previous materials, large variance in results at the 24h timepoint appeared to be sufficient to skew statistical analysis. As the results at the three earlier timepoints appear to show a clear dose-response effect, the ANOVA was repeated without the 24h data, and this confirmed a significant effect of dose on outcome ($p<0.0001^{****}$) but time-driven effect. Further examination of the data post-hoc using multiple comparisons showed that the effect of dose was significant from $1.875\mu\text{g}/\text{cm}^2$ at 2h ($p=0.0231^*$), $0.094\mu\text{g}/\text{cm}^2$ at 4h ($p=0.0277^*$) and $1.875\mu\text{g}/\text{cm}^2$ at 6h ($p<0.0001^{****}$).

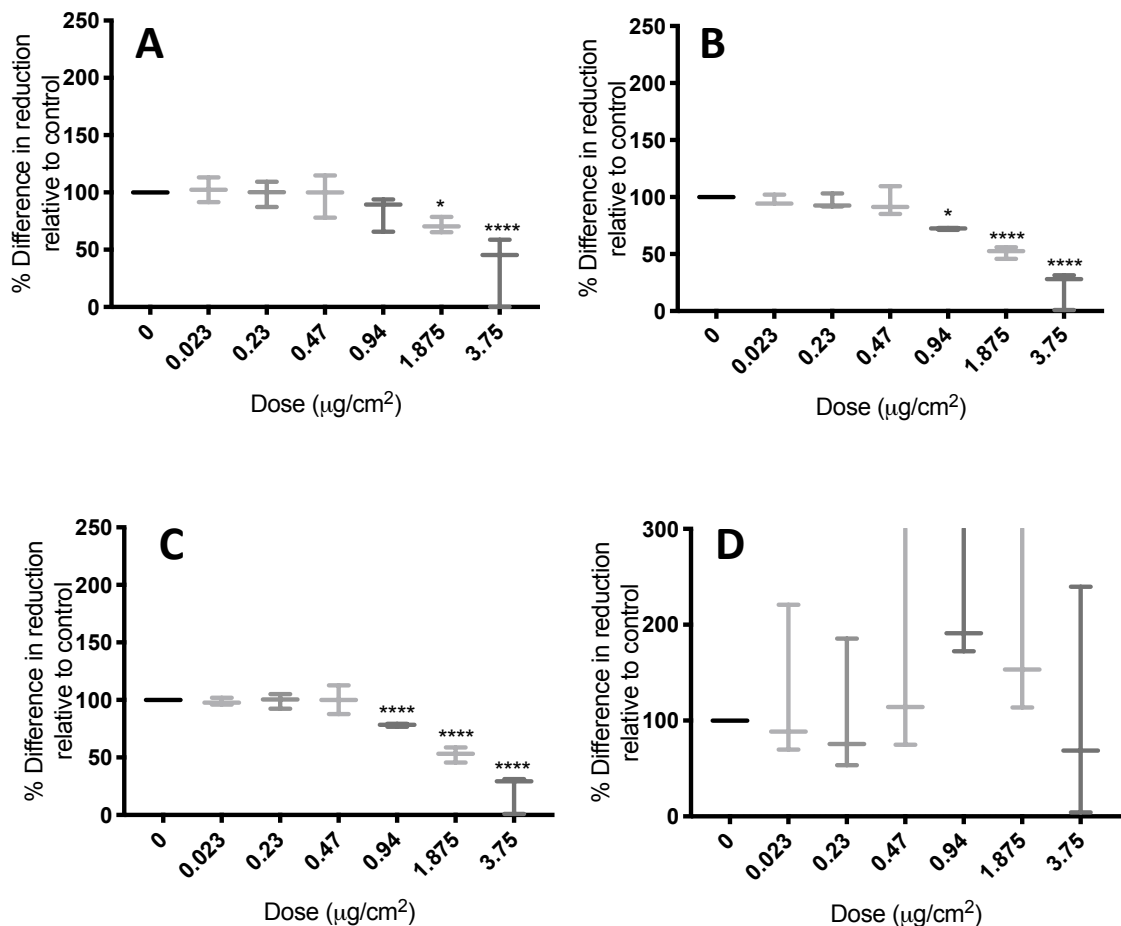


Figure 31: Timecourse assay following exposure to coated ZnO (NM-111) at the low dose range $0.037\mu\text{g}/\text{cm}^2$ to $60.24\mu\text{g}/\text{cm}^2$ in the presence of Alamar Blue ($n=3$). Timepoints represented: A = t2h, B = t4h, C = t6h, D = t24h. Note the y axis scale on (D) is increased to incorporate variance in readings. Where a statistically significant loss in viability of cells was identified compared to control, asterisks depict level of significance (* $p=0.05$, ** $p=0.01$, *** $p=0.001$ & **** $p=0.0001$).

TM3 Timecourse study - Silver (NM-300): High dose range

For NM-300, results show a wide range of viability with large variation and there is no observable pattern in the results (Fig 32). 2-way ANOVA confirmed that variance in the dataset meant that neither dose nor time had a significant effect on cells' ability to reduce Alamar blue.

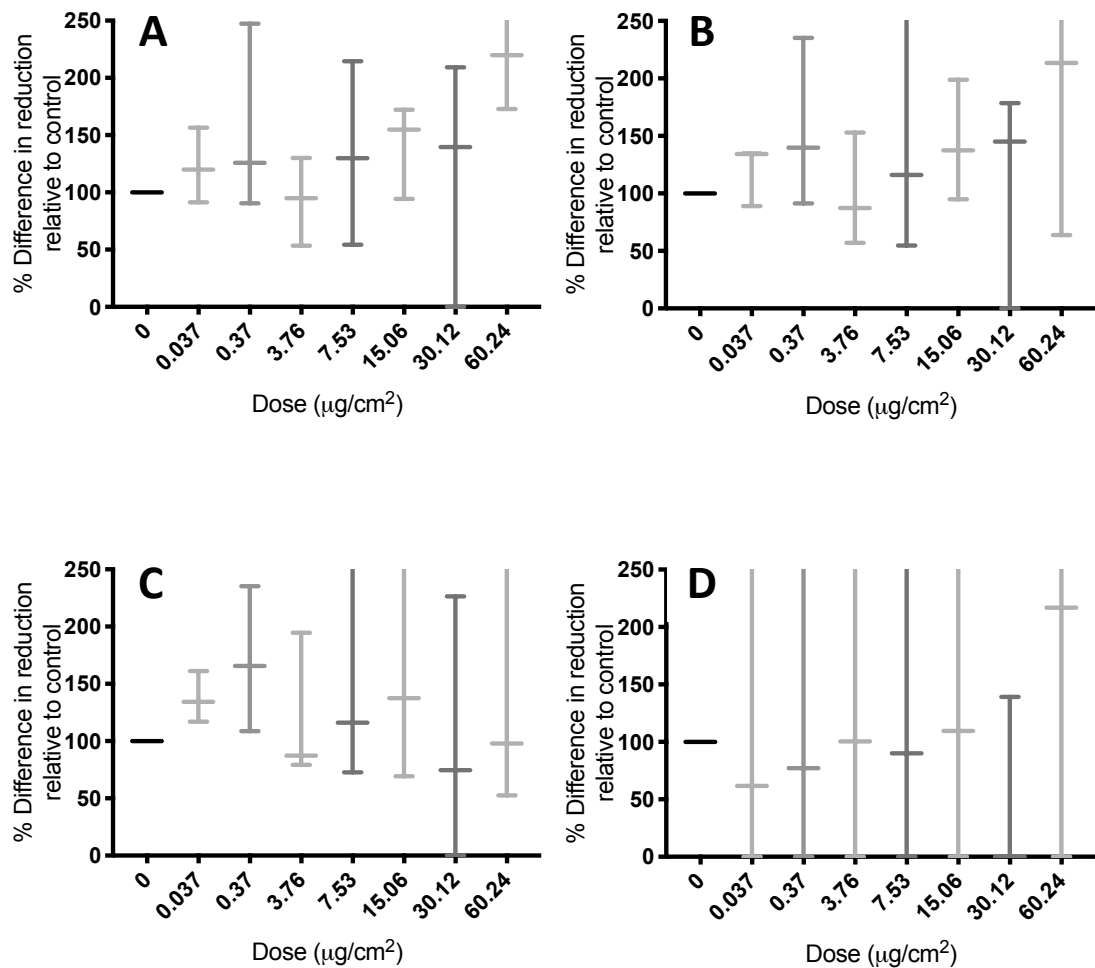


Figure 32: Timecourse assay following exposure to silver (NM-300) at the high dose range 0.037µg/cm² to 60.24µg/cm² in the presence of Alamar Blue (n=3). Timepoints represented: A = t2h, B = t4h, C = t6h, D = t24h. Where a statistically significant loss in viability of cells was identified compared to control, asterisks depict level of significance (* p=0.05, ** p=0.01, *** p=0.001 & **** p=0.0001).

TM3 Timecourse study - Silver (NM-300): Low dose range

At the low dose range, the NM-300 treated cells appear to show a slight increase in cellular reduction of Alamar blue followed by a decrease when compared to endogenous from 1.875 $\mu\text{g}/\text{cm}^2$ and above at the 2h timepoint (Fig 33). At 4h, this decrease appears to begin at a lower dose of 0.94 $\mu\text{g}/\text{cm}^2$. However, the 6h and 24h timepoints appear to show an initial increase in reduction of Alamar blue, followed by a decrease at the highest doses, albeit with large variance in data recorded around the mean. 2-way ANOVA of the full dataset showed a significant effect from both time ($p=0.023^{**}$) and dose ($p=0.0001^{***}$) on the results. Multiple comparisons seem to show a significant dose response within only the mid doses of 2h and 4h readings (the highest readings).

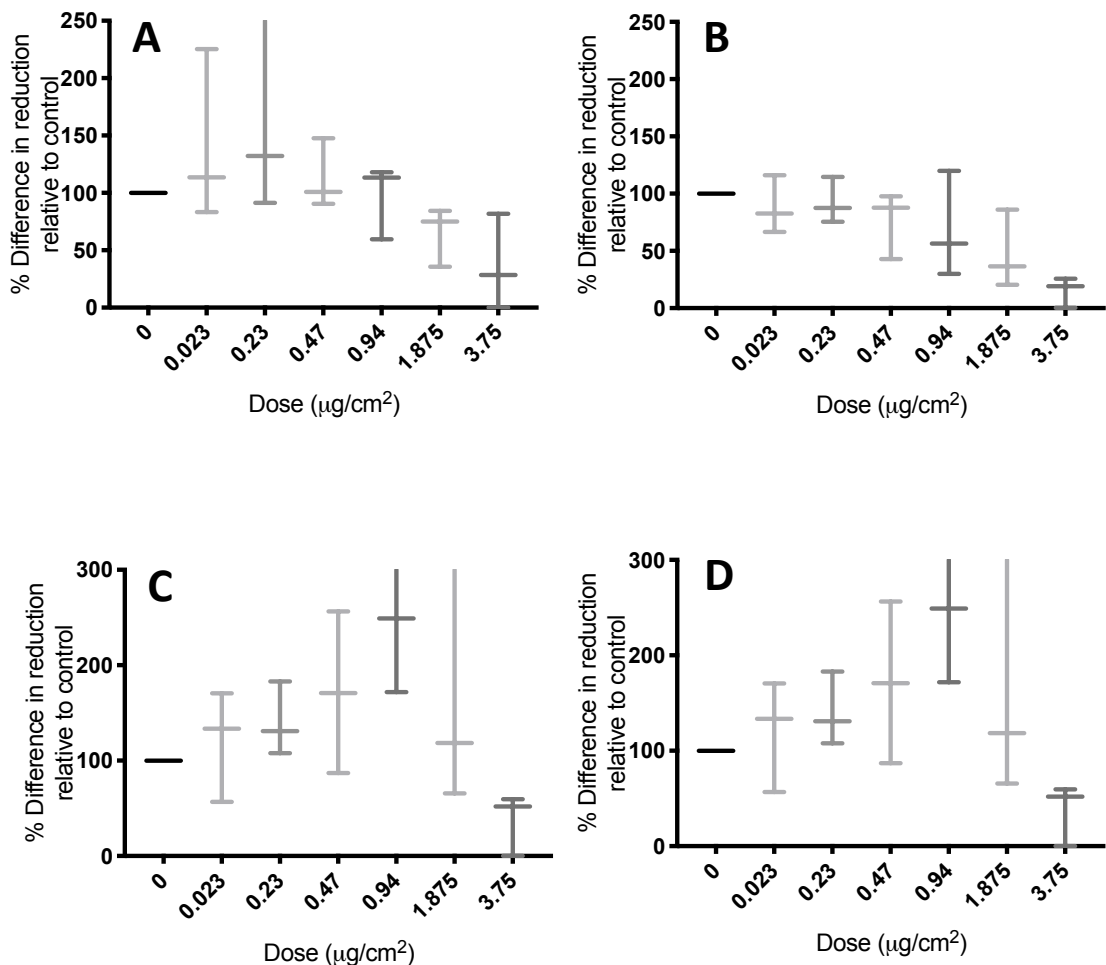


Figure 33: Timecourse assay following exposure to silver (NM-300) at the low dose range 0.037 $\mu\text{g}/\text{cm}^2$ to 60.24 $\mu\text{g}/\text{cm}^2$ in the presence of Alamar Blue ($n=3$). Timepoints represented: A = t2h, B = t4h, C = t6h, D = t24h. Note the y axis scale on (C & D) is increased to incorporate variance in readings. Where a statistically significant loss in viability of cells was identified compared to control, asterisks depict level of significance (* $p=0.05$, ** $p=0.01$, *** $p=0.001$ & **** $p=0.0001$).

TM3 Timecourse study – Silver dispersant (NM-300dis): Control testing

A single replicate AB assay was undertaken for NM-300dis (dispersant liquid only), to examine whether the dispersant could contribute to any observed toxicity. Appraisal of results indicates that dispersant alone had no effect on overall cell viability (Fig. 34). No statistical analysis was undertaken as this experiment was carried out as a single replicate.

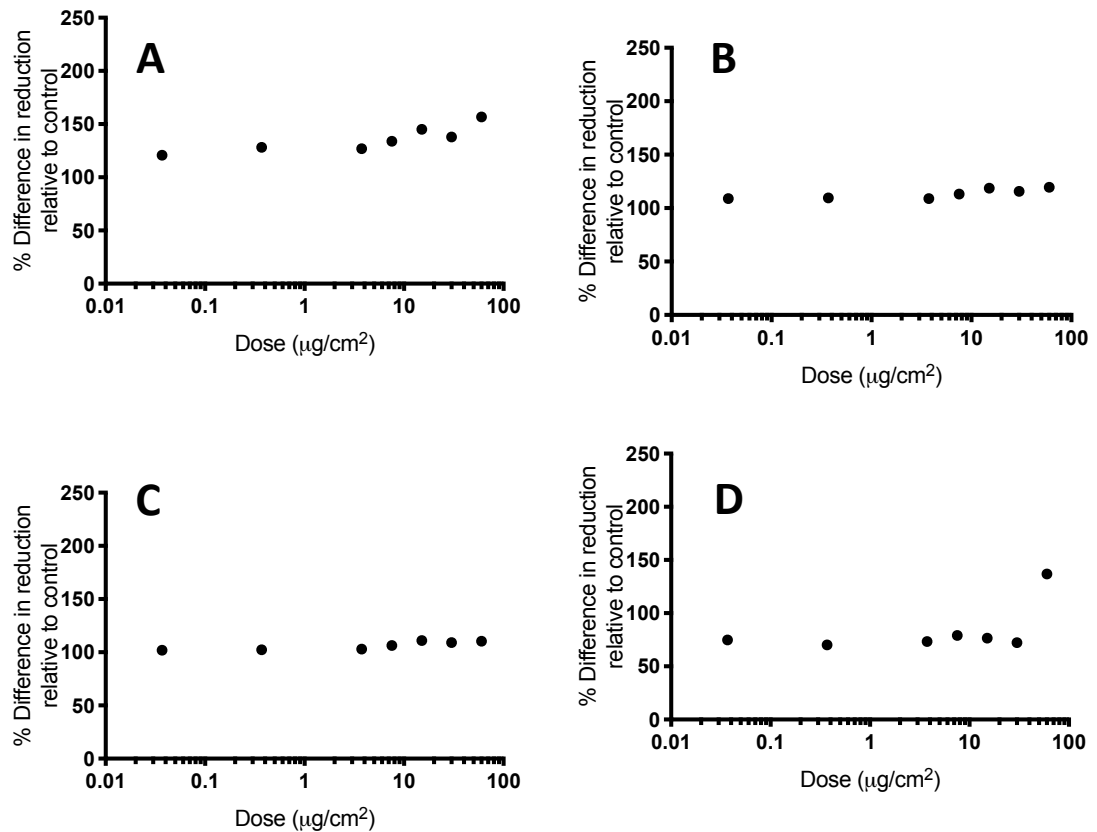


Figure 34: Timecourse assay following exposure to silver dispersant (NM-300dis) at the high dose range $0.037\mu\text{g}/\text{cm}^2$ to $60.24\mu\text{g}/\text{cm}^2$ in the presence of Alamar Blue (n=1). Timepoints represented: A = t2h, B = t4h, C = t6h, D = t24h. Where a statistically significant loss in viability of cells was identified compared to control, asterisks depict level of significance (* p=0.05, ** p=0.01, *** p=0.001 & **** p=0.0001).

Discussion

To begin work toward developing suitable *in vitro* methods by which to study nanotoxicity in the male reproductive system, basic toxicity testing was undertaken using an established panel of reference ENM and the mouse Leydig cell line, TM3. Following this, the influence of time- and dose- on response was investigated, and where possible an LC₅₀ was identified to guide development of further investigation into whether ENM alter normal cell function at sub-lethal doses. In parallel with this, the suitability of WST-1 and Alamar Blue assays for investigation of ENM toxicity *in vitro* was also considered.

Optimisation of protocols: assay interference and future endocrine work

The FBS used routinely in cell culture contains a number of growth factors and hormones involved in cell growth promotion. Because later work in this thesis aimed to examine endpoints relating to steroidogenesis and local function of receptors, enzymes and proteins related to the HPG axis, it was important to minimise interference in any results from such exogenous steroid, peptide and thyroid hormones, growth factors and other lipophilic materials via use of charcoal-stripped FBS.

Exploration of the impact of serum type on findings via the WST-1 assay revealed no major difference in results between charcoal-stripped FBS and standard FBS used alongside medium comprised of Dulbecco's Modified Eagle's Medium/Nutrient Mixture F-12 Ham 500ml with L-glutamine, 15mM HEPES, and sodium bicarbonate. This meant that all following experiments outlined within this thesis were undertaken using charcoal-stripped FBS, giving a higher confidence in the outcome of further work to establish the functional basis of any toxicity observed on endocrine endpoints.

It must be recognised that some ENM have been shown to absorb proteins and form a protein corona which may influence their uptake and fate (Kermanizadeh et al., 2013). However, it remains relevant to expose cells in medium containing some serum, as any ENM reaching the testis following exposure *in vivo* would be exposed to a multitude of proteins along the way. Therefore, we feel use of charcoal-stripped serum is a good

compromise between stunted cell growth in serum-free system and potentially dubious results to the outcome of planned endocrine endpoints via addition of traditional FBS.

The setup of the WST-1 cell proliferation and Alamar Blue timecourse assay was such that it was easy to identify any source of interference. Before analysis, each set of results was therefore examined for potential interference from ENM or other sources. In all WST-1 assays, the 'cells + WST-1' control showed that WST-1 dye had a marginal interference in readings, leading to small increases in % viability of cells relative to control. On this basis, all outputs were corrected for WST-1 during final analysis to ensure that results were not skewed. Interestingly, in those assays using NM-300 or AgNO₃, interference from ENM was also noted, as such, an additional correction for this interference was put in place. In all of the Alamar Blue assays undertaken, a low level of interference from ENM but no interference of Alamar blue was observed on the absorbance readings taken. Based on this, all results were corrected for ENM to ensure this did not skew results.

Interference of ENM with *in vitro* toxicity assays is a relatively commonly reported occurrence, especially where optical detection methods are used. In 2012, Kroll et al recommended that in each *in vitro* test system, evaluation for each single nanoparticle type should be undertaken, as ENM may interfere in classic cytotoxicity assays (such as the lactate dehydrogenase or MTT assays) in concentration- particle- and assay- specific manner (Kroll et al., 2012). Despite this, many studies published still make little attempt to include consideration of this potential effect, making its inclusion here was especially important. From these results it can be concluded that the assays produced a reproducible assessment of toxicity for the cell line and materials in question.

Cytotoxicity and time- and dose- dependent effects

A variety of ENM-specific outcomes were identified. For ease of consideration, these are reported per nanomaterial.

Titanium dioxide (NM-101, 103 & 104)

The first ENM tested were TiO₂ NM-101 (anatase), NM-103 (hydrophobic) and NM-104 (hydrophilic). Exposure to NM-101 showed no change in viability of cells, with little variation. Exposure to NM-103 and 104 showed a small decrease in viability to 73% at

the highest dose applied for NM-103 and no change to viability for NM-104. However, there was much greater variability in results recorded for these ENM, which most likely accounted for the decrease in average viability reported. This finding is in agreement with those reported for 8 other cell lines from 6 other systems/organs in the body as part of a major screening study published from this work in 2015, allowing the conclusion to be reached that the TiO₂ ENM tested were not cytotoxic (Farcas et al., 2015). Because results for NM-101 showed the least variation and greatest comparability to other organs/systems reported, it was selected as a control material for timecourse assays reported here, and future investigation of changes to TM3 cells at the functional level, reported in Chapter 4.

The Alamar Blue results for titanium dioxide NM-101 showed that of the two dose ranges tested, a significant effect on cells' ability to reduce AB was only observed for the highest two doses in the high dose range (30.12 and 60.24µg/cm²) from 2 hours onwards. Consultation of the literature suggests this toxicity may be linked to the materials' catalytic properties, which are in turn linked to its crystalline structure. TiO₂ comes in two main forms, anatase (as with NM-101) and rutile. It has been shown that as particles become smaller, their toxicity appears to increase, with anatase being more biologically active than rutile for the endpoints of cytotoxicity or oxidative DNA damage (Auffman et al., 2009). Therefore, although statistically significant, it is most likely that the findings are because of the enormous amount of TiO₂ added to the cells rather than because of any specific toxicity. Indeed, TiO₂ ENM are used within many consumer products such as sunscreens with no reported adverse effects to health.

Silica dioxide (NM-200 & 203)

Silica dioxide (NM-200 & 203) reported little change in viability of cells compared to control, except for NM-203 at the highest doses. The finding of a significant decrease in viability from control reported for NM-203 was likely due to the low standard deviation across replicates, which meant that any small variation in mean viability produced a significant result. As such, neither NM-200 nor NM-203 were considered to impact viability sufficiently to warrant their progression to subsequent sub-lethal toxicity studies, at least initially. Interestingly, a recently published study investigating the influence of mesoporous silica ENM on the WST-1 assay indicated that it occasionally

underestimated toxicity, leading to viabilities exceeding 100%. However, no such effect was identified here, suggesting that this may be either an ENM- or cell line- specific effect (Braun et al., 2018).

It is interesting that method of manufacture appears to have an effect on the toxicity, as precipitated SiO₂ (NM-200) did not decrease cell viability whereas thermally produced SiO₂. This result is comparable to that of Barkalina *et al*, who found no effect of mesoporous silica on the functions of mammalian boar sperm *in vitro* (Barkalina et al., 2014). Interestingly, when compared to other cell types from different organ systems, the effect of SiO₂ appears to be organ-dependent, as toxicity was identified to the MH-S alveolar macrophage cell line, and the mES embryonic stem cell line (Farcas et al., 2015).

Outcomes from *in vivo* studies report similar variation in findings, which appear to be dependent on the characteristics of ENM used, dose and exposure route. For example, Morishita *et al* found no adverse effects to testicular tissues following intravenous injection of 0.8mg 70nm or 300nm silica particles, and Bara *et al* found mesoporous silica nanoparticles (MSN) to be comparatively safer than zinc oxide ENM in swiss albino dams and pups following oral exposure to 50 or 250mg/kg does during gestation days 15-19 (Morishita et al., 2012, Bara et al., 2018). Conversely, Ren *et al* identified evidence of oxidative stress and adverse effects to sperm motility and normality following exposure of C57 mice to 57nm silica nanoparticles via tracheal perfusion. However, these effects appeared to be reversible, with animals recovering after a period of wash-out post dosing (Ren et al., 2016). Given this information, and with more time and resources, it would be interesting to investigate the potential for silica ENM to effect changes to TM3 cell line at a functional level in future.

Carbon nanotubes (NM-400, 401 and 403)

Appraisal of cytotoxicity for CNT showed no significant alteration in TM3 cell viability for NM-401, but a significant effect of ENM exposure for NM-400 and 403. Although absorbance readings did not suggest notable interference from CNTs to the assay outcome, it was noted that both NM-400 and 403 did not disperse well using the protocol applied, and that they appeared to settle out of suspension to form a visible

layer on top of cells when applied to the 96 well plate, that was hard to wash off before application of WST-1. To add to this, conflicting outcomes following use of the WST-1 assay have been previously reported in the literature, suggesting some interaction with the test dye (Gormley and Ghandehari, 2009). For this reason, it is hard to be confident that the reported effects are a direct effect of the ENM on TM3 cells; it can be speculated that significance in findings is more likely due to sedimentation of CNTs onto the cellular monolayer interfering with readings rather than through interaction of ENM with the cells themselves.

Converse to our findings *in vitro*, *in vivo* exposure of rodents to CNTs reports clear findings of testicular toxicity. For example, Nirmal *et al* exposed Wistar rats to 0.4, 2 or 10mg/kg hydroxyl-functionalised MWCNT (multi-walled CNT, diameter 10-20µm, length 10-30µm) for 15 does over 30 days, reporting adverse outcomes to the testis via histological analysis, an increase in oxidative stress and sperm abnormalities without a decrease in sperm viability, a finding that was echoed by Farombi *et al* following intraperitoneal injection of functionalised MWCNTs to mice (Nirmal *et al.*, 2017, Farombi *et al.*, 2016). Furthermore, it is suggested that the wide range of length, diameter and functionalisation used for investigation of CNTs driving the variety of outcomes reported, corroborated by the finding of differential toxicity between single-walled, double-walled and multi-walled CNTs in Syrian hamster embryo and lung cells (Darne *et al.*, 2014).

Due to this discrepancy in findings between our work *in vitro* and that reported *in vivo*, further consideration of dispersion protocol for CNTs, and methods by which to wash them from cells before reading absorbance using any optical reading detection system is advisable.

Copper Oxide

Exposure of TM3 cells to pristine copper oxide resulted in a clear dose-response toxicity, and following non-linear regression, an LC₅₀ value of 7.752µg/cm² was identified. This material was provided by partners in the SUN project, and their findings both *in vitro* and *in vivo* reflect this finding of toxicity. Ivask *et al* reported dose-response toxicity to the human T-lymphocyte cell line Jurkat following exposure to CuO (Ivask *et al.*, 2017).

Gosens *et al* reported pulmonary toxicity following a short-term inhalation exposure protocol (5 days) at 6h equivalent concentration of 0, 0.6, 2.4, 3.3, 6.3, and 13.2 mg/m³, which showed signs of recovery following a 22day wash-out period post exposure (Gosens et al., 2016). Given additional time, it would be very interesting to investigate further the potential mechanism of toxicity from CuO to TM3 cells, and compare this to histological findings from the testis of animals exposed in the study of Gosens *et al*, which were kindly provided to our group for future investigation and comparison.

Zinc Oxide (NM-110, 111 and ZnSO₄)

TM3 cells showed clear dose-response toxicity following exposure to both NM-110 and 111. Timecourse appraisal showed that for both ENM, this effect was dose- but not time-dependent, with a significant reduction in viability of TM3 cells identified at doses of 3.76µg/cm² (NM-110) and 1.88µg/cm² (NM-111) and above at 2,4 and 6h timepoints. Via non-linear regression, and subsequent exclusion of outliers it was possible to identify an LC₅₀ of 3.813µg/cm² for NM-110 and 6.052µg/cm² for NM-111. Further analysis of the data makes it highly likely that the results of the 2-way ANOVA were influenced by the outliers identified, and thus the difference in toxicity reported for NM-110 and 111 to that of the regression analysis. Using the LC₅₀ value calculated, and Dunnett's multiple comparison test as guidance, future investigation of the effects of NM-110 and 111 on functionality of TM3 cells will use sub-lethal doses of <3.76µg/cm².

Comparison of these results with those for similar assays undertaken on cell lines from other organs and tissues shows a similar toxicity to cells of the immune system (Raw 264.7 and MH-S Macrophage cell lines) and respiratory system (16HBE human bronchial cells). However, no toxicity was identified in HMDM monocyte-derived macrophages or Calu-3 lung cancer cells, implying potential for differing effects on cell types within each organ (Farcas et al., 2015). To support this, Vecchione *et al* published a study on developmental toxicity endpoints which highlighted differences in toxicity to murine fibroblasts (NIH3T3, representing differentiated tissue) and murine embryonic stem cells (mES, representing embryonic tissue) following exposure to NM-110 and 111. They reported that while mES cells lost viability following exposure to NM-110/111 at doses of above 10µg/ml, the viability of NIH3T3 was unaffected, supporting the idea that ENM may affect animals during development differently (Vecchione et al., 2013).

Interestingly, our results mirror those for the 16-HBE cell line, which indicate a slightly lower toxicity from NM-111 than NM-110. It would be worth considering whether this difference in toxicity could be due to a protective role for the triethoxycaprylsilane coating applied to NM-111. Unfortunately, of the available studies, none were identified which included other types of ZnO, nor that reported in detail the characteristics of the ENM used.

Silver (NM-300, NM-300dis & AgNO₃)

TM3 cells showed clear dose-response toxicity following exposure to both NM-300 and AgNO₃. 2-way ANOVA was unable to identify any clear link between either dose or time and response for the higher dose range, but a clear effect of time- and dose- was observed at the low dose range, with significant loss of viability in TM3 observed at 1.88µg/cm² and above at 2 hours, and 0.94µg/cm² at 4 hours. Due to aberrant readings in both the high dose range, and 6/24h timepoints of the low dose range, it may be suggested that NM-300 interferes with the assay at high doses. These findings were identical to those reported for the TM4 cell line, adding weight to this suggestion (Fulton and Hutchison, 2013). It may also be that the results are subject to interference by silver ions released from the NM-300 colloidal solution (discussed below). It is notable that the results at 4hours for NM300 differed significantly for the same dose (3.76 ug/cm²) between high- and low- dose ranges using the Alamar Blue assay. When comparing these to WST-1 results, which were undertaken at n=6 rather than n=3, it is clear that this dose is one which generally produced large fluctuations in response regardless of number of experimental replicates. This is most likely because this dose is around the point at which viability in cells began to drop drastically. Via non-linear regression, and subsequent exclusion of outliers it was possible to identify an LC₅₀ of 7.885 ug/cm² for NM-300, and 0.282 ug/cm² for AgNO₃. Based on these results, a maximum dose 3.75µg/cm² was planned for future work ensuring a sub-lethal dose was applied to cells.

Our findings are in agreement with those of Zhang et al, who saw a dose-dependent decrease in viability of both TM3 and TM4 cells, and an increase in reactive oxygen species formation following exposure to 10 and 20nm silver nanoparticles (Zhang et al., 2015a).

Interestingly, initial analysis of the data for NM-300dis indicated a significant loss of viability to cells following exposure, which required further investigation to understand. The Dunnett's multiple comparison test suggested a significant change in viability across doses in the middle of the range of exposures. Examining distribution of data at these vs the other doses revealed these doses exhibited less variation than the others tested, thus leading to a false indication that there was a significant departure from the untreated control. To check this hypothesis, these dose points were removed and the ANOVA re-run, this time reporting a finding of non-significance. As cells appeared healthy under the microscope and were not affected by the higher doses applied, it was concluded that dispersant did not influence toxicity of silver ENM.

Ionic influences on toxicity of metal ENM

Auffman *et al* previously reviewed the chemical stability of metallic NPs, highlighting direct release of metals in solution (dissolution) as one of three key ways ENM may effect toxicity (Auffman *et al.*, 2009). Thus, another important point for consideration is whether toxicity observed from metallic ENM is a particulate or ionic effect; for this reason ionic controls were implemented for zinc oxide and silver ENM.

It has previously been shown that ionic silver is toxic to development and has greater adverse effect than its particulate counterpart (Li *et al.*, 2010, Bar-Ilan *et al.*, 2009). Toxicity studies on the freshwater alga *Pseudokirneriella subcapitata* have shown comparable toxicity between 30nm ZnO and dissolved ZnCl₂ salts (Franklin *et al.*, 2007). The high surface area of metal-based ENM increases potential for metal ion release, and toxicity observed can be linked to the ionic content (Beer *et al.*, 2012). This is thought to be responsible for the antibiotic and antibacterial properties of silver, as these are linked to the release of Ag⁺ ions in solution, and subsequent binding of their surface atoms to electron donor groups containing sulphur, oxygen or nitrogen (Auffman *et al.*, 2009).

It is possible based on this to suggest that toxicity of metal oxide NPs such as NM-110, 111, 300 and CuO could be attributed to dissolution of ions in solution. However, as zinc- and copper-based ENM were provided in powder form and the silver in a colloidal solution, the implications of this need to be considered slightly differently as any dissolution of Zn⁺ or Cu²⁺ ions could only happen once in the prepared ENM dispersion,

whereas the silver colloid may have been releasing ions throughout its storage post manufacture.

It has been reported that ZnO ENM undergo fast dissolution, with evidence to suggest that 50-60% of NM-110 and 111 may be dissolved in cell medium after 24h (Kermanizadeh et al., 2013). This makes an ionic influence on observed toxicity possible, which certainly matches the similarity of decreased viability and LC₅₀ observed between ZnO ENM and its ionic control. Similarly, there is evidence to suggest that dissolution of CuO in cell culture medium is up to 40% (Ivask et al., 2017). Importantly, Ivask & colleagues reported that the dissolution of CuO applied at a concentration of 2µg/ml was similar to that of CuSO₄, suggesting strongly that the pristine CuO used in this research also underwent dissolution. They go on to suggest that dissolution and any subsequent transformation of ZnO and CuO ENM during testing may influence strongly the toxicities recorded (Ivask et al., 2017). Conversely, Kermanizadeh *et al* reported that less than 1% of NM-300 dissolved in medium following 24h (Kermanizadeh et al., 2013). This makes it less likely that the toxicity observed from NM-300 is due to the release of ions and may account in part for why the LC₅₀ values for AgNO₃ was much lower than that for NM-300.

Another important point to consider is that the toxicity of silver NPs increases during storage, due to slow dissolution. Kittler *et al* demonstrated that aged silver nanoparticles (after 1 month and 6 months of storage) caused complete cell death within primary human mesenchymal stem cells when compared to silver NPs only 3 days in age (Kittler et al., 2010). However, they also noted that their silver NPs were stored in an aqueous dispersion without any stabilising agents present, emphasising the importance of the inclusion of the stabilizing agents included in NM-300dis.

Investigation into ion release from NM-300 into its matrix has been demonstrated under storage conditions to be <0.01w/w%, but ion concentration was stable over the 12 month period of testing (Comero et al., 2011). This suggests it would be possible that the toxicity profile of NM-300 to change with increasing time in storage and thus greater dissolution of ions into solution. In addition, Comero *et al* also mention that there will

be some evaporation of the solution over time, meaning that the content of the solution becomes more potent over time.

During this period of research, logistical issues meant that NM-300 was stored for longer than recommended within the literature above. In combination with the knowledge about dissolution of Ag⁺ ions presented, this may mean that while the ionic contribution to NM-300 toxicity was less pronounced, latter results (timecourse assay) could be influenced by increased potency of the NM-300 solution. In future, it would be useful to re-run the timecourse assay with 'fresh' NN300, in order to appraise whether storage time did have any effect on outcome, which may explain potential differences in LC₅₀ values.

Issues encountered with Timecourse assays

Interestingly, the variation in findings at the 24hour timepoint for all four ENM tested was massive compared to the other timepoints in all three replicates, leading to a question over what may have caused this. Alamar Blue measures a change in cellular reduction capability, which could be due to cell death, cell cycle impairment, or decrease in cellular metabolism, the measured reduction of blue resazurin to red resorufin being undertaken via agents like NADH which are readily produced within viable cells. One paper which provides some insight into the possible reasoning for this is that of O'Brien et. al. (2000).

O'Brien *et al* tested primary rat hepatocytes, alongside HeLa and HepG2 cell lines using AB. They found that resazurin to resorufin reduction can go on to create a third highly reduced product – hydroresarufin. This final product is non-coloured and therefore doesn't give absorbance reading. Reduction of Resorufin to hydroresorufin could lead to aberrant results in tests as living cells which fully reduce resazurin will give a weaker signal than dying/dead cells which can't reduce the dye fully. They tested this using a HepG2 liver cell line and found that with a $t^{1/2}$ of 10 hours, measurements with a 26hour lag gave higher absorbance than that expected from a strict correlation between time and absorbance. To further investigate this, primary Hepatocytes were treated with control or the known toxicant sodium azide (NaN₃) with viability investigated using AB at a 2, 10 or 20% preparation. Absorbance readings showed that a lesser concentration

of AB dye led to a rapid shift to colourless in untreated cells. Thus, at a 2h timepoint, NaN_3 treated cells showed lower viability than untreated cells, but after 20 hours NaN_3 treated cells appeared to show a higher viability than untreated (especially at lower AB%). This was repeated for cells exposed to CuSO_4 as a point of comparison, and the same results were found (O'Brien et al., 2000).

Based on this, it is very possible that the pattern observed for NM-110, 111 and 300 of lower viability within untreated cells was due to complete reduction of dye to hydroresorufin, whereas the higher readings from treated cells was due to cell death/reduction in ability to metabolise the dye, and thus more partly reduced product being present in the media. In contrast, the WST-1 results, which followed an identical 24-hour exposure, gave an accurate representation of cell viability. Based on this it is plausible to conclude that Alamar Blue is not the ideal method by which to measure changes in viability over a longer period of exposure, and that the 24hour exposure point measured by WST-1 is suitable for further testing when combined with the lower dose range explored by the Alamar Blue assay. Ideally, it would be useful to repeat some of the shorter exposure times using WST-1 to provide a point of comparison for all timepoints measured and explore whether a 4 or 6h exposure would be most suitable for further testing of functional markers.

Conclusions and Future Development

In summary, two *in vitro* toxicity assays were optimised for investigation of an endocrine-active cell type via use of charcoal stripped serum, and it was found that once optimised the assays produced a reproducible assessment of toxicity for the cell line and ENM panel. Viability of TM3 cells following a 24-hour exposure to a panel of ENM gave a variety of results. Titanium dioxide (NM-101 Anatase, NM-103 hydrophilic & NM-104 hydrophobic), Silver dispersant (NM330Dis) and Multi-walled Carbon Nanotubes (NM-400, 401 and 403) were not found to be toxic to cells. Zinc Oxide (NM-110 coated & NM-111 uncoated), Silica Dioxide (NM-200 & 203), Silver (NM-300) and Copper Oxide were shown to impact upon cell viability at relatively low doses. For NM-110, 111, ZnSO_4 , NM-300, AgNO_3 and copper oxide, a non-linear log(inhibitor) vs response curve was plotted to identify an LC_{50} value to guide selection of dose for future sub-lethal functional studies. Consideration was given to the potential role of dissolution of ions from metallic

ENM in their observed toxicity. Recognition must also be offered to the role that differences in physico-chemical characteristics (hydrophobicity/philicity, size, coating, charge, production method etc.) may have in driving differential toxicities from materials with the same chemical identity.

As the same investigation was carried out in parallel for the TM4 Sertoli cell line within Edinburgh Napier University (Fulton and Hutchison, 2013), it is possible to present findings by WST-1 and Alamar Blue for both cell lines for comparison (Table 9).

As mentioned in this discussion, results for both TM3 and TM4 cells for NM-103 & 104 (TiO₂), NM-200 & 203 (SiO₂), and NM-110 and 111 (ZnO) have been published in a summary paper, bringing together evaluation of *in vitro* cytotoxicity of the ENM panel to 12 cellular models, representing 6 different target organs/systems: immune, respiratory, gastrointestinal, reproductive, hepatic systems and embryonic tissues (Farcas et al., 2015). The toxicity assessment was undertaken using 10 different assays for cytotoxicity, embryotoxicity, epithelial integrity, cytokine secretion and oxidative stress. To our knowledge, this is the first time that thorough physico-chemical characterisation ENM was combined with a standardised approach to dispersion, consideration of ENM behaviour in biological media, potential interference with assays and cell- and ENM- specific responses was reported in the published literature for such a large group of ENM, target organs/systems and endpoints.

Table 9: Summary of findings from WST-1 and Alamar Blue on Leydig (TM3) and Sertoli (TM4) cells. Results are reported as '-' where no toxicity was identified, '(-)' where toxicity was identified only at the highest possible dose *in vitro*, and '+' where clear toxicity was seen. Where possible, the dose over which a significant decrease in viability was seen is reported, and for those ENM eliciting a clear dose-response toxicity to TM3 cells, and LC₅₀ value is given.

Nanomaterial		Cytotoxicity TM3	Timecourse TM3	Cytotoxicity TM4	Timecourse TM4
Titanium Dioxide	NM-101	-	-	-	-
	NM-103	-	N/A	-	N/A
	NM-104	-	N/A	-	N/A
Silica Dioxide	NM-200	(-)	N/A	(-)	N/A
	NM-203	(-)	N/A	(-)	N/A
Zinc Oxide	NM-110	+	>1.875µg/cm ² , 4h LC ₅₀ 3.813µg/cm ²	+	>3.75µg/cm ² , 4h
	NM-111	+	>0.94µg/cm ² , 4h LC ₅₀ 6.052µg/cm ²	+	>3.75µg/ccm ² , 4h
	ZnSO ₄	+	N/A		
Silver	NM-300	+	>0.94µg/cm ² , 4h LC ₅₀ 7.885 µg/cm ²	+	>1.875µg/cm ² , 4h
	NM-300Dis	-	-	-	-
	AgNO ₃	+	N/A		
		LC ₅₀ 0.282µg/cm ²			
Copper Oxide	Pristine CuO	+	N/A	N/A	N/A
		LC ₅₀ 7.752µg/cm ²			
MWCNT	NM-400	(-)	N/A	N/A	N/A
	NM-401	(-)	N/A	N/A	N/A
	NM-403	(-)	N/A	N/A	N/A

To date, cytotoxicity assays for a panel of ENM have been successfully set up, optimised and tested for interference from ENM. This has produced data on Leydig cell viability

following exposure to ENM across a range of timepoints and highlighted a number of ENM for which it could be expected that exposure to the testis would result in a reduction in viable Leydig cell population, with resulting effects on androgen production, the regulation of spermatogenesis and even possibly adverse effects on BTB integrity. These assays allowed identification of a sub-lethal dose range in which to investigate functional changes in cells. There are a number of key functional and metabolic pathways within the Leydig Cell which could be affected following ENM exposure and lead to the observed reduced viability, as well as potential changes in the cells' key function – production of steroid hormones. Establishing these is the next step in establishing suitable *in vitro* models by which to appraise male reproductive nanotoxicology, and the subject of the next chapter.

Chapter 4: Functional changes to Leydig Cell behaviour following ENM Exposure

Introduction

Following examination of results from the WST-1 and Alamar Blue assays, three ENM were identified as being of interest for further examination of functional cellular responses; uncoated zinc oxide, coated zinc oxide and silver (NM-110, 111 and 300). For this, a No Observed Effects Limit (NOEL) was identified, and expression of several key proteins, receptors and enzymes in steroidogenesis were examined following treatment of TM3 cells with doses of ENM under the NOAL. This was initially undertaken by looking for alteration in expression of mRNA via RT-qPCR, and then by looking for any changes in cellular protein expression via Western blot. Results could then be compared to those from histological analysis on testicular samples from male Sprague-Dawley rats undertaken concurrently (reported within Chapter 5) to look for comparability between findings *in vitro* and *in vivo*.

A number of potential proteins, enzymes and receptors of interest were identified based on prior knowledge of the Leydig cell, steroidogenesis, and endocrine system regulation of male reproductive function (much of which is outlined within Chapter 1). These aligned with some of the key proteins investigated histologically, so that direct comparison of results could be made. To provide full rationalisation for the selection of each, the steroidogenic pathway within the Leydig cells of the testis is outlined in detail, together with commentary on available information relevant to ENM currently published.

Steroidogenesis & Selection of targets for measurement

The Leydig cell is the only testicular cell expressing all of the necessary enzymes for conversion of cholesterol to testosterone, these being cholesterol side chain cleavage (CYP11A1), 17 α -hydroxylase/C₁₇₋₂₀ lyase (CYP17A1), 3 β -hydroxysteroid dehydrogenase/ Δ 5-4 isomerase (HSDB3), and 17 β -hydroxysteroid dehydrogenase type 3 (HSD17B3) (Payne, 2007, O'Shaughnessy, 2017). Consequently, it is the sole site for conversion of 27-carbon cholesterol to 19-carbon steroid hormones such as

testosterone in this organ (O'Shaughnessy, 2017). As previously outlined, the production of testosterone is completely dependent on stimulation of LCs by luteinising hormone (LH). LH binds to high-affinity LH-receptors (LH-R) on the surface of LCs, activating a series of events which ultimately lead to the production of testosterone, which stimulates reproductive organ activity, controls actions in the periphery and maintains the male phenotype (Dufau and Tsai-Morris, 2007). As such, the LH-R is required for: i) normal function of the Hypothalamus-Pituitary-Gonad (HPG) axis via endocrine signalling, ii) management of paracrine interaction between Leydig and Sertoli cells, as well as iii) autocrine management of steroidogenesis and metabolic processes within the Leydig cells themselves.

The effects of ENM exposure on circulating LH levels and LH receptor expression are not extensively reported, nor does the literature reach any decisive conclusion. In relation to circulating LH levels, Kong *et al* reported no change to LH levels in male rats following nickel ENM exposure during a one generation reproductive toxicity test (Kong et al., 2014). Reyhani *et al* observed a dose-dependent decrease in LH levels following intraperitoneal injection of silver ENM (0.5-5mg/kg/day for 25 days), whereas no change in serum LH levels was detected by Mathias *et al* following silver ENM exposure of Wistar rats via oral gavage at 15 or 30µg/kg for 46 days, or by Garcia *et al* following exposure of CD1 mice to 1mg/kg silver NPs over 5 doses intravenously at 1mg/kg (Rezazadeh-Reyhani et al., 2015, Mathias et al., 2015). In relation to LH-R expression, only 1 study was identified: Bara et al (2018) reported an increase in LH-R expression following oral exposure to silica ENM in swiss albino mice, but not following zinc oxide ENM exposure via the same route (Bara et al., 2018).

Because of the both limited and contrasting information available from the existing literature, and as the initiator for the effects of LH on testosterone production, the first target selected was the luteinizing hormone (LH) receptor. A G-coupled transmembrane receptor (GCPR), the LH-R is found in abundance on the surface of Leydig cells (Chen et al., 2007). LH-R is within the superfamily of GCPRs with 7 membrane-spanning guanine nucleotide-binding domains and belongs to a sub-class which includes other receptors for pituitary hormones (Dufau, 1998). The LH-R is heterodimeric, and at the monomeric level contains α and β subunits; the 92 amino acid α subunit being common to the LH-

R, and other hormones including the human chorionic gonadotropin receptor, thyroid stimulating hormone receptor and the follicle-stimulating hormone receptor. Transcription of the 121 amino acid β subunit is therefore responsible for its unique functions and high receptor-binding capacity for LH (Choi and Smitz, 2014).

LH-R cDNA encodes a 75kDa glycoprotein, composed of two functional units: a heavily glycosylated extracellular (EC) hormone-binding domain which binds LH with high affinity, and the 7 membrane transmembrane/cytoplasmic module which anchors the receptor and transduces the signal initiated in the EC domain by coupling to G proteins (Jiang et al., 2014). The mature receptor is 80-90kDa in size, of which around 15kDa are made up of carbohydrate chains located at potential glycosylation sites on the EC domain (Dufau and Tsai-Morris, 2007).

Binding of LH to the LH-R induces binding of its cytosolic domain to a membrane-bound G protein, inducing exchange of bound guanosine 5'-diphosphate for guanosine 5'-triphosphate. In turn, this activates the α subunit of the G Protein to dissociate from its dimeric β - γ subunit and interact with Adenylyl cyclase to convert Adenosine Triphosphate (ATP) to cAMP, after which it re-associates with the β - γ subunit, restarting the cycle (Dufau and Tsai-Morris, 2007).

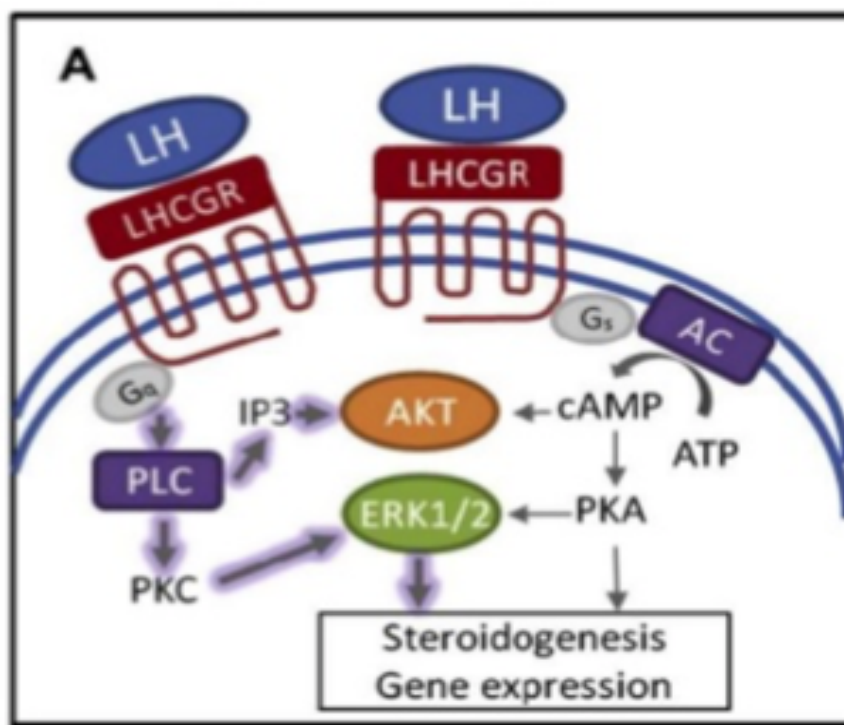


Figure 35: Luteinizing Hormone Receptor and its common second messenger pathways. LH = luteinizing hormone, G = G protein, AC = Adenylyl cyclase, ATP = Adenosine Triphosphate, cAMP = cyclic adenosine monophosphate, PKA= protein kinase A, PLC = phospholipid-specific phospholipase C, ERK 1/2= extracellular signal-regulated kinase, PKC = protein kinase C, AKT =protein kinase B. From (Choi and Smitz, 2014).

Cyclic adenosine monophosphate (cAMP) is the primary second messenger for LH-R in steroidogenic signal transduction, with the phospholipid-specific phospholipase C (PLC) and extracellular signal-regulated kinase (ERK) pathways also playing major roles (Fig. 35) (Choi and Smitz, 2014). This activation of cAMP is considered key to activation of steroidogenesis in temporally distinct manners, either acutely over minutes (via StaR activation and transfer of cholesterol to the inner mitochondrial membrane), or chronically over hours (via an increase in gene transcription for the enzymes p450_{sc}, P450_{c17}, 3 β -HSD and 17 β -HSD) (Kotula-Balak et al., 2012). TM3 cells have been shown to increase cAMP production in response to stimulation with LH, therefore it is considered that these cells possess active LH-Rs (Mather, 1980). Because of this LH-R expression was investigated for both RNA and protein-based work.

cAMP activates both protein kinase A (PKA) and B (AKT). Phosphorylation of proteins such as peripheral-type benzodiazepine receptor (PBR) and steroidogenic acute regulatory protein (StaR) via PKA is a key regulatory step in hormone-stimulated steroid

production. Both PBR and StaR have been implicated as holding important roles in translocation of cholesterol to the inner mitochondrial membrane, a constant supply of which is needed as a substrate for steroid hormone synthesis.

The primary source of cholesterol in all steroidogenic cells is cholesterol esters within lipid droplets. When this is depleted, cholesterol may be sourced from *de novo* synthesis or from exogenous lipoproteins (Fig. 36) (Chen et al., 2007). By comparison with adrenal cortex cells which use plasma lipoproteins as the major source of cholesterol, Leydig cells produce most of their own testosterone from lipid droplets, or *de novo* from acetate (the rate limiting enzyme in this process being 3-hydroxy-3-methylglutaryl-coenzyme (HMG CoA)). Carboxyesterase (ES-10) and hormone sensitive lipase (HSL) are also considered to play significant roles in mobilisation of cholesterol synthesised *de novo*. The Leydig cell may also import exogenous cholesterol from blood lipoproteins via the scavenger receptor class B type 1 (SR-B1), a receptor which is also stimulated by LH (Reaven et al., 2000).

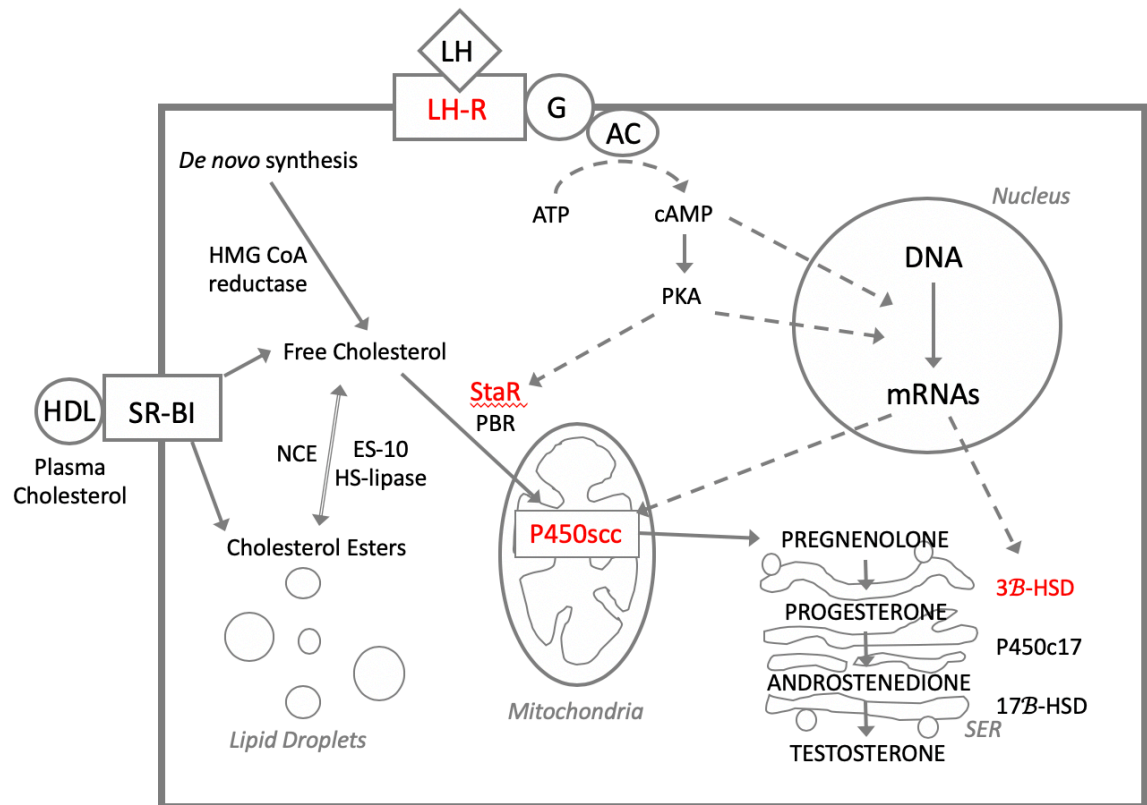


Figure 36: Location and role of selected key players in steroidogenesis within the Leydig cell. Regulatory and Steroidogenic pathways in the Leydig Cell. Highlighted are receptors, enzymes and molecules of interest which have been selected for further analysis via functional assays. LH-R: LH receptor, G: G protein, AC: Adenyl Cyclase, PKA: Protein Kinase A, StaR: Steroidogenic acute regulatory protein, PBR: Peripheral benzodiazepine receptor, Sr-BI: Scavenger receptor class B type 1, ES-10: Carboxyesterase, HS-lipase: hormone sensitive lipase, NCE: Neutral Cholesterol esterase. Image adapted from (Chen et al., 2007).

As cholesterol is hydrophobic and cannot simply diffuse across the aqueous intermembrane space of mitochondria, it is thought that StaR and PBR play coordinated roles in transport of cholesterol across the mitochondrial membrane (Chen et al., 2007). Discovered in the 1980s by Orme-Johnson & Pon, and later described in detail by Stocco *et al*, the 30kDa mitochondrial phosphoprotein StaR is considered to be the true rate limiter in steroidogenesis, controlling transport of cholesterol from the outer to the inner mitochondrial membrane (Clark and Stocco, 1996, Pon and Orme-Johnson, 1986). StaR is rapidly synthesised in response to stimulation of the cell to produce steroid by luteinising hormone, possibly via cAMP induced ERK pathway activity (Gyles et al., 2001). It was shown to be essential to steroidogenesis, as mutations in the StaR gene were shown to result in congenital lipoid adrenal hyperplasia (lipoid CAH), in which affected individuals are unable to produce adequate levels of steroids and suffered excessive cholesterol levels (Stocco, 2007). As such, StaR was selected as the second key target of

interest for investigation of the effects of ENM on steroid synthesis and function of the Leydig cell.

Whilst the exact mechanism of action for StaR remains debated, it is considered to be likely that it interacts with other mitochondrial outer membrane proteins such as StaR-binding protein and the Peripheral Benzodiazepine Receptor (PBR) to facilitate cholesterol transfer. The PBR receptor (more recently known as translocator protein TSPO) is a high affinity cholesterol binding protein present in high levels on the outer mitochondrial membrane, most likely acting as a channel for cholesterol transport (Papadopoulos et al., 2006). Stimulation with LH causes an increase in PBR ligand binding, which may be blocked by inhibition of PKA, suggesting cAMP induced phosphorylation may be involved (Chen et al., 2007).

It is proposed that StaR and PBR work in coordination, with StaR being a 'gatekeeper' managing and initiating transport of cholesterol, and PBR acting as the 'gate' through which it enters the mitochondria. However, with evidence both in support of and opposition to this proposal, it remains subject to much debate and certainly requires further investigation (Stocco, 2007). Previous studies have shown that StaR is expressed within TM3 cells and is affected by alterations in cellular environment as well as exposure to ENM (Zhang et al., 2015a). With such an important part in the steroidogenic pathway, StaR was examined both via RNA and protein work.

Once within the mitochondria, the first step in production of steroid hormones from cholesterol is its conversion to pregnenolone. This is catalysed by cholesterol side-chain cleavage enzyme (P450scc). P450scc is a member of the cytochrome P450 haem containing superfamily of enzymes (family 11, subfamily A, polypeptide 1), encoded by the gene *CYP11A1*. It is expressed on the inner mitochondrial membranes of Leydig cells, its synthesis being promoted in part by cAMP via LH stimulation. P450scc holds an important role as the rate-limiting enzymatic step in conversion of cholesterol to pregnenolone, and as such was selected as the third target of interest for investigation of ENM effects on Leydig cell function (Payne, 2007). It does this in the presence of NADPH and oxygen via a series of three monooxygenase reactions, which include 2 hydroxylations of cholesterol side chains, then cleavage of the bond between two

specific carbons, producing from 27-carbon cholesterol 21-carbon pregnenolone and isocaproaldehyde (Fig. 37). P450scc was investigated at the molecular level via RNA expression.

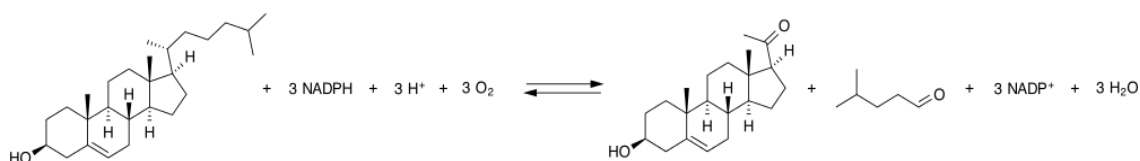


Figure 37: Conversion of cholesterol to pregnenolone by P450scc.

The literature reports few studies including investigation of *StaR* and P450scc following ENM exposure, and those available indicate that effect may be ENM dependent. One such study reported significant increases in expression of *CYP11A1* mRNA but no change in *Star* mRNA following intravenous injection of silver ENM in mice (Garcia et al., 2014). In another study, Mohamed *et al* aimed to investigate whether zinc oxide (ZnO) ENM may be protective to testicular function in animals exposed to nicotine. The group observed a decrease in both *StaR* and *CYP11A1* following nicotine treatment, that was potentiated past control with the addition of ZnO ENM. This indicates that ZnO ENM exposure may increase expression in both *StaR* and P450scc converse to the changes seen with silver exposure. A second paper from Bara et al (2018) includes measurement of *StaR* and *CYP11A1* expression following silica and zinc oxide ENM. This reports that in adult swiss albino mice exposed to zinc oxide and silica ENM gestationally (from gestational day 15-19), *StaR* expression was increased following both ZnO and silica exposure, while *CYP11A1* expression was increased following ZnO but decreased following silica exposure.

Pregnenolone diffuses from the mitochondria and moves to the smooth endoplasmic reticulum (SER) of LCs via methods which are largely unexplored to date (Sewer and Li, 2008). Once in the SER, pregnenolone is converted to 21-carbon progesterone by the hydroxysteroid dehydrogenase enzyme 3 β -hydroxysteroid (3 β -HSD). 3 β -HSD is a membrane-bound enzyme present in mitochondrial and microsomal membranes, of which there are multiple isoforms; in total 6 have been isolated and characterised to date (Kotula-Balak et al., 2012). Within rodent Leydig cells, variant 1 of 3 β -HSD catalyses one step in the biosynthesis of testosterone from pregnenolone, by converting the Δ 5-

3β -hydroxysteroid pregnenolone to the Δ^5 -3-ketosteroid progesterone in the presence of NADPH. Its human counterpart is 3β -HSD variant 2. Zhang et al reported significant downregulation of 3β -HSD in male somatic and spermatogonial stem cells following exposure to silver ENM (Zhang et al., 2015a).

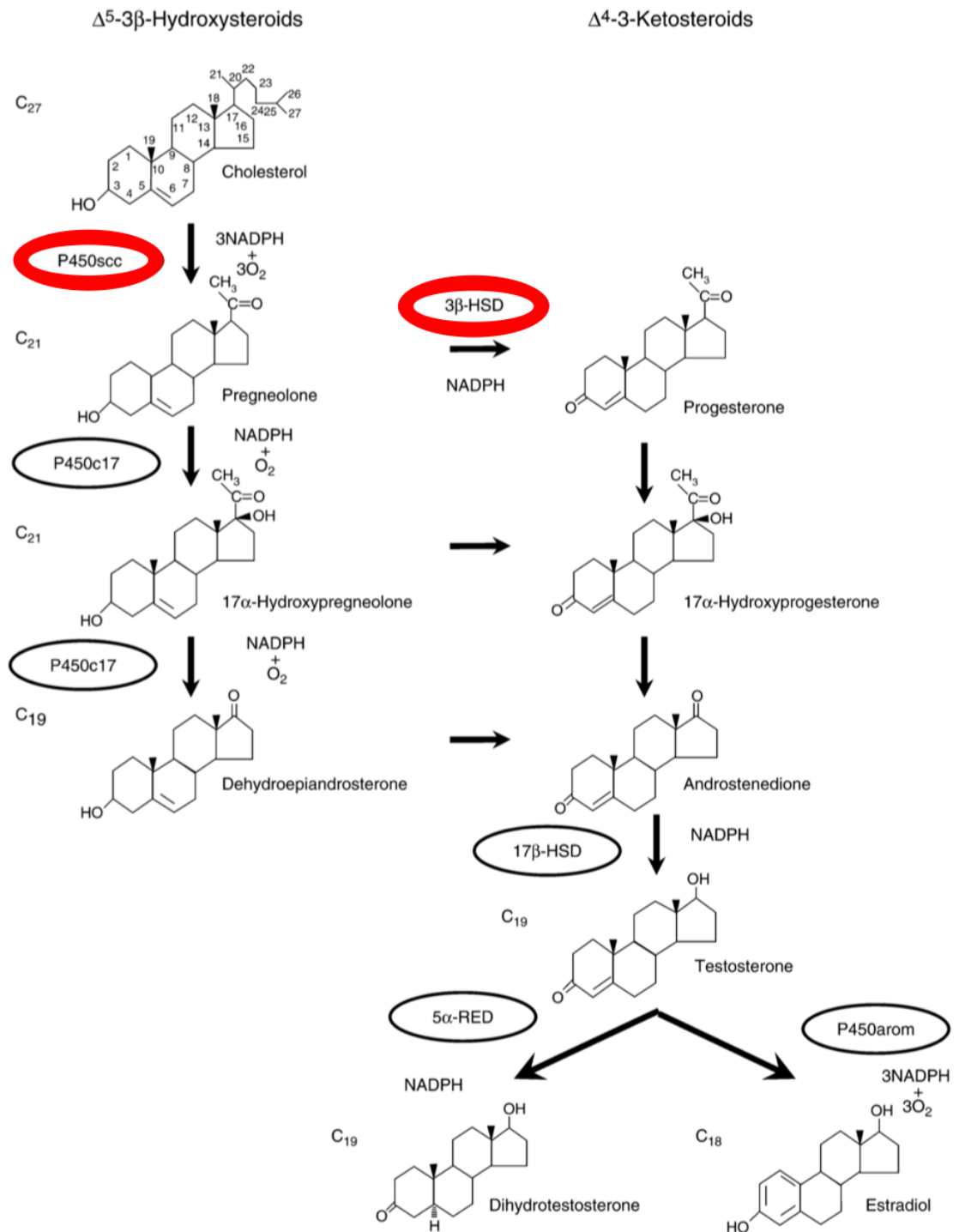


Figure 38: Key steroid biosynthetic pathways in Leydig cells. Enzymes examined using protein and RNA work are highlighted in red. P450scc = side chain cleavage enzyme; 3β -HSD = 3β -hydroxysteroid. Reproduced from Payne (2007).

To complete synthesis of testosterone (T), 21-carbon progesterone is converted to 19-carbon androstenedione via catalysis with CYP17, and finally to the 19-carbon T via catalysis with 17 β -hydroxysteroid (17 β -HSD). T may be further metabolised by 5 α -reductase (5 α R) to dihydrotestosterone (DHT), or the enzyme CYP19A1 (encoding aromatase enzyme) to oestradiol (Fig. 38). For the purposes of this work, testosterone and dihydrotestosterone are considered to be the most important hormones in sexual maturation and maintenance of the male phenotype (Payne, 2007).

The literature reports that CD1 mice exposed to silver ENM at 1mg/kg via intravenous injection showed significant upregulation of 3 β -HSD (*Hsd3b1*) expression (Garcia et al., 2014). Conversely, Jia et al (2014) reported no change in 3 β -HSD expression following oral exposure of pubertal Kunming mice despite observing clear adverse effects on testicular morphology and a decrease in expression of 17 β -HSD. To help fill a clear gap in the data, and as a key step in the final synthesis of testosterone (T) within Leydig cells, 3 β -HSD v1 was investigated at the molecular level via RNA expression.

Upon synthesis within the Leydig cell, T can act both locally and systemically. Systemically, T contributes to negative feedback within the HPG axis, controlling reproductive function. It is also involved with the HPA (Hypothalamic Pituitary Adrenal) axis, influences sexual activity, promotes muscle growth and helps to manage platelet aggregation in the blood. Locally, T has an important role in managing spermatogenesis via its paracrine action on Sertoli cells within testicular seminiferous tubules. In addition, adult LCs have been shown to express Androgen Receptors (AR) at variable levels in both rodents and humans, and so can be responsive to autocrine androgen signalling from T (Eacker and Braun, 2007). This may be for a number of reasons, including controlling LC number and steroidogenic enzyme production (O'Hara et al., 2015). Within target tissues both systemically and locally, T can act directly to mediate changes by binding to the Androgen receptor, or it may act indirectly following conversion to other active steroid hormones.

Also known as NR3C4 (nuclear receptor subfamily 3, group C, member 4), the AR is activated by binding androgenic hormones, testosterone or dihydrotestosterone in the cytoplasm. Once bound, a conformational change in the receptor causes dissociation of

heat shock proteins which transport from the cytosol into the cell nucleus and then dimerize, before binding to its hormone response element on DNA, causing an up- or down-regulation of specific gene transcription. As such, its primary role is as a DNA-binding transcription factor that regulates gene expression. In addition, AR has also been shown to have a second mode of action, which is independent of interaction with DNA. This involves interaction with signal transduction proteins in the cytoplasm, causing rapid changes in cell function such as alteration in ion transport, or indirect secondary changes to gene transcription for example via phosphorylation of other transcription factors (Fig. 39).

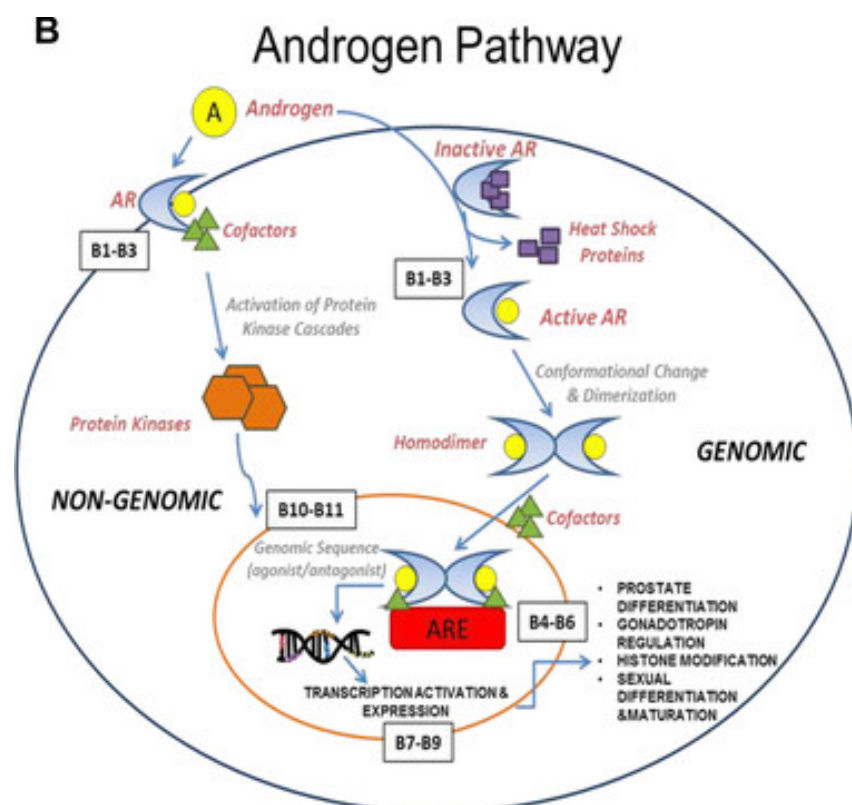


Figure 39: Androgen Receptor genomic and non-genomic mechanisms of action. From (Silva et al., 2015)

Within the literature, only one study examining the effects of ENM on AR expression was identified. Jia et al (2014) reported no change to AR mRNA expression in pubertal Kunming mice exposed to TiO₂ orally at various doses (Jia et al., 2014). *In vitro*, Kang et al recently reported that exposing human prostate cells to silver ENM disrupted AR transactivation (triggering of gene expression via signalling cascades following AR

binding of T or DHT). The mechanism of action suggested was that silver ENM may bind to dihydrotestosterone, thus inhibiting its ability to bind to the AR (Kang and Park, 2018). It is also known that endocrine disrupting chemicals such as brominated flame-retardants are capable of altering AR expression, therefore investigation of AR expression following ENM exposure appears both valid and needed (Kharlyngdoh et al., 2018). TM3 cells are able to produce testosterone, therefore examining whether they possess AR is relevant (Musa et al., 2000). As it wasn't clear from the literature whether TM3 cells have active ARs, it was decided that AR would be examined via protein analysis to establish whether it was present.

Objectives

In order to build on results from the basic cytotoxicity assays undertaken within Chapter 3, it was necessary to investigate the functional effects of ENM exposure on TM3 cells *in vitro*. The outcomes of this could then be compared to those recorded following exposure of animals *in vivo* (Chapter 5).

Research questions to be addressed were:

1. Does exposure to zinc oxide and silver ENM lead to changes in mRNA expression encoding for a number of key markers of endocrine function in TM3 cells (LH-R, StaR, P450scc & 3 β -HSD)?
2. Does exposure to zinc oxide and silver ENM lead to changes in protein expression for a number of key markers of endocrine function in TM3 cells (LH-R, StaR & AR)?

The aim of the work was therefore to elucidate whether TM3 exposure to zinc or silver based ENM caused changes in RNA or protein expression for key markers of reproductive function *in vitro* that could be compared to results gathered from concurrent analysis being undertaken on testicular samples from animals exposed *in vivo* (chapter 5).

Materials and Methods

RNA Expression via RP-qPCR

To examine RNA expression, Reverse Transcriptase quantitative Polymerase Chain Reaction (RT-qPCR) was used. RT-qPCR using an intercalating dye such as SYBR® Green is an attractive prospect for pilot experiments such as this, as it is fast, inexpensive and the technique is relatively easy to master. SYBR® Green is an asymmetrical cyanine dye, which fluoresces when intercalated with double stranded cDNA. The cDNA-dye complex absorbs blue light ($\lambda_{\text{max}} = 497 \text{ nm}$) and emits green light ($\lambda_{\text{max}} = 520 \text{ nm}$). RT-qPCR was undertaken according to the guidelines for minimum information for publication of quantitative RT-PCR experiments (MIQE) (Taylor, 2010). For RNA work, primers were designed based on available published literature and through NCBI-NIH Primer-BLAST.

RNA Extraction

Preparation of RNA for PCR was undertaken using TM3 cells exposed to NM-110, NM-111 and NM-300 as follows. Cells were cultured for 24 hours in 6 well plates at a density of 2.75×10^5 cells/well. This resulted in a final cell number which was sufficient for extraction of RNA using the Qiagen RNeasy kit, which requires a maximum of 1×10^7 cells as a pellet. Cells were treated with ENM at sub-lethal doses (0,4 and $8 \mu\text{g/ml}$, or 0, 1.26 and $2.52 \mu\text{g/cm}^2$ as determined in Chapter 3) and incubated for a further 24 hours. It should be noted that these ENM were used out with the 1 week recommended opening time, due to the limited availability of materials and the time it took to carry out experimentation. To disrupt and homogenise the cells, $350 \mu\text{l}$ Buffer RLT from the kit (guanidine-isothiocyanate containing lysis buffer which disrupts cell membrane, linearizes nucleic acids and destabilises RNAses) was added to wells after removal of the medium, and the lysate transferred to an Eppendorf tube. A further $350 \mu\text{l}$ of 70% ethanol was then added and mixed well, before $700 \mu\text{l}$ of sample (including precipitate) was transferred to an RNeasy spin column placed in a 2ml collection tube, and centrifuged in an Eppendorf 5415R centrifuge for 15 seconds at 8161 xg to bind total RNA to the column and wash off buffer RLT. Flow through was discarded.

On-column DNase digestion was undertaken using a Qiagen DNase On-Column Digestion kit. Initially, $350 \mu\text{l}$ of buffer RW1 was added to the column. Buffer RW1

contains a guanidine salt, as well as ethanol, and is used as a stringent washing buffer that efficiently removes biomolecules such as carbohydrates, proteins, fatty acids etc., that are non-specifically bound to the silica membrane. At the same time, RNA molecules larger than 200 bases remain bound to the column. Once added, the column was centrifuged for 15s at 8161 xg and flow-through discarded. DNase incubation mix was prepared by suspending 10µl DNase I stock solution to 70µl Buffer RDD in mini Eppendorf. The mixture was applied directly to the spin column membrane and incubated at room temperature for 15min. 350µl of buffer RPE – a mild washing buffer which removes traces of salts present on the column from earlier buffers - was added to the column which was centrifuged for 15s at 8161 xg and the flow-through discarded. Two further washes with buffer RPE were then undertaken as above, before the column was placed into a new 2ml collection tube and centrifuged at full speed for 1 minute to dry the membrane.

The RNeasy column was placed into a new 1.5ml collection tube, before 30-50µl of RNase-free water was added to the column membrane. The column was then centrifuged for 1minute at 8161 xg to elute the RNA into a collection tube, before quantification and storage at -20°C.

RNA Quantification and Quality check

Following collection of RNA, basic quantification was done via photometric analysis using a Thermo Fisher Nanodrop 2000 spectrophotometer. In short, 2µl of RNase-free water was added to the instrument measuring platform to provide a blank, followed by 2µl of purified RNA. Quantity was determined by absorbance at 260nm, and purity as a ratio between absorbance readings at 260 and 280nm (pure RNA having a ratio of between 1.9 and 2.1).

Additional quantification and integrity readings were undertaken via chip-based gel electrophoresis using the Agilent Bioanalyzer 2100. Chip-based electrophoresis uses the chip as an integrated electrical circuit, with each electrode from the machine's cartridge providing independent power. The system drives charged molecules, such as RNA, along a voltage gradient which pushes them through a sieving polymer matrix, separating molecules by size, with the smaller ones migrating faster than the larger ones. Detection

is by laser-induced fluorescence (LIF), with dye molecules intercalating with RNA strands. The resulting gel image and details from the electropherogram (plot of fluorescence intensity vs size/migration) can then be compared to a ladder containing components with known sizes to determine molecule size. Quantification is achieved by comparing the area under the upper marker (markers are internal standards) to the sample peak areas. As the concentration of the upper marker is known, sample concentration can be calculated. Integrity of the RNA sample is achieved by determining ribosomal ratio, and the presence/absence of degradation products.

To prepare samples for the bioanalyzer, 2 μ l of each sample was pipetted into small Eppendorf tubes. For those samples with an indicated concentration of >500ng/ μ l, samples were diluted 1:1 with RNase free water to ensure accurate readings (1.5 μ l sample:1.5 μ l RNase free water). Samples were then heat denatured for 2minutes at 70°C. 65 μ l of Agilent RNA 6000 nanogel matrix was vortexed for 10 seconds, before 1 μ l of RNA 6000 nanodye concentrate was added. The gel-dye matrix was then vortexed to mix further, before being spun in a centrifuge for 10 minutes at 15996 xg. A 16-pin bayonet electrode cartridge was loaded into a priming station, and 9 μ l of gel-Dye matrix placed into the bottom of the relevant well, before being syringe pressurised for 30 seconds. 9 μ l of gel-dye matrix was then loaded to two other wells, alongside a further well containing 5 μ l of the RNA 6000 nanomarker to complete chip preparation. Once the chip was ready, 1 μ l of sample was pipetted into the base of each well, and 1 μ l of ladder added to a final well, as per a pre-prepared chip layout plan. The chip was placed on an IKA Vortex mixer and well contents mixed for 1min at 2400rpm before reading was undertaken on the Bioanalyzer. The resulting output provided graphed marker and 2 ribosomal peaks (18s and 28s), together with RNA concentration (ng/ μ l), rRNA ratio (28s:18s) and RNA Integrity number (on a scale of 1-10).

Reverse Transcription

To perform PCR using RNA as a template, RNA must first be reverse-transcribed to complementary DNA (cDNA) in a reverse transcription (RT) reaction. This was carried out as a 1-step RT-PCR reaction using PrimerDesign Reverse transcriptase premix-2™, and RT negative control premix for controls. A final concentration of 5ng/ μ l was required for the PCR reaction. Therefore, in order to prepare enough cDNA to perform all PCR

using samples that were reverse-transcribed in the same reaction, the volume required to undertake full analysis was calculated (including 10% extra in case of pipetting or other user errors) using results from the RNA quantification, and the RT reaction planned based on this (Appendix 3).

For the RT reaction, the work area was prepared by decontaminating with RNase Zap™, and nuclease-free pipettes and plastics used in all handling and transfer. The pre-calculated volume of RNA sample was added to 20µl of RT premix 2 into 0.2µl thin wall reaction tubes, including RNase-free water where required to balance the reaction volume (volume can be varied without affecting the efficiency of the RT reaction). Samples were then incubated in a thermal cycler at 42°C for 20 minutes for the RT reaction to occur, then 72°C for 10 minutes to heat inactivate any other products. Based on the calculations, the resultant cDNA was finally diluted with RNase-free water in order to adjust it to 5ng/µl concentration required for PCR, before being stored at -20°C until required.

geNorm Pilot Experiment for Reference Gene Selection

Use of multiple stable housekeeping (stable reference) genes (HKG) is the method of choice for RT-qPCR (Vandesompele et al., 2002). In order to select the most appropriate reference genes for use during PCR, a geNorm reference gene selection kit containing a 12 gene panel was used. geNorm is a recognised gold standard in the industry for selection of reference genes from which to normalise experimental data. The gene panel provided for *mus musculus* cell lines is:

- Mus musculus actin, beta, cytoplasmic (ACTB), mRNA;
- Mus musculus glyceraldehyde-3-phosphate dehydrogenase (GAPDH), mRNA;
- Mus musculus ubiquitin C (UBC), mRNA;
- Mus musculus beta-2 microglobulin (B2M), mRNA;
- Mus musculus phospholipase A2 (YWHAZ), mRNA;
- Mus musculus ribosomal protein L13a (RPL13A), mRNA;
- Mus musculus calnexin (CANX), mRNA;
- Mus musculus cytochrome c-1 (CYC1), mRNA;
- Mus musculus succinate dehydrogenase complex, subunit A (SDHA), mRNA;
- Mus musculus 18S rRNA gene;
- Mus musculus eukaryotic translation initiation factor 4A2 (EIF4A2), mRNA; and

- Mus musculus ATP synthase subunit (ATP5B), mRNA.

The PCR laminar flow hood was prepared by cleaning with RNase Zap™, and the area, plus all plastics and pipettes further sterilized using UV light before work commenced. To prepare the primers, they were first pulse spun

Table 10: PCR Reaction mix preparation (per well) as provided by PrimerDesign. *working concentration of primers = 300nM in a 20µl reaction.

Component	Vol. for 1 reaction
Resuspended primer mix	1µl*
PrimerDesign 2x PrecisionPLUS™ Mastermix	10µl
RNAse/DNAse free water	4µl

to ensure that dry primer mix was at the base of the Eppendorf tube, then re-suspended using 200µl primer mix contained in the kit. PCR reaction mix was prepared using Primer design 2x PrecisionPLUS™ qPCR Mastermix with SYBR green (Table 10). Once the reaction mix was prepared, 15µl was pipetted into each well on a Primer Design BrightWhite qPCR plate. Following this, 5µl of diluted cDNA at 5ng/µl concentration was added to each well according to a pre-prepared plate plan. The plate was sealed with an optical seal and centrifuged for 1 minute at 19 xg to mix well contents, before being transferred to a StepOne™ qPCR system, and run according to the thermal cycling conditions outlined within figure 40. During this, three main steps are undertaken repeatedly: i) denaturation; heating of samples to 95°C to denature template DNA, disrupting hydrogen bonds and interactions holding base pairs together, ii) annealing; cooling to around 60°C to allow primers to base pair (anneal) to complementary regions on the template, and iii) extension; where temperature is increased to allow the polymerase to extend the primer to form a nascent DNA strand. After completion of 40 cycles, the cycler holds temperature between 4°C and 10°C to maintain integrity of the products.

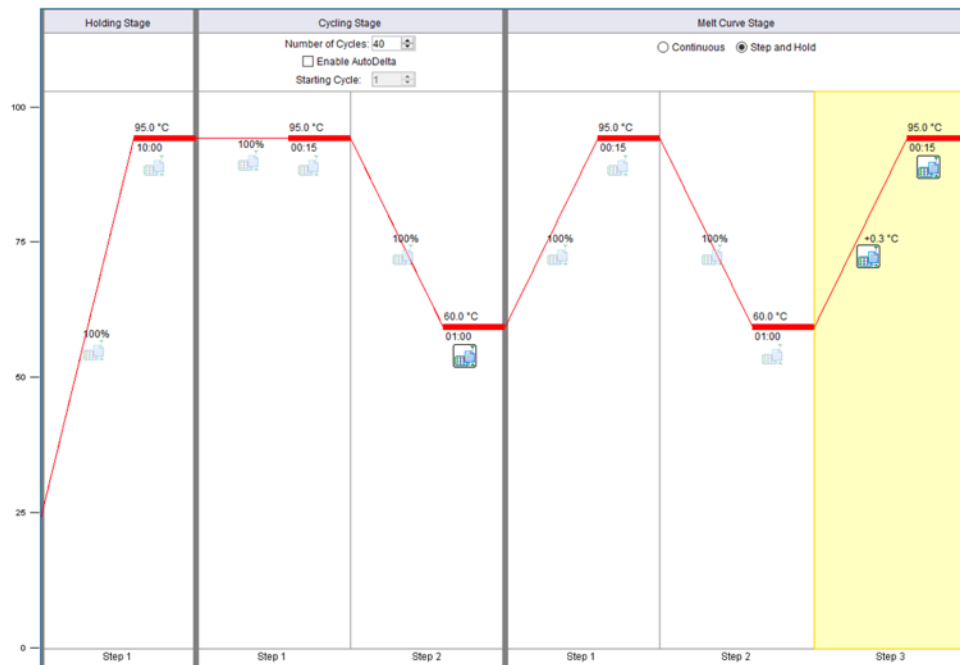


Figure 40: Amplification conditions for PCR

Results were then analysed using qbase^{PLUS} software, a programme based on Microsoft Excel which incorporates data quality controls and uses an advanced relative quantification model with efficiency correction, multiple reference gene normalization, inter-run calibration and error propagation along each step of the calculations (Hellemans et al., 2007). This ranked housekeeper genes (HKG) in order of stability of expression, providing reference values for acceptable gene stability (geNorm M value), and the results were used to dictate reference genes used for later PCR.

Primer Design & Efficiency testing

Following an extensive literature search, primers were designed based on published literature and via cross-reference to NCBI-NIH Primer-BLAST, a free-to-use online offering which helps users make primers that are specific to the intended PCR target. Primer-BLAST uses algorithms to help with primer choice, and screens these against a database which helps to avoid selection of non-specific amplifications (Ye et al., 2012).

Table 11: Primers designed for PCR work

Primer Identity		Amplicon characteristics				
Name	Variant	Accession Number	Primer Sequence	Size (base pairs)	Tm (°C)	GC content (%)
LH-R	-	NM_013582	F: CTCGCCCGACTATCTCTCAC	20	61.4	60
			R: ACGACCTCATTAAGTCCCCTG	21	59.8	
StaR	-	NM_011485	F: GCAGCAGGCAACCTGGTG	18	60.5	66.7
			R: TGATTGTCTTCGGCAGCC	18	56.0	
CYP11A1	Subfamily A, Polypeptide 1, Transcript Variant 1	NM_019779	F: ACATGGCCAAGATGGTACAGTTG	23	60.6	47.8
			R: ACGAAGCACCAGGTCATTAC	21	59.8	
3β-HSD	Transcript variant 1	NM_008293	F: TTCCAGGCAGACCATCCTA	20	59.4	55
			R: TCTGTTCTCGTGGCCATTC	20	59.4	

The final primer designs were procured from Eurofins genomics (Table 11). Primers were provided as separate Forward and Reverse preparations. Upon arrival, primer tubes were first pulse spun to ensure that dry primer mix was at the base of the Eppendorf tube. They were then re-suspended a volume of RNase/DNase free water, calculated to provide a starting concentration of 100pMol/μl. To ensure complete

Table 12: User-supplied PCR reaction mix preparation/well

Component	1 Reaction
Resuspended Eurofins primer mix @6pMol/ul (F+R)	2ul
PrimerDesign 2x PrecisionPLUS™ Mastermix	10ul
RNase/DNase free water	3ul
Template (25ng)	5ul @5ng/μl
Final volume	15ul

resuspension, each tube was vortexed, then allowed to stand for 5 minutes before being vortexed again and stored at -20°C when not in use. Primer Design required 6pMol of forward and 6pMol of reverse primer for a PCR reaction mix using Primer Design Mastermix, therefore a 6pMol/ μ l solution was prepared, and F and R primers were mixed just prior to addition to the mix (Table 12).

For the calculation of gene expression via the delta delta Ct method used ($\Delta\Delta C_T$), it is assumed that PCR primer efficiencies are comparable between the gene of interest (GOI) and the housekeeper gene(s) (HKG). In order to ensure that this assumption is valid, primer efficiencies were calculated using a standard curve. Ideal primer efficiency is between 90-110%. To prepare the standard curve, a sample of untreated cDNA was diluted in RNase-free water according to table 13.

Table 13: Serial Dilutions of untreated cDNA to generate standard curve for primer efficiency determination

Tube	Sample	Volume sample	Volume RNase-free water
A	Stock cDNA	85ul	0 μ l
B	1/10 dilution	8.5ul tube A	76.5 μ l
C	1/100 dilution	8.5ul tube B	76.5 μ l
D	1/1000 dilution	8.5ul tube C	76.5 μ l
E	1/10,000 dilution	8.5ul tube D	76.5 μ l

RT-qPCR was performed under the same conditions as the GENORM analysis (Figure 40), with each sample in technical and biological triplicate per GOI, and results were analysed within Microsoft Excel.

In addition, a further set of custom-designed primers was obtained from Primer Design (Table 14). These primers have guaranteed efficiency of >90% and are suitable for use with the delta Ct method without need for mathematical correction. To prepare the primers, they were first pulse spun to ensure that dry primer mix was at the base of the Eppendorf tube, then re-suspended in 660 μ l RNase/DNase free water contained in the

kit. To ensure complete resuspension, each tube was vortexed, then allowed to stand for 5 minutes before being vortexed again and stored at -20°C when not in use.

Table 14: Primer Design Custom-designed primers

Primer Identity			Amplicon characteristics				
Name	Variant	Accession Number	Primer Sequence	Size (base pairs)	Amplicon Length	Tm (°C)	GC content (%)
LH-R	-	NM_013582	F: TTCACCCAAGACTCCAATG	21	96	56.4	47.6
			R: AGCCAAATCAACACCTAAGG	21		56.4	
StaR	-	NM_011485.5	F: TGGCTGCTCAGTATTGACCTG	21	92	52.4	52.4
			R: AGGTGGTTGGCGAACTCTATC	21		52.4	
CYP11A1	Subfamily A, Polypeptide 1, Transcript Variant 1	NM_019779	F: TGCTGTCTACCAGATGTTCCAC	22	89	57.5	50
			R: CCTTCCAGGTCTTAGTTCTGAGG	23		57.5	
3β-HSD	Transcript variant 1	NM_008293	F: CCCCTGCTCAGAGACAAACATA	22	125	57.2	50
			R: AAGGCAAGATATGATTTAGGAC	27		57.3	
			TGAA				

PCR

Once all preparatory work had been completed and the process optimised, the final experimental PCR was carried out for the GENORM panel analysis for both the Primer Design GOI primer set, as well as GAPDH ACTB and YWHAZ HKGs. Each PCR reaction was prepared according to Table 15. A standard plate setup was adhered to for each gene, which included each treatment in triplicate, each sample in biological triplicate, as well as no template controls (NTC) using RNase-free water, and no reverse transcriptase control (NRT) using RNA samples which underwent thermal cycling in the absence of

reverse transcriptase (Primer Design noRT). Once the reaction mix was prepared, 15µl was pipetted into each well on a Primer Design BrightWhite qPCR plate. Following this, 5ul of diluted cDNA at 5ng/µl concentration was added to each well according to the plate setup plan (Table 15). The plate was sealed with an optical seal and centrifuged for 1 minute at 19 xg to mix well contents, before being transferred to a StepOne qPCR system and run according to the amplification conditions outlined within Fig. 40. Results were then analysed using Microsoft Excel and Graphpad Prism.

Table 15: PCR reaction mix, prepared according to protocol from PrimerDesign.

Components	Vol. for 1 reaction
PrecisionPLUS	10µl
Primer/Probe mix	1µl
Template (25ng)	5µl
RNAse/DNAse free water	4µl
Final Volume	20µl

Protein Expression via Western Blot

To investigate protein expression, SDS-PAGE gel electrophoresis followed by Western Blot was undertaken, using both fluorescent and horseradish peroxidase conjugated secondary antibodies. For the protein work, antibodies were selected that matched to some of those used for histological analysis of animal tissues following ENM exposure *in vivo* and procured from Santa Cruz biotechnology.

Protein Extraction

Preparation of protein samples for Western blotting was undertaken for ENM-110, 111 and 300 as follows. TM3 cells were cultured for 24 hours in a 6 well plate at a density of 2.75×10^5 cells/well, either with or without addition of testosterone to allow determination of whether the cells were stimulated in any way following hormone exposure. This was done by adding 3µl of 1nM T or ethanol vehicle to each well to give final concentration of 9nM in each well of the plate. Cells were treated with ENM at sub-lethal doses (0,1,2,4,6 and 8µg/ml, equating to 0, 0.32, 0.63, 1.26, 1.89 and 2.52 µg/cm²) and incubated for a further 24 hours. Following this, plates were washed with 1ml phosphate buffered saline (PBS) on ice twice, scraped and transferred to ice cold tubes. Tubes were centrifuged at 146 xg for 5 minutes at 4° C. PBS was removed, and the

pellet re-suspended in 3x its own volume of lysis buffer containing HALT protein inhibitor cocktail (Thermo Scientific #87786), before being incubated on ice for 20 minutes. Following incubation, tubes were centrifuged at 13,793 xg at 4°C for 5 minutes. The supernatant was then removed, and a Bradford assay performed to determine protein content before storing samples at -80°C.

The Bradford assay

The Bradford assay is a colorimetric protein assay, based on the shift in absorbance of Coomassie Brilliant Blue dye. Under acidic conditions the red form of the dye is converted into its bluer form to bind to the protein being assayed. When protein binds to the dye, it stabilizes the blue form of the Coomassie dye. Consequently, the amount of the dye-protein complex present in solution is a measure of the protein concentration and can be estimated by measuring its absorbance at 600nm. Reference standards were prepared from 0 - 1500µg/ml protein. 5µl standards and protein extract samples (diluted 1:5) were added to a 96 well plate, followed by 250µl Bradford reagent. After 5 minutes of incubation at room temperature, the plate was read at 600nm and the absorbance of samples vs standards was used to determine the protein concentration of each sample. All readings were adjusted against the absorbance of a zero standard.

Western Blot

Western blotting is a technique in which gel electrophoresis is used to separate macromolecules such as proteins in a sample by size (kDa). Introduced in 1979 by Towbin *et al*, blotting involves the transfer of proteins from gel to a nitrocellulose or polyvinylidene difluoride (PVDF) membrane and blocking to prevent nonspecific binding (Towbin et al., 1979). The membrane is then probed with primary antibodies specific to the target protein of interest, and a secondary antibody specific to the host species of the primary in order to produce a detectable signal. Detection may be undertaken via a number of established methods, including colourimetric reactions, fluorescence and chemiluminescence (ThermoFisher-Scientific, 2019b).

Fluorescence Detection via LiCor

Fluorescence-based systems for detection of proteins are based on conjugation of fluorophores (fluorescent molecules) to secondary antibodies, which attach to the

primary antibody on the protein of interest (Fig. 43, right). Within the detection system, a light source emits high energy photons and excites the fluorophore, allowing it to leave ground state (S_0) and enter a higher energy state (S'_1). Some of this energy dissipates allowing the fluorophore will enter a relaxed state (S_1). Finally, a photon of light at a slightly lower energy and longer wavelength than the light source itself is emitted (due to the energy dissipation that has already occurred), returning the fluorophore to ground state again (S_0). The emitted light signal is captured by a camera to produce the final image.

For fluorescent detection, 0.75mm thickness gels were prepared in the lab following an in-house protocol (Frazer, 2014). Later these were later replaced by mini-PROTEAN® TGX™ pre-cast gels, purchased from BioRad in order to reduce preparation time on each blot. Protein samples were prepared at 1µg/ml (sufficient for 10µg protein/lane) in loading sample buffer and boiled for 5 minutes at 95° C for 5 minutes. 10µl of sample was then loaded to each lane of the gel, with a final lane containing 4ul PageRuler™ Plus pre-stained Protein ladder (10-250kDa). Electrophoresis was run at 100V for 90minutes (or until the protein ladder reached the end of the gel). Gels were then removed, and transfer to nitrocellulose membrane was undertaken for 1 hour at 100V with the tank on ice.

Once transfer was complete, the nitrocellulose membrane was blocked in Odyssey Blocking Buffer diluted 1:1 with PBS for 1-2 hours at room temperature. Odyssey blocking buffer is a mammalian protein-free blocker in PBS, which helps to prevent non-specific protein binding as the membranes have a high affinity for proteins. Following blocking, the primary antibody of interest and reference antibody (Actin) were prepared according to the dilutions outlined within Table 16 (page 163).

The membrane was cut in half, and the Ab of interest added to one membrane, while the reference Ab was added to the other. Incubation took place overnight at 4° C on a laboratory rocker to ensure distribution of the antibodies across the membranes. The following morning, the membrane was rinsed for 4 cycles of 5 minutes with 1x PBS-Tween (PBS-T) on a rocker at room temperature, before incubation with a fluorescent secondary antibody (Odyssey antibody prepared in Odyssey blocking buffer with 0.1%

Tween) at room temperature for 1 hour in the dark with shaking. Following a further rinse cycle with PBS-T, a final rinse with PBS was undertaken before reading the membranes on an Odyssey infrared imaging system (Li-Cor) in both 700 and 800 channel settings and undertaking further analysis using Image Studio Lite software.

Enhanced Chemiluminescence (ECL) Detection via GBox

Chemiluminescent Western blotting was used for some blots, as it is a highly sensitive detection system for looking at single proteins and issues were encountered with detection on the fluorescent LiCor system. The selected system is luminol-based, using horseradish peroxidase (HRP) conjugated secondary antibodies. In the presence of HRP and peroxidase buffer, the luminol in the reaction mix applied oxidises to an excited-state product called 3-aminophthalate which emits light as it decays. (Fig. 43).

Sample preparation and electrophoresis was identical to that used for LiCor fluorescent detection. However, gels were prepared according to a plan which allowed one membrane to be stained for all 4 antibodies (Fig. 42 and 43).

Once the gel was run, PVDF membrane was activated in 100% methanol for 5 minutes, then rinsed in blotting buffer. Transfer was undertaken at 100V for 60minutes with the tank on ice. Once transfer was complete, the PVDF membrane was blocked in a solution of PBS-tween containing 10% Marvel (milk powder containing the phosphoprotein casein which binds to unoccupied sites on the membrane) for 1-2 hours at room temperature. Primary antibodies were prepared as in Table 16, membranes were cut down the centre of each ladder, and incubated with separate primary antibodies overnight at 4°C on a rocker.

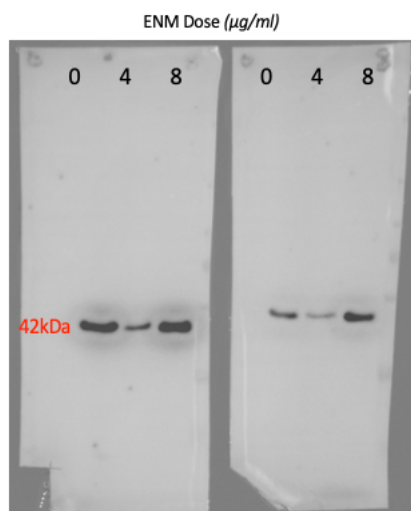


Figure 41: Example ECL Actin stain (NM-110 & NM-111 n=1). 0,4 and 8µg/µl represent doses of 0, 1.26 and 2.52µg/cm²

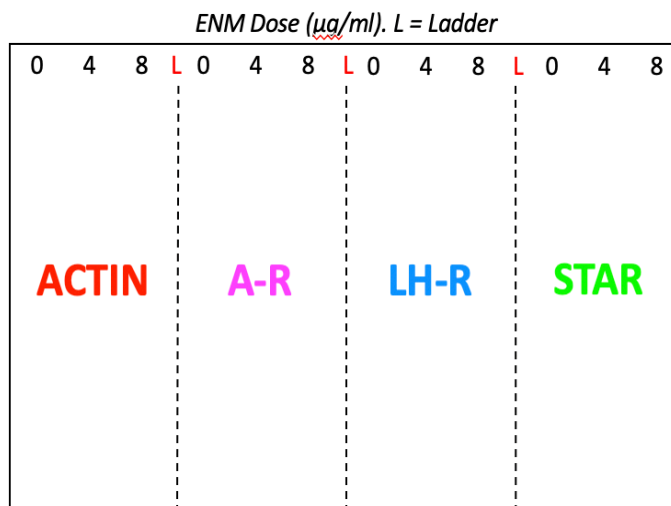


Figure 42: Gel/Membrane layout for staining against 4 antibodies and analysis by ECL. 0, 4 and 8µg/µl represent doses of 0, 1,26 and 2.52µg/cm².

The following day, the membrane was rinsed with PBS-tween (0.05% tween) and washed for 4x5 minutes (applying fresh buffer each time). The secondary antibodies were prepared (in PBS-Tween 0.05% with 5% marvel) and incubated with the membrane for 1 hour at room temperature with shaking. As these secondary antibodies were horseradish peroxidase conjugated, this incubation did not need to be in the dark. Following a further rinse cycle with PBS-T (rinse, followed by 4x5minute wash), the membrane was rinsed with PBS to remove residual tween.

Amersham ECL Prime Western Blotting Reagents were prepared according to manufacturer's specification (GE Healthcare Life Sciences), with aliquots of both luminol and peroxidase solution being allowed to warm to room temperature before use (luminol solution was kept in the dark until application to the membrane). ECL reagents were mixed just prior to use, then carefully pipetted onto the membrane laid on a clear plastic surface in preparation for imaging. Imaging was undertaken using the GBox Chemi Gel Doc using GeneSys software for automatic optimization of the sensitive image capture step. Subsequent analysis was undertaken using Image J software.

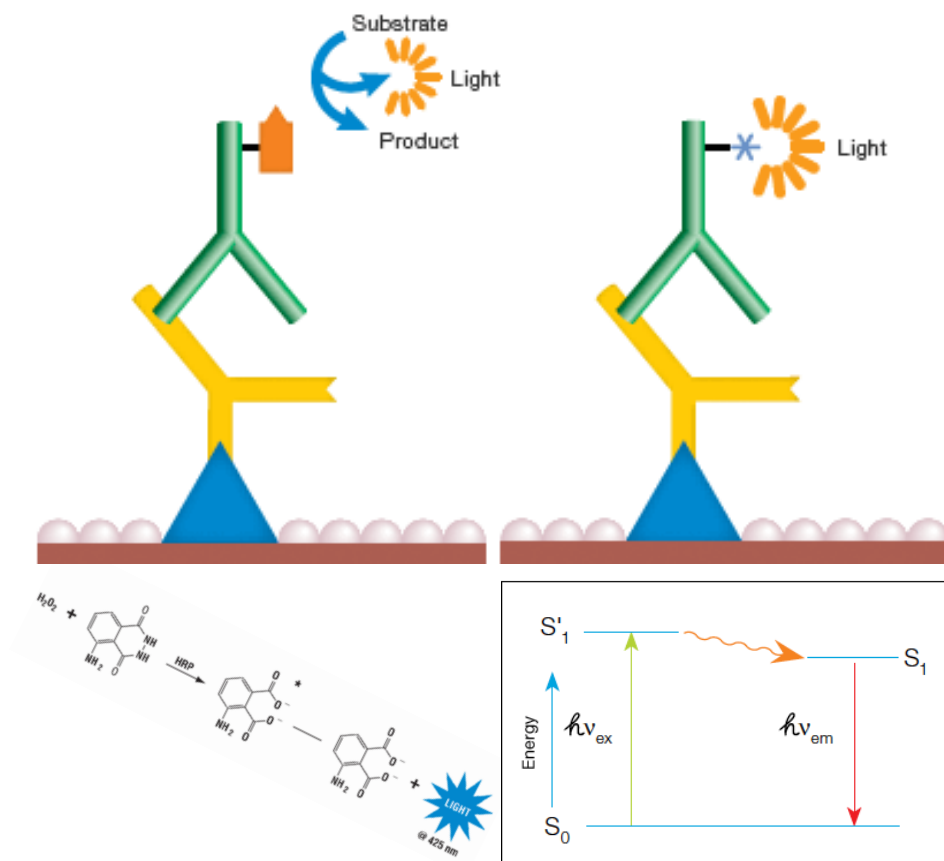


Figure 43: Western Blot detection methods. LHS is enhanced chemiluminescence as used with the GBox system, the equation representing the chemical change required to produce light. RHS is fluorescence as used with the LiCor system, the lower portion of the image representing excitation of a fluorophore bound to a secondary antibody and its subsequent release of light. Image compiled from resources provided by BioRad and GE Life Sciences.

Table 16: Antibody Preparation for Western Blotting analysis. Detailed is primary antibody and its preparation for detection in either fluorescent (LiCor) or ECL (GBox) based systems, along with secondary antibodies and their respective preparation for each detection method.

1° ANTIBODY	RAISED IN	MOLECULAR WEIGHT (kDa)	Preparation (Fluorescent)	Preparation (ECL)	2° ANTIBODY (Fluorescent)	Preparation (Fluorescent)	2° ANTIBODY (ECL)	Preparation (ECL)
Actin (Santa Cruz)	Goat Polyclonal	42kDa	1:10,000 2ul in 10ml Odyssey BB +0.1%Tween	1:10,000 2ul in 10ml PBS-T with 10% Marvel	Alexa-Fluor Donkey α Goat	1:10,000 1ul in 10ml Odyssey BB +0.1%Tween	Dako Rabbit α Goat	1:5000 2ul in 10ml PBS 0.05%tween + 5% Marvel
LH-R (Santa Cruz)	Rabbit Polyclonal	85kDa	1:200 50ul in 10ml Odyssey BB +0.1%Tween	1:200 50ul in 10ml PBS-T with 10% Marvel	Alexa-Fluor Goat α Rabbit	1:10,000 1ul in 10ml Odyssey BB +0.1%Tween	Dako Goat α Rabbit	1:5000 2ul in 10ml PBS 0.05%tween + 5% Marvel
AR (Santa Cruz)	Rabbit Polyclonal	110kDa	1:100 50ul in 5ml Odyssey BB +0.1%Tween	1:100 50ul in 5ml TBS-T w.10% Marvel	Alexa-Fluor Goat α Rabbit	1:10,000 1ul in 10ml Odyssey BB +0.1%Tween	Dako Goat α Rabbit	1:5000 2ul in 10ml PBS 0.05%tween + 5% Marvel
StaR (Santa Cruz)	Goat Polyclonal	30kDa	1:100 50ul in 5ml Odyssey BB +0.1%Tween	1:100 50ul in 5ml TBS-T w.10% Marvel	Alexa-Fluor Donkey α Goat	1:10,000 1ul in 10ml Odyssey BB +0.1%Tween	Dako Rabbit α Goat	1:5000 2ul in 10ml PBS 0.05%tween + 5% Marvel

Statistical Analysis

Calculations to determine components for PCR reactions based on RNA concentration measurements were undertaken in Microsoft Excel.

geNorm pilot experiment data was inputted to qbase+ software, which uses the full dataset for all 12 potential HKGs to calculate the gene expression stability measure 'M' for a reference gene as the average pairwise variation 'V' for that gene with all other tested reference genes. Stepwise exclusion of the gene with the highest M value allows ranking of the tested genes according to their expression stability, based on the principles and calculations described previously by Vandesompele et al. (Vandesompele et al., 2002).

Calculation of Primer efficiency was undertaken in Microsoft Excel by calculating average Ct values for each serial dilution of primer, alongside the log of each sample dilution, then using this to produce an R² value for the slope of the regression between the two. Primer efficiency was then calculated as a percentage value using the following equation:

$$\text{Primer Efficiency}(\%) = \left(10^{-\frac{1}{\text{slope}}} - 1\right) * 100$$

PCR analysis produced data files within StepOne software, which were exported to Microsoft Excel. These files contained comprehensive raw information and readings on melt temperatures, multicomponent data, amplification data and cycle thresholds (C_t). From this, C_t values for each sample in triplicate were used to calculate a mean Ct value per sample. These values were used to calculate relative changes in gene expression via the ΔΔC_t method (Hellemans et al., 2007, Livak and Schmittgen, 2001).

In order to calculate fold change in expression, a geometric mean Ct value for each RNA sample was calculated from the mean Ct values across the three HKGs. This was then subtracted from the mean Ct value of the corresponding GOI, to produce a ΔC_t value. ΔΔC_t was then calculated by subtracting the ΔC_t of the experimental control from the ΔC_t of the treated sample. This was converted into a fold difference in gene expression using the following equation (Livak and Schmittgen, 2001):

$$\text{Fold Difference in gene expression} = 2^{-(\Delta\Delta C_t)}$$

The fold difference was then logged to the base 2 in order to normalise the fold change for display as either positive or negative according to whether expression increased or decreased. Once ΔC_T and log fold change were derived, these were transferred to Graphpad Prism v7; ΔC_T values were used for 1-way ANOVA with post-hoc Tukey's test used to determine statistical significance of any changes observed, and log fold change values were used to plot the outcomes graphically.

Densitometry plots from Western Blots were analysed for fluorescent detection via Image Studio Lite (LI-COR Biotechnology), and for ECL via Image J. In short, the blot image was adjusted so that bands were clearly visible on the image. The area around each band was then selected, background intensity subtracted, and the intensity of the selected bands imported to Microsoft Excel and Graphpad Prism for further analysis and graphing.

Results

RNA Quantification and Integrity

Initial analysis of RNA quantity was undertaken via spectrophotometric analysis using a Thermo-Fisher Nanodrop 2000 spectrophotometer. This was used to guide sample preparation for more accurate analysis using chip-based electrophoresis on the Agilent Bioanalyzer 2100. The bioanalyzer uses laser-induced fluorescence detection to produce both densitometry plots (Fig. 44) and electropherograms which are used to calculate RNA quantity (concentration: ng/ μ l) and RNA integrity number (RIN).

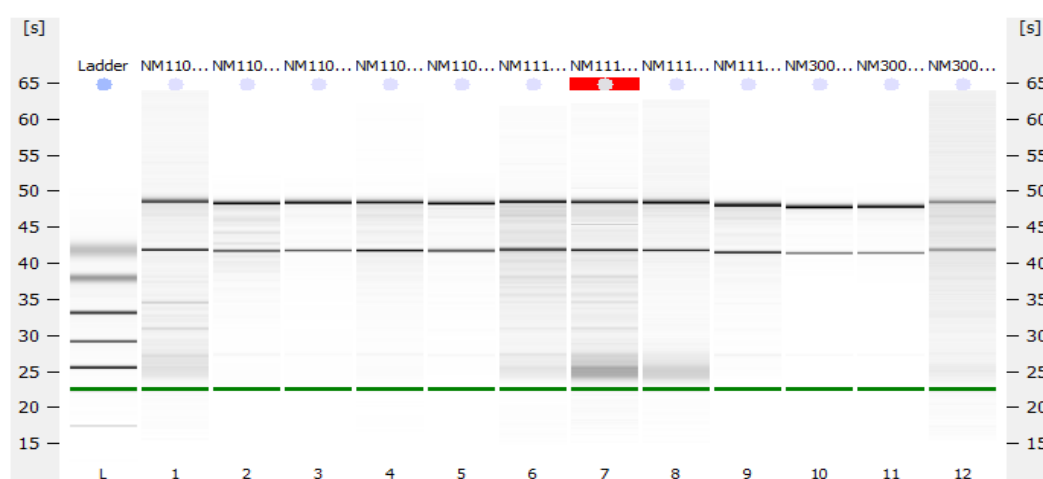


Figure 44: Densitometry plot of chip-based electrophoresis for RNA samples from cells treated with NNM-110 and NM-111 Zin Oxide nanoparticles.

Quantification was undertaken by 2100 Expert software, which uses a ladder containing components of known sizes to plot a standard curve of migration time vs. molecule size, alongside data from the internal standard 'RNA 6000 nanomarker' to align the ladder data and correct for drift effects over the course of each chip run. These known values are then used to quantify the concentration of each RNA sample on the chip in ng/ μ l. The RNA Integrity Number (RIN), a measure of integrity of total RNA samples is also produced, using Agilent Biotechnologies' proprietary method which appraises the entire electrophoretic trace of the sample, including presence or absence of degradation products. Generally, it is considered that an RIN of >7 indicates good quality RNA.

The results (Appendix 4) show that whilst the Nanodrop is a useful initial indication on presence or absence of RNA in an extracted sample and its purity, concentration reported tended in many cases to be a lower estimate of RNA content than those

obtained when the sample underwent detailed quantification using the Bioanalyzer. RNA concentrations were found to be sufficient to proceed with PCR in 24/27 samples, and consistently high RNA integrity scores (RIN) indicated that RNA extraction had been successfully undertaken to the required standard. For cell treated with NM-300 at $2.52\mu\text{g}/\text{cm}^2$ aberrant readings were recorded, indicating that the cells and their RNA content were potentially degraded. This finding was in line with the results discussed within chapter 3, which indicated that although $2.52\mu\text{g}/\text{cm}^2$ was considered to be a sub-lethal dose of NM-300, the nature of the NM preparation meant that over time, ionic silver was released from the nanoparticles, leading to an increase in potency with storage which in turn reduces the threshold for loss of cell viability.

GENORM 12 Gene Panel Analysis

geNorm analysis on 18 representative samples against 12 target genes was completed using qbase+ software. Analysis confirmed the run layout was correct, with all samples measured in the same run against a given reference target. Results of the analysis showed that the optimal number of reference targets in this experimental situation is 3, as geNorm average pairwise variation $V < 0.15$ when comparing a normalization factor based on the 3 or 4 most stable targets (Fig. 45). As such, the optimal normalization factor can be calculated as the geometric mean of reference targets GAPDH, ACTB and YWHAZ. High reference target stability was observed (average geNorm $M \leq 0.5$). This is typically seen when evaluating candidate reference targets on a homogeneous set of samples (e.g. untreated cultured cells, or blood from normal individuals). Fig. 46 & 47 show the stable expression and behaviour of all three selected housekeeper genes.

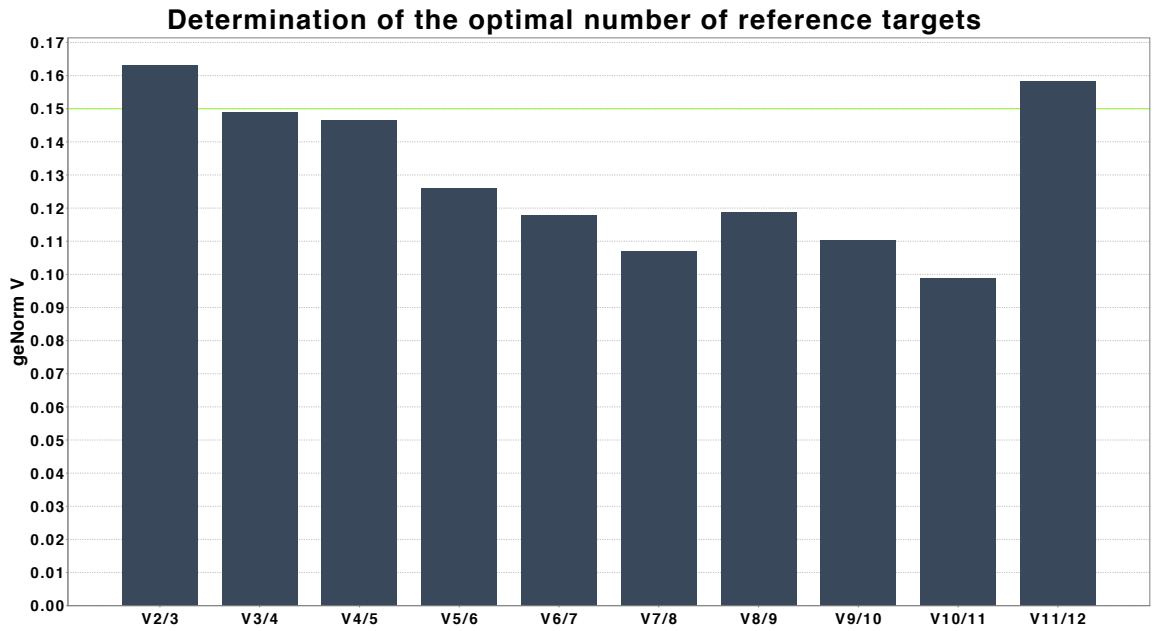


Figure 45: geNorm pairwise variation across 12 potential reference genes. Optimal number of targets confirmed to be 3, with $V < 0.15$ for this number (sample $n=18$).

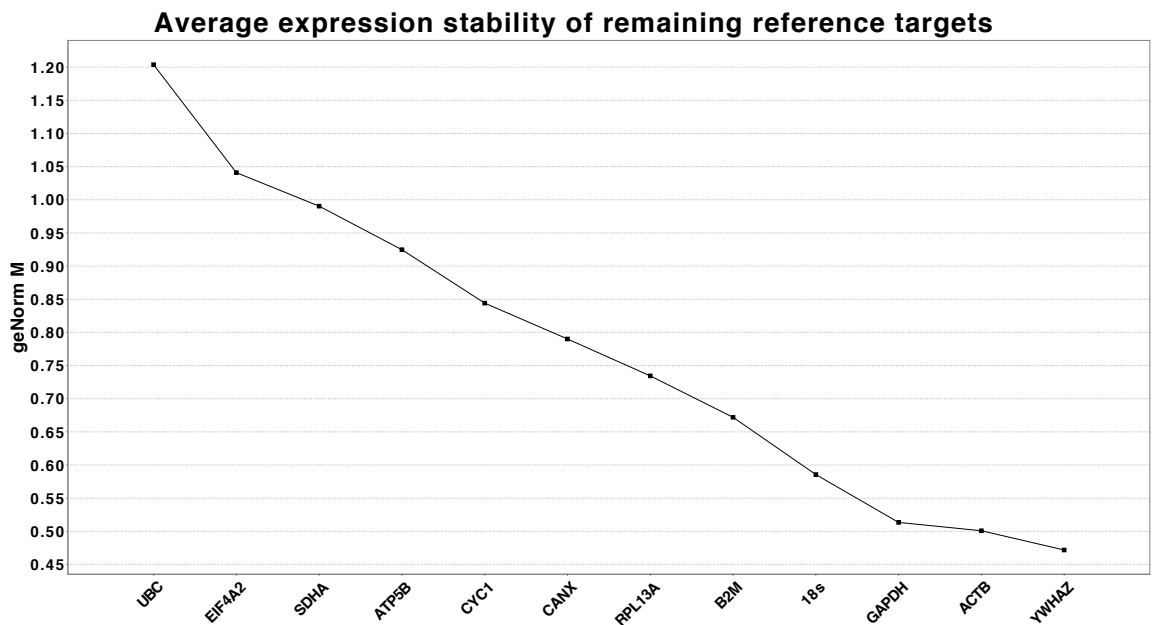


Figure 46: geNorm M values for 12 panel kit. GAPDH, ACTB and YWHAZ were confirmed as having the most stable expression across all samples tested (sample $n=18$).

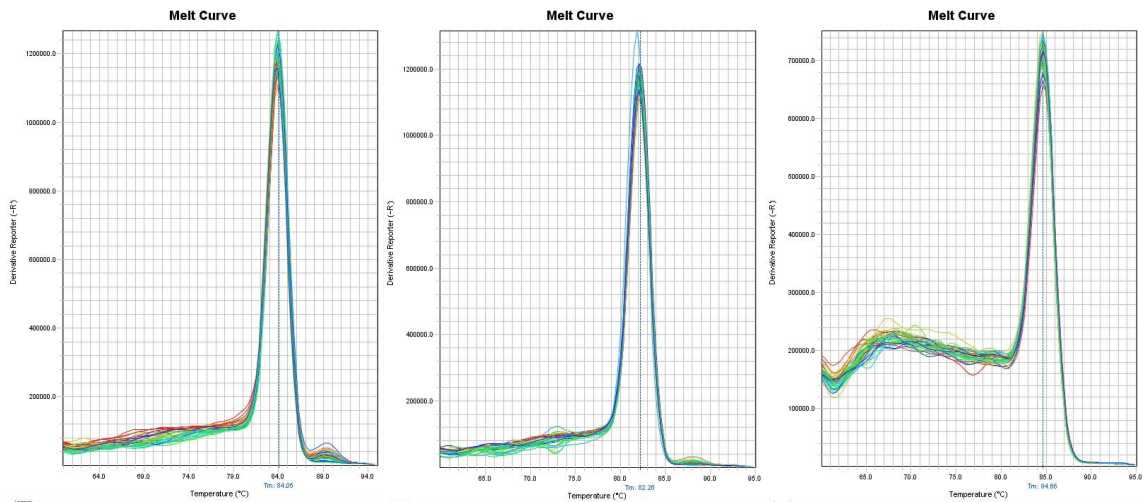


Figure 47: Melt Curves for GAPDH, YWHAZ and ACTB (L to R) as selected using geNorm analysis.

Primer Efficiency testing

Efficiency testing was undertaken for each of the primers designed based on published literature and using NCI – NIH Primer –BLAST was undertaken. If primer efficiency is 100% then Ct values in 10-fold dilutions will be 3.3 cycles apart, representing a 2-fold change for each change in Ct. Desirable primer efficiencies lie between 90% and 110%. However, initial analysis of the amplification plots and melt curves generated indicated that there may be issues with the primers, as all except StaR showed late and unevenly distributed cycle amplification, and melt curves were not clean in appearance (Fig. 48). Further analysis of the Ct values showed that primer efficiency was poor, with calculated efficiencies varying hugely between primers and all indicating R^2 values far lower than the desired >0.90 (Table 17).

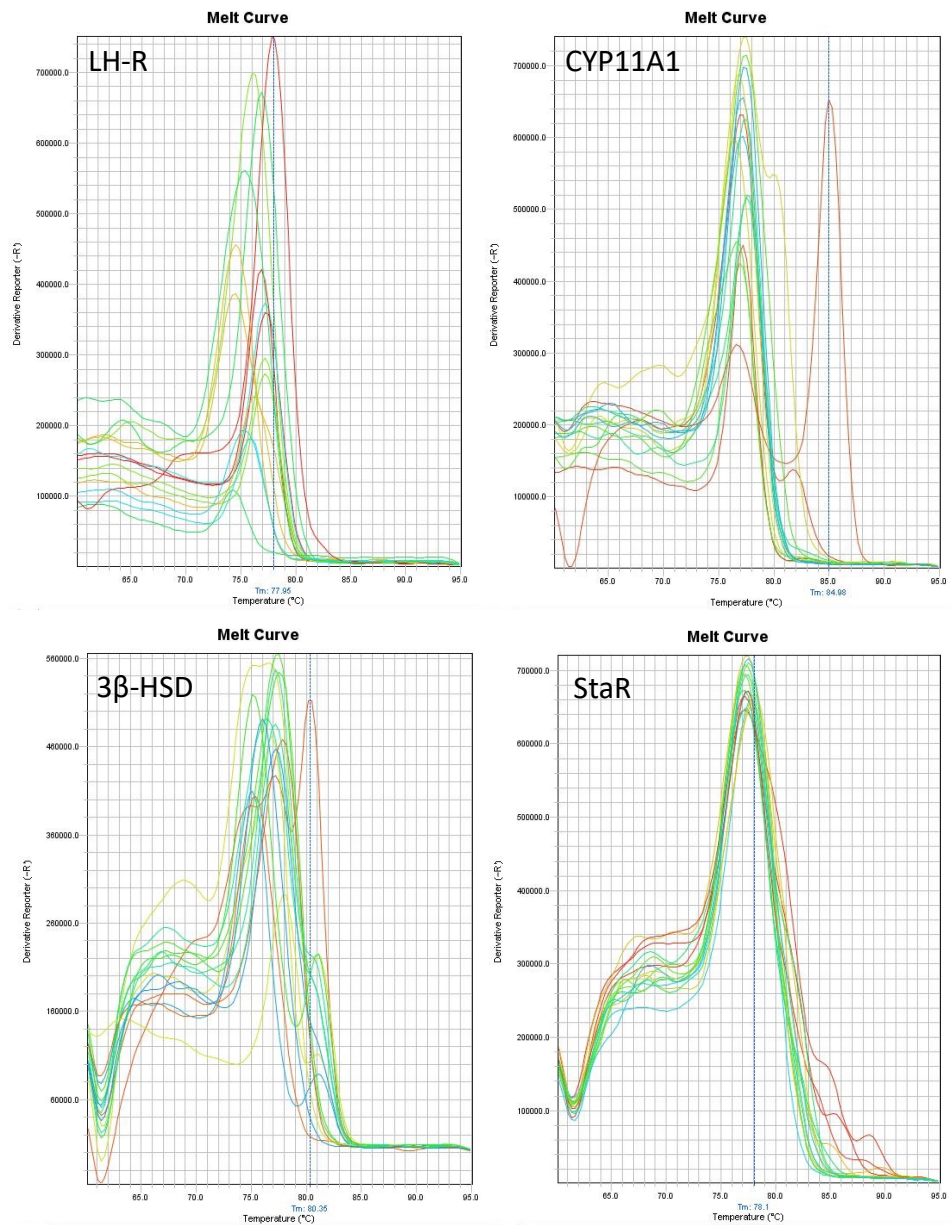


Figure 48: Melt curves generated during primer efficiency testing.

Table 17: Efficiency testing of Primers sourced from Literature and Primer-BLAST searching

Primer	Slope	R Squared	Plot
LH-R	-0.51	0.69	
CYP11A1	-0.15	0.28	
3β-HSD	-0.23	0.31	
StaR	0.06	0.59	

Because of the issues encountered despite extensive research and planning and use of primers which were mostly already published in the literature, the decision was made to move to using custom-designed primers from PrimerDesign.

PCR

Analysis of the output from RT-qPCR using PrimerDesign custom primers revealed several interesting findings. Initial analysis of the Amplification Plots and Melt Curves confirmed that the primers were behaving as predicted, with amplification plots showing reliable cycle threshold (Ct), and clear single-peak melt curves, indicating the primers were working well and with good

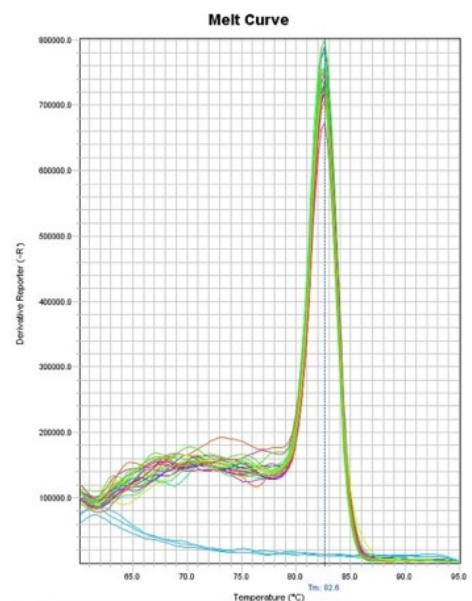


Figure 49: Example melt curve for PrimerDesign custom primer. Curve shown is for StaR. Blue region at base is no template control data.

efficiency (Fig.49). Ct values were converted to fold-change in gene expression, and results graphed. The change in gene expression is shown as the log to the base 2 of fold difference in expression order to allow display as either positive or negative according to whether expression increased or decreased.

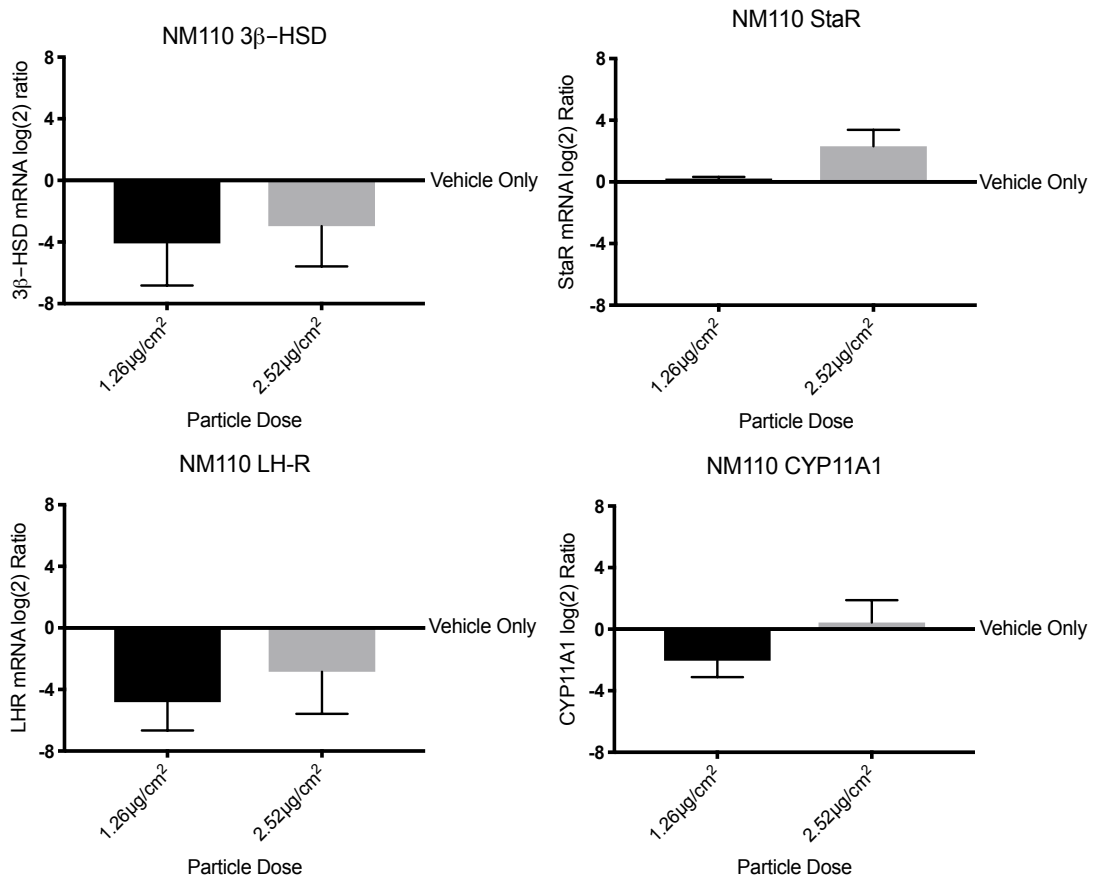


Figure 50: mRNA expression from TM3 cells exposed to NM-110 shown as log₂ ratio fold difference compared to vehicle

For NM-110 uncoated zinc oxide, it appeared that there was a small reduction in expression of 3β-HSD, LH-R and CYP11A1. There was little to no change recorded in expression for StaR recorded (Fig. 50). Statistical analysis of these results showed that no changes were significant when tested using 1-way ANOVA (Table 18, p175) implying that overall for this sample size there is little evidence for a change in expression from any of the genes tested. 0, 4 and 8 μg/μl represent doses of 0, 1.26 and 2.52 μg/cm².

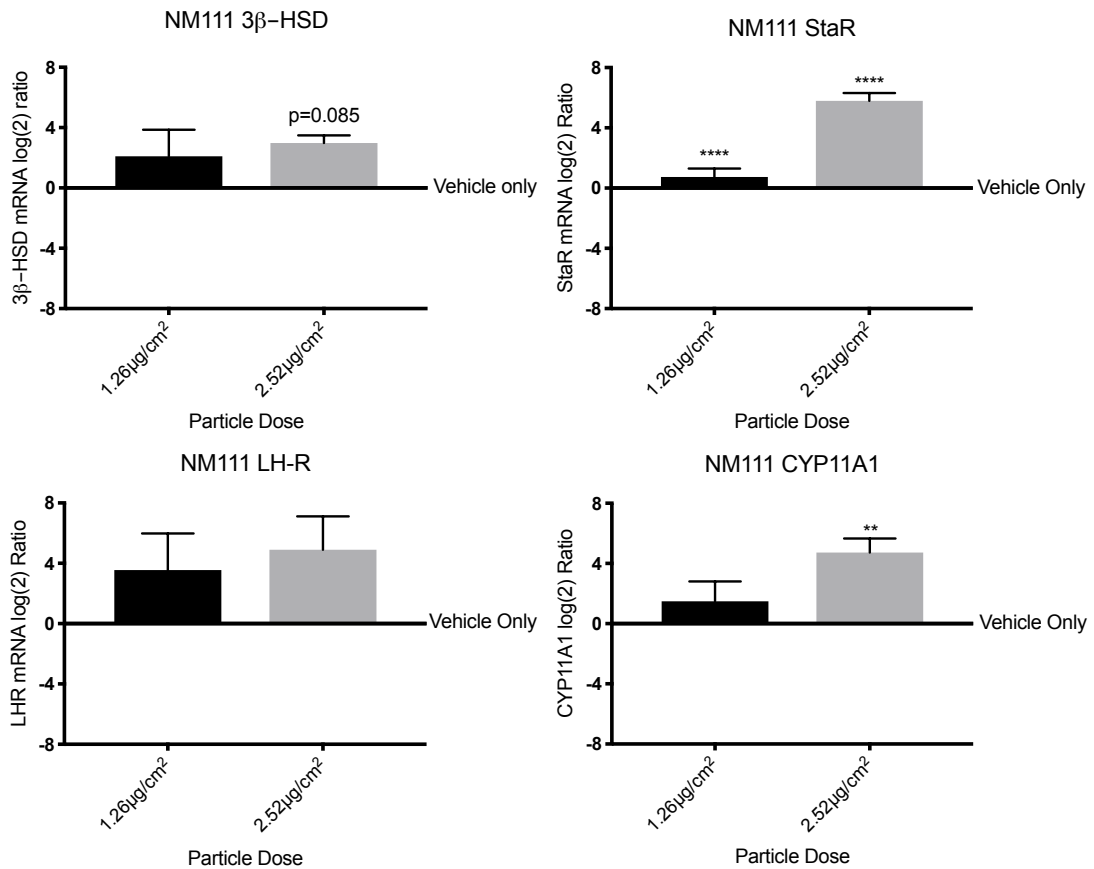


Figure 51: mRNA expression from TM3 cells exposed to NM-111 shown as log₂ ratio fold difference compared to vehicle

For NM-111 uncoated zinc oxide, visual analysis of the graphed data appeared to show an increase in expression for all genes with increasing dose of nanomaterial applied (Fig.51). This was further investigated by ANOVA and Tukey's post-hoc analysis (Table 18), which showed that for StaR the change in expression was significant from 1.26 μg/cm², and for CYP11A1 the change in expression was significant from 2.52 μg/cm². However, for LH-R and 3β-HSD, no significant change in expression was found. It was notable that for 3β-HSD the probability of a difference in expression was 0.085, which indicates a 90% confidence level in changed expression compared to vehicle.

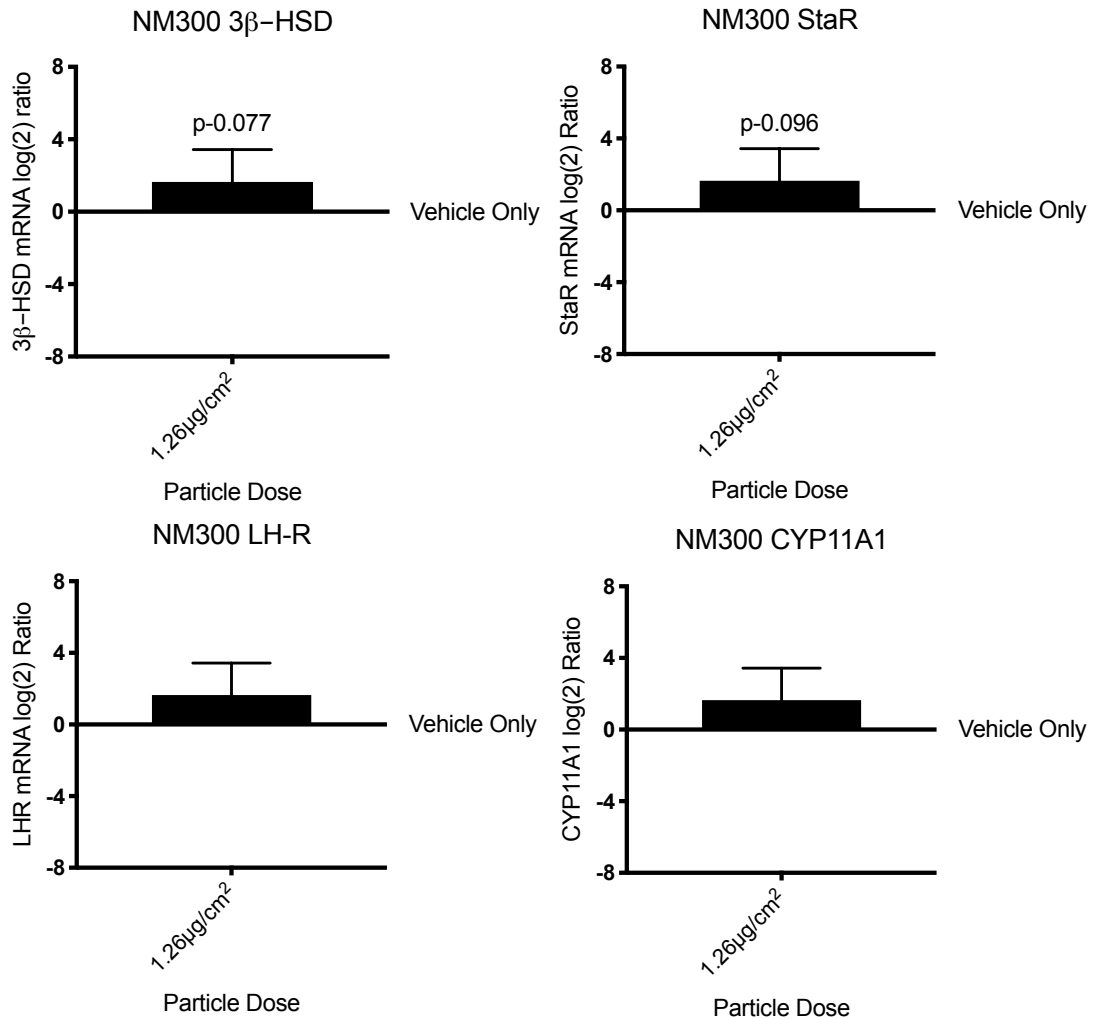


Figure 52: mRNA expression from TM3 cells exposed to NM-300 shown as log(2) ratio fold difference compared to vehicle. Graphs show only lower dose (4μg/μl or 1.26μg/cm²) data because cells treated with 8μg/μl (2.52μg/cm²) did not yield any RNA.

For NM-300 silver, all genes appeared to show an increase in expression in treated cells compared to control (Fig. 52). However, despite the trend in the data, none were shown to be significant by one-way ANOVA (Table 18). However, it was notable that for StaR and 3β -HSD the probabilities of a difference in expression were 0.096 and 0.077 respectively, which indicates a 90% confidence level in changed expression compared to vehicle. For this dataset, no Tukey's multiple comparison test was undertaken due to the lack of RNA for TM3 cells treated with 2.52μg/cm² NM-300.

Table 18: Statistical analysis of RT-qPCR for 4 GOI in TM3 cells treated with NM-110, NM-111 and NM-300. It is worth noting that as little RNA was detected in samples treated with 8µg/µl NM-300, no Tukey's multiple comparisons test was completed.

GOI	NM-110		NM-111		NM-300
	ANOVA Result	Tukey Result	ANOVA Result	Tukey Result	ANOVA Result
StaR	p=0.096	0v4 p=0.9787 0v8 p=0.1153 4v8 p=0.1484	Sig**** p<0.0001	Significant* 0v4 p=0.2863 0v8 p<0.0001**** 4v8 p<0.0001****	n/s p=0.0966
LH-R	p=0.260	0v4 p=0.2374 0v8 p=0.5585 4v8 p=0.7430	n/s p>0.070	n/s 0v4 p=0.2241 0v8 p=0.0909 4v8 p=0.7666	n/s p=0.303
CYP11A1	p=0.676	0v4 p=0.7681 0v8 p=0.9881 4v8 p=0.6854	Sig** p=0.004	Significant* 0v4 p=0.2704 0v8 p=0.0036** 4v8 p=0.0211*	n/s p=0.4718
3b-HSD-1	p=0.285	0v4 p=0.2774 0v8 p=0.4733 4v8 p=0.8898	n/s p=0.091	n/s 0v4 p=0.2316 0v8 p=0.0858 4v8 p=0.7266	n/s p=0.077

Western Blotting

The standards against which protein quantity was estimated showed accuracy in preparation, with a linear regression R² fit of 0.9849 (Fig. 53). Protein concentration readings were used to prepare 200µl 'Western-ready' sample aliquots at a concentration of 10µg in a 10µl volume, complete with loading sample buffer and 10% DTT.

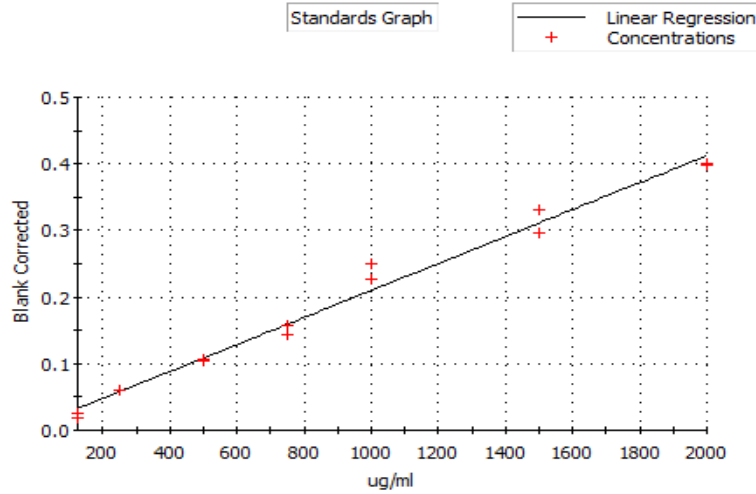


Figure 53: Standards for derivation of protein concentration from prepared samples obtained via Bradford assay. Linear regression R^2 fit of 0.9849.

The first antibody examined was the LH receptor, with Actin as the reference antibody using the LiCor fluorescent system. TM3 cells treated with NM-110 were selected as the first for examination by Western blot. The initial gels for NM-110 exposed cells n1, n2 and n3 which were supplemented with testosterone are shown in Fig. 54. Interestingly, two rows of clearer bands were present around 85kDa for LH-R.

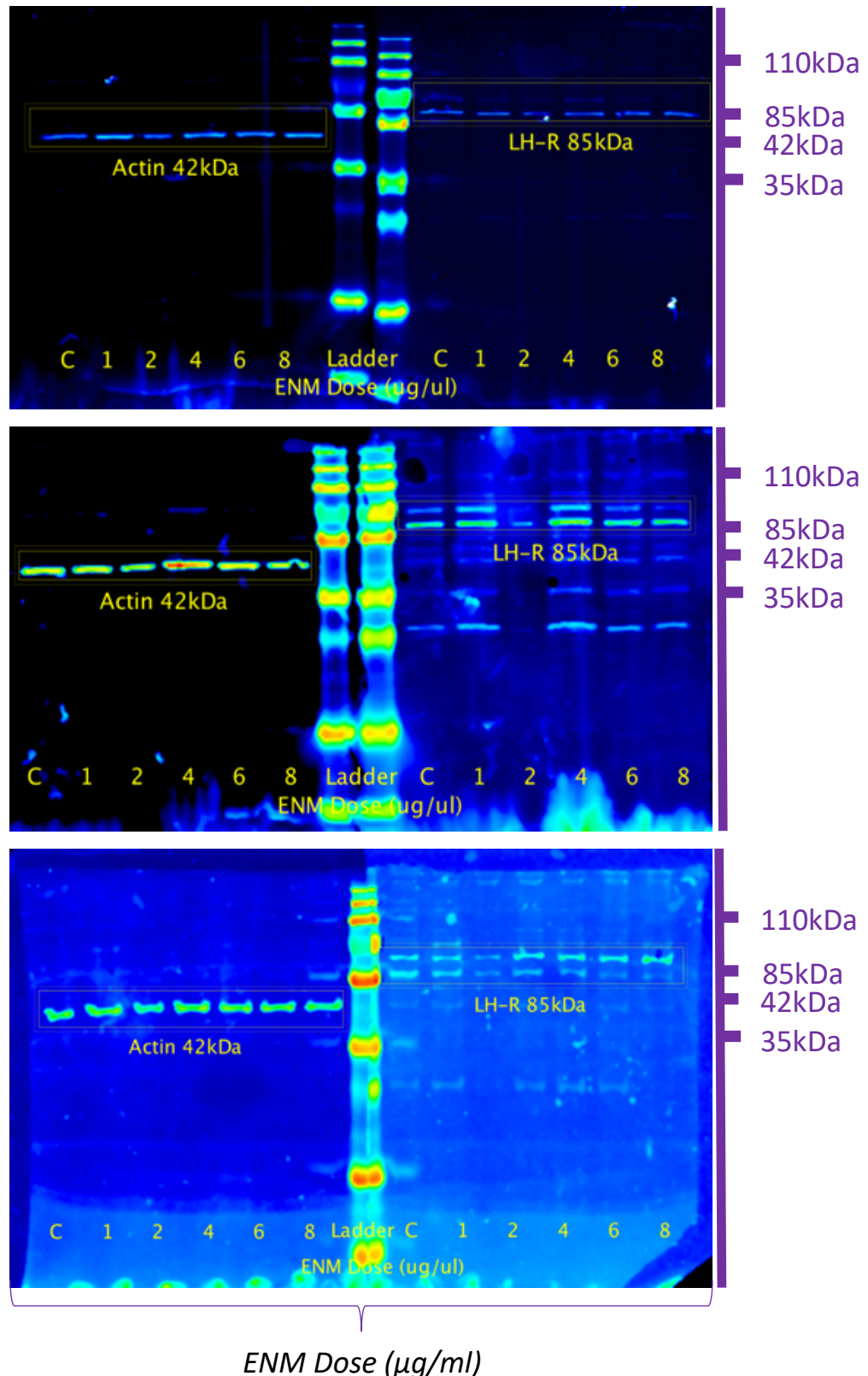


Figure 54: Western blot analysis for expression of Actin (LHS of membrane) and LH-R (RHS of membrane) recorded on LiCor using fluorescent secondary antibodies. A) NM-110 n1 +T, B) NM-110 n2 +T, C) NM-110 n3 +T. 0,1,2,4,6 and 8μg/ml represent 0, 0.32, 0.63, 1.26, 1.89 and 2.52 μg/cm² doses.

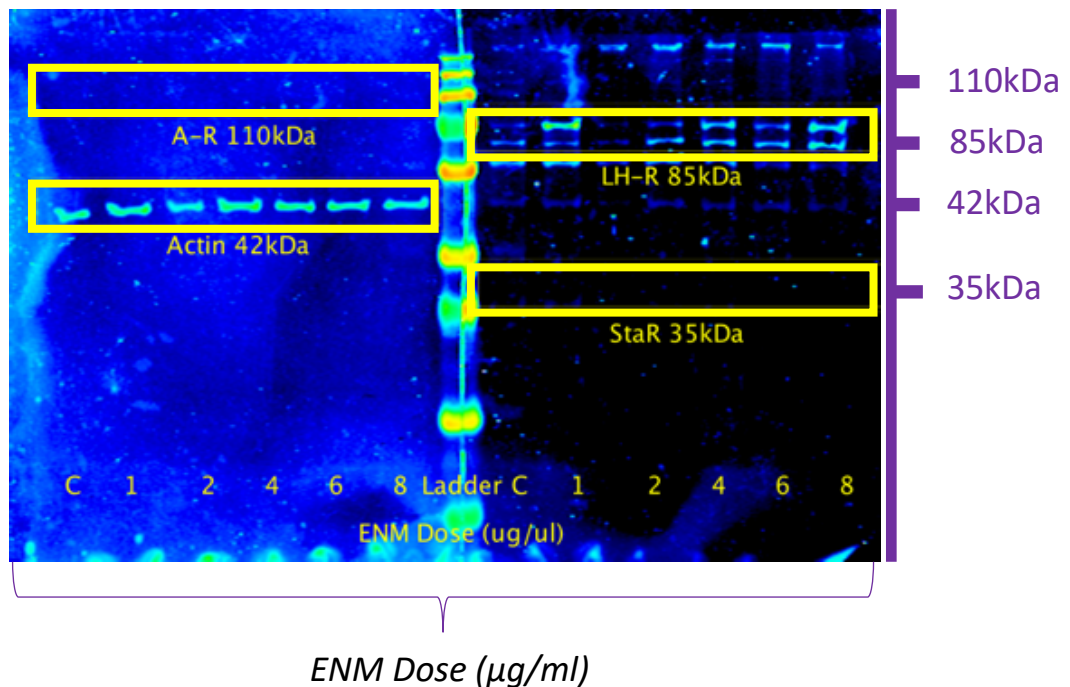


Figure 55: Example of Western blot for NM-110 n3 +T, originally probed for LH-R and Actin, which was unsuccessfully re-probed for Androgen Receptor and StaR. Locations where these antibodies should have been are shown on the image for illustration. 0,1,2,4,6 and 8 $\mu\text{g/ml}$ represent 0, 0.32, 0.63, 1.26, 1.89 and 2.52 $\mu\text{g/cm}^2$ doses.

Whilst initial Western blots using this system were promising, further runs examining LH-R Expression and using different Antibodies (AR, StaR) revealed a lack of reliability for LH-R and sensitivity issues with detection for AR and StaR (Fig. 55).

Due to the sensitivity problems on the LiCor system, an alternative detection method was attempted using enhanced chemiluminescence (ECL). In order to ensure that pilot experiments for all antibodies were tested using this system, a simplified treatment protocol was used, which examined only control, 1.26 $\mu\text{g/cm}^2$ and 2.52 $\mu\text{g/cm}^2$ treatments and did not include any testosterone treatment of cells. Results showed that Actin expression was reliable, indicating that gel preparation, electrophoresis, transfer, antibody incubation and ECL reaction had been undertaken to a satisfactory standard. ECL allowed reliable detection of Androgen Receptor (AR) expression across all samples. However, LH-R and StaR were not detectable using this method (Fig. 56).

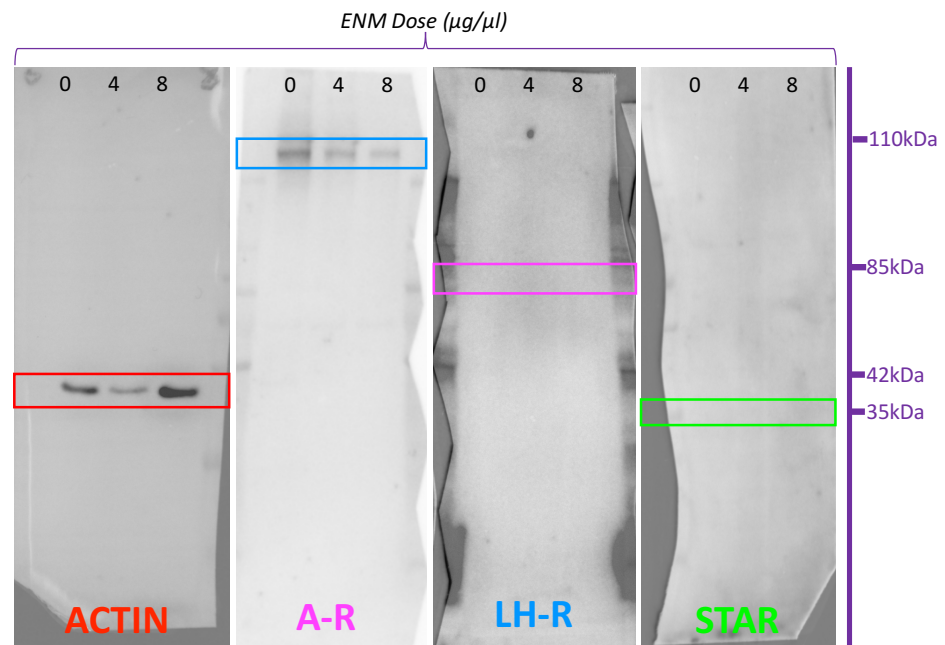


Figure 56: Representative ECL capture of antibody stains. L to R: Actin, AR, LH-R & StaR. 0,4 and 8μg/ml represent 0, 1.26 and 2.52 μg/cm² doses

For Androgen receptor, ImageJ was used to obtain densitometry readings for all samples, and these were normalised as a % of Actin expression. Initial examination of the data suggested that there may be a dose-dependent decrease in AR expression following exposure to all three ENM tested (Fig. 57). However, variation was high, and analysis via ANOVA confirmed that there was no significance in the findings because of this (NM-110, $p=0.8603$, NM-111 $p=0.2365$, NM-300 $p=0.7550$). In order to understand this trend further, additional Westerns would be required to reduce variation and improve the statistical power of the ANOVA.

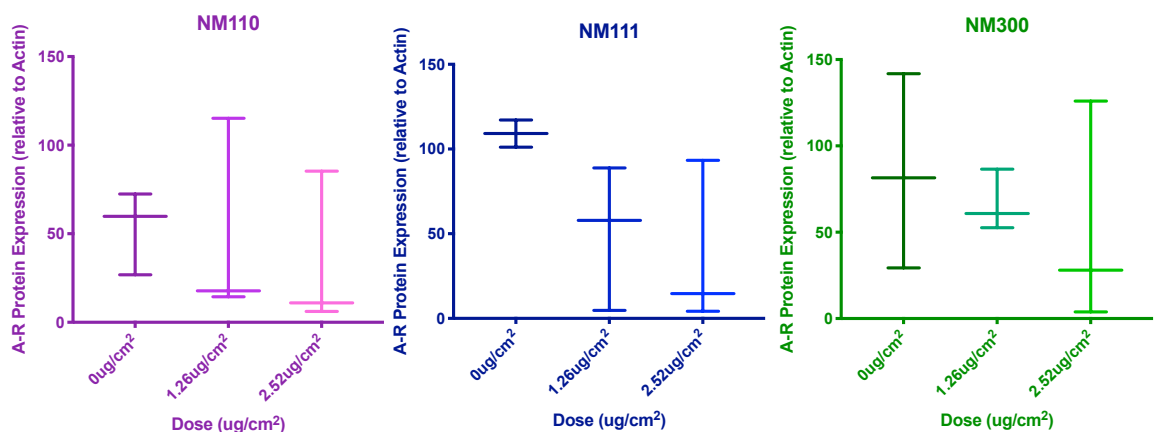


Figure 57: Mean expression of AR in TM3 cells treated with NM-110, 111 and 300 as a % of Actin expression in the same sample. $n=3$.

Discussion

Within this chapter, TM3 cells were exposed to sub-lethal doses of two zinc oxide (NM-110 and 111) and one silver (NM-300) ENM. There were 2 research questions to be addressed: i) Does exposure to zinc oxide and silver ENM lead to changes in RNA expression for a number of key markers of endocrine function in TM3 cells (LH-R, StaR, P450scc & 3 β -HSD)?, and ii) Does exposure to zinc oxide and silver ENM lead to changes in protein expression for a number of key markers of function in TM3 cells (LH-R, StaR & AR)? Through these questions, the overall aim was to understand further whether ENM exposure caused changes in RNA or protein expression for key markers of reproductive function *in vitro*, and to compare these results to those gathered from concurrent analysis being undertaken on testicular samples from animals exposed *in vivo* (chapter 5). PCR and Western blot analysis revealed a number of findings, which are summarised in Table 19.

Table 19: Summary of findings from PCR and Western analysis of RNA and Protein expression in TM3 cells

Marker	Nanomaterial	RNA Expression	Protein Expression
LH Receptor (<i>Lhr</i>)	NM-110	↓	?
	NM-111	↑	?
	NM-300	↑	?
Androgen Receptor	NM-110	N/A	↓
	NM-111	N/A	↓
	NM-300	N/A	↓
StaR (<i>Star</i>)	NM-110	↑	?
	NM-111	↑	?
	NM-300	↑	?
CYP11A1 (<i>Cyp11a1</i>)	NM-110	↓	N/A
	NM-111	↑	N/A
	NM-300	↑	N/A
3 β -HSD (<i>Hsd3b1</i>)	NM-110	↓	N/A
	NM-111	↑	N/A
	NM-300	↑	N/A

PCR analysis for RNA expression

Due to sample size and associated variation, analysis of RNA expression via PCR did not produce any statistically significant outcomes for the genes tested. However, some interesting trends were apparent. For NM-110, it appeared that there was a decrease in expression of LH-R, CYP11A1 and 3 β -HSD, and an increase in StaR. For NM-111 and NM-300, an increase was seen across all GOIs tested. From a biological perspective, this indicates the potential for alterations to steroidogenesis within TM3 cells.

LH-R expression

LH-R expression was decreased following NM-110 exposure but increased following NM-111 and NM-300 exposure. Both downregulation and upregulation of the LH-R can lead to decreases in fertility levels (Narayan, 2015). Downregulation may lead to low testosterone levels, associated detrimental effects to Sertoli cell function and ultimately spermatogenesis. In addition, a lack of negative feedback to the HPG axis by testosterone may result in unimpeded production of GnRH, in itself leading to excess production of LH and FSH at the adenohypophysis and later downregulation of the whole system over time. Unregulated upregulation is also associated with detrimental effects; activating mutations in the LH-R having been associated with Leydig cell hyperplasia and high circulating levels of LH (Narayan, 2015).

From the available literature, only one study was identified that recorded LH-R expression following ENM exposure, and like our work, it reported varied findings. Bara *et al* exposed pregnant swiss albino mice to mesoporous silica and zinc oxide (ZnO) ENM at doses between 50 and 250mg/kg via oral gavage on gestational day 15-18 and examined both dams and their offspring (at 6 months age). In dams, they saw increased LH-R expression in mesoporous silica nanoparticle (MSN) exposed animals, but no change in ZnO exposed. In their offspring, LH-R levels were again unchanged by ZnO exposure, but this time were decreased following MSN exposure compared to control (Bara *et al.*, 2018). The authors did not offer speculation on why LH-R expression was altered differently between dams and offspring. However, it is clear that ENM interfered with the normal LH-R expression in all animals tested.

Based on the data available to date, it would be unfitting to try and draw any conclusions over these potential changes in LH-R expression. However, it is important to recognise

that there is a potential here for ENM exposure to cause alterations in LH-R expression independent of trophic drive. In order to investigate this further, it would be interesting to repeat the study with a greater replicate number, elucidate via Western blot whether these changes were translated into final production of LH-R and examine the mechanism of action responsible. Comparison of the changes in LH-R to the work undertaken *in vivo* is also important in order to see whether findings *in vitro* reflect those *in vivo*.

Should repeated studies confirm changed expression of LH-R, one possibility for next steps could be to examine expression of both LH-R and the peptide hormone insulin-like peptide 3 (INSL-3) in primary Leydig cells. INSL-3 is secreted by Leydig cells but is not directly influenced by the pulsatile action of the HPG axis nor acutely regulated by LH or cAMP in adult animals (its responsiveness to HPG axis and Leydig cell events in immature or old animals is different) (Ivell et al., 2014). It acts on specific receptors on the Leydig cell to modulate steroidogenesis (RXFP2 receptors) and appears to be part of a feed-forward mechanism to 'buffer' the production of steroids following LH-R stimulation, and seems to act in a similar way in ovarian follicular theca cells (the female equivalent of Leydig cells) (Ivell et al., 2014). As INSL-3 appears not to fluctuate as much as androgens, and its role in the gonads is in part to buffer fluctuations in output from the HPG axis, examining this alongside LH-R in primary cells could give an interesting picture of the effect of ENM exposure on both, and whether (at least acutely) INSL-3 may act to help 'level out' any impact on the HPG axis and spermatogenesis via LH-R up- or down-regulation.

StaR expression

All ENM treatments led to a potential increase in expression of StaR, the key rate limiting protein in cholesterol transport for testosterone production. Zhang *et al* reported a downregulation in expression of TM3 and TM4 cells to StaR following exposure to silver nanoparticles (Zhang et al., 2015a). However, three *in vivo* studies suggest that changes to StaR expression following ENM exposure may vary. The first described StaR expression in TM3 cells following treatment with nano TiO₂, diesel exhaust particles (DEP) or carbon black (CB) (Komatsu et al., 2008). They reported no change in expression of StaR following treatment with 10 or 30 µg/ml TiO₂, but an increase in expression

compared to control following treatment with DEP or CB. Bara *et al* also evaluated StaR expression following oral exposure to ZnO or MSN (see above for detailed outline of the experiment), and found a decrease in StaR expression in dams following ENM exposure, but an increase in their male pups (Bara et al., 2018). Garcia *et al* reported no change in StaR expression following exposure of CD1 mice to a series of 5 injections of citrate coated silver ENM (10nm) at 1mg/kg (Garcia et al., 2014).

Again, it appears that response to ENM exposure varies dependent on the ENM used, and that there is variation in the available literature in terms of ENM used, dose applied, and exposure route selected. Had additional time been available, it would have been useful to undertake additional TM3 cell treatments and harvest additional RNA to hopefully add more power to the outcome found for this (and other) genes of interest.

CYP11A1 expression

CYP11A1 is the gene encoding for P450_{scc}, the enzymatic rate limiter in steroidogenesis responsible for conversion of cholesterol to progesterone within the mitochondria of Leydig cells. A number of other studies have reported changes in CYP11A1 expression following ENM exposure. Jia *et al* reported no change in CYP11A1 expression following oral exposure of pubertal Kunming mice to titanium dioxide nanoparticles at between 10 and 250mg/kg doses, a finding in agreement with Zhang et al, who reported no change in CYP11A1 expression of TM3 cells following exposure to silver ENM at a pre-determined LC₅₀ concentration (Zhang et al., 2015a). However, Garcia *et al* reported an increase in CYP11A1 expression following exposure of CD1 mice to citrate coated nano-silver (10nm) via a series of 5 injections at 1mg/kg, (Garcia et al., 2014). Similarly Zhang *et al* reported an increased expression in CYP11A1 following exposure of neonatal ICR mice to silver nanoparticles post-natal days 8 – 21 and a period of wash-out period of up to 80 days (Zhang et al., 2015b).

Whilst our findings and those from studies examining the effects of silver ENM *in vitro* differ, they are in agreement with the outcomes of studies reported *in vivo*, making this pilot data potentially promising. To build this dataset, the next logical step would be to undertake further testing with an appropriate antibody for CYP11A1 *in vitro* on TM3 cells via Western blot, and *in vivo* on tissue from animals exposed to the same ENM via

immunohistochemistry to see whether this increase in CYP11A1 expression resulted in a higher production of P450_{scc}. Should CYP11A1 be upregulated and resultant P450_{scc} levels higher, this would indicate a potential for disruption of steroid hormone synthesis following NM-300 exposure. It would also be relevant to consider testing other types of silver ENM on the same tissue, to try and determine why our results differed from those of Zhang *et al.*

3 β -HSD Expression

3 β -HSD is responsible for conversion of pregnenolone to progesterone within the smooth endoplasmic reticulum of Leydig Cells. Following a similar pattern to CYP11A1, expression of 3 β -HSD was decreased following exposure to NM-110 but increased following exposure to NM-111 and NM-300. The published literature reports varied outcomes for expression of 3 β -HSD following ENM exposure, although *in vitro* mechanistic studies are scarce. Garcia *et al* (outlined above) reported an increase in 3 β -HSD following intravenous exposure to silver ENM, whereas Jia *et al* (also outlined above) reported no change in 3 β -HSD following oral exposure of mice to nano-TiO₂ (Jia *et al.*, 2014, Garcia *et al.*, 2014). As with the other genes of interest reported here, the effect of ENM exposure appears to be nanomaterial-specific. However, dysregulation of 3 β -HSD regardless of whether via upregulation or downregulation indicates a potential for disruption of normal steroidogenesis. It would be useful to investigate this further, via PCR, Western blot for protein analysis and immunohistochemistry for detection of the enzyme in tissues exposed to ENM (provided in chapter 5).

Another interesting avenue of research would be to examine expression of 17 β -HSD expression, as the final step in production of testosterone from androstenedione. However, this would require use of primary Leydig cells as there is not yet a cell line (TM3, MA-10, Mlhc-1 etc.) known to express 17 β -HSD, and therefore suitable for investigation of the later steps of spermatogenesis (Engeli *et al.*, 2018).

The importance of ENM coating in understanding response to zinc oxide exposure

The differences in changes to expression of genes encoding LH-R, P450_{scc} and 3 β -HSD following exposure to NM-110 and 111 (uncoated and coated zinc oxide) is interesting, as it highlights the importance differing physico-chemical properties may play in

creating different outcomes for hazard testing in materials with the same chemical identity. As reported within Chapter 2, NM-110 is uncoated zinc oxide, with an average primary particle size of 100nm. In contrast, NM-111 is coated with triethoxycaprylylsilane, a silicone-based material that gives it a hydrophobic coating. Generally speaking, coating an ENM is used to either functionalise the materials in some way (for example to help with even dispersion), or to attempt to reduce their relative toxicity.

Whilst no other published work was found relating to NM-110 or 111 exposure and reproductive toxicity, a few relevant studies were identified which considered the role of ZnO coatings in toxicity. Following exposure of mice to a single dose of NM-110 and 111 via intratracheal instillation, Gosens *et al* reported differing outcomes for lung and liver endpoints depending on ENM (Gosens et al., 2015). NM-111 coated ZnO resulted in greater inflammatory responses than NM-110, which the authors suggested could be via release of triethoxycaprylylsilane from the ENM over time or due to the fact that NM-111 was more stable allowing for longer persistence in the body and increased inflammation by comparison to NM-110.

Interestingly, another study undertaken by Osmond-McLeod and colleagues reported exposure of human hepatic stellate cells to 30µg/ml NM-110 or 111 for 24 hours (Osmond McLeod, 2014). NM-110 exposure resulted in modulation of multiple cell stress signalling pathways known to regulate cellular responses to abiotic stresses, mechanisms responsible for control of cell survival or apoptosis and senescence, together with a loss of cell viability. In contrast, exposure to NM-111 and ionic zinc control (ZnSO₄) had little to no effect on the cells. The authors suggested that in this instance, the triethoxycaprylylsilane of NM-111 was protective against ZnO toxicity to this cell line *in vitro*. Following application of silica coating, Chia & Leong also reported a reduction in toxicity of Zinc oxide nanoparticles (which had been pre-processed in various synthetic gastrointestinal fluids at acidic pH) to two types of gastrointestinal cell lines (Chia and Leong, 2016).

The authors postulated that silica coating of ZnO may be protective against toxicity from ZnO particles or Zn ions released via dissolution. Gosens *et al* also noted the importance

of pH in the solubility and subsequent dissolution of zinc ions from ZnO ENM. They suggest that in their study, much of the NM-110 and 111 underwent almost complete dissolution and therefore the increased toxicity from NM-110 exposure may be an ionic effect rather than particulate. This hypothesis does seem to agree with the results seen from these studies, despite the fact that neither Gosens nor Chia reported use of a pre-wetting step in preparation of ZnO solutions for treatment of cells, bringing into question the actual dose of ZnO reaching cells, given its relatively low solubility in water alone.

In relation to the present research, there is insufficient evidence to allow a conclusion to be reached on the exact reason for the difference in RNA expression between the two types of ZnO ENM. Given the evidence above, an obvious next step would be to examine the rate of dissolution of zinc ions from NM-110 and 111 in the cell culture medium used for TM3 cells, in order to understand extent to which dissolution of ions may contribute to observed changes in RNA expression and subsequent cellular toxicity. To elucidate further events at the cellular level, it would also be interesting to undertake assays on TM3 cells examining endpoints relating to cellular stress and death (such as NFκB, ATM/ATR, mTOR, AKT, and MAPK signalling pathways), or generation of reactive oxygen species.

Technical Challenges with PCR

PCR also generated a number of problems and technical questions. The first of these was the notable observation that cells treated with $2.52\mu\text{g}/\text{cm}^2$ NM-300 did not produce any useable RNA. This finding was in line with the results discussed in Chapter 3, which indicated that although $2.52\mu\text{g}/\text{cm}^2$ was considered to be a sub-lethal dose of NM-300, the nature of the NM preparation meant that over time, ionic silver was released from the nanoparticles, leading to an increase in potency with storage which in turn reduces the threshold for loss of cell viability. The nature of the work involved in this thesis meant that the PCR analysis was undertaken some time after the original cytotoxicity assays, and as availability of ENM was limited, stock vials of NM-300 therefore had to be used that had been open for longer than was advised within the protocol for their handling and use (outlined in Chapter 2). Therefore, it is likely that this increased toxicity was due to an increase in potency over time.

The original Primers designed from a review of the literature and cross-check in Primer-BLAST were not deemed to be suitable for use following efficiency testing. Consideration of why this may have happened led to a number of possibilities. The first was that sample preparation and pipetting were inaccurate. However, a second run of the efficiency experiment yielded identical results where all other PCR experiments were successful, therefore operator error was unlikely to be the problem.

Secondly, RNA that contains PCR inhibitory compounds such as sample preparation reagents, or excessive protein can lead to partial or complete inhibition of PCR. However, as RNA was analysed by both Nanodrop and Bioanalyzer and quality found to be high, it is unlikely that this was the case. gDNA contamination can produce unexpected amplicons and interfere with expected efficiency. However, no-RT controls showed zero amplification, therefore gDNA contamination was ruled out.

The fourth was that the primer design was not optimal, despite using BLAST to identify a unique sequence and cross check those primers which had been sourced from the literature. All primers were within the optimal length of 18-22 bases, which allows adequate specificity but is short enough for primers to anneal to template at the annealing temperature. Optimal amplicon length is 100-150bp; the longest primer, *Star*, was 247bp in length which may have contributed to the sub-optimal results. Fifth, in relation to GC content, ideal content is between 40% and 60%. Again, *Star* had a slightly high GC content of 66% which may have had some influence. Sixth, both LH-R and 3 β -HSD had some repeats and runs of single bases which may be contributing factors to misprimers. The biggest indicator that mis-primers or primer-dimers are causative of issues is from examination of melt curve plots. Normally, melt curves will show a single distinct peak in the plot of the negative derivative of fluorescence vs. temperature (as shown for the housekeeper genes). However, for these primers multiple peaks were present, indicating off-amplicon products were present. Finally, further examination of the T_m for each primer (the temperature at which one-half of the primer DNA duplex will dissociate to become single stranded) showed that melting temperature was slightly lower (2-3°C) than the low temperature range set on the StepOne™ default cycle. This could also have been a contributing factor to the erratic amplification observed,

although it was not an inhibitory factor for the Primer Design primer set, so is unlikely to be the single reason for failure of the original primer set.

Western Blot Analysis

Initial Western blot analysis using fluorescent detection methods proved problematic. As cells were not passaged more than 10 times in their preparation for protein extraction, and all protein was extracted from passage-matched cell populations, this is not likely to be due to accumulated differences in cell protein expression profiles. However, it may be that modified subtypes of the protein were present. Following a time-consuming re-appraisal of the methods used with no improvement, the decision to move from Fluorescent to ECL based Western detection was made as it is considered to be a more sensitive detection system for weakly expressed antibodies. However, despite clean electrophoresis and clear detection of housekeeper genes & AR, there were still issues with detection of LH-R and StaR. There are three possible reasons for this: i) that the proteins selected are not expressed within the TM3 cell line, ii) that despite careful selection, the specific antibodies used for this experiment were not suitable for detecting the isoform of protein expressed, or iii) that the specific antibodies used were not suitable for a Western endpoint, or for the cell line. As detection of LH-R was possible via the fluorescent detection system, it is more likely that issues with the particular antibody purchased are responsible than a lack of expression in this case. As it was not possible to detect StaR using either fluorescent or chemiluminescent secondary antibodies, it was concluded that this antibody was not suitable for Western blot analysis, despite having been sold as such. It would therefore be appropriate to repeat the Western study protocol with fresh antibodies from a different supplier to see whether better results could be gathered.

Whilst the Western based protein work was problematic, initial findings from ECL detection of AR showed what appeared to be a decrease in expression following exposure to ENM. Interestingly, work undertaken at Edinburgh Napier University in parallel with this research also generated Western blots for AR using protein extracted from TM4 Sertoli cells with some success. Figures 58 and 59 show expression of AR following exposure to NM-110 & 111 (n=3), and NM-300 (n=1) (Young et al., 2014).

All three graphs show a downward trend in AR expression with increasing dose of NM-110, 111 and 300. For zinc oxide (NM-110 and 111), the original measurements provided were used to undertake statistical analysis. Neither NM-110 nor NM-111 were found to be significantly different to control at any dose via one-way ANOVA (NM-110 $p=0.2053$; NM-111 $p=0.051$). This was most likely due to the large variation recorded in results. To understand this further, it would be useful to repeat Western analysis for all three ENM in order to build a more powerful set of data on which to undertake statistical analysis for significance of ENM effect on AR expression.

There is little to no published literature against which to compare or contrast these findings. As Androgen Receptor is important in the development and progression of prostate cancer, some papers are available which describe research into the potential role of functionalised ENM as constructs onto which to build AR inhibitors as targeted medication in prostate cancer patients (Reznikov et al., 2015). Interestingly, one cancer therapy focussed study of the LNCaP prostate cancer cell line reports suppression of prostate cancer cell growth following exposure to selenium nanoparticles. The authors suggest that this is mediated via AR and the Akt/Mdm2 (apoptotic) pathways (Kong, 2012).

As investigation of the effects of ENM exposure on the expression of androgen receptors appears to remain a little investigated avenue of research. It would be relevant to pursue this avenue further *in vitro*, perhaps using alternative cell lines (Mltc-1 or MA-10) as comparison or expanding the work to primary Leydig and Sertoli cells. In any case, it would be useful to consider use of an alternative antibody for AR in any future work, as following issues with immunohistochemical analysis of tissues exposed to ENM *in vivo* it was suspected that the quality of this antibody quality was questionable.

Based on this scarcity of published work, to our knowledge this downward trend in AR expression seen following exposure to two types of zinc oxide ENM (NM-110 and 111) on TM4 Sertoli cells, and silver ENM (NM-300) on TM3 Leydig and TM4 Sertoli cells is being shown for the first time. Despite being pilot data, and a clear need to build a larger dataset to provide sufficient power to the data for good statistical analysis, this is an

interesting outcome, with clear implications for spermatogenesis, regulation of the HPG axis and male fertility if confirmed.

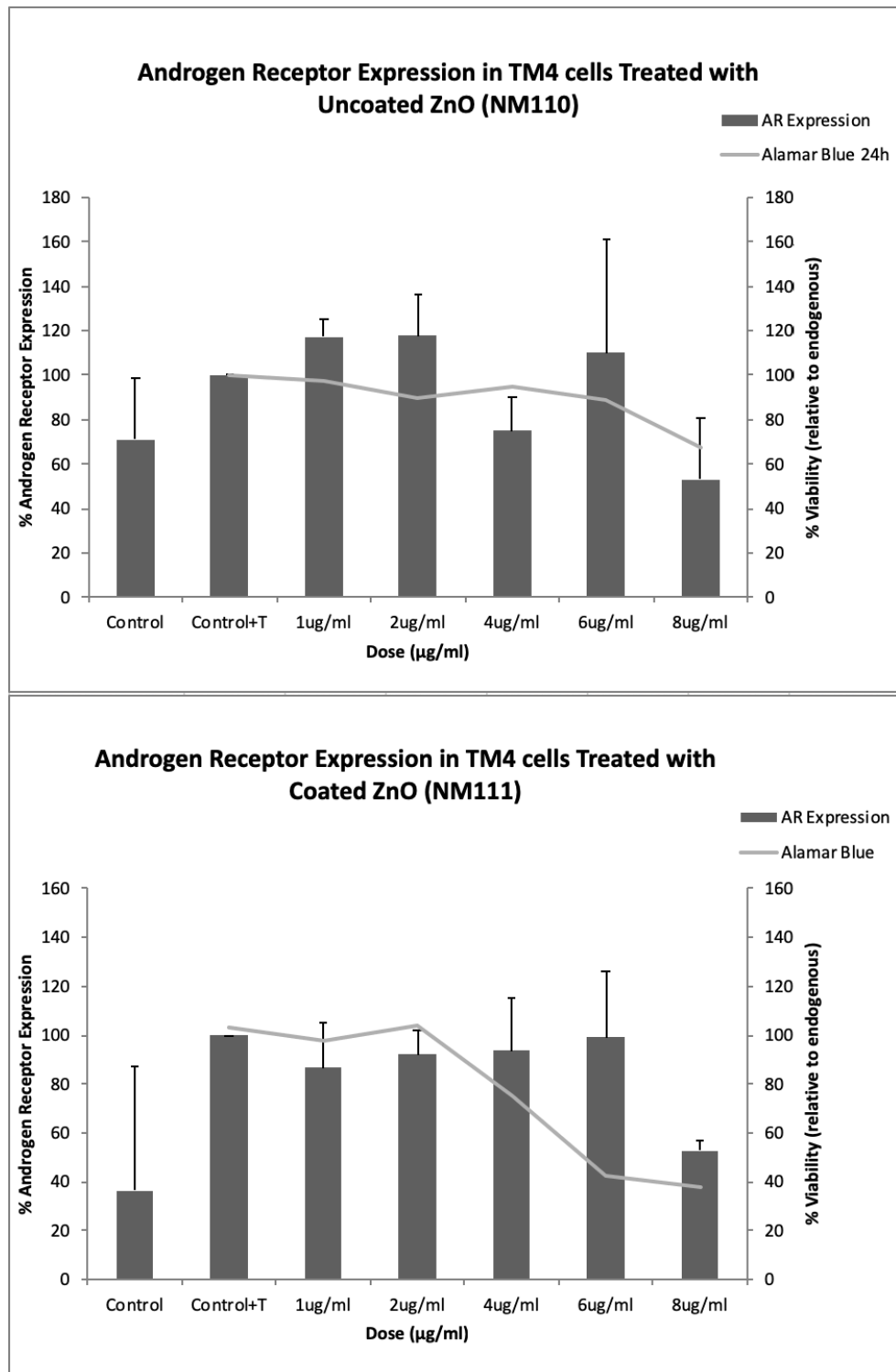


Figure 58: Androgen Receptor expression in TM4 cells treated with NM-110 and NM-111 (uncoated and coated) Zinc Oxide at doses of 0, 1, 2, 4, 6 and 8µg/ml, equivalent to 0, 0.32, 0.63, 1.26, 1.89 and 2.52µg/cm² in the presence of testosterone stimulation. Receptor expression is expressed as a % of β-Actin expression in control sample to which testosterone stimulus has been added (Control+T). AR expression is overlaid with cell viability (% relative to control) following 24 hours of exposure to ENM, recorded using the Alamar Blue assay. N=3. (Young & Fulton, 2014).

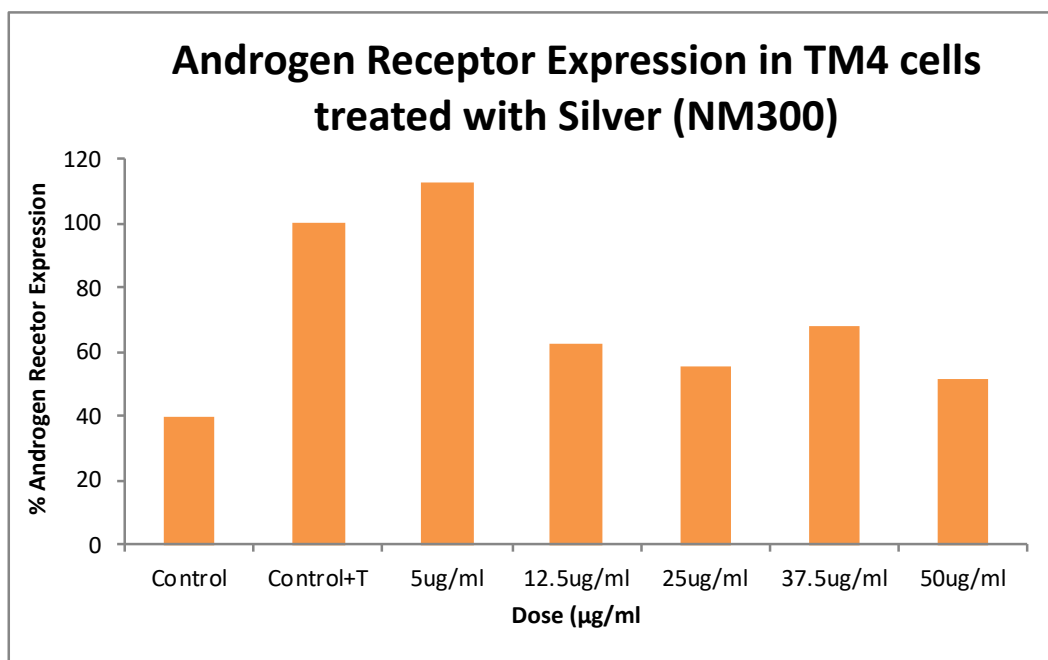


Figure 59: Androgen Receptor expression in TM4 cells treated with silver ENM (NM-300) at doses of 0, 1, 2, 4, 6 and 8 µg/ml, equivalent to 0, 0.32, 0.63, 1.26, 1.89 and 2.52 µg/cm² in the presence of testosterone stimulation. Receptor expression is expressed as a % of β-Actin expression in control sample to which testosterone stimulus has been added (Control+T). N=1. (Young & Fulton, 2014).

Final conclusions and Next steps

Analysis of RNA and protein expression for the receptor mediating pituitary release of LH and thus stimulation of reproductive function (LH-R), rate limiting proteins and enzymes in conversion of cholesterol to testosterone (StaR, CYP11A1 and 3β-HSD), and the receptor mediating the effects of testosterone directly on spermatogenesis within seminiferous tubules and on Leydig cells via autocrine action (AR) revealed some interesting preliminary results. These imply that ENM may alter Leydig cell function at sub-lethal concentrations, potentially impacting spermatogenesis, the HPG axis and fertility. There is also evidence to suggest effects may be nanomaterial specific, reinforcing important questions for the risk assessment community around the role of physico-chemical characteristics in altering sub-lethal changes to cell function in materials that would be classed as the same chemically. Whilst none of the results from these pilot tests are sufficiently powerful to make any definite claims about changes to the function of TM3 Leydig cells, a potential effect has been demonstrated and further research to expand on this is clearly warranted.

Various specific avenues of research have been outlined earlier; however, one obvious next step would be to repeat ENM exposure on primary Leydig cells and perform a testosterone assay on cell supernatants. This is not possible with TM3 cells due to their aforementioned inability to convert androstenedione to testosterone, however, it may be possible that measurement of androstenedione could be used as an alternative. Accurate measurement of testosterone could be achieved using mass spectroscopy and as the endpoint in steroidogenesis, would offer a definitive answer to whether Leydig cells were functioning normally following ENM exposure. Results could then be directly compared to results of a similar assay *in vivo*. Unfortunately, time and resource constraints meant that this was not possible within the duration of this research.

A further potential line of investigation could be to conduct a series of experiments comparing the effects of ENM exposure on Leydig, follicular theca cells and adrenal cortical cells. Theca cells are the equivalent of Leydig cells within the female reproductive system, and adrenal cortical cells are responsible for steroid, mineralocorticoid and glucocorticoid synthesis within the adrenal glands. As all three cell types are responsible for production of steroids essential for endocrine system function, any potential disruption to this process could have important systemic effects.

The results of *in vitro* assessment give hope that this could be used as a predictor of *in vivo* endpoint measurements, as presented in this discussion. There is more work to be done, and there is a need to be a check on the best and most appropriate cell line to work up as a potential OECD TG of the future. These mechanistic studies do not stand alone but can help toxicologists identify target cells that may influence endocrine function.

Results *in vitro* can now be compared to those generated from analysis of tissues taken from animals exposed to the same panel of ENM to identify whether the *in vitro* work is a suitable substitute or guide for predicting hazard *in vivo*.

Chapter 5: Histological analysis of changes to rat testis following exposure to ENM

Introduction

In addition to understanding of the effects of engineered nanomaterials (ENM) on animal cell lines *in vitro*, it is important to understand effects *in vivo*, in order to form a comparison between the two and establish suitability of *in vitro* testing for predicting effect *in vivo*. To allow this, animals were exposed to some of the same ENM *in vivo* by MARINA project partners in the Netherlands, and testicular tissue from these animals provided to Edinburgh Napier University for histological analysis.

Following fixation and processing, testicular tissue samples from Sprague-Dawley rats exposed to a panel of silver and silica ENM via oral gavage were shipped from RIKILT, Wageningen, Netherlands to Edinburgh Napier University. After sectioning, tissues were stained using haematoxylin and eosin and examined in detail for morphological and stereological changes, as well undergoing immunohistochemical stains to determine activity in various receptors and enzymes considered to play important roles in spermatogenesis.

In order to establish whether exposure to ENM caused any morphological or functional changes, it is first important to have a more detailed understanding of normal testicular morphology and the spermatogenic cycle. Although basic testicular morphology is explained within the introductory chapter of this thesis, testicular toxicity most often manifests as subtle changes in the detail of its morphology. Changes in testicular morphology may be examined via various histological techniques. Histology has proven indispensable in furthering understanding of both general biology and pathology, and histopathology allows examination of tissue post mortem for changes due to chemical or environmental exposure through an animals' life.

Testicular Morphology in detail

As previously outlined, the testis is a complex structure, composed of convoluted seminiferous tubules separated by interstitial tissue (Fig. 60). It has been reported from detailed morphological analysis that 82.4% of the volume is occupied by seminiferous tubules, 15.7% by interstitial tissue, and 1.9% by the capsule (Mori, 1980).

The interstitium is formed from populations of Leydig cells, testicular macrophages, fibroblasts, mast cells, blood vessels, nerves, lymphatic vessels and connective tissue. Leydig cells are polyhedral cells, which tend to cluster together around blood capillaries. They make up around 2.7% of testicular volume, and represent around 17% of the interstitial tissue in rats, although this percentage varies from species to species (Creasy and Chapin, 2013, Mori, 1980). As the major site for synthesis of testosterone they are a key component in the HPG axis, responsible for regulation of reproductive function (Fig. 60).

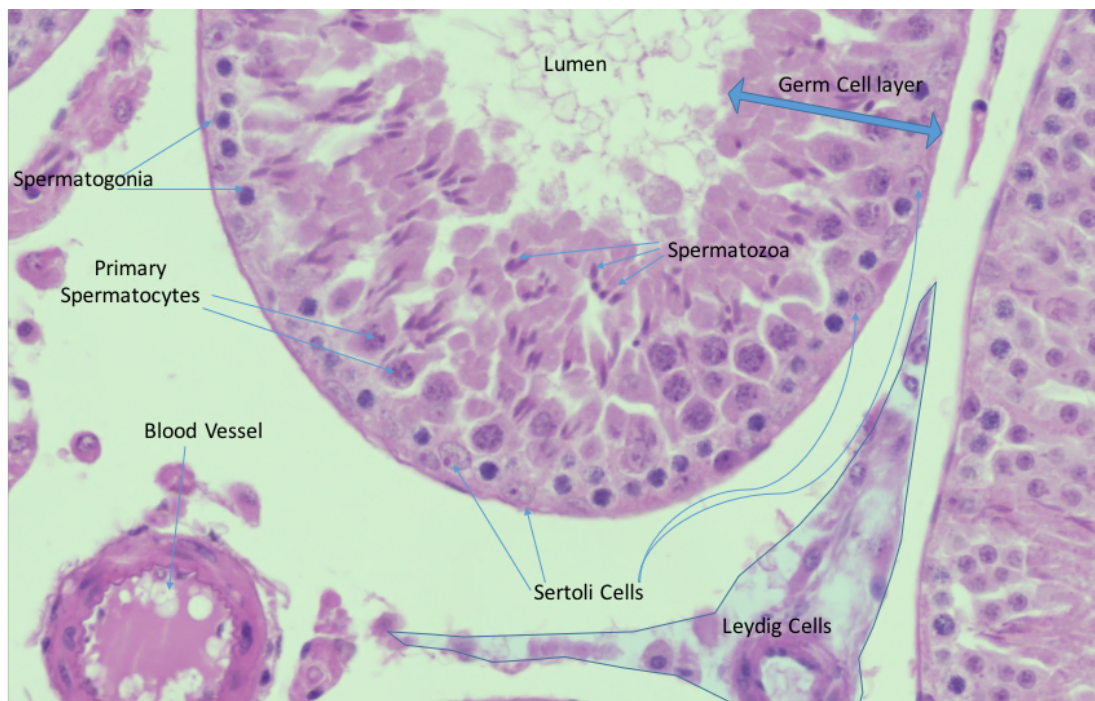


Figure 60: Generalised morphology of the testes. The interstitial compartment contains Leydig Cells, Blood vessels and capillaries, as well as lymphatic vessels and testicular macrophages (not visible). The seminiferous tubules, lined by peritubular myoid cells, are composed of two compartments – the basal and adluminal compartments. Within these, germ cells develop through spermatogenesis, a process which is managed by Sertoli cells, before being shed into the central lumen at spermiation.

Testicular macrophages are the principle immune cells within the testis, but in addition to response to infection are also involved in regulation of spermatogenesis, steroidogenesis and other homeostatic functions of the testis (Winnall and Hedger,

2013). They are a distinct subset of mononuclear phagocytes and are made up of two populations. The first are of embryonic origin, present from the beginning of life and associated mainly with Leydig cells. The second have their origins in bone marrow, and are found on the surface of seminiferous tubules, appearing around puberty (Mossadegh-Keller et al., 2017).

Intertubular and peritubular capillaries run parallel to or around seminiferous tubules, supplying oxygen, nutrients and important endocrine messengers. The lymphatic channels between Leydig and peritubular cells on the seminiferous tubules are responsible for removal of interstitial fluid containing waste from tissues, and also form an accessory return route for blood plasma. Importantly, they also play a vital role in the immune system, being the primary site for cells relating to adaptive immunity (e.g. T cells and B cells). Relatively free equilibration occurs between the interstitial tissue, lymph and blood vessels, but penetration through the seminiferous tubule wall into its basal compartment is limited, and the barrier between the basal and adluminal compartments (within which sperm develop) is tightly controlled by the Blood Testis Barrier (BTB).

The seminiferous tubules themselves are surrounded by peritubular myoid cells (PTM). These have various functions, including forming a loose part of the BTB, and having paracrine regulatory interactions with Sertoli and Leydig cells. They also contain actin filaments which are thought to contract in order to create peristaltic waves that help move developing spermatozoa and testicular fluids during spermatogenesis (Creasy and Chapin, 2013). Between the PTM cells and the internal cell populations of each tubule lies a basement membrane.

Sertoli cells (SC) rest on the basement membrane of tubules, attached by hemidesmosomes. They are large euchromatic cells which are irregular but columnar in shape, with thin cytoplasmic 'arms' which protrude toward the tubule lumen at various distances depending on the stage of spermatogenesis ongoing in that particular locale (Fig. 61). Sertoli cells have a multitude of functions, including:

- i) Maintenance of homeostasis within stem cell populations, and transport of micronutrients to developing sperm. Germ cells are completely reliant on

Sertoli cells for nutrients, being unable to produce their own. SC provide lactate and/or pyruvate to spermatocytes and spermatids, and α -keto acids to germ cells.

- ii) Establishing germ cell adhesions and communication via ectoplasmic specializations called tubulobulbular complexes. SC are also responsible for 'moving' developing sperm through the seminiferous tubule (detailed further below).
- iii) Phagocytosing the waste products of spermatogenesis from seminiferous tubules. As well as losing many of its organelles, the cytoplasmic volume of a spermatid is reduced around 70% during its development. This is left behind in tubules in residual bodies (which may be seen as dark coloured autophagic vacuoles under a light microscope). SCs phagocytose and digest these.
- iv) Initiation and response to endocrine signals. SC are targets for FSH and testosterone, transducing those endocrine signals and other cellular cues into paracrine regulation of germ cells, and forming an important part of the HPG axis by themselves producing activin and inhibin which feedback to control androgen and FSH release.
- v) Initiation and regulation of the cycle of the seminiferous epithelium (see below).
- vi) Maintaining the Blood-Testis Barrier (see below).
- vii) Inhibiting autoimmune reactions to autoimmunogenic sperm and maintaining immune privilege in the testis via the Blood-Testis barrier.

These roles are summarised within Fig. 61. Disturbance of any of these is likely to impair spermatogenesis, and potentially affect fertility.

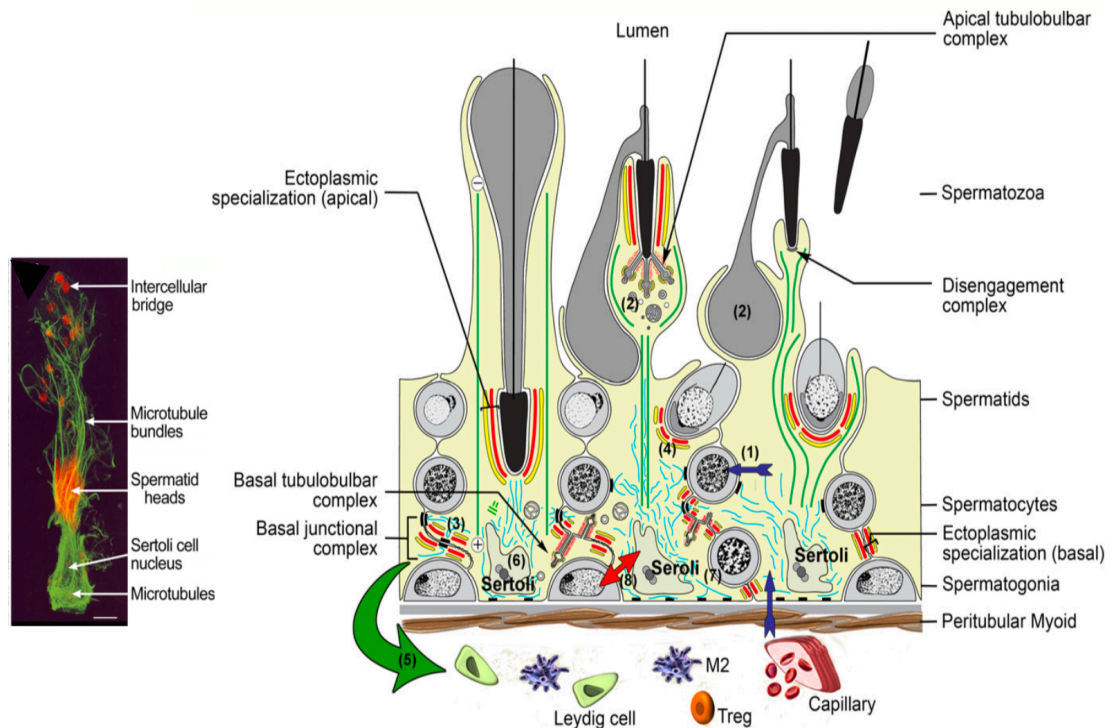


Figure 61: Illustration of Sertoli cell morphology via immunofluorescent microscopy (IF) (left) and schematic representation of its interaction with germ cells at different stages during spermatogenesis together with other key functions (right). The IF image shows a Sertoli cell isolated *in vitro* (with attached elongating spermatids). Cell is labelled for filamentous actin (red) and somatic cell-specific tubulin (green). The cytoplasmic arms wrap germ cells with thin processes which nurture cells through their differentiation. They do this via specialised cell-cell junctions between sertoli cells and germ cells (or other sertoli cells) called ectoplasmic specializations, labelled red around the spermatid heads. Bar = 10 μ m. The image showing sertoli cell interaction and functions details the many functions it serves: (1) transport of micronutrients across the junctional complex; (2) management of waste and recycled leftover cytoplasm during germ cell development; (3) maintenance of the blood-testis barrier (BTB); (4) establishment of germ cell adhesions and communication; (5) inhibition of immune reactions and maintenance of immune privilege; (6) initiation and response to endocrine signalling pathways; (7) initiation and regulation of the cycle of the seminiferous epithelium; and (8) maintenance of stem cell homeostasis. The autoimmunogenic germ cells remain sequestered within the adluminal compartment behind the BTB, surrounded by Sertoli cells which secrete immunoregulatory factors (5) to modify any immune response. Treg = T cells, M2 = macrophages. Images reproduced from Franca et. al. (2016).

Spermatozoa themselves develop within the adluminal compartment of tubules, separated from the rest of the testis by the blood-testis-barrier (BTB). This develops fully during puberty and is formed by a series of 4 different cell junctions which encircle each Sertoli cell – gap junctions (GJ), tight junctions (TJ), ectoplasmic specialisations, and desmosomes (Fig. 62). TJs are the most important component of the BTB, acting in a ‘gate and fence’ function; the gate preventing passage of water, solutes and larger molecules, and the fence controlling movement of proteins and lipids (Mruk and Cheng, 2015). Their regulation is multifaceted, involving hormones, cytokines, the presence of germ cells and a number of key proteins. Preleptene and Leptene spermatocytes pass through these TJs at the commencement of the seminiferous tubule cycle (as explained

within spermatogenesis subsection). Sertoli-Sertoli and Sertoli-Germ cell attachments are facilitated by ectoplasmic specialisations, the basal part of which also helps to form the BTB. Desmosomes are cell-cell junctions that help to ensure adhesion of adjacent cells, whereas GJs are cell-cell channels that allow passage of metabolites, ions, second messengers and other small molecules (Mruk and Cheng, 2015, Creasy and Chapin, 2013).

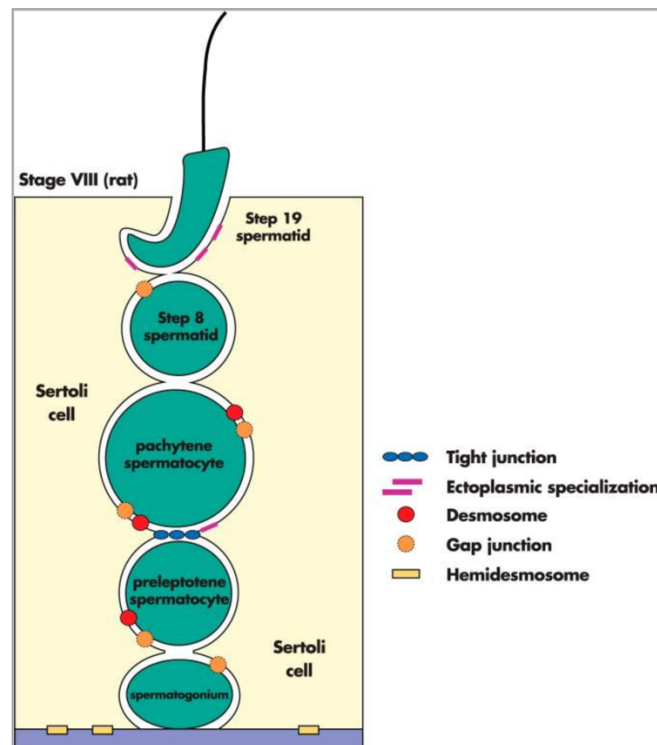


Figure 62: Illustration of the different kinds of cellular junction in the epithelium of rat seminiferous tubules. 4 types of junction are represented: tight junctions, ectoplasmic specialisations, desmosomes, and gap junctions. Each plays a crucial but slightly different role in maintenance of the BTB. Image reproduced from Mruk & Cheng (2015).

The BTB is important for two main reasons. First, it acts to maintain seminiferous tubules as an immune-privileged area of the body by stopping developing sperm from leaking out into the surrounding space. This is important because sperm themselves are autoimmunogenic, i.e. capable of eliciting an immune response which can generate antispermatozoal antibodies or developing autoimmune reactions such as autoallergic orchiditis, both of which result in reduced fertility. Second, the BTB separates the intratubular and intertubular fluids, allowing spermatogenesis to occur in a chemically controlled microenvironment (Johnson and Everitt, 2000).

Spermatogenesis

Spermatogenesis is a cyclical process by which diploid germ cells gradually transform into mature haploid spermatozoa within seminiferous tubules. Its etymology is within the Greek language, '*sperma*' meaning seed, '*kytos*' meaning cell, and '*genesis*' meaning production. It initiates on postnatal day 5 in the rat and broadly speaking, occurs in three main phases: i) mitotic proliferation of cells, ii) meiotic division of cells to generate genetic diversity and halve chromosome number, and iii) cytodifferentiation which packages haploid chromosomes for delivery to the oocyte (Johnson and Everitt, 2000, Mruk and Cheng, 2015). This is summarised within Fig. 63 and outlined in more detail below.

i) The basement membrane of seminiferous tubules is lined with spermatogonial stem cells, which form a reservoir of self-regenerating stem cells and support continual sperm production through the majority of male life (Oatley and Brinster, 2006). At intervals, groups of cells called A1 spermatogonia emerge, marking the beginning of a spermatogenic cycle. These undergo mitotic divisions at around 42-hour intervals, producing clones. In the rat there are 6 mitotic divisions, leading to a maximum clone size of 64 cells (although cell death means this may be much lower). This pool of cells may be sub-classified into A-4 spermatogonia (1st three mitotic divisions), Intermediate after the 4th mitosis, and B after the 5th division. Type B spermatogonia then form resting primary spermatocytes (preleptotene spermatocytes) after a final 6th division. Whilst complete karyokinesis ensures that nuclear division is complete in each of these mitotic divisions, cytokinesis is incomplete, therefore all primary spermatocytes derived from one A1 spermatogonium are linked by thin cytoplasmic bridges, forming a large syncytium. This remains in place throughout the meiotic divisions that follow, and individual cells are only released as mature spermatozoa.

ii) During the second phase, resting preleptotene spermatocytes are found lining the basal intratubular compartment of the seminiferous tubules. These move into the adluminal intratubular compartment by disrupting the tight junctions between adjacent Sertoli cells. They then enter a prolonged meiotic prophase, moving through leptotene, zygotene, pachytene and diplotene stages, with characteristic morphologies depicting the state of their chromatin. At this point, their genetic material is shuffled, and they

become particularly sensitive to damage (especially during pachytene). At the first of two meiotic divisions, homologous chromosomes separate to opposite ends of the cells, then cytokinesis yields two haploid secondary spermatocytes. A second meiotic division then yields early round spermatids. At this stage, the cells remain linked syncytially via cytoplasmic bridges.

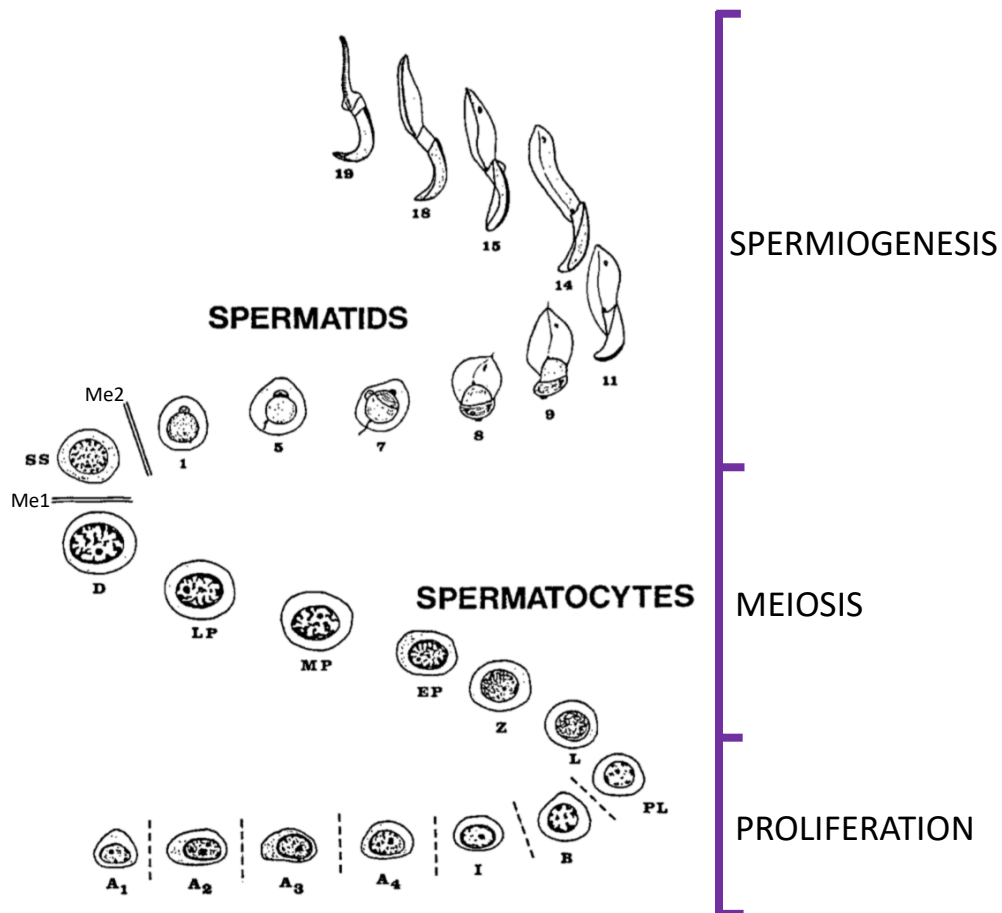


Figure 63: Germ cell development through spermatogenesis in the rat. The Proliferation phase includes 6 mitotic divisions from A1-A4 type spermatogonia, Intermediate (I), B type (B) and finally preleptotene spermatocytes (PL). Meiosis begins with small Leptotene spermatocytes (L) entering prophase, cell enlarging through Zygotene (Z), early- mid- and late Pachytene (EP, MP, LP) spermatocytes. Diplotene spermatocytes (D) then undergo the first meiotic division (Me1) to produce Secondary Spermatocytes (SS). After the second meiotic division (Me2), haploid cells begin to differentiate by forming round spermatids (RS) which represent steps 1-7 of spermatid development. RS become Elongating Spermatids from step 8 when the tail of the spermatozoa starts to form, continuing to differentiate until step 19 where they are considered to be mature spermatozoa and ready for release. Image adapted from Creasy, 1997.

iii) During the final phase, spermatids undergo the 19-step process of spermiogenesis (Fig. 63). This involves major cytoplasmic remodelling of the spermatid to take it from a round to elongated state. The resulting spermatozoa have elongated tails containing mitochondria to allow propulsion. The head of the spermatozoa, containing compacted haploid chromosomes, also has an acrosome which acts as an 'enzymatic knife' to aid

passage toward an oocyte. When spermatozoa are completely formed, the cytoplasmic bridges between them break, and they are released into the lumen at spermiation. The residual bodies left behind at this stage are in effect dustbins for residue of cytoplasm that is superfluous to requirements; these are phagocytosed by Sertoli cells after sperm are released.

Structural support and movement of germ cells is imperative to successful spermatogenesis. Sertoli cells play a critical role in managing this process, disassembling the junctional complexes on the luminal side and forming new ones on the basal side of the germ cell, effectively 'moving' it into the adluminal compartment. This dynamic mobilisation can be thought of like hospital theatre doors – to maintain a safe environment, when one set of doors are open, the others must be closed. The process is repeated as these germ cells develop, with germ cells moving down the adluminal compartment to the luminal edge midway through development, then back toward the Sertoli cell nucleus, before elongation and final release as spermatozoa (Creasy and Chapin, 2013, Mruk and Cheng, 2015).

The spermatogenic cycle in the rat

Within the rat, the spermatogenic cycle is generally broken down into 14 identifiable stages based on morphological markers, as first described by Leblond and Clermont in 1952 (Leblond and Clermont, 1952). Each stage contains a set population of developing spermatogonia, spermatocytes, round and elongating spermatids (Fig. 64). Although division into 14 stages is arbitrary, the cycle of spermatogenesis is a specifically timed developmental process; it takes 12.9 days in the Sprague-Dawley rat (10 days in humans) to see all 14 stages at any one location in a seminiferous tubule.

The actual time taken for the complete process of spermatogenesis whereby basal spermatogonia reach the final stage of spermatid development represents 4.5 spermatogenic cycles, which is 56 days in Sprague-Dawley rats (Creasy, 1997) or around 74 days in man, although it has been reported that spermatozoa may start to be shed as early as postnatal day 42 in the rat (Creasy and Chapin, 2013). Because seminiferous tubules are folded repeatedly within the testis, any section of testicular tissue typically

reveals hundreds of tubule cross-sections, all at one of the 14 stages of spermatogenesis.

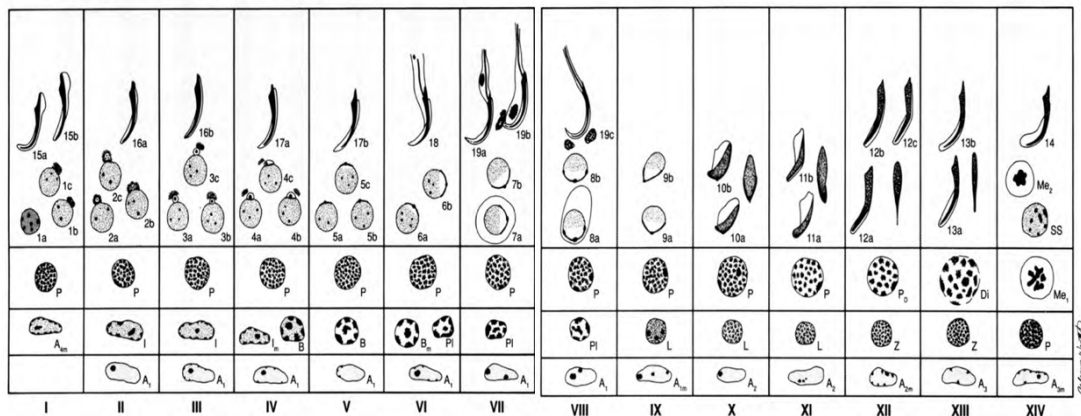


Figure 64: Stages of the spermatogenic cycle within the rat. To show the transitional characteristics, cell nuclei are depicted. Stages are identifiable by roman numerals. Steps of development from round spermatids to mature spermatozoa are labelled using letters and numbers. Round spermatids are seen within steps 1-8 of sperm development, and elongating spermatids from step 9-19. Mitosis is indicated by 'M' and meiosis by 'Me1' or 'Me2'. Spermatogonia are depicted as A, I or B type. Spermatocytes are depicted as preleptotene (PL), Leptotene (L), Zygotene (Z), Pachytene (P), Diplotene (Di) and Secondary (SS). Image reproduced from Hess (1990).

Based on a thorough understanding of testicular morphology and the spermatogenic cycle, the available literature was consulted for evidence of adverse testicular effects following ENM exposure. A number of studies examining the potential effects of ENM on male reproductive health using histological techniques have been published, reporting a variety of exposure routes, analysis techniques and outcomes. From the growing body of literature, studies using an experimental approach similar to that employed within the current chapter (oral exposure, silica or silver based ENM) are the focus of this section.

Effects of ENM on male reproductive health following Oral Exposure

Several authors report distribution of nanoparticles to the testis and subsequent detrimental effects to the testis following oral exposure regimes within rodents. (Jia et al., 2014) examined the effect of pubertal TiO₂ ENM exposure on testosterone synthesis and spermatogenesis in 60 Kunming mice. TiO₂ NPs 25nm in size were given orally to groups of mice at doses of either 10, 50 or 250mg/kg for 42 days from post-natal day 28-70. Abnormalities measured in epididymal sperm were much higher in exposed animal. The authors also reported a loss of developing spermatogonia within the seminiferous tubule germ cell layer at the highest dose, and the presence of vacuoles at all doses.

(Hong et al., 2015) exposed ICR mice aged 5 weeks to either 2.5, 5 or 10mg/kg bodyweight TiO₂ ENM 5-6nm in size (equivalent to around 0.15-0.7g of TiO₂ in humans 60-70kg bodyweight) daily via oral gavage for 60 days. Histopathology revealed lesions in the testis and epididymis, with reduction in sperm motility, quantity and increases in abnormal sperm recorded. Within the testis, seminiferous tubule germ cell layer was seen to be depleted, with reduced numbers of Leydig cells and mature sperm, and presence of pyknotic nuclei, spermatolysis and severe disorganisation of the tissue.

(Moridian et al., 2015) exposed 32 NMRI mice aged 6-8 weeks orally to either 5, 50 or 300mg/kg ZnO NPs daily for 35 consecutive days (equal to one sperm cycle in mouse). They reported significant decreases in serum testosterone levels in the 50 & 300 mg/kg dose groups, and a slight decrease in the 5mg/kg group. The diameter of seminiferous tubules was measured; a small decrease in size was reported for 5mg/kg alongside a significant reduction in size compared to control in the 50/300mg/kg group. In the 50/300 mg/kg groups, the total volume of seminiferous tubules, interstitial tissue and Leydig cell number were also significantly lower than control. The authors suggested the decrease in serum testosterone could be due to the loss of Leydig Cells

Silica NPs

Studies specifically examining silica ENM report mixed findings in relation to whether silica either accumulates within the testis or causes detrimental effects. In relation to distribution of silica nanoparticles to the testis, the findings of van der Zande *et al* are key, as they concern the same animals from which tissue samples were used in this chapter of research (van der Zande et al., 2014a). Silica nanoparticle treatments (28-day oral exposure to 100, 500 or 1000mg/kg bodyweight NM202 or 100, 1000 or 2500 mg/kg bodyweight SAS silica nanoparticles) did not reveal any significant accumulation in the testis compared to control. However, this does not mean that the tissues were not exposed to nanoparticulate silica during the experimental regime, rather it confirms that there was no accumulation of silica in the organ.

Of those studies published that included morphological evaluation of the testis without finding any histological changes, notable is that of (Morishita et al., 2012) who examined distribution and histologic effects of amorphous nanosilica (nSi) in Balb/c mice testis. An

initial protocol established that nano silica were able to enter the testis (being detected via TEM in the nuclei of spermatocytes). Following this, ENM were injected with either 0.4mg or 0.8mg 70nm nano silica (nSP70) via the tail vein every other day for 4 doses in total. The testes were collected 48 hours or 1 week after the last administration, and histological examination revealed no changes compared to control. Likewise, a study undertaken by Kim et al in 2006 revealed no histological findings following exposure of mice to magnetic silica nanoparticles via intraperitoneal injection (Kim et al., 2006).

Some studies have reported reversible effects, with histological and biochemical markers of toxicity returning to normal after a recovery period. Xu and colleagues investigated intravenous exposure of ICR mice (8 weeks old) to 65nm nSi ENM at a dose of 20mg/kg every 3 days, a total of 5 times over 13-day period. Animals were sacrificed at 15, 35 or 60 days after the 1st dose. The authors reported reversible negative changes to oxidative stress markers and quality/quantity of epididymal sperm, observed at 15/35 days, but not 60 days. They found no changes to acrosome integrity, sperm number, spermatogonia number or levels of testosterone, LH or FSH. These findings led them to the conclusion that damage following nSi exposure is transient and reversible (Xu et al., 2014).

Similar to Xu, Ren *et al* reported reversible damage to the testis in C57 mice exposed to 57nm Si ENM by tracheal perfusion over 15 doses (2mg/kg every 3 days for 45 days). Animals sacrificed at the end of the dosing regimen showed focal areas of seminiferous tubules with a thin germ cell layer, vacuolisation and exfoliation or sloughing of cells into the lumen. At this time point, sperm motility and normality in the epididymis was decreased compared to control, an increased number of spermatocytes were found to be undergoing apoptosis, and there were raised levels of markers related to oxidative stress (MDA and 3-NT). Conversely, animals sacrificed following a 1-month wash-out period were not different to control (Ren et al., 2016).

Although most studies concerning exposure to silica nanoparticles in pubertal or adult rodents reported either no adverse outcome, or reversible adverse effects, a recent study suggests that prenatal exposure to nano silica may lead to negative reproductive outcomes in pups. Bara *et al* investigated reported negative outcomes relating to

testicular morphology and hormone levels within 6-month old swiss albino mice exposed to mesoporous silica ENM *in utero*. Dams were exposed via oral gavage at either 50 or 250mg/kg bodyweight between gestational days 15 and 19. The high dose group showed changes in testicular morphology, with prominent epithelial vacuolization, decrease in seminiferous tubule diameter and alterations to the spermatogenic process visible. Testosterone levels were measured as decreased in this group compared to control, however StaR expression was increased, and P450scc, LH-R, 17b-HSD and P450c17 expression decreased. No changes were measured within the low-dose group, indicating a threshold of effect between the two (Bara et al., 2018).

Silver NPs

The literature concerning the effects of silver nanoparticle exposure is far wider than that for silica, and it appears to be more widely accepted that silver nanoparticles generally result in adverse effects to male reproductive organs following short, medium or long-term exposure.

Of primary importance are the findings of Van der Zande *et al*, as tissue samples from their study are used within this chapter of research (van der Zande et al., 2012). By contrast to their findings for silica, their evaluation of the distribution, elimination and toxicity of <20nm silver nanoparticles within Sprague-Dawley rats following 28 days of oral exposure (at 90mg/kg daily) reported distribution to and accumulation within the testis of silver nanoparticles. It is important to note that silver concentrations were highly correlated to the amount of Ag⁺ ion present in the silver nanoparticle suspension, further analysis on which suggested that silver ion distribution was far greater than silver nanoparticle. Nonetheless, Ag nanoparticles were also present, and interestingly, not cleared from the testis after an 8-week period of wash-out.

Research published by Kim *et al* in 2008 further substantiates the findings of Van der Zande. Following 28-day oral exposure of Sprague-Dawley rats to 30, 300 or 1000 mg/kg bodyweight silver nanoparticles (50-70nm) according to OECD TG407, all tissues from exposed groups showed a statistically significant ($p < 0.1$) dose-dependent increase in silver concentration (Kim et al., 2008). Additionally, in 2010, Kim *et al* tested oral toxicity of 56nm silver nanoparticles over a sub-chronic 90-day period, according to OECD

TG408. Following daily exposure of 5-week-old specific-pathogen free (SPF) Fisher 344 rats to 30, 125 or 500mg/kg silver, a dose-dependent accumulation of particles was seen in all tissues examined, including the testis (Kim et al., 2010). Finally, Lee and colleagues went on to demonstrate that not only were silver nanoparticles able to accumulate in the testis, it was likely that their biopersistence was greater than seen by van der Zande *et al.* Following 28 days' oral exposure in Sprague-Dawley rats, the group allowed animals to recover for up to 4 months before testing for silver content in their organs. They saw accumulation and persistence of Ag nanoparticles in the brain and testis of the animals with no sign of clearance. This was contrary to all other organs tested, which showed a gradual decrease over the 4-month recovery period (Lee et al., 2013).

Based on these studies, it can be assumed with relative confidence that silver nanoparticles are able to enter and accumulate within the testis following oral exposure, potentially affecting homeostasis and leading to adverse effects. This outcome is mirrored within studies examining exposure via alternative routes, with silver distribution to the testis of rats and mice reported following intravenous administration (Dziendzikowska et al., 2012, Garcia et al., 2014, Wang et al., 2013), intraperitoneal administration (Wang et al., 2013), and transdermal uptake (Pfurtscheller et al., 2014).

Of the many available studies, a few specifically concern effects of Ag NPs following oral exposure. Miresmaeili *et al* evaluated the effects of Ag NPs on the acrosomal reaction and spermatogenic cells in rats following oral gavage exposure every 12 hours over one cycle of spermatogenesis (48 days). Rats were exposed to either 25, 50, 100 or 200 mg/kg bodyweight. A triple stain for the acrosome reaction showed a significant difference between control and treated animals in relation to live vs dead sperm quantities and to the ability of sperm to undergo the acrosome reaction (key for fertilization of oocytes). No change in Sertoli cell number was seen, and a reduction in spermatogonia cells was only observed in the highest dose group. However, animals receiving doses from 50-200mg/kg all showed significant reduction in number of primary spermatocytes and spermatids and spermatozoa (Miresmaeili et al., 2013).

In relation to longer-term exposures, Thakur *et al* administered 10-12-week-old Wistar rats Ag NPs at 20ug/kg daily for 90days. Histological examination of testicular tissue

revealed disorganisation and atrophy of seminiferous tubule germinal epithelia, loss of spermatogenic cells (especially spermatocytes and spermatids) and exfoliation of germ cells into the lumen. Some Sertoli Cell Only (SCO) tubules were present, and very few mature spermatozoa were seen. TEM analysis showed damage to tubular basement membrane, and apoptotic germ cells, with separation from basal laminae. Sertoli cells showed dissociation of nuclei from the basal portion, vacuoles in the cytoplasm and presence of silver NPs and lysosomal bodies. Spermatogonia, round spermatids, elongating and plus mature spermatids were all noted to be adversely affected (Thakur et al., 2014)

Two studies examining pre-pubertal effects of Ag NP exposure in male Wistar rats reported similar findings to those in adult animals. Sleiman *et al* exposed pre-pubertal Wistar rats via oral gavage to 60nm Ag NPs at either 50 or 15ug/kg bodyweight from post-natal day (PND) 23-53, sacrificing at the end of exposure or after 5 weeks of wash-out at PND90. Exposure delayed puberty onset in both treatment groups compared to control. A reduction in total and daily sperm production was seen at PND53 for the high dose group, and both groups at PND90. Morphometric analysis showed disorganisation of the seminiferous tubule epithelium, sloughing of germ cells and debris into the lumen. However, no significant difference in epithelial height or lumen/tubule diameter was recorded, and no change in serum testosterone or oestradiol concentrations from control observed at either PND53 or 90 (Sleiman et al., 2013).

Mathias *et al* examined a slightly longer period of exposure to Ag NPs during prepubertal development. 30 Wistar rats were dosed orally with 60nm Ag NPs at either 15 or 30ug/kg/day from PND12 to PND58, with sacrifice after 44 days of wash-out at PND102. Like Sleiman et al, they observed that onset of puberty was delayed in treated animals. Acrosomal integrity and sperm plasma membrane integrity (measured by eosin-y and nigrosin staining) decreased in a dose dependent manner, while the number of sperm abnormalities increased. Again, no change on serum hormone levels (testosterone, LH, FSH and oestradiol) was recorded (Mathias et al., 2015).

Several other studies concerning alternative routes of exposure have also reported relevant histological outcomes. Rezazadeh-Reyhani *et al* found alterations in

seminiferous tubular diameter and spermiogenesis index compared to control in animals exposed intraperitoneally to 50-60nm silver nanoparticles at doses from 0.5-5mg/kg daily for 25 days (Rezazadeh-Reyhani et al., 2015). Similarly, a 2014 paper from Garcia *et al* described various changes in seminiferous epithelial morphology, including germ cell apoptosis and a reduction in Leydig cell numbers following intravenous injection of 1mg/kg 10nm silver NPs to CD1 mice for 12 days (Garcia et al., 2014). Interestingly, Castellini *et al* reported no adverse morphological observations following a single intravenous injection of 0.6mg/kg bodyweight silver nanoparticles (40nm), despite finding damage to sperm. Conversely, (Fathi et al., 2018) observed a significant reduction in number of spermatogonia, Sertoli and Leydig cells in Wistar rats exposed via a single intraperitoneal injection (Castellini et al., 2014).

In summary, it is clear that both Si and Ag NPs are able to reach the testis following oral exposure, with multiple sources reporting testicular accumulation of Ag NPs with little clearance over time. Mixed outcomes reported following silica exposure indicate a potential for adverse morphological and functional effects, which may be resolved over time. Conversely, almost all studies on silver ENM indicate it is likely to cause adverse effects on both testicular morphology and function.

Based on the available literature, it is clear that thorough histopathological analysis is able to form a cornerstone in establishing effect (where present) of ENM on the testis. Some studies also attempted to use stereological methods to produce a semi-quantitative evaluation of either epididymal sperm or the seminiferous tubule and its contents. Additionally, numerous studies have examined sperm morphology, motility and abnormalities as the end product of spermatogenesis. To compliment this, serum, blood or homogenized tissue samples are often used to determine hormone level changes, or expression of RNA or proteins indicative of changes in steroidogenesis, components of the HPG axis or important proteins, enzymes and receptors for maintaining testicular homeostasis during spermatogenesis. Additionally, immunohistochemical staining of tissues for key proteins, enzymes and receptors to the functioning of the testis forms another useful and commonly applied route of investigation to further understand functional aspects of testicular biology following ENM exposure.

Objectives

In order to build further understanding of the potential adverse effects of engineered nanomaterial exposure on male reproduction, processed paraffin-embedded testis from Sprague-Dawley rats exposed to one of 2 types of silica dioxide, 2 types of silver ENM, silver ions or vehicle were procured from animals following a 28-day oral exposure protocol.

The research questions to be addressed were:

1. Does exposure to silver and silica ENM lead to morphological changes in the testes of treated animals?
2. Could semi-quantitative, systematic, stereological analysis of tissue reveal any measurable changes to the cycle of the seminiferous epithelium indicative of altered function following ENM exposure?
3. Could exposure to silver and silica ENM lead to any functional changes in the steroidogenic pathway or other key elements of the HPG axis within the testis?
4. Were any identified changes in tissues from animals exposed *in vivo* comparable to findings from previous work undertaken *in vitro*?

The aims for analysis were therefore twofold:

- i) to undertake a qualitative analysis of testicular morphology, together with an evaluation of stain intensity for various receptors, proteins and enzymes involved in steroidogenesis and its regulation, and
- ii) to further build understanding of morphological changes using a semi-quantitative, stereological analysis of the tissue.

A two-pronged qualitative analysis was developed, consisting of a detailed morphological analysis to uncover any changes (subtle or gross) to the testicular structure which may indicate toxicity. This was followed by immunohistochemical investigation of key receptors, proteins and enzymes to provide an indication on whether functional aspects of steroidogenesis and the HPG axis were altered following exposure. In order to provide a semi-quantitative appraisal of any effects, a stereological analysis was also designed.

Materials and Methods

Testicular tissues from rats used in two *in vivo* studies on the effects of ENM were provided by RIKILT, Netherlands. The testes were one of a number of major organs that were collected during a wider study, other organs included brain, liver, kidneys, spleen and sections of the intestine. This work was undertaken in accordance with the national guidelines for the care and use of laboratory animals under approval of the Dutch welfare committee. Of the organs collected, Edinburgh Napier University received a selection of paraffin embedded samples of kidney, liver, testis, brain and spleen. In this thesis, only testicular samples were considered. Exact details of the *in vivo* protocols for animal treatment, organ collection and preparation for histology is outlined below.

Animal study I: Silver nanoparticle treatments

The first study concerned exposure to three types of silver based ENM: NM-300, a JRC standardised nanoparticle used within the MARINA project; Nano Amor, an industrially available silver nanoparticle; and silver nitrate ions (AgNO_3) used as an ionic control. Details of all nanoparticles used are outlined within Table 20. Six-week old male Sprague-Dawley rats weighing ~245g each at the start of experimental work were purchased from Harlan (Horst, the Netherlands). Animals were housed in polycarbonate cages and acclimatised to a 12h light/dark reversed cycle for 2 weeks. Room temperature was ~20°C with a relative humidity of ~55%. Food and water was provided *ad libitum* except for a 2hr fasting period before each treatment. Rats were randomly divided into 5 groups of 5 for treatment:

1. NM-300 Ag < 20; 90 mg/kg bw
2. Nano Amor Ag < 15-PVP; 90 mg/kg bw,
3. AgNO_3 9 mg/kg bw,
4. Ctrl-Ag < 20, and
5. Ctrl-Ag < 15-PVP / AgNO_3 .

In addition, the remaining rats were randomly divided into 3 groups (n = 5) to study the wash-out until day 36, and into another 3 groups (n = 5) to study the wash-out until day 84. These wash-out groups for day 36 and 84 received equal treatments as group 1-3.

All animals were exposed daily for 28 days by oral gavage, at a dosing volume of 3.3ml/kg bodyweight. The suspensions and solutions were directly administered to the lower

oesophagus after 2 hours of fasting to prevent a reflux reaction. At day 29 the first 5 groups were euthanised by CO₂/O₂ inhalation and the organs excised aseptically, weighed and placed on ice. The washout groups were sacrificed at day 84 and organs collected using the same protocol. Animals were provided to Edinburgh Napier university after fixation in 10% neutral-buffered formalin, and subsequent dehydration in a series of ethanol and embedding in paraffin.

Table 20: Nanomaterials used in animal treatments

ENM	Type of Material	Form	Primary particle size and specific surface area	Additional info
JRC NM-300k	Coated Silver NPs from JRC representative manufactured nanomaterial panel	Suspension	<20nm	Dispersed in matrix of stabilizing agents polyoxyethylene glycerol trioleate (4%) and Tween 20 (4%) in H ₂ O.
Nano Amor	Commercially available coated nanosilver from Nanostructured & Amorphous Materials Inc.	Dry powder	<15nm	75% PVP. Final concentration 27mg/ml suspended in LC/MS grade water.
AgNO ₃	Ionic silver control, Sigma Aldrich	Dry powder	-	Final concentration 2.7mg/ml suspended in LC/MS grade water.
SAS	Synthetic Amorphous Silica	Dry Powder	Primary particle size: 7nm SSA: 380m ² /g ^a	Hydrophilic pyrogenic At least 89% of the material was >100nm in SEM analysis
NM202	Silica Dioxide	Dry Powder	Primary particle size: 10-25nm SSA: 200m ² /g ^a	Hydrophilic pyrogenic At least 78% of the material was >100nm in SEM analysis

Animal study II: silica nanoparticle treatments

The second animal study concerned exposure to two types of silica nanoparticulates: NM202, a JRC standardised nanomaterial used within the MARINA project; and SAS, a synthetic silica nanoparticle which is industrially available. Six-week-old male rats purchased from Harlan (Horst, the Netherlands) were housed individually in polycarbonate cages to allow control over feed. Animals were acclimatised to a 12h light/dark reversed cycle for 3 weeks prior to experiment at a room temperature of

~20°C with a relative humidity of ~55%. Feed and water were given *ad libitum*, except for a 2-hour fasting period before the prepared feed was offered to the animals, and the following exposure period.

Animals were an average bodyweight of ~280g at commencement of the experiment. They were randomly divided into 10 groups (n=5), made up of seven groups to be fed SAS or NM-202 in different dosages or vehicle for 28 days, and 3 groups which were fed either vehicle control or the highest doses SAS or NM-202 for 84 days. The groups for 28-day exposure were: 1) SAS; 100 mg/kg bw/day, 2) SAS; 1000 mg/kg bw/day, 3) SAS; 2500 mg/kg bw/day, 4) NM-202; 100 mg/kg bw/day; 5) NM-202; 500 mg/kg bw/day; 6) NM-202; 1000 mg/kg bw/day and 7) control. For the 84-day exposure, the groups were divided into: 8) SAS; 2500 mg/kg bw/day, 9) NM-202; 1000 mg/kg/day and 10) control.

The dosages selected were chosen to reflect previously observed LOAEL of 1500 mg/kg bw/day for SAS (van der Zande et al., 2014a) The medium and high doses of NM202 were chosen to be lower than those of SAS, because the material characterization showed a higher fraction of silica in the nano-size range in the feed matrix for NM-202. All treatments were offered prepared food with SAS, NM202 or vehicle.

Rats were allowed to consume all feed prepared with either vehicle, NM202 or SAS, and thereafter were immediately offered standard feed pellets again. During the course of the study, it was noted by the technical staff undertaking the experiment that the rats ate all silica containing food mixtures or vehicle mixtures within the exposure period of two hours.

One day after the last exposure (day 29) animals in groups 1-7 were euthanized by CO₂/O₂ inhalation and organs were excised aseptically, weighed and placed on ice. Animal testes were provided to Edinburgh Napier university after fixation in 10% neutral-buffered formalin, and subsequent dehydration in a series of ethanol and embedding in paraffin. Animals from groups 8-10 underwent an 84-day exposure. However, the testes of these groups were not made available to Edinburgh Napier University for further analysis.

Selection of Tissue and its Preparation

Upon arrival at Edinburgh Napier University, tissue samples were organised and catalogued (Table 21). The tissue samples selected for analysis were control animals, along with those treated with silver ENM, and those treated with silica NM202. These were chosen as they provided a direct comparison between the *in vitro* testing already completed and the *in vivo* work which had been undertaken. Whilst analysis of the full complement of tissues provided would have been ideal, time constraints meant that a focussed set needed to be chosen.

Table 21: Tissue Samples selected for analysis from those provided by RIKILT.

Treatment	Animal #	Dose	Washout Y/N	Sacrifice Day
CONTROL	J13	Vehicle only	Y	85
CONTROL	J20	Vehicle only	Y	85
CONTROL	J22	Vehicle only	Y	85
CONTROL	J28	Vehicle only	Y	85
CONTROL	J44	Vehicle only	Y	85
NM-300K	G31	90 mg/kg bw/day	Y	78
NM-300K	G32	90 mg/kg bw/day	Y	78
NM-300K	G33	90 mg/kg bw/day	Y	78
NM-300K	G34	90 mg/kg bw/day	Y	78
NM-300K	G35	90 mg/kg bw/day	Y	78
Nano Amor	I41	90 mg/kg bw/day	Y	78
Nano Amor	I42	90 mg/kg bw/day	Y	78
Nano Amor	I43	90 mg/kg bw/day	Y	78
Nano Amor	I44	90 mg/kg bw/day	Y	78
Nano Amor	I45	90 mg/kg bw/day	Y	78
AgNO ₃	K51	09 mg/kg bw/day	Y	78
AgNO ₃	K52	09 mg/kg bw/day	Y	78
AgNO ₃	K53	09 mg/kg bw/day	Y	78
AgNO ₃	K54	09 mg/kg bw/day	Y	78
AgNO ₃	K55	09 mg/kg bw/day	Y	78
CONTROL	G16	Vehicle only	N	29
CONTROL	G31	Vehicle only	N	29
CONTROL	G36	Vehicle only	N	29
CONTROL	G38	Vehicle only	N	29
CONTROL	G40	Vehicle only	N	29
202 LOW	D24	100mg/kg bw/day	N	29
202 LOW	D33	100mg/kg bw/day	N	29
202 LOW	D35	100mg/kg bw/day	N	29
202 LOW	D41	100mg/kg bw/day	N	29
202 LOW	D47	100mg/kg bw/day	N	29
202 MEDIUM	E7	500mg/kg bw/day	N	29
202 MEDIUM	E9	500mg/kg bw/day	N	29
202 MEDIUM	E26	500mg/kg bw/day	N	29
202 MEDIUM	E27	500mg/kg bw/day	N	29
202 MEDIUM	E34	500mg/kg bw/day	N	29
202 HIGH	F4	1000mg/kg/bw/day	N	29
202 HIGH	F5	1000mg/kg/bw/day	N	29
202 HIGH	F10	1000mg/kg/bw/day	N	29
202 HIGH	F29	1000mg/kg/bw/day	N	29
202 HIGH	F46	1000mg/kg/bw/day	N	29

202 HIGH	F4	1000mg/kg/bw/day	N	29
202 HIGH	F5	1000mg/kg/bw/day	N	29
202 HIGH	F10	1000mg/kg/bw/day	N	29
202 HIGH	F29	1000mg/kg/bw/day	N	29
202 HIGH	F46	1000mg/kg/bw/day	N	29
202 HIGH	I1	1000mg/kg/bw/day	Y	85
202 HIGH	I8	1000mg/kg/bw/day	Y	85
202 HIGH	I23	1000mg/kg/bw/day	Y	85
202 HIGH	I42	1000mg/kg/bw/day	Y	85
202 HIGH	I45	1000mg/kg/bw/day	Y	85

To prepare tissues for analysis, 15 non-consecutive sagittal 5µm sections from the testis of each animal were cut from each paraffin embedded block using a Leica RM2125RT rotary microtome, floated onto ThermoFisher Superfrost™ glass slides using a water bath set to 42°C (which electro-statically attract tissue to reduce loss during staining) before being dried in an oven overnight at 60°C.

Tissues were then examined for morphological and functional markers of change using qualitative morphological and stain intensity analyses and semi-quantitative stereological analysis, to allow a validation of results obtained from *in vitro* studies. This was completed using first Haematoxylin and Eosin staining and then Immunohistochemical stains for antibodies identified to be of interest.

Haematoxylin and Eosin (H&E) staining

H&E staining involves application of haematoxylin (a basic dye) and eosin (an acidic dye) to prepared tissue samples in order to stain cellular structures and make them easily viewable for analysis down a microscope. Haematoxylin is comprised of hemalum (a complex formed from aluminium ions and hematein). Hematein is an oxidation product of haematoxylin. When tissue is exposed to haematoxylin, it stains acidic (basophilic) structures such as the nucleus purple. Eosin is a fluorescent acidic dye which acts as a counterstain to haematoxylin by binding to basic (eosinophilic) structures like proteins within the cytoplasm and staining them shades of red to pink. The end result is a clear stain of intracellular structures which shows nuclei as blue to blue/black, cytoplasm in deep pink, and red blood cells and eosinophilic granules in bright orange/red.

Haematoxylin and Eosin staining protocol

To stain tissues using H&E, slides were first brought to a hydrated state through xylene and diminishing grades of alcohol to water. This ensures removal of all paraffin as this is hydrophobic and prevents staining with aqueous reagents such as H&E. Slides were stained with haematoxylin (Mayer's Haematoxylin, Cellpath UK) for 5 minutes in a bath on a laboratory rocker, then washed with tap water for 30secs-1min, before being dipped in 1% acid alcohol solution to remove any background staining and washed in water again. If necessary, they were then 'blued up' in warm Scott's tap water substitute (Cellpath UK) – a weakly alkaline solution which assists in bringing out the blue staining on the nuclei. An eosin Y based counterstain (mixture of 8-parts 1% Aqueous Eosin and 1-part Putt's Eosin, both from Cellpath UK) was then applied as a bath for 5 minutes, slides were washed in water for 30sec-1minute to remove all Eosin, and then dehydrated through alcohol and xylene baths before applying pertex mounting glue and coverslips. The staining protocol including times for immersion of slides in each solution is summarised within Table 22.

Table 22: Haematoxylin and Eosin staining protocol

1. Rehydration		2. H & E Stain		3. Dehydration	
Solution	Time	Solution	Time	Solution	Time
Xylene (de-wax 1)	3min	Mayer's Haematoxylin	5min	Methylated spirit	1min
Xylene (de-wax 2)	2min	Water wash	30sec-1min	Ethanol 2 (70%)	2min
Ethanol 1 (90%)	2min	1% acid alcohol	1-3 quick dips	Ethanol 3 (90%)	1min
Methylated spirit	1min	Water wash	30sec-1min	Xylene (clearing)	1min
Water	30sec-1min	Scott's tap water substitute	1min	Xylene (coverslip)	5min
		Water wash	30sec-1min		
		Eosin	5min		
		Water wash	30sec-1min		

Immunohistochemistry

Immunohistochemistry (IHC) is based on the interaction of target antigens with specific antibodies tagged with a visible label and this enables the visual localization of specific cellular components within tissue. For this endpoint, the peroxidase enzyme based-system making use of biotin labelling and formation of an avidin-biotin complex was selected. This system therefore allows sensitive visualisation of the cellular target (antigen) via 4 key steps (outlined in Fig. 65):

1. Binding of the primary antibody of interest to the protein/receptor of interest on the tissue,
2. Binding of a biotinylated secondary antibody to the primary antibody,
3. Binding of an avidin-biotinylated peroxidase enzyme complex (ABC) to the biotin attached to the secondary antibody to increase signal, and finally
4. Addition of an enzyme substrate (DAB) in order to label the antigen, in this case via development of a colorimetric reaction from clear to brown.

A panel of antibodies were selected for investigation to compliment the functional analysis carried out *in vitro*, and the optimal dilution determined for the tissue samples. These are outlined within Table 23.

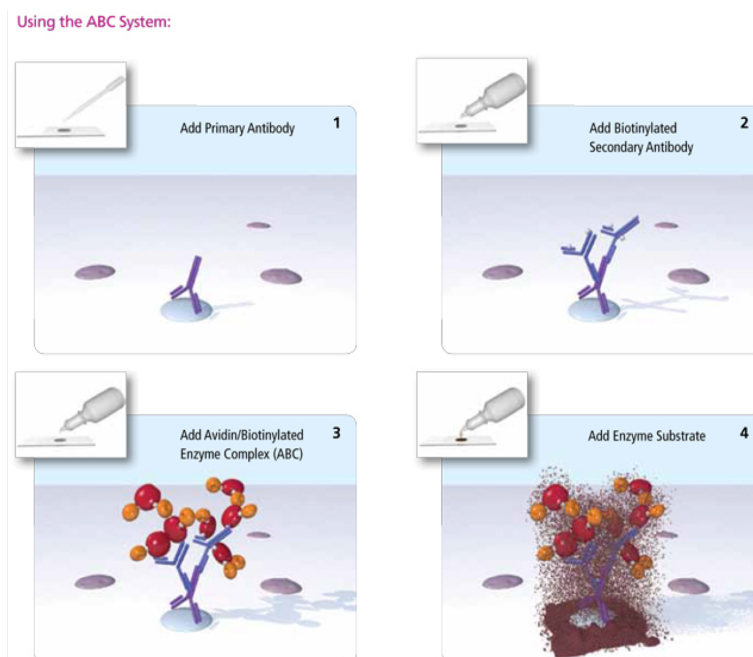


Figure 65: Biotin labelled immunohistochemistry. Source: Vector Labs (VectorLaboratories, 2018).

Table 23: Panel of Antibodies selected for examination of tissues collected by immunohistochemistry.

ANTIBODY	DETECTS	PRODUCER	RAISED IN	1°Ab Dilution	SECONDARY ANTIBODY
Luteinising Hormone Receptor (LH-R)	Luteinising hormone receptor, indicative of Leydig Cell function	Santa Cruz	Rabbit Polyclonal	1:50	Vector Labs: biotinylated universal anti-mouse/rabbit IgG secondary antibody
Androgen Receptor (AR)	Androgen receptor, abundant within healthy Sertoli Cells	Santa Cruz	Rabbit Polyclonal	1:50	Vector Labs: biotinylated universal anti-mouse/rabbit IgG secondary antibody
Steroidogenic acute Regulatory Protein (StaR)	Regulation of steroid hormone synthesis by Leydig Cells	Santa Cruz	Goat Polyclonal	1:50	Vector Labs: Biotinylated Universal Pan-Specific Antibody (Horse Anti-Mouse/Rabbit/Goat IgG)
3-β-hydroxysteroid dehydrogenase (3β-HSD)	Regulation of steroid hormone synthesis by Leydig Cells	Santa Cruz	Goat Polyclonal	1:50	Vector Labs: Biotinylated Universal Pan-Specific Antibody (Horse Anti-Mouse/Rabbit/Goat IgG)
Deleted in AZoospermia-like protein (DAZL)	Present within Germ cells and crucial to achievement and maintenance of spermatogenesis	Santa Cruz	Goat Polyclonal	1:250	Vector Labs: Biotinylated Universal Pan-Specific Antibody (Horse Anti-Mouse/Rabbit/Goat IgG)
Mouse Anti-Rat Granulocytes RP-1	Reacts with rat peritoneal and peripheral blood neutrophils if present	BD Biosciences	Mouse monoclonal	1:50	Vector Labs: biotinylated universal anti-mouse/rabbit IgG secondary antibody

It is notable that two new antibodies were introduced in addition to those already used within the *in vitro* work, namely *Dazl* and RP-1. *Dazl* was used to measure germ cell development within the spermatogenic cycle (something which was not possible in the individual cell lines used *in vitro*), and RP-1 was employed to investigate whether inflammatory effects observed within the testicular interstitium were due to immune system response. To undertake immunohistochemical staining for each of the above, slides were taken through the four key steps of immunohistochemical staining as follows:

1. Dehydration, antigen retrieval and peroxidase blocking

Slides were first dewaxed and hydrated using xylene and graded alcohols to water as per the hydration steps employed for H&E staining (Table 22). They were then microwaved in citrate buffer to allow antigen retrieval whereby cross-linking of proteins which occurs during the fixing steps of sample preparation is reversed in order to unmask the epitope of interest. Following this, they were blocked in 3% peroxidase solution for 20 minutes to suppress endogenous peroxidase activity, which would cleave the substrate and lead to background staining caused by non-specific binding of the antibody.

2. Serum blocking and antiserum binding

A Tris-Buffered Saline wash (a solution which is close to physiological pH of 7.4) was prepared by diluting 0.1M Tris (10x) with water and sodium chloride. Following a wash with TBS, a further 30-minute block for non-specific binding was undertaken using normal horse serum (2.5%, Vector labs). A PAP pen was then used to seal the space around tissue on each slide, the primary antibody selected was diluted appropriately in normal horse serum and applied before slides were incubated in a humidified chamber overnight at 4°C.

3. Binding of Secondary antibody and ABC complex

The following day, primary antibody was washed from slides using PBS-Tween (0.1%). Negative controls were washed separately to avoid any cross-reaction with primary Antibody. Slides were then incubated with an appropriate secondary Antibody (Table 23) for 60 minutes at room temperature. A further wash was undertaken with TBS before incubation with Avidin-Biotin Complex (ABC complex, Vector Labs) for 60 minutes to enable substrate binding (Fig. 20).

4. Addition of DAB substrate and colorimetric reaction to visualise results

DAB staining Following a final 5-minute TBS wash, DAB substrate (3,3'-Diaminobenzidine, Vector Labs) was prepared and applied to the slides to determine antibody localisation. When colour development was deemed sufficient, the colour reaction was stopped by rinsing slides in water for 5 minutes. They were then counterstained with haematoxylin and then dehydrated through graded alcohols to

xylene for final mounting using Pertex mounting medium (Cellpath UK). Sections for all control and treated animals were run for each antibody at the same time and under the same conditions to ensure comparability.

Image Capture

Once slides were prepared, a Zeiss slide scanner (Axio Scan.Z1, accessed at Institute of Aquaculture, Stirling University) was used to digitise all specimens. The scanner uses an automated process to create high quality virtual slides in a reliable, reproducible way. The slide library was then catalogued in preparation for morphological and stereological analysis using the software packages Zeiss Zen Blue v2.3 for morphological analysis, and ImagePro Premier v8 (Media Cybernetics) for stereological measurements.

Virtual slide preparation for Morphological Analysis

Qualitative morphological analysis to identify treatment effects was undertaken on H&E stained slides. Every virtual slide prepared was scanned within Zen blue software to appraise general appearance, and 2-4 representative images at varying magnifications taken of each in preparation for analysis.

Virtual slide preparation for Stereological analysis I: basic analysis

Five snapshot images were taken from H&E stained slides at 50x magnification using Zen Blue to produce five subset virtual slides saved as Carl Zeiss Image (czi) files, which unlike many other image formats, retain metadata that allow the user to zoom into much higher magnifications in order to undertake detailed analysis at a later time. To ensure that analysis was as consistent and unbiased as possible, these were taken as subset images from each pole of the slide, plus the centre (Fig. 66). Images were then white balanced to remove unrealistic colour casts from the light source at imaging using pre-sets within Zen, and a scale bar was applied to each for

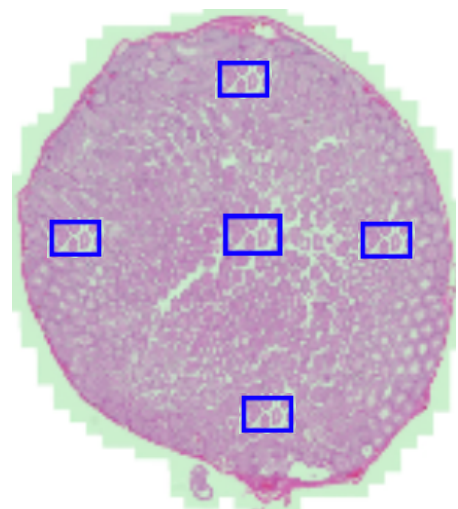


Figure 66: Subset image preparation from tissue sections within Zen. A 50x magnification was applied, then 5 subset images were captured from the 4 poles of the section plus the middle.

reference. At this stage the virtual subsets of slides were blinded by a person uninvolved in the work to minimise bias in analysis.

Virtual slide preparation for Stereological analysis II: staging and related measurements

Subsequently, a second stereological analysis of slides was undertaken (rationale outlined below) which included staging of tubules on each virtual slide before measurement of key parameters. To enable this, a similar protocol was followed as for analysis I, but using Dazl antibody stained slides to assist in identification of tubule stage.

Morphological analysis of tissues

One virtual slide per animal in each treatment or control group was analysed for general appearance, structure and morphology of the seminiferous tubules, Leydig and interstitial cells. Commentary was prepared based on observations and any morphological changes of note. This was then used to guide subsequent immunohistochemical and quantitative analysis.

Immunohistochemical Analysis:

Virtual slides were evaluated subjectively but systematically. Initially the intensity of immunostaining was noted for each animal on a scale from negative through weakly, moderate to strongly positive, and overstained. Although staining intensity was noted, it was not considered to be a quantitative measure of immunostaining, as the colourimetric reaction seen with DAB does not represent a linear relationship between concentration of compound and absorbance. This is because DAB does not follow the Beer-Lambert law as it is not a true absorber of light, but rather scatters it with a broad, featureless spectrum (van der Loos, 2008). Thus, darkness of DAB stain is not directly related to amount of reaction product. Based on this, intensity of staining was used as a qualitative indicator only and any inferences on potential alteration in steroidogenic potential were made in conjunction with those from the western blot and RNA analysis (Chapter 4).

Stereological analysis of tubules I: basic measurements

Initially, blinded H&E images were imported to ImagePro Premier software and the scale bar used to calibrate measurements. On each image, all tubules that were fully visible within the screen were then measured for diameter across the shortest point of the cross-section, and germ cell layer thickness from the edge of the tubule to the inner edge of the germ cell layer. Measurements were exported to Microsoft Excel and compiled before transfer to Graphpad Prism v7 for statistical analysis.

Stereological analysis of tubules II: staging and related measurements

Following processing of initial results, it was clear that the stage of the seminiferous epithelium at which each tubule was played a major role in the tubule diameter, lumen volume and germ cell layer thickness observed. Therefore, a second analysis was carried out which took into account stage, following guidance set out by Creasy et. al. (Creasy, 1997). As this analysis was far more detailed, only silver treated animals and controls were analysed, with plans to include animals from the silica study at a later date. The analysis required several key steps in order to be successful:

1. Tubule staging, assisted by
2. Dazl immunostaining intensity measurement, then
3. Measurement of tubule diameter and lumen volume,
4. Measurement of additional relevant parameters, including internal luminal volume (where cell sloughing into the lumen was present), and allocation a shape class (round, elliptical or elongated).

Each step is outlined in full within the sub-sections below.

1. Staging of tubules

Identification of tubule stage was undertaken within Zen Blue software, and systematically labelled within this programme before export to Image Pro Premier for measurement. Staging of tubules was supported by development of a decision key to assist with accuracy and consistency. This was adapted from several sources, initially referencing Leblond's seminal paper defining the stages of the cycle of the seminiferous

epithelium in the rat (Leblond and Clermont, 1952), and then using work from Hess which provided a detailed overview of each stage and its characteristics (Hess, 1990, Meistrich and Hess, 2013), alongside OECD prepared guidance on the histopathological evaluation of the male reproductive system (OECD, accessed 2017). The final decision key and supporting data are outlined within Tables 24 and 25. It is important to note that because of previously recognised challenges with assigning stages I-IV using classical histology methods such as paraffin sectioning, these stages were grouped together for this analysis.

2. Dazl immunohistochemical stain intensity

To assist staging, analysis of the staining intensity of Dazl protein was also undertaken for each tubule on each virtual slide. Dazl is a crucial factor for achievement and maintenance of spermatogenesis, and its expression is known to vary within germ cell populations in the testis. Rocchietti-March *et al* reported weak but specific Dazl staining in the cytoplasm of intermediate and B Spermatogonia, primary spermatocytes during Prelepotene to Zygotene stages, and in the acrosomal region and around elongating spermatids. They also observed strong specific staining in the cytoplasm of primary spermatocytes, which was lost in Diplotene spermatocytes (Rocchietti-March *et al.*, 2000). It was hoped that this stage-specific Dazl staining would provide a further support to ensuring accuracy in staging of tubules for stereological analysis. Expected Dazl stain intensity was therefore outlined alongside key germ cell populations within Table 25, to be used alongside the primary decision key (Table 24) to support staging of tubules.










Tubules on each virtual slide were evaluated subjectively but systematically so that the intensity of immunostaining was appraised for each animal on a scale from negative (0) through weakly (1), moderate (2) to strongly (3) positive, and (4) overstained. Results were then exported to excel for initial analysis, before being imported to Graphpad Prism v7 for final analysis and graphing. The final graphed result for Dazl stain was overlaid onto each graph produced of measured tubule diameter and lumen volume per treatment to illustrate the supportive relationship between Dazl stain and tubule stage.

Table 24: Key cell populations, distinguishing features, morphological and stereological identifiers present at each stage of the seminiferous tubule cycle used in staging tubules for morphological and stereological analysis.

Initial Question:		Are 2 steps of spermatids present (round and elongating)?		YES: stages I – VIII / NO: stage IX - XIV		
If YES to question 1:		Are elongated spermatids located near lumen?		NO: late I-V / YES: Late VI-VIII		
Stage in Cycle	Spermatid Step	Spermatid populations present	SPERMATID Step Distinguishing Features	Germ cell types Present	Morphology Notes	Stereological analysis Notes
I	1, 15	Round + Elongating Spermatids	15: Pronounced curve of nuclear apex and bulge in caudal region, located midway between lumen and basal membrane	A1 Spermatogonia Pachytene spermatocytes	Earlier P spermatocytes are closer to basement membrane and darker in appearance	Tubule diameter ↑ stages I-IV Germ Cell Epithelium Volume ↑ stages XIV-V of next cycle
II	2,16	Round + Elongating Spermatids	16: located midway between lumen and basal membrane	A1 Spermatogonia Intermediate Spermatogonia Pachytene spermatocytes	Earlier P spermatocytes are closer to basement membrane and darker in appearance	Tubule diameter ↑ stages I-IV Germ Cell Epithelium Volume ↑ stages XIV-V of next cycle
III	3, 16	Round + Elongating Spermatids	16: located midway between lumen and basal membrane	A1 Spermatogonia Intermediate Spermatogonia Pachytene spermatocytes	Earlier P spermatocytes are closer to basement membrane and darker in appearance	Tubule diameter ↑ stages I-IV Germ Cell Epithelium Volume ↑ stages XIV-V of next cycle
IV	4, 17	Round + Elongating Spermatids	17: located midway between lumen and basal membrane	A1 Spermatogonia Intermediate Spermatogonia B Spermatogonia Pachytene spermatocytes	Earlier P spermatocytes are closer to basement membrane and darker in appearance	Tubule diameter ↑ stages I-IV Germ Cell Epithelium Volume ↑ stages XIV-V of next cycle
V	5, 17	Round + Elongating Spermatids	5: Slightly curved head cap from acrosomic system (Ac) 17: located midway between lumen and basal membrane	A1 Spermatogonia Intermediate Spermatogonia B Spermatogonia Pachytene spermatocytes	B type Spermatogonia present against basement membrane	Lumen volume ↑ stages V-VIII Germ Cell Epithelium Volume ↑ stages XIV-V of next cycle

VI	6, 18	Round + Elongating Spermatis	Presence of mitotic figures Step 18 spermatis	A1 Spermatogonia B Spermatogonia Prelepotene spermatocytes Pachytene spermatocytes	PL spermatocytes are squashed and have 'dots' in them	Lumen volume ↑stages V-VIII Germ Cell Epithelium volume ↓ stages V-VII
VII	7, 19	Round + Elongating Spermatis	Elongating spermatis line luminal border Step 19 spermatis	A1 Spermatogonia Prelepotene spermatocytes Pachytene spermatocytes	Later P spermatocytes are larger and move toward lumen Basophilic granules present in cytoplasm	Tubule diameter ↑stages VII-VIII Lumen volume ↑stages V-VIII Germ Cell Epithelium volume ↓ stages V-VII
VIII	8	Round Spermatis	Step 19 spermatis Line luminal border	A1 Spermatogonia Prelepotene spermatocytes	Residual bodies present around lumen	Tubule diameter ↑stages VII-VIII Lumen volume ↑stages V-VIII
IX	9	Elongating Spermatis	No late spermatis present 9: spermatis all appear round	Lepotene Spermatis Possibly some residual prelepotene spermatocytes	More Lepotene than prelepotene Residual bodies in epithelium	Tubule diameter ↓stage VIII-IX Lumen volume ↓ stage VIII-IX
X	10	Elongating Spermatis	No late spermatis present 10: slight elongation starting to show	Lepotene Spermatis	Residual bodies have disappeared	
XI	11	Elongating Spermatis	11: Ac hooks off at angle and spermatis present in clumps	Lepotene Spermatis	Distinct bundles of elongating spermatis present	
XII	12	Elongating Spermatis	12: more elongated and narrow than (11)	Zygotene spermatocytes Pachytene spermatocytes	Some Diplotene spermatocytes may be present	
XIII	13	Elongating Spermatis	13: bulge of spermatis head now present	Zygotene spermatocytes Diplotene Spermatis	Large number of Diplotene spermatocytes present	
XIV	14	Elongating Spermatis	14: spermatis appear more 'hooked' than (13)	Pachytene spermatocytes 2ndary Spermatis Meiosis Occurring	Meiotic figures present Some secondary spermatocytes may be visible	Germ Cell Epithelium Volume ↑ stages XIV-V of next cycle

Table 25: Key cell populations present at each stage the seminiferous cycle in tubules to support decision key outlined within table 24 for staging of tubules for morphological and stereological analysis. Relative expected Dazl protein immunohistochemical stain is also noted at the base of the table, based on Rocchietti-March et. al. (2000). Images reproduced from Hess (Hess, 1990).

Germ cell type		Present in stage? Y/N													
Name	Morphology	I	II	III	IV	V	VI	VII	VIII	IX	X	XI	XII	XIII	XIV
Intermediate Spermatogonia			Y	Y	Y	Y									
B Spermatogonia					Y	Y	Y								
Preleptotene								Y	Y	Y					
Leptotene										Y	Y	Y			
Zygotene													Y	Y	
Pachytene: LHS early RHS late		Y Early	Y Early	Y Early	Y Early	Y Early	Y Early	Y Early	Y Early	Y Early	Y Late	Y Late	Y Late		Y Early
Diplotene													Y	Y	
Meiotic															Y
Secondary Spermatocytes															Y (in some)
Expected Dazl Stain Intensity		-	-	-	-	+	++	+++	+++	++	+	+	-	-	-

3. Stereological Measurements within Image Pro Premier

Once virtual slides including annotation for tubule stage were imported to Image Pro Premier, the scale bar was used to calibrate measurements. Each tubule was then systematically measured for diameter and lumen volume. Diameter was measured across the shortest point of the tubule cross-section, and luminal volume measured by drawing a region of interest (ROI) around the edge of the luminal space, from which Image Pro Premier calculated volume in $\mu\text{m}/\text{cm}^2$ (Fig. 67).

4. Measurement of additional parameters and classification of tubule shape

In some of the treated animals, sloughing of cells into the central lumen of the tubule was observed (Fig. 68). Where this occurred, an internal diameter was taken and used to generate a second set of volumes, corrected for internal sloughing of cells. This second set of measurements were later used within the statistical analysis to elucidate whether taking into account cells sloughed into the lumen altered any outcomes observed.

Finally, all tubules were annotated as to whether they were round, elliptical, or elongated in shape, in order to later check whether tubule shape influenced outcomes relating to the lumen volume measured (Fig. 69). All measurements were then exported

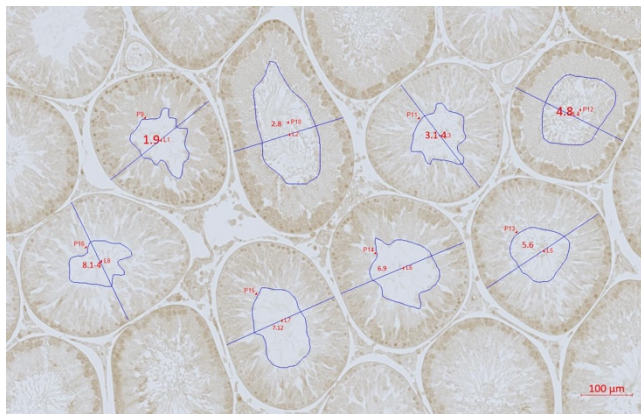


Figure 67: Example of annotation and measurement process for stage, tubule diameter and lumen volume applied to all sample images. Tubules were staged and marked sequentially with "number.stage" in Zen Blue, before being exported to ImagePro Premier. Tubule diameter was then measured across the shortest transverse cross-section of tubule, and lumen volume calculated by drawing an ROI around the edge of the lumen space in each tubule. Representative image is from animal I43 within the Nano Amor treatment group, taken from the west pole of the slide.

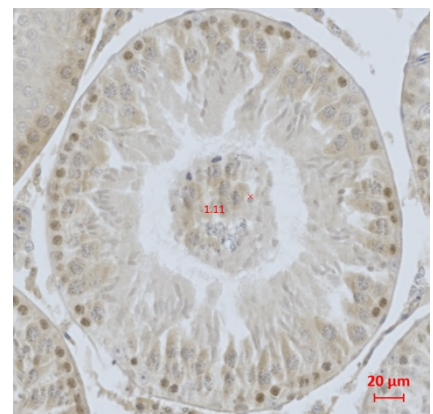


Figure 68: Representative image of tubule containing cells that have sloughed into the centre of the lumen. Where this was present, both the overall luminal volume and the inner luminal volume were calculated within Image Pro Premier, in order to provide aid analysis of whether taking into account cell sloughing altered any outcomes observed relating to treatment.

to Microsoft Excel and compiled before transfer to Graphpad Prism v7 and SAS for statistical analysis.

Statistical Analysis

Statistical analysis for this chapter was initially begun in Graphpad prism v7, and all of the statistical findings reported within the initial stereological analysis (stereological analysis I) were calculated within this programme. However, due to limitations discovered in dealing with uneven numbers of replicates such as those generated from observational recordings during the second part of the stereological analysis (which linked tubule stage to treatment, tubule shape and presence/lack of sloughed cells alongside measured outcomes), analysis was switched from Prism into SAS. To complete the analysis, Statistical Analysis Software (SAS) version 9.4 was used for the statistical outputs, while graphical representations of datasets were prepared in Graphpad prism.

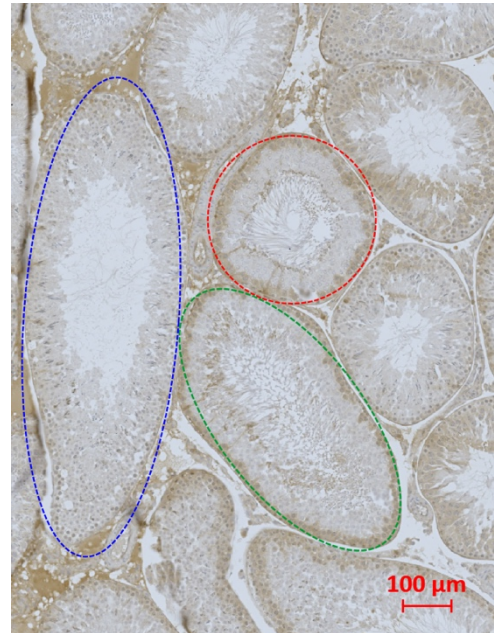


Figure 69: Representative image captured from a control animal to illustrate the differences in tubule shape captured on each section or virtual slide. Red = round tubule cut exactly perpendicular to the direction it is running in, green = elliptical tubule, cut at an oblique angle to the direction of the tubule, blue = elongated tube, cut on a sagittal plane to the direction of the tube.

Analysis within SAS was completed using a mixed model for repeated measures data. Mixed models are a type of linear regression model that take into consideration variation that is not generalizable to the independent (fixed) variables (such as treatment, tubule stage etc). These are enhancements on classical linear regression models that accommodate the fact that animal responses are not completely without variance, and as such contain both fixed and random effects, allowing for a more flexible approach to correlated data (Seltman, 2018). They also allow for uneven numbers of data within each dataset, which meant it is possible to analyse a dataset generated from observations and containing uneven numbers of observed tubule diameters and lumen volumes per stage and per animal.

Within this model animal was the random effect, tubule stage, treatment, shape etc. were fixed effects, and the response was lumen volume or tubule diameter. Having animal as the random effect accounts for the fact that this inherently contains variation i.e. each animal will respond slightly differently to treatment, something that would generally result in errors forbidden by the assumptions of a standard ANOVA or regression model. Inclusion of fixed and random effects therefore partitions the variability in a regression approach for observations that are correlated. Allowing for these allows the correlated variability of animal response to be 'soaked up'. This means the remaining variability is classed as heteroscedastic, uncorrelated and normal error, which allows the use of least squared regression techniques to finish the estimation of result (Barter, 2018).

In short, for each outcome of interest, the model calculates a resulting coefficient or estimate (which is similar to an average but takes into account assumptions made by the model), by fitting a regression line to each factor (e.g. stage or treatment) within each level (animal), then averaging the regression to obtain an overall effect of treatment on result. For example, when comparing tubule diameters between the d29 and d85 control animals, the model examining the effect of treatment and stage (factors) on tubule diameter (result) would be:

$$\textit{Tubule Diameter} = \textit{stage (11 possible)} + \textit{treatment (2 possible)}$$

For each of the possible choices with each factor (stage or treatment), the estimate is the intercept of the model's fit plus the estimate of factor 1 (stage) plus the estimate of factor 2 (treatment). Thus, if the average tubule diameter calculated within the model was 257.21µm, the estimate of stage I-IV was -5.439µm and the estimate of treatment d29 was -27.026µm, then the calculated Tubule Diameter estimate for stage I-IV within control d29 animals would be:

$$\begin{aligned} \text{Tubule diameter } \textit{stage I-IV d29} &= 257.21 + -5.439 + -27.026 \\ &= 224.745\mu\text{m} \end{aligned}$$

At this stage, the model would make a final adjustment for the proportional amount of observations that have contributed to each factor vs the overall dataset size, and thus

the final 'weighted average' produced would account for smaller numbers of observations against certain factors.

Results

Morphological analysis of control tissues

An initial examination of slides from control animals prepared with H&E stain revealed tissue with regularly shaped seminiferous tubules at various stages of spermatogenesis, interspersed with interstitial Leydig cells, capillaries and blood vessels.

As depicted within Fig. 70, the seminiferous tubules had a well-defined outer tunica propria, with tubular myoid cells lining the basal lamina of the tubules. The epithelium was comprised of Sertoli cells and a developing germ cell layer containing sperm at various stages of maturation. Within these images, which depict a stage VII tubule (A) and a stage VIII tubule (B), the least mature primary spermatogonia (A, intermediate and B type – Fig. 71 contains a clear view of an A type spermatogonia) were present at the basement membrane, with spermatocytes alongside them in varying stages of development from primary to secondary (preleptene and pachytene visible within Fig. 70). Round and elongating spermatids were situated midway between basement membrane and lumen, and mature spermatids when present passed toward the central lumen before being released at stage VIII of the tubule's cycle (spermiation). Image B shows the migration of Sertoli cells toward the central lumen, which occurs at stage VIII.

The interstitial cell population of Leydig cells, capillaries and blood vessels all appeared to be healthy. Fig.71 shows the polyhedral layout of Leydig cells around both capillaries and blood vessels in the interstitial space. Adult Leydig cells are not exclusively arranged in clusters but do tend to stay in close association a blood supply, as shown within the image.

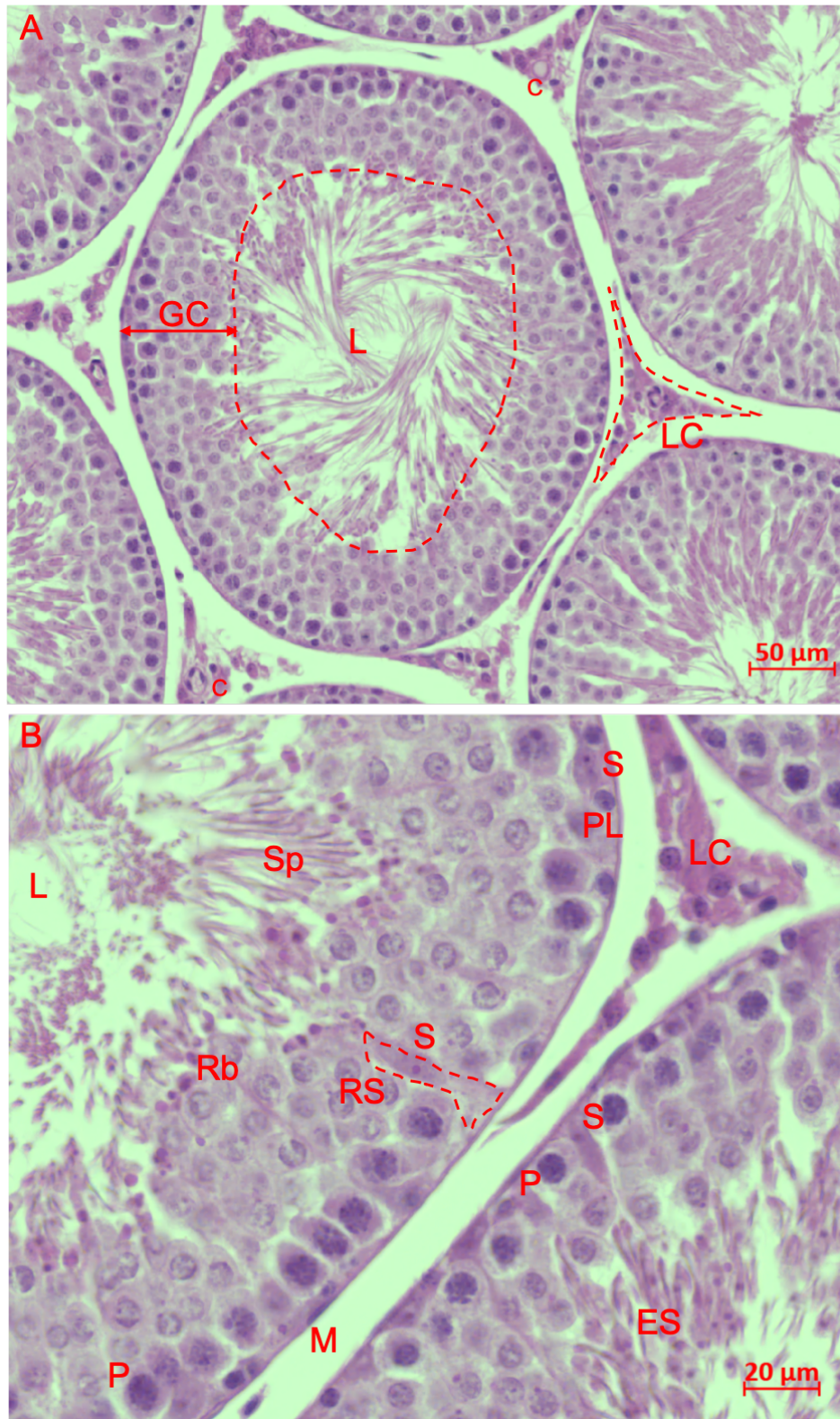


Figure 70: Representative morphology of healthy rat testis, taken from control animal (H&E stained). A: general layout of round seminiferous tubules, interspersed with polyhedral Leydig cells and blood vessels/capillaries. The tubule in the centre of the image is at stage VII. Scale bar represents 50µm. B: higher magnification representation of the same image. Scale bar represents 20µm. C = capillary; LC = Leydig Cell; GC = Germ Cell layer; L = Lumen; Rb = Residual Bodies; S = Sertoli cell; M = Peritubular Myoid Cell; P = Pachytene spermatocyte; PL = Preleptotene Spermatocyte; RS = Round Spermatid; ES = Elongating Spermatid; Sp = mature Spermatozoa.

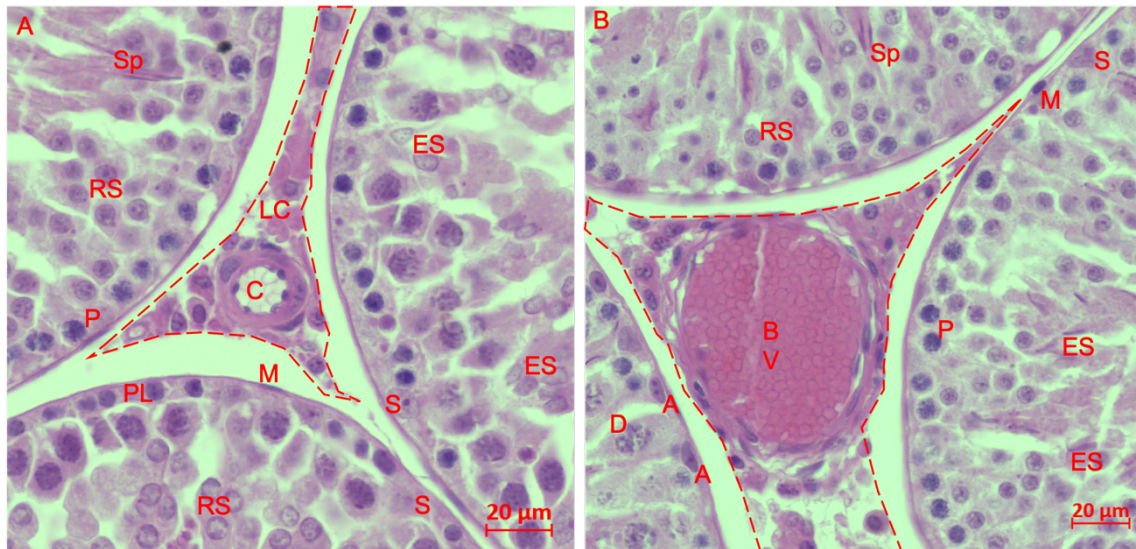


Figure 71: Generalised morphology of healthy rat testis with focus on interstitial cell populations. A: adult Leydig cell populations surrounding a capillary. B: adult Leydig cells lying in close association to a larger blood vessel containing red blood cells. Scale bar represents 20µm. C = capillary; BV = blood vessel; LC = Leydig Cell; S = Sertoli cell; M = Peritubular Myoid Cell; A= type A spermatogonia; P = Pachytene spermatocyte; PL = Preleptene Spermatocyte; D = Diplotene spermatocyte; RS = Round Spermatid; ES = Elongating Spermatid; Sp = mature Spermatozoa.

Morphological analysis of treated tissues

Silica dioxide treated animals (NM202)

Analysis of tissue from animals treated with silica dioxide - NM202 - at low, medium and high doses revealed no obvious morphological changes compared to control tissue. The layout of the testis was well structured, with seminiferous tubules at various stages of the seminiferous epithelium cycle, and the polyhedral collections of Leydig cells and other interstitial contents appeared normal (Fig. 72).

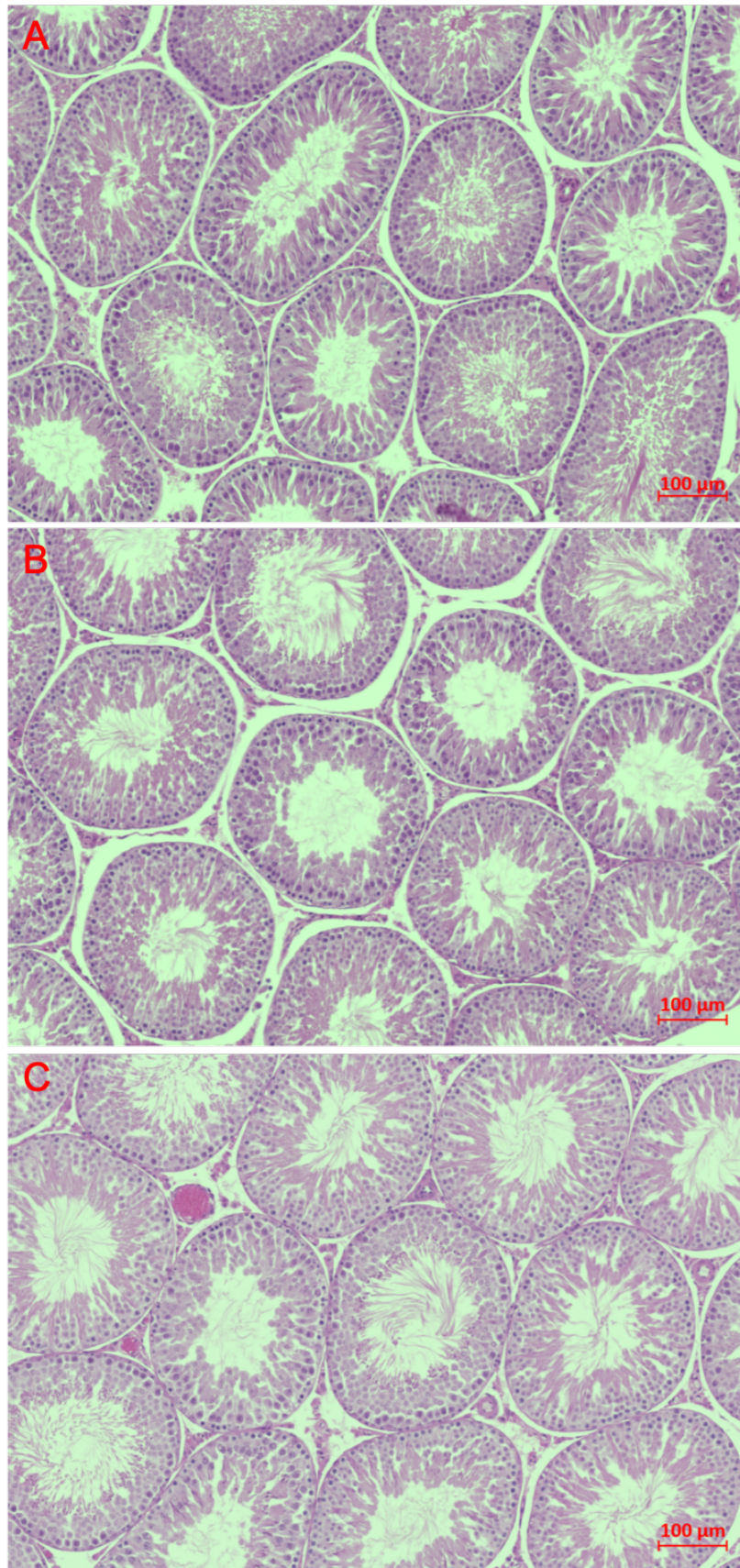


Figure 72: Generalised morphology of rat testis from animals treated with NM202 silica dioxide. Morphology appears unaltered when compared to control, indicating no major structural disturbances to the testis of these animal following treatment at any dose level. A) NM202 low dose; B) NM202 medium dose; C) NM202 high dose. Scale bar represents 100µm.

Silver treated animals (NM-300)

Animals treated with NM-300 silver showed focal areas of generalised dysmorphism across the testicular sections. Examination of these areas revealed the presence of generalised disorganisation within tubule germ cells, with partial degeneration/atrophy of germ cells being visible (Fig. 73). In many tubules, this was accompanied by the presence of pyknotic nuclei which are very dark in appearance and indicate the cell is undergoing apoptosis (Fig. 73).

In some tubules, there was a complete loss of lumen and general tubular architecture present (Fig. 74). In places, this was accompanied by an accumulation of disorganised cells out with the tubules themselves. Although it was not possible to undertake examination and further testing to prove the presence of immune cell infiltration, these interstitial changes did appear similar to those seen with inflammation (Fig. 75). This effect was exclusively within the interstitium, and not observed within the tubules.

In a few stage IX and X tubules, mature step 19 spermatids could be seen at the basement membrane of the tubule (Fig. 76). Retention of step 19 spermatids is recognised as a sensitive marker of toxicity within stage XI and X tubules. Within a few distinct tubules, appearance of much larger cells which could be developing multinucleated giant cells was noted (Fig. 77).

In tubules which maintained a more structured architecture, exfoliation of germ cells into the central lumen (considered a sensitive indicator of spermatogenic disturbance) was a widespread observation (Fig. 74). In mature rats there are normally very few sloughed cells, therefore this is considered a sensitive indicator of spermatogenic disturbance in the testis (Creasy et al., 2012).

It is important to note that where tubules appeared to be normal, organisation of germ cells was unaffected, and tubules from stage I-XIV were present, including stage VIII tubules at spermiation and stage XIV tubules with active meiosis underway. This is further supported by the observation from one animal where epididymal tissue was present on the slide, ducts appeared healthy and contained mature spermatozoa.

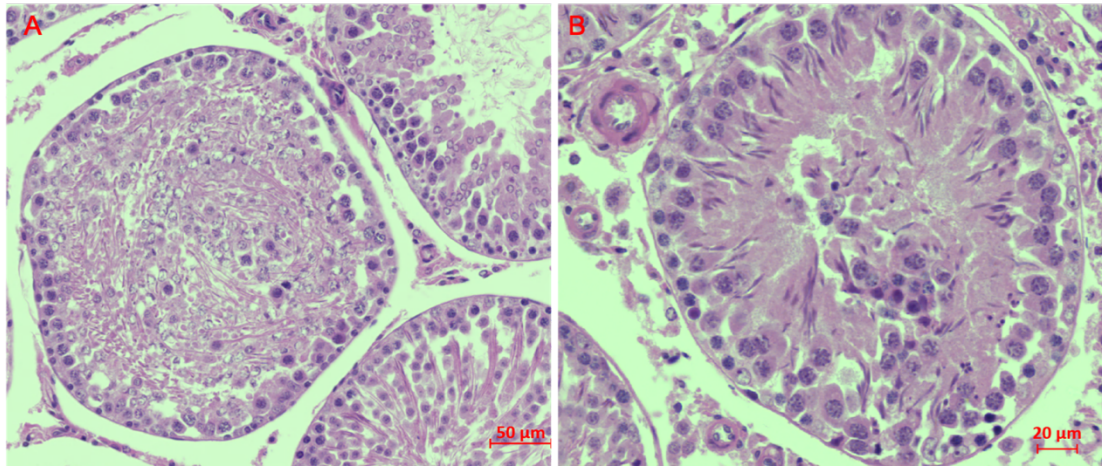


Figure 73: Image captured from an animal treated with NM-300 silver nanoparticles. A) generalised loss of tubular architecture in some tubules and maintenance of normal architecture in others (left- and right-hand side of image). Within this image, round spermatids appear to be degenerating, as illustrated by their patchy appearance. B) presence of pyknotic nuclei (very dark cells where chromatin in the nucleus is condensed and undergoing apoptosis). Scale bar represents 50 μ m in A, and 20 μ m in B.

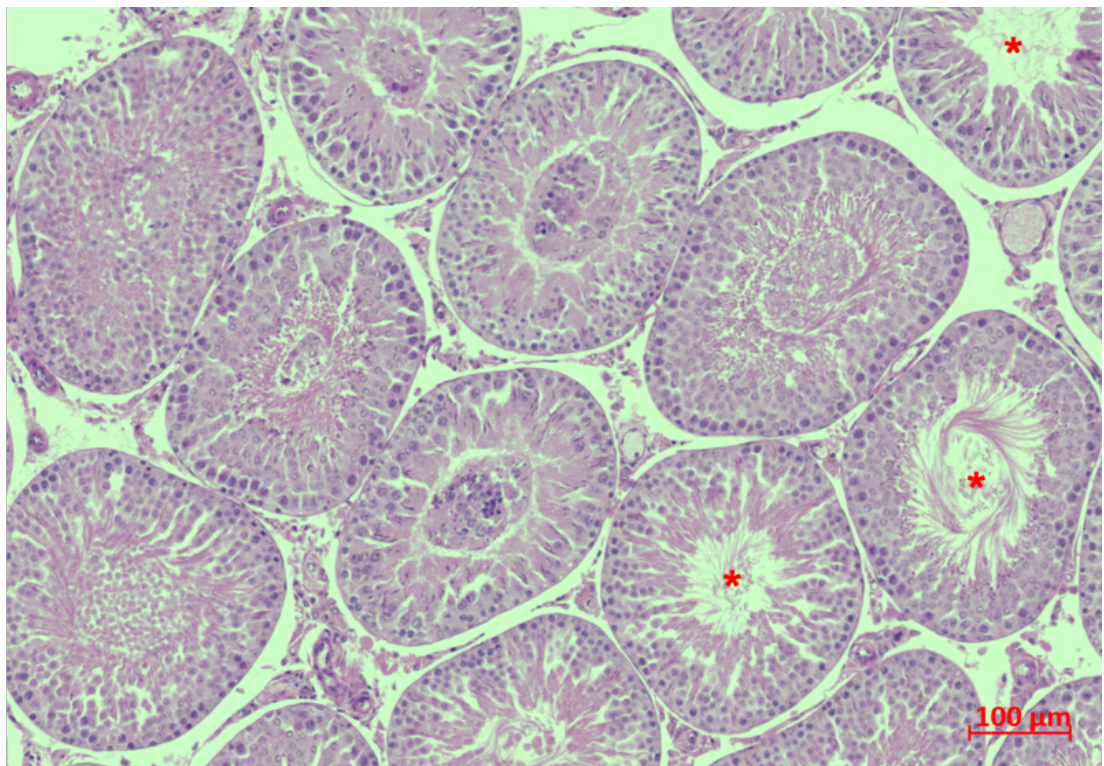


Figure 74: Image captured from an animal treated with NM-300, illustrating area of focal dysmorphism in tubules, alongside tubules which appear to be healthy and showing normal germ cell populations and architecture (red asterisks). Scale bar represents 100 μ m.

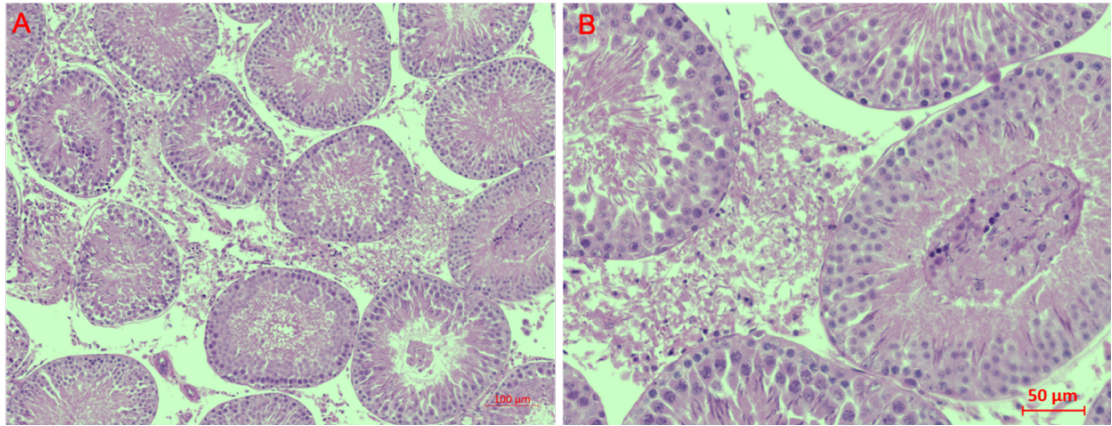


Figure 75: Image captured from an animal treated with NM-300 silver nanoparticles, illustrating generalised loss of tubular architecture accompanied by inflammation within the interstitium. Image B offers a higher magnification view on both tubule and interstitium contents. Scale bar represents 100µm in A, and 50µm in B.

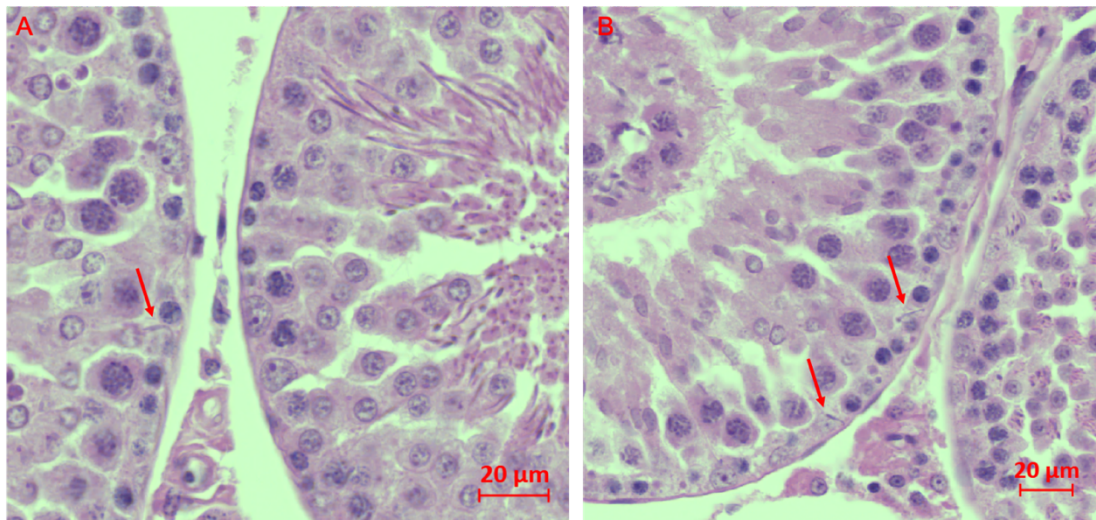


Figure 76: Images captured from an animal treated with NM-300 silver nanoparticles, showing retention of mature step 19 spermatids in stage IX (A) and X (B) tubules (red arrows). Retention of mature spermatids after spermiation at stage VIII is a sensitive indicator of toxicity. Scale bar represents 20µm.

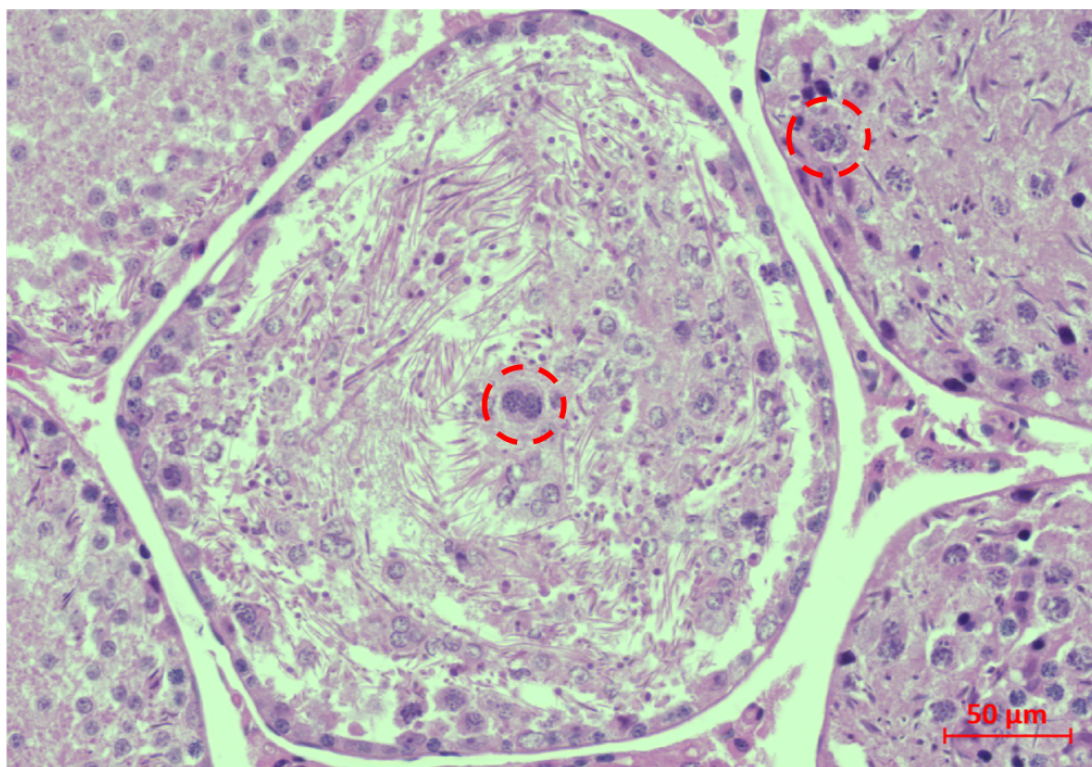


Figure 77: Images from an animal treated with NM-300 silver nanoparticles, showing what could be development of multinucleated giant cells within morphologically degenerative tubules (red circles). Scale bar represents 50 μ m.

Silver treated animals (AgNO₃)

As with NM-300 treated animals, those exposed to AgNO₃ silver showed focal areas of generalised dysmorphism across testicular sections, including a complete loss of lumen and general tubular architecture and presence of pyknotic nuclei (Fig. 78). The dysmorphism seen within AgNO₃ exposed animals was on the whole more widespread than in those exposed to NM-300 or Nano Amor, morphologically abnormal tubules often being much higher in number than those that were normal in appearance.

Evidence of hyperplasia within Leydig cells of the tubular interstitium was found in some animals and was associated almost exclusively with tubules which had completely lost their internal architecture (Fig. 79). It manifested in a focal manner, as a collection of Leydig cells with a diameter equal to or more than half of an average seminiferous tubule, with no compression of the surrounding tissue, as per the agreed criteria for Leydig Cell hyperplasia from the Society of Toxicologic Pathologists (McConnell et al., 1992).

There was no evidence of mature spermatid retention in stage IX and X tubules or giant cell formation. However, a very few distinct tubules were noted to be almost completely lacking in germ cells, being lined primarily by Sertoli cells (fig. 80). Again, in those tubules which maintained a more structured architecture, exfoliation of germ cells into the central lumen was a widespread observation Fig. 81). Where tubules appeared to be normal, organisation of germ cells was unaffected, and tubules from stage I-XIV were present.

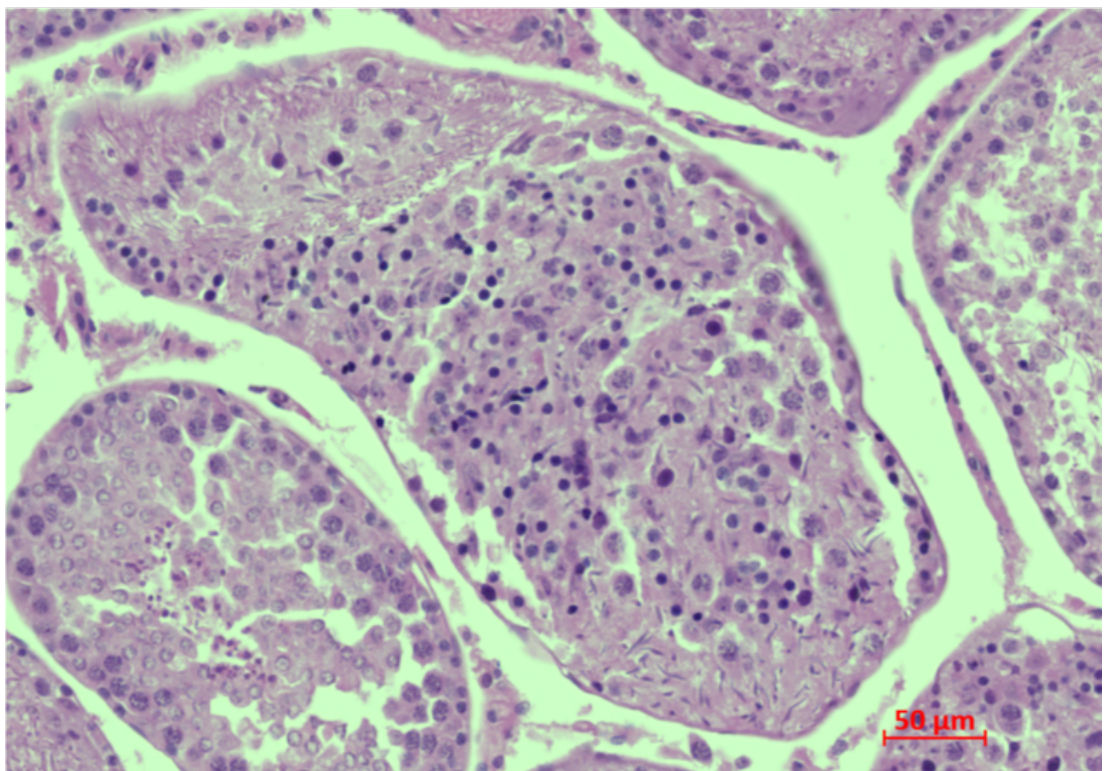


Figure 78: Representative image of focal dysmorphism within AgNO_3 exposed animal. Generalised loss of cellular architecture, and presence of pyknotic nuclei (very dark cells where chromatin in the nucleus is condensed and undergoing apoptosis) may be seen throughout the tubule. Scale bar represents 50 μm .

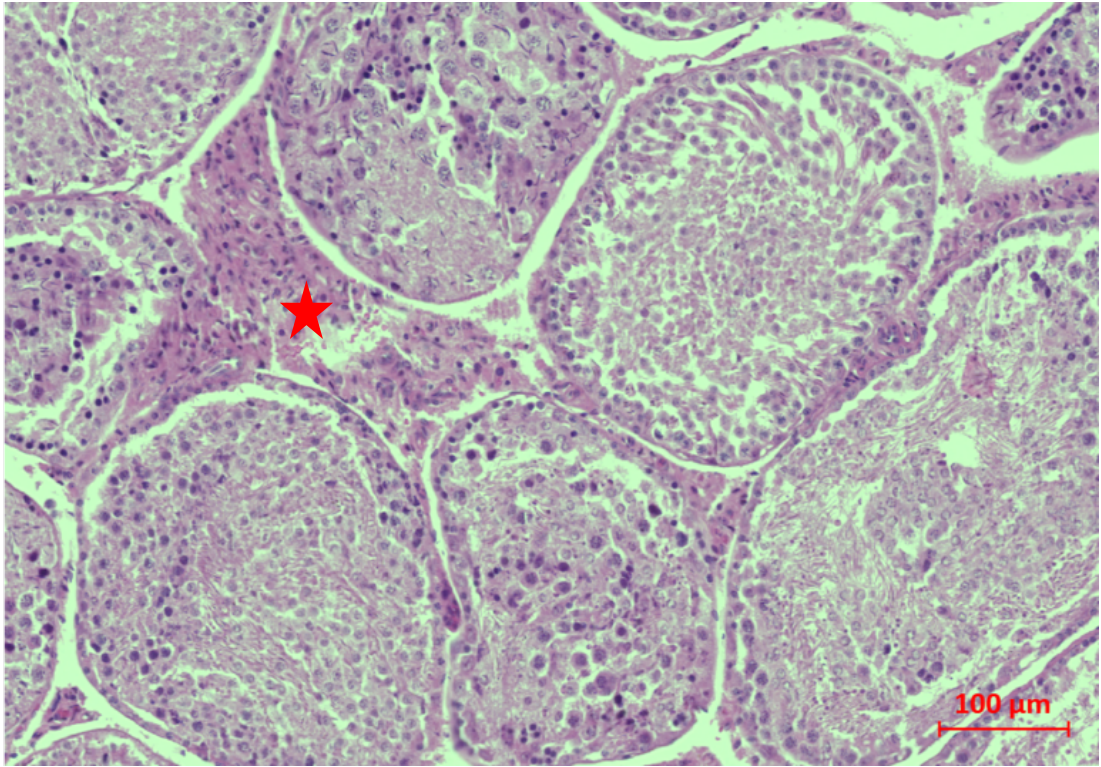


Figure 79: Representative image of morphologically abnormal tubules with LC hyperplasia in the interstitium within AgNO₃ exposed animal (highlighted with star). Scale bar represents 100µm.

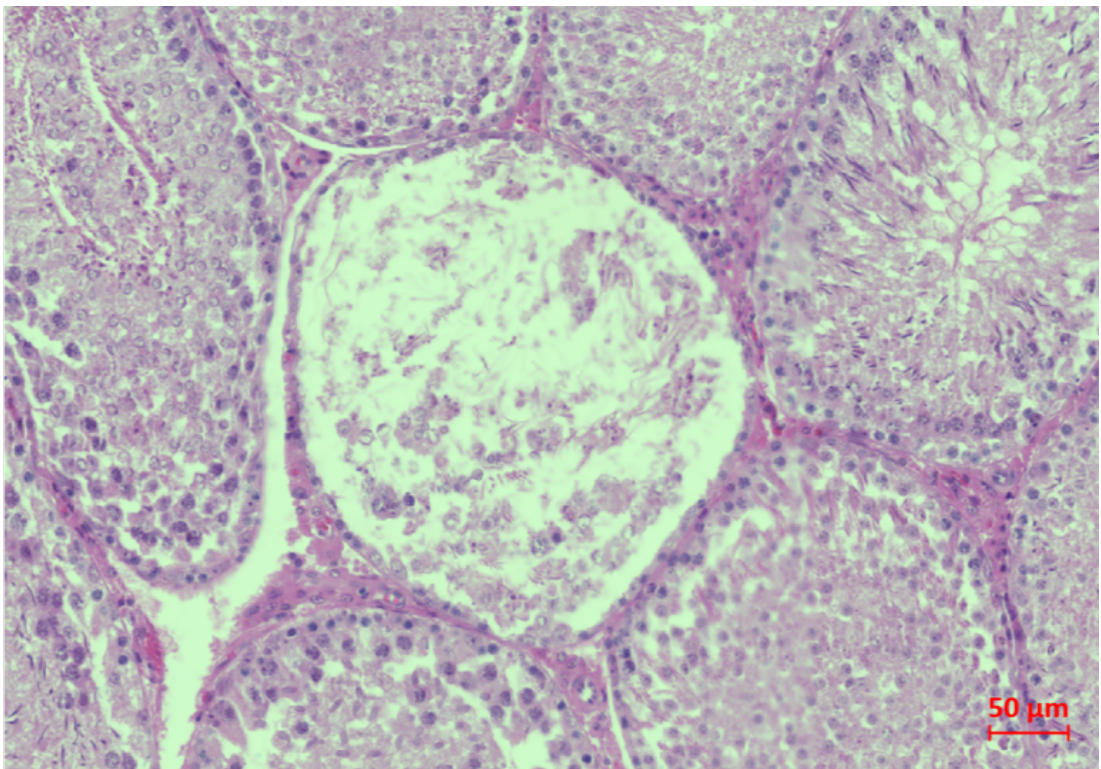


Figure 80: Tubule observed within AgNO₃ exposed animal containing almost no germ cells, those cells left lining the basement membrane are primarily sertoli cells. Scale bar represents 50µm.

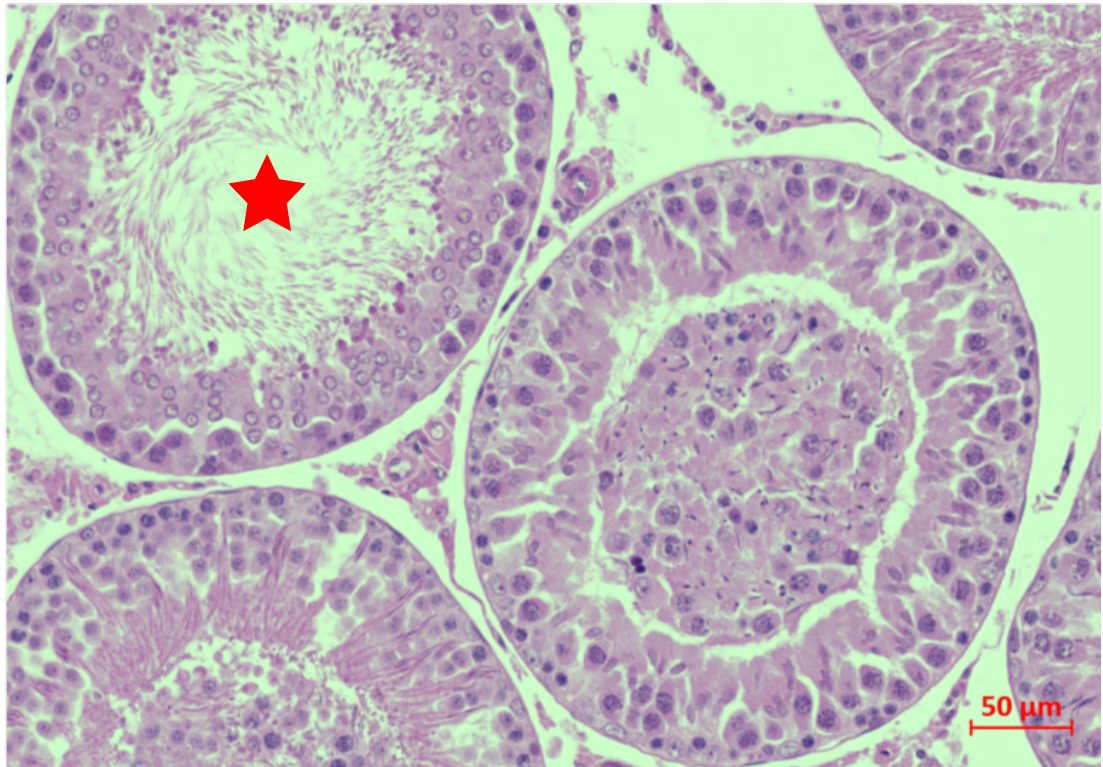


Figure 81: Sloughing of tubular contents into central lumen, observed within AgNO₃ exposed animals. As with other silver treatments, morphologically disturbed tubules were often seen alongside tubules which were healthy in appearance (star). Scale bar represents 50μm.

Silver treated animals (Nano Amor)

As with the other silver treatments, animals exposed to Nano Amor silver showed focal areas of generalised dysmorphism across testicular sections. This included complete loss of lumen, general tubular architecture and presence of pyknotic nuclei (Fig. 82). Additionally, some tubules appeared to show dilation of the lumen, having a thinner epithelium containing a normal compliment of germ cells (Fig. 83). Tubules at stages IX to XIV generally have a much smaller lumen volume than those at earlier stages of the seminiferous epithelial cycle (Wing and Christensen, 1982). As the tubules within Fig. 83 are stages X and XII (left and right-hand side of image B) it is therefore unlikely for the lumen to be so large under normal circumstances.

Focal areas of dysmorphism were more widespread than in NM-300 exposed animals; as with AgNO₃ treated animals there were some slides where morphologically abnormal tissue was more prevalent than normal. There was no evidence of inflammation or Leydig cell hyperplasia within the interstitium, mature spermatid retention in stage IX and X tubules or giant cell formation. However, potential arrest of germ cell development was noted, namely by the presence of step 12 spermatids within a stage

XIV tubule in which step 14 spermatids would be expected (Fig. 84). In those tubules which maintained a more structured architecture, exfoliation of germ cells into the central lumen was a widespread observation (Fig. 83). Where tubules appeared to be normal, organisation of germ cells was unaffected, and tubules from stage I-XIV were present.

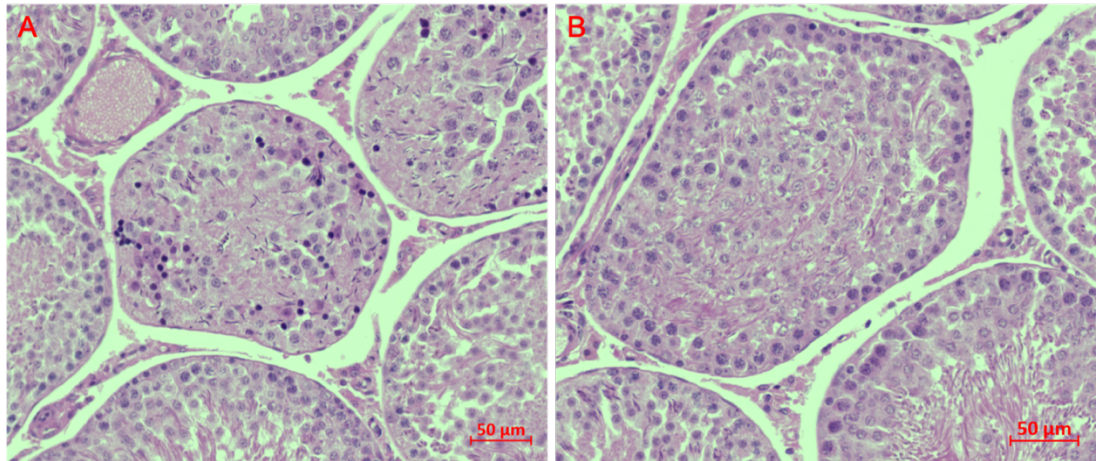


Figure 82: Representative images of focal dysmorphism within Nano Amor exposed animal. Generalised loss of cellular architecture is observable within both tubules, these again being situated adjacent to other tubules which appear to be morphologically normal. A number of pyknotic nuclei, identifiable as very dark cells where chromatin in the nucleus is condensed and undergoing apoptosis are also visible on image A. Scale bar represents 50µm.

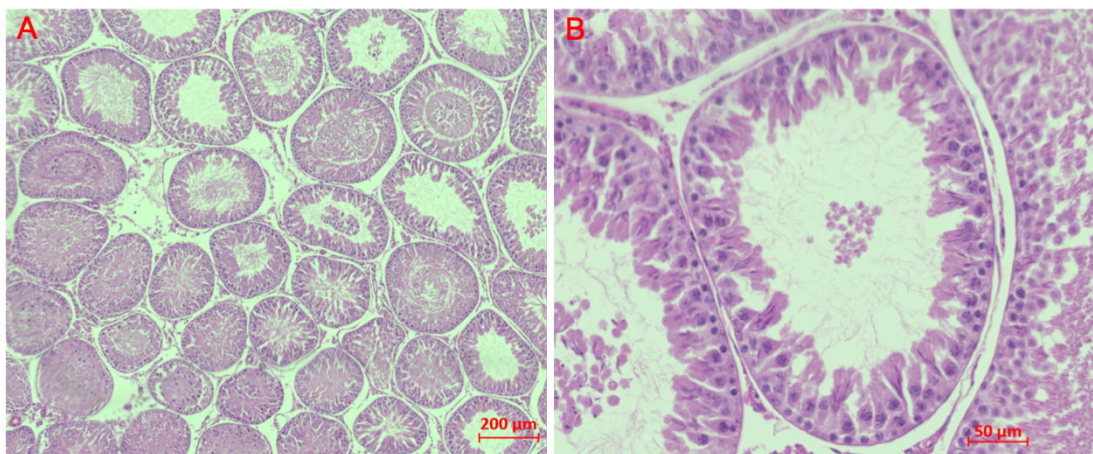


Figure 83: Representative images of Nano Amor treated animals where dilated tubule lumens are present. A) tubules with dilated lumen may be seen alongside other tubules with sloughing of germ cell contents into the central lumen, or complete obliteration of lumen and tubular architecture. B) Higher magnification view of tubules at multiple stages with dilated lumens, and some moderate sloughing of germ cell contents. Germ cell layer around the tubule edge appears to be otherwise normal in appearance. Scale bar represents 200µm in image A, and 50µm in image B.

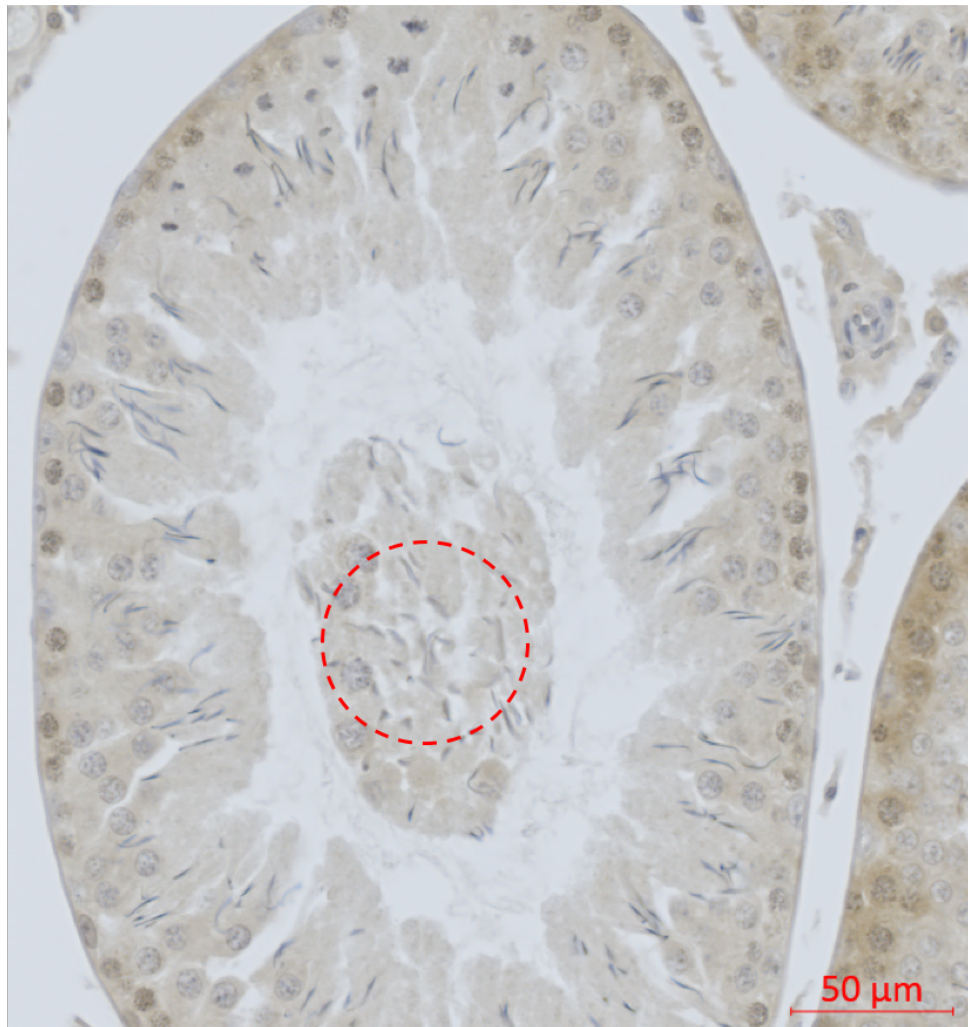


Figure 84: Tubule observed within animal exposed to Nano Amor which appeared to have retention of step 11 elongating spermatids within the lumen of a stage XIV tubule. Tubule stage is identifiable by presence of meiotic bodies in top portion. Step 11 spermatids may be seen in the very centre of the cells sloughed into the lumen, identifiable as being step 11 due to the protrusion of the acrosome and apex at a sharp angle from the caudal portion of the nucleus. Spermatids seen from step 13 to 15 have a more hooked appearance, with highly condensed (appearing darker) and pointed nuclei.

Immunohistochemical analysis of tissues

To further elucidate possible mechanisms of toxicity following silver nanoparticle exposure, immunohistochemical staining of tubules was undertaken. Preliminary work was carried out to optimise the IHC protocol for AR, LH-R, 3 β -HSD, Dazl StaR and RP-1 antibodies. Following this initial work, a full complement of IHC on all animals was completed for LH-R, AR, Dazl and StaR.

3 β -HSD

Staining for 3 β -HSD was carried out as part of a preliminary screen of antibodies to give an indication of overall tissue health and steroidogenic capability. Moderate 3 β -HSD expression was found within all interstitial cells (Leydig cells) of all sections sampled (red

arrows, Fig. 85), indicating that this enzyme was present within all tissues and unaffected by any silver NP treatment.

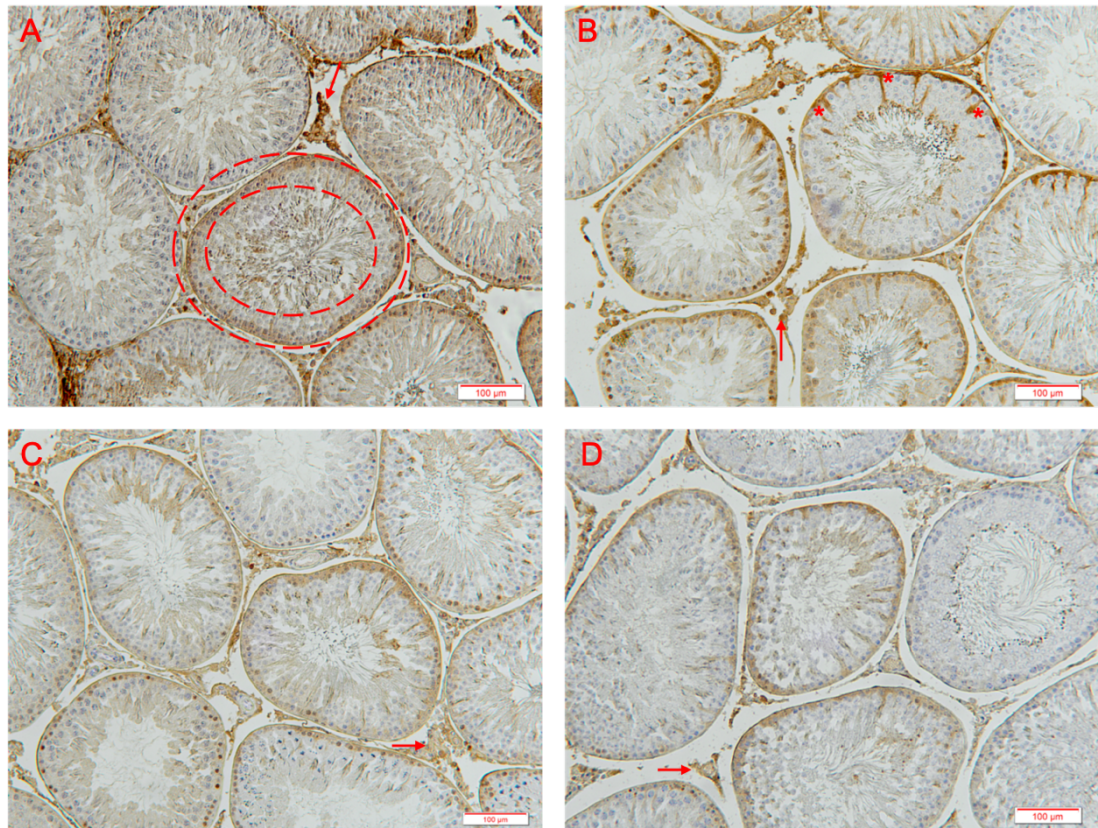


Figure 85: Representative images of immunohistochemical staining for 3b-HSD within rat testis tissue following 3-4 minutes of DAB exposure and colorimetric reaction development. Scale bar represents 100µm. A) AgNO₃, B) Nano Amor, C) NM-300 & D) Control. Red arrows show staining localised to Leydig cells in the interstitium. Asterisks and red circle denote background staining within AgNO₃ and Nano Amor treated animals that was visible throughout many of the sections analysed.

There was some inconsistency in DAB staining across the samples and some suspected overstaining occurring in AgNO₃ and NM-300 treated animals, as evidenced by the spill-over staining onto the peritubular myoid cells, basement membrane and Sertoli cells within these tissue sections (red circle Fig. 85 outlines tubule with basal lamina staining on an AgNO₃ animal slide, and asterisks denote Sertoli cell staining on animal treated with Nano Amor). On the whole this gave the slides the appearance of being more intensely stained on these treatments than on NM-300 treated or control animal. In reality however, this disparity in staining was present across all slides analysed and was likely due to a sub-optimal primary antibody. For this reason, and because StaR worked

well one optimised, 3 β -HSD staining was not undertaken in a full complement of tissue samples.

LH-R

Examination of the IHC for Luteinising hormone receptor showed a clear Leydig cell specific staining, localised to the Leydig cell cytoplasm, within the interstitium surrounding seminiferous tubules across both control and treated animals (red arrows, Fig. 86). Following optimisation of the protocol, background or non-specific staining was minimised. It appeared that as staining intensity was relatively comparable at a moderate to intense level across control, Nano Amor and AgNO₃ treated animals, with a slightly lesser intensity being present on NM-300 treated samples. It is worth noting that staining for LH-R was unaffected in those animals exhibiting focal areas of dysmorphism within testicular tissue. As such, although morphologically abnormal, it may be considered that LH receptors within the Leydig cells surrounding affected tubules were unaffected (Fig. 87).

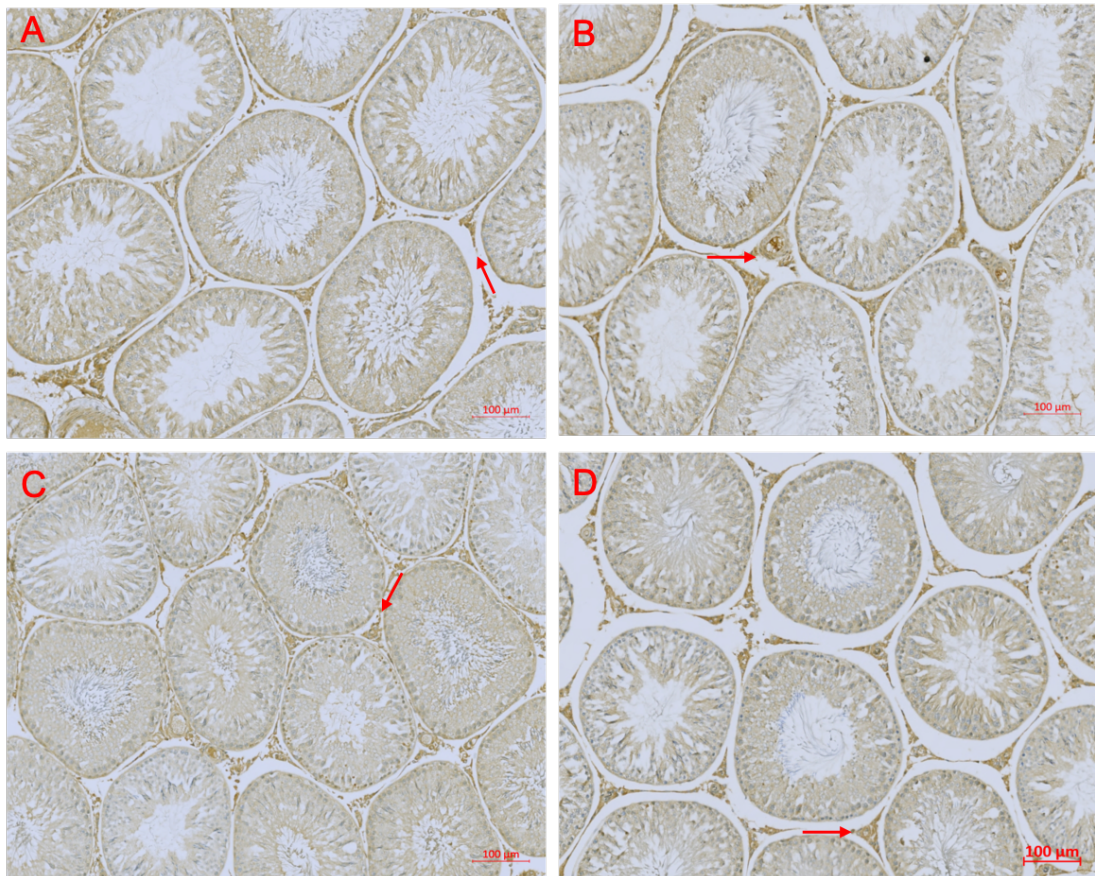


Figure 86: Representative images of immunohistochemical staining for LH-R within rat testis tissue following 3-4 minutes of DAB exposure and colorimetric reaction development. Scale bar represents 100 μ m. A) AgNO₃, B) Nano Amor, C) NM-300 & D) Control. Red arrows show staining localised to Leydig cells located within in the interstitium between seminiferous tubules.

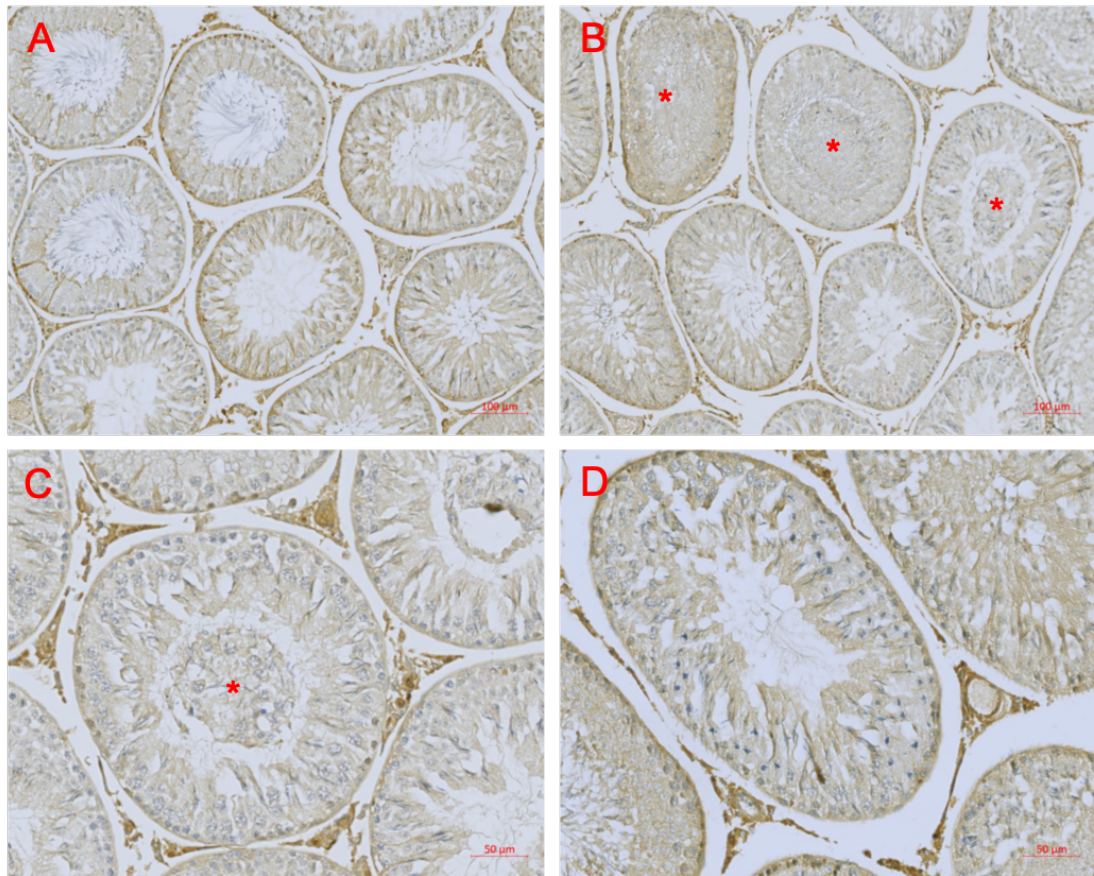


Figure 87: Representative images of LH-R stained tissue captured from animals treated with nanoparticulate silver. Images A & B are both captured from one animal (I44) treated with Nano Amor; A shows a healthy area of testicular tissue; image B shows an area of focal dysmorphism within the same slide (red asterisks). Image C shows a stage XII seminiferous tubule from an NM-300 treated animal which clearly has degenerating tissue sloughing into the lumen, while image D shows meiotic divisions of a stage XIV tubule an animal treated with AgNO_3 . It is notable that LH-R specific staining is comparable and localised to the Leydig cells of all images. Scale bar represents $100\mu\text{m}$ in A & B, and $50\mu\text{m}$ in C & D.

AR

Representative images of the completed immunohistochemical stains for androgen receptor are depicted within Fig. 88. It was possible to identify some intense Sertoli cell specific staining in areas of the control tissue, with moderate to intense nuclear staining being seen in silver treated animals, indicating that androgen receptors were present on the cells and able to bind substrate.

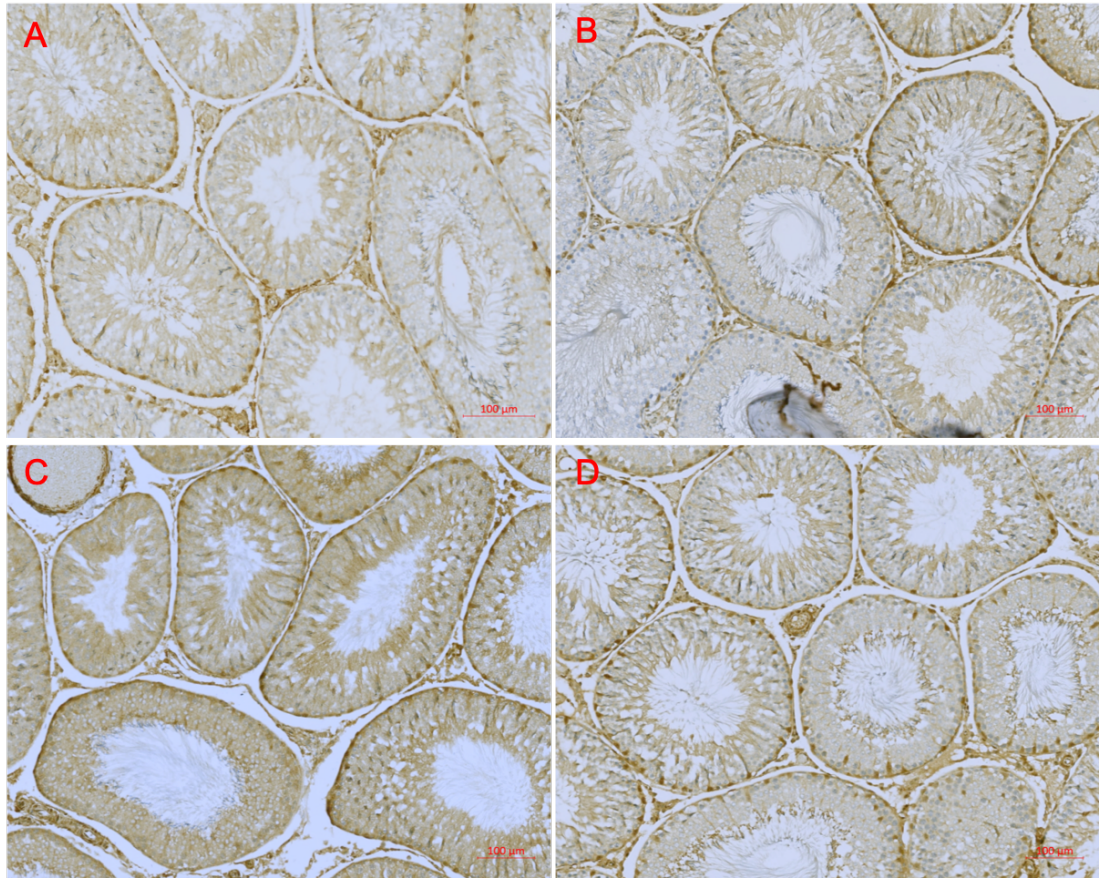


Figure 88: Representative images of immunohistochemical staining for AR within rat testis tissue following 9 minutes of DAB exposure and colorimetric reaction development. AR positive Sertoli cell staining is visible as 'rings' of dots around the outer edge of the seminiferous epithelium in tubules. Some clear background staining of tissue is visible within the NM-300 treated image, this was present through many of the slides. Scale bar represents 100μm. A) AgNO₃, B) Nano Amor, C) NM-300 & D) Control.

Closer observation of the androgen receptor immunostaining shows that although patchy, the AR stain clearly extends not only to Sertoli cells, but also Leydig and peritubular myoid cells, a finding reported widely in the literature (Fig. 89). Again, similar staining was present in both control and silver treated animals despite high background stain on some slides.

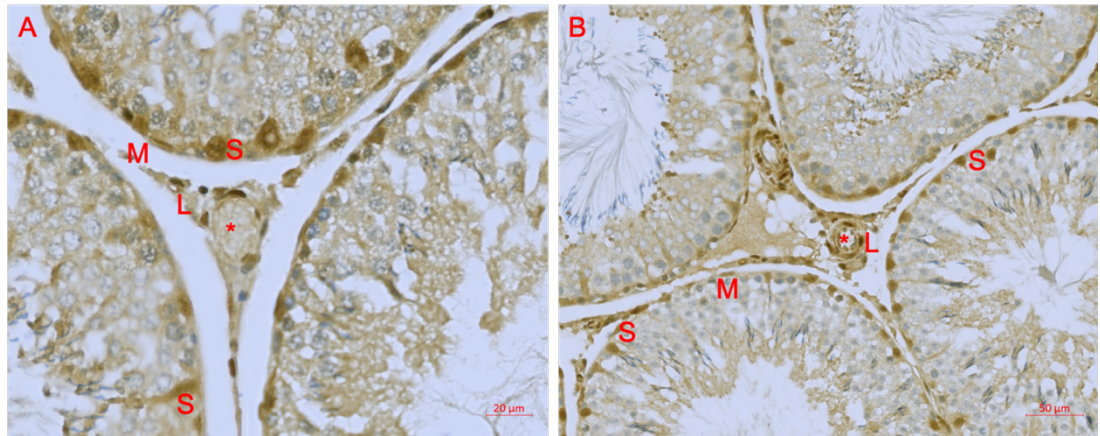


Figure 89: A close magnification view of tissue from an A) Silver treated (Nano Amor, I43) and b) control (J20) animal following IHC staining for AR. Both show clear staining for AR across a number of cell types. M = peritubular myoid cell (long and thin in shape), S = Sertoli cell (round in shape), L = Leydig cell, Asterisk = capillary. Scale bars show 20 μ m (LHS) and 50 μ m (RHS) respectively.

Figure 90 shows in further detail the Sertoli cell staining on an NM-300 treated animal. Image A shows clear moderate to intense AR staining in a healthy stage VIII tubule, where Sertoli cell nuclei are seen to migrate from the basement membrane toward the central lumen to support release of mature spermatids. Image B depicts moderate stain for AR within an unhealthy stage VII tubule, found in another area of the same slide. In this image, sloughing of cells into the central lumen of the tubule can clearly be seen, along with clear positive staining of Sertoli cells for AR (at the basement membrane pre-migration).

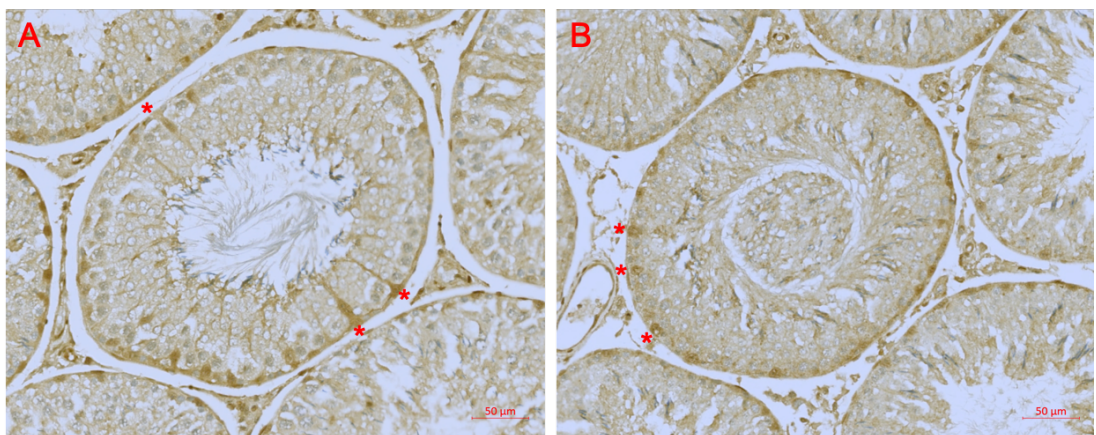


Figure 90: Two images captured from an animal treated with NM-300, following IHC staining for AR. Image A shows a healthy stage VIII tubule, with red asterisks indicating staining of Sertoli cells that have migrated toward the central lumen to assist in release of mature spermatids at Spermiation. Image B shows an unhealthy stage VII tubule within a focal area of dysmorphism from the same slide. Despite the tubule appearing to be abnormal, it is notable that positive AR staining is still present around the basement membrane of the tubule (red asterisks).

StaR

A clear cytoplasmic stain for StaR was present within Leydig cell populations of all animals, both treated and control, although some issues were encountered with background staining (visible within A & C, Fig. 91). It appeared that this staining was of a higher intensity in silver treated animals than in control.

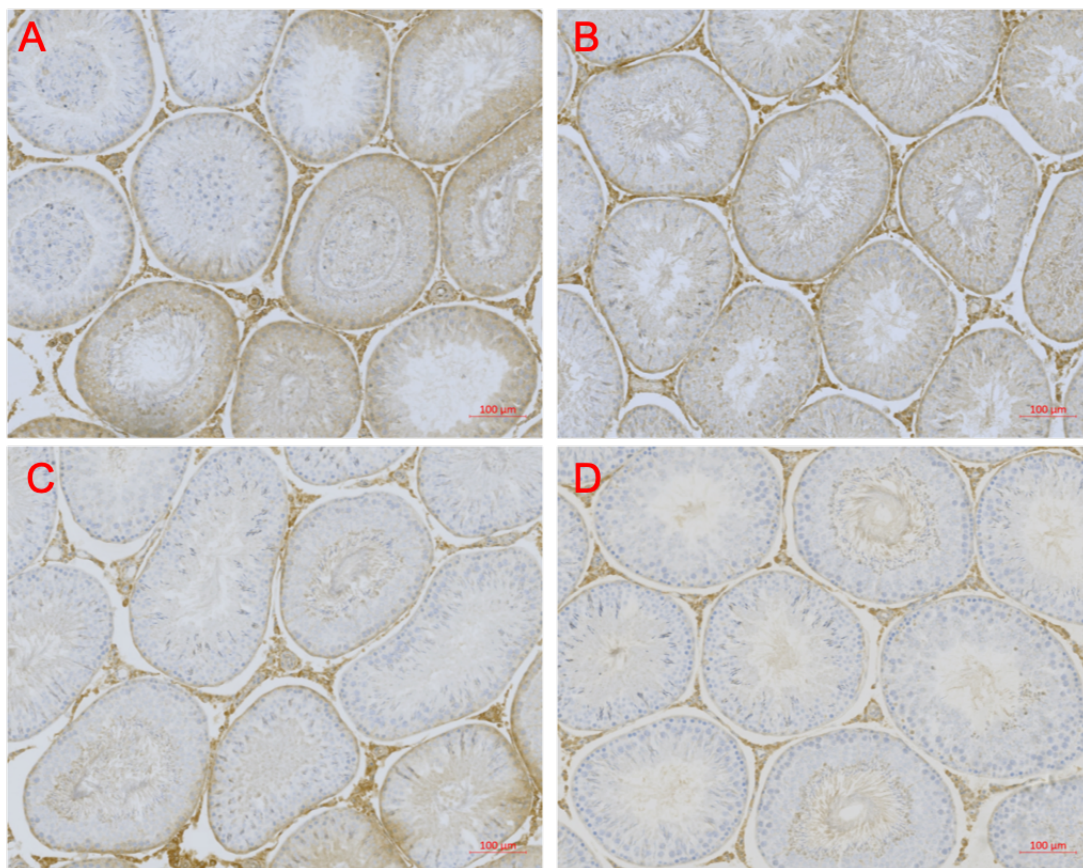


Figure 91: Representative images of immunohistochemical staining for StaR within rat testis tissue following 3 minutes of DAB exposure and colorimetric reaction development. Scale bar represents 100µm. A) AgNO₃, B) Nano Amor, C) NM-300 & D) Control. Areas of generalised over-staining are visible on the right-hand side of image A and the bottom right corner of image C.

Within AgNO₃ treated tissues, StaR appeared to stain the acrosomal cap region of developing round spermatids in some areas (Fig. 92). This may be due to a generalised over-staining in areas of the tissue sections, but nonetheless is worth noting.

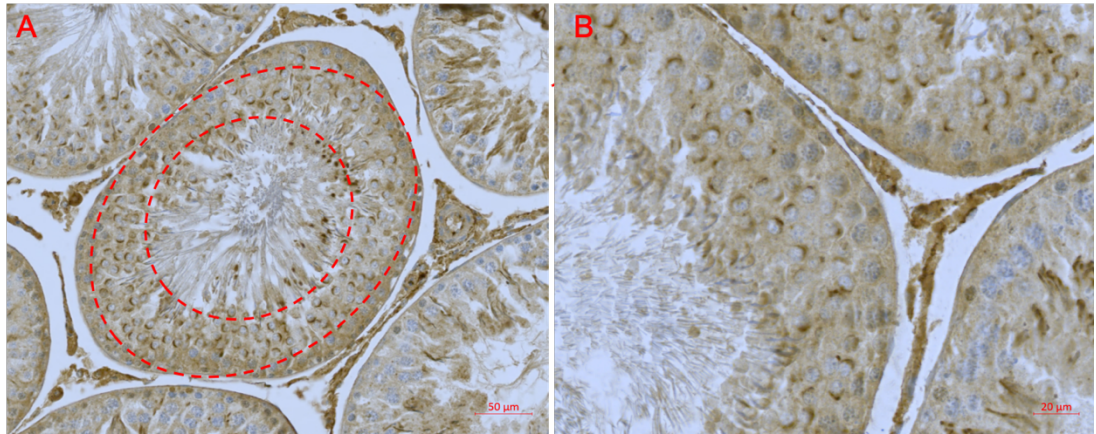


Figure 92: Two images captured from animals treated with AgNO₃, and following IHC staining for StaR. Image A shows a healthy stage V-VI tubule, with red dashes outlining the area in which round spermatid acrosomal caps have been stained (animal K52). Image B shows a closer view of this staining in a different animal (K54). Scale bar represents 50µm on A and 20µm on B.

Dazl

Dazl protein stains with varied localisation and intensity dependent on the stage of spermatogenesis at which each tubule is captured, and therefore staining is not expected to be uniform across the whole tissue sample at the target cells of interest. As predicted, staining was not regular across the slide but was definitely positive. Figure 93 illustrates this variation in staining intensity, which appeared to be linked to tubule stage, with tubules around Spermiation (stage VIII) showing the most intense staining. Moderate intensity staining was observed in tubules pre- or post- spermiation (stages VI-VII or IX-XI), and no stain was seen in either early (stage I-V) or late (stage XIII-XIV) tubules.

To check whether the areas of focal dysmorphism present in treated animals altered Dazl staining, slides with clear disruption present were examined for Dazl stain to see whether it was altered in any way from tubules with a normal morphological appearance. Despite very clear morphological changes being present, Dazl stain on affected and unaffected tubules was comparable (Fig. 94). Dazl provided differential staining according to stage that was not changed within tubules with major morphological disruption. As a result, Dazl stain intensity can be used to support tubule stage identification for further stereological analysis. and was used to assist with staging and stereological analysis of tubules.

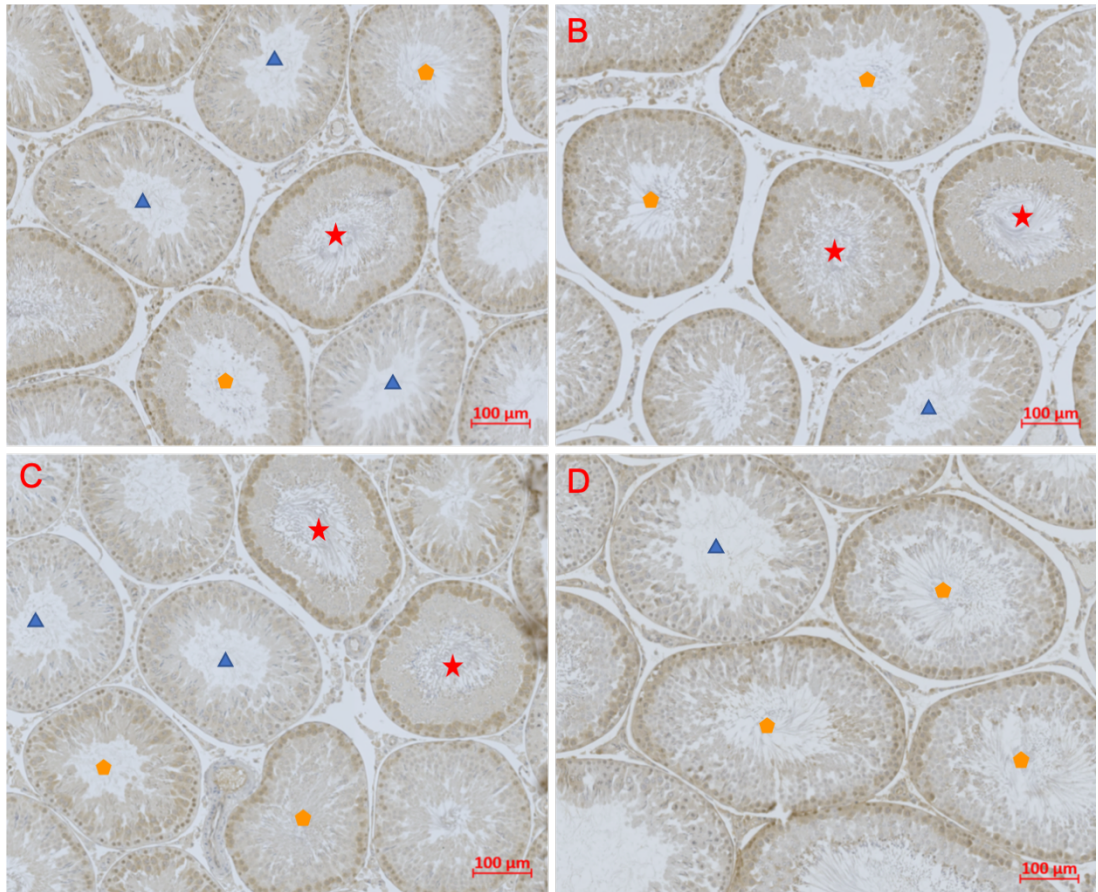


Figure 93: Representative images of immunohistochemical staining for Dazl within rat testis tissue following 3.5 minutes of DAB exposure and colorimetric reaction development. Scale bar represents 100µm. Tubules are marked to indicate i) heavily stained tubules undergoing Spermiation at stage VII (red stars), ii) moderately stained tubules pre- or post- Spermiation at stages VI-VII or IX-XI (orange pentagons), or iii) unstained tubules at the start (stage I-V) or end (stage XII-IV) of the cycle of the seminiferous epithelium (blue triangles). A) AgNO₃, B) Nano Amor, C) NM-300 & D) Control.

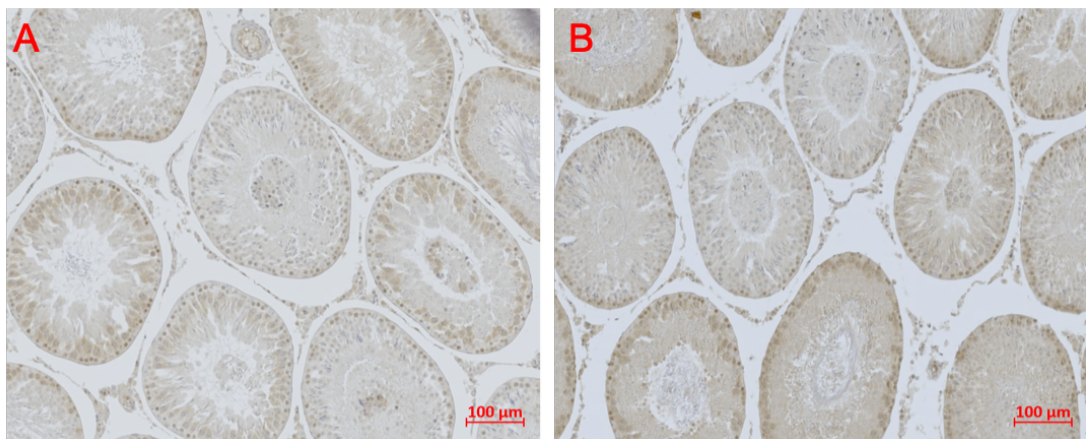


Figure 94: Two images captured from animals treated with NM-300 (left) AgNO₃ (right) following IHC staining for Dazl Scale bar represents 100µm. Both images show clear focal areas of dysmorphism within testicular sections. It is notable that Dazl staining was not affected by morphological disturbance, unless germ cells were completely absent from tubules. Thus, it was possible to use Dazl staining to assist with staging of damaged tubules.

RP-1

A granulocyte specific antibody (RP-1) was used to explore the possibility of neutrophil involvement around damaged tubules. Figure 95 shows representative images of tissues stained for RP-1 containing clear areas of morphological dysmorphism. Although some of the sloughed cell populations stained intensely with haematoxylin, no DAB positive stain for RP-1 was present.

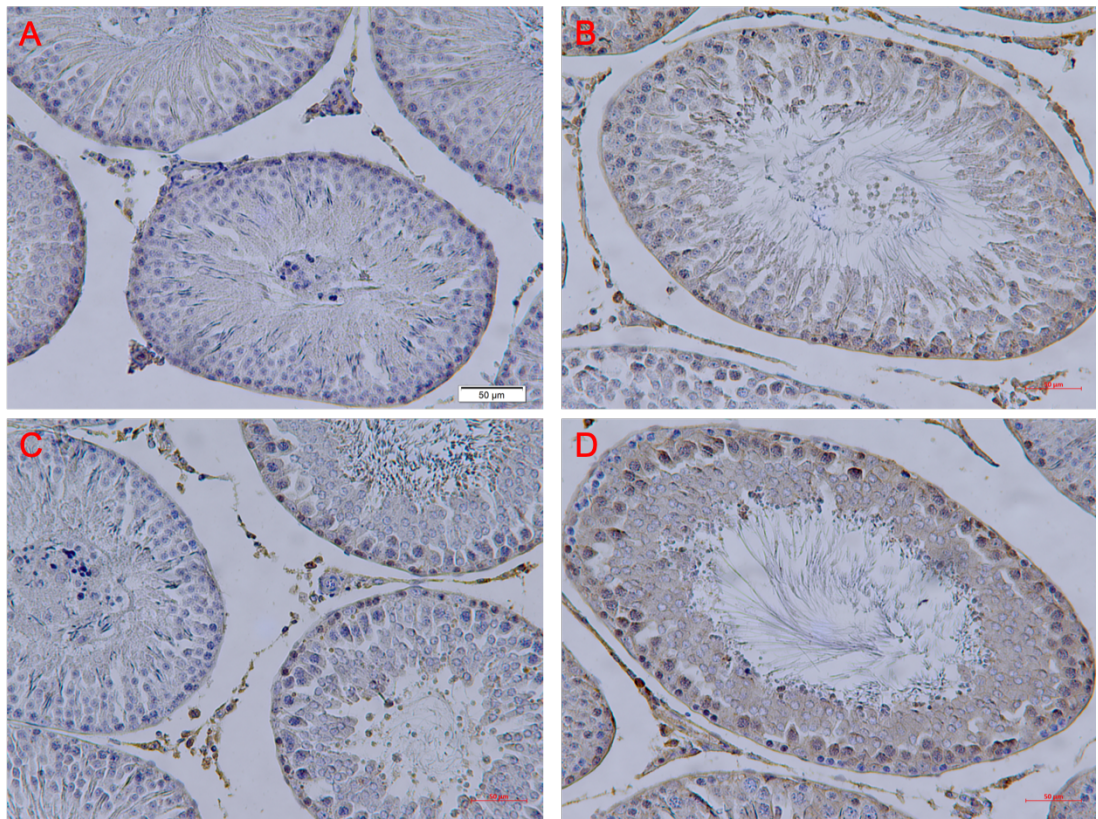


Figure 95: Representative images of immunohistochemical staining for RP-1 within rat testis tissue following 3.5 minutes of DAB exposure and colorimetric reaction development. Scale bar represents 50μm. Images were selected as they show tubules which include cells either sloughed into the central lumen, or cells which have invaded that tubular lumen which would stain positively for RP-1 should they be neutrophils. A) AgNO₃, B) Nano Amor, C) NM-300 & D) Control.

Stereological analysis of tubules I: semi-quantitative analysis

Count data

Within the first analysis of samples, a total of 2,054 tubules were measured for diameter and germ cell thickness. Of these, 915 were control, 193 were NM-300 treated, 186 were AgNO₃ treated, 203 were Nano Amor treated, 178 were low dose NM202, 199 were medium dose NM202 and 180 were high dose NM202.

Comparison of Control data

Control data fell into two animal groups: group G animal were sacrificed at 29 days on completion of dosing, and group J at 85 days following a 6-week wash-out period. As the control animals were sacrificed at more than one time, initial analysis was completed to check that tubule diameter and germ cell layer thickness measurements were comparable across the two sets of results. An unpaired t-test on the data revealed that there was a significant difference between the two groups for tubule diameter P-value of <0.0001**** (confidence interval 34.41 to 47.25) but not for germ cell layer thickness (P-value 0.9291) (Fig. 96).

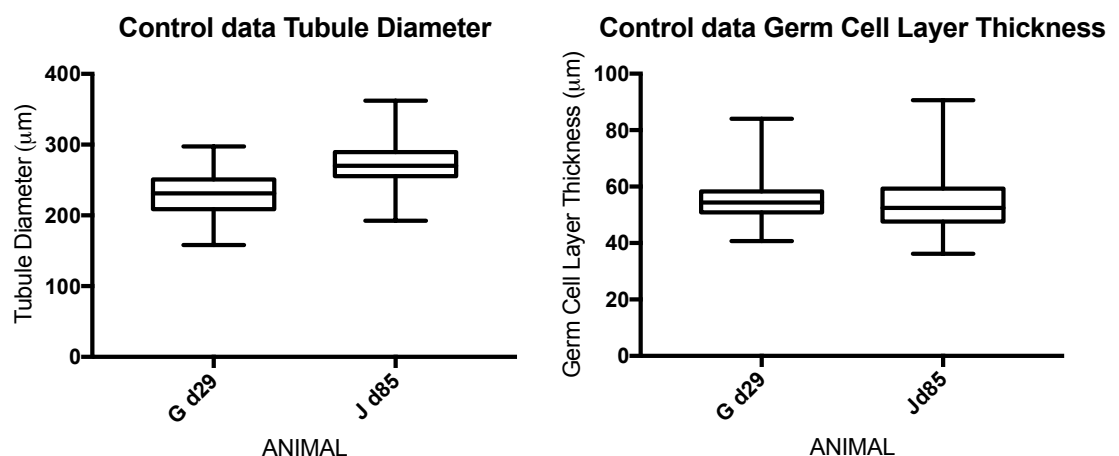


Figure 96: Summary of Control datasets for animals sacrificed at day 29 and day 85. Left: Tubule Diameter. Right: Germ Cell Layer Thickness. A significant difference was found between the two groups for tubule diameter ($P < 0.0001$) but not germ cell layer thickness.

As a result, the two control datasets were separated for further comparison to the treatment data. For completeness of analysis all animals were compared to both control groups.

Initial Measurement results: tubule diameter

Results of the data collected on tubule diameter for each animal was graphed per treatment (Fig. 97). Initial appraisal of the graphed data did not reveal any particular patterns of measured diameter with treatment, other than the observation that control animals sacrificed at day 85 (control J) appeared to have a higher tubule diameter than those sacrificed at day 29 (control G), and that NM202 medium dose had apparently low variability in the tubule diameters recorded, with its box and whiskers plot showing a short box and minimal whiskers (Fig. 97 plot h).

A one-way ANOVA on all treatments compared to d29 control (group G) showed no significant difference ($p=0.4880$). A subsequent Dunnett's multiple comparisons test showed statistical difference between control G and Nano Amor ($p=0.0481^*$), control G and NM202 Low dose ($p=0.0361^*$), and control G and NM202 High dose ($p=0.0381^*$).

The finding of significant differences in tubule diameter between control animals sacrificed at the same timepoint to those treated with NM202 (day 29) suggests that there may be some effect of treatment here. However, this finding was not replicated in NM202 treated animals receiving medium or high doses, and it is possible to speculate that this is the case because on the whole measurements collected from animals treated with NM202 medium held far less variation than the other treatments (Fig. 97 plot h).

There were no significant differences in tubule diameter between all treatments and controls (d29 control $p=0.5682$ and d85 $p=0.8112$).

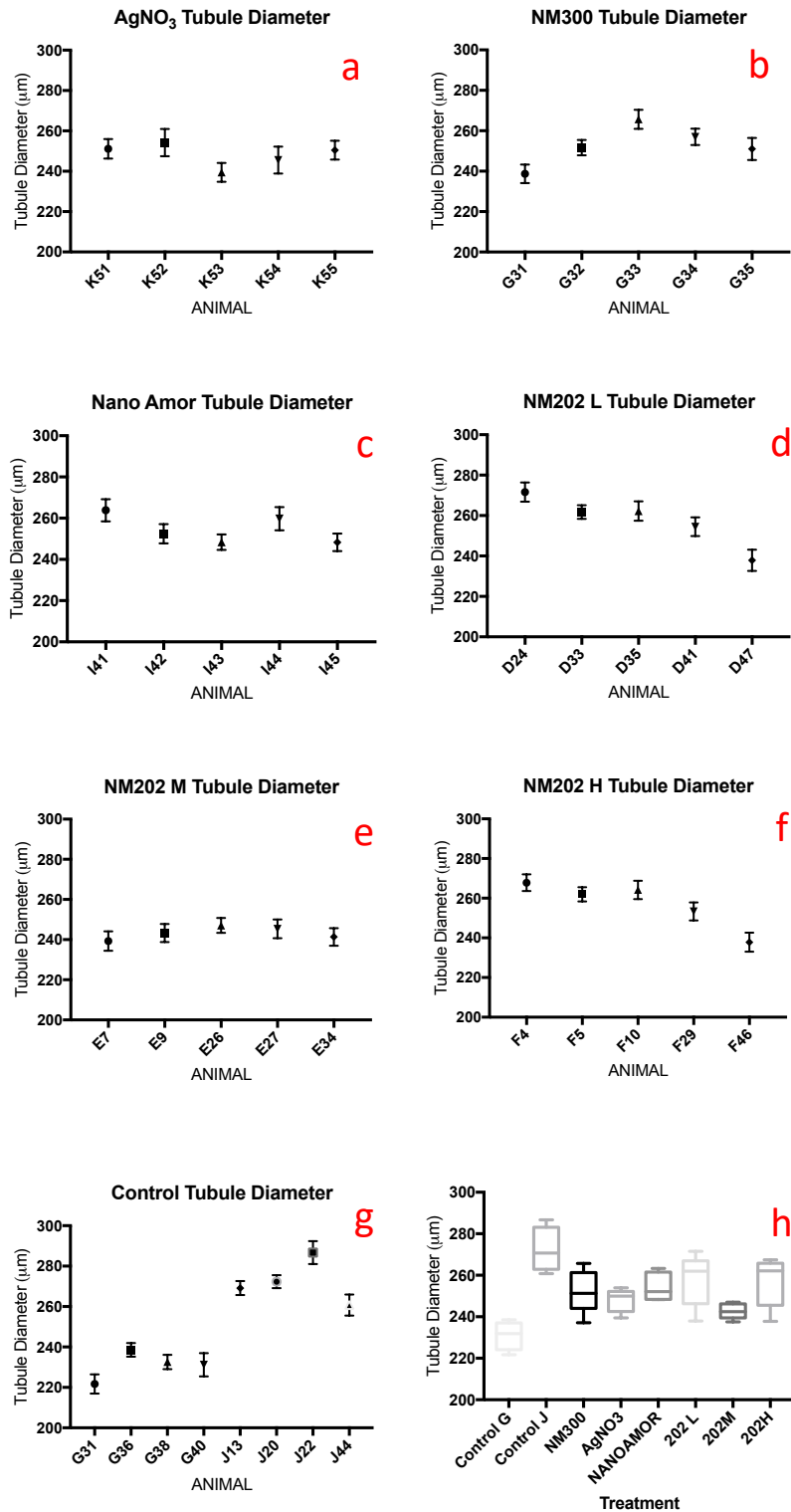


Figure 97: Tubule Diameter measurements (+/- SEM) from all treatments. Each treatment had 5 animals except control for which there were 8 animals. From Top to bottom: a) AgNO₃ (tubules measured n=186), b) NM-300 (tubules measured n=193), c) Nano Amor (tubules measured n=203), d) NM202 low dose (tubules measured n=178), e) NM202 medium dose (tubules measured n=199), f) NM202 high dose (tubules measured n=180), g) Control (tubules measured n=915), and h) all treatments compared to control shown as a box and whiskers plot illustrating minimum to maximum values and median for each group.

Initial measurement results: germ cell layer thickness

Results of the data collected on tubule diameter for each animal is presented in Fig. 98. The graphed data did not reveal any particular patterns of germ cell layer thickness according to treatment, other than the identification of a possible outlier in the observation that one animal (I44) treated with Nano Amor appeared to have unusually higher germ cell layer thickness measurements compared to other animals in this group.

There were no significant differences in tubule diameter between all treatments and controls (d29 control $p=0.5682$ and d85 $p=0.8112$). The lack of significance when comparing silver treated animals sacrificed to controls sacrificed at a similar timepoint (day 78 treated and day 85 control) shows that there was no change in tubule diameter compared to control at this timepoint and in these treatment groups.

As morphological and immunohistochemical analysis (undertaken concomitantly with the initial stereological analysis) had highlighted significant changes in tubule diameter, germ cell layer and central lumen structure, a second stereological analysis was undertaken to elucidate whether taking into account seminiferous epithelium stage influenced findings.

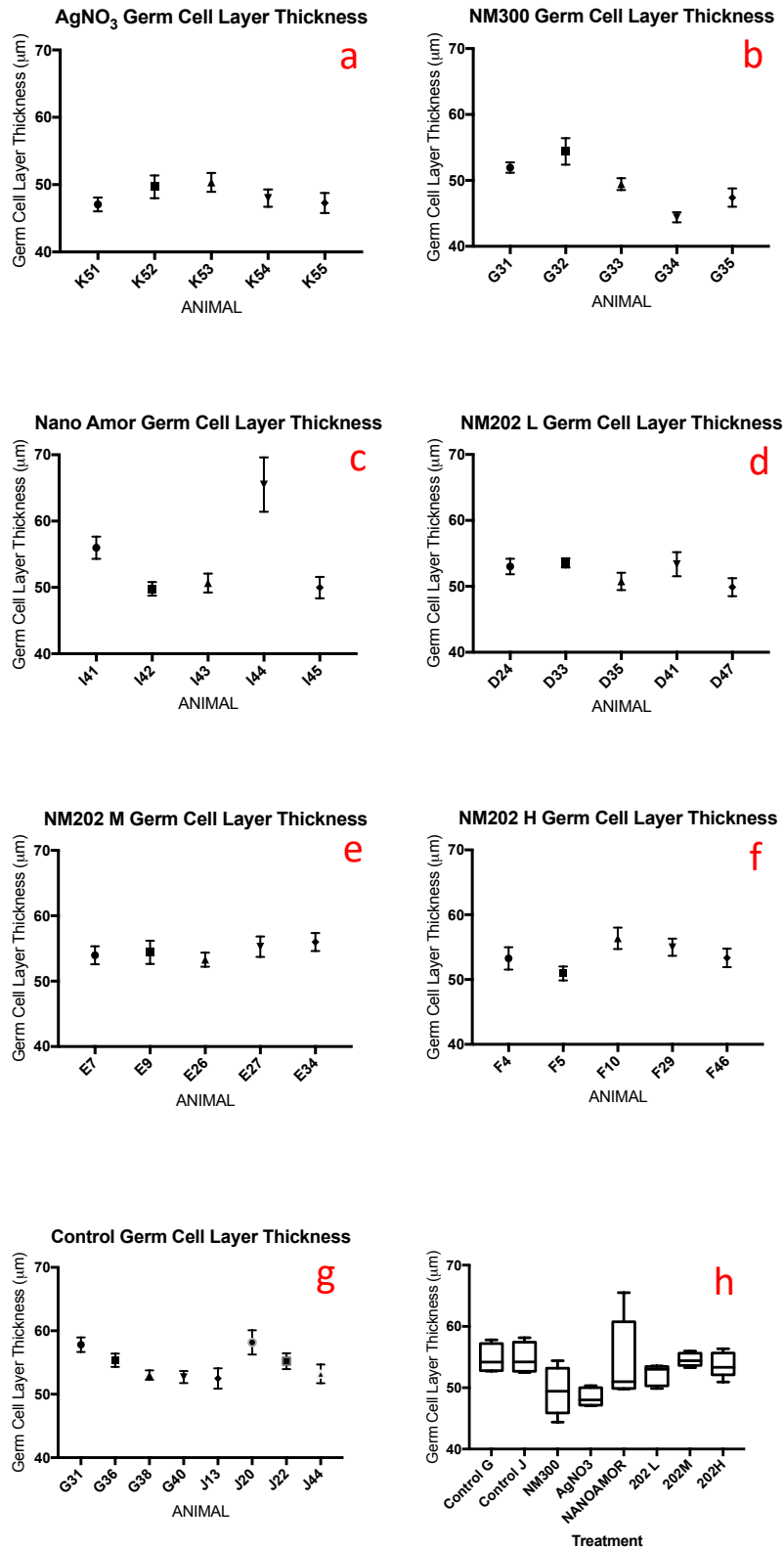


Figure 98: Germ Cell layer thickness measurements (+/- SEM) from all treatments. Each treatment had 5 animals except control for which there were 8 animals. From Top to bottom: a) AgNO₃ (tubules measured n=186), b) NM-300 (tubules measured n=193), c) Nano Amor (tubules measured n=203), d) NM202 low dose (tubules measured n=178), e) NM202 medium dose (tubules measured n=199), f) NM202 high dose (tubules measured n=180), g) Control (tubules measured n=915), and h) all treatments compared to control shown as a box and whiskers plot illustrating minimum to maximum values and median for each group.

Identification of Tubule Stage

Using the decision key adapted from Hess, representative photographs of tubules across the 14 stages of seminiferous epithelium in the rat were identified (Hess, 1990). Representative photographs of key stages identified in the cycle of the seminiferous epithelium of the rat (I-XIV), viewed in paraffin embedded sections were prepared (Fig. 99).

Stage I-IV

Stage I, II, III and IV tubules are almost impossible to differentiate in paraffin sections as staging is dependent on a clear view of the golgi apparatus in early round spermatids, something which it has been recognised is difficult to identify in paraffin sections (Hess, 1990). As a result, for this analysis, tubules were grouped into stages I-IV. Generally, tubules within this group contain both round and elongated spermatids, the elongated spermatids being late in appearance (step 15-17). Pachytene spermatocytes appear smaller in size than later stages, and populations of A, I and B type Spermatogonia are visible in places.

Stage V

In stage V tubules, clusters of late spermatid nuclei may be seen deep in the tubular epithelium close or adjacent to Sertoli cell nuclei. Most Spermatogonia present are type B rather than A or I.

Stage VI

In stage VI tubules, late spermatids are no longer at the epithelium adjacent to Sertoli cells but are instead moved closer to the central lumen and often seen in clusters.

Stage VII

When tubules reach stage VII, late spermatid nuclei line up around the luminal border, and large basophilic granules become visible around the nuclei. On the epithelial border of the tubule, B type Spermatogonia have been replaced by Prelepotene spermatocytes.

Stage VIII

To differentiate stage VII from VIII, two key observations were utilised: i) release of some spermatids into the lumen, ii) Sertoli nucleus orientated perpendicular to the epithelial border and extended toward the central lumen of the tubule.

Stage IX

Within stage IX tubules, mature spermatids are missing entirely from the luminal border, but perhaps a few step 19 spermatids still visible within the centre of the lumen. This gives the lumen an 'empty' appearance. Large residual bodies are present throughout the epithelium, and Leptotene spermatocytes are more prominent as a population than preleptotene.

Stage X

Stage X tubules are distinguishable from stage IX as the round spermatids present start to elongate at this point. Close inspection shows that the cap of the elongating spermatids deviates at a sharp angle to the nucleus, with a blunted appearance at the tip. Pachytene spermatocytes at this stage start to enlarge in size.

Stage XI

In stage XI tubules, the head cap of the elongating spermatid forms a much narrower tubular protrusion at an angle to the nucleus, and spermatids are present in distinctive bundles. Pachytene spermatocytes continue to appear enlarged and more granular in appearance.

Stage XII

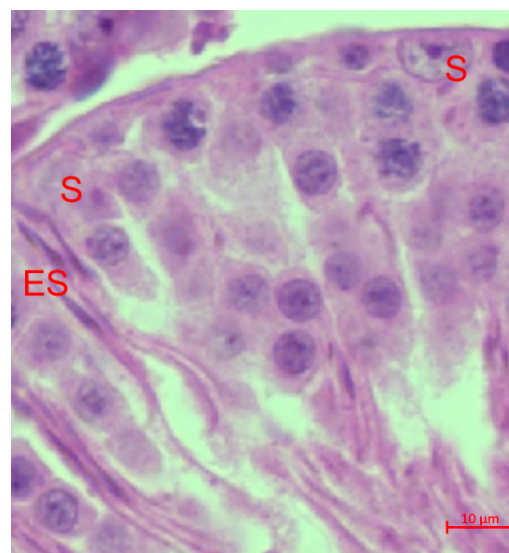
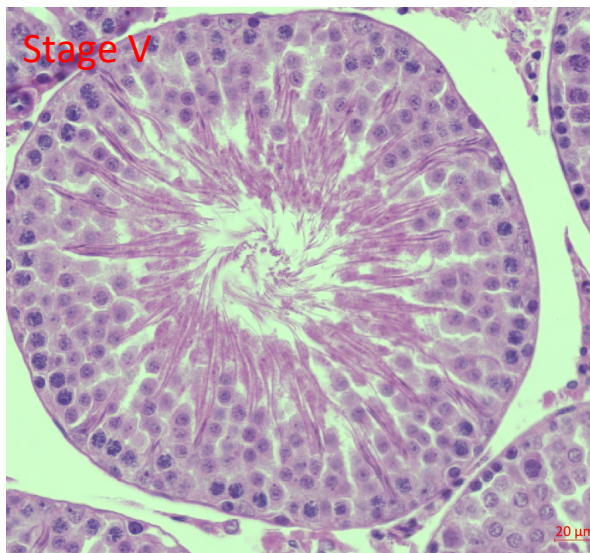
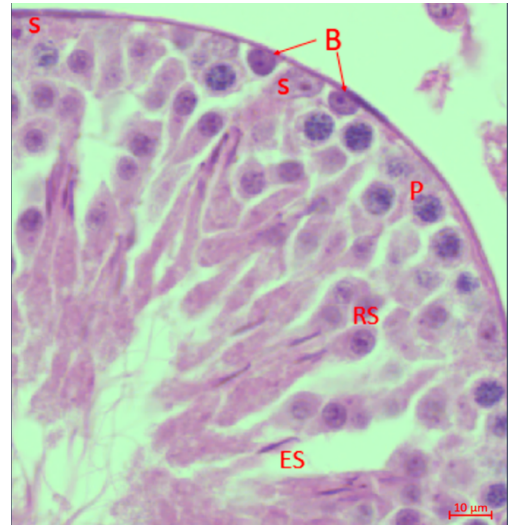
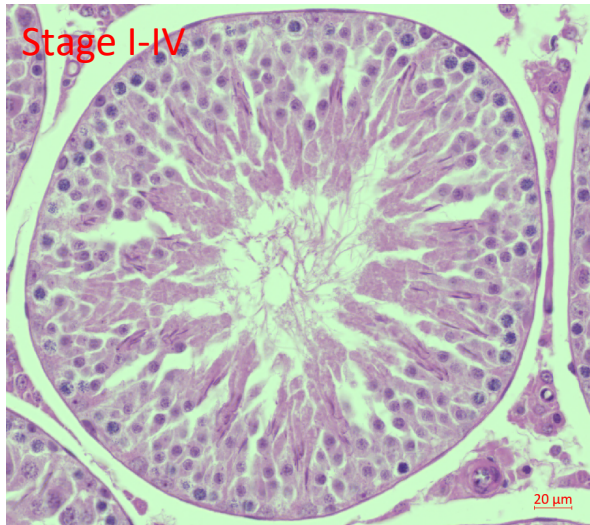
At stage XII, the tail of the elongating spermatid is longer, narrow and slightly curved. Both enlarged late Pachytene spermatocytes, and Diplotene spermatocytes are visible within the epithelium, alongside symmetrical round, dark Zygotene spermatocytes.

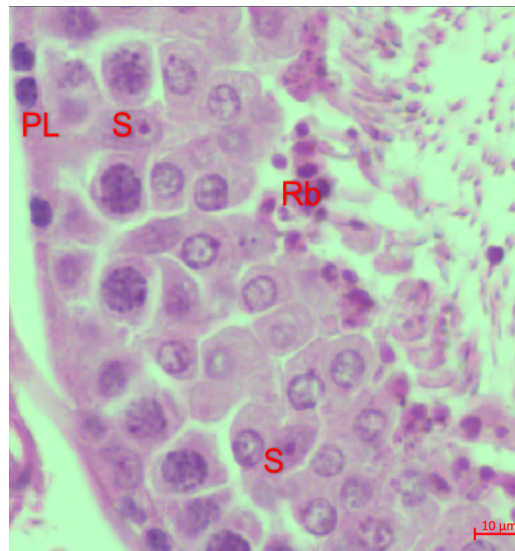
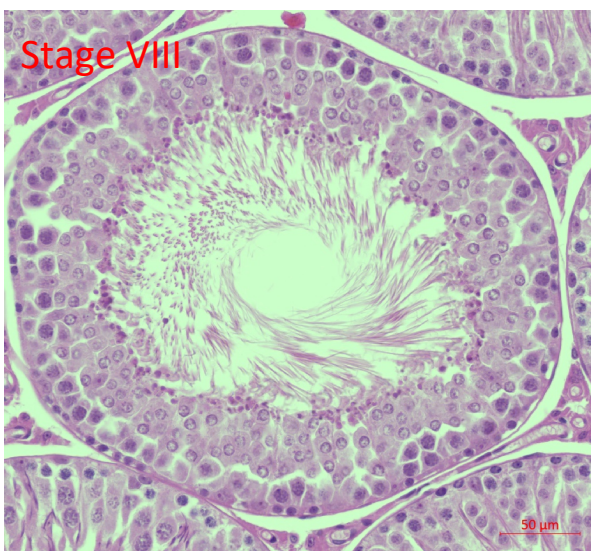
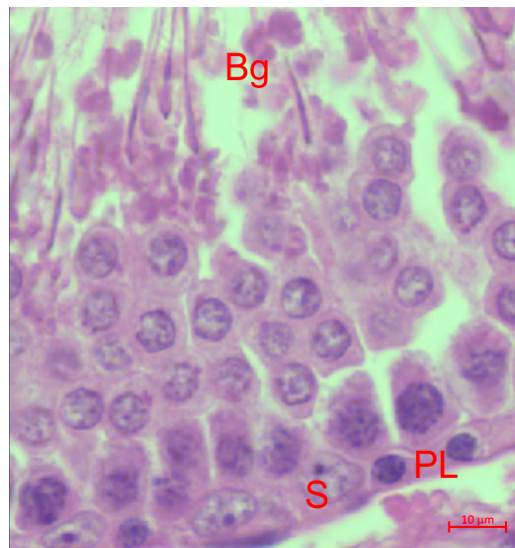
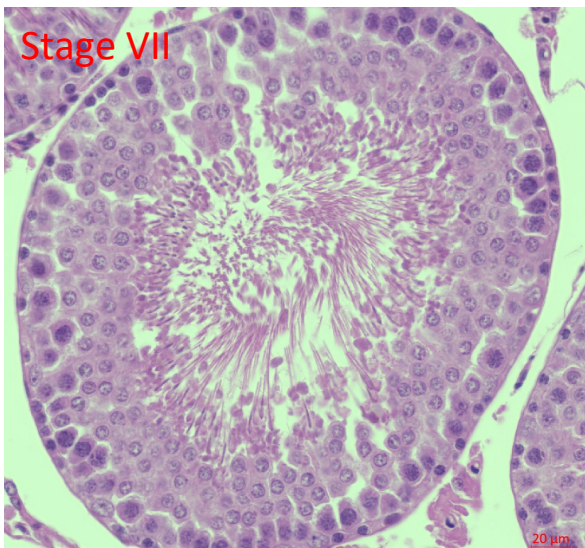
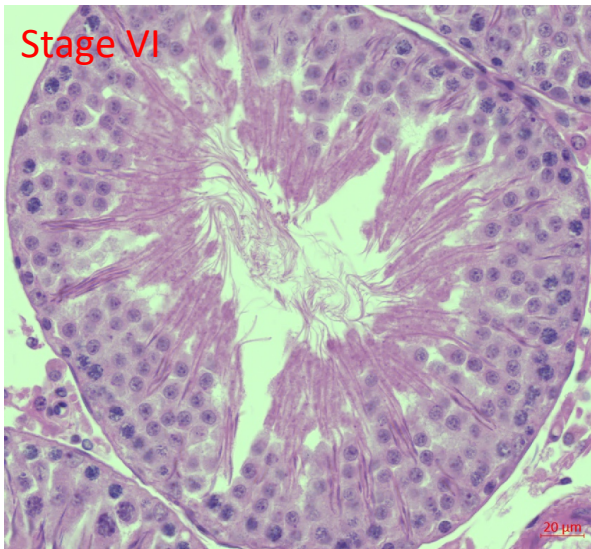
Stage XIII

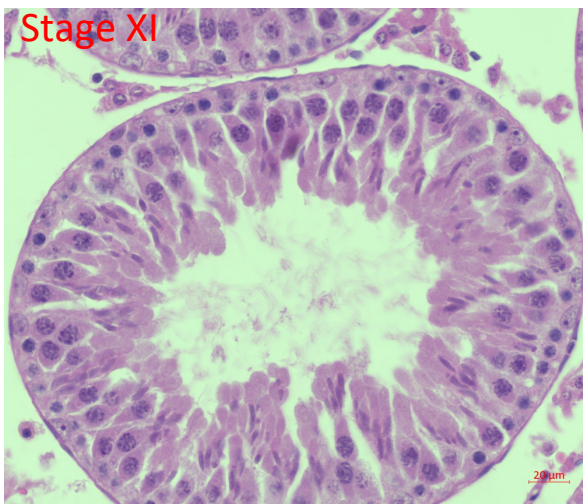
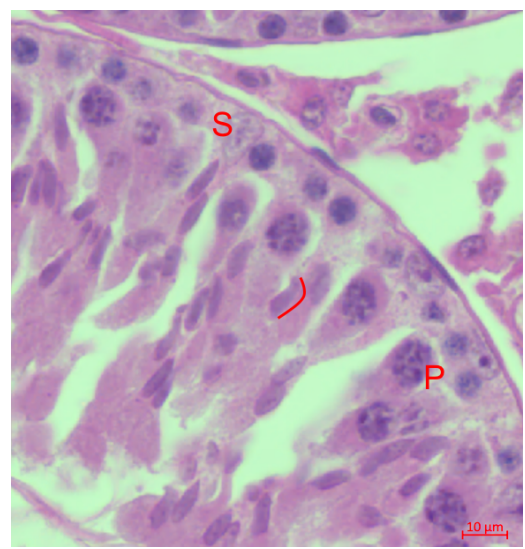
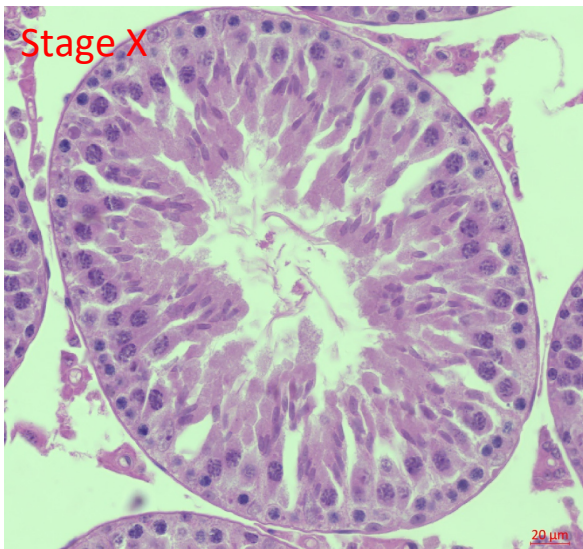
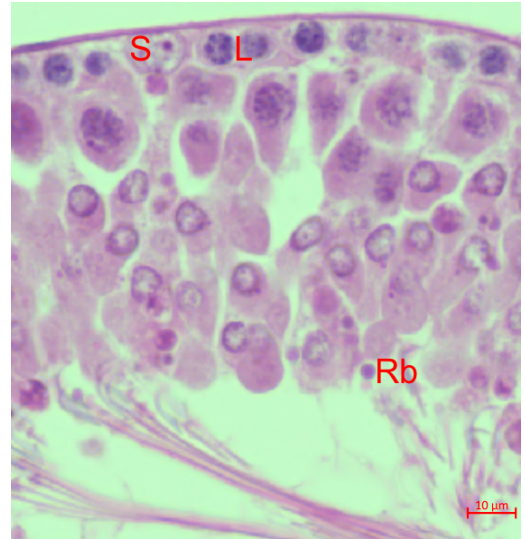
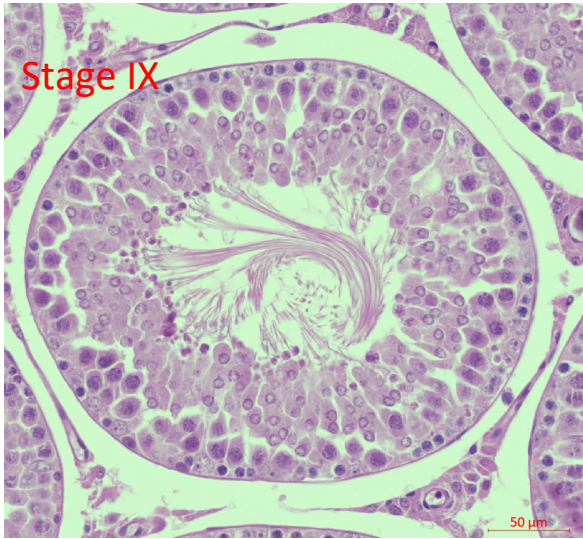
By stage XIII, large numbers of Diplotene spermatocytes are present with large nuclei with dispersed clumps of chromatin. Elongating spermatids in stage XIII tubules are now very thin.

Stage XIV

Stage XIV tubules are easily identifiable by the presence of meiotic figures where the Diplotene spermatocytes were previously.







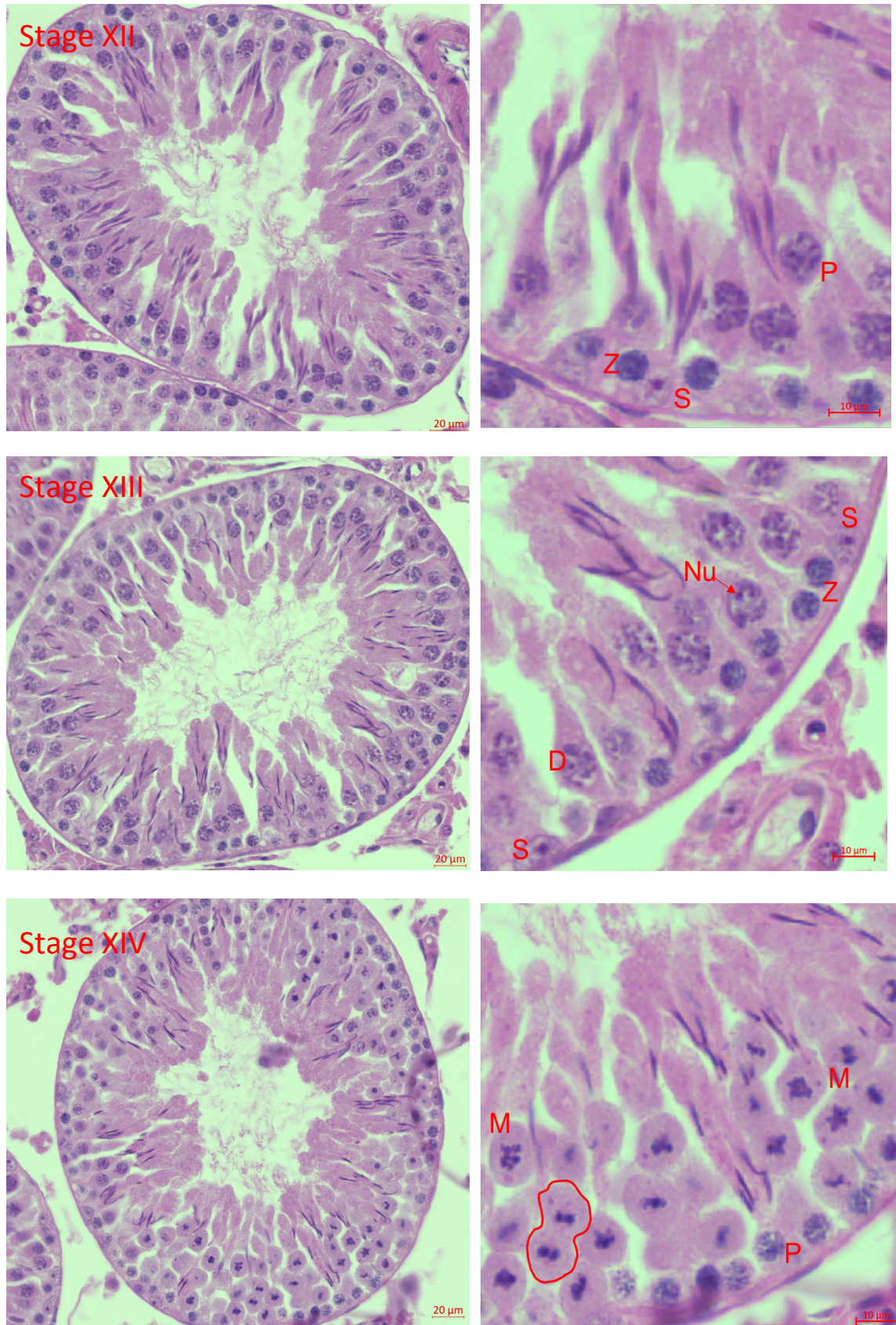


Figure 99: Illustrative examples of tubule staging from I – XIV, according to decision key and criteria specified within the literature. Scale bar represents 50μm on left-hand side images and 10μm on the right-hand side. S (Sertoli cell nucleus); A (type-A spermatogonia); I (intermediate spermatogonia); B (type-B spermatogonia); PL (preleptotene spermatocyte); P (pachytene spermatocyte); L (leptotene spermatocyte); Z (zygotene spermatocyte); D (diplotene spermatocyte); SS (secondary spermatocyte); Nu (Nucleus); ES (Elongating Spermatid); RS (Round Spermatid).

Number of observations

In total 718 tubules were measured across all samples using a randomised approach; 167 were control tubules (23.25%), 171 were AgNO₃ treated (23.8%), 192 were NM-300 treated (26.8%) and 188 were Nano Amor treated (26.2%). A breakdown of tubule counts per stage, per group is included in Table 26.

Table 26: Count data for tubule observations made per stage of spermatogenesis assigned across i) all data pooled, and ii) each treatment group

Stage	Number of tubules counted				
	Total population	Control	NM-300	AgNO ₃	Nano Amor
I-IV	80	25 (15.0)	18 (9.4)	20 (11.7)	17 (9.0)
V	47	9 (5.4)	7 (3.6)	16 (9.4)	15 (8.0)
VI	71	16 (9.6)	15 (7.8)	20 (11.7)	20 (10.6)
VII	100	22 (13.2)	35 (18.2)	18 (10.5)	25 (13.3)
VIII	129	28 (16.8)	38 (19.8)	30 (17.5)	33 (17.6)
IX	83	23 (13.8)	21 (10.9)	21 (12.3)	18 (9.6)
X	25	7 (4.2)	5 (2.6)	6 (3.5)	7 (3.7)
XI	51	11 (6.6)	15 (7.8)	11 (6.4)	14 (7.4)
XII	58	9 (5.4)	23 (12.0)	10 (5.8)	16 (8.5)
XIII	38	11 (6.6)	5 (2.6)	13 (7.6)	9 (4.8)
XIV	36	6 (3.6)	10 (5.2)	6 (3.5)	14 (7.4)
TOTAL	718	167	192	171	188

Dazl staining intensity and tubule stage

In order to assist with accurate staging of tubules, a sample from each animal underwent immunohistochemical staining using the Dazl antibody. As Dazl stains the germ cell layer differentially depending on the cell populations within each tubule and thus its stage in the spermatogenic cycle, it was expected that intensity of the resulting DAB stain would alter with stage of tubule. If this was the case, the stain intensity observed would assist

in the identification of tubule stage and later analysis. Initial examination of staged tubules according to Dazl stain showed what appears to be a clear pattern of increasing then decreasing stain intensity as the tubules move through the cycle of the seminiferous epithelium (Fig. 100).

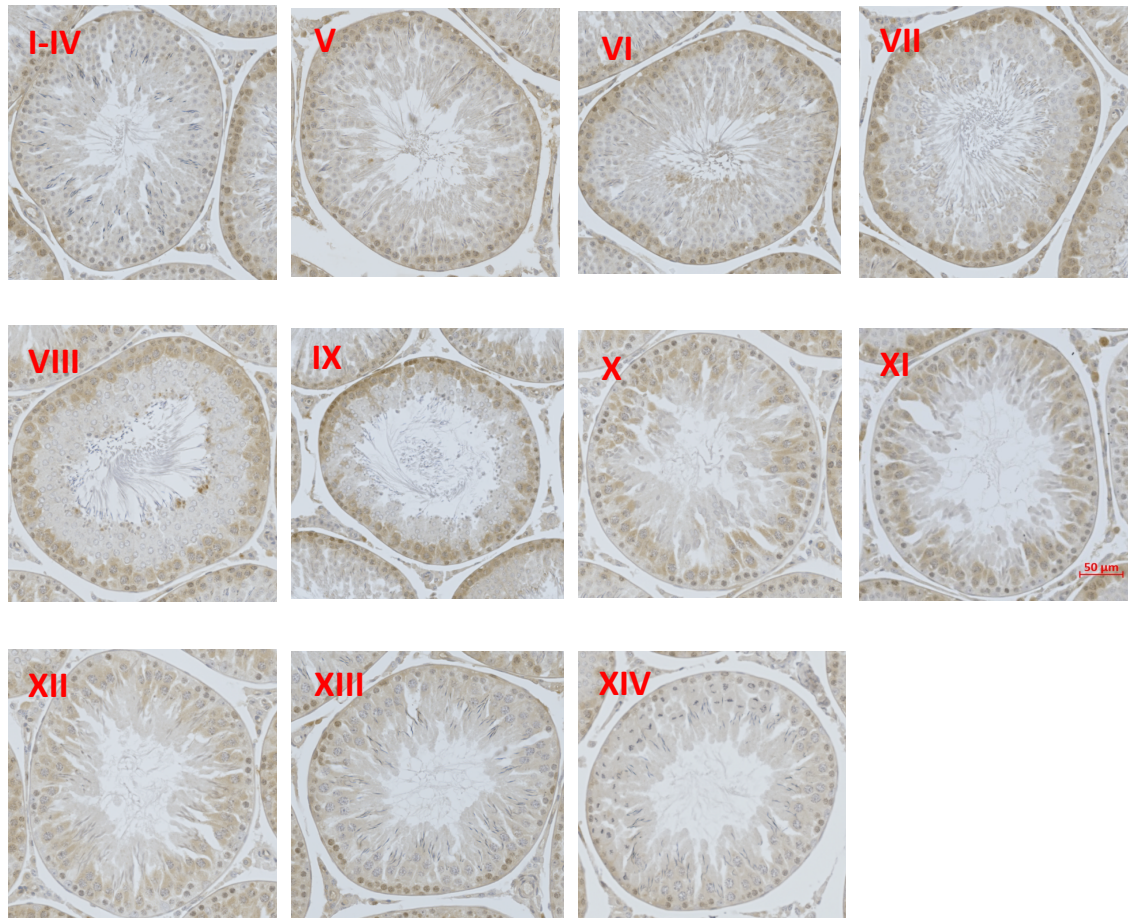


Figure 100: Development of Dazl staining according to tubule stage (shown in red). Intensity of Dazl stain increases from stage V-VII, peaks at stage VIII, then decreases from stage IX-XI, and is not present through stages XIII-IV of the next cycle. It is a useful stain to aid accuracy of staging tubules. Scale bar represents 50µm.

Figure 101 shows DAB stain intensity for Dazl as a % of the total number of tubules identified for each stage of the spermatogenic cycle in control animals (n=5). The stage-specific Dazl stain increased in intensity from stage V-VIII, decreased from stage IX-XII and showed no DAB stain from stage XIII-IV, matching findings from Nicholas *et. al.* and Rocchietti-March *et. al.* on Dazl expression in rodent testicular seminiferous epithelium (Nicholas *et al.*, 2009, Rocchietti-March *et al.*, 2000) Dazl immunostaining was therefore confirmed to be a useful measure to assist with accurate staging, and subsequent morphological and semi-quantitative analysis of tubules.

Evaluation of control data

As the control animals were sacrificed at more than one time, initial statistics focussed on whether tubule diameter and lumen volume measurements were comparable across the two times. Testing of the hypothesis that control data was the same regardless of sacrifice date resulted in P-values of 0.3407 for tubule diameter, and 0.6083 for lumen volume, with all 95% confidence intervals crossing zero, confirming that there was no statistical difference between the two groups (Tables 28 and 29).

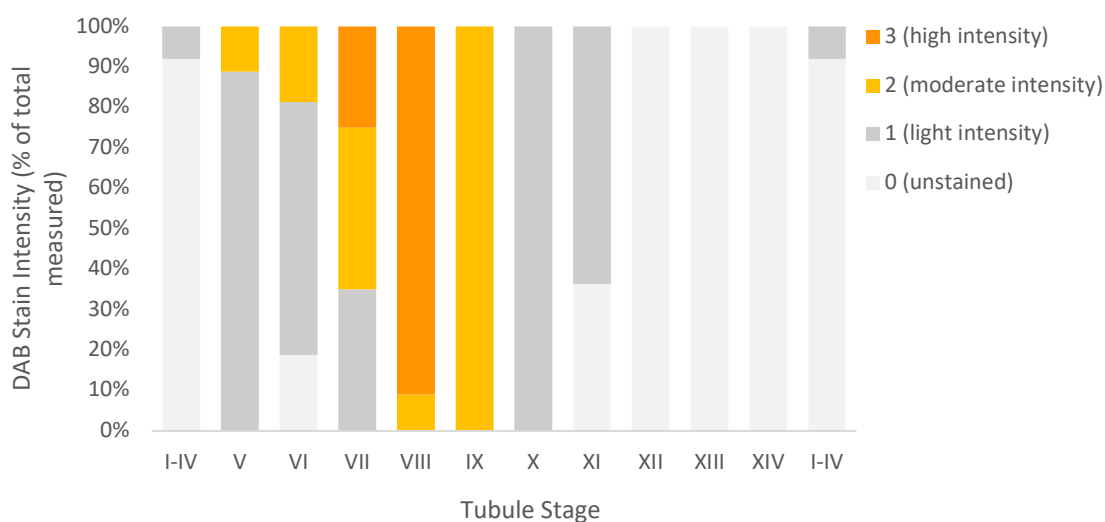


Figure 101: DAB stain intensity for Dazl antibody as % of total counts according to stage of tubule in control animals (n=5).

Table 27: comparison of control data from animals harvested at day 29 compared to day 85 for tubule diameter, generated using a mixed-model where animal is the random effect and stage and day are fixed effects. Estimates reported by the model for day29 and 85 are shown in the first two rows of the table, with the difference between these and associated p-value reported in the bottom row. N= 167.

Sample	Estimate (SD)	95% CI	P-value
C d29	225.49 (15.554)	[175.99, 274.99]	
C d85	253.19 (19.075)	[192.49, 313.90]	
C d29 - d85	-27.70 (24.623)	[-106.06, 50.66]	0.3424

Table 28: comparison of control data from animals harvested at day 29 compared to day 85 for lumen volume, generated using a mixed-model where animal is the random effect and stage and day are fixed effects. Estimates reported by the model for day29 and 85 are shown in the first two rows of the table, with the difference between these and associated p-value reported in the bottom row. N=167.

Sample	Estimate (SD)	95% CI	P-value
C d29	12799.68 (1936.8)	[6635.94, 18963.43]	
C d85	14581.94 (2380.6)	[7005.86, 22158.01]	
C d29 - d85	-1782.25 (3072.4)	[-11559.89, 7995.38]	0.6026

Cross-evaluation of control data with published data to determine reliability

Once it was established that control samples were not statistically different, tubule diameter and lumen volume measurements from control animals were pooled and plotted according to stage (Fig. 102). The graphed measurements are clearly comparable with data previously published by Wing & Christensen, also using Sprague-Dawley rats (Fig. 103) (Wing and Christensen, 1982).

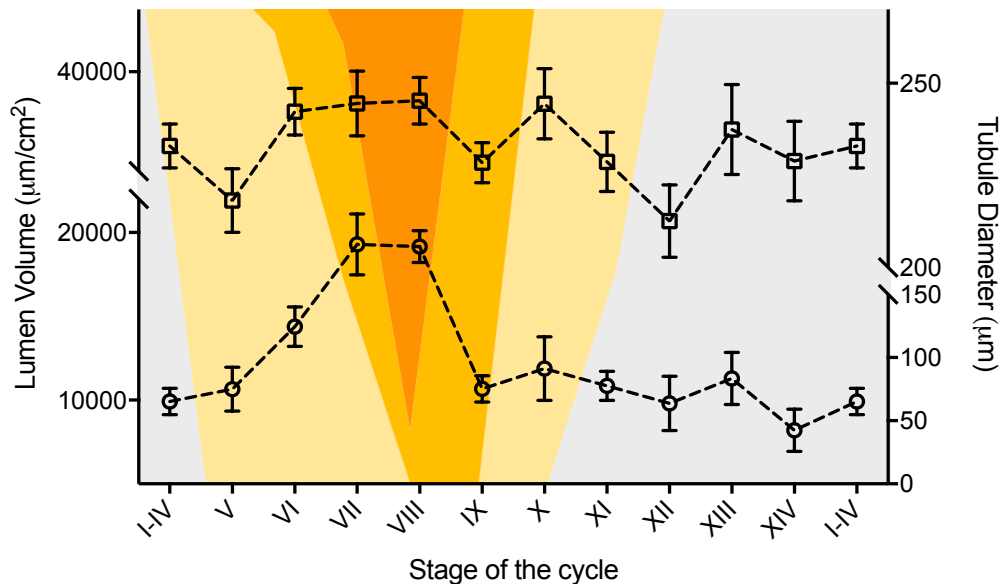


Figure 102: Diameter of the seminiferous tubule (squares) and volume of the lumen (circles) at various stages of the seminiferous epithelium cycle, superimposed onto the *Dazl* immunostaining intensity scores recorded. Each value represents the mean of 5 animals (plotted +/- SEM for comparison to figure 40). NB. lumen volume is expressed directly as recorded ($\mu\text{m}^2/\text{cm}^2$), with the influence of tubule shape on volume observed considered later within this analysis.

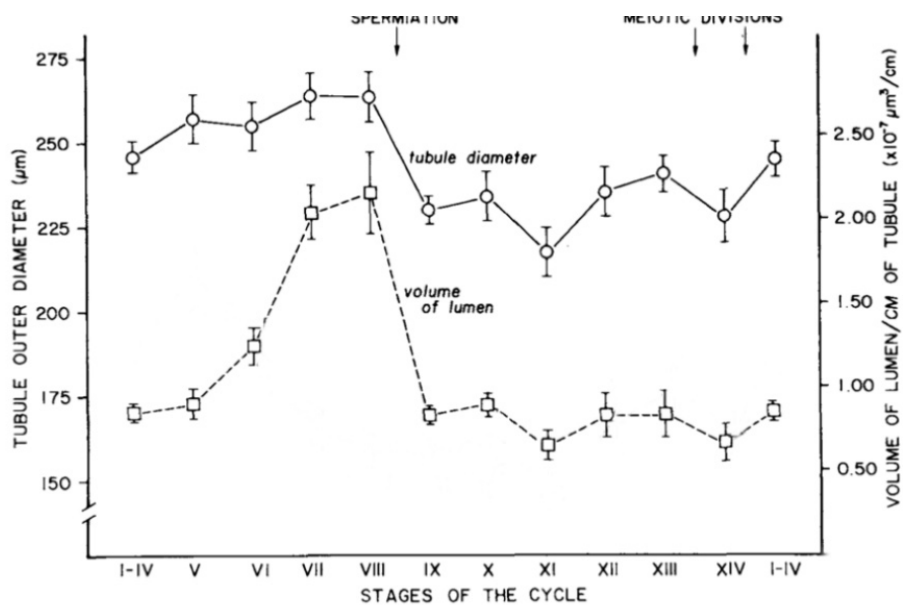


Figure 103: Diameter of the seminiferous tubule and volume of the lumen per unit length of seminiferous tubule at various stages of the cycle. Each value represents the mean of four animals (plotted +/- SEM). Wing & Christensen, 1982. NB. lumen volume is expressed per unit length of the seminiferous tubule, probably in order to try and correct for shape differences between tubule.

Closer inspection shows that lumen volume changes replicated exactly the pattern in Wing & Christensen's data, with a large rise in mean lumen volume from stage V-VIII, and a sharp drop at stage IX following spermiation. Interestingly, Standard Error of the Mean (SEM) values reported also followed a very similar pattern, with the lowest variation being seen at stage I-IV and IX.

Tubule diameter changes show a similar pattern to that reported by Wing & Christensen, with some small but notable differences. From stage I-IV to V, Wing & Christensen reported an increase in tubule diameter, whereas the data collected in this work showed a small drop. In addition, the decrease in diameter between stages VIII and IX following spermiation was more pronounced in the 1982 paper than in the current work.

Tubule Diameter Analysis

Analysis of tubule diameter by treatment produced some interesting findings. Initially, tubule diameter was plotted according to stage for all treatments, and overlaid on the Dazl stain intensity scores recorded for each tubule within each treatment (Fig. 104). The data showed that the pattern of Dazl expression did not change with treatment. However, mean diameter recorded at each stage did not follow the same pattern as seen within control animals. However, statistical analysis using a mixed model yielded P-values of 0.5025 (AgNO₃ – control), 0.7286 (NM-300 – control) and 0.3390 (Nano Amor – control), with all 95% confidence intervals crossing zero. Therefore, no significant difference was found between treated animals and control (Table 29).

As stages VII, VIII and IX surround a key event in the seminiferous epithelium cycle (representing before, during and immediately after spermiation), further analysis was undertaken to investigate these stages in isolation. Comparison of diameter measurements from treated animals at stages VII, VIII and IX (together, and then in isolation) to control did not change the outcome – no significant difference was seen to control in any of the three stages within each treatment (Table 30).

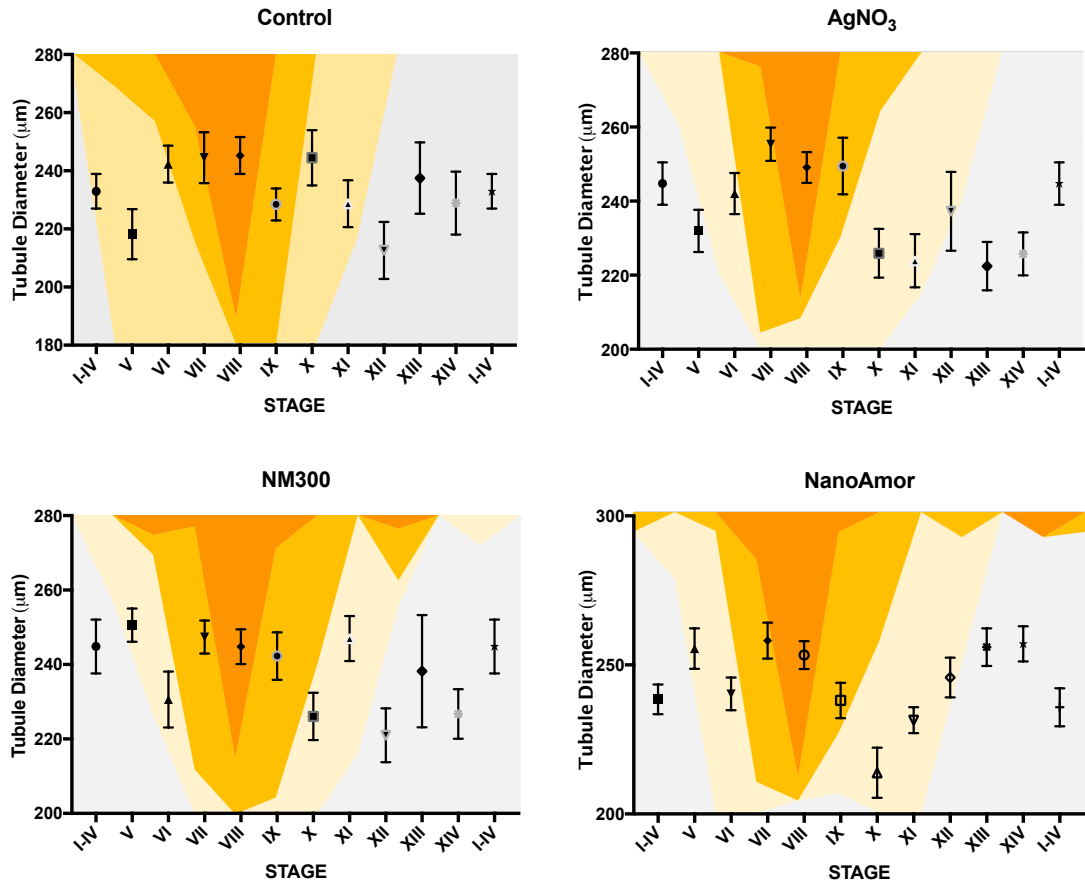


Figure 104: Average Seminiferous Tubule Diameter (+/- SEM) overlaid on Dazl staining intensity scores, both according to stage of the seminiferous tubule cycle. Dazl staining intensity scores followed the same pattern regardless of whether animals were exposed to engineered nanomaterials or not. Tubule diameters recorded showed some alteration from the pattern recorded in control animals.

Table 29: Comparison of tubule diameter in treated animals to controls generated using a mixed-model where animal is the random effect and tubule stage and treatment are fixed effects. Estimates together with their standard deviation and 90% confidence interval are reported by the model for each treatment are shown in the first 4 rows of the table; the difference between each treatment and control and associated p-value are reported in the bottom 3 rows.

	Estimate (SD)	95% CI	P-value
AgNO ₃	243.76 (7.362)	[228.15, 259.37]	
Control	236.62 (7.368)	[221.00, 252.23]	
NM-300	240.29 (7.335)	[224.74, 255.84]	
Nano Amor	246.86 (7.335)	[231.32, 262.41]	
AgNO ₃ - Control	7.14 (10.414)	[-14.93, 29.22]	0.5025
NM-300 - Control	3.67 (10.399)	[-18.37, 25.72]	0.7286
Nano Amor - Control	10.25 (10.399)	[-11.80, 32.29]	0.3390

Table 30: Comparison of tubule diameter in treated animals to controls for key stages of the seminiferous epithelium cycle. Results generated using a mixed-model where animal is the random effect and tubule stage and treatment are fixed effects. Estimates together with their standard deviation and 90% confidence interval are reported by the model for each treatment are shown in the first 4 rows of the table; the difference between each treatment and control and associated p-value are reported in the bottom 3 rows.

	Stage VII, VIII, IX			Stage VII			Stage VIII			Stage IX		
	Estimate (SD)	95% CI	P-value	Estimate (SD)	95% CI	P-value	Estimate (SD)	95% CI	P-value	Estimate (SD)	95% CI	P-value
AgNO₃	253.53 (8.256)	[236.03, 271.04]		257.46 (11.162)	[233.80, 281.12]		256.58 (9.880)	[235.63, 277.52]		247.55 (8.433)	[229.68, 265.43]	
Control	240.66 (8.225)	[223.23, 258.10]		237.90 (10.712)	[215.19, 260.61]		246.18 (9.931)	[225.13, 267.24]		230.63 (8.286)	[213.06, 248.20]	
NM-300	243.46 (8.085)	[226.32, 260.60]		247.14 (9.866)	[226.22, 268.06]		242.54 (9.713)	[221.95, 263.13]		240.69 (8.316)	[223.07, 258.32]	
Nano Amor	251.91 (8.209)	[234.51, 269.31]		262.55 (10.313)	[240.69, 284.41]		252.22 (9.846)	[231.35, 273.09]		237.88 (8.754)	[219.33, 256.44]	
AgNO₃ - Control	12.87 (11.651)	[-11.83, 37.57]	0.2857	19.55 (15.471)	[-13.24, 52.35]	0.2243	10.39 (14.009)	[-19.30, 40.09]	0.4689	16.92 (11.823)	[-8.14, 41.99]	0.1715
NM-300 - Control	2.79 (11.536)	[-21.66, 27.25]	0.8117	9.24 (14.563)	[-21.64, 40.11]	0.5349	-3.64 (13.891)	[-33.09, 25.81]	0.7965	10.07 (11.739)	[-14.82, 34.95]	0.4039
Nano Amor - Control	11.25 (11.622)	[-13.39, 35.89]	0.3475	24.64 (14.869)	[-6.88, 56.16]	0.1169	6.03 (13.985)	[-23.61, 35.68]	0.6719	7.25 (12.054)	[-18.30, 32.81]	0.5557

Lumen Volume by stage analysis:

Lumen volume was plotted according to stage for all treatments, and overlaid on the Dazl stain intensity scores recorded for each tubule within each treatment (Fig. 105). The data showed that the general pattern of Dazl expression did not alter with treatment. However, mean lumen volume recorded at each stage did not follow the same pattern as control animals. Within all treated animals, there appeared to be a small drop in lumen volume from stage V to VI, where in control animals lumen volume was increasing. The increase in lumen volume between stage VI and VII therefore looked much greater by comparison to control. There was also a higher lumen volume at stage VII than VIII for NM-300 and Nano Amor treated animals than in control, where stage VII and VIII tubules had a similar average volume. In addition, it appeared that maximal lumen volume reached at spermiation (stage VIII) was marginally higher in treated animals compared to control, and the decrease in volume between stage VIII and IX smaller than control in AgNO₃ treated animals.

Statistical analysis using a mixed model where animal was the random effect, and tubule stage and treatment fixed effects yielded P-values of 0.5025 (AgNO₃ – control), 0.7286 (NM-300 – control) and 0.3390 (Nano Amor – control) with all 95% confidence intervals crossing zero. Thus, despite the differences in graphed data, no significant difference was found between treated animals and control (Table 31).

As stages VII, VIII and IX surround a key event in the seminiferous epithelium cycle (representing before, during and immediately after spermiation), and deviation from control data was seen in treated animals, further analysis was undertaken to investigate whether looking at these stages in isolation revealed any subtle effects taking place. Testing of diameter measurements from treated animals at stages VII, VIII and IX as (a sub-group) against control did not change the outcome – no significant difference was seen to control in any of the three stages within each treatment (Table 32). However, testing of stage VII, VIII and IX separately against control showed some differences. Within stage VII, Nano Amor treated animals were statistically different to control ($p=0.0431^*$), and within stage IX AgNO₃ treated animals were statistically different to control ($p=0.0365^*$).

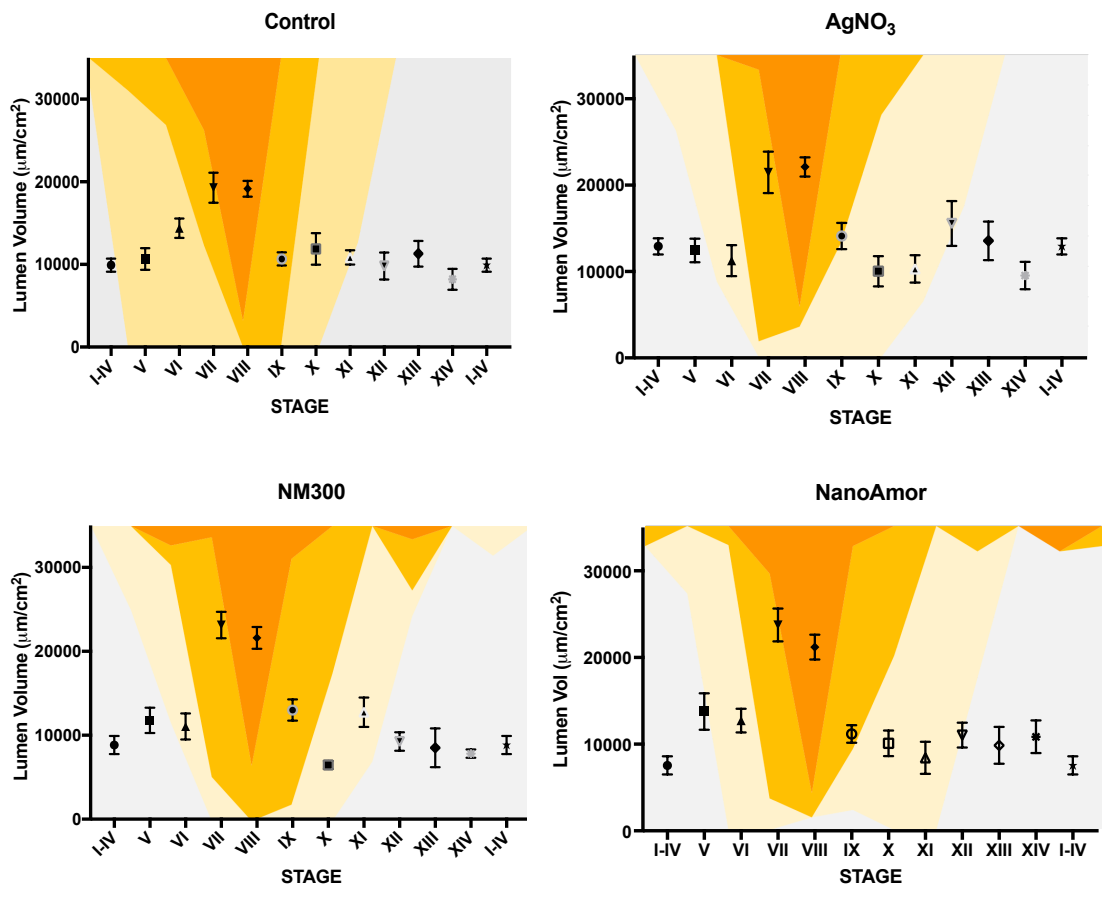


Figure 105: Average Lumen Volume (+/- SEM) overlaid on Dazl staining intensity scores, both according to stage of the seminiferous tubule cycle. Dazl staining intensity scores followed the same pattern regardless of whether animals were exposed to engineered nanomaterials or not. Tubule diameters recorded showed some alteration from the pattern recorded in control animals.

Table 31: Comparison of lumen volume in treated animals to controls generated using a mixed-model where animal is the random effect and tubule stage and treatment are fixed effects. Estimates together with their standard deviation and 90% confidence interval are reported by the model for each treatment are shown in the first 4 rows of the table; the difference between each treatment and control and associated p-value are reported in the bottom 3 rows.

	Estimate (SD)	95% CI	P-value
AgNO3	21283.18 (1753.0)	[17566.94, 24999.41]	
Control	16916.95 (1742.0)	[13224.09, 20609.81]	
NM-300	19716.64 (1692.1)	[16129.49, 23303.80]	
Nano Amor	20746.67 (1735.7)	[17067.22, 24426.11]	
AgNO3 - Control	4366.23 (2470.4)	[-870.89, 9603.34]	0.0962
NM-300 - Control	2799.69 (2429.5)	[-2350.52, 7949.91]	0.2661
Nano Amor - Control	3829.72 (2459.6)	[-1384.48, 9043.91]	0.1390

Table 32: Comparison of lumen volume in treated animals to controls for key stages of the seminiferous epithelium cycle. Results generated using a mixed-model where animal is the random effect and tubule stage and treatment are fixed effects. Estimates together with their standard deviation and 90% confidence interval are reported by the model for each treatment are shown in the first 4 rows of the table; the difference between each treatment and control and associated p-value are reported in the bottom 3 rows.

	Stage VII, VIII, IX			Stage VII			Stage VIII			Stage IX		
	Estimate (SD)	95% CI	P-value	Estimate (SD)	95% CI	P-value	Estimate (SD)	95% CI	P-value	Estimate (SD)	95% CI	P-value
AgNO₃	21283.18 (1753.0)	[17566.94, 24999.41]		21370.98 (2600.7)	[15857.67, 26884.29]		26062.07 (2578.7)	[20595.45, 31528.70]		14173.10 (1112.1)	[11815.56, 16530.65]	
Control	16916.95 (1742.0)	[13224.09, 20609.81]		18437.00 (2418.2)	[13310.62, 23563.38]		19171.15 (2592.6)	[13674.99, 24667.32]		10663.14 (1062.6)	[8410.43, 12915.85]	
NM-300	19716.64 (1692.1)	[16129.49, 23303.80]		23154.85 (2043.7)	[18822.42, 27487.29]		21211.28 (2533.0)	[15841.56, 26581.00]		13007.90 (1112.1)	[10650.35, 15365.44]	
Nano Amor	20746.67 (1735.7)	[17067.22, 24426.11]		25716.73 (2264.1)	[20917.11, 30516.34]		22084.68 (2569.0)	16638.63, 27530.72]		12393.78 (1201.2)	[9847.34, 14940.22]	
AgNO₃ - Control	4366.23 (2470.4)	[-870.89, 9603.34]	0.0962	2933.97 (3551.3)	[-4594.40, 10462.35]	0.4209	6890.92 (3656.7)	[-860.97, 14642.81]	0.0778	3509.96 (1538.2)	[249.17, 6770.75]	0.0365
NM-300 - Control	2799.69 (2429.5)	[-2350.52, 7949.91]	0.2661	4717.85 (3166.1)	[-1994.06, 11429.76]	0.1556	2040.12 (3624.6)	[-5643.74, 9723.98]	0.5813	2344.76 (1538.2)	[-916.03, 5605.55]	0.1469
Nano Amor - Control	3829.72 (2459.6)	[-1384.48, 9043.91]	0.139	7279.72 (3312.7)	[257.18, 14302.26]	0.0431	2913.52 (3649.9)	[-4823.87, 10650.91]	0.4364	1730.64 (1603.8)	[-1669.23, 5130.50]	0.2965

Whilst staging and measuring tubules, it was observed that some presented with what appeared to be populations of sloughed cells within the tubular epithelium. A check of the data revealed that of the 718 tubules measured, only 41 had sloughing of cells into the lumen (some 6% of the total). Of these, none were measured within control animals, leading to the consideration that they were a treatment associated effect. Within treated animals, 11.7% of AgNO₃ treated tubules, 6% of NM-300 treated tubules, and 5.6% of Nano Amor treated tubules contained sloughing into the lumen (Table 33).

Table 33: Count data for tubules measured with and without sloughing of cells into the luminal area.

Treatment	Tubules without sloughing	Tubules with sloughing	% of total tubules with sloughing
Control	167	0	0
AgNO₃	151	20	11.7
NM-300	181	11	6
Nano Amor	178	10	5.6

Further examination of the counts to include treatment and stage showed a generalised spread of tubules with sloughing across all treated animals, with no observable pattern of occurrence (Table 34).

Table 34: Count data for tubules measured with and without sloughing of cells into the luminal area according to Stage of spermatogenesis. + = sloughing present, - = no sloughing

Stage	Sloughing	Control	AgNO ₃	NM-300	Nano Amor
I-IV	+	0	4	1	0
	-	25	16	17	17
V	+	0	1	0	1
	-	9	15	7	14
VI	+	0	1	1	0
	-	16	19	14	20
VII	+	0	0	1	1
	-	22	18	34	24
VIII	+	0	1	1	1
	-	28	29	37	32
IX	+	0	0	2	1
	-	23	21	19	17
X	+	0	0	0	0
	-	7	6	5	7
XI	+	0	3	2	3
	-	11	8	13	11
XII	+	0	4	3	1
	-	9	6	20	15
XIII	+	0	6	0	1
	-	11	7	5	8
XIV	+	0	0	0	1
	-	6	6	10	13

As it was possible that sloughing of cells into the central lumen of tubules could potentially affect the lumen volume recorded, further investigation into the potential effect of lumen volume changes on outcome was undertaken. An additional dataset was prepared, in which the lumen volume of tubules with sloughing into the central lumen was calculated by taking overall volume, then subtracting the inner volume of sloughed cells. The dataset was then re-tested against control to establish whether taking into account lumen volume adjusted for sloughing affected the outcome. Table 35 outlines the outcomes of this test, which confirmed that treated animals were not statistically different to control with this adjustment, producing p values of 0.5129 for AgNO₃, 0.8893 for NM-300 and 0.4779 for Nano Amor with all 95% confidence intervals crossing zero.

Table 35: Comparison of lumen volume in treated animals to controls, where lumen volume was corrected for cells sloughed into the central lumen. Generated using a mixed-model where animal is the random effect and tubule stage and treatment are fixed effects. Estimates together with their standard deviation and 90% confidence interval are reported by the model for each treatment are shown in the first 4 rows of the table; the difference between each treatment and control and associated p-value are reported in the bottom 3 rows.

	Estimate (SD)	95% CI	P-value
AgNO₃	15061.73 (1352.4)	[12194.75, 17928.71]	
Control	13808.58 (1355.0)	[10936.12, 16681.05]	
NM-300	14078.35 (1340.5)	[11236.58, 16920.12]	
Nano Amor	15194.43 (1340.6)	[12352.46, 18036.40]	
AgNO₃ - Control	1253.15 (1913.7)	[-2803.75, 5310.05]	0.5219
NM-300 - Control	269.77 (1907.0)	[-3772.82, 4312.35]	0.8893
Nano Amor - Control	1385.85 (1907.1)	[-2656.95, 5428.65]	0.4779

The effect of tubule shape on recorded values

As tubule diameter and lumen volume were recorded, tubule shape was also noted in order to allow consideration of whether shape affected the values recorded and correct for this if necessary. Of the 718 tubules measured, 287 (39.9%) were round, 366 (44.2%) were intermediate and 65 (9.01%) were elongated. Table 36 outlines the count data for tubule shape according to treatment. The proportional representation of each tubule shape was similar across all treatments.

Table 36: Count data for shape of tubules measured across all treatments. Round tubules were uniform in shape and diameter, Intermediate tubules were more polyhedral than round, with some elongation and difference in diameter dependent on axis measured, Elongated tubules were clearly longer than wide with an oval or sausage shaped appearance. Numbers within brackets represent % of treatment total (columns), while numbers out with brackets represent % of shape total (rows).

	Control	AgNO ₃	NM-300	Nano Amor
Round	91 (53.2)	80 (47.9)	90 (47.9)	105 (54.7)
Intermediate	59 (34.5)	71 (42.5)	88 (46.8)	69 (35.9)
Elongated	21 (12.3)	16 (9.6)	10 (5.3)	18 (9.4)

Statistical analysis for Tubule Diameter and Lumen Volume recorded for tubules when categorised according to shape is summarised in Table 37. As expected, there was a significant shape-dependent difference ($p < 0.001$ or $p < 0.0001$) in both tubule diameter and lumen volume dependent on shape of tubule. The only exception was a no significant finding for tubule diameter between intermediate and round tubules.

Table 37: Comparison of shape effects on tubule diameter and luminal volume. Analysis conducted using a mixed model, where animal was the random effect and shape was the fixed effect.

		Estimate (SD)	95% C.I.	P-value
Tubule Diameter	Round	237.68 (3.690)	[230.44, 244.93]	
	Intermediate	233.44 (4.671)	[224.27, 242.61]	
	Oval	249.20 (3.753)	[241.83, 256.57]	
	Intermediate-Round	4.25 (3.448)	[-2.52, 11.02]	0.2185
	Intermediate-Oval	-11.52 (2.009)	[-15.46, -7.57]	<0.0001
	Oval-Round	-15.76 (3.509)	[-22.65, -8.87]	<0.0001
Lumen Volume	Round	15119.91 (602.12)	13937.69, 16302.14]	
	Intermediate	20455.97 (928.98)	[18631.99, 22279.96]	
	Oval	13717.68 (625.42)	[12489.71, 14945.65]	
	Intermediate-Round	-5336.06 (851.26)	[-7007.44, -3664.68]	<0.0001
	Intermediate-Oval	1402.23 (496.35)	[427.70, 2376.77]	0.0049
	Oval-Round	6738.29 (866.61)	[5036.76, 8439.82]	<0.0001

Because there was a significant difference between tubule populations when categorised according to shape, statistical analysis was re-run for the round and intermediate shape groups to investigate whether tubule shape had any effect on outcome when comparing

Table 38: Re-testing tubule diameter and lumen volume measurements in treated animals to controls for round and intermediate shaped tubules. Results generated using a mixed-model where animal is the random effect and tubule stage and treatment are fixed effects. Estimates together with their standard deviation and 90% confidence interval are reported by the model for each treatment are shown in the first 4 rows of the; the difference between each treatment and control and associated p-value are reported in the next 3 rows.

		Round only			Intermediate only		
		Estimate (SD)	95% CI	P-value	Estimate (SD)	95% CI	P-value
Tubule Diameter	AgNO ₃	250.84 (7.569)	[234.80, 266.89]		240.14 (7.721)	[223.77, 256.50]	
	Control	241.36 (7.357)	[225.76, 256.96]		233.03 (7.839)	[216.41, 249.65]	
	NM-300	245.45 (7.373)	[229.82, 261.08]		238.95 (7.676)	[222.68, 255.23]	
	Nano Amor	256.60 (7.242)	[241.25, 271.96]		238.48 (7.737)	[222.08, 254.89]	
	AgNO ₃ - Control	9.48 (10.550)	[-12.88, 31.85]	0.3821	7.11 (11.004)	[-16.22, 30.44]	0.5275
	NM-300 - Control	4.09 (10.425)	[-18.01, 26.19]	0.7001	5.92 (10.968)	[-17.33, 29.17]	0.5967
	Nano Amor - Control	15.24 (10.341)	[-6.68, 37.17]	0.1598	5.45 (11.020)	[-17.91, 28.81]	0.6274
Lumen Volume	AgNO ₃	14095.43 (1257.2)	[11430.24, 16760.63]		15873.83 (1179.9)	[13372.52, 18375.13]	
	Control	12579.85 (1189.9)	[10057.46, 15102.24]		13438.16 (1215.8)	[10860.8, 16015.47]	
	NM-300	12479.88 (1196.3)	[9943.81, 15015.96]		14612.56 (1163.0)	[12147.16, 17077.95]	
	Nano Amor	14351.35 (1144.4)	[11925.32, 16777.38]		16397.08 (1185.1)	[13884.85, 18909.31]	
	AgNO ₃ - Control	1515.58 (1728.8)	[-2149.24, 5180.41]	0.3936	2435.66 (1694.9)	[-1157.40, 6028.73]	0.17
	NM-300 - Control	-99.97 (1691.0)	[-3684.80, 3484.86]	0.9536	1174.40 (1681.5)	[-2390.19, 4738.99]	0.4949
	Nano Amor - Control	1771.50 (1657.9)	[-1743.06, 5286.06]	0.3011	2958.92 (1699.8)	[-644.56, 6562.39]	0.1009

control animals to those treated with silver. Elongated tubules were not tested as the sample size was so small.

Table 38 summarises the results of testing control vs treated for i) round tubules only and ii) intermediate tubules only. Tubule diameter testing for round tubules only gave p values of 0.3821 (AgNO₃), 0.7001 (NM-300) and 0.1598 (Nano Amor), and 0.5275 (AgNO₃), 0.5967 (NM-300) and 0.6274 (Nano Amor) with all 95% confidence intervals crossing zero. Lumen volume testing for round tubules only gave p values of 0.3936 (AgNO₃), 0.9536 (NM-300) and 0.3011 (Nano Amor), and 0.17 (AgNO₃), 0.4949 (NM-300) and 0.1009 (Nano Amor) with all 95% confidence intervals crossing zero. Therefore, despite tubule shape having a significant effect on the diameter and volume recorded during stereological analysis, consideration of each tubule shape alone did not alter the finding of no significance for treatment being different to control.

Discussion

This chapter examined tissues from animals exposed to one type of silica nanomaterial (NM202) and two ENM and silver ions (NM-300, Nano Amor and AgNO₃). The research questions it addressed were four-fold: i) to establish whether there were morphological alterations in ENM treated tissues, ii) to understand whether these could be evaluated in a semi-quantitative manner through systematic application of stereological analysis, iii) to establish whether exposure to ENM could lead to any changes in functionality of steroidogenic pathways or the wider HPG axis in the testis, and iv) to compare results to those reported *in vitro* for comparability and validation.

Morphological analysis of tissues for changes post-ENM exposure

Morphological analysis of tissues revealed a variety of findings, including focal dysmorphism, degeneration of germ cells, presence of pyknotic nuclei, disorganisation and possible hyperplasia of interstitial content, retention of spermatids and sloughing of germ cells, many of which were in agreement with the published literature, but some which were to our knowledge are being shown for the first time, especially in such detail. Table 39 summarises the key findings from morphological examination for ease of comparison.

Table 39: Summary of morphological changes observed within tissue samples from animals in two studies: i) animals treated with low, medium or high dose of NM202 silica nanoparticles; ii) animals treated with one of three different types of silver nanoparticle (NM-300, Nano Amor and silver ions AgNO₃)

	Dysmorphism	Germ Cell degeneration / atrophy	Pyknotic germ cell Nuclei (apoptosis)	Giant Cells	Interstitial effects	Germ Cell Sloughing	Germ Cell layer atrophy / SC only tubules	Spermatid retention
Control	-	-	-	-	-	-	-	-
NM202 L	-	-	-	-	-	-	-	-
NM202 M	-	-	-	-	-	-	-	-
NM202 H	-	-	-	-	-	-	-	-
Silver Nano Amor	Y (widespread)	Y	Y	-	-	Y	Y	Y
Silver NM-300	Y (focal)	Y	Y	Y	Inflammation-like changes	Y	-	Y
Silver AgNO₃	Y (focal)	Y	Y	-	Leydig Cell Hyperplasia	Y	Y	-

Morphological evaluation of testicular tissue collected following 28-day oral exposure to nanoparticulate silica dioxide (NM202) at low, medium and high concentrations did not reveal any changes from control. This is similar to the findings of Morishita et al (2012) in Balb/c mice following intravenous injection, and Kim et al (2006) who injected mice intraperitoneally with 50nm silica nanoparticles (Morishita et al., 2012, Kim et al., 2006).

As discussed within the introductory section of this chapter, other published literature suggests that there may be a transient adverse reversible effect on the testis following oral nano-silica exposure (Xu et al., 2014, Ren et al., 2016). However, this was not seen within the current work. As all tissue samples examined in this body of work were taken from animals sacrificed at day 29, for completeness (and given time) it could be interesting to examine additional stored tissues from NM202 high dose animals sacrificed following 6 weeks of wash-out (day 85). However, as no onset of effect was observed at d29, it remains unlikely that morphological changes would manifest at a later date.

One key reason for the differences in morphological finding between our work, and some of the published literature is that whilst all of the nanomaterials used were classified as nano-silica, they were different sizes, prepared using a different synthesis

method, which invariably leads to variation in final composition and physico-chemical properties. The NM202 used within this research was a standardised representative nanomaterial, as selected by the OECD, and had been through extensive characterisation both by the Joint Research Centre (who produced the particles), and van der Zande *et al* from whose study tissues were harvested (van der Zande *et al.*, 2014a, Rasmussen *et al.*, 2013). It is described as a hydrophilic, pyrogenic synthetic amorphous silica with a primary particle size between 10 and 25 nm, a specific surface area of 200 m²/g, and a purity ≥99.9%. By comparison, the nanoparticles used within the published literature are much larger. For example, Morishita *et al* used silica nanoparticles with a reported particle diameter of 300nm, much larger size than those meeting the EU definition of a nanomaterial, Kim *et al* (2006) used 50nm silica-coated magnetic nanoparticles, Xu *et al* (2014) used 65nm silica nanoparticles, while Ren *et al* (2016) used 57nm silica nanoparticles (Morishita *et al.*, 2012, Kim *et al.*, 2006, Xu *et al.*, 2014, Ren *et al.*, 2016). Without the same nanomaterial from the same production batch being used in other published work, it is difficult to draw any firm conclusions around true comparability and could certainly lead to differences in histopathological outcome following exposure.

Another potential reason for the difference in both our findings and those in the published literature could be related to exposure route: studies reported here used a diverse range of exposure routes from direct testicular injection, through intraperitoneal injection, oral feeding and tracheal perfusion. Additionally, the interaction of nanoparticles with the biological fluids via formation of a 'protein corona' plays an increasingly recognised role in its Adsorption, Distribution, Metabolism and Excretion (ADME) profile, and the protein coronae which form around particles will differ greatly depending on what it comes into contact with i.e. blood, intestinal content, lung mucosa etc (Lundqvist *et al.*, 2008). It is beyond the scope of this thesis to provide further investigation of these effects; however, it is pertinent to recognise their importance.

All animals exposed to nanoparticulate silver exhibited adverse morphological changes, but the detail of these changes was material dependent and subtly different between each nanoparticle exposure (Table 39). In all silver exposed animals, there were areas of

clear focal dysmorphism and disorganisation of tubular content. Tubular degeneration (& atrophy) is widely recognised as a common manifestation of toxicological injury in the testis, which can be mediated through Germ cell or Sertoli cell injury, hormone disruption or vascular effects (Creasy et al., 2012). As in many tubules Sertoli cells appeared to be intact and regular in appearance, and there was little further evidence of vascular injury, it is possible that this was mediated through hormonal influence.

Within degenerative tubules, pyknotic nuclei were present, indicating cells undergoing rapid cell death over and above the normal cell attrition that is expected during spermatogenesis. Apoptosis of germ cells is an important function that acts to limit germ cell populations in the testis, with up to 75% of germ cells being discarded through this process to ensure that the resultant spermatozoa are viable (Shaha et al., 2010). Germ cell apoptosis is regulated via a multitude of proteins and enzymes that induce or inhibit the process (Meena et al., 2015). The exact mechanism to trigger apoptosis varies between direct toxicity (germ cell injury) and indirect toxicity (Sertoli cell injury). At the simplest level, it is initiated through two key pathways; the intrinsic mitochondrial pathway which is primarily activated via Mitochondria outer membrane permeabilization proteins Bax and Bcl-xL, and the extrinsic pathway activated via the 'death receptor' FAS (Lee et al., 1997). Downstream, caspases then act as the final executors of apoptosis (Fig. 106). The FAS pathway is utilised by Sertoli cells, activated via the FAS ligand FASL acting on Fas, a transmembrane receptor protein expressed by germ cells (Lee et al., 1997, Creasy et al., 2012). The Bax or Bcl-xL pathways would therefore be routes of apoptotic cell death associated with direct germ cell injury. Yoo *et al* previously reported Fas upregulation and caspase-dependent apoptotic cell death in human liver, breast and lung cell lines following exposure to TiO₂ ENM (Yoo et al., 2012). In addition, adding an antioxidant (N-acetyl-L-cysteine) suppressed upregulation of Fas, activation of Bax and subsequent cell death. Furthermore, Ma *et al* reported activation of apoptotic cell death in a variety of cell types, following exposure to a number of ENM (titanium dioxide, copper, silica dioxide, zinc oxide and CNTs). This included activation of caspase 3/8/9 in testicular Leydig and Sertoli cells (TM3 and TM4) following exposure to silver ENM (Ma and Yang, 2016).

As a next step, it would be interesting to investigate the presence of caspases either via immunoreactivity or PCR, or changes in expression of FAS/Bax (via western blot or PCR) in order to further understand the detail of the effect observed. Nonetheless, the presence of pyknotic nuclei in germ cell populations out with those traditionally expected during germ cell development is a clear indicator that silver nanomaterials have an adverse effect on germ cells in the testis.

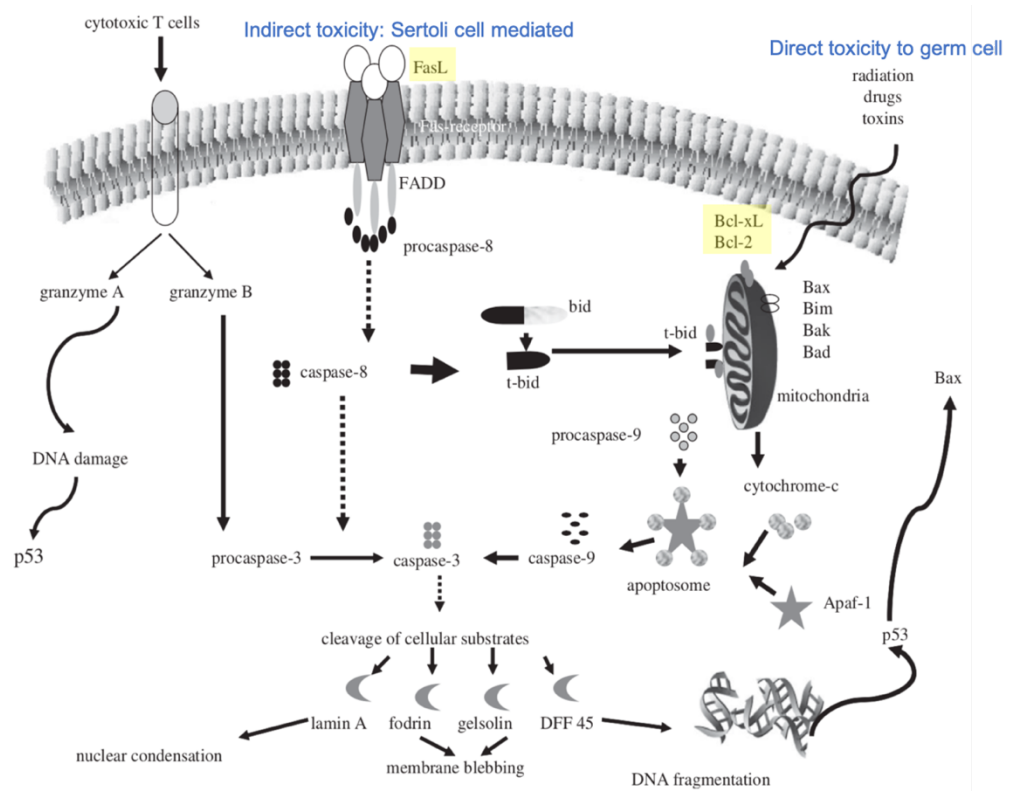


Figure 106: Key apoptotic pathways within cells. Adapted from (Igney and Krammer, 2002).

The presence of sloughing or exfoliation of germ cells into the central lumen of tubules in all animals exposed to nanoparticulate silver, an observation also reported in much of the literature (Sleiman et al., 2013, Thakur et al., 2014, Ahmed et al., 2017), is considered to be a sensitive indicator of spermatogenic disturbance (Creasy et al., 2012). It is acknowledged that in mature animals presence of exfoliated or sloughing of cells into the lumen without seminiferous epithelial architectural disorder (or cell debris in the epididymis, which unfortunately it was not possible to look for as separate epididymal samples were not provided) has been linked to possible handling or fixation artefacts in the literature (Foley, 2001, Creasy et al., 2012). However, it is reasonable to

conclude that this is unlikely to be the case here, as all tissues were fixed simultaneously using the same protocol, and this effect is only seen within treated animals.

Sloughing of cells can be due to a number of processes. Ahmed et al (2018) suggested it could be due to effects of silver nanoparticles on filaments of Sertoli cells, leading to abnormal development in elongating spermatids. Creasy et al (2012) reflect a similar viewpoint, suggesting that in the case of known toxicants like colchicine and carbendazim, extensive sloughing of adluminal germ cells is due to effects on microtubules that form the Sertoli cell cytoplasm (Creasy et al., 2012). Another possibility is disruption to the cytoplasmic syncytium linking developing spermatogonia, leading to early release of developing spermatids. To help understand the effect further it would be interesting to look further into both the microtubules of Sertoli cells, and intercellular bridge formation around developing spermatozoa. A number of possible avenues are available to understand further Sertoli cell cytoskeletal integrity, including visualisation of occludin, ZO-1 or actin-related proteins responsible for cell-cell junction, microtubule and microfilament formation. To investigate intercellular bridge formation around developing spermatozoa, it could be interesting to examine expression of testis-expressed gene 14 (TEX14), which is known to be required for formation of intercellular bridges during meiosis, and kinetochore-microtubules attachment during mitosis (Kim et al., 2015).

Interstitial effects were observed in animals treated with NM-300 and AgNO₃, albeit slightly different in their manifestation and likely origin. NM-300 treated animals had what seemed like inflammatory changes in the tubular interstitium, whilst AgNO₃ treated animals showed evidence of Leydig Cell hyperplasia. Inflammation is typically associated with infiltration of immune cells (macrophages, dendritic cells and T cells), alongside secretion of pro-inflammatory cytokines, or, if localised to around the vascular system it may also be a sign of necrosis. As the changes observed in NM-300 treated animals were not associated with the visible vascular system, it is unlikely to be associated with any vascular injury or necrotic event. Interestingly, Park et al (2010) observed an increase in a panel of inflammatory cytokines following 28 day repeat oral dosing of ICR mice to silver (42nm). It has previously been demonstrated that pro-inflammatory cytokines are able to influence tight junction molecule expression and

distribution, thus increasing the permeability of the BTB (Pérez et al., 2013). Thus, presence of interstitial inflammation could be considered a 'warning sign' of potential tubular effects or BTB damage should inflammation be chronic. In this study we have identified a possible negative endpoint; it would be interesting to investigate the underlying mechanism using a similar cytokine assay on our own tissue to see whether these changes are truly inflammatory in nature.

Occurrence of Leydig cell hyperplasia in AgNO₃ treated animals, while relatively common in some rat strains such as F344, is less frequent in Sprague-Dawley rats (generally <6% of animals), suggesting that this finding was not coincidental (Creasy et al., 2012). Hyperplasia observation was focal in nature, with LCs increased in size and number. Hyperplasia is seen in response to a range of chemically diverse drugs, and is often associated with disruption of the HPG axis, via interference with LC control mechanisms at a variety of points (Creasy et al., 2012). In many cases, LC hyperplasia and later tumorigenesis is associated with high circulating levels of LH, which causes LC mitosis, hyperplasia and eventually adenoma. However, a similar effect may be achieved through disruption of intratesticular testosterone or other hormones in the HPG, affecting paracrine feedback on LC proliferation (Creasy et al., 2012). To further investigate its causality through future study, a measurement of circulating hormones in treated animals at the start and end of dosing, and after a 6-week wash-out would be required.

Interestingly, NM-300 was also the only treatment in which multinucleated giant cells were identified. Giant cells are usually made up of round spermatids or pachytene spermatocytes fused together into a large cell in response to infection or foreign bodies, and often alongside more widely observed tubular degeneration. It is believed that these form when cytoplasmic bridges between cells in the syncytium of developing germ cells are damaged and open, allowing cytoplasmic fusion and a slow form of cell death, although they are usually TUNEL negative indicating DNA remains intact within (Creasy et al., 2012, Creasy et al., 2014b). Giant cells are often more prevalent in immature animals, and as these rats were peri-pubertal it is worth considering whether their presence was linked to the animals' age, although as no such bodies were seen in control animals it is likely this could be a treatment effect. The giant cells observed do not show

signs of acrosomal cap adherence, as is often seen when round spermatids are involved (Singh and Abe, 1987). Because only 1 testis from each animal was obtained, it is not possible to comment on whether this finding is unilateral or bilateral. However, as germ cell degeneration was present throughout all sections, this may be seen as a further generalised indicator of toxicity to the testis following NM-300 exposure.

In Nano Amor treated animals, tubules with dilated luminal volume were observed. Within affected tubules, a normal but compressed compliment of germ cells was present. According to Creasy et al, such dilation may be due to “decreased reabsorption of fluid in the efferent ducts, efferent duct blockage, decreased emptying of fluid from the seminiferous tubules, or increased production of seminiferous tubule fluid by the Sertoli cells” (Creasy et al., 2014a). Creasy *et al* go on to state that tubular dilation is reported in a number of chemicals including the fungicide carbendazim, leukotriene inhibitors and endothelin antagonists. Dilation being caused by decreased emptying of seminiferous tubules or efferent duct blockage is corroborated by the observation of step 11 elongating spermatids sloughed from the germ cell layer being retained in the tubular lumen of a stage XIV tubule. Creasy et al (2014a) go on to comment that dilation is usually seen as a precursor of complete tubular atrophy, as was observed in AgNO₃ treated animals. Thus, it may be that had examination of Nano Amor treated animals been undertaken following a longer period of wash-out, more tubules devoid of a germ cell layer would have been observed.

In AgNO₃ treated animals, tubules were visible which had undergone complete germ cell layer atrophy, being lined only by Sertoli cells (Sertoli Cell Only or SCO tubules). Although SCO tubules can occur as an incidental finding in mice and rats at all ages (Creasy et al., 2012, Foley, 2001), no SCO tubules were observed in control animals, and it is considered an end-stage lesion and has previously been reported as a common outcome following exposure to known reproductive toxicants such as phthalates (Hutchison et al., 2008). For this reason, it is a notable finding and contributes to the emerging picture of silver nanoparticulate toxicity to the testis, especially when considering that the dilated tubular lumens seen in Nano Amor treated animals would likely also develop into SCO tubules.

The final noteworthy finding in silver exposed animals was that of mature spermatid (step 19) retention in stage IX and X tubules within animals exposed to NM-300. Under normal circumstances, step 19 spermatids are released from the germ cell syncytium during stage VIII of the spermatogenic cycle. Retention of spermatids is therefore an indicator of some failure in spermiation. Retained spermatids are usually pulled to the basal cytoplasm of tubules and phagocytosed by Sertoli cells, therefore retention is usually seen as a morphologically subtle but important finding, exactly as reported in the findings of the current chapter (Creasy et al., 2014c). Retention may be due to disturbances in Sertoli cells, reduced testosterone levels (as spermiation is testosterone dependent) or abnormalities in germ cell development (Creasy et al., 2012). It often results in reduced epididymal sperm count, increased numbers of sperm abnormalities, and potential effects on fertility (Creasy et al., 2014c). From this study we have reported spermatid retention as a possible marker of toxicity following an ENM exposure. In future studies it would be good to further elucidate the reason for this. Examination of Sertoli cell viability, along with hormonal assays would be a preferred approach, should blood samples or fresh tissue have been available from the animals exposed.

It is important to recognise that whilst many of the published papers examining histopathology following silver nanoparticle exposure note vacuolisation of the seminiferous tubules as an outcome, this was not seen within the present study. Vacuolisation often occurs in the Sertoli cell basal cytoplasm as an early indicator of morphological injury. Creasy et al (2014) note that this phenomenon is usually seen in studies of 28 days or less in duration as a precursor of germ cell degeneration (Creasy et al., 2014d). As the animals in this study were subject to a 28-day exposure followed by 6-week wash out and germ cell degeneration was well established, it is likely that this is why vacuolisation was not observed.

It is notable that some of the morphological changes reported within this chapter are similar to those found in tissues from animals exposed to the known endocrine disruptors phthalates. It would be interesting to look more closely for similarities between the manifestation of their toxicities to see whether any further information or lessons could be brought to the hazard assessment of ENM from phthalates.

In addition to the work undertaken in this study, some of the testicular tissue was also examined for morphological changes at the University of Wageningen using the Johnsen score. This system examines at least 100 seminiferous tubules, grading the level of sperm maturation between 1 and 10 according to the most advanced germ cell present (Table 40). A total score is then determined by dividing the total score by the number of tubules evaluated (Dohle et al., 2012).

Table 40: Johnsen score grading system for testicular morphology

Score	Morphological Identifiers
10	Full spermatogenesis
9	Slightly impaired spermatogenesis, many late spermatids, disorganized epithelium
8	Less than five spermatozoa per tubule, few late spermatids
7	No spermatozoa, no late spermatids, many early spermatids
6	No spermatozoa, no late spermatids, few early spermatids
5	No spermatozoa or spermatids, many spermatocytes
4	No spermatozoa or spermatids, few spermatocytes
3	Spermatogonia only
2	No germinal cells, Sertoli cells only
1	No seminiferous epithelium

From 100 seminiferous tubules counted, Wageningen University's Johnsen score outcomes are outlined alongside the observed % incidence of cells undergoing apoptosis (Table 41) (Bouwmeester, 2014). These results corroborate further our findings, showing both a clear effect on spermatogenesis, increased incidence of apoptotic cells in animals exposed to nanoparticulate vs control.

Table 41: Results of Johnsen scores on spermatogenesis in animals exposed to two types of silver ENM, silver ions and vehicle control. Unpublished data received via personal communication (Bouwmeester and van der Zande, 2015)

Treatment	Johnson score		% of apoptotic cells
	10	9	
Control	100		0
NM-300 (20nm)	36.6	63.4	8.2
Nano Amor (15nm)	25	75	27.6
AgNO3	92.2	7.8	7.6

Semi-quantitative stereological analysis of tissues

Establishment of whether stereological analysis could reveal any measurable changes to the cycle of the seminiferous epithelium indicative of altered function proved to be challenging but ultimately rewarding. Initial analysis of 2,054 measurements of tubule

diameter and germ cell layer thickness measurements revealed no true statistical difference from control day29 or day85 for any treatment. However, re-examining tissue sections from selected treatments (silver only) to take into account tubule stage alongside tubular diameter and lumen volume resulted in not only a useful protocol for further research into the area, but also a clearer picture on the nuances of any effects.

As *Dazl* immunostaining intensity proved to be a useful and accurate indicator of seminiferous tubule stage, and as staining was not affected by any treatment, it was possible to use this to group tubules according to staining intensity (I-IV and XII-XIV show no stain, V, VI, X and XI have a light intensity stain, VII and IX shows a moderate stain and VIII a high intensity of staining). From these groupings, a decision key including key cell populations, morphological and stereological identifiers was then used to assign them to individual stages for stereological analysis. Following initial analysis on comparability of control data, measurements collated from 167 tubules for tubule diameter and lumen volume in control animals was shown to be directly comparable to measurements previously published for Sprague-Dawley rats (Wing and Christensen, 1982). This comparability offered a high level of confidence in its representation of tubule diameter and lumen volume within a healthy population of rats. To our knowledge, this is the first time this hybrid method for staging has been implemented and reported, as no other evidence for it has been identified from the literature. As such, this forms a useful reference methodology by which to undertake future work in the area.

Analysis of tubule diameter using a mixed model revealed no statistical difference between control and treated animals for NM-300, Nano Amor or AgNO₃. Even when analysis was limited to key stages around spermiation (where changes in tubular diameter are known to be greater), no change from control was seen. Based on this, it is possible to suggest that whilst silver nanoparticle exposure produces varied adverse morphological outcomes, there is no change tubule diameter when measured stereologically. This observation aligns with the data reporting that dysmorphia was seen to be focal, as it may be that this type of gross analysis may not be sensitive enough to detect partial changes.

Visual analysis of lumen volume initially suggested some changes from control in certain treatments, with a decrease in lumen volume from stage V – VI in all treated animals that was not present in control, and a higher lumen volume in NM-300 and Nano Amor treated animals around stage VII and VIII than in other treatments or control. However, statistical analysis of the full dataset using a mixed model resulted in non-significant outcomes. More detailed analysis did however reveal some significant stage-specific changes in Nano Amor tubules at stage VII and AgNO₃ tubules at stage IX when compared to control data at the same stage.

Stage VII tubules are in immediate preparation for spermiation, therefore alteration in their stereology at this important point in the spermatogenic cycle could be indicative of problems in the tubule. Interestingly, this finding matches the observation of lumen dilation from the morphological examination of tissues, discussed in the previous section, and adds weight to the argument that Nano Amor causes adverse effects on spermatogenesis in a rodent model. An increase in stage IX lumen volume compared to control in AgNO₃ treated animals may be linked to the morphological observation of tubular atrophy. It would be interesting to cross-examine the two datasets to see whether the observation of tubular atrophy is limited to stage IX tubules in the morphological analysis.

To provide further detail on the observation of germ cell sloughing seen in the initial morphological examination, count data on sloughing of cells from the overall population of tubules examined was produced. This confirmed sloughing to be treatment-associated, being present in none of the control tubules, 11% of AgNO₃ treated animals, and 6% of NM-300 and Nano Amor treated animals. To check that sloughed cells did not interfere with the stereological findings for lumen volume, re-analysis of data corrected for sloughed cell volume was undertaken, confirming that this was not the case. Thus, it is possible to conclude that the germ cell sloughing seen is a focal, treatment-associated effect, and that it does not influence the outcome of stereological measurement of lumen volume.

Finally, to provide reassurance that tubule shape did not interfere with findings, analysis of results was re-run taking into account tubule shape recorded. This confirmed that

although tubule shape was a significant effect, the overall outcome was no different to the previous analysis in terms of significance of difference between control and treated animals.

It is interesting to note at this stage that of the published literature which mentioned morphometric or stereological measurements as part of its analysis (Sleiman et al., 2013, Rezazadeh-Reyhani et al., 2015, Bara et al., 2018, Garcia et al., 2014) that none appeared to take into consideration tubule stage in interpreting the results. Creasy considers that the ability to identify tubular stages to be essential in undertaking a sensitive examination of testicular histopathology (Creasy, 1997). Indeed, OECD test guidelines 421 and 422 (relating to reproduction/developmental toxicity screening test and the combined repeated dose toxicity study with the reproductive/developmental toxicity screening test) state that *“detailed histological examination should be performed on the ovaries, testes and epididymides (with special emphasis on stages of spermatogenesis and histopathology of interstitial testicular cell structure) of the animals of the highest dose group and the control group”*, although tubular staging is not mentioned in TG416, the 2 generation reproductive toxicity study, or TG433, the extended one-generation reproductive toxicity study (OECD, 1983, OECD, 2015, OECD, 2001, OECD, 2011). In addition, the ICH S5 for evaluation of DART in pharmaceuticals states that *“A detailed qualitative microscopic evaluation with awareness of the spermatogenic cycle is sufficient to detect effects on spermatogenesis. A quantitative analysis of spermatogenic stages (i.e., staging) is not generally recommended but can be useful to further characterize any identified effects.”*, but there is a lack of guidance as to how to undertake such an evaluation (EMA, 2017). Creasy recommends that as a minimum, morphological examination alongside semi-quantitative inspection of tubular diameter or cell counts of individual cell populations (with a minimum replicate number of 10-15 tubules for tubular diameter or 10 tubules for cell population counts where there are 10 rats in a group) should be undertaken (Creasy, 1997). Based on this, and my own findings within this chapter, it would be possible to question the accuracy of the outcomes described within much of the literature where stereological analysis was reported. Rather though, this serves to highlight the robustness of the analysis

undertaken within this study; to our knowledge this is the first time such a detailed evaluation has been completed in the area.

Functional analysis of tissues following ENM exposure via Immunohistochemistry

To explore the potential for ENM exposure to interfere with the steroidogenic pathway or other elements of the HPG axis, immunohistochemical staining for a number of important enzymes, receptors and proteins was undertaken. The results are discussed, alongside an evaluation against findings *in vitro* for comparability.

The first to be examined was 3 β -HSD, an enzyme involved in the conversion of pregnenolone to testosterone within the smooth endoplasmic reticulum of the Leydig cell. Whilst good staining of Leydig cells was observed in all samples, some non-specific staining was present in all sections. Such high background staining could be due to a number of possible factors, including slide preparation, peroxidase quenching, the biotin block applied, the serum block, inadequate washing or indeed the primary and secondary antibodies used. As a uniform approach was used to all IHC and almost all other tissues were successful, it could be speculated that the primary antibody being sub-optimal for this approach is the most likely explanation. However, the presence of relatively uniform moderate staining intensity across Leydig cell populations indicates that 3 β -HSD was present and therefore that its expression was not hugely affected by nanoparticle exposure.

Luteinising hormone receptor expression appeared to have a comparable moderate to intense staining level across control, Nano Amor and AgNO₃ treated animals, with a lesser intensity of staining being present on NM-300 treated samples. Its expression also appeared to be unaffected by dysmorphism following silver exposure, as clear LH-R staining was present in Leydig cells surrounding morphologically abnormal tubules. As such, it could be considered that luteinising hormone receptor expression was not hugely affected by any silver treatment bar NM-300, and that in theory LH stimulation from the anterior pituitary would therefore be successful in commencing production of androgens. The slightly lowered expression of LH-R within NM-300 exposed animals indicates a potential knock-on effect on steroidogenesis and subsequent production of viable sperm. In addition, a lack of LH-R would lead to a downstream loss of negative

feedback to the pituitary to reduce LH production, potentially interfering with the overall HPG axis.

Bara *et al* reported no change in LH-R expression of offspring following zinc oxide ENM exposure *in utero*, but a decrease in LH-R expression following exposure to silica under the same conditions (Bara et al., 2018). No studies reporting LH-R expression following silver ENM exposure were identified. Interestingly, the results of PCR on Leydig cells treated with NM-300 *in vitro* indicated an increase in LH-R expression compared to control. With variability like this reported, it is possible that effects on the LH-R may be ENM specific due to differing physico-chemical parameters. In our case, it may also be possible that the discrepancy between what we observed *in vivo* and *in vitro* is due to the isolated nature of TM3 cells in culture. It would be relevant and important to investigate ENM effects on Leydig cells as part of a co-culture system in future to see if better comparability could be achieved *in vitro* to *in vivo*.

Androgen Receptor immunohistochemistry revealed moderate to intense staining in both control and treated animals. In principle, this indicates that treatment with silver nanoparticles or ions does not prevent Sertoli cells from responding to testosterone released from Leydig cells and thus should be able to support spermatogenesis. The only published literature examining AR expression following ENM exposure was that of Jia *et al*, which reported no change in AR expression within male mice following TiO₂ exposure to 25nm TiO₂ at 10, 50 or 250 mg/kg for 42 days spanning puberty (Jia et al., 2014). However, this result is for a different ENM, and the results of the western blots used to determine protein expression *in vitro* within chapter 4 indicate a potential increase in AR expression on TM3 Leydig cells.

One potential reason for the disparity in results was that this particular IHC staining protocol was one of the hardest to optimise. Despite several attempts with slight adjustments to antibody incubation times, washes and blocking, a lengthened DAB development time of 9 minutes was required in order to see any Sertoli cell specific staining. Unfortunately, this also led to a high level of background stain. As such it is reasonable to suggest that the primary antibody used in this instance was not ideal for this particular application, despite it being sold as suitable for IHC in rodents in principle.

In addition, the issues previously reported with Western Blotting make it difficult to reach an informed conclusion on biological reasons for this difference. It would be interesting to repeat this work with an alternative AR antibody to see whether more conclusive results could be found.

As a key rate-limiting step in steroidogenesis, immunostaining with StaR reveals much about the testis' ability to convert cholesterol to testosterone (via pregnenolone) within Leydig cells. The presence of increased intensity of cytoplasmic staining within Leydig cells of all treated animals compared to controls, indicates that StaR was present and likely able to mediate the transfer of cholesterol from the outer mitochondrial membrane to inner mitochondrial membrane for conversion to pregnenolone. A comparable finding of StaR upregulation following silver NM-300 exposure was recorded *in vitro* using PCR analysis (Chapter 4).

StaR expression is widely accepted as being regulated by the cAMP/PKA signalling cascade; however, cAMP/PKA-independent events have also been shown to play a role in regulation of StaR. For example, growth factors, macrophage derived factors, chloride ions, calcium messenger systems and macrophage-derived factors have all been shown to enhance StaR expression independently of cAMP/PKA (Manna et al., 2016). Upregulation of StaR expression has previously been linked to excessive production of free radicals and reactive oxygen species, although the exact method of upregulation may vary (Manna et al., 2016). Long term potentiation of StaR expression could lead to excessive cholesterol transport within cells, almost causing a 'bottle neck' for its subsequent conversion to pregnenolone by P450_{scc}, or further down the pathway to testosterone production.

PCR analysis within chapter 4 indicated CYP11A1, the gene encoding P450_{scc} may also be upregulated by exposure to NM-300 silver ENM, a finding which is echoed within published work reporting exposures to neonatal and adult rodents *in vivo*. For example, Garcia *et al* observed an increased in CYP11A1 expression following IV injection of 1mg/kg bodyweight silver ENM to CD-1 mice over 12 days (Garcia et al., 2014). Similarly, following intraperitoneal exposure of neonatal ICR mice from postnatal

day 8-15, Zhang *et al* recorded upregulation of CYP11A1 (Zhang et al., 2015a, Garcia et al., 2014).

A question may then be posed about changes in production of subsequent enzymes involved in the conversion of pregnenolone to testosterone, and where a bottle-neck would appear should one form. It would be interesting to examine P450_{scc} expression within the tissue samples to deduce whether this upregulation in expression seen *in vitro* was mirrored *in vivo*.

Interestingly, Garcia *et al* reported a concomitant increase in CYP11A1 and 3 β -HSD expression following IV exposure to silver ENM (summarised previously within this chapter), but no change in expression of genes involved in cholesterol synthesis from intracellular lipids (HMGCR), *de novo* cholesterol synthesis (HMGCS), cholesterol transfer across the mitochondrial border (StaR and Tspo – mitochondrial translator protein), or enzymes involved in conversion of cholesterol to testosterone (CYP17A1, CYP19A1 and 17 β -HSD) (Garcia et al., 2014). This indicates that there may well be a bottle-neck in synthesis of testosterone following upregulation of P450_{scc}. As initial IHC work undertaken for this thesis indicated 3 β -HSD expression did not appear to be changed, time and funding permitting, it would also be interesting to re-visit IHC for 3 β -HSD and other key enzymes above involved in testosterone synthesis on the tissues available, alongside examining its expression in TM3 cells *in vitro* using further PCR. The only enzyme it would not be possible to examine through TM3 cells is 17 β -HSD, as it has been shown clearly that this is not expressed within this cell line, or other representative cell lines (Engeli et al., 2018).

Y chromosomal DAZ (deleted in azoospermia) and its autosomal homologue *Dazl* (deleted in azoospermia-like) genes are exclusively expressed in germ cells, and are considered to be crucial to achievement and maintenance of spermatogenesis (Rocchietti-March et al., 2000). Using *Dazl* expression to assist with staging of tubules was unhampered by morphological changes following nanomaterial exposure, unless germ cells were missing altogether from tubules. It is notable that despite *Dazl* expression being seemingly unchanged by silver ENM exposure in this experiment, Ahmed *et al* reported a down-regulation of *Dazl* in albino rats exposed to silver

nanoparticles over 28 days at a dose of 100mg/kg/day (Ahmed et al., 2017). Following our observation of sertoli cell only (SCO) tubule formation in AgNO₃ treated animals, presence of lumen dilation in Nano Amor treated animals, alongside our previous comments on the fact that SCO tubules are an end-stage lesion, and knowledge that silver ENM are retained in the testis for long periods of time, it would be interesting in a future study to look at whether extending the wash-out period of animals post exposure before examination would result in i) a higher incidence of SCO tubules, and ii) any associated down-regulation of *Dazl*.

Following the observation of cell populations within the central lumen of some tubules, one explanatory avenue considered was whether any infiltration of immune cells into the testicular area had occurred. This was considered as some sloughed cells present within the tubular lumen appeared to have masses within them that appeared similar to the lobular nuclei seen within mature neutrophils.

Unlike macrophages, eosinophils and dendritic cells which are found in varying numbers in the seminiferous tubule interstitium, granulocytic neutrophils are not found in the rodent testis under normal conditions. However, they play an important part in the body's response to infection or damage and their presence would be an indicator that the animals' immune systems were attempting to respond to presence of something potentially harmful. As the testicular tubules themselves are an immune privileged site, the body's 'normal' immune system cells being kept outside of tubules by the blood-testis barrier to prevent autoimmune response to the immunogenic spermatids being triggered, the presence of any immune cells within tubules themselves would be a sign the BTB itself had become compromised in some way.

IHC for RP-1 showed no specific localisation, indicating that this particular immune cell type was not present within the tissue samples, or that the antibody was not optimal for this application (indeed, its producer BD Pharmingen suggests a slight variant on the antibody that was available to me for optimal immunohistochemical staining). However, it may be possible that other immune cells were present, particularly in light of the inflammation noted around tubules in NM-300 and AgNO₃ treated animals. Alternative antibodies would be required to investigate this further.

It is worth recognising that despite morphological changes in silver ENM exposed animals being widespread, their focal nature could well mean that no drastic change in overall expression of proteins, enzymes and hormones related to normal testicular physiology would be evident. As much of the dysmorphism observed was interspersed with areas of tissue that were completely normal in appearance, it is highly possible that this is the case here. It is also worth noting that focal morphological changes are a well-recognised trait in many reproductive toxicants. For example, known endocrine disruptors such as phthalates have been shown to result in a clear pattern of focal dysgenesis within testicular tissue, with varying impacts on fertility depending on severity and spread of the dysmorphic areas (Hutchison et al., 2008).

Conclusions, Future thoughts and ideas

The changes described within tissues from animals exposed *in vivo* makes a clear case for ENM being causative of adverse effects on the testis. There are a number of areas for further investigation which would be well worth pursuing.

Initially, in order to generate a full complement of data for comparison to *in vitro* work, it would be useful to complete IHC analysis on tissues from silica treated animals. A further set of testicular tissues procured from animals exposed to nano copper oxide via a short-term inhalation protocol were also obtained during the course of this work. In order to compare effects *in vivo* to those generated from exposing cell lines to CuO *in vitro*, morphological, stereological and immunohistochemical analysis of these tissues would be required.

To further understand effects of *in vivo* ENM exposure on Sertoli and Leydig cell structure and function, further IHC could be planned using antibodies as markers of cellular integrity, cytostructure and microfilament structure (such as vimentin, occludin, ZO-1, actin-related proteins, or testis-expressed gene 14 TEX14, as discussed previously). As the inflammation noted in some tissue samples is often associated with immune system influx (as discussed previously). Should investigation of cellular integrity provide further evidence for injury to the BTB, the risk of autoimmune action on developing spermatozoa, or adhesion of antibodies to the sperm surface that prevent it

fusing with an oocyte would be much higher. It would therefore be important to in more detail at additional IHC markers for components of the immune system.

The identification of pyknotic nuclei in many of the treated testicular samples indicated apoptosis was ongoing. To further understand the extent of apoptotic changes, the dead-end TUNEL assay could be used. Further understanding of the mechanism by which apoptosis was ongoing could then be considered using caspase assays (via confocal microscopy), or further IHC staining for Bax or FAS. Additionally, as much of the published work indicates the major role oxidative stress and inflammation hold in mediating ENM toxicity at the cellular level, it would be interesting to investigate markers of oxidative stress (GSH, GPx, Lipid Peroxidase etc.), and cytokines and myeloperoxidase activity as inflammatory biomarkers.

Working in such a heavily regulated system, it also is important to explore further endpoints to see whether the effects at cellular level appear to be from toxicity or endocrine disruption. As a fundamental theme throughout this thesis, and being key to spermatogenesis and general testicular health, it would be pertinent as a next step to explore hormone circulation to look for potential effects on steroid hormones and the HPG axis. It is for this reason that many of the published papers in the area focus on measuring circulating hormone levels. It is important to note here that the levels of testosterone in the testis are often many-fold higher than in the systemic circulation, and the two values are not necessarily strictly correlated (Creasy and Chapin, 2013). Thus, measuring intratesticular alongside systemic hormone levels would be an optimal approach.

In future work, systemic hormone levels could be measured via serum or blood collection, while testicular hormone levels could be undertaken via homogenisation of testicular tissue, both of which would be followed by ELISA, Radio Immunoassay or mass spectrometry. If it had been possible to influence this aspect of the original animal studies used in this chapter of research, collection of both blood and fresh testicular tissue from the animals used in this work would have been ideal in order to understand clearly the effect of ENM exposure on systemic and local hormone levels. Changes in

circulating or local hormone levels would provide a useful indicator as to the involvement of endocrine disruption in the effects seen.

Finally, it is important to recognise that not all mechanistic changes lead to phenotypic alterations. For example, sperm number may drop without any change to sperm function (leading to almost no change in fertility), conversely sperm number could be unaltered, while incidence of abnormalities rises (leading to sub-fertility). For this reason, it would be important in future work to include examination of sperm as the final endpoint for male reproductive function. The current study used only one testicle provided from each animal; any future work could easily include either use of the other testicle to examine sperm or use of the epididymis of the same testicle for the same.

Analysis of epididymal morphology (prepared using Bouins fixative to preserve structure) can provide an initial indication of ENM effects on spermatozoa. Investigation of sperm motility is possible via simple analysis using a haemocytometer, or more comprehensive computer assisted sperm analysis (CASA). Morphology of sperm can be examined using Eosin Y staining, and evaluation of DNA fragmentation in sperm heads could be achieved using flow cytometry of acridine orange stained samples.

Chapter 6: Discussion

The purpose of this thesis was to investigate the toxicity of ENM to the male reproductive system with a focus on development of non-animal testing approaches in line with the 3Rs principle. Using a panel of commonly used reference engineered nanomaterials, alongside some highly relevant commercially available materials, the research aimed to: i) establish suitable assays for screening ENM for cytotoxicity and the effects of time- and dose- on effect; ii) investigate functional cellular parameters relevant to fertility and endocrine health, iii) examine in detail morphological and functional markers of effect in tissues from animals exposed to some of the same ENM, and iv) compare results generated *in vitro* to those *in vivo* to guide a decision on the suitability of *in vitro* testing to predict outcomes *in vivo*. The overall objective was therefore to take initial steps in formation of an integrated approach to testing and assessment (IATA) for male DART following exposure to nanomaterials.

Establishing suitable assays for high-throughput screening of ENM cytotoxicity

The first step in achieving these objectives was to establish reliable and reproducible assays by which to screen ENM for toxicity *in vitro*, including consideration of potential for interference from ENM. The cytotoxicity assay (WST-1) was optimised and shown to be both reliable and reproducible in this respect for short term exposures, an outcome that is in agreement with another recently published appraisal using different ENM (Mannerström et al., 2016). The timecourse toxicity assay (Alamar Blue) clearly revealed the importance of exposure time *in vitro* in driving effect and was again shown to be suitable for use with ENM for short term exposures with some caveats, including the use of robust controls to identify ENM-specific interference. To validate this assay further, it would be useful to investigate further the influence of the highly reduced form of resazurin on the assay's output, in order to provide further confidence in results generated.

Following from these findings using TM3 and TM4 cells, it would next be interesting to establish relative responses to the same panel of ENM from other available male

reproductive cell lines (Mlhc-1, MA-10 etc), to check further for reproducibility of the assays established, comparability of results, and to open opportunities to identify cells that have appropriate endocrine genes for further functional assessment. This would help to produce a reliable benchmark against which to compare findings for cytotoxicity of other ENM, helping to resolve one aspect of observed variability between studies.

Importantly, results from the assays established within this research were also compared to those from other cell lines from a further nine cellular models (representing 6 organs within the body) for six of the ENM tested (Farcal et al., 2015). Results from the male testicular cell lines TM3 and TM4 were found to be generally comparable with outcomes reported from 7/9 cell lines for TiO₂ (NM-103 & 104), 5/6 cell lines reported for ZnO (NM-110 & 111), and 3/5 cell lines reported for SiO₂ (NM-200 & 203). Any differences in results stemmed from lung macrophage (Raw 264.7 and MH-S mouse alveolar macrophages) and embryonic cell lines (NIH/3T3 & mES cells), both of which appeared to be highly sensitive to challenge from ENM. This further emphasises the importance of considering a panel of cell lines of varying sensitivity in future toxicity assessments. It also highlights the potential for ENM with varying characteristics (manufacturing technique, physical form, coating, size) to generate differing outcomes from toxicity tests. This was, to our knowledge, the first time such comparative work had been undertaken, and it was very encouraging to see so much general agreement amongst datasets.

A number of important considerations for future *in vitro* assays contributing to hazard assessment of ENM were highlighted through the present study. The first is to establish whether ENM may interfere with the assay being used, especially in the case of those reliant on optical readings. The second is to elucidate whether the actual dose delivered to cells reflects that added to the test system, as highlighted by Cohen et al (2014), and from observations on the apparent sedimentation of CNTs on top of cells highlighted in the present research (Cohen et al., 2014). Third, for all metallic ENM, the role of ionic dissolution and further transformation of ENM in biological media must be considered, and relevant ionic controls built into any research planned. Fourth, as highlighted from the results of assays using NM-300, consideration of whether transformation of ENM in biological media results in altered behaviour is recommended, something which may be

directly linked to the question of whether 'aged' ENM (later in their life-cycle) behave differently to pristine ENM. At the most basic level, building in robust ionic controls for all metallic ENM into future studies is strongly recommended. In addition, use of both 'pristine' and 'aged' ENM which have either been in storage (for colloids especially) and/or in biological media for some time may be important. Thorough physico-chemical characterisation of materials available would assist with many of these issues. At the most basic level, for metallic ENM, characterisation of the percentage of dissolution of ions within the exposure medium before and during any experiment undertaken would be highly useful. This requires a multidisciplinary approach to be applied to hazard testing, but such information allows for a fuller understanding of the results from each assay.

Application of these considerations in future work will not only allow for greater confidence in results generated, but ultimately also contribute to building robustly validated rankings of materials, for example via comparison of the same material with differing physico-chemical properties (as reported here), or through comparing the same material through stages of its life-cycle.

Evaluation of cellular parameters related to fertility and endocrine function

Loss of viability in TM3 and TM4 cells was established following exposure to a sub-set of the ENM panel. Knowing that metabolic activity was affected, consideration of whether ENM exposure led to effects on cell related to fertility and endocrine function was then undertaken. At a transcriptional level, it was demonstrated that genes related to Leydig Cell function and its important role in steroidogenesis from cholesterol may be interrupted or altered. It was possible to identify via measurement of protein expression that the TM3 cell expresses androgen receptor, confirming that TM3 is both potentially responsive to stimulation with testosterone *in vitro*. Protein expression work also confirmed that exposure to ENM altered both the ability of TM3 and TM4 express AR.

It is important to recognise that the data reported for RNA and protein expression was very much from a time-limited pilot dataset. As a next step, further work to optimise the assays used to determine protein expression should be undertaken. In this, it would be

important to include a wider panel of protein antibodies, reflective of the genes investigated via RNA analysis in future work (using different antibodies where those selected previously were shown to be ineffective). Once established, expansion of protein expression analysis to a wider panel of testicular Leydig cell lines would not only contribute toward development of reliable and reproducible approaches to measuring protein expression across the panel, but also enable robust comparison between results generated. In line with previous comments, this may also contribute to identification of a cell line with additional appropriate genes for a more extensive endocrine assessment.

Together, these findings are important as they add to previous work which has suggested a potential role for ENM as endocrine disruptors, clearly warranting a more thorough analysis with a wider panel ENM, genes/proteins and cells. Two potentially important genes involved in the management of steroidogenesis to include alongside LHR, StaR, CYP11A1 and 3 β -HSD could be i) 17 β -HSD, as the enzyme responsible for final conversion of androstenedione (AD) to testosterone, and ii) INSL-3, a hormone which has been identified as a potentially important new diagnostic tool in identifying late-onset hypogonadism, as it plays an interesting role in modulation of steroidogenesis following LHR stimulation but is not directly influenced by the trophic drive of the HPG axis (Ivell and Anand-Ivell, 2009, Ivell et al., 2014). In implementing this, it is important to note that at the current time, none of the commonly used murine LC lines are capable of converting exogenous AD to T, most likely because they do not express the variant of 17 β -HSD required to do so (Engeli et al., 2018).

It has been reported that both that MA-10 and mLTC-1 LC lines are capable of producing progesterone, which accords with observations of high progesterone production in the original tumour from which they are derived (Odermatt et al., 2016). This may make it possible to measure progesterone as an indicator of whether ENM interfere with the initial steps in steroidogenesis by interference with LHR, cAMP and PKA dependent signalling, or direct inhibition of StaR, CYP11a1 or 3 β -HSD. This would preferably be achieved via mass spectrometry (GC-MS/MS or LC-MS/MS), which has been shown to be both more sensitive and reliable than RIA- or ELISA- based methods (Stanczyk et al., 2007). Such interference has already been demonstrated for other ED chemicals such as bisphenol-A using MA-10 cells, and the TM3 cell line is frequently used to study the

impact of environmental pollutants and EDs such as diethylstilbestrol on steroidogenesis (Odermatt et al., 2016). A remaining problem based on the available evidence is that evaluation of ENM interference with later stages of steroidogenesis is not currently possible. To overcome this issue, it may therefore be necessary to undertake future work using primary cells isolated from rodent testicular tissue. If this were the case, not only could RNA expression and protein expression be measured, but it would be possible to use hormone assays to establish whether exposure to ENM altered actual production of Testosterone or Inhibin by LC and SC respectively.

It would also be possible at this stage to expand the panel of Sertoli cells to provide a more complete understanding of the effects of ENM exposure on SC function, via measurement of selected genes related to i) endocrine function and ii) cytoskeletal integrity and thus BTB function. Endocrine function could be indicated by measurement of Inhibin (to investigate ability of the SC to feedback on FSH secretion) and androgen binding protein (ABP, which has a role in managing germ cell development). BTB integrity could be investigated by measuring ZO-1, Occludin or other actin-related proteins. To make analysis of BTB interference more robust, inclusion of measurement of transmembrane electrical resistance (TEER), could also be considered, on the basis that if TEER is reduced significantly following exposure, the BTB may be compromised.

Although out with the scope of the current research, in future it would also be important to build understanding of the MoA by which ENM may be eliciting effects, for both cell lines. Addition of assay/s measuring endpoints relative to reactive oxygen species generation, oxidative stress and apoptotic pathway activation would be relevant and justified. This would help in particular with comparison of results *in vitro* to *in vivo*.

With the knowledge that ENM have the potential to disrupt endocrine production and signalling, development of biologically-relevant models to establish endocrine disruption potential from ENM exposure is important. These could be undertaken through a number of different approaches. The most simplistic would be to apply media from ENM treated LC (potentially containing signalling molecules released from the cells) to TM4 cells, and measurement of relevant gene expression (outlined above). Another approach would be to use a 3D co-culture model, incorporating LC and SC

alongside germ cells. Development of such co-culture systems has already been reported using primary cells isolated from immature rats (Wegner et al., 2013). Some researchers have attempted to overcome the obvious requirement for animal sacrifice in primary cell culture through co-culturing TM3 LC and TM4 SC lines, alongside the germ cell line C18-4, isolated from Balb/c mice (Yin et al., 2017). However, in relation to evaluation of endocrine endpoints the obvious limitation of this is the fact that LC are unlikely to be able to produce T / DHT, at least via its principal pathway of synthesis.

Another possible route by which endocrine signalling between cell types could be considered is through use of microfluidic 'endocrine system on a chip' models. One such model, developed by Nguyen et al (2017), used a co-culture microfluidic system containing intestinal-pancreatic cells to measure the effect of glucose on production of glucagon-like peptide-1 (GLP-1) from the intestinal L-cell line (GLUTag) and insulin from the pancreatic β -cell line (INS-1), with the future aim of using the system to screen drugs for the treatment of diabetes (Nguyen et al., 2017). Modelling using key cells from the male reproductive system and associated organs in the endocrine feedback loops that control it (e.g. pituitary & hypothalamic cells) comes with many challenges, the most obvious being identification of cell lines which are fully active in terms of hormone production and response, identification of a suitable medium that provides appropriate nourishment for each organ on the system, and provision of necessary substrates for production of signalling molecules by the cells in culture (Eddie et al., 2014).

An over-arching consideration in interpretation of results (both *in vitro* and *in vivo*) is the interaction of ENM with the biological environment into which they enter, formation of a dynamic biocorona and its subsequent influence on observed effect. Lai *et al* (2017) investigated interaction of gold and silver ENM with human plasma. They identified over 300 individual proteins on the coronae, of which >80% of which was comprised of the 20 most abundant biological proteins known (Lai et al., 2017). Through their analysis, they were able to elucidate that differing ENM characteristics such as surface charge and core material played a significant role in determining bio-corona composition. Likewise, the net charge of protein molecules also influenced their interaction with ENM. Such observations imply that it is entirely possible effects of ENM may be altered significantly by their bio-coronae. It is unlikely that any biocorona formed in cell culture

be the same as that formed *in vivo*, bringing into question how this influence could potentially be managed when comparing results *in vitro* to those *in vivo*.

An alternative consideration relating to the interaction of ENM with their surroundings in biological environments is the potential for ENM to interact with biological molecules and in turn, interfere with their ability to interact with one another e.g. signalling molecules with their receptors, or antibodies with proteins of interest in an assay. Noteworthy in consideration of this paradigm is the work of Findlay et al (2017), who demonstrated that carbon nanoparticles inhibit the antimicrobial activity of human cathelicidin peptide LL-37 even at low concentrations of exposure (Findlay et al., 2017). On examination of the underlying MoA, they identified that carbon NP were able to not only bind to LL-37 (observed via a change in aerodynamic diameter), but that once adsorbed to the surface they caused a change in structure of the peptide and associated loss of antimicrobial action. The authors also hypothesised that this NP-peptide interaction may have been one of the reasons for a loss of physically detectable peptide in some of the assays they conducted, a consideration which could also be applied to the protein detection work undertaken in the current research.

Based on the above, in relation to investigation of endocrine disruption events following ENM exposure, it could therefore be hypothesised that ENM-biomolecule interactions may either i) interact with proteins at hormone-active sites to influence hormone binding, ii) interact directly with hormones to alter them in some way, potentially leading to decreased (or increased) activity at their targets, or even iii) attach to hormones and other relevant molecules and 'piggy-back' around the body, adding further complexity to understanding their biokinetics (as from this study it was possible to demonstrate that following oral exposure, ENM translocate from the GI tract to testis, amongst other organs). As ENM interactions with biological molecules and bio-corona formation will no doubt differ *in vitro* and *in vivo*, these reflections bring forward a multitude of further questions which are not possible to answer at the current time, but which must be continually revisited and reconsidered as the field of research develops.

These considerations not only demonstrate the huge value of *in vitro* work which may be used to establish better understanding of ENM effects and interactions with the male

reproductive system, but also highlight the currently remaining requirement for the downstream use of animal models in establishing DART for ENM.

Histological appraisal of relevant fertility & endocrine endpoints in animals exposed to ENM *in vivo*

Detailed examination of morphological and functional markers of effect in tissues from animals exposed orally over 28-days to a sub-set of the ENM panel first and foremost led to development of a new methodology for staging of testicular tissue in toxicity studies. The hybrid technique combined Dazl immunostaining (to quickly allow grouping of seminiferous tubule stage) with a decision key (incorporating key cell populations, morphological and stereological identifiers) to assign individual stage. This technique may be applied easily and ensures a high level of accuracy in determining tubule stage without necessarily requiring the many years of experience usually needed to undertake such an evaluation. Importantly, this approach allowed consideration of tubule stage to be taken into account more readily when undertaking histopathological analysis, something which the author and others have found to be key in the correct interpretation of stereological and morphological evaluations. It is strongly recommended that this robust approach is applied in research pertaining to appraisal of testicular histopathology.

Such considerations are under-recognised in both published nanotoxicology research, and within the test guidelines themselves (for all industries). A further major recommendation arising from this research is to ensure consideration of tubule stage in appraising histopathological endpoints in the testis, and that not only the importance of tubule stage be recognised in test guidelines for DART testing in industrial or pharmaceutical settings, but that further guidance for its application and interpretation be provided.

A third important outcome of this work was the appraisal of morphological and stereological impact of ENM exposure to testicular tissue following a 28-day oral exposure regimen, which to our knowledge was achieved a level of detail far greater than any previously described.

Interestingly, through this evaluation it was possible to demonstrate clearly that those animals exposed to silica dioxide showed no unfavourable morphological outcomes, a finding that was in agreement with the work *in vitro*, but not in all published literature *in vivo*. Further examination of the evidence suggested that this was due to a combination of factors, including physical characteristics of the ENM reported & the fact that many used were not technically ENM at all owing to their larger sizes, the doses administered, exposure routes used and associated differences in ADME/toxicokinetic profile that followed.

It was possible to confirm that all animals treated with silver suffered adverse changes within their testicular tissue following exposure, which were maintained even after a 6-week period of wash out, a finding which aligns completely with both that of van der Zande et al (2012), who confirmed that silver ENM accumulated in the testis and were not excreted following this recovery period, and our own findings *in vitro* (van der Zande et al., 2012). Stereological analysis showed no alteration in tubule diameter with stage following exposure to ENM, indicating that at a structural level there was no link between tubule diameter and effect observed. However, it was possible to identify some very specific changes in lumen volume. These included increases compared to control for stage VII tubules in Nano Amor treated animals, and an increase in volume for stage IX tubules in treated animals, both of which indicate potential disruption of tubules associated with spermiation (stage VIII).

Whilst the recording of adverse morphological outcomes were consistently recorded in all animals treated with silver, there were some differences between the pattern of results recorded depending on the type of silver to which animals were exposed, allowing the building of a better picture of how differing physico-chemical characteristics may alter biological response and outcomes.

Effects common to all animals included generalised tubular dysmorphism, presence of pyknotic nuclei, degeneration of germ cell populations and sloughing of tubular contents into the central lumen, all of which are widely accepted indicators of testicular toxicity, and relatively sensitive indicators of a disturbance in spermatogenesis, either via direct injury or disturbances in the HPG axis. Sertoli cells are known to be relatively

robust, and as many appeared intact, it could be suggested it is more likely these effects were mediated via endocrine disturbances. However, further appraisal of key parameters in SC and BTB structure, alongside investigation into whether SC cell injury would help provide a more complete understanding of these effects and the underlying cause.

One interesting difference in tubular content between silver treatments we highlighted was the retention of spermatids identified in testes from NM-300 and Nano Amor treated animals, but not in AgNO₃ treated animals. Spermatid retention is related to problems with spermiation, forming an extremely sensitive indicator of toxicity which implicates endocrine disturbance, as spermiation is mediated via testosterone acting on SC, adding further weight to the suggestion of endocrine disturbance as a cause for observed effects. This finding also allows some conjecture that these effects may be primarily mediated via particles not ions, although it would be unwise to draw any further inferences from this supposition without further investigation.

A further specific difference between tubules was the observation of tubule dilation in Nano Amor treated animals. This is considered to be a manifestation of problems with tubule emptying and is in alignment with the finding of step 11 spermatid retention and sloughing of tubule content without its apparent efflux, and that of increased lumen volume compared to control in tubules immediately prior to spermiation (stage VII). Dilation is also a known precursor of complete tubular atrophy and, as discussed previously, it may be that should animals have been sacrificed later an increased incidence of this would have been observed. Interestingly, Nano Amor exposed animals also presented with germ cell layer atrophy, a precursor of development of SCO tubules. As AgNO₃ exposure led to identification of SCO tubules, this may suggest that should the observed toxicity be mediated by ions rather than particles, more chronic exposure to Nano Amor may lead to a similar outcome. In support of this posit, van der Zande et al (2012) noted that the soluble silver content to which rats were exposed could potentially be up to 4x higher for Nano Amor, owing to its greater dissolution of Ag⁺ ions over the 7 day period tested (45% vs 3% for NM-300) (van der Zande et al., 2012). This is further supported by the findings of Kittler et al (2010) who observed that PVP-coated silver ENM released more Ag⁺ ions than citrate capped Ag ENM of the same size (Kittler

et al., 2010). Taking into account the fact that NM-300 is citrate-capped, this may offer a plausible reason for the lack of tubule dilation or SCO tubules recorded in animals exposed to this ENM and suggests that such effects may be mediated by ions rather than particles. These observations would require further analysis before any final conclusions could be reached. However, As LC dysfunction (and resultant lowered testosterone levels) have been associated with a long-term risk of not only decreased fertility, but also systemic inflammation and metabolic syndrome, developing further understanding of the effect observed here is of clear importance (Bandak et al., 2017).

In addition to tubular effects, further key differences were observed in the interstitium, for example, presentation of NM-300 treated animals with generalised inflammation. As already discussed, inflammation is generally associated with immune influx and cytokine secretion, which in turn can lead to an increase in permeability of the BTB. Should exposure to silver be chronic rather than sub-chronic in nature, a potential for downstream compromise of the BTB and associated access of immune cells to adluminal compartment, leading to an autoimmune response to spermatozoa could be posited. This would require further investigation over a longer period of exposure and inclusion of assays to appraise caspase and immune cell populations, but would be justified given the strong evidence presented. A further outcome highlighted was that animals exposed to AgNO₃ were the only group to show evidence of Leydig cell hyperplasia. As a known sensitive indicator of disturbance in the HPG axis, and precursor of testicular adenoma, this new finding is particularly relevant.

Taken together, these results indicate strongly a role for silver ENM as reproductive toxicants and as potential endocrine disruptors. Evaluation of endocrine function via immunohistochemical analysis further aided in reaching this conclusion. It was possible to show an increase in StaR expression following exposure to both silver ENM and ionic AgNO₃, a decrease in LHR expression following NM-300 exposure (but not Nano Amor or AgNO₃), and no change to AR expression following any treatment. Results indicated that further optimisation of antibodies may be required, which would be undertaken at the commencement of any future research. However, a clear case is presented for further investigation of endocrine-relevant endpoints following ENM exposure, using either an expanded range of antibodies (comparable to those discussed for work *in*

vitro), or preferably, via measurement of hormone levels from both testicular tissue homogenates and blood samples, to measure local and systemic effects respectively.

As previously highlighted, mechanical changes in tissues do not always manifest as phenotypic changes, as the body is often capable of compensating for damage to a certain extent. This is especially relevant as the tissue effects identified were localised in their nature. To assist in this, an additional endpoint which can be strongly recommended for future studies would be the inclusion of sperm analysis from both testicular and epididymal samples. This would allow for consideration of whether the focal areas of dysgenesis contributed to a decrease in sperm normality, motility and function, (via CASA, Eosin Y stain and acridine orange respectively) and therefore their potential to fertilise an oocyte.

Comparison of results *in vitro* to *in vivo*

The penultimate aim from the data accumulated was to compare results generated *in vitro* to those *in vivo* to guide a decision on the suitability of *in vitro* testing to predict outcomes *in vivo*. Of the ENM panel selected for examination at the commencement of this work, the most comprehensive analysis was undertaken for silver, and results are summarised in Table 42.

Table 42: Comparative summary of findings for silver ENM. Where cells are blank, no assay was performed for this endpoint. AR = Androgen Receptor, LHR = Luteinising Hormone Receptor, WB = Western Blot, IHC = Immunohistochemistry, PCR = Polymerase Chain Reaction. *=additional result for Androgen Receptor expression, generated from pilot data using TM4 cells.

Cell/Animal model		Endpoint & Assay		Silver			
				300	AgNO ₃	Nano Amor	300dis
Murine <i>In vitro</i>	TM3 Leydig	Cytotoxicity	WST-1	+	+		-
		Timecourse	Alamar Blue	LC ₅₀ 7.88µg/cm ² >0.94µg/cm ² 4h	LC ₅₀ 0.282µg/cm ²		
	TM4 Sertoli	Cytotoxicity	WST-1	+			
		Timecourse	Alamar Blue	>1.875µg/cm ² 4h			
<i>In vitro</i> (murine TM3) <i>In vivo</i> (Sprague-Dawley rat)		AR expression	WB (<i>in vitro</i>) IHC (<i>in vivo</i>)	↓ ↓*	•	•	•
		LHR expression	PCR (<i>in vitro</i>) IHC (<i>in vivo</i>)	↑	↓	•	•
		StaR expression	PCR (<i>in vitro</i>) IHC (<i>in vivo</i>)	↑	↑	↑	↑
		CYP11A1 expression	PCR (<i>in vitro</i>)	↑			
		3β-HSD expression	PCR (<i>in vitro</i>) IHC (<i>in vivo</i>)	↑	?	?	?

The data clearly show that identification of cytotoxicity *in vitro* using the WST-1 test was able to predict adverse outcomes following exposure *in vivo*. As no previous studies concomitantly examining the same male reproductive nanotoxicity endpoints *in vitro* and *in vivo* have been identified, this comparison is being reported for the first time. It represents an encouraging first step in the development of future IATAs to reduce the use of animals in DART for ENM.

It was also possible to observe changes in expression of StaR observed following a sub-acute exposure to NM-300 via oral gavage *in vivo*, based on outcomes from PCR on TM3 LC *in vitro*. Three published studies were found with which to compare this outcome. Garcia et al (2014) found a non-significant increase of StaR expression in CD1 mice (measured via PCR), following 12 day IV exposure to 14nm Ag ENM (Garcia et al., 2014).

By comparison, Zhang *et al* (2015a&b) showed in two separate studies that while exposure to 10 and 20nm Ag NPs decreased expression of StaR in TM3 cells following 24hr exposure *in vitro*, but that 4 doses of ~15nm Ag NPs to neonatal mice over 15 days increased expression at a low dose (1mg/kg) but decreased expression *in vivo* at a higher dose (5mg/kg) (Zhang *et al.*, 2015a, Zhang *et al.*, 2015b). Despite the ENM used in each study being of similar sizes, they were all from different sources and held different characteristics, making it difficult to draw a direct comparison between the data *in vitro*, and even harder to reach conclusion on effects of Ag ENM on StaR expression when considering the data *in vivo*, given that the ENM were different from either study *in vitro*. However, this does serve to highlight the importance of use of reference material, and of considering not only ENM characteristics, but exposure length, dose and animal model and maturity in interpretation of results. Had such a reference material been employed for these studies, it would have been easier to usefully compare the outcomes of the three.

Evaluation of AR expression led to some interesting findings. *in vitro*, NM-300 exposure appeared to decrease in expression of AR in TM3 and TM4 cells. Results *in vitro* are in agreement with those published by Zhang (2015), showing a decrease in AR expression in TM4 cells following Ag ENM exposure (Zhang *et al.*, 2015a). The outcome is not only interesting because of the alignment with other published work on testicular cell lines *in vitro*, but because it confirms for the first time that ENM are able to alter expression of AR in the TM3 Leydig cell. By comparison to the outcomes generated *in vitro* no change in expression of AR was observed *in vivo*. However, discussed in Chapter 5, issues with specificity of the antibody used led to problems in drawing conclusions on the relevance of this disparity in findings. There is a strong possibility that with further optimisation and use of an alternative antibody the results generated may be different. As no published *in vivo* studies using silver ENM were identified against which to compare this, further work to optimise the protocol for AR IHC is strongly recommended, in order to draw a definitive conclusion on comparability *in vitro* to *in vivo*.

One clear difference between findings *in vitro* and *in vivo* was for LHR. PCR *in vitro* reported a non-significant increase in expression of LHR in TM3 cells following exposure

to NM-300, whereas IHC *in vivo* reported a slight decrease. Based on this data alone, it appears that the current methods employed to examine TM3 cells may not be particularly accurate in predicting changes to LHR expression *in vivo*. It would be well worth repeating evaluation of LHR expression using both TM3 cells *in vitro* and the tissues exposed *in vivo*, to look for reproducibility before drawing any final conclusions. Ultimately though, hormone assays to measure circulating LHR from future studies *in vivo* would be the most robust method by which to measure this and compare outcomes to those *in vitro* in future.

One steroidogenic enzyme for which no clear *in vitro in vivo* comparison was possible was 3 β -HSD. Whilst a slight increase in expression was observed *in vitro*, (non-significant), it was not possible to optimise the antibody used to evaluate tissues from animals exposed *in vivo*. Development of this aspect of the research would be justified as a next step, especially as results from other studies *in vitro* and *in vivo* currently reveal contrasting results. Further work to understand the potential for comparability between the two would be recommended before any final conclusions can be made.

Although evaluation of P450scc (protein) or CYP11A1 (gene) expression was not conducted *in vivo*, it was encouraging to see that our results matched those of Garcia *et al*, who identified a clear increase in CYP11A1 expression following Ag ENM exposure *in vivo* (details of study described above) (Garcia *et al.*, 2014). Interestingly, Zhang *et al* did not find a significant change in expression of CYP11A1 when they exposed TM3 cells to 10 μ g/ μ l 10 or 20nm Ag ENM (Zhang *et al.*, 2015a). Again, it is difficult to draw an exact comparison between the datasets when the ENM tested are not exactly the same. In order to understand this further, it would be very interesting to undertake IHC for P450scc or CYP11A1 on the tissues from animals exposed *in vivo* to see whether they matched those generated *in vitro*.

In summary, appraisal of silver ENM cytotoxicity using testicular cell lines *in vitro* have been shown to be predictive of adverse outcomes recorded *in vivo* following exposure to the same ENM. Some clear comparability between functional and endocrine markers of testicular health was identified (e.g. increased expression of StaR). There is however a clear need to develop further methods for appraisal of other endpoints in both

systems. For completeness of this comparative evaluation, it would be useful to expose TM4 cells to AgNO₃ to establish cytotoxicity, a timecourse for effect, together with appraisal of the full complement of endocrine endpoints, as would appraisal of Nano Amor for both cell lines *in vitro* (something which was not possible during this research as no access to a Nano Amor preparation was available).

Should further funding be procured with which to continue this research, expansion of the comparative dataset with minimal time, expense and no additional animal burden would be possible by examination of pristine CuO. Tissues from a short-term inhalation exposure *in vivo* are available, as is more of the ENM with which to appraise functional and endocrine parameters *in vitro*. This would, relatively quickly, add further data to the dataset from an alternative ENM and exposure protocol, with which to examine ability of outcomes *in vitro* to predict those measured *in vivo*. Following this, evaluation of additional ENM could be added *in vitro*, alongside additional cell lines from multiple animal types, allowing for identification of commonality or differences across species and thus potentially animal models. Following careful appraisal and comparison of results, further work *in vivo* could then be added where its use in building a comparative model is justified without question.

In conducting any future research, there are a number of considerations and limitations from the design of the current that ideally should be considered and improved on where possible. For most of these, there may not be either i) any solution or ii) a solution which is not high cost and high effort at the current time, but their continued consideration in design of future work is nonetheless warranted.

The first is that for this research, the exposure times *in vitro* do not match those *in vivo* (24h vs 28-days). It is important to consider for future research how a more accurate representation for longer-term exposure could be achieved *in vitro*. This remains a problem that is recognised by the scientific community, and for which currently there is no immediate solution. On one hand, it would be possible to simply apply repeated doses of ENM following the same regimen as applied *in vivo*. On the other, this would still not represent the system *in vivo* as it applies only to an isolated cell line, with no ability to interact with other cells from the same organ. Use of microfluidics systems as

mentioned earlier may be one way this could be tackled; however, this would require considerable further time and effort to develop into a working system. The second is the potential influence of the spermatogenic cycle on outcomes reported *in vivo*. As the spermatogenic cycle in a rat lasts ~12 days, and development of basal spermatogonia to mature spermatozoa takes ~56days, it may be that exposure duration has an even more important impact for male reproductive endpoints than in other organs. Finally, as discussed, the influence of biocorona on ENM interactions *in vitro* and *in vivo* remains an important consideration for any study.

Finally, alongside the shorter-term animal studies that have been undertaken to date, consideration of longer term, low level exposure regimens in animal research should be given. On average, is far more likely that humans will come into contact with small doses of ENM over a much longer time (potentially with 'spikes' of exposure) than larger doses in a short time period, potentially leading to cumulative effects on fertility. Epidemiological studies of the link between exposure to larger particles in air pollution (PM) and spontaneous pregnancy loss have identified a significant link between the two, both for short-term, and longer-term exposures (Carrington, 2019). It may therefore be argued that as clear reproductive effects from particulate matter are already proven, further investigation for their nano- counterparts using an animal model *in vivo* is both relevant and justified at the current time.

Formation of an integrated approach to testing and assessment (IATA) for male DART following exposure to nanomaterials.

The final aim of this thesis was to propose a framework on which to develop an Integrated Approach to Testing and Assessment (IATA) for male reproductive toxicity from ENM. Similar approaches are beginning to emerge in other regulatory frameworks to assist with both maximising the impact of available data and reduce and/or refine the use of animals in testing where possible. For example, ICH S5 details an integrated testing strategy (ITS) for detection of adverse effects on embryo-foetal development, ECHA includes a simple ITS for sampling strategy and preparation for testing human health endpoints with ENM, and the OECD recently published a guidance document on defined approaches to be used within Integrated approaches to testing and assessment (ECHA, 2017, OECD, 2016, EMA, 2017).

The proposed IATA is outlined overleaf. It must be recognised that this is a starting point, and further refinement, development and additions will be necessary as knowledge in the area is grown. However, to our knowledge, this is the first time production of such an ENM-specific IATA has been undertaken for male reproductive toxicity endpoints.

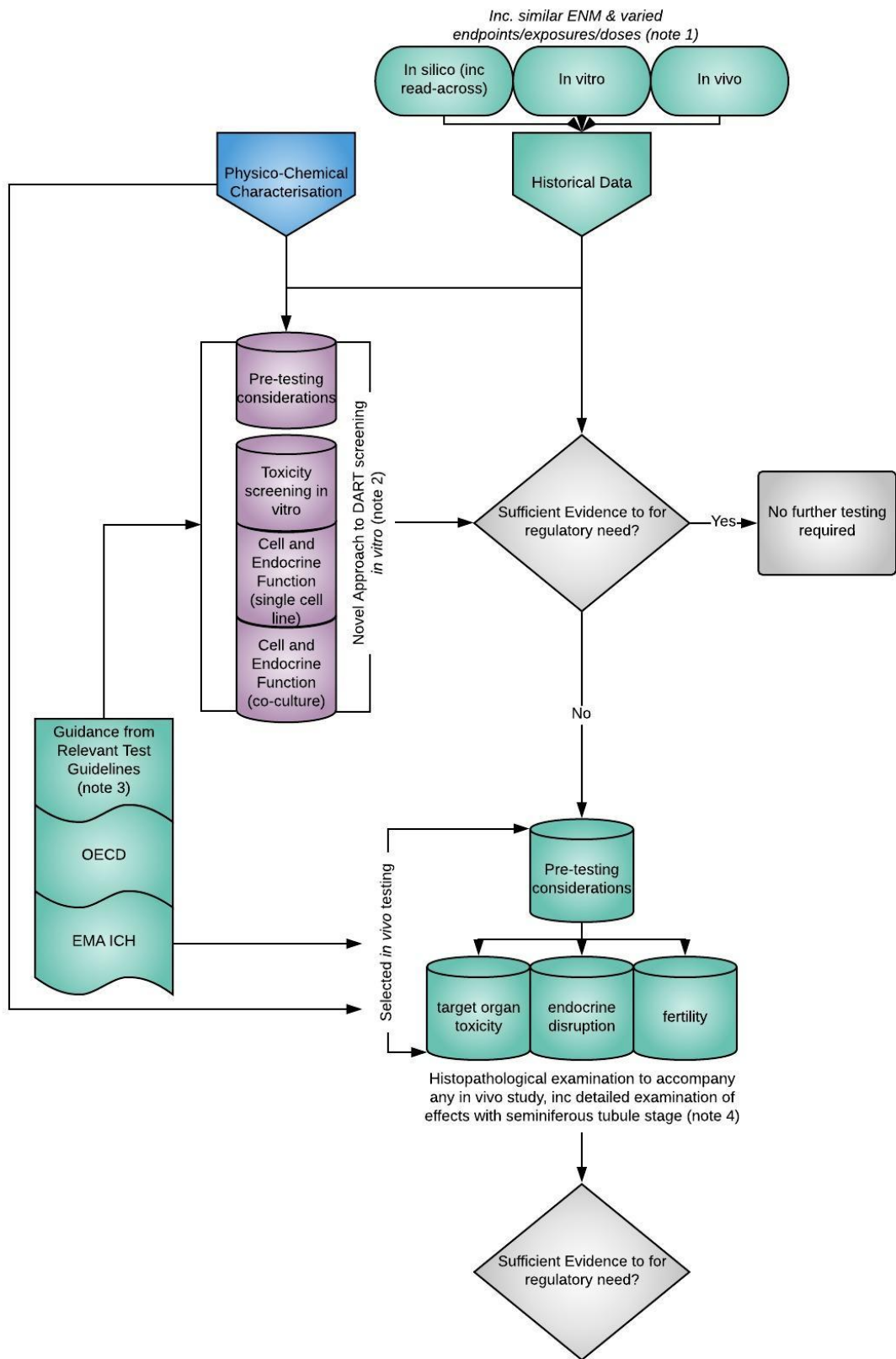


Figure 107: Proposed IATA for consideration of male DART following ENM exposure

Note 1: The use of *in silico* models for ENM is on the whole yet to be established. However, development of Quantitative Structure Activity Relationships (QSARs), Physiologically Based Pharmacokinetic Models (PBPK) are under development and useful output should be available soon. The use of grouping an read-across should also be considered at this stage, but is only applicable to certain ENM under REACH, details of which may be found in ECHA Appendix R7-1 for nanomaterials applicable to Chapter R71a Endpoint specific guidance (ECHA, 2017).

Note 2: DART screening *in vitro* should be undertaken according to guidelines detailed in Fig. 108.

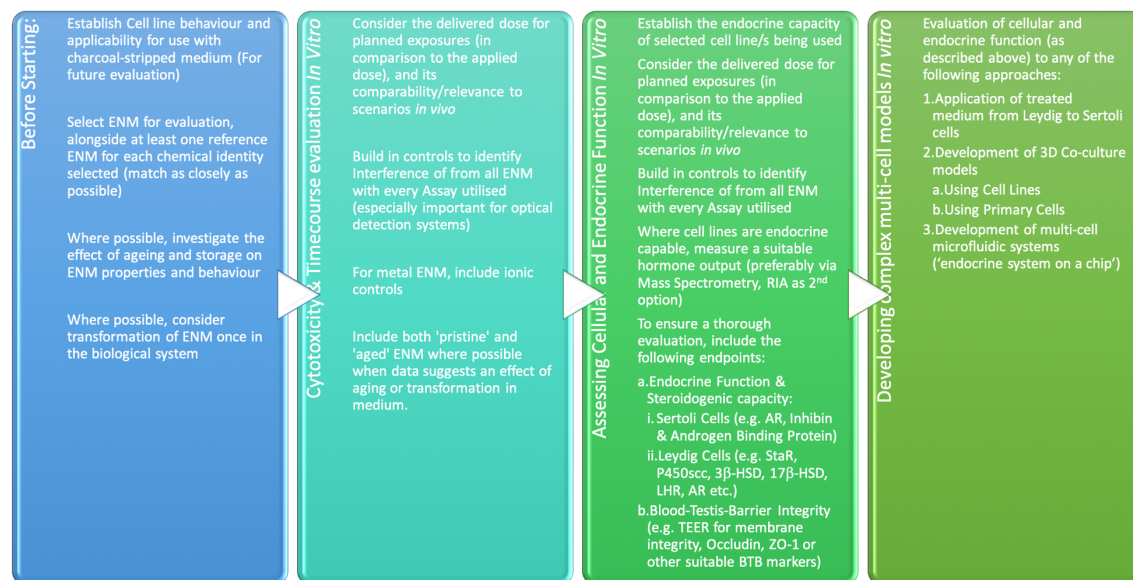


Figure 108: Proposed IATA, Note 1. Detail on requirements for *In vitro* toxicity testing endpoints.

Note 3: Alongside the traditional test guidelines, the following guidance should be consulted to ensure robust study design:

- PHARMACEUTICALS: ICH S5 (R3) Guideline on Reproductive Toxicology (EMA, 2017)
- CHEMICALS: ECHA Appendix R7-1 for nanomaterials applicable to Chapter R71a Endpoint specific guidance (ECHA, 2017)
- OECD Revised guidance document No 150: Standardised test guideline for evaluating chemicals for endocrine disruption (OECD, 2018b)
- OECD Guidance document on good *in vitro* method practices (GIVMP) (OECD, 2018a)
- Series on Testing & Assessment No 178: Review paper on novel *in vitro* and *in vivo* screening and testing methods and endpoints for evaluating endocrine disruptors (2012)
- Series on Testing & Assessment No 255: Guidance Document on defined approaches to be used within Integrated approaches to testing and assessment (OECD, 2016)

Note 4: Analysis of stage using hybrid technique combining Dazl immunostaining with a decision key (for key cell populations, morphological and stereological identifiers). Method outlined in full within Chapter 4.

Conclusions and Future work

Reports of reduced serum testosterone levels, a decline in sperm morphology & motility, and an increase in use of assisted reproductive techniques, all indicate clearly that male fertility rates are in decline in the Western world (Odermatt et al., 2016, Rolland et al., 2013). With fertility now below the replacement level in some countries, it has never been more important to understand and manage potential threats to reproductive health (Makarow and Hojgaard, 2010).

To this end, this research has aimed to assess the toxicity of engineered nanomaterials in the male reproductive system and develop an improved testing strategy for hazard assessment. Assays to evaluate cytotoxicity and the effect of time- and dose- on effect were established and optimised for ENM. A panel of ENM were then evaluated for toxicity to male testicular cell lines. For the first time, these results were compared to those from multiple other cell lines representing six organs in the body and found to be generally in agreement. It was possible to conclude that the assays used were suitable for screening ENM for toxicity to the male reproductive system in a reliable and reproducible manner.

Functional assessment of cell lines *in vitro* provided a deeper understanding of the response of TM3 and TM4 cell lines to acute ENM exposure. Comparison of outcomes to tissues from animals exposed *in vivo* indicated that for a selected ENM (silver), screening tests *in vitro* were capable of predicting toxicity *in vivo*. Furthermore, whilst future work will refine the approach and establish fully the comparability between functional endpoints *in vitro* and *in vivo*, it was possible to generate sufficient data to conclude that silver ENM are both potential male reproductive toxicants and an endocrine disruptor.

To develop this work programme further, a number of key steps could be taken to strengthen and develop the findings so far. A first step would be to expand testing *in vitro* to a panel of cell lines both from the same animal to compare reproducibility of results, and different animals to examine the potential for cross-species differences in response. As the potential for ENM to translocate to and accumulate within the testis has been demonstrated (van der Zande et al., 2012, van der Zande et al., 2014a),

evaluation of cellular integrity in single cell culture, and interaction of the ENM panel with cell co-cultures would be warranted, especially for parameters related to the integrity of the BTB. In order to facilitate more accurate measurement of endpoints related to fertility, cell integrity and endocrine function at sub-lethal doses, development of a model using Primary cells in co-culture is justified, as this would allow (amongst other things) direct evaluation of hormone levels rather than reliance on RNA or protein expression in estimation of effect. Collection of hormone levels (both intratesticular and circulating) from future animal studies would enable a direct comparison between results *in vitro* and *in vivo* and allow for a more accurate evaluation of comparability between the two. Evaluation of additional testicular samples from animals treated with an alternative ENM *in vivo* would also be useful in building an evidence base for comparing *in vitro* to *in vivo* (for example, animals exposed to CuO short-term). The potential for a long-term low-exposure animal model should be also be seriously considered as a method through which to evaluate realistic ENM exposures. Such developments could then easily be fed into further development and refinement of the proposed IATA detailed above.

As toxicology models *in vitro* have not been well explored, this plan both ensures development of relevant new findings for male DART endpoints following ENM exposure, and an active contribution to develop a protocol that regulators would in future accept as a validated pre-screening technique, further supporting refinement and reduction of the use of animals in testing.

The work in this thesis has made a significant contribution to developing the underlying knowledge on ENM as potential reproductive toxicants and endocrine disruptors and has contributed to development of an initial IATA framework through which to refine and reduce the number of animals used in regulatory DART testing.

Reference List

2011. *Reproductive and Developmental Toxicology*, USA, Elsevier.
2012. DETAILED REVIEW PAPER ON THE STATE OF THE SCIENCE ON NOVEL IN VITRO AND IN VIVO SCREENING AND TESTING METHODS AND ENDPOINTS FOR EVALUATING ENDOCRINE DISRUPTORS. *OECD Environment, Health and Safety Publications Series on Testing and Assessment No. 178*. Paris: OECD Publishing.
- AHAMED, M., KARNS, M., GOODSON, M., ROWE, J., HUSSAIN, S. M., SCHLAGER, J. J. & HONG, Y. 2008. DNA damage response to different surface chemistry of silver nanoparticles in mammalian cells. *Toxicol Appl Pharmacol*, 233, 404-410.
- AHMED, S. M., ABDELRAHMAN, S. A. & SHALABY, S. M. 2017. Evaluating the effect of silver nanoparticles on testes of adult albino rats (histological, immunohistochemical and biochemical study). *J Mol Histol*, 48, 9-27.
- AITKEN R.J, HANKIN SM, ROSS B, TRAN CL, STONE V, FERNANDES TF, DONALDSON K, DUFFIN R, CHAUDHRY Q, WILKINS TA, WILKINS SA, LEVY LS, ROCKS SA & A, M. 2009. EMERGNANO: A review of completed and near completed environment, health and safety research on nanomaterials and nanotechnology. Report TM/09/01. Edinburgh, UK.: Institute of Occupational Medicine (IOM).
- AITKEN, R. J., ROSS, B. L., PETERS, S. A. K., GEERTSMA, R. E., BLEEKER, E., WIJNHOFEN, S. W. P., TOUFEKTSIAN, M.-C. & NOWACK, B. 2011. Nanotechnology EHS Landscape Document, Report on ObservatoryNANO FP7 project (Contract number 218528). ObservatoryNANO FP7: EC.
- ASARE, N., INSTANES, C., SANDBERG, W. J., REFSNES, M., SCHWARZE, P., KRUSZEWSKI, M. & BRUNBORG, G. 2012. Cytotoxic and genotoxic effects of silver nanoparticles in testicular cells. *Toxicology*, 291, 65-72.
- AUFFMAN, M., ROSE, J., WEISNER, M. & BOTTERO, J.-Y. 2009. Chemical stability of metallic nanoparticles: A parameter controlling their potential cellular toxicity in vitro. *Environmental Pollution*, 157.
- BAI, Y., ZHANG, Y., ZHANG, J., MU, Q., ZHANG, W., BUTCH, E. R., SNYDER, S. E. & YAN, B. 2010. Repeated administrations of carbon nanotubes in male mice cause reversible testis damage without affecting fertility. *Nat Nanotechnol*, 5, 683-689.
- BANDAK, M., JORGENSEN, N., JUUL, A., LAURITSEN, J., OTURAI, P. S., MORTENSEN, J., HOJMAN, P., HELGE, J. W. & DAUGAARD, G. 2017. Leydig cell dysfunction, systemic inflammation and metabolic syndrome in long-term testicular cancer survivors. *Eur J Cancer*, 84, 9-17.
- BAR-ILAN, O., ALBRECHT, R. M., FAKO, V. E. & FURGESON, D. Y. 2009. Toxicity assessments of multisized gold and silver nanoparticles in zebrafish embryos. *Small*, 5, 1897-910.
- BARA, N., ESHWARMOORTHY, M., SUBAHARAN, K. & KAUL, G. 2018. Mesoporous silica nanoparticle is comparatively safer than zinc oxide nanoparticle which can cause profound steroidogenic effects on pregnant mice and male offspring exposed in utero. *Toxicol Ind Health*, 34, 507-524.
- BARKALINA, N., JONES, C., KASHIR, J., COOTE, S., HUANG, X., MORRISON, R., TOWNLEY, H. & COWARD, K. 2014. Effects of mesoporous silica nanoparticles upon the function of mammalian sperm in vitro. *Nanomedicine: Nanotechnology, Biology and Medicine*, 10, 859-870.
- BARKHORDARI, A., HEKMATIMOGHADDAM, S., JEBALI, A., KHALILI, M. A., TALEBI, A. R. & NOORANI, M. 2013. Effect of zinc oxide nanoparticles on viability of human spermatozoa. *Iranian Journal of Reproductive Medicine*, 11, 767-771.
- BARRETT, K. E., BARMAN, S. M., BROOKS, H. L. & JASON, X. J. 2019. *Ganong's Review Of Medical Physiology, Twenty Sixth Edition*, McGraw-Hill Education.

- BARTER, R. 2018. Fixed, Mixed, and Random Effects. *Practical Statistics* [Online]. Available from: <https://rlbarter.github.io/Practical-Statistics/2017/03/03/fixed-mixed-and-random-effects/> [Accessed October 18th 2018].
- BEEKHUIJZEN, M. 2017. The era of 3Rs implementation in developmental and reproductive toxicity (DART) testing: Current overview and future perspectives. *Reprod Toxicol*, 72, 86-96.
- BEEKHUIJZEN, M. 2018. *DEVELOPMENTAL AND REPRODUCTIVE TOXICOLOGY (DART) TESTING: THE NEXT GENERATION*. PhD, Utrecht University.
- BEER, C., FOLDBJERG, R., HAYASHI, Y., SUTHERLAND, D. S. & AUTRUP, H. 2012. Toxicity of silver nanoparticles - nanoparticle or silver ion? *Toxicol Lett*, 208, 286-92.
- BEN-DAVID MAKHLUF, S., QASEM, R., RUBINSTEIN, S., GEDANKEN, A. & BREITBART, H. 2006. Loading magnetic nanoparticles into sperm cells does not affect their functionality. *Langmuir*, 22, 9480-2.
- BHIMJI, S. S. & LESLIE, S. W. 2018. Anatomy, Abdomen and Pelvis, Testicle. *StatPearls [Internet]*. Treasure Island (FL): StatPearls Publishing.
- BOISEN, A. M., SHIPLEY, T., JACKSON, P., HOUGAARD, K. S., WALLIN, H., YAUK, C. L. & VOGEL, U. 2012. NanoTiO₂ (UV-Titan) does not induce ESTR mutations in the germline of prenatally exposed female mice. *Part Fibre Toxicol*, 9, 19.
- BOUWMEESTER, H. 2014. *RE: Johnsen scoring: outcome and potential effects*. Type to ROSS, B. L.
- BOUWMEESTER, H., LYNCH, I., MARVIN, H. J., DAWSON, K. A., BERGES, M., BRAGUER, D., BYRNE, H. J., CASEY, A., CHAMBERS, G., CLIFT, M. J., ELIA, G., FERNANDES, T. F., FJELLSBO, L. B., HATTO, P., JUILLERAT, L., KLEIN, C., KREYLING, W. G., NICKEL, C., RIEDIKER, M. & STONE, V. 2011. Minimal analytical characterization of engineered nanomaterials needed for hazard assessment in biological matrices. *Nanotoxicology*, 5, 1-11.
- BOUWMEESTER, H. & VAN DER ZANDE, M. 2015. *RE: Johnsen Scores for Sprague-Dawley rats exposed in vivo to silver nanoparticulates*. Type to ROSS, B. L.
- BRAUN, K., STÜRZEL, C. M., BISKUPEK, J., KAISER, U., KIRCHHOFF, F. & LINDÉN, M. 2018. Comparison of different cytotoxicity assays for in vitro evaluation of mesoporous silica nanoparticles. *Toxicology in Vitro*, 52, 214-221.
- BRAYDICH-STOLLE, L., HUSSAIN, S., SCHLAGER, J. J. & HOFMANN, M. C. 2005. In vitro cytotoxicity of nanoparticles in mammalian germline stem cells. *Toxicol Sci*, 88, 412-9.
- BRAYDICH-STOLLE, L. K., LUCAS, B., SCHRAND, A., MURDOCK, R. C., LEE, T., SCHLAGER, J. J., HUSSAIN, S. M. & HOFMANN, M.-C. 2010. Silver nanoparticles disrupt GDNF/Fyn kinase signaling in spermatogonial stem cells. *Toxicological Sciences*, 116, 577-589.
- BUZULUKOV, Y. P., GMOSHINSKI, I. V., ANTSIFEROVA, A. A., DEMIN, V. A., DEMIN, V. F. & KASHKAROV, P. K. 2017. Accumulation of Silver Nanoparticles in Brain and Testes during Long-Term Ingestion to Mammals. *Nano Hybrids and Composites*, 13, 199-205.
- CARREAU, S., BOURAIMA-LELONG, H. & DELALANDE, C. 2011. Estrogens in male germ cells. *Spermatogenesis*, 1, 90-94.
- CARREAU, S., DELALANDE, C., SILANDRE, D., BOURGUIBA, S. & LAMBARD, S. 2006. Aromatase and estrogen receptors in male reproduction. *Molecular and Cellular Endocrinology*, 246, 65-68.
- CARRINGTON, D. 2019. Air pollution 'as bad as smoking in increasing risk of miscarriage'. *The Guardian*.
- CASTELLINI, C., RUGGERI, S., MATTIOLI, S., BERNARDINI, G., MACCHIONI, L., MORETTI, E. & COLLODEL, G. 2014. Long-term effects of silver nanoparticles on reproductive activity of rabbit buck. *Syst Biol Reprod Med*, 60, 143-50.
- CEFIC 2012. Synthetic Amorphous Silica (SAS) Factsheet. Brussels: European Chemical Industry Council – Cefic aisbl.

- CHEN, G., MRUK, D. D., XIA, W., BONANOMI, M., SILVESTRINI, B. & CHENG, C. Y. 2016. Effective Delivery of Male Contraceptives Behind the Blood- Testis Barrier (BTB) – Lesson from Adjudin. *Current medicinal chemistry*, 23, 701-713.
- CHEN, H., MIDZAK, A., LUO, L. & ZIRKIN, B. 2007. Aging and the decline of androgen production. In: PAYNE, A. (ed.) *The Leydig Cell in Health and Disease*. Totowa, New Jersey: Humana Press.
- CHEN, Y., XUE, Z., ZHENG, D., XIA, K., ZHAO, Y., LIU, T., LONG, Z. & XIA, J. 2003. Sodium chloride modified silica nanoparticles as a non-viral vector with a high efficiency of DNA transfer into cells. *Curr Gene Ther*, 3, 273-9.
- CHENG, J., CHAN, C. M., VECA, L. M., POON, W. L., CHAN, P. K., QU, L., SUN, Y. P. & CHENG, S. H. 2009. Acute and long-term effects after single loading of functionalized multi-walled carbon nanotubes into zebrafish (*Danio rerio*). *Toxicol Appl Pharmacol*, 235, 216-25.
- CHIA, S. L. & LEONG, D. T. 2016. Reducing ZnO nanoparticles toxicity through silica coating. *Heliyon*, 2, e00177.
- CHOI, J. & SMITZ, J. 2014. Luteinizing hormone and human chorionic gonadotropin: origins of difference. *Mol Cell Endocrinol*, 383, 203-13.
- CLARK, B. J. & STOCOCO, D. M. 1996. StAR-A Tissue Specific Acute Mediator of Steroidogenesis. *TEM*, 7.
- COHEN, J. M., TEEGUARDEN, J. G. & DEMOKRITOU, P. 2014. An integrated approach for the in vitro dosimetry of engineered nanomaterials. *Particle and fibre toxicity*, 11.
- COLOGNATO, R., PARK, M., WICK, P. & DE JONG, W. H. 2012. Interactions with the human body. In: FADEEL, B., PIETROIUSTI, A. & SHVEDOVA, A. (eds.) *Adverse Effects of Engineered Nanomaterials*. USA: Elsevier.
- COMERO, S., KLEIN, C., STAHLMECKE, B., ROMAZANOV, J., KUHLBUSCH, T. A. J., VAN DOREN, E., WICK, P., LOCORO, G., KOERDEL, W., GAWLIK, B., MAST, J., KRUG, H., HUND-RINKE, K., FRIEDRICH, S., MAIER, G., WERNER, J. & LINSINGER, T. 2011. NM-300 Silver Characterisation, Stability, Homogeneity. Joint Research Council.
- COTOGNO, G., TOTARO, S., RASMUSSEN, K., PIANELLA, F., RONCAGLIA, M., OLSSON, H., RIEGO SINTES, J. & CRUTZEN, H. 2016. The JRC Nanomaterials Repository: Safe handling of nanomaterials in the sub-sampling facility. *JRC Technical Reports*. Luxembourg: Joint Research Centre.
- CREASY, D., BUBE, A., DE RIJK, E., KANDORI, H., KUWAHARA, M., MASSON, R., NOLTE, T., REAMS, R., REGAN, K., REHM, S., ROGERSON, P. & WHITNEY, K. 2012. Proliferative and nonproliferative lesions of the rat and mouse male reproductive system. *Toxicol Pathol*, 40, 40S-121S.
- CREASY, D., MARONPOT, R. R. & GIRI, D. K. 2014a. *Testis, Seminiferous Tubule - Dilation* [Online]. National Toxicology Program: US department of Health and Human services. Available: https://ntp.niehs.nih.gov/nnl/male_reproductive/testis/setubdilata/index.htm [Accessed 12.12.18 2018].
- CREASY, D., MARONPOT, R. R. & GIRI, D. K. 2014b. *Testis, Seminiferous tubule – Giant cells* [Online]. National Toxicology Program: US Department of Health and Human Services. Available: https://ntp.niehs.nih.gov/nnl/male_reproductive/testis/setubmgcel/index.htm [Accessed 12/12/18 2018].
- CREASY, D., MARONPOT, R. R. & GIRI, D. K. 2014c. *Testis, Seminiferous tubule – Retention, Spermatio* [Online]. National Toxicology Program: US department of Health and Human services. Available: https://ntp.niehs.nih.gov/nnl/male_reproductive/testis/setubreten/testis_seminiferous_tubule-retention_spermatio_508.pdf [Accessed 12.12.18 2018].
- CREASY, D., MARONPOT, R. R. & GIRI, D. K. 2014d. *Testis, Seminiferous tubule – Vacuolation* [Online]. National Toxicology Program: US Department of Health and Human Services.

Available: https://ntp.niehs.nih.gov/nnl/male_reproductive/testis/setubvac/index.htm [Accessed 12.12.18 2018].

- CREASY, D. M. 1997. Evaluation of testicular toxicity in safety evaluation studies: the appropriate use of spermatogenic staging. *Toxicol Pathol*, 25, 119-31.
- CREASY, D. M. & CHAPIN, R. E. 2013. Male Reproductive System. *Haschek and Rousseaux's Handbook of Toxicologic Pathology*.
- DARNE, C., TERZETTI, F., COULAIS, C., FONTANA, C., BINET, S., GATE, L. & GUICHARD, Y. 2014. Cytotoxicity and genotoxicity of panel of single- and multiwalled carbon nanotubes: in vitro effects on normal Syrian hamster embryo and immortalized v79 hamster lung cells. *J Toxicol*, 2014, 872195.
- DE MATTEIS, V., CASCIONE, M., BRUNETTI, V., TOMA, C. C. & RINALDI, R. 2016. Toxicity assessment of anatase and rutile titanium dioxide nanoparticles: The role of degradation in different pH conditions and light exposure. *Toxicology in Vitro*, 37.
- DOHLE, G. R., ELZANATY, S. & VAN CASTEREN, N. J. 2012. Testicular biopsy: clinical practice and interpretation. *Asian J Androl*, 14, 88-93.
- DONALDSON, K., STONE, V., TRAN, C. L., KREYLING, W. & BORM, P. J. 2004. Nanotoxicology. *Occup Environ Med*, 61, 727-8.
- DUFAU, M. 1998. The Lutenizing Hormone Receptor. *Annual Reviews of Physiology*, 60.
- DUFAU, M. L. & TSAI-MORRIS, C.-H. 2007. 16: The Luteinizing Hormone Receptor. In: PAYNE, A. & HARDY, M. P. (eds.) *The Leydig Cell in Health and Disease*. Totowa, New Jersey: Humana Press.
- DURNEV, A. D., SOLOMINA, A. S., DAUGEL-DAUGE, N. O., ZHANATAEV, A. K., SHREDER, E. D., NEMOVA, E. P., SHREDER, O. V., VELIGURA, V. A., OSMINKINA, L. A., TIMOSHENKO, V. Y. & SEREDENIN, S. B. 2010. Evaluation of genotoxicity and reproductive toxicity of silicon nanocrystals. *Bull Exp Biol Med*, 149, 445-9.
- DZIENDZIKOWSKA, K., GROMADZKA-OSTROWSKA, J., LANKOFF, A., OCZKOWSKI, M., KRAWCZYNSKA, A., CHWASTOWSKA, J., SADOWSKA-BRATEK, M., CHAJDUK, E., WOJEWODZKA, M., DUSINSKA, M. & KRUSZEWSKI, M. 2012. Time-dependent biodistribution and excretion of silver nanoparticles in male Wistar rats. *J Appl Toxicol*, 32, 920-8.
- EACKER, S. M. & BRAUN, R. E. 2007. Androgen Receptor in Leydig Cell Function and Development. In: PAYNE, A. & HARDY, M. P. (eds.) *The Leydig Cell in Health and Disease*. Totowa, NJ: Humana Press.
- EC 2006. REGULATION (EC) No 1907/2006 on the Registration, Evaluation, Authorisation and Restriction of Chemicals (REACH) In: COUNCIL, E. P. A. (ed.) *No 1907/2006*. Brussels: European Parliament.
- EC 2008. Regulation 1272/2008 on Classification Labelling and Packaging of Substances In: COUNCIL, E. P. A. O. T. (ed.) *1272/2008*. Brussels: European Commission
- EC 2011. RECOMMENDATIONS: COMMISSION RECOMMENDATION of 18 October 2011 on the definition of nanomaterial (2011/696/EU), L 275/38. Official Journal of the European Union: European Commission.
- EC 2014. Data requirements for active substances, in accordance with Regulation (EC) No 1107/2009 of the European Parliament and of the Council concerning the placing of plant protection products on the market. In: COUNCIL, E. P. A. O. T. (ed.) *No 283/2013*. Brussels: European Commission.
- EC 2018. Regulation (EC) No 1907/2006 of the European Parliament and of the Council on the Registration, Evaluation, Authorisation and Restriction of Chemicals (REACH) as regards Annexes I, III, VI, VII, VIII, IX, X, XI, and XII to address nanoforms of substances. In: EUROPEAN PARLIAMENT AND OF THE COUNCIL ON THE REGISTRATION, E., AUTHORISATION AND RESTRICTION OF CHEMICALS (REACH) (ed.) *2018/1881*. Brussels: European Commission.

- ECHA 2008. Guidance on information requirements and chemical safety assessment, Chapter R.7a: Endpoint specific advice. Helsinki: European Chemicals Agency.
- ECHA 2017. Appendix R7-1 for nanomaterials applicable to Chapter R7a Endpoint specific guidance, version 2.0. *Guidance on information requirements and chemical safety assessment*. Finland: European Chemicals Agency.
- EDDIE, S. L., KIM, J. J., WOODRUFF, T. K. & BURDETTE, J. E. 2014. Microphysiological modeling of the reproductive tract: a fertile endeavor. *Exp Biol Med (Maywood)*, 239, 1192-202.
- EMA 2017. ICH S5 (R3) guideline on reproductive toxicology: detection of toxicity to reproduction for human pharmaceuticals. European Medicines Agency.
- ENGELI, R. T., FÜRSTENBERGER, C., KRATSCHMAR, D. V. & ODERMATT, A. 2018. Currently available murine Leydig cell lines can be applied to study early steps of steroidogenesis but not testosterone synthesis. *Heliyon*, 4.
- EPA 2000. OPPTS 870.3550 Reproduction/ Developmental Toxicity Screening Test. *EPA Health Effects Test Guidelines*.
- EPA. 2019. *Series 870 - Health Effects Test Guidelines* [Online]. EPA website: US Government Available: <https://www.epa.gov/test-guidelines-pesticides-and-toxic-substances/series-870-health-effects-test-guidelines> [Accessed 16/1/19 2019].
- EVANS, T. & GANJAM, V. K. 2011. Reproductive and Developmental Toxicology. In: GUPTA, R. C. (ed.) *Reproductive and Developmental Toxicology*. USA: Elsevier.
- FARCAL, L., ANDON, F. T., DI CRISTO, L., ROTOLI, B. M., BUSSOLATI, O., BERGAMASCHI, A., MECH, A., HARTMANN, N., PONIT, J., KINSER-OVASKAINEN, A., ROSSI, F., RASMUSSEN, K., RIEGO SINTES, J., OOMEN, A. G., BOS, P., CHEN, R., CHEN, C., BAI, R., ROCKS, L., FULTON, N., ROSS, B. L., HUTCHISON, G. R., TRAN, C. L., MUES, S., OSSIG, R., SCHNEKENBURGER, J., CAMPAGNOLO, L., VECCHIONE, L., PIETROIUSTI, A. & FADEEL, B. 2015. Comprehensive in vitro toxicity testing of a panel of representative oxide nanomaterials: first steps towards an intelligent testing strategy. *PLOS ONE*, In press.
- FAROMBI, E. O., ADEDARA, I. A., FORCADOS, G. E., ANAO, O. O., AGBOWO, A. & PATLOLLA, A. K. 2016. Responses of testis, epididymis, and sperm of pubertal rats exposed to functionalized multiwalled carbon nanotubes. *Environ Toxicol*, 31, 543-51.
- FATHI, N., HOSEINIPANAH, S. M., ALIZADEH, Z., ASSARI, M. J., MOGHIMBEIGI, A., MORTAZAVI, M., HOSSEINI, M. H. & BAHMANZADEH, M. 2018. The effect of silver nanoparticles on the reproductive system of adult male rats: A morphological, histological and DNA integrity study. *Adv Clin Exp Med*.
- FDA 1966. Guidelines for reproduction and studies for safety evaluation of drugs for human use. Bureau of Drugs, Rockville, MD.
- FINDLAY, F., POHL, J., SVOBODA, P., SHAKAMURI, P., MCLEAN, K., INGLIS, N. F., PROUDFOOT, L. & BARLOW, P. G. 2017. Carbon Nanoparticles Inhibit the Antimicrobial Activities of the Human Cathelicidin LL-37 through Structural Alteration. *J Immunol*, 199, 2483-2490.
- FOLEY, G. L. 2001. Overview of male reproductive pathology. *Toxicol Pathol*, 29, 49-63.
- FRANKLIN, N. M., ROGERS, N. J., APTE, S. C., BATLEY, G. E., GADD, G. E. & CASEY, P. S. 2007. Comparative Toxicity of Nanoparticulate ZnO, Bulk ZnO, and ZnCl₂ to a Freshwater Microalga (*Pseudokirchneriella subcapitata*): The Importance of Particle Solubility. *Environmental Science and Technology*, 41.
- FRAZER, J. 2014. *RE: Western Blotting Analysis Protocol*. Type to ROSS, B. L.
- FULTON, N. & HUTCHISON, G. H. 2012. *RE: TM3 and TM4 passage number and cell response*. Type to L, R. B.
- FULTON, N. & HUTCHISON, G. H. 2013. *RE: Response of TM4 cells to ENM exposure: cell proliferation and timecourse assays* Type to ROSS, B. L.
- GARCIA, T. X., COSTA, G. M. J., FRANÇA, L. R. & HOFMANN, M.-C. 2014. Sub-acute intravenous administration of silver nanoparticles in male mice alters Leydig cell function and testosterone levels. *Reproductive Toxicology*, 45, 59-70.

- GORE, A. C., CREWS, D., DOAN, L. L., LA MERRILL, M., PATISAUL, H. & ZOTA, A. 2014. INTRODUCTION TO ENDOCRINE DISRUPTING CHEMICALS (EDCs). Endocrine Society / IPEN.
- GORMLEY, A. J. & GHANDEHARI, H. 2009. Evaluation of Toxicity of Nanostructures in Biological Systems. In: SAHU, S. C. & CASCIANO, D. A. (eds.) *Nanotoxicity: From In Vivo and In Vitro Models to Health Risks*. Wiley.
- GOSENS, I., CASSEE, F. R., ZANELLA, M., MANODORI, L., BRUNELLI, A., COSTA, A. L., BOKKERS, B. G., DE JONG, W. H., BROWN, D., HRISTOZOV, D. & STONE, V. 2016. Organ burden and pulmonary toxicity of nano-sized copper (II) oxide particles after short-term inhalation exposure. *Nanotoxicology*, 10, 1084-95.
- GOSENS, I., KERMANIZADEH, A., JACOBSEN, N. R., LENZ, A. G., BOKKERS, B., DE JONG, W. H., KRYSZEK, P., TRAN, L., STONE, V., WALLIN, H., STOEGER, T. & CASSEE, F. R. 2015. Comparative hazard identification by a single dose lung exposure of zinc oxide and silver nanomaterials in mice. *PLoS One*, 10, e0126934.
- GROMADZKA-OSTROWSKA, J., DZIENDZIKOWSKA, K., LANKOFF, A., DOBRZYNSKA, M., INSTANES, C., BRUNBORG, G., GAJOWIK, A., RADZIKOWSKA, J., WOJEWODZKA, M. & KRUSZEWSKI, M. 2012. Silver nanoparticles effects on epididymal sperm in rats. *Toxicol Lett*, 214, 251-8.
- GUPTA, R. C. 2011. Introduction. In: C, G. R. (ed.) *Reproductive and Developmental Toxicology*. USA: Elsevier.
- GYLES, S. L., BURNS, C. J., WHITEHOUSE, B. J., SUGDEN, D., MARSH, P. J., PERSAUD, S. J. & JONES, P. M. 2001. ERKs regulate cyclic AMP-induced steroid synthesis through transcription of the steroidogenic acute regulatory (StAR) gene. *J Biol Chem*, 276, 34888-95.
- HAN, Z., YAN, Q., GE, W., LIU, Z.-G., GURUNATHAN, S., DE FELICI, M., SHEN, W. & ZHANG, X.-F. 2016. Cytotoxic effects of ZnO nanoparticles on mouse testicular cells. *International Journal of Nanomedicine*, Volume 11, 5187-5203.
- HANKIN, S. M., TRAN, C. L., ROSS, B., DONALDSON, K., STONE, V. & CHAUDHRY, Q. 2008. CELL PEN: A study to identify the physico-chemical factors controlling the capacity of nanoparticles to penetrate cells. Defra Research Report CB0407. UK: Defra.
- HARRIS, G. W. 1955. *Neural control of the Pituitary Gland.*, London, Edward Arnold.
- HARTMANN, N., JENSEN, K. A., BAUN, A., RASMUSSEN, K., RAUSCHER, H., TANTRA, R., CUPI, D., GILLILAND, D., PIANELLA, F. & RIEGO SINTES, J. 2015. Techniques and protocols for dispersing nanoparticle powders in aqueous media – (what) are we ready to harmonise? *J Toxicol Environ Health B Crit Rev.* , 18, 299-326.
- HELLEMANS, J., MORTIER, G., DE PAEPE, A., SPELEMAN, F. & VANDESOMPELE, J. 2007. qBase relative quantification framework and software for management and automated analysis of real-time quantitative PCR data. *Genome Biol*, 8, R19.
- HESS, R. A. 1990. Quantitative and Qualitative Characteristics of the Stages and Transitions in the Cycle of the Rat Seminiferous Epithelium: Light Microscopic Observations of Perfusion-Fixed and Plastic-Embedded Testes1. *Biology of Reproduction*, 43, 525-542.
- HONG, F., SI, W., ZHAO, X., WANG, L., ZHOU, Y., CHEN, M., GE, Y., ZHANG, Q., WANG, Y. & ZHANG, J. 2015. TiO₂ Nanoparticle Exposure Decreases Spermatogenesis via Biochemical Dysfunctions in the Testis of Male Mice. *J Agric Food Chem*, 63, 7084-92.
- HOUGAARD, K. S., JACKSON, P., JENSEN, K. A., SLOTH, J. J., LOSCHNER, K., LARSEN, E. H., BIRKEDAL, R. K., VIBENHOLT, A., BOISEN, A. M., WALLIN, H. & VOGEL, U. 2010. Effects of prenatal exposure to surface-coated nanosized titanium dioxide (UV-Titan). A study in mice. *Part Fibre Toxicol*, 7, 16.
- HUTCHISON, G. R., SCOTT, H. M., WALKER, M., MCKINNELL, C. & FERRARA, D. 2008. Sertoli cell development and function in an animal model of testicular dysgenesis syndrome. *Biology of Reproduction*, 78, 352-360.

- IGNEY, F. H. & KRAMMER, P. H. 2002. Death and anti-death: Tumor resistance to apoptosis. *Nature Reviews Cancer*, 2, 227-288.
- IVASK, A., SCHECKEL, K. G., KAPRUWAN, P., STONE, V., YIN, H., VOELCKER, N. H. & LOMBI, E. 2017. Complete transformation of ZnO and CuO nanoparticles in culture medium and lymphocyte cells during toxicity testing. *Nanotoxicology*, 11, 150-156.
- IVELL, R. & ANAND-IVELL, R. 2009. Biology of insulin-like factor 3 in human reproduction. *Hum Reprod Update*, 15, 463-76.
- IVELL, R., HENG, K. & ANAND-IVELL, R. 2014. Insulin-Like Factor 3 and the HPG Axis in the Male. *Front Endocrinol (Lausanne)*, 5, 6.
- JACKSON, P., HALAPPANAVAR, S., HOUGAARD, K. S., WILLIAMS, A., MADSEN, A. M., LAMSON, J. S., ANDERSEN, O., YAUK, C., WALLIN, H. & VOGEL, U. 2011. Maternal inhalation of surface-coated nanosized titanium dioxide (UV-Titan) in C57BL/6 mice: effects in prenatally exposed offspring on hepatic DNA damage and gene expression. *Nanotoxicology*.
- JIA, F., SUN, Z., YAN, X., ZHOU, B. & WANG, J. 2014. Effect of pubertal nano-TiO₂ exposure on testosterone synthesis and spermatogenesis in mice. *Arch Toxicol*, 88, 781-8.
- JIANG, X., DIAS, J. A. & HE, X. 2014. Structural biology of glycoprotein hormones and their receptors: insights to signaling. *Mol Cell Endocrinol*, 382, 424-451.
- JO, E., SEO, G., KWON, J. T., LEE, M., LEE, B., EOM, I., KIM, P. & CHOI, K. 2013. Exposure to zinc oxide nanoparticles affects reproductive development and biodistribution in offspring rats. *J Toxicol Sci*, 38, 525-30.
- JOBLING, M. S., HUTCHISON, G. R., VAN DER DRIESCHE, S. & SHARPE, R. 2011. Effects of Di(n-butyl) phthalate exposure on fetal rat germ cell number and differentiation: identification of age-specific windows of vulnerability. *International Journal of Andrology*, 34, e386–e396.
- JOHNSON, M. & EVERITT, B. J. 2000. *Essential Reproduction, 5th Edition*, Blackwell Science Ltd.
- JOHNSTON, H. J., HUTCHISON, G., CHRISTENSEN, F. M., PETERS, S., HANKIN, S. & STONE, V. 2010. A review of the in vivo and in vitro toxicity of silver and gold particulates: particle attributes and biological mechanisms responsible for the observed toxicity. *Crit Rev Toxicol*, 40, 328-46.
- JRC 2011. List of materials in the Joint Research Council Nanomaterials (NM) Repository. http://ihcp.jrc.ec.europa.eu/our_activities/nanotechnology/nanomaterials-repository/list_materials_JRC_rep_oct_2011.pdf: JRC.
- KANG, J. S. & PARK, J. W. 2018. Insight on cytotoxic effects of silver nanoparticles: Alternative androgenic transactivation by adsorption with DHT. *Sci Total Environ*, 618, 712-717.
- KERMANIZADEH, A., VRANIC, S., BOLAND, S., MOREAU, K., BAEZA-SQUIBAN, A., GAISER, B., ANDRZEJCZUK, L. & STONE, V. 2013. An in vitro assessment of panel of engineered nanomaterials using a human renal cell line: cytotoxicity, pro-inflammatory response, oxidative stress and genotoxicity. *BMC Nephrology*, 14, 1-12.
- KHARLYNGDOH, J. B., PRADHAN, A. & OLSSON, P. E. 2018. Androgen receptor modulation following combination exposure to brominated flame-retardants. *Sci Rep*, 8, 4843.
- KHORSANDI, L., ORAZIZADEH, M., MORADI-GHARIBVAND, N., HEMADI, M. & MANSOURI, E. 2017. Beneficial effects of quercetin on titanium dioxide nanoparticles induced spermatogenesis defects in mice. *Environ Sci Pollut Res Int*, 24, 5595-5606.
- KIM, H. J., YOON, J., MATSUURA, A., NA, J. H., LEE, W. K., KIM, H., CHOI, J. W., PARK, J. E., PARK, S. J., KIM, K. T., CHANG, R., LEE, B. I., YU, Y. G., SHIN, Y. K., JEONG, C., RHEE, K. & LEE, H. H. 2015. Structural and biochemical insights into the role of testis-expressed gene 14 (TEX14) in forming the stable intercellular bridges of germ cells. *Proc Natl Acad Sci U S A*, 112, 12372-7.

- KIM, J. S., YOON, T. J., YU, K. N., KIM, B. G., PARK, S. J., KIM, H. W., LEE, K. H., PARK, S. B., LEE, J. K. & CHO, M. H. 2006. Toxicity and tissue distribution of magnetic nanoparticles in mice. *Toxicol Sci*, 89, 338-47.
- KIM, Y. S., KIM, J. S., CHO, H. S., RHA, D. S., KIM, J. M., PARK, J. D., CHOI, B. S., LIM, R., CHANG, H. K. & CHUNG, Y. H. 2008. Twenty-eight-day oral toxicity, genotoxicity, and gender-related tissue distribution of silver nanoparticles in Sprague-Dawley rats. *Inhal Toxicol*, 20, 575-583.
- KIM, Y. S., SONG, M. Y., PARK, J. D., SONG, K. S., RYU, H. R., CHUNG, Y. H., CHANG, H. K., LEE, J. H., OH, K. H., KELMAN, B. J., HWWANG, I. K. & YU, I. J. 2010. Subchronic oral toxicity of silver nanoparticles. *Particle and fibre toxicity*, 7.
- KITTLER, S., GREULICH, C., DIENDORF, J., KÖLLER, M. & EPPLE, M. 2010. Toxicity of Silver Nanoparticles Increases during Storage Because of Slow Dissolution under Release of Silver Ions. *Chemistry of Materials*, 22, 4548-4554.
- KOMATSU, T., TABATA, M., KUBO-IRIE, M., SHIMIZU, T., SUZUKI, K., NIHEI, Y. & TAKEDA, K. 2008. The effects of nanoparticles on mouse testis Leydig cells in vitro. *Toxicol In Vitro*, 22, 1825-31.
- KONG, L. 2012. Institute of High Energy Physics, Beijing: The suppression of prostate LNCaP cancer cells growth by Selenium nanoparticles through Akt/Mdm2/AR controlled apoptosis In: ASHTON ACTON, Q. (ed.) *Steroid Receptors—Advances in Research and Application: 2012 Edition*. ScholarlyEditions.
- KONG, L., TANG, M., ZHANG, T., WANG, D., HU, K., LU, W., WEI, C., LIANG, G. & PU, Y. 2014. Nickel nanoparticles exposure and reproductive toxicity in healthy adult rats. *Int J Mol Sci*, 15, 21253-69.
- KOTULA-BALAK, M., HEJMEJ, A. & BILINSKI, B. 2012. Hydroxysteroid Dehydrogenases – Localization, Function and Regulation in the Testis. *Dehydrogenases*.
- KROLL, A., PILLUKAT, M. H., HAHN, D. & SCHNEKENBURGER, J. 2012. Interference of engineered nanoparticles with in vitro toxicity assays. *Arch Toxicol*, 86, 1123-36.
- LAI, W., WANG, Q., LI, L., HU, Z., CHEN, J. & FANG, Q. 2017. Interaction of gold and silver nanoparticles with human plasma: Analysis of protein corona reveals specific binding patterns. *Colloids and Surfaces B: Biointerfaces*, 152, 317-325.
- LAN, Z. & YANG, W.-X. 2012. Nanoparticles and spermatogenesis: how do nanoparticles affect spermatogenesis and penetrate the blood-testis barrier. *Nanomedicine*, 7, 579-596.
- LAYALI, E., THAHMASBPOUR, E. & JORSARAEI, S. G. A. 2016. Effects of Silver Nanoparticles on Lipid Peroxidation and Quality of Sperm Parameters in Male Rats. *J Babol Univ Med Sci*, 18, 48-55.
- LEBLOND, C. P. & CLERMONT, Y. 1952. DEFINITION OF THE STAGES OF THE CYCLE OF THE SEMINIFEROUS EPITHELIUM IN THE RAT. *Annals of the New York Academy of Sciences*, 55.
- LEE, J., RICHBURG, J. H., YOUNKIN, S. C. & BOEKELHEIDE, K. 1997. The Fas System Is a Key Regulator of Germ Cell Apoptosis in the Testis. *Endocrinology*, 138, 2081-2088.
- LEE, J. H., KIM, Y. S., SONG, K. S., RYU, H. R., SUNG, J. H., PARK, J. D., PARK, H. M., SONG, N. W., SHIN, B. S., MARSHAK, D., AHN, K., LEE, J. E. & YU, I. J. 2013. Biopersistence of silver nanoparticles in tissues from Sprague-Dawley rats. *Particle and fibre toxicity*, 10.
- LEE, K. J., NALLATHAMBY, P. D., BROWNING, L. M., OSGOOD, C. J. & XU, X. H. 2007. In vivo imaging of transport and biocompatibility of single silver nanoparticles in early development of zebrafish embryos. *ACS Nano*, 1, 133-43.
- LI, P. W., KUO, T. H., CHANG, J. H., YEH, J. M. & CHAN, W. H. 2010. Induction of cytotoxicity and apoptosis in mouse blastocysts by silver nanoparticles. *Toxicol Lett*, 197, 82-7.
- LIVAK, K. J. & SCHMITTGEN, T. D. 2001. Analysis of relative gene expression data using real-time quantitative PCR and the 2(-Delta Delta C(T)) Method. *Methods*, 25, 402-8.

- LUNDQVIST, M., STIGLER, J., ELIA, G., LYNCH, I., CEDERVALL, T. & DAWSON, K. A. 2008. Nanoparticle size and surface properties determine the protein corona with possible implications for biological impacts. *Proc Natl Acad Sci U S A*, 105, 14265-70.
- LYNCH, I. & DAWSON, K. 2008. Protein-nanoparticle interactions. *Nano Today*, 3, 40-47.
- MA, D.-D. & YANG, W.-X. 2016. Engineered nanoparticles induce cell apoptosis: potential for cancer therapy. *Oncotarget*, 7.
- MAKAROW, M. & HOJGAARD, L. 2010. Male reproductive health. Its impacts in relation to general wellbeing and low European fertility rates. *European Science Foundation. Science policy briefing*, 40.
- MANNA, P. R., STETSON, C. L., SLOMINSKI, A. T. & PRUITT, K. 2016. Role of the steroidogenic acute regulatory protein in health and disease. *Endocrine*, 51, 7-21.
- MANNERSTRÖM, M., ZOU, J., TOIMELA, T., PYYKKÖ, I. & HEINONEN, T. 2016. The applicability of conventional cytotoxicity assays to predict safety/toxicity of mesoporous silica nanoparticles, silver and gold nanoparticles and multi-walled carbon nanotubes. *Toxicology in Vitro*, 37, 113-120.
- MATHER, J. P. 1980. Establishment and characterization of two distinct mouse testicular epithelial cell lines. *Biol Reprod*, 23, 243-52.
- MATHER, J. P., ZHUANG, L. Z., PEREZ-INFANTE, V. & PHILLIPS, D. M. 1982. Culture of testicular cells in hormone-supplemented serum-free medium. *Ann N Y Acad Sci*, 383, 44-68.
- MATHIAS, F. T., ROMANO, R. M., KIZYS, M. M., KASAMATSU, T., GIANNOCCO, G., CHIAMOLERA, M. I., DIAS-DA-SILVA, M. R. & ROMANO, M. A. 2015. Daily exposure to silver nanoparticles during prepubertal development decreases adult sperm and reproductive parameters. *Nanotoxicology*, 9, 64-70.
- MCCONNELL, R. F., WESTEN, H. H., ULLAND, B. M., BOSLAND, M. C. & WARD, J. 1992. Proliferative lesions of the testes in rats with selected examples from mice URG-3. *Guides for Toxicologic Pathology*. Washington, DC.: STP/ARP/AFIP
- MEENA, R., KAJAL, K. & R, P. 2015. Cytotoxic and genotoxic effects of titanium dioxide nanoparticles in testicular cells of male wistar rat. *Appl Biochem Biotechnol*, 175, 825-40.
- MEISTRICH, M. L. & HESS, R. A. 2013. Assessment of spermatogenesis through staging of seminiferous tubules. *Methods Mol Biol*, 927, 299-307.
- MIRESMAEILI, S. M., HALVAEI, I., FESAHAAT, F., FALLAH, A., NIKONAHAD, N. & TAHERINEJAD, M. 2013. Evaluating the role of silver nanoparticles on acrosomal reaction and spermatogenic cells in rat. *Iranian Journal of Reproductive Medicine*, 11, 423-430.
- MOHAMED, D. A. & ABDELRAHMAN, S. A. 2018. The possible protective role of zinc oxide nanoparticles (ZnONPs) on testicular and epididymal structure and sperm parameters in nicotine-treated adult rats (a histological and biochemical study). *Cell Tissue Res*.
- MORETTI, E., TERZUOLI, G., RENIERI, T., IACOPONI, F., CASTELLINI, C., GIORDANO, C. & COLLODEL, G. 2013. In vitro effect of gold and silver nanoparticles on human spermatozoa. *Andrologia*, 45, 392-6.
- MORI, H. 1980. Morphometric analysis of Leydig cells in the normal rat testis. *The Journal of Cell Biology*, 84, 340-354.
- MORIDIAN, M., KHORSANDI, L. & TALEBI, A. R. 2015. Morphometric and stereological assessment of the effects of zinc oxide nanoparticles on the mouse testicular tissue. *Bratisl Lek Listy*, 116, 321-325.
- MORISHITA, Y., YOSHIOKA, Y., SATOH, H., NOJIRI, N., NAGANO, K., ABE, Y., KAMADA, H., TSUNODA, S., NABESHI, H., YOSHIKAWA, T. & TSUTSUMI, Y. 2012. Distribution and histologic effects of intravenously administered amorphous nanosilica particles in the testes of mice. *Biochem Biophys Res Commun*, 420, 297-301.
- MOSSADEGH-KELLER, N., GENTEK, R., GIMENEZ, G., BIGOT, S., MAILFERT, S. & SIEWEKE, M. H. 2017. Developmental origin and maintenance of distinct testicular macrophage populations. *J Exp Med*, 214, 2829-2841.

- MOTZKUS, C., GAIE-LEVREL, F., AUSSET, P., MAILLÉ, M., BACCILE, N., VASLIN-REIMANN, S., IDRAC, J., OSTER, D., FISCHER, N. & MACÉ, T. 2014. Impact of batch variability on physicochemical properties of manufactured TiO₂ and SiO₂ nanopowders. *Powder Technology*, 267, 39-53.
- MRUK, D. D. & CHENG, C. Y. 2015. The Mammalian Blood-Testis Barrier: Its Biology and Regulation. *Endocr Rev*, 36, 564-91.
- MUSA, R. M., RTAKENAKA, I., KONISHI, R. & TOKUDA, M. 2000. Effects of Luteinizing Hormone, Follicle-Stimulating Hormone, and Epidermal Growth Factor on Expression and Kinase Activity of Cyclin-Dependent Kinase 5 in Leydig TM3 and Sertoli TM4 Cell Lines. *Journal of Andrology*, 21.
- NAPIERSKA, D., THOMASSEN, L., LISON, D., MARTENS, J. & HOET, P. 2010. The nanosilica hazard: another variable entity. *Part Fibre Toxicol*, 7, 39.
- NARAYAN, P. 2015. Genetic Models for the Study of Luteinizing Hormone Receptor Function. *Front Endocrinol (Lausanne)*, 6, 152.
- NETTER, F. 1997. *The Netter collection of medical illustrations, Volume 2, Reproductive System*, Philadelphia, Saunders Elsevier.
- NGUYEN, D. T., VAN NOORT, D., JEONG, I. K. & PARK, S. 2017. Endocrine system on chip for a diabetes treatment model. *Biofabrication*, 9, 015021.
- NICHOLAS, C. R., XU, E. Y., BANANI, S. F., HAMMER, R. E., HAMRA, F. K. & REIJO PERA, R. A. 2009. Characterization of a Dazl-GFP germ cell-specific reporter. *Genesis*, 47, 74-84.
- NIRMAL, N. K., AWASTHI, K. K. & JOHN, P. J. 2017. Effects of hydroxyl-functionalized multiwalled carbon nanotubes on sperm health and testes of Wistar rats. *Toxicology and Industrial Health*, 33, 519-529.
- O'HARA, L., MCINNES, K., SIMITSIDELLIS, I., MORGAN, S., ATANASSOVA, N., SLOWIKOWSKA-HILCZER, J., KULA, K., SZARRAS-CZAPNIK, M., MILNE, L., MITCHELL, R. T. & SMITH, L. B. 2015. Autocrine androgen action is essential for Leydig cell maturation and function, and protects against late-onset Leydig cell apoptosis in both mice and men. *FASEB J*, 29, 894-910.
- O'BRIEN, J., WILSON, I., ORTON, T. & POGNAN, F. 2000. Investigation of the Alamar Blue (resazurin) fluorescent dye for the assessment of mammalian cell cytotoxicity. *European Journal of Biochemistry*, 267.
- O'SHAUGHNESSY, P. J. 2017. The Human Leydig Cell. *Male Hypogonadism*.
- OATLEY, J. M. & BRINSTER, R. L. 2006. Spermatogonial Stem Cells. *Methods in Enzymology*, 419, 259-282.
- OBERDORSTER, G., ELDER, A. & RINDERKNECHT, A. 2009. Nanoparticles and the brain: cause for concern? *J Nanosci Nanotechnol*, 9, 4996-5007.
- OBERDORSTER, G., OBERDORSTER, E. & OBERDORSTER, J. 2005. Nanotoxicology: an emerging discipline evolving from studies of ultrafine particles. *Environ Health Perspect*, 113, 823-39.
- ODERMATT, A., STRAJHAR, P. & ENGELI, R. T. 2016. Disruption of steroidogenesis: Cell models for mechanistic investigations and as screening tools. *J Steroid Biochem Mol Biol*, 158, 9-21.
- OECD 1983. *Test No. 415: One-Generation Reproduction Toxicity Study*, OECD Publishing.
- OECD 2001. *Test No. 416: Two-Generation Reproduction Toxicity*, OECD Publishing.
- OECD 2010. LIST OF MANUFACTURED NANOMATERIALS AND LIST OF ENDPOINTS FOR PHASE ONE OF THE SPONSORSHIP PROGRAMME FOR THE TESTING OF MANUFACTURED NANOMATERIALS: REVISION. *Series on the Safety of Manufactured Nanomaterials, No. 27*. Paris: Organisation for Economic Co-operation and Development (OECD).
- OECD 2011. *Test No. 443: Extended One-Generation Reproductive Toxicity Study*, OECD Publishing.
- OECD 2015. *Test No. 421: Reproduction/Developmental Toxicity Screening Test*, OECD Publishing.

- OECD 2016. GUIDANCE DOCUMENT ON THE REPORTING OF DEFINED APPROACHES TO BE USED WITHIN INTEGRATED APPROACHES TO TESTING AND ASSESSMENT. *Series on Testing & Assessment No. 255*. Paris: OECD Publishing.
- OECD 2018a. Guidance Document on Good In Vitro Method Practices (GIVIMP). *OECD Series on Testing and Assessment, No. 286*. Paris: OECD Publishing.
- OECD 2018b. Revised Guidance Document 150 on Standardised Test Guidelines for Evaluating Chemicals for Endocrine Disruption. *OECD Series on Testing and Assessment*. Paris: OECD.
- OECD accessed 2017. OECD Histology Guide: Part 2: Male Reproductive System.
- ORAZIZADEH, M., KHORSANDI, L., ABSALAN, F., HASHEMITABAR, M. & DANESHI, E. 2014. Effect of beta-carotene on titanium oxide nanoparticles-induced testicular toxicity in mice. *J Assist Reprod Genet*, 31, 561-8.
- OSMOND MCLEOD, M. J. 2014. Surface Coatings Protect against the In vitro Toxicity of Zinc Oxide Nanoparticles in Human Hepatic Stellate Cells. *Journal of Nanomedicine & Nanotechnology*, 05.
- PAPADOPOULOS, V., BARALDI, M., GUILARTE, T. R., KNUDSEN, T. B., LACAPÈRE, J., LINDEMANN, P., NORENBORG, M. D., NUTT, D., WEIZMAN, A., ZHANG, M.-R. & GAVISH, M. 2006. Translocator protein (18 kDa): new nomenclature for the peripheral-type benzodiazepine receptor based on its structure and molecular function. *Trends in Pharmacological Sciences*, 27, 402-409.
- PARK, E. J., BAE, E., YI, J., KIM, Y., CHOI, K., LEE, S. H., YOON, J., LEE, B. C. & PARK, K. 2010. Repeated-dose toxicity and inflammatory responses in mice by oral administration of silver nanoparticles. *Environ Toxicol Pharmacol*, 30, 162-8.
- PARK, M. V., ANNEMA, W., SALVATI, A., LESNIAK, A., ELSAESSER, A., BARNES, C., MCKERR, G., HOWARD, C. V., LYNCH, I., DAWSON, K. A., PIERSMA, A. H. & DE JONG, W. H. 2009. In vitro developmental toxicity test detects inhibition of stem cell differentiation by silica nanoparticles. *Toxicol Appl Pharmacol*, 240, 108-16.
- PAWAR, K. & KAUL, G. 2012. Toxicity of titanium oxide nanoparticles causes functionality and DNA damage in buffalo (*Bubalus bubalis*) sperm in vitro. *Toxicol Ind Health*.
- PAYNE, A. 2007. Steroidogenic Enzymes in Leydig Cells. In: PAYNE, A. & HARDY, M. P. (eds.) *The Leydig Cell in Health and Disease*. Totowa New Jersey: Humana Press.
- PÉREZ, C. V., THEAS, M. S., JACOBO, P. V., JARAZO-DIRTRICH, S., GUAZZONE, V. A. & LUSTIF, L. 2013. Dual role of immune cells in the testis: Protective or pathogenic for germ cells? *Spermatogenesis*, 3.
- PFURTSCHELLER, K., PETNEHAZY, T., GOESSLER, W., BUBALO, V., KAMOLZ, L. P. & TROP, M. 2014. Transdermal uptake and organ distribution of silver from two different wound dressings in rats after a burn trauma. *Wound Repair and Regeneration*, 22, 654-659.
- PIETROIUSTI, A., CAMPAGNOLO, L. & FADEEL, B. 2013. Interactions of engineered nanoparticles with organs protected by internal biological barriers. *Small*, 9, 1557-72.
- PLANT, T. M. 2015. 60 YEARS OF NEUROENDOCRINOLOGY: The hypothalamo-pituitary-gonadal axis. *J Endocrinol*, 226, T41-54.
- PON, L. A. & ORME-JOHNSON, N. R. 1986. Acute stimulation of steroidogenesis in corpus luteum and adrenal cortex by peptide hormones. Rapid induction of a similar protein in both tissues. *The Journal of Biological Chemistry*, 261, 6594-6599.
- POWERS, C. M., SLOTKIN, T. A., SEIDLER, F. J., BADIREDDY, A. R. & PADILLA, S. 2011. Silver nanoparticles alter zebrafish development and larval behavior: distinct roles for particle size, coating and composition. *Neurotoxicol Teratol*, 33, 708-14.
- POWERS, C. M., YEN, J., LINNEY, E. A., SEIDLER, F. J. & SLOTKIN, T. A. 2010. Silver exposure in developing zebrafish (*Danio rerio*): persistent effects on larval behavior and survival. *Neurotoxicol Teratol*, 32, 391-7.
- RASMUSSEN, K., MAST, J., DE TEMMERMAN, P.-J., VERLEYSSEN, E., WAEGENEERS, N., VAN STEEN, F., PIZZOLON, J. C., DE TEMMERMAN, L., VAN DOREN, E., JENSEN, K. A.,

- BIRKEDAL, R. K., CLAUSEN, L. P. W., KEMBOUCHE, Y., THIERIET, N., SPALLA, O., GUIOT, C., ROUSSET, D., WITSCHGER, O., BAU, S., BIANCHI, B., SHIVACHEV, B., DIMOWA, L., NIKOLOVA, R., NIHTIANOVA, D., TARASSOV, M., PETROV, O., BAKARDJIEVA, S., MOTZKUS, C., LABARRAQUE, G., OSTER, C., COTOGNO, G. & GAILLIARD, C. 2014. Multi-walled Carbon Nanotubes, NM-400, NM-401, NM-402, NM-403: Characterisation and Physico-Chemical Properties. *JRC Science and Policy Reports*. Luxembourg: Joint Research Centre, European Commission.
- RASMUSSEN, K., MECH, A., GILLIAND, G., PIANELLA, F., CECCONE, G., COTOHNO, G., RAUSCHER, H., GIBSON, N., STAMM, H., MARST, J., DE TEMMERMAN, P.-J., WARGENEERS, N., VAN DOREN, E., JENSEN, K. A., BIRKEDAL, R. K., LEVIN, M., NIELSEN, S. H., KOPONEN, I. K., CLAUSEN, P. A., KEMBOUCHE, Y., THEIRIET, N., SPALLA, O., GUIOT, C., ROUSSET, D., WITSCHGER, O., BAU, S., BIANCHI, B. & SHICHEV, B. 2013. Synthetic Amorphous Silicon Dioxide (NM-200, NM-201, NM-202, NM-203, NM-204): Characterisation and Physico-Chemical Properties. *JRC Repository: NM-Series of Representative Manufactured Nanomaterials*. Italy: Joint Research Council, European Commission.
- REAVEN, E., ZHAN, L., NOMOTO, A., LEERS-SUCHETA, S. & AZHAR, S. 2000. Expression and microvillar localization of scavenger receptor class B, type I (SR-BI) and selective cholesteryl ester uptake in Leydig cells from rat testis. *Journal of Lipid Research*, 41.
- REN, L., ZHANG, J., ZOU, Y., ZHANG, L., WEI, J., SHI, Z., LI, Y., GUO, C., SUN, Z. & ZHOU, X. 2016. Silica nanoparticles induce reversible damage of spermatogenic cells via RIPK1 signal pathways in C57 mice. *Int J Nanomedicine*, 11, 2251-64.
- RESEARCHANDMARKETS 2018. Global Nanotechnology Market (by Component and Applications), Funding & Investment, Patent Analysis and 27 Companies Profile & Recent Developments - Forecast to 2024. ResearchAndMarkets.com: iGATE Research.
- REZAZADEH-REYHANI, Z., RAZI, M., MALEKINEJAD, H. & SADRKHANLOU, R. 2015. Cytotoxic effect of nanosilver particles on testicular tissue: Evidence for biochemical stress and Hsp70-2 protein expression. *Environ Toxicol Pharmacol*, 40, 626-38.
- REZNIKOV, A. G., SALIVONYK, O. A., SOTKIS, A. G. & SHUBA, Y. M. 2015. ASSESSMENT OF GOLD NANOPARTICLE EFFECT ON PROSTATE CANCER LNCaP CELLS. *Experimental Oncology*, 37, 100-104.
- RIEGO SINTES, J. 2015. MARINA Reference Materials (WP3): Reference Dossiers with industrial, scientific and regulatory relevance. In: TRAN, C. L. (ed.). UK: IOM.
- ROCCHIETTI-MARCH, M., WEINBAUER, G. F., PAGE, E., NIESCHLAG, E. & GROMOLL, J. 2000. Dazl protein expression in adult rat testis is up-regulated at meiosis and not hormonally regulated. *International journal of andrology*, 23, 51-56.
- ROCCO, M. C. 2005. National Nanotechnology Initiative at Five Years: from concept to reality. *Discovery Lecture Series 2006, Purdue University*. Nanohub.
- ROCHE 2011. Cell Proliferation Reagent WST-1. Sigma Aldrich Online: Roche Diagnostics.
- ROLLAND, M., LE MOAL, J., WAGNER, V., ROYERE, D. & DE MOUZON, J. 2013. Decline in semen concentration and morphology in a sample of 26,609 men close to general population between 1989 and 2005 in France. *Hum Reprod*, 28, 462-70.
- RS-RAE 2004. *Nanoscience and nanotechnologies: opportunities and uncertainties*. Latimer Trend Ltd, Plymouth, UK.
- RUSSEL, W. M. S. & BURCH, R. L. 1959. *The Principles of Humane Experimental Technique*, London, Meuthen.
- SAVOLAINEN, K., ALENIUS, H., NORPPA, H., PYLKKANEN, L., TUOMI, T. & KASPER, G. 2010. Risk assessment of engineered nanomaterials and nanotechnologies--a review. *Toxicology*, 269, 92-104.
- SCHLATT, S. & EHMCKE, J. 2014. Regulation of spermatogenesis: An evolutionary biologist's perspective. *Seminars in Cell & Developmental Biology*, 29, 2-16.
- SELTMAN, H. J. 2018. Experimental Design and Analysis. Carnegie Mellon University.

- SEWER, M. B. & LI, D. 2008. Regulation of steroid hormone biosynthesis by the cytoskeleton. *Lipids*, 43, 1109-15.
- SHAHA, C., TRIPATHI, R. & MISHRA, D. P. 2010. Male germ cell apoptosis: regulation and biology. *Philos Trans R Soc Lond B Biol Sci*, 365, 1501-15.
- SHARPE, R. 1983. LOCAL CONTROL OF TESTICULAR FUNCTION. *Quarterly Journal of Experimental Physiology*, 68, 265-287.
- SHERBET, D. P. & AUCHUS, R. J. 2007. Peripheral Testosterone Metabolism. In: PAYNE, A. & HARDY, M. P. (eds.) *The Leydig Cell in Health and Disease*. Totowa, NJ: Humana Press.
- SILVA, M. J., PHAM, N., LEWIS, C., IYER, S., KWOK, E., SOLOMON, G. & ZIESE, L. 2015. A Comparison of ToxCast Test Results with In Vivo and Other In Vitro Endpoints for Neuro, Endocrine, and Developmental Toxicities: A Case Study Using Endosulfan and Methidathion. *Birth Defects Research Part B Developmental and Reproductive Toxicology online* 2.
- SINGH, S. K. & ABE, K. 1987. Light and electron microscopic observations of giant cells in the mouse testis after efferent duct ligation. *Archives of histology japan*, 50, 579-585.
- SLEIMAN, H. K., ROMANO, R. M., OLIVEIRA, C. A. D. & ROMANO, M. A. 2013. Effects of Prepubertal Exposure to Silver Nanoparticles on Reproductive Parameters in Adult Male Wistar Rats. *Journal of Toxicology and Environmental Health, Part A*, 76, 1023-1032.
- SMITH, M. A., MICHAEL, R., ARAVINDAN, R. G., DASH, S., SHAH, S. I., GALILEO, D. S. & MARTIN-DELEON, P. A. 2015. Anatase titanium dioxide nanoparticles in mice: evidence for induced structural and functional sperm defects after short-, but not long-, term exposure. *Asian J Androl*, 17, 261-8.
- SPA, M. N. 2014. Deliverable 1.3: Aquisition of pristine nanomaterials and their integration into products. *Sustainable Nanotechnologies (SUN)*. MBN Nanomaterials SPA.
- SPIELMANN, H. 2009. The way forward in reproductive/developmental toxicity testing. *Altern Lab Anim*, 37, 641-56.
- STANCZYK, F. Z., LEE, J. S. & SANTEN, R. J. 2007. Standardization of steroid hormone assays: why, how, and when? *Cancer Epidemiol Biomarkers Prev*, 16, 1713-9.
- STOCCO, D. M. 2007. The role of StaR in Leydig Cell Steroidogenesis In: PAYNE, A. & HARDING, J. (eds.) *The Leydig Cell in Health and Disease*. Totowa, New Jersey: Humana Press.
- TAKEDA, K., SUZUKI, K., ISHIHARA, A., KUBO-IRIE, M., FUJIMOTO, R., TABATA, M., OSHIO, S., NIHEI, Y., IHARA, T. & SUGAMATA, M. 2009. Nanoparticles transferred from pregnant mice to their offspring can damage the genital and cranial nerve systems. *J Health Sci*, 55, 95 - 102.
- TALEBI, A. R., KHORSANDI, L. & MORIDIAN, M. 2013. The effect of zinc oxide nanoparticles on mouse spermatogenesis. *J Assist Reprod Genet*, 30, 1203-9.
- TASSINARI, R., CUBADDA, F., MORACCI, G., AURELI, F., D'AMATO, M., VALERI, M., DE BERARDIS, B., RAGGI, A., MANTOVANI, A., PASSERI, D., ROSSI, M. & MARANGHI, F. 2013. Oral, short-term exposure to titanium dioxide nanoparticles in Sprague-Dawley rat: focus on reproductive and endocrine systems and spleen. *Nanotoxicology*.
- TAYLOR, S. 2010. A Practical Guide to Publishing RT-qPCR Data That Conform to the MIQE Guidelines. *American Biotechnology Laboratory*, 28.
- TAYLOR, U., GARRELS, W., BARCHANSKI, A., PETERSON, S., SAJTI, L., LUCAS-HAHN, A., GAMRAD, L., BAULAIN, U., KLEIN, S., KUES, W. A., BARCIKOWSKI, S. & RATH, D. 2014. Injection of ligand-free gold and silver nanoparticles into murine embryos does not impact pre-implantation development. *Beilstein J Nanotechnol*, 5, 677-88.
- TEEGUARDEN, J. G., HINDERLITER, P. M., ORR, G., THRALL, B. D. & POUNDS, J. G. 2007. Particokinetics in vitro: dosimetry considerations for in vitro nanoparticle toxicity assessments. *Toxicol Sci*, 95, 300-12.
- THAKUR, M., GUPTA, H., SINGH, D., MOHANTY, I. R., MAHESWARI, U., VANAGE, G. & JOSHI, D. S. 2014. Histopathological and ultra structural effects of nanoparticles on rat testis

- following 90 days (Chronic study) of repeated oral administration. *Journal of Nanobiotechnology*, 12.
- THERMOFISHER-SCIENTIFIC. 2019a. *Charcoal Stripped Fetal Bovine Serum* [Online]. Available: <https://www.thermofisher.com/uk/en/home/life-science/cell-culture/mammalian-cell-culture/fbs/specialty-serum/charcoal-stripped-fbs.html> [Accessed].
- THERMOFISHER-SCIENTIFIC. 2019b. *Overview of Western Blotting* [Online]. UK: Thermo Fisher Scientific. Available: <https://www.thermofisher.com/uk/en/home/life-science/protein-biology/protein-biology-learning-center/protein-biology-resource-library/pierce-protein-methods/overview-western-blotting.html> [Accessed January 3rd 2019].
- TOWBIN, H., STAHELIN, T. & GORDON, J. 1979. Electrophoretic Transfer of Proteins from Polyacrylamide Gels to Nitrocellulose Sheets: Procedure and Some Applications. *PNAS*, 76, 4350-4354.
- TRAN CL, H. S., ROSS B, AITKEN RJ, JONES AD, DONALDSON K, STONE V, TANTRA R 2008. An outline scoping study to determine whether high aspect ratio nanoparticles (HARN) should raise the same concerns as do asbestos fibres. Report on DEFRA project CB0406. Defra.
- UNECE 2005. United Nations Economic Commission for Europe Globally Harmonized System for Classification and Labelling of Chemicals (GHS), Chapter 3. 7. Reproductive Toxicity. New York/Geneva: United Nations.
- VAN DER LOOS, C. M. 2008. Multiple immunoenzyme staining: methods and visualizations for the observation with spectral imaging. *J Histochem Cytochem*, 56, 313-28.
- VAN DER ZANDE, M., VANDEBRIEL, R. J., GROOT, M. J., KRAMER, E., HERRERA RIVERA, Z., RASMUSSEN, K., OSSENKOPPELE, J. S., TROMP, P., GREMMER, E. R., PETERS, R. J., HENDRIKSEN, P. J., MARVIN, H. J., R.L.A.P., H., PEIJNENBURG, A. A. & BOUWMEESTER, H. 2014a. Sub-chronic toxicity study in rats orally exposed to nanostructured silica. *Particle and fibre toxicity*, 11.
- VAN DER ZANDE, M., VANDEBRIEL, R. J., GROOT, M. J., KRAMER, E., RIVERA, Z. H., RASMUSSEN, K., OSSENKOPPELE, J. S., TROMP, P., GREMMER, E. R., PETERS, R. J., HENDRIKSEN, P. J., MARVIN, H. J., PEIJNENBURG, A. A. & BOUWMEESTER, H. 2014b. Supporting Information: Sub-chronic Toxicity Study in Rats Orally Exposed to Nanostructured Silica. *Particle and fibre toxicity*, 11.
- VAN DER ZANDE, M., VANDEBRIEL, R. J., VAN DOREN, E., KRAMER, E., HERRERA RIVERA, Z., SERRANO-ROJERO, C. S., GREMMER, E. R., MAST, J., PETERS, R. J., HOLLMAN, P. C., HENDRIKSEN, P. J., MARVIN, H. J., PEIJNENBURG, A. A. & BOUWMEESTER, H. 2012. Distribution, elimination, and toxicity of silver nanoparticles and silver ions in rats after 28-day oral exposure. *ACS Nano*, 6, 7427-42.
- VANDESOMPELE, J., DE PRETER, K., PATTYN, F., POPPE, B., VAN ROY, N., DE PAEPE, A. & SPELEMAN, F. 2002. Accurate normalization of real-time quantitative RT-PCR data by geometric averaging of multiple internal control genes. *Genome Biology*, 3.
- VECCHIONE, L., MASSIMIANI, M., CAMAIONI, A., SIFRANI, L., MAGRINI, A., PIETROIUSTI, A. & CAMPAGNOLO, L. 2013. A comparative study of metal oxide nanoparticles embryotoxicity using the embryonic stem cell test. *Bionanomaterials*, 14, 61-64.
- VECTORLABORATORIES. 2018. *Vectastain Elite ABC HRP System* [Online]. Maravai LifeSciences Available: <https://vectorlabs.com/vectastain-elite-abc-kit-universal-r-t-u-ready-to-use.html> [Accessed October 17th 2018].
- WANG, Z., QU, G., SU, L., WANG, L., YANG, Z., JIANG, J., LUI, S. & JIANG, G. 2013. Evaluation of the Biological Fate and the Transport Through Biological Barriers of Nanosilver in Mice. *Current Pharmaceutical Design*, 19.
- WEGNER, S., HONG, S., YU, X. & FAUSTMAN, E. M. 2013. Preparation of rodent testis co-cultures. *Curr Protoc Toxicol*, Chapter 16, Unit 16 10.
- WING, T.-U. & CHRISTENSEN, A. K. 1982. Morphometric Studies on Rat Seminiferous Tubules. *The American Journal of Anatomy*, 165.

- WINNALL, W. R. & HEDGER, M. P. 2013. Phenotypic and functional heterogeneity of the testicular macrophage population: a new regulatory model. *Journal of Reproductive Immunology*, 97, 147-158.
- WIWANITKIT, V., SEREEMASPUN, A. & ROJANATHANES, R. 2009. Effect of gold nanoparticles on spermatozoa: the first world report. *Fertil Steril*, 91, e7-8.
- XU, Y., WANG, N., YU, Y., LI, Y., LI, Y. B., YU, Y. B., ZHOU, X. Q. & SUN, Z. W. 2014. Exposure to silica nanoparticles causes reversible damage of the spermatogenic process in mice. *PLoS One*, 9, e101572.
- YAMASHITA, K., YOSHIOKA, Y., HIGASHISAKA, K., MIMURA, K., MORISHITA, Y., NOZAKI, M., YOSHIDA, T., OGURA, T., NABESHI, H., NAGANO, K., ABE, Y., KAMADA, H., MONOBE, Y., IMAZAWA, T., AOSHIMA, H., SHISHIDO, K., KAWAI, Y., MAYUMI, T., TSUNODA, S., ITOH, N., YOSHIKAWA, T., YANAGIHARA, I., SAITO, S. & TSUTSUMI, Y. 2011. Silica and titanium dioxide nanoparticles cause pregnancy complications in mice. *Nat Nanotechnol*, 6, 321-8.
- YE, L., YONG, K. T., LIU, L., ROY, I., HU, R., ZHU, J., CAI, H., LAW, W. C., LIU, J., WANG, K., LIU, J., LIU, Y., HU, Y., ZHANG, X., SWIHART, M. T. & PRASAD, P. N. 2012. A pilot study in non-human primates shows no adverse response to intravenous injection of quantum dots. *Nat Nanotechnol*, 7, 453-8.
- YIN, L., WEI, H., LIANG, S. & YU, X. 2017. From the Cover: An Animal-Free In Vitro Three-Dimensional Testicular Cell Coculture Model for Evaluating Male Reproductive Toxicants. *Toxicol Sci*, 159, 307-326.
- YOISUNGNERN, T., CHOI, Y. J., HAN, J. W., KANG, M. H., DAS, J., GURUNATHAN, S., KWON, D. N., CHO, S. G., PARK, C., CHANG, W. K., CHANG, B. S., PARNPAI, R. & KIM, J. H. 2015. Internalization of silver nanoparticles into mouse spermatozoa results in poor fertilization and compromised embryo development. *Sci Rep*, 5, 11170.
- YOO, K. C., YOON, C. H., KWON, D., HYUN, K. H., WOO, S. J., KIM, R. K., LIM, E. J., SUH, Y., KIM, M. J., YOON, T. H. & LEE, S. J. 2012. Titanium dioxide induces apoptotic cell death through reactive oxygen species-mediated Fas upregulation and Bax activation. *Int J Nanomedicine*, 7, 1203-14.
- YOUNG, L. E., FULTON, N. & HUTCHISON, G. H. 2014. *RE: Expression of A-R following exposure to uncoated and coated zinc oxide engineered nanoparticles (NM110 & 111) and silver nanoparticles (NM300)*. Type to ROSS, B. L.
- ZHANG, H., YANG, D., YANG, H. & LIU, H. 2008. Effect on conception and offspring development in female parental rats following intratracheal instillation of nano-C/ZnO and C-ZnO composite nanoparticles. *Wei Sheng Yan Jiu*, 37, 654-6.
- ZHANG, X. F., CHOI, Y. J., HAN, J. W., KIM, E., PARK, J. H., GURUNATHAN, S. & KIM, J. H. 2015a. Differential nanoreprotoxicity of silver nanoparticles in male somatic cells and spermatogonial stem cells. *Int J Nanomedicine*, 10, 1335-57.
- ZHANG, X. F., GURUNATHAN, S. & KIM, J. H. 2015b. Effects of silver nanoparticles on neonatal testis development in mice. *International journal of nanomedicine*, 2015.
- ZHU, X., WANG, J., ZHANG, X., CHANG, Y. & CHEN, Y. 2009. The impact of ZnO nanoparticle aggregates on the embryonic development of zebrafish (*Danio rerio*). *Nanotechnology*, 20, 195103.

RESEARCH ARTICLE

Comprehensive *In Vitro* Toxicity Testing of a Panel of Representative Oxide Nanomaterials: First Steps towards an Intelligent Testing Strategy

Lucian Farcas¹, Fernando Torres Andón¹, Luisana Di Cristo², Bianca Maria Rotoli³, Ovidio Bussolati³, Enrico Bergamaschi², Agnieszka Mech⁴, Nanna B. Hartmann^{4,5}, Kirsten Rasmussen⁴, Juan Riego-Sintes⁴, Jessica Ponti⁴, Agnieszka Kinsner-Ovaskainen⁴, François Rossi⁴, Agnes Oomen⁶, Peter Bos⁶, Rui Chen⁷, Ru Bai⁷, Chunying Chen⁷, Louise Rocks⁸, Norma Fulton⁹, Bryony Ross^{9,10}, Gary Hutchison⁹, Lang Tran¹⁰, Sarah Mues¹¹, Rainer Ossig¹¹, Jürgen Schneckeburger¹¹, Luisa Campagnolo¹², Lucia Vecchione¹², Antonio Pietroiusti¹², Bengt Fadeel^{1*}



CrossMark
click for updates

 OPEN ACCESS

Citation: Farcas L, Torres Andón F, Di Cristo L, Rotoli BM, Bussolati O, Bergamaschi E, et al. (2015) Comprehensive *In Vitro* Toxicity Testing of a Panel of Representative Oxide Nanomaterials: First Steps towards an Intelligent Testing Strategy. PLoS ONE 10(5): e0127174. doi:10.1371/journal.pone.0127174

Academic Editor: Donghui Zhu, North Carolina A&T State University, UNITED STATES

Received: January 22, 2015

Accepted: April 13, 2015

Published: May 21, 2015

Copyright: © 2015 Farcas et al. This is an open access article distributed under the terms of the [Creative Commons Attribution License](https://creativecommons.org/licenses/by/4.0/), which permits unrestricted use, distribution, and reproduction in any medium, provided the original author and source are credited.

Data Availability Statement: All relevant data are within the paper and its Supporting Information files.

Funding: The study was supported by the European Commission Seventh Framework Programme Project FP7-MARINA (Grant No. 263215; www.marina-fp7.eu). The funders had no role in study design, data collection and analysis, decision to publish, or preparation of the manuscript.

Competing Interests: The authors have declared that no competing interests exist.

1 Division of Molecular Toxicology, Institute of Environmental Medicine, Karolinska Institutet, Stockholm, Sweden, **2** Department of Clinical and Experimental Medicine, University of Parma, Parma, Italy, **3** Department of Biomedical, Biotechnological and Translational Sciences, University of Parma, Parma, Italy, **4** Nanobiosciences Unit, Institute for Health and Consumer Protection, European Commission—Joint Research Centre, Ispra, Italy, **5** Technical University of Denmark, Kongens Lyngby, Denmark, **6** National Institute for Public Health and the Environment, Bilthoven, The Netherlands, **7** Chinese Academy of Sciences Key Laboratory for Biomedical Effects of Nanomaterials and Nanosafety, National Center for Nanoscience & Technology of China, Beijing, P. R. China, **8** Centre for BioNano Interactions, School of Chemistry and Chemical Biology, University College Dublin, Belfield, Dublin, Ireland, **9** Centre for Nano Safety, Edinburgh Napier University, Edinburgh, United Kingdom, **10** Institute of Occupational Medicine, Edinburgh, United Kingdom, **11** Biomedizinisches Technologiezentrum, Westfälische Wilhelms-Universität, Münster, Germany, **12** Department of Biomedicine and Prevention, University of Rome Tor Vergata, Rome, Italy

* bengt.fadeel@ki.se

Abstract

Nanomaterials (NMs) display many unique and useful physico-chemical properties. However, reliable approaches are needed for risk assessment of NMs. The present study was performed in the FP7-MARINA project, with the objective to identify and evaluate *in vitro* test methods for toxicity assessment in order to facilitate the development of an intelligent testing strategy (ITS). Six representative oxide NMs provided by the EC-JRC Nanomaterials Repository were tested in nine laboratories. The *in vitro* toxicity of NMs was evaluated in 12 cellular models representing 6 different target organs/systems (immune system, respiratory system, gastrointestinal system, reproductive organs, kidney and embryonic tissues). The toxicity assessment was conducted using 10 different assays for cytotoxicity, embryotoxicity, epithelial integrity, cytokine secretion and oxidative stress. Thorough physico-chemical characterization was performed for all tested NMs. Commercially relevant NMs with different physico-chemical properties were selected: two TiO₂ NMs with different surface chemistry – hydrophilic (NM-103) and hydrophobic (NM-104), two forms of ZnO – uncoated (NM-110) and coated with triethoxycapryl silane (NM-111) and two SiO₂ NMs produced by two different manufacturing techniques – precipitated (NM-200) and pyrogenic (NM-203). Cell

Appendix 2: Experimental Outline for WST-1 & Alamar Blue assays

	1	2	3	4	5	6	7	8	9	10	11	12
A	0 ¹	0.125	1.25	12.5	25	50	100	200	200 + Triton ⁵	Media + Triton ²		
B	0 ¹	0.125	1.25	12.5	25	50	100	200	200 + Triton ⁵	Media + Triton ²		
C	0 ¹	0.125	1.25	12.5	25	50	100	200	200 + Triton ⁵	Media + Triton ²		
D	0	0.125 ⁶	1.25 ⁶	12.5 ⁶	25 ⁶	50 ⁶	100 ⁶	200 ⁶	200 + Triton	Control + Triton		
E	0	0.125 ⁶	1.25 ⁶	12.5 ⁶	25 ⁶	50 ⁶	100 ⁶	200 ⁶	200 + Triton	Control + Triton		
F	0	0.125 ⁶	1.25 ⁶	12.5 ⁶	25 ⁶	50 ⁶	100 ⁶	200 ⁶	200 + Triton	Control + Triton		
G	0 ³	0.125 ⁴	1.25 ⁴	12.5 ⁴	25 ⁴	50 ⁴	100 ⁴	200 ⁴	200 + Triton	Control + Triton		
H	0 ³	0.125 ⁴	1.25 ⁴	12.5 ⁴	25 ⁴	50 ⁴	100 ⁴	200 ⁴	200 + Triton	Control + Triton		

	<ol style="list-style-type: none"> 1. Add 200µl TM3 cells to wells A-C. Incubate for 24 hrs. 2. Remove media. Add prepared treatments to wells in triplicate. Incubate for 24 hrs. 3. Remove and store supernatants from TM3 cells, pooling triplicate wells. 4. Add 90µl DMEM+10µl WST-1 to these wells for WST-1 Assay.
	<ol style="list-style-type: none"> 1. Add 200µl of TM3 cells to wells D-F. Incubate for 24 hrs. 2. Remove media. Add prepared treatments to wells in triplicate. Incubate for 24 hrs. 3. Remove and store supernatants from TM3 cells, pooling triplicate wells. 4. Add 100µl of DMEM to each well. No WST-1.
	<ol style="list-style-type: none"> 1. Leave wells empty for the first 24hrs. 2. Add prepared treatments for the next 24 hrs. 3. Remove and store supernatants from TM3 cells, pooling triplicate wells. 4. Leave wells empty for WST-1 assay.

Figure 109: Experimental design for WST-1 assay, based on a 96 well plate. Plate rows are annotated A-H, and columns 1-12. Protocol denoted by grey shading, is noted in superscript and outlined in full within the body of the text.

Appendix 3: Preparation of RNA samples for PCR

Table 43: Sample preparation for PCR

RT Reaction setup: <i>Each reaction set to make 2000ng cDNA where possible</i>							Final PCR Reaction setup: <i>Final concentration of 5ng/μl per well</i>			
Nanomaterial	Sample	RNA Quantity ng/μl	VOLUME TO ADD (μl)	RNase free H2O to add	cDNA quantity after RT (ng)	Total Reaction Volume (μl)	Concentration cDNA (ng/μl)	Final Volume required for 5ng/μl concentration	Vol cDNA (μl)	Vol H2O (μl)
NM-300	n1 0μg/cm ²	394.03	5.08	3.92	2000	29	68.96551724	400	29	371
NM-300	n1 1.26μg/cm ²	145.7862	9	0	1312.0758	29	45.2439931	262.41516	30	233.41516
NM-300	n1 2.52μg/cm ²	-	-	-	-	-	-	-	-	-
NM-300	n2 0μg/cm ²	716.0984	2.79	6.21	2000	29	68.96551724	400	29	371
NM-300	n2 1.26μg/cm ²	759.9938	2.63	6.37	2000	29	68.96551724	400	29	371
NM-300	n2 2.52μg/cm ²	-	-	-	-	-	-	-	-	-
NM-300	n3 0μg/cm ²	1257.97	1.59	7.41	2000	29	68.96551724	400	29	371
NM-300	n3 1.26μg/cm ²	470.7	4.25	4.75	2000	29	68.96551724	400	29	371
NM-300	n3 2.52μg/cm ²	-	-	-	-	-	-	-	-	-
NM-110	n1 0μg/cm ²	208.03	9	0	1872.27	29	64.56103448	374.454	29	345.454
NM-110	n1 1.26μg/cm ²	182.04	9	0	1638.36	29	56.49517241	327.672	29	298.672
NM-110	n1 2.52μg/cm ²	383.94	5.21	3.79	2000	29	68.96551724	400	29	371
NM-110	n2 0μg/cm ²	371.64	5.38	3.62	2000	29	68.96551724	400	29	371
NM-110	n2 1.26μg/cm ²	171.4	9	0	1542.6	29	53.19310345	308.52	29	279.52
NM-110	n2 2.52μg/cm ²	357.77	5.59	3.41	2000	29	68.96551724	400	29	371
NM-110	n3 0μg/cm ²	830.03	2.41	6.59	2000	29	68.96551724	400	29	371
NM-110	n3 1.26μg/cm ²	578.6	3.46	5.54	2000	29	68.96551724	400	29	371
NM-110	n3 2.52μg/cm ²	358.755	5.57	3.43	2001	29	68.96551724	400	30	371
NM-111	n1 0μg/cm ²	473.45	4.22	4.78	2000	29	68.96551724	400	29	371
NM-111	n1 1.26μg/cm ²	372.32	5.37	3.63	2000	29	68.96551724	400	29	371
NM-111	n1 2.52μg/cm ²	135.26	9	0	1217.34	29	41.97724138	243.468	29	214.468
NM-111	n2 0μg/cm ²	750.36	2.67	6.33	2000	29	68.96551724	400		371
NM-111	n2 1.26μg/cm ²	1137.38	1.76	7.24	2000	29	68.96551724	400		371
NM-111	n2 2.52μg/cm ²	376.3	5.31	3.69	2001	29	68.96551724	400		371
NM-111	n3 0μg/cm ²	237.86	8.41	0.59	2000	29	68.96551724	400	29	371
NM-111	n3 1.26μg/cm ²	458.95	4.36	4.64	2000	29	68.96551724	400	29	371
NM-111	n3 2.52μg/cm ²	241.29	8.29	0.71	2000	29	68.96551724	400	29	371

Appendix 4: RNA Sample Quantification & Integrity Scoring

Table 44: RNA sample quantification and integrity scoring using spectrophotometry and chip-based gel electrophoresis.

ENM	Sample	NANODROP		BIOANALYZER	
		RNA Concentration (ng/ μ l)	RNA Purity (A260/A280)	RNA Concentration (ng/ μ l)	RNA integrity number (RIN)
NM-300	n1 0 μ g/cm ²	524.9	2.07	394.03	10
NM-300	n1 1.26 μ g/cm ²	112.3	2.07	145.7862	9.3
NM-300	n1 2.52 μ g/cm ²	2.14	(no reading)	<3	N/A
NM-300	n2 0 μ g/cm ²	539	2.09	716.0984	9.6
NM-300	n2 1.26 μ g/cm ²	572.2	2.11	759.9938	9.7
NM-300	n2 2.52 μ g/cm ²	45.8	2.05	-	N/A
NM-300	n3 0 μ g/cm ²	458.3	2.08	1257.97	10
NM-300	n3 1.26 μ g/cm ²	182.3	2.09	470.7	10
NM-300	n3 2.52 μ g/cm ²	14.1	(no reading)	-	N/A
NM-110	n1 0 μ g/cm ²	262.9	2.08	208.03	7.5
NM-110	n1 1.26 μ g/cm ²	173.9	2.08	182.04	9.5
NM-110	n1 2.52 μ g/cm ²	316	2.07	383.94	9.7
NM-110	n2 0 μ g/cm ²	193.3	2.08	371.64	9.9
NM-110	n2 1.26 μ g/cm ²	141.9	2.06	171.4	9.8
NM-110	n2 2.52 μ g/cm ²	268.7	2.11	357.77	9.2
NM-110	n3 0 μ g/cm ²	913.9	2.10	830.03	10
NM-110	n3 1.26 μ g/cm ²	290.4	2.10	578.6	9.3
NM-110	n3 2.52 μ g/cm ²	263.1	2.10	358.755	8.1
NM-111	n1 0 μ g/cm ²	420.2	2.11	473.45	10
NM-111	n1 1.26 μ g/cm ²	427.4	2.11	372.32	10
NM-111	n1 2.52 μ g/cm ²	157.8	2.08	135.26	9.6
NM-111	n2 0 μ g/cm ²	598.4	2.11	750.36	10
NM-111	n2 1.26 μ g/cm ²	857.2	2.09	1137.38	10
NM-111	n2 2.52 μ g/cm ²	179.2	2.07	376.3	8.9
NM-111	n3 0 μ g/cm ²	179.6	2.11	237.86	10
NM-111	n3 1.26 μ g/cm ²	844.6	2.07	458.95	10
NM-111	n3 2.52 μ g/cm ²	175.1	2.07	241.29	9.7